



MINISTÉRIO DO EQUIPAMENTO SOCIAL

# Laboratório Nacional de Engenharia Civil

---

## ACCURATE NUMERICAL MODELING OF ADVECTION-DOMINATED TRANSPORT OF PASSIVE SCALARS

A Contribution

Lisboa, Junho de 1986

---

António Eugénio de Melo Baptista

Tese apresentada a concurso para a obtenção do grau  
de especialista e acesso à categoria de investigador auxiliar  
do Laboratório Nacional de Engenharia Civil

---

I&D  
TESE  
HIDRÁULICA

MINISTERIO DAS OBRAS PUBLICAS, TRANSPORTES E COMUNICAÇÕES  
LABORATORIO NACIONAL DE ENGENHARIA CIVIL

DEPARTAMENTO DE HIDRAULICA  
NÚCLEO DE ESTUARIOS

Proc. 64/13/7398

ACCURATE NUMERICAL MODELING OF ADVECTION-DOMINATED TRANSPORT OF PASSIVE SCALARS  
A Contribution

António Eugénio de Melo Baptista

Tese apresentada ao concurso para acesso a investigador auxiliar e obtenção do grau de especialista do Laboratório Nacional de Engenharia Civil

Lisboa, Junho de 1986

7/7/86



To the memory of my father



Computer modelling in the area of hydraulic and coastal engineering is a very strongly integrated area of endeavour [...]. The remarkable achievements obtained in this area have led to further demands from the side of practice and new efforts on the side of the modellers to meet this demand. Looking at this situation from the research point of view, one might describe the area of modelling which is rather well understood and where the predictive capabilities are well-established as 'the white area'. There is also a very large area which is so little understood and where predictive capability is so low that one could describe it as 'the black area'. In between these areas is a considerable 'grey area', merging into white on the one side and black on the other. As research progresses, the white area expands and the black is invaded further by the grey, but a grey area still remains in the middle. [...]. It is the duty of every organisation in the modelling business to ascertain, through its research, just how 'grey' its models are in any actual application and to communicate the extent of this 'greyiness' [...].

in "Computer modelling: a warning", by the Section for the Use of Computers on Hydraulics and Water Resources, of the IAHR (THE DOCK & HARBOUR AUTHORITY, MARCH 1986)

The solution of first-order hyperbolic problems is schizophrenic [...].

in LAPIDUS and PINDER 1982, pg. 619



## ABSTRACT

This work presents a systematic study, based on both formal analysis and numerical experimentation, of the accuracy and stability of the solution of the advection-dominated transport equation by an Eulerian-Lagrangian method (ELM). The method splits the transport equation into advection and diffusion components, solving the former by the backwards method of characteristics (BMC), and the latter by a Galerkin finite element method.

The space-interpolation procedure associated to the BMC is shown to be critical for the overall accuracy, and alternative interpolation schemes (some of which first proposed) are compared. A combination of compact and non-compact Lagrange interpolation schemes is suggested to be a potential best choice.

The BMC is shown to be, for proper choices of the interpolation procedure, consistent, stable, convergent and accurate; some other choices lead, however, to instability or inconsistency.

The dependence of the accuracy of the BMC on the number of time steps required to reach a fixed total time is firmly established. Taking less and larger time steps is shown to typically improve accuracy (a both unusual and very convenient behavior); in the range of very small Courant numbers, however, accuracy is quasi-independent of the time step, which avoids divergence.

The effect of grid non-uniformity and multi-dimensionality on the feasibility and accuracy of the BMC is briefly examined. All considered interpolation procedures are shown to be sensitive to grid non-uniformity, but the BMC performs well as long as the grid distortion is not excessive; further work is deemed necessary to establish proper criteria on this regard. Multi-dimensional grids pose special difficulties only for non-compact interpolation schemes, and when associated to unstructured non-uniformity; the combination of compact and non-compact schemes, in the solution of a same problem, should considerably alleviate such difficulties, which also demands further work.

The presence of physical diffusion is shown to improve both the solution of the advection step and the overall accuracy of the reference ELM.

Finally, the application of the reference ELM (in a particular form, based on compact interpolation schemes alone), to the solution of selected case studies of pollutant transport in coastal waters, is discussed and its usefulness demonstrated. In particular, the method is shown to allow long-term (several tides) simulations at moderate cost, even for large and complex grids, and to avoid the need for artificially high diffusivities as a numerical stabilizer or smoother; both in general and in these two specific accounts, the reference ELM reveals a superior performance relative to conventional Eulerian methods (e.g., Galerkin or Petrov-Galerkin finite element methods, applied to the undecoupled transport equation)





## SUMÁRIO

Apresenta-se um estudo sistemático, baseado simultaneamente em análises formais e em experimentação numérica, da precisão e estabilidade da solução da equação de transporte por um método Euleriana-Lagrangeana (MEL). O método decompõe a equação de transporte em equações separadas de advecção e de difusão, resolvendo a primeira pelo método das características regressivas no tempo (MCR), e a segunda por um método de elementos finitos, do tipo Galerkin.

Mostra-se que as interpolações no espaço requeridas pelo MCR são um factor limitativo da precisão global do MEL, e comparam-se diversas técnicas alternativas de interpolação, algumas das quais originais. A combinação de esquemas compactos e não-compactos de interpolação, baseados em polinómios de Lagrange, é apontada como uma potencial solução óptima.

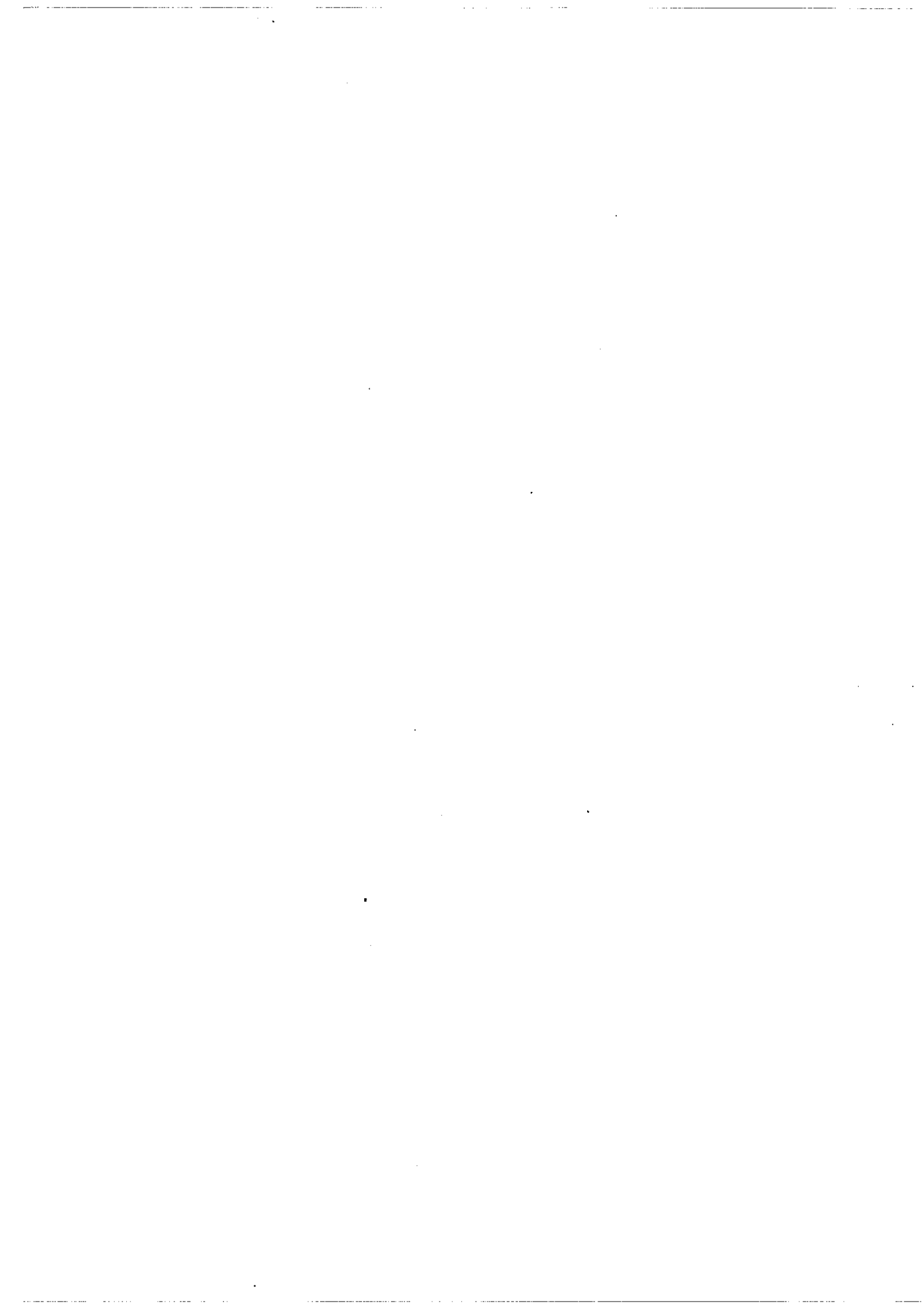
Demonstra-se que, para uma adequada escolha do esquema de interpolação, o MCR é consistente, estável e convergente e tem boas características de precisão. Escolhas inadequadas do esquema de interpolação podem, no entanto, causar instabilidade e inconsistência.

Estabelece-se a dependência da precisão do MCR no passo de cálculo, mostrando-se que essa precisão aumenta, em geral (para um tempo total fixo), quando se reduz o número de passos de cálculo, isto é, quando se aumenta o passo de cálculo (uma propriedade simultaneamente pouco habitual e muito conveniente). No entanto, na gama de valores muito pequenos do Número de Courant, a precisão é praticamente independente do passo de cálculo, o que evita que o método se torne divergente.

Analisa-se brevemente o efeito de malhas irregulares e pluri-dimensionais sobre a aplicabilidade e precisão do MCR. Apesar de sensível à irregularidade da malha, o método mantém boas características de precisão desde que as distorções geométricas não sejam excessivas. Malhas pluri-dimensionais, quando simultaneamente irregulares, levantam problemas específicos de aplicabilidade de esquemas não-compactos de interpolação; esses problemas poderão ser resolvidos através da utilização conjugada de esquemas compactos e não-compactos, para um mesmo problema. Investigação adicional é ainda requerida nestas áreas.

Mostra-se ainda que a presença de mecanismos físicos de difusão beneficia tanta a precisão da solução da equação de advecção como a precisão global do MEL.

Finalmente, demonstra-se a eficácia da aplicação do MEL (numa forma particular, restricta a esquemas de interpolação compactos) à simulação do transporte de poluentes em águas costeiras. O método permite, em particular, realizar simulações longas (várias marés) a custos moderados, mesmo para malhas irregulares com elevado número de nós, e, também, evitar a necessidade do uso de difusividades artificiais como garante de estabilidade; em geral, e nestes dois aspectos em particular, o método revela-se superior a métodos Eulerianos, mais convencionais (por exemplo, métodos de elementos finitos, do tipo Galerkin ou Petrov-Galerkin, aplicados à equação de transporte indivisa).



## ACKNOWLEDGEMENTS

This work was performed at the Estuaries Division of the Hydraulics Department of Laboratório Nacional de Engenharia Civil (LNEC), as a part of the research project "Modelação matemática da hidrodinâmica e qualidade da água em estuários" (Mathematical modeling of hydrodynamics and water quality in estuaries), sponsored by PIDDAC (Plano de Investimentos e de Despesas de Desenvolvimento da administração Central).

The work, presented in fulfillment of the requirements for my access to the category of Investigador Auxiliar do LNEC, integrates a cycle that was initiated at Massachusetts Institute of Technology (with my degree of Master of Science in Civil Engineering, in 1984), and that will be formally closed with the submission to the same University of a thesis in fulfillment of the requirements for the degree of Doctor of Philosophy.

Throughout this cycle, I have received financial support from a number of Institutions, which I now gratefully acknowledge:

- LNEC awarded me a paid leave during my stay at MIT (from August 1982 to June 1984), and has, since then, and within the severe constraints of the available budget, assisted in my periodic visits to MIT.
- NATO Committee on the Challenges of Modern Society, who, through the Pilot Study "Use of remote sensing in setting up models designed to anticipate maritime pollution movements" (to which this work is a contribution), awarded me a grant that has made possible the technical contacts that are essential to carry out the research.
- Comissão INVOTAN, who supported my tuition as a non-resident student at MIT, and partially supported two of the visits to MIT, for meetings with my PhD Thesis Committee (since September 85). INVOTAN had also provided partial support for living expenses during my first year of resident work at MIT (1982/1983).
- Massachusetts Institute of Technology, who provided me with a Research Assistantship during my work towards the Master of Science degree (1982/1984); and Comissão Cultural Luso-Americana, who supported my travelling expenses in the same period.

In addition to the specific support concerning my academic program at MIT, LNEC has, for the past eight years, provided conditions for the improvement of my academic and scientific background, and for the development of systematic research (of which this work is a part). While my acknowledgement is extensive to the present Director and to the previous Director, and to the present and the previous Heads of the Hydraulics Department, the confidence and encouragement of Mr. Pires Elias, Head of the Estuaries Division, and of Messrs. Júlio Barceló and Mr. Reis de Carvalho, former Heads of the same Division, are stressed and worth particular appreciation.

My advisors at Massachusetts Institute of Technology, Drs. E. Eric Adams and Keith D. Stolzenbach (who is also a member of the jury for evaluation of this thesis), have provided healthy technical discussion and constant encouragement and friendship, throughout the whole cycle of this research. Their serious yet uncomplicated way of doing and promoting research has been an excellent motivation and should be an example to follow.

A number of my colleagues and support staff at LNEC have assisted me throughout the preparation of this thesis. I would like to emphasize the contributions of:

- Mr. Geadas Cabaço, a technician at the Estuaries Division, who has been working with me for the past six years, and, once more, revealed his extraordinary competence, skilness and dedication to work. He directly contributed to this thesis in a variety of essential ways, which included: performing endless computer runs, coding and debugging computer programs (e.g., most of the figures were generated with his plotting codes), and correcting text, figures and tables.
- Mr. Areias Capitão, a Research Trainee Officer, at the Estuaries Division, who alleviated me from a significant part of my work on ongoing projects, and, in the later phase of the thesis, provided a decisive assistance in some of the calculations and, very specially, in the endless work of reviewing the manuscript, correcting the typing in the word processor, and correcting figures and tables. His human and professional qualities are acknowledged.
- Dr. Mendes de Carvalho, a Senior Research Officer at the Harbor and Beaches Division, who provided useful discussion on part of the material of Chapter 4, and made a patient revision of my american-english (remaining mistakes are my sole responsibility).
- Mr. Fernando Mendes, from the Graphic Arts of LNEC, who was responsible for the very efficient and fast preparation of the thesis brochure.
- Mssrs. Fernando Brito and João Vale, trainee technicians at the Estuaries Division, who did a patient and skilled job in the drawing and preparation of the figures, and in the respective corrections. Mr. Brito also did a significant part of the word processing work.

Thanks are also due to Dr. Afonso Covas, from the Harbor and Beaches Division, who accepted to be a member of the jury for evaluation of this thesis.

Several of my colleagues and support staff at LNEC, while not contributing directly to this work, have provided assistance in different phases of my activity in this Laboratory. I wish to express my sincere appreciation to them, and, in particular, to Mssrs. Eduardo Oliveira, David Leite, Oliveira Costa, João Cunha, among the former, and Mr. Ildemundo Martins and his team, among the latter.

Finally, very special thanks are due my mother, brother and sister-in-law, who have been strongly supportive throughout the times; to my loving and very special wife, a source of strenght (who, as usual, gave an hand in the drawing of part of the figures); and to our son, a 21 month old source of charm and fun.

Ten years after his death, this thesis is dedicated to the memory of my father.

**ACCURATE NUMERICAL MODELING OF ADVECTION-DOMINATED TRANSPORT OF PASSIVE SCALARS  
A contribution**

**TABLE OF CONTENTS**

**CHAPTER 1: INTRODUCTION**

1.1 MOTIVATION AND OBJECTIVES .....	3
1.2 RESEARCH OUTLINE AND TEXT ORGANIZATION .....	4

**CHAPTER 2: BACKGROUND**

2.1 MATHEMATICAL STATEMENT OF THE TRANSPORT PROBLEM .....	9
2.1.1 Governing equation for three-dimensional transport .....	9
2.1.2 Governing equation for two-dimensional (depth-averaged) transport ...	11
2.1.3 Initial and boundary conditions .....	13
2.2 ON THE ROLE OF ADVECTION AND DIFFUSION .....	16
2.3 ON THE MATHEMATICAL NATURE OF THE TRANSPORT EQUATION .....	19
2.4 REVIEW OF NUMERICAL SOLUTION METHODS FOR THE TRANSPORT EQUATION .....	21
2.4.1 Introduction .....	21
2.4.2 Eulerian methods .....	21
2.4.3 Eulerian-Lagrangian methods .....	24

**CHAPTER 3: DESCRIPTION OF A REFERENCE EULERIAN-LAGRANGIAN METHOD**

3.1. INTRODUCTION .....	31
3.2 THE SPLITTING OF ADVECTION AND DIFFUSION .....	32
3.2.1 Standard approach .....	32
3.2.2 Modified approach .....	33
3.2.3 Splitting errors .....	34
3.3 SOLUTION OF THE DIFFUSION EQUATION .....	36

3.3.1 Introduction .....	36
3.3.2 The weighted-residual statement .....	36
3.3.3 The finite element formulation .....	38
3.3.4 Time-discretization scheme. Solution strategy .....	48
3.4 SOLUTION OF THE ADVECTION EQUATION .....	41
3.4.1 Introduction .....	41
3.4.2 The stepwise particle tracking .....	41
3.4.3 The interpolation step .....	43
3.5 INTRODUCTORY DISCUSSION ON ACCURACY AND STABILITY .....	45

#### CHAPTER 4: ACCURACY AND STABILITY ANALYSIS OF THE BACKWARDS METHOD OF CHARACTERISTICS

4.1 INTRODUCTION .....	49
4.2 CONSTANT ADVECTION IN ONE-DIMENSIONAL UNIFORM GRIDS .....	50
4.2.1 Introduction .....	50
4.2.2 Truncation errors .....	52
4.2.3 Amplitude and phase errors .....	55
4.2.3.1 General remarks .....	55
4.2.3.2 The case of interpolation schemes with linear core elements .....	55
4.2.3.2.1 Theoretical framework .....	55
4.2.3.2.2 Characteristics of errors per time step .....	58
4.2.3.2.3 Characteristics of errors after N time steps .....	60
4.2.3.3 Interpolation schemes with quadratic and higher order core elements.....	61
4.2.3.3.1 Theoretical framework .....	61
4.2.3.3.2 Characteristics of errors in the first time step .....	63
4.2.3.3.3 Characteristics of errors after N time steps .....	64
4.2.4 Global accuracy .....	65
4.2.4.1 General remarks .....	65
4.2.4.2 Mass preservation .....	66
4.2.4.3 Numerical dissipation and dispersion .....	67

4.2.4.4	Dependence of the global accuracy on controlling parameters .....	68
4.2.5	Consistency, stability and convergence .....	69
4.2.5.1	General remarks .....	69
4.2.5.2	Stability .....	69
4.2.5.3	Convergence .....	70
4.3	EXTENSION TO NON-UNIFORM ONE-DIMENSIONAL GRIDS .....	73
4.3.1	General remarks .....	73
4.3.2	Extension of the definition of the interpolation schemes .....	73
4.3.3	Set-up of a numerical experiment and analysis of results .....	73
4.4	EXTENSION TO TWO DIMENSIONS .....	76
4.4.1	The case of straight orthogonal grids .....	76
4.4.2	The case of unstructured grids .....	77
4.5	REMARKS ON THE SELECTION OF THE INTERPOLATION SCHEME .....	79

**CHAPTER 5: GENERAL PROPERTIES OF EULERIAN-LAGRANGIAN METHODS**

5.1	INTRODUCTION .....	85
5.2	DEPENDENCE OF ACCURACY ON THE RELATIVE IMPORTANCE OF ADVECTION AND DIFFUSION .....	86
5.3	ON THE CHOICE OF THE TIME STEP .....	88

**CHAPTER 6: THE NUMERICAL MODELING OF POLLUTANT TRANSPORT IN COASTAL  
WATERS REVISITED**

6.1	INTRODUCTION .....	95
6.2	OUTLINE OF THE TRANSPORT PROBLEM .....	96
6.3	REVIEW OF THE TRANSPORT MODEL ELA .....	98
6.3.1	Motivation .....	98
6.3.2	Formulation .....	99
6.4	REVIEW OF SELECTED APPLICATIONS .....	100
6.4.1	Sludge dumping in Massachusetts Bay .....	100
6.4.2	Heat disposal from the Brayton Point Generating Station .....	101



6.4.3 Sludge disposal in Boston Harbor ..... 104

6.5 DISCUSSION OF THE GENERAL PERFORMANCE AND FURTHER IMPROVEMENTS FOR  
ELA ..... 106

**CHAPTER 7: CONCLUSIONS**

7.1 NUMERICAL SOLUTION OF THE TRANSPORT EQUATION BY EULERIAN-LAGRANGIAN  
METHODS ..... 113

7.2 NUMERICAL MODELING OF POLLUTANT TRANSPORT IN COASTAL WATERS ..... 115

**REFERENCES** ..... 117

**FIGURES**

**TABLES**

**APPENDICES**

- A. REFERENCE TEST PROBLEMS FOR THE CONVECTION-DIFFUSION FORUM
- B. A NOTE ON THE CIRCULATION MODELS TEA AND TEANL
- C. SOURCE REPRESENTATION IN A NUMERICAL TRANSPORT MODEL

ACCURATE NUMERICAL MODELING OF ADVECTION-DOMINATED TRANSPORT OF PASSIVE SCALARS  
A contribution

LIST OF FIGURES

Chapter 2

1. Definition sketch for a 2-D quasi-horizontal flow
2. Diagrammatic representation of hyperbolic and parabolic partial differential equations
3. The double-step, implicit-explicit second order scheme: (a) Finite-difference discretization; (b) Numerical dispersion characteristics (the method has no amplitude errors); (c) Application to the advection of a cosine-hill

Chapter 3

1. Statement of the 2-D transport problem. Definition sketch
2. General solution procedure for the reference Eulerian-Lagrangian method. Illustrative sketch
3. Solution of the advection equation. Illustrative sketch
4. Particle tracking. Illustrative sketch

Chapter 4

1. Definition of alternative interpolation schemes for the Backwards Method of Characteristics
2. Amplifying factors as a function of  $\alpha$  and  $L_m/\Delta x$  (first time step)
3. Phase errors as a function of  $\alpha$  and  $L_m/\Delta x$  (first time step)
4. Celerity ratios as a function of  $\alpha$  and  $L_m/\Delta x$  (first time step)
5. Statistics of the amplifying factors as a function of  $L_m/\Delta x$  (first time step)

6. Amplifying factors as a function of  $L_m/\Delta x$  ( $\kappa=0.5$ ), after N time steps (N=10,100,1000,10000)
7. Amplifying factors as a function of  $L_m/\Delta x$  ( $\kappa=0.0625$ ), after N time steps (N=10,100,1000,10000)
8. Amplifying factors as a function of  $L_m/\Delta x$  ( $\kappa=0.24$ ), after N time steps (N=10,100,1000,10000)
9. Amplifying factors as a function of  $L_m/\Delta x$ , after a sequence of N randomly generated time steps (N=100,1000,10000)
10. Amplifying factors per time step ( $L_m/\Delta x=3, 4, 5$ ), as a function of the number of time steps, for interpolation schemes with quadratic core elements
11. Amplitude and phase errors in BMC solutions of the uniform advection of a Gauss-hill ( $Cu=0.24$ ;  $N=100$ ;  $\sigma_0/\Delta x=1.32$ ;  $t=T=9600$ )
12. BMC solutions for the uniform advection of a Gauss-hill ( $Cu=0.24$ ;  $N=100$ ;  $\sigma_0/\Delta x=1.32$ ;  $t=T=9600$ )
13. BMC solutions for the uniform advection of a Gauss-hill ( $Cu=0.24$ ;  $N=100$ ;  $\sigma_0/\Delta x=1.6$ ;  $t=T=9600$ )
14. BMC solutions for the uniform advection of a Gauss-hill ( $Cu=0.24$ ;  $N=100$ ;  $\sigma_0/\Delta x=2.0$ ;  $t=T=9600$ )
15. BMC solutions for the uniform advection of a Gauss-hill ( $Cu=0.024$ ;  $N=1000$ ;  $\sigma_0/\Delta x=1.32$ ;  $t=T=9600$ )
16. BMC solutions for the uniform advection of a Gauss-hill ( $Cu=0.024$ ;  $N=1000$ ;  $\sigma_0/\Delta x=1.6$ ;  $t=T=9600$ )
17. BMC solutions for the uniform advection of a Gauss-hill ( $Cu=0.024$ ;  $N=1000$ ;  $\sigma_0/\Delta x=2.0$ ;  $t=T=9600$ )
18. BMC solutions for the uniform advection of a Gauss-hill ( $Cu=0.125$ ;  $N=100$ ;  $\sigma_0/\Delta x=1.32$ ;  $t=T=5000$ )
19. BMC solutions for the uniform advection of a Gauss-hill ( $Cu=0.125$ ;  $N=100$ ;  $\sigma_0/\Delta x=1.6$ ;  $t=T=5000$ )
20. BMC solutions for the uniform advection of a Gauss-hill ( $Cu=0.125$ ;  $N=100$ ;  $\sigma_0/\Delta x=2.0$ ;  $t=T=5000$ )
21. BMC solutions for the uniform advection of a Gauss-hill ( $Cu=0.375$ ;  $N=100$ ;  $\sigma_0/\Delta x=1.32$ ;  $t=T=15000$ )
22. BMC solutions for the uniform advection of a Gauss-hill ( $Cu=0.375$ ;  $N=100$ ;  $\sigma_0/\Delta x=1.6$ ;  $t=T=15000$ )
23. BMC solutions for the uniform advection of a Gauss-hill ( $Cu=0.375$ ;  $N=100$ ;  $\sigma_0/\Delta x=2.0$ ;  $t=T=15000$ )
24. BMC solutions for the uniform advection of a Gauss-hill ( $Cu=1.2$ ;  $N=20$ ;  $\sigma_0/\Delta x=1.32$ ;  $t=T=9600$ )

25. BMC solutions for the uniform advection of a Gauss-hill ( $Cu=2.4$ ;  $N=10$ ;  $\sigma_0/\Delta x=1.32$ ;  $t=T=9600$ )
26. BMC solutions for the uniform advection of a Gauss-hill ( $Cu=4.8$ ;  $N=5$ ;  $\sigma_0/\Delta x=1.32$ ;  $t=T=9600$ )
27. Mean square error as a function of the number of time steps required to reach a fixed total time ( $Cu=24/N$ ,  $t=T=9600$ )
28. Mean square error as a function of the number of time steps required to reach a fixed total time ( $Cu=50/N$ ,  $t=T=20000$ )
29. Mean square error as a function of the grid discretization ( $Cu=0.096/\Delta x$ ;  $N=50000$ ;  $t=T=9600$ ;  $\sigma_0=264$ )
30. Mean square error as a function of the grid discretization ( $Cu=0.2/\Delta x$ ;  $N=50000$ ;  $t=T=20000$ ;  $\sigma_0=264$ )
31. Definition of the non-uniform grids considered in section 4.3
32. Effect of different elementary mappings in the accuracy of BMC solutions for non-uniform grids
33. BMC solutions for the uniform advection of a Gauss-hill in grids of type 1 ( $N=100$ ;  $t=T=9600$ ;  $\sigma_0=264$ ;  $u=0.5$ )
34. BMC solutions for the uniform advection of a Gauss-hill in grids of type 1 ( $N=100$ ;  $t=T=9600$ ;  $\sigma_0=400$ ;  $u=0.5$ )
35. BMC solutions for the uniform advection of a Gauss-hill in grids of type 2 ( $N=100$ ;  $t=T=9600$ ;  $\sigma_0=264$ ;  $u=0.5$ )
36. BMC solutions for the uniform advection of a Gauss-hill in grids of type 2 ( $N=100$ ;  $t=T=9600$ ;  $\sigma_0=400$ ;  $u=0.5$ )
37. BMC solutions for the uniform advection of a Gauss-hill in grids of type 3 ( $N=100$ ;  $t=T=9600$ ;  $\sigma_0=264$ ;  $u=0.5$ )
38. BMC solutions for the uniform advection of a Gauss-hill in grids of type 3 ( $N=100$ ;  $t=T=9600$ ;  $\sigma_0=400$ ;  $u=0.5$ )
39. BMC solutions for the uniform advection of a Gauss-hill in grids of type 4 ( $N=100$ ;  $t=T=9600$ ;  $\sigma_0=264$ ;  $u=0.5$ )
40. BMC solutions for the uniform advection of a Gauss-hill in grids of type 4 ( $N=100$ ;  $t=T=9600$ ;  $\sigma_0=400$ ;  $u=0.5$ )
41. BMC solutions for the uniform advection of a Gauss-hill in grids of type 5 ( $N=100$ ;  $t=T=9600$ ;  $\sigma_0=264$ ;  $u=0.5$ )
42. BMC solutions for the uniform advection of a Gauss-hill in grids of type 5 ( $N=100$ ;  $t=T=9600$ ;  $\sigma_0=400$ ;  $u=0.5$ )
43. Interpolation schemes in 2-D straight orthogonal grids. Illustrative sketch

44. BMC solutions for the 2-D advection of a Gauss-hill in a flow field in rigid-body rotation. Concentration profiles after one revolution ( $W=2\pi/3000$ ;  $N=30$ ;  $\sigma_x=\sigma_y=264$ )
45. BMC solutions for the 2-D advection of a cone-hill in a flow field in rigid-body rotation. Concentration profiles after one revolution ( $W=2\pi/3000$ ;  $N=30$ ;  $l=800$ )
46. Extension of non-compact interpolation schemes to 2-D unstructured grids. Illustration of a possible ambiguity in the identification of nodes contributing to the interpolation
47. Extension of non-compact interpolation schemes to 2-D unstructured grids. Illustration of difficulties in mapping global into local coordinates
48. Extension of non-compact interpolation schemes to 2-D unstructured grids. Illustration of the interpolation procedure in global coordinates

## Chapter 5

1. ELM solutions for the transport of a Gauss-hill in a uniform flow. An illustration of the accuracy dependence on  $Pe$  ( $Cu=0.24$ ;  $N=100$ ;  $\sigma_0/\Delta x=1.32$ ;  $t=T=9600$ )
2. ELM solutions for the transport of a Gauss-hill in a uniform flow, using the 3P-LI3. An illustration of the accuracy dependence on  $N$ , for different  $Pe$ ,  $Cu$ ,  $Di$  ( $\sigma_0/\Delta x=1.32$ ;  $t=T=9600$ )
3. ELM solutions for the transport of a Gauss-hill in a uniform flow, using the 5P-LR3. An illustration of the accuracy dependence on  $N$ , for different  $Pe$ ,  $Cu$ ,  $Di$  ( $\sigma_0/\Delta x=1.32$ ;  $t=T=9600$ )
4. ELM solutions for the transport of a Gauss-hill in a uniform flow, using the 5P-HL3. An illustration of the accuracy dependence on  $N$ , for different  $Pe$ ,  $Cu$ ,  $Di$  ( $\sigma_0/\Delta x=1.32$ ;  $t=T=9600$ )
5. ELM solutions for the transport of a Gauss-hill in a uniform flow, using the 8P-PL2. An illustration of the accuracy dependence on  $N$ , for different  $Pe$ ,  $Cu$ ,  $Di$  ( $\sigma_0/\Delta x=1.32$ ;  $t=T=9600$ )
6. Mean square error as a function of the number of time steps required to reach a fixed total time ( $\sigma_0/\Delta x=1.32$ ;  $t=T=9600$ )
7. Qualitative cost function for the reference ELM
8. Qualitative cost and accuracy functions, for the reference ELM

## Chapter 6

1. Heat dispersion in the water environment. Identification of zones of analysis and of transport processes

2. Massachusetts Bay. Finite element grid
3. Massachusetts Bay. Flow field at maximum ebb
4. Massachusetts Bay. Flow field at maximum flood
5. Massachusetts Bay. Sludge plumes for dumping at Site 1
6. Massachusetts Bay. Sludge plumes for dumping at Site 2
7. Brayton Point. Complete finite element grid for Mt. Hope Bay
8. Brayton Point. Detail of the finite element grid near the discharge
9. Brayton Point. Circulation computed by TEA at maximum ebb
10. Brayton Point. Detail of circulation computed by TEA at high tide
11. Brayton Point. Detail of circulation computed by TEA at maximum ebb
12. Brayton Point. Finite element grid for transport calculations
13. Brayton Point. Excess temperature at high tide and maximum ebb
14. Major sources of pollution to Boston Harbor
15. Boston Harbor application. Finite element grid for Massachusetts Bay
16. Boston Harbor application. Detail of the finite element grid in the zone of the Harbor
17. Current velocities in the Boston Harbor 4 1/2 hours after low tide
18. Simulated concentrations (parts-per-trillion) in Boston Harbor at high water slack ( $E_x=E_y=10\text{m}^2/\text{sec}$ ;  $K=10\text{ cm/hr}$ ; variable source strength)
19. Total mass in the domain versus number of time steps ( $\Delta t=3.1\text{ hrs}$ ;  $E_x=E_y=60\text{m}^2/\text{s}$ ;  $K=1\text{cm/hr}$ ;  $CoQo=13.4\text{ Kg/day}$ )

ACCURATE NUMERICAL MODELING OF ADVECTION-DOMINATED TRANSPORT OF PASSIVE SCALARS  
A contribution

LIST OF TABLES

Chapter 4

1. Truncation errors for alternative interpolation schemes (general case)
2. Truncation errors for alternative interpolation schemes (case of  $\beta < 1$ , i.e.,  $\alpha = \beta = u\Delta t/\Delta x$ )
3. Amplitude and phase errors of the BMC for alternative interpolation schemes (first time step)
4. Complementary functions for the propagation of amplitude and phase errors for interpolation schemes with quadratic core elements
5. Accuracy measures for the BMC solution of the uniform advection of a Gauss-hill (problems of the Convection-Diffusion Forum).
6. Fourier representation of different instantaneous sources, in the domain  $x \in [0, 13600]$ .
7. Standard interpolation functions and isoparametric mappings for 1-D elements
8. Improved interpolation functions and isoparametric mappings for 1-D elements
9. Accuracy measures for the BMC solution of the uniform advection of a Gauss-hill in irregular grids ( $u=0.5$ ;  $t=T=9600$ ;  $N=100$ )
10. Standard interpolation functions and isoparametric mappings for triangular elements
11. Standard interpolation functions and isoparametric mappings for quadrangular elements
12. Improved interpolation functions and isoparametric mappings for 9-nodes quadrangular elements
13. Number of nodes and operations associated to alternative interpolation schemes (uniform grids)

## Chapter 5

1. Accuracy measures for the transport of a Gauss-hill in a uniform flow. An illustration of the dependence on  $Pe$  ( $Cu=0.24$ ;  $N=100$ ;  $\sigma_0/\Delta x=1.32$ ;  $t=T=9600$ )
2. Accuracy measures for the transport of a Gauss-hill in a uniform flow, using the 3P-PL13. An illustration of the dependence on  $N$ , for different  $Pe$ ,  $Cu$ ,  $Di$  ( $\sigma_0/\Delta x=1.32$ ;  $t=T=9600$ )
3. Accuracy measures for the transport of a Gauss-hill in a uniform flow, using the 5P-LR3. An illustration of the dependence on  $N$ , for different  $Pe$ ,  $Cu$ ,  $Di$  ( $\sigma_0/\Delta x=1.32$ ;  $t=T=9600$ )
4. Accuracy measures for the transport of a Gauss-hill in a uniform flow, using the 5P-HL3. An illustration of the dependence on  $N$ , for different  $Pe$ ,  $Cu$ ,  $Di$  ( $\sigma_0/\Delta x=1.32$ ;  $t=T=9600$ )
5. Accuracy measures for the transport of a Gauss-hill in a uniform flow, using the 8P-PL2. An illustration of the dependence on  $N$ , for different  $Pe$ ,  $Cu$ ,  $Di$  ( $\sigma_0/\Delta x=1.32$ ;  $t=T=9600$ )
6. CPU time (seconds) for the solution of the advection-diffusion reference problem





CHAPTER 1  
INTRODUCTION



## 1.1. MOTIVATION AND OBJECTIVES

Computer modeling is a powerful tool for the analysis of a variety of problems in Hydraulics and Environmental Engineering, as long as it is properly used. However, it is too easy to misuse a computer model, as it is well illustrated by the article by the IAHR Section for the Use of Computers on Hydraulics and Water Resources, published under the title "Computer modelling: a warning" in the March 1986 edition of THE DOCK AND HARBOR AUTHORITY.

The role of research institutions, such as LNEC, is of key importance in making computer modeling a useful rather than a dangerous tool. Such role should include identifying priority areas for fundamental and applied research, effectively carrying out and exploring the results of such research, and promoting a wide divulgation of both successes and failures among the technical and scientific communities.

One of the areas where the misuse of computer modeling is a permanent risk is that of the simulation of the transport of passive scalars in coastal waters. Indeed, the complexity of the relevant physical mechanisms, the diversity of important time and space scales, and the complexity and cost of field data collection and processing, contribute to make computer modeling in this area specially uncontrolled, and therefore, highly subject to errors.

In recent years, a variety of efforts have been made to overcome the inherent deficiencies of currently accepted conceptual formulations and numerical solution techniques. Other efforts have concentrated on making the already available tools safer and easier to use, through recommendations and the establishment of practical user's criteria. Also, efforts have been made to improve our ability to collect and interpret field data, at affordable costs.

The emphasis of the present work has been placed on basic research in the area of the numerical solution of the advection-dominated transport equation. This equation has been a major challenge in computational fluid dynamics since ever, and valid contributions to the understanding and overcoming of the deficiencies of available methods are in increasingly great demand, in various technical domains.

Our general objective is to contribute to improve the current ability to solve the transport equation through what has come to be known as Eulerian-Lagrangian techniques, and to establish a solid formal knowledge of the properties of these increasingly popular techniques (so as to assist their application to practical problems).

## 1.2. RESEARCH OUTLINE AND TEXT ORGANIZATION

The report includes seven Chapters and three Appendices. This first Chapter introduces the work, by describing the motivation and general objectives, and by outlining the contents of the different Chapters and Appendices.

Chapter 2 provides background information and discussion. The physical problem of the transport of a passive scalar is stated in mathematical form, for 3-D and 2-D quasi-horizontal flows (section 2.1), the relative role of the two leading physical mechanisms for transport (advection and diffusion) and the nature of the mathematical problem are discussed (sections 2.2 and 2.3, respectively), and the most representative techniques for the numerical solution of the transport equation are reviewed (section 2.4). Section 2.1 is largely based on a previous, but still unpublished work (ADAMS and BAPTISTA 1986), while section 2.4 extends and updates BAPTISTA 1984.

Eulerian-Lagrangian methods (ELM) are identified in section 2.4 as an effective alternative to conventional Eulerian methods. Chapter 3 describes a reference ELM that generalizes the method proposed by BAPTISTA 1984. This method splits the transport equation in advection and diffusion components, solving the former by a backwards method of characteristics (BMC) and the latter by a finite element Galerkin method. Particularly relevant as an extension of the previous work is the relaxation of the constraint of a same interpolation scheme applying for both advection and diffusion.

An introductory discussion of the accuracy of the reference ELM (section 3.5) identifies the solution of the advection equation, and, in particular, the associated interpolation procedure, as the potential major source of errors. Hence, Chapter 4 addresses in detail the accuracy of the adopted BMC. Formal analysis and numerical experimentation provide insight into the relevant error mechanisms and on the relative performance of alternative interpolation schemes. Emphasis is given to the simple case of advection in 1-D uniform grids, as to allow a systematic analysis. Extensions to non-uniform and to two-dimensional grids are however presented as an important complement. Several alternative interpolation schemes (some of them first proposed through this research) are considered in the analysis, which is effective in comparing schemes and in identifying upper bounds in the accuracy of the BMC.

Chapter 5 analyzes general properties of ELM, for a selected range of alternative interpolation schemes for advection. The influence of diffusion in the solution of the global transport equation is discussed, and shown to typically correspond to an improvement of accuracy (section 5.2). Also, the time step that leads to optimal accuracy is shown to be a function of the relative importance of advection and diffusion, and the selection of the most cost-effective time step is briefly discussed (section 5.3).

Chapter 6 links findings of earlier chapters to the application that constitutes the motivation for the present research: the modeling of the physical mechanisms determining the fate of

passive scalars (e.g., pollutants and water quality indicators) in coastal waters. Three case studies (BAPTISTA 1984, BAPTISTA et al. 1984 and KOSSIK 1986) where a 2-D depth-averaged Eulerian-Lagrangian transport model, ELA (BAPTISTA 1984), was used as a fundamental tool, are critically reviewed, and the improvements that should be introduced to ELA following the present research are discussed.

Chapter 7 summarizes the relevant conclusions of the present research, and outlines further work, both at the level of basic research and of engineering applications.

The Appendices provide complementary information to the material described in the text. Appendices A and C reproduce material presented to the VI International Conference on Finite Elements in Water Resources, held at LNEC, between June 1-5, 1986: the statement of reference problems and accuracy measures for a specialized Forum on the advection-dominated transport equation (Convection-Diffusion Forum), and a paper on the representation of sources in transport models, respectively. Appendix B briefly refers to the companion circulation models, TEA and TEANL, for the transport model ELA.



CHAPTER 2  
BACKGROUND





## 2.1 MATHEMATICAL STATEMENT OF THE TRANSPORT PROBLEM

### 2.1.1 Governing equation for three-dimensional transport

The fate of a substance introduced in a host fluid is governed by the principle of mass conservation. In the absence of internal sources and sinks, this principle, applied over an elementary volume of fluid, states that

"the rate of increase of mass within the elementary volume equals the net inflow of mass through the boundaries of the elementary volume".

This principle is mathematically expressed by the partial differential equation (PDE)

$$\frac{\partial c}{\partial t} = - \sum_{i=1,2,3} \frac{\partial q_i}{\partial x_i} \quad (2.1)$$

where summation is implied over repeated indices, and

$c(x,y,z,t)$  - is the substance concentration  
 $q_i(x,y,z,t)$  - is the mass flux in the  $i$ -direction  
 $t$  - is the time coordinate  
 $x=x_1, y=x_2, z=x_3$  - are the spatial coordinates

We note that a volumetric definition of concentration was adopted, i.e.

$$c = \frac{\text{mass of substance}}{\text{volume of solution}} \quad (2.2)$$

This definition is related to the alternative massic definition

$$c_m = \frac{\text{mass of substance}}{\text{mass of solution}} \quad (2.3)$$

through

$$c = \rho \cdot c_m \quad (2.4)$$

where  $\rho$  is the density of the solution.

Two mechanisms promote mass flux across the volume boundaries: advection, defined as the transport of mass by the fluid motion; and molecular diffusion, defined as the transport of mass by the Brownian motion of molecules within the fluid.

The mass flux in the  $i$ -direction is defined by

$$q_i = u_i c + q_{di} \quad (2.5)$$

where  $u_i c$  represents the flux by advection ( $u_i$  being a velocity), and  $q_{di}$  the flux by molecular diffusion.

Molecular diffusion is governed by Fick's law, which states that

"the flux of mass in a given direction, due to molecular diffusion, is proportional to the gradient of concentration in that direction",

In differential form, this is expressed as

$$q_{di} = -D \frac{\partial c}{\partial x_i} \quad (2.6)$$

where the minus sign indicates that transport is from high to low concentrations. The proportionality constant,  $D$ , is called molecular diffusivity and has dimensions of square length per time. The molecular diffusivity is isotropic, and its actual value depends on the molecular structure of the substance and the host fluid, on their relative concentrations, and on the temperature and pressure of the system.

Replacing Eqs. 2.5 and 2.6 into 2.1, we obtain the three dimensional transport equation

$$\frac{\partial c}{\partial t} + \frac{\partial}{\partial x_i} (u_i c) = \frac{\partial}{\partial x_i} \left( D \frac{\partial c}{\partial x_i} \right) \quad \{i=1,2,3\} \quad (2.7)$$

written in terms of instantaneous values of concentration and flow characteristics. While general, this form is inconvenient in turbulent flows (which includes, in particular, most natural flows). Indeed, turbulent flows exhibit random fluctuations over the time-scale of turbulence, which we seldom know how, and often do not care, to represent.

Hence, for turbulence flows, this governing equation is more often used in the form involving mean turbulent quantities, which is derived through the concept of Reynolds-averaging.

With this objective, instantaneous quantities are represented by the sum of an average value (over the time-scale of turbulence) and a deviation from the average; for velocity and concentration

$$u_i = \bar{u}_i + u_i' \quad (2.8)$$

$$c = \bar{c} + c' \quad (2.9)$$

where the bars denote time-average and the primes denote deviation from the average.

Introducing Eqs. 2.8 and 2.9 into 2.7, and averaging the latter over the time-scale of turbulence, we obtain the 3-D Reynolds transport equation

$$\frac{\partial \bar{c}}{\partial t} + \frac{\partial (\bar{u}_i \bar{c})}{\partial x_i} = \frac{\partial}{\partial x_i} \left( D \frac{\partial \bar{c}}{\partial x_i} \right) - \frac{\partial}{\partial x_i} \overline{(u_i' c')} \quad \{i=1,2,3\} \quad (2.10)$$

We note that three new unknowns (the double correlations  $\overline{u_i' c'}$  in the three dimensions of space) are introduced; each correlation represents a mass flux, due to random fluctuations of concentration over the time-scale of the turbulent motion. Specification of these unknowns is required to close the problem (turbulence closure), and remains as one of the greatest challenges in modern modeling of turbulent flow and transport.

Turbulence closure is often attempted either by introducing new equations (e.g. for turbulent kinetic energy, or for turbulent kinetic energy and its dissipation:  $k$  and  $k-\epsilon$  models, respectively), or by using some ad-hoc assumption on the form of the unknown turbulent fluxes.

Very often, the approach adopted in engineering practice is of the latter type, involving an analogy with Fick's law for molecular diffusion, based on Prandtl's mixing length argument. In this approach, the turbulent mass flux in the  $i$ -direction is expressed as

$$q_{ii} = \overline{u_i' c'} = -K_{(i)} \frac{\partial \bar{c}}{\partial x_i} \quad (2.11)$$

where  $K_{(i)}$  is the eddy diffusivity in the  $i$ -direction, which must be specified or computed from known quantities (the brackets indicate that  $i$  is not a summable index). Eddy diffusion coefficients are generally several orders of magnitude larger than molecular diffusion coefficients and, unlike molecular diffusion, they depend on the flow characteristics. Hence, in general, they are neither isotropic nor homogeneous.

Recognizing that  $K_{(i)} \gg D$  and dropping the overbar, Eq. 2.11 may be substituted into Eq. 2.10 to yield

$$\frac{\partial c}{\partial t} + \frac{\partial}{\partial x_i} (u_i c) = \frac{\partial}{\partial x_i} \left( K_{(i)} \frac{\partial c}{\partial x_i} \right) + S \quad \{i=1,2,3\} \quad (2.12)$$

where, for the sake of generality, we added a term  $S$ , representing the rate of production or loss of mass per unit volume by internal sources or sinks.

### 2.1.2 Governing equation for two-dimensional (depth-averaged) transport

In many natural flows, motion in the vertical direction is much smaller than in the horizontal. For such flows, Eq. 2.12 may be simplified by vertical averaging. We will consider the case of a quasi-horizontal flow, defined over a depth  $h(x,y,z,t)$  between

adjacent interfaces  $\eta_1(x,y,z,t)$  and  $\eta_2(x,y,z,t)$  as shown in Fig. 2.1.

Integration of Eq. 2.12 over depth leads to

$$\int_{\eta_2}^{\eta_1} \frac{\partial c}{\partial t} dz + \int_{\eta_2}^{\eta_1} \frac{\partial}{\partial x_j} (u_j c) dz + cw \Big|_{\eta_2}^{\eta_1} = \int_{\eta_2}^{\eta_1} \frac{\partial}{\partial x_j} \left( K_{(j)} \frac{\partial c}{\partial x_j} \right) dz + \left( K_z \frac{\partial c}{\partial z} \right) \Big|_{\eta_2}^{\eta_1} + \int_{\eta_2}^{\eta_1} S dz \quad (2.13) \quad \{j=1,2\}$$

Using Leibnitz's rule, and rearranging, gives

$$\frac{\partial}{\partial t} \int_{\eta_2}^{\eta_1} c dz + \frac{\partial}{\partial x_j} \int_{\eta_2}^{\eta_1} u_j c dz = \frac{\partial}{\partial x_j} \int_{\eta_2}^{\eta_1} \left( K_{(j)} \frac{\partial c}{\partial x_j} \right) dz + \phi_{\eta_1} - \phi_{\eta_2} + \int_{\eta_2}^{\eta_1} S dz \quad (2.14)$$

where  $\phi_{\eta_m}$  (with  $m=1,2$ ) is mathematically described by

$$\phi_{\eta_m} = \left\{ c \left( \frac{\partial \eta_m}{\partial t} + u_j \frac{\partial \eta_m}{\partial x_j} - w \right) - \left( K_{(j)} \frac{\partial c}{\partial x_j} \frac{\partial \eta_m}{\partial x_j} + K_z \frac{\partial c}{\partial z} \right) \right\}_{\eta_m} \quad (2.15)$$

Physically,  $\phi_{\eta_m}$  represents the mass flux across the interface  $z=\eta_m(x,y,t)$ , the first and second terms of Eq. 2.15 being, respectively, advective and diffusive flux components.

Fluxes across interfaces are problem-specific (e.g., advective fluxes are null for impermeable interfaces, and diffusive fluxes are null for fully-reflective surfaces), and must be specified in a case-by-case basis, as vertical boundary conditions.

To treat the other terms of Eq. 2.14, we introduce the notation

$$r(x,y,t) = \langle r \rangle + r''(x,y,z,t) \quad (2.16)$$

with

$$\langle r \rangle = \frac{1}{h} \int_{\eta_2}^{\eta_1} r dz \quad (2.17)$$

and

$$\int_{\eta_2}^{\eta_1} r'' dz = 0 \quad (2.18)$$

where  $r$  is a dummy variable that may represent  $u$ ,  $c$  or  $K$ ;  $\langle \rangle$  denotes a depth-averaged value, and the double prime denotes a deviation from the average. Eq. 2.14 may then be rewritten as

$$\frac{\partial}{\partial t} (h \langle c \rangle) + \frac{\partial}{\partial x_j} (h \langle u_j \rangle \langle c \rangle) = \frac{\partial}{\partial x_j} \left[ h \left( \langle K_{(j)} \rangle \left\langle \frac{\partial c}{\partial x_j} \right\rangle + \langle K''_{(j)} \rangle \frac{\partial c''}{\partial x_j} \right) \right] - \frac{\partial}{\partial x_j} (h \langle u'_j c'' \rangle) + \phi_{\eta_1} - \phi_{\eta_2} + h \langle S \rangle \quad \{j=1,2\} \quad (2.19)$$

Note that new unknowns, in the form  $\langle u'_j c'' \rangle$  and  $\langle K''_{(j)} \rangle \langle \partial c'' / \partial x_j \rangle$ , were introduced by the vertical integration. These unknowns represent horizontal mass fluxes, due to differential advection

(shear) and diffusion over depth. By analogy with turbulent diffusion, these fluxes are assumed to be of the form

$$\langle u_j'' c'' \rangle - \langle K_{ij}'' \frac{\partial c''}{\partial x_j} \rangle = -K_{ij}^* \frac{\partial \langle c \rangle}{\partial x_i} \quad (2.20)$$

where the vertical shear diffusion coefficients,  $K_{ij}^*$ , must be specified or computed from known quantities.

Inserting Eq. 2.20 into Eq. 2.19, and dropping " and  $\langle \rangle$ , leads to the 2-D (depth-averaged) transport equation

$$\frac{\partial}{\partial t} (hc) + \frac{\partial}{\partial x_j} (hu_j c) = \frac{\partial}{\partial x_j} \left( E_{ij} h \frac{\partial c}{\partial x_i} \right) + \phi_{n_1} - \phi_{n_2} + Sh \quad \{i,j=1,2\} \quad (2.21)$$

where the diffusion coefficients  $E_{ij}$  result from lumping together the eddy and horizontal shear diffusion coefficients.

The above form of the transport equation is known as the conservative form. Making explicit use of the 2-D continuity equation

$$\frac{\partial h}{\partial t} + \frac{\partial (hu_j)}{\partial x_j} = 0 \quad \{j=1,2\} \quad (2.22)$$

we can derive the non-conservative form

$$\frac{\partial c}{\partial t} + u_j \frac{\partial c}{\partial x_j} = \frac{1}{h} \frac{\partial}{\partial x_j} \left[ E_{ij} h \frac{\partial c}{\partial x_i} \right] + \frac{1}{h} \left[ \phi_{n_1} - \phi_{n_2} \right] + S \quad \{i,j=1,2\} \quad (2.23)$$

### 2.1.3. Initial and boundary conditions

The mathematical formulation of a physical problem is not complete until proper initial and boundary conditions are specified. General forms for these conditions are

$$c(x, y, t) = c_0(x, y) \quad \text{at } t=0, \text{ in } \Omega \quad (2.24)$$

and

$$(1-\alpha) [q_n(x, y, t) - Q^*(x, y, t)] + \alpha(x, y, t) [c(x, y, t) - C^*(x, y, t)] = 0 \quad (2.25)$$

at  $t > 0$ , on  $\Gamma$

where  $\Omega$  and  $\Gamma$  denote the computational domain and its boundary,  $c_0$ ,  $C^*$  and  $Q^*$  are prescribed functions, and  $\alpha$  controls the type of boundary condition: e.g., a prescribed concentration condition if  $\alpha=1$ , a prescribed flux condition if  $\alpha=0$ . The variable  $q_n$  represents the mass flux along  $\hat{n}$ , the direction normal to the boundary, and is given by (assuming  $E_{ij}=0$  for  $i \neq j$ )

$$q_n = \left[ \beta uhc - (1-\beta) h E_x \frac{\partial c}{\partial x} \right] \cos(\hat{n}, \hat{x}) + \left[ \beta vhc - (1-\beta) h E_y \frac{\partial c}{\partial y} \right] \cos(\hat{n}, \hat{y}) \quad (2.26)$$

where  $\beta$  controls the kind of flux to be prescribed: e.g., advective flux if  $\beta=1$ , diffusive flux if  $\beta=0$ .

On closed (or land) boundaries, a flux condition is usually used ( $\alpha=0$ ). As normal velocities must be zero on these boundaries, advected fluxes are implicitly zero. Dispersive fluxes, however, must be specified, and Eq. 2.24 becomes

$$-\left( h E_x \frac{\partial c}{\partial x} \cos(\hat{n}, \hat{x}) + h E_y \frac{\partial c}{\partial y} \cos(\hat{n}, \hat{y}) \right) = Q^* \quad (2.27)$$

The value of  $Q^*$  depends on the reflectivity of the boundary as regards the tracer. When a full reflection may be assumed,  $Q^*=0$ .

Open boundaries are much more difficult to handle, and no uniformly accepted procedure exists. For inflow boundaries concentration is usually prescribed ( $\alpha=1$ ), in the form

$$c(x, y, t) = C^*(x, y, t) \quad (2.28)$$

but it may be more convenient (e.g., in the vicinity of effluent discharges in a receiving water body), to prescribe advective fluxes ( $\alpha=0$ ,  $\beta=1$ ), in the form

$$uc \cos(\hat{n}, \hat{x}) + vc \cos(\hat{n}, \hat{y}) = Q^* \quad (2.29)$$

In outflow boundaries, a flux condition ( $\alpha=0$ ,  $\beta=0$ ), in the form

$$E_x \frac{\partial c}{\partial x} \cos(\hat{n}, \hat{x}) + E_y \frac{\partial c}{\partial y} \cos(\hat{n}, \hat{y}) = 0 \quad (2.30)$$

is often used, to indicate that only (unspecified) advective fluxes occur. Eq. 2.30 is, however, only valid if concentration gradients are negligible near the outflow boundary, which, in some real problems (e.g., diffusion of effluents in a receiving water body) can be achieved by considering a large enough computational domain.

Taking again as a reference the problem of effluent dispersal in a receiving water body, the specification of the values of  $C^*$  or  $Q^*$  required at inflow boundaries (Eqs. 2.28 or 2.29) is relatively easy if the currents are unidirectional (even so, difficulties will arise when the background concentration field is not trivial). In the presence of reversing currents specification of  $C^*$  or  $Q^*$  becomes quite hard, though, because the mass that leaves the computational domain in the outflow phase will reenter in the inflow phase and must be taken into account. Several approaches to this problem have been proposed, the least arbitrary being to consider a large enough domain, in order to

reduce outflow concentrations to background level; unfortunately practical limitations concerning CPU time and memory capacity sometimes prevent this approach.

When a 2-D (depth-averaged) formulation is used, the mass flux normal to the surface and to the bottom constitute vertical boundary conditions, that must be specified in addition to the horizontal conditions described by Eq. 2.25. Often, these fluxes are rather unimportant, and may be set equal to zero. Typical exceptions include thermal energy and dissolved gases, which are exchanged with the atmosphere, and sediments which are deposited and re-suspended at the bottom.

A thorough review of heat exchange mechanisms is presented in ADAMS et al. 1981; volatilization and reaeration mechanisms have been summarized in BRUTSAERT and JIRKA 1984; and vertical fluxes of sediments are discussed in VANONI 1977. The reader is referred to these works for information on the specification of vertical mass fluxes.



## 2.2 ON THE ROLE OF ADVECTION AND DIFFUSION

From the derivation of the 2-D (depth-averaged) transport equation, it should be clear that advection and diffusion are not staunching mechanisms, the actual meaning of each depending on the time and space scales that we elect to explicitly represent in a given formulation.

To illustrate concepts, and provide insight on the relative importance of these mechanisms, we loosely approximate a continuum host fluid of a passive scalar, in turbulent motion, through an "infinite" set of equal fluid parcels, each of infinitesimal (although larger than the scale of Brownian motion) size. Mass of the scalar is associated to each parcel according to some initial distribution, and we examine the changes that take place as time progresses.

If we look at the problem through the three-dimensional instantaneous form of the transport equation (Eq. 2.7) we identify the transport mechanisms as being advection by the instantaneous flow and molecular diffusion.

Advection redistributes mass through the displacement of fluid parcels, which follow the flow; the original amount of mass in each parcel is strictly preserved. It is useful, at this point, to consider the carrying flow as a superposition of three components: a uniform component, a shear component (associated with the deviations from uniformity that refer to space and associated time scales larger than what is loosely called the scale of the turbulent fluctuations) and a fluctuating component (associated with the deviations from uniformity within the scale of the turbulent fluctuations). While the uniform component moves parcels in a rigid-body-like way, the non-uniform components rearrange the position of the parcels relative to each other: a deterministic rearrangement over large scales, in the case of the shear component, and a random rearrangement over small scales, in the case of the fluctuating component.

Diffusion, in turn, redistributes mass by actually exchanging it between adjacent parcels, through Brownian motion at the molecular level; no parcel displacements are involved. Mass exchange is set in a way that tends to smooth out existing gradients (i.e., mass goes from parcels with higher content to parcels with lower content), and the exchange rate is proportional to the driving gradients.

For passive scalars, diffusion does not affect advection. However, advection by the non-uniform components of the carrying flow may significantly affect the efficiency of diffusion. Indeed, the relative position of fluid parcels is changed by non-uniform advection, which establishes new parcel neighborhoods: if parcels with high mass content are all brought closer to each other, diffusion becomes less efficient; conversely, if such parcels are spread over larger regions, diffusion becomes more efficient. Typically, non-uniform advection enhances global diffusion, although it may inhibit diffusion locally.

We now take the three-dimensional form of the equation for mean turbulent transport, Eq. 2.12. Both advective and diffusive

mechanisms are, again, present.

Now, however, advection is associated only with the mean turbulent flow (uniform and shear components), and the effect of the fluctuating component of the flow is represented as a turbulent diffusion. As pointed out earlier, turbulent diffusion is typically several orders of magnitude more efficient than molecular diffusion, and the latter can therefore be dropped from the governing equation.

Because diffusion implies exchange of mass between fluid parcels, we immediately recognize, from earlier discussion, that the size of the parcels that we can look at has increased: parcels are still small, but they must be larger than the scales associated with turbulent fluctuation.

We lost resolution, but we gained convenience. Indeed, we avoided the explicit representation of the fluctuating component of the flow, which is particularly hard to handle. This approximation may constitute the difference between feasibility and unfeasibility in the modeling of turbulent flow and transport(1).

Let us now consider the two-dimensional equation for mean turbulent transport, Eq. 2.21. Advection is associated only with the uniform component and with a part of the shear component of the flow. Indeed, the effect of vertical shear is represented as a diffusion mechanism (vertical-shear diffusion) and added to the turbulent diffusion.

Again, we lose resolution (the horizontal size of the fluid parcels is still constrained only by the scale of the turbulent fluctuations, but the vertical size must be the flow depth) to gain convenience (we avoid the explicit representation of the vertical flow and of the vertical variation of the horizontal flow).

Computational savings related to depth-averaging are much less impressive than those achieved by Reynolds - averaging, but are still significant (may be one to two orders of magnitude in CPU and memory requirements). Although advanced computers already exist that make feasible the computational effort for the solution of three-dimensional mean turbulent transport problems, depth-averaging (or an alternative space averaging) is still often useful or even the only sensible or feasible approach

---

(1) To illustrate this statement, we reproduce from WHITE 1974 the following reasoning based on figures given by EMMONS 1970: for the relatively simple problem of turbulent flow in a pipe, a computer solution revealing the turbulence structure of the flow, at a Reynolds number of  $10^7$  would require  $10^{22}$  operations; at the computer speed of 10 microseconds per operation (representative of computers in the seventies), this would require  $10^{17}$  seconds, or  $3 \times 10^9$  years (about one fifth of the age of the universe); since we are probably limited by the speed of light to an "ultimate" computer speed of 1 nanosecond per operation, our fastest foreseeable computation would take  $3.2 \times 10^4$  years (over 500 generations).

(because of: limitations of the computer actually available; detail that can be achieved in the specification of boundary conditions; accuracy of available numerical solution techniques; etc).

It should be emphasized that Eq.2.21 assumes that the horizontal plan is represented as a continuum; however, the numerical solution of this equation involves the discretization of the horizontal plan, through the set-up of a grid. While in some cases (e.g., for finite-element methods) unambiguous interpolation functions hold within each grid element, some space- (and associated time-) scales of the flow are, again, omitted or ill-represented. This further reduces our ability to directly represent advection, and should, again, be compensated by the introduction of an additional diffusion mechanism: now, the sub-grid scale horizontal shear diffusion (DEARDORFF 1971, CHRISTODOULOU et al. 1976).

Relevant questions are how to evaluate the diffusion coefficient that is actually going to be used in the computations, and how important has diffusion become relative to advection.

Clearly, the answers depend on the specific problem and on the model (dimensionality and form of the equations; solution technique and its spatial refinement) that one elects to use; this is discussed in further detail by ADAMS and BARTISTA 1986, who address the empirical determination of diffusion coefficients, in the context of coastal and oceanic flows.

### 2.3. ON THE MATHEMATICAL NATURE OF THE TRANSPORT EQUATION

The detailed analysis of the mathematical nature of the transport equation is beyond the scope of this work. The following brief discussion should, however, be helpful to the understanding of problems arising in the numerical solution of this equation, and are a motivation for Eulerian-Lagrangian methods.

We take as a reference, without loss of conceptual generality, the 1-D partial differential equation

$$\frac{\partial c}{\partial t} + A(x,t) \frac{\partial c}{\partial x} = B(x,t) \frac{\partial^2 c}{\partial x^2} + C(x,t) c + D(x,t) \quad (2.31)$$

where the coefficients  $B(x,t)$ ,  $A(x,t)$  - representing, respectively, diffusion and advection (or advection plus non-uniform diffusion, see Chapter 3) - are of special interest.

This equation is linear, as revealed by the functional dependence of the coefficients A through D (1). Hence, the extensive body of knowledge available on linear PDE applies, and some general properties may be assumed.

In particular, it is easily recognized that Eq. 2.31 has a considerably different behaviour, depending on whether  $B(x,t)$  is or is not null. Indeed, when  $B(x,t) \neq 0$ , the equation is a second-order parabolic PDE, while it becomes a first-order hyperbolic PDE when  $B(x,t) = 0$  (2).

Hence, when  $B(x,t) \neq 0$ , Eq. 2.31 has a single family of horizontal characteristic lines (or, to be more precise, two coincident - thus necessarily horizontal - families), and is associated with the initial and boundary conditions diagrammatically represented in Fig. 2.2(a). The function  $c(x,t)$  is determined, at any given location of space and time, by all the initial data plus the data on the boundaries which are on or below the relevant characteristic line. Hence, in particular, at any given time,  $t$ , solutions at different space locations are all interrelated.

---

(1) A  $n$ th-order PDE is nonlinear when its coefficients depend on  $n$ th-order derivatives of the dependent variable; it is quasi-linear when they depend on  $m$ th-order derivatives, with  $m < n$ ; and it is linear when they depend on the independent variables alone.

(2) Second-order linear or quasi-linear PDE of the general form

$$a(\cdot) \frac{\partial^2 v}{\partial y^2} + b(\cdot) \frac{\partial^2 v}{\partial y \partial z} + c(\cdot) \frac{\partial^2 v}{\partial z^2} + d(\cdot) \frac{\partial v}{\partial y} + e(\cdot) \frac{\partial v}{\partial z} + f(\cdot)v + g(\cdot) = 0 \quad (2.32)$$

where  $(\cdot)$  represents some functional dependence, are classified as hyperbolic if  $b^2 > 4ac$ , as parabolic if  $b^2 = 4ac$  and as elliptic if  $b^2 < 4ac$  (e.g., LAPIDUS and PINDER 1982, pgs. 12-13). The above criterion does not give any useful information for first-order PDE; however, hyperbolic equations are identified as those for which the Cauchy problem is well-posed (JEFFREY 1976, pg. 42), which is the case of Eq. 2.31 when  $B(x,t) = 0$ .

When  $B(x,t)=0$ , Eq. 2.31 has, again, a single family of characteristic lines. Now, however, this number results from the order of the equation, and not from the coincidence of two families of lines; hence, in particular, the characteristic lines do not have to be (and are not, except in the uninteresting case of  $A(x,t)=\infty$ ) horizontal. The requirements on initial and boundary conditions, and the domain of dependence of the solution, are now completely different, as illustrated in Fig. 2.2(b). In particular, we note that the relevant initial or boundary conditions fully determine the solution along each characteristic line.

The transition between the parabolic and the hyperbolic behaviour of the equation is, from the above discussion, discontinuous (associated to a singularity at  $B(x,t)=0$ ). Although this is formally so, the actual behaviour of the solutions is hypothesized to change gradually as diffusion becomes less and less important with regard to advection. This is in agreement with the physics of the transport phenomena, and may justify the frustrating experience of many modellers, in the last decades, while solving numerically the advection-dominated transport equation.

Hence, the idea of splitting the transport into a purely parabolic diffusion equation and a purely hyperbolic advection equation, and solving each by a different method, becomes appealing, and has indeed been increasingly explored (section 2.4).

## 2.4 REVIEW OF NUMERICAL SOLUTION METHODS FOR THE TRANSPORT EQUATION

### 2.4.1 Introduction

The transport equation has been solved by several different numerical methods, which may be classified into three broad categories: Eulerian, Lagrangian and Eulerian-Lagrangian.

Eulerian methods (EM) solve the Eulerian form of the transport equation, at the nodes of a fixed grid. This requires the simultaneous solution of hyperbolic (advective) and parabolic (diffusive) operators, which has proved to be a hard task when the former dominate the latter. Indeed, when advection dominates, "centered" EM often generate spurious spatial oscillations (wiggles) while "upwind" and "balanced-dissipation" EM introduce significant numerical damping.

Lagrangian methods (LM) avoid the explicit treatment of hyperbolic operators by solving the Lagrangian form of the transport equation in grids moving with the flow. This approach is potentially very accurate, but is made unattractive or unfeasible in many situations of interest (e.g., continuous sources and complex reversing flows) due to practical difficulties associated with the grid displacement and deformation.

Eulerian-Lagrangian methods (ELM) retain the convenience of a fixed grid, but, at some point of the numerical procedure, a part or the whole transport equation is treated in a Lagrangian form, in order to avoid the explicit treatment of hyperbolic operators. Reported results from ELM are rather promising, showing that wiggles and numerical damping can be greatly reduced, even for very strongly advection-dominated problems.

Discussion in the next paragraphs concentrates on EM (still the most used in engineering practice), and on ELM (which are becoming increasingly used).

### 2.4.2 Eulerian methods

Methods in this category are typically based on the set-up and solution of a single system of algebraic equations, where both advective and diffusive terms are represented; unknowns are the concentrations at a finite number of fixed locations (nodes) in the computational domain. The transformation of the original differential equation into such a system of algebraic equations is usually achieved using either finite difference methods (FDM) or finite element methods (FEM).

Relative merits of FDM and FEM have been widely discussed for several years. While few widely accepted conclusions have been reached, it is usually recognized that FEM

- handle more efficiently the description of complicated land boundaries, as well as internal grid refinements;

- are more consistent in the treatment of boundary conditions and in the set-up of interpolation procedures over the whole computational domain;

while FDM

- are more intuitive to formulate, and tend to require less memory and CPU time, for a similar number of nodes;

- result in significantly easier procedures concerning preparation and input of data.

The option between FEM and FDM, while of practical importance, plays a secondary role in what the fundamental difficulties of the accurate solution of the transport equation are concerned. Indeed, as we shall see, each FDM has what can be considered a FEM "equivalent", sharing the same type of fundamental abilities and limitations.

FDM have been used in the solution of the transport equation since the late 1950's. They typically discretize the computational domain through the use of an orthogonal grid (stretching transformations have however been increasingly used to provide some grid refinement or specific shaping). Over each grid element, the differential transport equation is replaced by an algebraic equation, where both the space- and time-derivatives are approximated by finite-differences. The resulting system of algebraic equations is adjusted to take into account the appropriate boundary conditions, and is then solved to give the nodal concentrations.

Initial FDM used centered schemes to approximate both the advection and the diffusion terms. These methods, however, lead often to strong parasitic spatial oscillations (wiggles), specially for large Courant numbers (i.e., often in the range of practically feasible  $\Delta x$ ,  $\Delta t$ ). In a careful (although too specific) formal analysis in the context of a one-dimensional, steady problem, with Dirichlet boundary conditions specified at the two boundaries, ROACHE 1976 (pp. 161-165) showed that wiggles are, in this case, caused by a singularity at low  $D/u$  (the numerical equivalent of the singularity at  $D=0$  of the behavior of the exact solution, discussed in section 2.3). According to Roache, a perturbation is generated at the outflow boundary, for Peclet numbers,  $Pe=u\Delta x/D$ , larger than 2, and propagates to the whole domain.

Experience shows, however, that wiggles may have a broader range of origins. A more general statement is (see discussion in Chapter 4) that wiggles are the consequence of phase errors at short wavelengths; hence, wiggles will occur whenever such wavelengths are of significance in the true solution (which relates to insufficient discretization), and are not artificially damped by the numerical algorithm.

As centered FDM are often associated with small damping but significant phase errors at short wavelengths (e.g., see Fourier analysis by HOLLY 1975), they should, indeed, promote

wiggles, except when physical diffusion is strong enough to smooth out sharp (relative to the grid discretization) gradients.

As a remedy for wiggles in advection-dominated problems with sharp gradients, more recent FDM have used centered finite-differences only for the diffusion terms, replacing the advective derivatives by upwind differences. Upwinding methods do avoid wiggles; however, this is done by very strongly damping short wavelengths; for linear approximations, a numerical diffusion is explicitly introduced (as easily shown by Taylor series expansion), which often overshadows physical diffusion.

BOOK et al. 1975 proposed, as an alternative to "brute-force" upwinding, the elimination of wiggles through the controlled addition of (unsteady, non-uniform and non-isotropic) artificial diffusion (Flux-Corrected Transport FD Method) to numerical solutions obtained with centered differences. This and similar techniques lead also to a re-statement of the physical problem, and can loosely be seen as forms of "intelligent", but often relatively expensive, upwinding.

FEM have become popular for the solution of the transport equation since the early 1970's. The computational domain is divided into elements of convenient shape, such as triangles or quadrilaterals. Within each element information is concentrated at nodes, but may be unambiguously interpolated to the interior using pre-selected interpolation functions. The original partial differential equation is then transformed into a system of ordinary differential equations in time, using a weighted residual method. Numerical integration of this system leads finally to a system of algebraic equations, whose solution gives the nodal values of the concentration field.

The use of the weighted residual method requires the definition of elementary weighted residuals, resulting from the integration over each element of the errors made in approximating the actual concentration field, weighted by pre-selected weighting functions; the sum over the whole computational domain of the elementary residuals is then forced to be zero, to minimize the approximation errors. Different FEM result from different choices of interpolation and weighting functions. In the early 1970's, most FEM solved the transport equation using the same interpolation and weighting functions; such methods are known as Galerkin-FEM (GA-FEM).

GA-FEM lead to "centered" approximations of the advective terms, and present the same limitation as centered FDM: wiggles are produced when short wavelengths are significant, and are not progressively damped by physical diffusion (Peclet number above a critical value). The increase of the order of the interpolation functions from linear to quadratic seems to have a significant effect on accuracy (e.g. NORONHA and BAKER 1986), but is unable to fully avoid wiggles. Users of GA-FEM (e.g. LEIMKULHER 1974) have tried to extend the application of the method to advection-dominated problems with sharp gradients, through the adoption of uniform diffusion coefficients which are 1 to 2 orders of magnitude larger than the physical ones (which is a rough re-statement of the physical problem).



In the late 1970's several attempts were made to account for the flow direction, i.e., to "upwind" FEM. Petrov-Galerkin FEM (PG-FEM), as presented by CHRISTIE et al. 1976, and extended by HEINRICH et al. 1977 and HEINRICH and ZIENZIEWICZ 1977 constitute one such attempt which has been successful in avoiding wiggles. In these methods, the weighting functions are not equal to the interpolation functions, but are obtained from them by a change in shape that increases the relative weight of upstream information in a way that depends on the element geometry and the flow characteristics. Limitations of PG-FEM methods include (a) introduction of numerical damping (close similarity with upwinding FDM); (b) increased computational effort required to generate weighting functions from interpolation functions, at each element and at each time step, and (c) difficulty in handling elements which are not quadrilaterals.

A different upwinding procedure (much in the line of the Flux-Corrected Transport Method in FDM) was proposed in HUGHES 1979 for 1-D, and was extended to 2-D by HUGHES and BROOKS 1979 and by KELLY et al. 1980. In this procedure, the weighting and interpolation functions are equal, like in standard GA-FEM. However, an artificial anisotropic diffusion term, equivalent to the one that is implicitly introduced by the PG-FEM, is computed and added to each element at each time step. Methods using this procedure have not received a unique designation, but are often referred to as Balanced-Dissipation-FEM (BD-FEM). Results of BD-FEM have been reported as indistinguishable from results obtained with PG-FEM, for a few simple test cases. However, BD-FEM are much less expensive and are more easily applied to elements of any shape and dimensionality; for complex flows, they should also lead to a more controlled type of upwinding, resulting in enhanced accuracy.

A final comment on Eulerian methods is that none of them can be safely applied for large Courant numbers. As a general rule, explicit methods become unstable for  $Cu > 1$  (the classical Courant-Lewy stability criterion), while implicit methods, even if stable, tend to significantly lose accuracy above the same limit.

#### 2.4.3 Eulerian-Lagrangian Methods

We now analyze key aspects of ELM. A distinction will be made between ELM based on the concept of "concentration" (ELM/C), ELM based on the concept of "particle" (ELM/P) and on ELM involving both concepts (ELM/CP).

Typically, ELM/C split the transport equation into an advection and a diffusion equations, solving the former by a point-to-point transfer method (e.g., a backwards method of characteristics) and the latter by some conventional global discrete element technique (e.g., finite elements or finite-differences). ELM implementations based on this conceptual approach include those reported by LEITH 1965, HOLLY and PREISSMAN 1977, BENQUE et al. 1980, NEUMAN and SOREK 1982, GLASS and RODI 1982, HOLLY and POLATERA 1984, HOLLY and KOMATSU 1984, BAPTISTA 1984, BAPTISTA et al. 1985 and KOMATSU et al. 1984.

Two major general splitting approaches have been used. The most common of these approaches (of which the technique described in Chapter 3 is an example) applies to the time-discretized form of the transport equation, while the approach suggested by NEUMAN and SOREK 1982 applies to the differential form of the equation. The latter approach is attractive for its formal elegance, potential accuracy, and independence relative to time-discretization schemes; however, when advection is dominant, it apparently generates systematic (although localized) errors in the diffusion step and, therefore its practical advantage over the more conventional former approach is yet to be demonstrated.

The solution of the advection equation by a point-to-point transfer method is based on the fact that the concentration of a particle following the flow remains constant, if advection is the only transport mechanism. Most often, the method takes the form of (a) assigning at each new time step,  $n$ , a particle to each node of the computational grid, (b) following each particle backwards along characteristic lines defined by the flow, until reaching time step  $n-1$ , where concentrations at the foot of each characteristic line are computed, by interpolation between known nodal values, and (c) assigning such concentrations to the corresponding grid nodes at time  $n$ ; Chapter 3 provides further details of this procedure.

Two major tasks are clearly involved: the particle backtracking and the interpolation to find concentrations at the feet of the characteristic lines.

Very accurate particle tracking algorithms were developed both for simply structured and for complexly structured or unstructured grids (e.g. see Chapter 3). The computational cost of these algorithms increases significantly with the complexity of the grid and of the flow field, but accuracy may be kept excellent within affordable costs.

The interpolation procedure to find the concentrations at the feet of the characteristic lines has proved much harder to handle. A variety of interpolation schemes have been or can be considered; however, even if several of these schemes allow ELM/C to reduce (when compared to EM) the range of dimensionless wavelengths that are affected by significant amplitude and phase errors, no scheme can claim to be free of a "critical" wavelength, which may still be constraining for a number of applications. A comprehensive discussion of the absolute and relative merits and limitations of alternative interpolation schemes is presented in Chapter 4.

Meanwhile, most ELM/C handle accurately the solution of the diffusion equation, by using a conventional centered FD or FE technique. We note that the solution is global (i.e., involves all the grid nodes simultaneously), which implies that large systems of equations must be solved at each time step. The size of these systems has not proved to be a serious problem in 2-D, because they are often nicely banded and symmetric, and because most of the above mentioned ELM/C are implicit, allowing for large time steps (i.e., reducing the number of required solutions of the system of equations). However, in 3-D applications the global solution of the diffusion step will become a major problem

in terms of computer costs and memory requirements.

CHENG et al. 1984 proposed a ELM/C that is slightly different, conceptually, from the preceding ones. The whole transport equation is written in Lagrangian form, and solved by a backwards method of characteristics in which diffusion is treated as a correction term. The assignment of a particle to each grid node and its backtracking with the flow is shared with preceding ELM/C; however, the concentration at the feet of the characteristic lines is computed by a weighted-average of the concentrations at points defining a physically-based mixing region; the concentration at each of these points is obtained by interpolation between nodal values.

Cheng's approach has the merit of providing a non-global solution of the diffusion, which may prove highly valuable in a 3-D context. Also, it allows a natural treatment of non-isotropic diffusion. Reported accuracy and mass preservation characteristics are promising, at the same level of precedent ELM/C. However, restrictions should have to be applied to the maximum allowable time step, to keep on with accuracy, and this may strongly limit the method's efficiency.

ELM/P (e.g. PRICKETT 1981) are based on a conceptually different approach: particles are introduced in the domain (which was previously discretized in a convenient way) in a number and location related to the initial concentration field; these particles are moved forward with the flow (the flow should represent both "advection" and "diffusion" and is typically described in an Eulerian form); whenever convenient, the number and location of the particles is processed back to the form of concentrations, as to give the instantaneous concentration field.

ELM/P are natural, and physically sound. They inherently avoid the issue of short dimensionless wavelengths, and therefore handle accurately sharp gradients and small (as compared to the grid size) sources of mass, which ELM/C can not do. Also, they are rather versatile, being equally suited for the analysis of concentrations fields, residual transport and field experiments.

However, ELM/P have some potential problems. Clearly, they are not inherently conservative: mass conservation relies only on accuracy, both requiring that a very large (and sometimes unfeasible) number of particles be tracked, and that a fine support grid be used for the conversion between number and location of particles and concentration. Also, if the "advective" part of the carrying flow may be "easily" found by means of a complementary circulation model, the same is not true for the "diffusive" part (which we will call pseudo-velocities).

Approaches to handle the pseudo-velocities range from purely deterministic to partially statistical methods. LANGE 1978, after some manipulation of the theory of diffusion, proposed deterministic pseudo-velocities in the form

$$U_i = - \frac{K}{C} \frac{\Delta C}{\Delta x_i} \quad (2.33)$$

where  $U_i$  is the pseudo-velocity in the  $i$ -direction,  $K$  is a conventional eddy diffusivity coefficient, and  $C$  is the concentration, expressed in terms of the number of particles. In this deterministic method, the motion of a single particle is affected by the whole concentration field, i.e., by the positions of the other particles.

Statistical approaches rely on associating the pseudo-velocities to random perturbations of the motion of individual particles. Again, this may be made by resorting to the eddy diffusivity concept, and using it as to define the statistics of the random motion (e.g., as suggested by CSANADY 1973); or in a more fundamental way, by extracting the statistics of the random motion from Eulerian records of the flow (ZANNETTI 1984).

The ELM/CP proposed by NEUMAN 1984 constitutes a hybrid and very promising novel approach. A ELM/C formulation is used everywhere in the domain, except near gradients too sharp to be handled accurately this way; a ELM/P formulation is adopted in these cases (just for the advection equation). With this approach, most of the computational effort is based on a fixed reference grid; forward tracking of particles is required only in specific regions of time and space, and therefore involve only an affordable number of particles. Principal gray areas for this approach include: mass preservation; efficient and consistent detection of sharp gradients; and accurate procedures for mapping concentrations from particles to the nodes of the fixed grid (we note that this mapping must be performed each time step, previous to the solution of the diffusion equation). All these gray areas may become harder to handle for complex flows than they are for the simple flows that have been used so far to demonstrate the effectiveness of the approach.

ELM overcome in a natural way the limitation on the Courant number referred to for EM. This will be discussed in Chapter 4, in the context of the reference ELM/C described in Chapter 3, and constitutes a fundamental advantage of ELM over EM.



CHAPTER 3

DESCRIPTION OF A REFERENCE EULERIAN-LAGRANGIAN  
METHOD



### 3.1. INTRODUCTION

This Chapter describes an Eulerian-Lagrangian numerical method (a ELM/C in the terminology of Chapter 2), that generalizes the method described in BAPTISTA 1984.

The transport equation is time-discretized and split into advection and diffusion components; the advection equation is then solved by a Backwards Method of Characteristics (BMC), while the diffusion equation is solved by a Galerkin FEM. Fig. 3.2 illustrates the general procedure.

The description of the method motivates and provides a reference framework for subsequent chapters. Chapters 4 and 5, which deal with fundamental aspects of the accuracy of ELM/C solutions of the transport equation, benefit from the general presentation and discussion. Meanwhile, Chapter 6, which discusses the performance of ELA, an Eulerian-Lagrangian model for the 2-D simulation of pollutant transport in coastal waters, benefits from the specific references made to the formulation of such model.

While the discussion is presented in a 2-D context, conceptual extension to 3-D or particularization to 1-D is straightforward.



## 3.2 THE SPLITTING OF ADVECTION AND DIFFUSION

### 3.2.1 Standard approach

We recall, from Chapter 2, the non-conservative form of the 2-D (depth-averaged) transport equation, rewritten as

$$\frac{\partial c}{\partial t} + u_i \frac{\partial c}{\partial x_i} = \frac{1}{h} \frac{\partial}{\partial x_j} [E_{ij} h \frac{\partial c}{\partial x_i}] + \phi \quad \{i,j=1,2\} \quad (3.1)$$

and approximate the time derivative by

$$\frac{\partial c}{\partial t} = \frac{c^n - c^{n-1}}{\Delta t} \quad (3.2)$$

where  $n$  represents current time, and  $n-1$  represents a previous time,  $\Delta t$  apart. A truncation error, of the form

$$\epsilon = -\frac{\Delta t}{2} \frac{\partial^2 c}{\partial t^2} - \frac{\Delta t^2}{6} \frac{\partial^3 c}{\partial t^3} + \dots \quad (3.3)$$

is introduced.

Defining an auxiliary variable  $c^f$ , and making use of the linearity of the equation, we decompose Eq. 3.1 into time-discrete advection and diffusion equations of the form

$$\frac{c^f - c^{n-1}}{\Delta t} + u_i \frac{\partial c}{\partial x_i} = 0 \quad (3.4)$$

$$\frac{c^n - c^f}{\Delta t} = \frac{1}{h} \frac{\partial}{\partial x_j} (h E_{ij} \frac{\partial c}{\partial x_i}) + \phi \quad (3.5)$$

where we leave undetermined, for the moment, the time of evaluation of the different terms.

The variable  $c^f$  may be interpreted as the concentration that would be obtained at time  $n$ , if the only transport mechanism between  $n-1$  and  $n$  was advection by the velocity  $u_i$ . However,  $c^f$  can not be rigidly identified with time  $n$ , as it becomes an initial condition for the solution of the diffusion equation.

The initial (at the beginning of each step) and boundary conditions of the full problem may be written in discretized form, as

$$c = c^{n-1} \quad \text{at } n-1, \text{ in } \Omega \quad (3.6)$$

$$c^n = \bar{c} \quad \text{at } n, \text{ on } \Gamma_1 \quad (3.7)$$

$$q_n^n = \bar{q}_n \quad \text{at } n, \text{ on } \Gamma_2 \quad (3.8)$$

Using the auxiliary variable  $c^f$ , we again take advantage of the linearity of the problem to obtain the equivalent two following sets of conditions

- for advection:

$$c = c^{n-1} \quad \text{at } n-1, \text{ in } \Omega \quad (3.9)$$

$$c^f = \bar{c} \quad \text{at } n, \text{ on } \Gamma_1 \quad (3.10)$$

- for diffusion:

$$c = c^f \quad \text{at } n-1, \text{ in } \Omega \quad (3.11)$$

$$c^n = c^f \quad \text{at } n, \text{ on } \Gamma_1 \quad (3.12)$$

$$q_n^n = \bar{q}_n \quad \text{at } n, \text{ on } \Gamma_2 \quad (3.13)$$

### 3.2.2. Modified approach

In the general case where  $hE_{ij}$  is space-dependent, the decomposition defined by Eqs. 3.4 and 3.5 does not avoid the presence of hyperbolic components in the diffusion equation, as it becomes clear by expanding the derivatives in the R.H.S. of Eq. 3.5:

$$\frac{1}{h} \frac{\partial}{\partial x_j} \left[ E_{ij} h \frac{\partial c}{\partial x_i} \right] = E_{ij} \frac{\partial^2 c}{\partial x_i \partial x_j} + \frac{1}{h} \frac{\partial}{\partial x_j} (h E_{ij}) \frac{\partial c}{\partial x_i} \quad (3.14)$$

This is formally inconsistent with the purpose of the decomposition, and may become a source of inaccuracies if, in the R.H.S. of Eq. 3.14, the hyperbolic terms dominate the parabolic ones (e.g., due to large gradients in the flow depth).

Even if this is not a typical situation, BAPTISTA 1984 suggested an alternative splitting approach (which was the one effectively used in ELA), defined by

$$\frac{c^f - c^{n-1}}{\Delta t} + u_i^* \frac{\partial c}{\partial x_i} = 0 \quad (3.15)$$

$$\frac{c^n - c^f}{\Delta t} = E_{ij} \frac{\partial^2 c}{\partial x_i \partial x_j} + \varphi \quad (3.16)$$

The pseudo-velocity,  $u_i^*$ ,

$$u_i^* = u_i - \frac{1}{h} \frac{\partial}{\partial x_j} (h E_{ij}) \quad (3.17)$$

now introduced, represents non-uniform effects on diffusive transport.

Whether this modified splitting approach should, or should not, be used instead of the standard approach has to be decided in a case-by-case basis.

### 3.2.3. Splitting errors

Both Eqs. 3.4 and 3.5 (or, alternatively, Eqs. 3.15 and 3.16), are to be solved between times  $n-1$  and  $n$ ; they are not, however, solved simultaneously, which should involve some approximation, i.e., a splitting error. This error is now discussed in the context of the standard splitting approach, conclusions extending in a straightforward way to the modified approach of section 3.2.2. For simplicity, we assume a steady flow.

For convenience, we assume first that Eq. 3.1 is to be solved in a fully implicit way, i.e.,

$$\frac{c^n - c^{n-1}}{\Delta t} + \left\{ u_i \frac{\partial c}{\partial x_i} \right\}_n = \left\{ \frac{1}{h} \frac{\partial}{\partial x_i} [E_{ij} h \frac{\partial c}{\partial x_j}] \right\}_n + \{\varphi\}_n \quad (3.18)$$

Consistently, we would then have

$$\frac{c^{\dagger} - c^{n-1}}{\Delta t} + \left\{ u_i \frac{\partial c}{\partial x_i} \right\}_n = 0 \quad (3.19)$$

and

$$\frac{c^n - c^{\dagger}}{\Delta t} = \left\{ \frac{1}{h} \frac{\partial}{\partial x_i} [E_{ij} h \frac{\partial c}{\partial x_j}] \right\}_n + \{\varphi\}_n \quad (3.20)$$

Adding Eqs 3.19 and 3.20, to get

$$\frac{c^n - c^{n-1}}{\Delta t} + \left\{ u_i \frac{\partial c}{\partial x_i} \right\}_n = \left\{ \frac{1}{h} \frac{\partial}{\partial x_i} [E_{ij} h \frac{\partial c}{\partial x_j}] \right\}_n + \{\varphi\}_n \quad (3.21)$$

and replacing in this equation  $c^{\dagger}$ , as given by Eq. 3.20, leads to

$$\frac{c^n - c^{n-1}}{\Delta t} + \left\{ u_i \frac{\partial c}{\partial x_i} \right\}_n = \left\{ \frac{1}{h} \frac{\partial}{\partial x_i} [E_{ij} h \frac{\partial c}{\partial x_j}] \right\}_n + \{\varphi\}_n + \Delta t \left\{ u_k \frac{\partial}{\partial x_k} \left[ \frac{1}{h} \frac{\partial}{\partial x_i} (E_{ij} h \frac{\partial c}{\partial x_j}) + \varphi \right] \right\}_n \quad (3.22)$$

which recovers Eq. 3.18 except for a  $O(\Delta t)$  term, which represents the additional error introduced by the splitting. We note that this error is of the same order of the truncation error associated with the discretization of the time derivative  $\partial c / \partial t$ .

Errors of this same order are introduced by the splitting defined by Eqs. 3.4 and 3.5, for alternative semi-implicit or explicit solutions of Eq. 3.1, with a single exception: when the first of the splitted equations is solved explicitly while the second is solved implicitly, the splitting introduces no additional error.

We take, for illustration, the case where advection is solved explicitly previous to diffusion, which is solved implicitly. The full equation, Eq. 3.1, becomes

$$\frac{c^n - c^{n-1}}{\Delta t} + \left\{ v_i \frac{\partial c}{\partial x_i} \right\}_{n-1} = \left\{ \frac{1}{h} \frac{\partial}{\partial x_i} \left[ E_{ij} h \frac{\partial c}{\partial x_j} \right] \right\}_n + \left\{ \varphi \right\}_n \quad (3.23)$$

and, consistently, Eqs. 3.4 and 3.5 become

$$\frac{c^f - c^{n-1}}{\Delta t} + \left\{ v_i \frac{\partial c}{\partial x_i} \right\}_{n-1} = 0 \quad (3.24)$$

and

$$\frac{c^n - c^f}{\Delta t} = \left\{ \frac{1}{h} \frac{\partial}{\partial x_i} \left[ E_{ij} h \frac{\partial c}{\partial x_j} \right] \right\}_n \quad (3.25)$$

Simple examination indicates, that, indeed, addition of Eqs. 3.24 and 3.25 reproduces Eq. 3.23 exactly.

The time discretization scheme adopted in our reference ELM will follow Eq. 3.23 and, therefore, the previous analysis suggests that no splitting error occurs. However, for unsteady flows, the above analysis does not fully hold, and some splitting error (which we expect to be minor) should actually be introduced.

*em sui modis esse indicat...*

### 3.3. SOLUTION OF THE DIFFUSION EQUATION

#### 3.3.1 Introduction

Most centered FDM and FEM will provide appropriate solutions for the diffusion equation. We have adopted a standard FEM, based on a weighted residual Galerkin formulation, with an implicit time-discretization.

The choice of a FEM rather than a FDM was decided on the basis of the superior ability of the former to deal with unstructured grids in irregular domains, which is important for the transport model ELA.

The choice of an implicit rather than explicit time-discretization scheme is based on more fundamental arguments, representing a natural attempt not to constrain one of the great advantages of ELM: their inherent ability to solve the advection equation using large  $\Delta t$ .

The next sections describe the adopted solution technique for diffusion.

#### 3.3.2 The Weighted-Residual Statement

The diffusion problem will be stated (Fig. 3.1) as governed by the differential equation (1)

$$\frac{\partial c}{\partial t} = \frac{1}{h} \frac{\partial}{\partial x_j} \left[ E_{ij} h \frac{\partial c}{\partial x_i} \right] + \phi \quad (3.26)$$

with initial conditions

$$c(x, y, t) = \bar{c}_0(x, y) \quad \text{at } t=0, \text{ in } \Omega \quad (3.27)$$

and boundary conditions

$$c(x, y, t) = \bar{c}(x, y, t) \quad \text{at } t>0, \text{ on } \Gamma_1 \quad (3.28)$$

$$q_n(x, y, t) = \bar{q}_n(x, y, t) \quad \text{at } t>0, \text{ on } \Gamma_2 \quad (3.29)$$

---

(1) Formally, the problem should be stated in the time-discrete form that results from the splitting of operators. The non-discretized form is adopted for the sake of simplicity; a consistent time-discretization will be used in section 3.3.4.

The term of production or loss of mass by internal sources or sinks,  $Q(c,x,y,t)$  will be taken in the form (appropriate for ELA)

$$Q = -k c + p \quad (3.30)$$

with  $p$  representing a source, and  $kc$  a first-order decay.

A discrete representation of the space-domain is adopted, such that the concentration is approximated by

$$c(x,y,t) \approx \hat{c}(x,y,t) = \bar{c}(x,y,t) + \sum_{j=1}^{N_T} \alpha_j(t) \phi^j(x,y) \quad (3.31)$$

where

- $\hat{c}(x,y,t)$  - denotes approximation due to the spatial discretization
- $\bar{c}(x,y,t)$  - is zero outside  $\Gamma_1$ , and is known everywhere on  $\Gamma_1$
- $\alpha_j(t)$  - are unknown coefficients
- $\phi^j(x,y)$  - are known interpolation functions
- $N_T$  - is the number of nodes in the domain

This approximation introduces residuals over  $\mathcal{R}$ ,  $\Gamma_1$  and  $\Gamma_2$ , defined as

$$R(x,y) = \frac{\partial \hat{c}}{\partial t} - \frac{1}{h} \frac{\partial}{\partial x_j} \left[ \epsilon_{ij} h \frac{\partial \hat{c}}{\partial x_i} \right] + k \hat{c} - p \quad \text{in } \mathcal{R} \quad (3.32)$$

$$T(x,y) = \hat{c} - \bar{c} \quad (3.33)$$

$$S(x,y) = \bar{q}_n - \hat{q}_n \quad (3.34)$$

We will satisfy the essential boundary condition Eq. 3.29 exactly, which implies that the residual  $T(x,y)$  and the functions  $\phi^j$  must vanish identically on  $\Gamma_1$ . The errors in  $\mathcal{R}$  and on  $\Gamma_2$  will be minimized in a weighting residual sense, by letting

$$W = \iint_{\mathcal{R}} w R(x,y) dA + \int_{\Gamma_2} w S(x,y) ds = 0 \quad (3.35)$$

where  $W$  is the weighted-residual over the domain, and  $w$  is an arbitrary weighting function.

Introducing the definitions of the residuals  $R(x,y)$  and  $S(x,y)$  into Eq. 3.35, the weighted residual over the whole domain becomes

$$W = \iint_{\Omega} \left\{ w \frac{\partial \hat{c}}{\partial t} - E_{ij} w \frac{\partial^2 \hat{c}}{\partial x_i \partial x_j} - \frac{w}{h} \frac{\partial}{\partial x_j} (h E_{ij}) \frac{\partial \hat{c}}{\partial x_i} + k w \hat{c} - w p \right\} dA + \int_{\Gamma_2} w (\bar{q}_n - \hat{q}_n) ds \quad (3.36)$$

Integration by parts of the term involving second derivatives, and re-arrangement, leads to the balanced weak form of the weighted residual statement retained for our finite element formulation:

$$W = \iint_{\Omega} \left\{ w \frac{\partial \hat{c}}{\partial t} + E_{ij} \frac{\partial w}{\partial x_i} \frac{\partial \hat{c}}{\partial x_j} - \frac{w}{h} \frac{\partial}{\partial x_j} (h E_{ij}) \frac{\partial \hat{c}}{\partial x_i} + k w \hat{c} - w p \right\} dA + \int_{\Gamma_1} w \hat{q}_n ds + \int_{\Gamma_2} w \bar{q}_n ds = 0 \quad (3.37)$$

This statement takes, when the modified splitting approach of section 3.2.2 is adopted, the simpler form

$$W = \iint_{\Omega} \left\{ w \frac{\partial \hat{c}}{\partial t} + E_{ij} \frac{\partial w}{\partial x_i} \frac{\partial \hat{c}}{\partial x_j} + k w \hat{c} - w p \right\} dA + \int_{\Gamma_1} w \hat{q}_n ds + \int_{\Gamma_2} w \bar{q}_n ds = 0 \quad (3.38)$$

### 3.3.3 The FEM Formulation

As in any FEM formulation, the domain is divided into elements. The weighted residual over the domain,  $W$ , which is required to vanish by Eq. 3.37, is evaluated as the sum of the elementary residuals,  $W^e$ .

Following a Galerkin approach, we will restrict the weighting functions to have the same shape as the interpolation functions, over each element. Clearly, the weighting functions must now vanish on  $\Gamma_2$ , as the interpolation functions do. Therefore, the integral over  $\Gamma_2$  on the right-hand of the weighted residual statement,  $\int_{\Gamma_2} w \bar{q}_n ds$ , vanishes identically. Also, we may write over an element, in a way consistent with Eq. 3.31,

$$\hat{c} = \underline{\phi}(x,y) \underline{\alpha}_e(t) \quad (3.39)$$

$$w = \underline{\phi}(x,y) \underline{w}_e(t) \equiv \underline{w}_e^T(t) \underline{\phi}^T(x,y) \quad (3.40)$$

where  $\underline{\alpha}_e$  and  $\underline{w}_e$  are column vectors containing the nodal concentrations and the (arbitrary) nodal weights;  $\underline{\phi}$  is a row vector containing the interpolations functions.

The weighted residual over an element then becomes:

$$W^e = \underline{w}_e^T \left\{ \left( \iint_{\Omega_e} \underline{\phi}^T \underline{\phi} dA \right) \frac{\partial \underline{\alpha}_e}{\partial t} + \left( \iint_{\Omega_e} E_{ij} \frac{\partial \underline{\phi}^T}{\partial x_i} \frac{\partial \underline{\phi}}{\partial x_j} dA + \iint_{\Omega_e} \frac{\underline{\phi}^T}{h} \frac{\partial}{\partial x_j} (h E_{ij}) \frac{\partial \underline{\phi}}{\partial x_i} dA \right) \underline{\alpha}_e + \left( \iint_{\Omega_e} k \underline{\phi}^T \underline{\phi} dA \right) \underline{\alpha}_e - \iint_{\Omega_e} \underline{\phi}^T p dA + \int_{\Gamma_2} \underline{\phi}^T \bar{q}_n ds \right\} \quad (3.41)$$

or equivalently,

$$\underline{W}^e = \underline{w}_e^T \{ \underline{M}_e \dot{\underline{a}}_e + (\underline{A}_e + \underline{B}_e) \underline{a}_e - \underline{P}_e \} \quad (3.42)$$

where

$$\underline{M}_e = \iint_{\Omega_e} \underline{\phi}^T \underline{\phi} \, dA \quad (3.43)$$

$$\underline{A}_e = \iint_{\Omega_e} \left\{ E_{ij} \frac{\partial \underline{\phi}^T}{\partial x_i} \frac{\partial \underline{\phi}}{\partial x_j} + \frac{\underline{\phi}^T}{h} \frac{\partial}{\partial x_i} (h E_{ij}) \frac{\partial \underline{\phi}}{\partial x_i} \right\} dA \quad (3.44)$$

$$\underline{B}_e = \iint_{\Omega_e} k \underline{\phi}^T \underline{\phi} \, dA \quad (3.45)$$

$$\underline{P}_e = \iint_{\Omega_e} \underline{\phi}^T \underline{p} \, dA - \int_{\Gamma_2} \underline{\phi}^T \bar{q}_n \, ds \quad (3.46)$$

When the modified splitting approach of section 3.2.2 is adopted, matrix  $\underline{A}$  takes the simpler form

$$\underline{A}_e = \iint_{\Omega_e} E_{ij} \frac{\partial \underline{\phi}^T}{\partial x_i} \frac{\partial \underline{\phi}}{\partial x_j} \, dA \quad (3.47)$$

The sum, over the whole domain, of the individual contributions of the elements to the global weighted residual leads to the system of ordinary differential equations

$$\underline{M} \dot{\underline{a}} + (\underline{B} + \underline{A}) \underline{a} = \underline{P} \quad (3.48)$$

where each global matrix represents the assemblage of the corresponding elementary matrices (which should be previously computed using standard integration procedures).

In the above formulation, we implicitly assume that concentration is the single dependent variable of the problem (in particular, avoiding concentration derivatives as additional variables). This deliberately restricts the choice of the elementary interpolation functions, which are selected to be Lagrange interpolations. As the highest derivatives involved in the selected weighted residual statement are of first order, space-continuity requires that these functions be first-derivative square integrable, i.e., have piece-wise continuous first derivatives. In addition, convergence in the mean-square sense requires that, within each element, the interpolation functions be at least linear.

The choice of the actual interpolation function is much less of



an issue here (where even linear interpolations will lead to satisfactory accuracy, if properly used) than it is for the solution of advection. As both choices should be consistent (although not necessarily the same), we leave open, for the moment, the possibility of using up to cubic Lagrange interpolation functions, reserving further discussion for section 3.4.3.

### 3.3.4 Time-Discretization Scheme. Solution Strategy

To transform Eq. 3.48 into a system of algebraic equations, we adopt the implicit time-discretization scheme

$$[\underline{M} + \Delta t(\underline{A}^n + \underline{B}^n)] \underline{\alpha}^n = \underline{M} \underline{\alpha}^f + \Delta t \underline{P}^n \quad (3.49)$$

where superscripts n and f denote current time and "previous" time (after the advection equation has been solved). This scheme is unconditionally stable and is consistent with the splitting procedures described in section 3.2.

From the analysis of Eqs. 3.43 through 3.45, we recognize that  $\underline{M}$  is always a symmetric, time-independent matrix, while matrices  $\underline{A}$  and  $\underline{B}$  may be non-symmetric and time-dependent. However,  $\underline{A}$  will be time-independent if  $E_{ij}$  and  $h$  are both constant, or  $E_{ij}$  is constant and  $h$  uniform over each single element; and will be symmetric if  $E_{ij}$  and  $h$  are both uniform over each element, and, in addition,  $E_{ij} = E_{ji}$ . Also,  $\underline{B}$  will be time-independent if  $K$  is constant, and will be symmetric if  $K$  is uniform over each element.

We note that when the modified splitting approach of section 3.2.2. is used,  $\underline{A}$  is fully independent of  $h$ , and therefore requirements for symmetry and time-independence are associated with the characteristics of  $E_{ij}$ , alone. In many situations of practical interest (e.g., pollutant transport in estuaries and coastal waters), requirements on  $E_{ij}$  are much more easily satisfied than requirements on  $h$ , which constitutes a potential advantage of the modified over the standard splitting approach.

The best strategy for the solution of the system of algebraic equations represented by Eq. 3.49 depends on the actual characteristics of the matrix  $\underline{Z} = \underline{M} + \Delta t(\underline{A}^n + \underline{B}^n)$ .

In the formulation adopted for ELA,  $\underline{Z}$  is symmetric and time-independent (a consequence of the adoption of the splitting approach of section 3.2.2, and of constant, element-wise uniform  $E_{ij}$  ( $=E_{ji}$ ) and  $K$ ). To take advantage of this property, we have solved the system by using an  $LL^T$ -decomposition. The decomposition of  $\underline{Z}$  is done only once, at the beginning of the computations; at each specific time step, the required operations are limited to updating the load vector,  $\underline{P}$ , and performing appropriate forward and backward substitutions to obtain the vector of nodal concentrations.

### 3.4. SOLUTION OF THE ADVECTION EQUATION

#### 3.4.1. Introduction

In continuous form, the advection equation may be written as

$$\frac{Dc}{Dt} \equiv \frac{\partial c}{\partial t} + U_i \frac{\partial c}{\partial x_i} = 0 \quad (3.50)$$

where  $U=U_1, V=U_2$  are actual  $(u,v)$  or pseudo  $(u^*,v^*)$  velocities (depending on whether non-uniform diffusion was or was not accounted for during the diffusion step). This simply states that the concentration of a particle following the  $(U,V)$  flow remains constant along the trajectories or characteristic lines defined by

$$\frac{dx_i}{dt} = U_i(x,y,t) \quad (3.51)$$

We will use this property to solve the equation. In each time step, we allocate a fluid particle to each node of the finite element grid used to solve the diffusion equation, and we proceed as illustrated below.

Consider, at time  $n$ , the particle at node  $j$ , located at  $P \equiv (x_j, y_j)$  - Fig. 3.3. This particle was previously at position  $(P', n-1)$ , having been driven from there by the flow, along a characteristic line. Tracking the characteristic line backwards, we can determine  $P'$ , and then determine  $c(P', n-1)$  by spatial interpolation at time  $n-1$  (where the concentrations at the nodes of the finite element grid are known). But by Eq. 3.50,  $c(P, n) = c(P', n-1)$  and the problem is solved for node  $j$ ; the procedure must now be repeated for each of the remaining nodes.

The same basic procedure applies even if an inflow boundary is crossed during the back-tracking (case of node  $Q$ , Fig. 3.3). Now, however, the concentration at  $(Q, n)$  is imposed directly from the boundary condition, i.e.,  $c(Q, n) \equiv \bar{c}(Q', n-\theta)$ . In outflow or closed boundaries the back-trajectory of a particle is towards the interior of the domain, and boundary conditions are not required.

The approach described has been called "backwards method of characteristics (BMC)" (designation which we will adopt), "stepwise method of characteristics", "reverse method of characteristics" or "streakline method". It clearly includes two main tasks:

- the stepwise back-tracking of particles along the characteristic lines, between time  $n$  and time  $n-1$  (or until an inflow boundary is crossed);
- the spatial interpolation required to find the concentration carried along each characteristic line.

#### 3.4.2 The Stepwise Particle Tracking

The stepwise tracking of a particle constitutes an initial-value

problem, governed by the set of ordinary differential equations

$$\frac{dx_i}{dt} = U_i(x,y,t) \quad \{i=1,2\} \quad (3.52)$$

which must be solved backwards in time, with boundary conditions

$$x_i = \bar{x}_i \quad \text{at time } n \quad (3.53)$$

In most FEM, the driving flow field (u,v,h) is given explicitly at the nodes of a (often irregular) grid, but elementary interpolation functions allow the unambiguous definition of (U,V) in the whole domain. Also, most FE circulation models only compute the flow field at fixed times, requiring time-interpolation procedures to complete the flow description. Exceptions include models based on frequency-domain approaches, that explicitly establish the time dependence of u, v, h.

We now describe an element-by-element tracking algorithm that accounts for the need of an element-based spatial interpolation of the flow field, and is flexible to accommodate time-interpolation procedures when required.

We will refer to Fig. 3.4 to describe this algorithm. Consider a particle at position (P,n) where P coincides with a node of the finite element grid; at time n-1 this particle was at (P<sup>'''</sup>,n-1), which we want to determine. We first follow the particle backwards along its characteristic line, until position (P',n-β<sub>1</sub>). As only element K<sub>1</sub> is involved, we may write:

$$u_i(x,y,t) = \sum_{l=1}^m \psi_l(x,y;K_1) u_{il}(t;K_1) \quad (3.54)$$

$$h(x,y,t) = \sum_{l=1}^m \tau_l(x,y;K_1) h_l(t;K_1) \quad (3.55)$$

$$E_{ij}(x,y,t) = \sum_{l=1}^m \theta_l(x,y;K_1) E_{ijl}(t;K_1) \quad (3.56)$$

where  $\psi_l$ ,  $\tau_l$  and  $\theta_l$  are elementary interpolation functions;  $u_{il}$ ,  $h_l$  and  $E_{ijl}$  represent nodal values; and m is the number of nodes of the element. If the nodal quantities  $u_{il}$ ,  $h_l$  and  $E_{ijl}$  are known at all times between n and n-β<sub>1</sub> (either directly or by time interpolation),  $U_i$  may be computed everywhere.

Once U,V are defined, the solution of the initial-value problem governed by Eqs. 3.52 and 3.53 determines (P',n-β<sub>1</sub>). From the several numerical solution techniques available for such solution, we selected a 4th order Runge-Kutta (R-K) method, with

constant time-stepping. The R-K time step,  $\delta t^{K_1}$  (which is a fraction of, and should not be confused with, the BMC time step) is automatically selected so as to limit the theoretical truncation error per R-K step to a prescribed value. Once  $(P', n - \beta_1)$  is obtained, an evaluation of  $(P, n)$  given  $(P', n - \beta_1)$  is performed, to assess the total error introduced between consecutive BMC instants  $n$  and  $n - \beta_1$ ; if the total error is not found satisfactory, the time-step is reset (reduced to an half), and the tracking between  $(P, n)$  and  $(P', n - \beta_1)$  is repeated.

Once  $(P', n - \beta_1)$  is known within satisfactory accuracy, the functions  $U$  and  $V$  are replaced by equivalent ones applying over element  $K_2$ , and the particle is tracked along this element, back to  $(P'', n - \beta_2)$ . The tracking is accomplished as before; a new Runge-Kutta time step  $\delta t^{K_2}$  is selected in an attempt to account for the variation of the flow characteristics from element to element.

The element-by-element tracking is continued until time  $n-1$  is reached, or a boundary is crossed (whichever happens first).

The actual implementation of the algorithm just described was originally made for grids involving straight triangles, with linear interpolations for the flow characteristics and quadratic interpolations for concentrations (which is consistent with the formulation of ELA). Alternative versions of this algorithm, applying to grids involving (a) subparametric quadratic triangles and rectangles, and (b) isoparametric triangles and rectangles, were formulated and its coding and testing initiated, as a step for the extension of ELA (see Chapter 6).

### 3.4.3 The Interpolation Scheme

Consider again the finite element grid shown in Fig. 3.4. Assume that  $(P''''', n-1)$  was found by the particle tracking procedure, and lies in element  $K_4$ , say.

The concentration at  $(P''''', n-1)$  will not, in general, be explicitly known. However, concentrations at the nodes of element  $K_4$  are known at time  $n-1$ , and can, therefore, be interpolated to the interior of each element.

The finite element approximation used to solve the diffusion equation inherently supplies a consistent way of interpolating concentrations over the elements, i.e.,

$$c(P, n) = c(P''''', n-1) = \sum_{i=1}^m \phi_i(x, y; K_4) c_i^{(n-1)}(K_4) \quad (3.57)$$

where  $\phi_i(x, y; K_4)$  are the Lagrange interpolation functions associated with the finite element approximation for concentrations;  $c_i$  are nodal concentrations; and  $m$  is the number of nodes of the element.

While natural and convenient, this choice of interpolation functions has accuracy limitations. Indeed (see Chapter 4), linear interpolations lead to excessive numerical damping (in a

way much similar to upwind Eulerian methods), and cubic and higher order interpolations lead to instability. Quadratic interpolations seem to be the optimal choice within the class, and were adopted in BAPTISTA 1984 and in the actual implementation of ELA (where the interpolation functions for concentration are defined over subparametric six-node triangles); however, this still allows for non-negligible numerical damping and dispersion.

Chapter 4 explores the idea of improving the accuracy of the BMC (hence ELM/C) by resorting to interpolation functions that, while consistent with the finite element approximation for the diffusion step, are more performing than such Lagrange polynomials.

As it will be seen, considerable accuracy improvements can be achieved for advection-dominated problems involving sharp gradients, but always at the expense of additional complexity (both conceptual and practical).

In particular, some of the most promising interpolation schemes are not compact, i.e, they have a domain of validity smaller than their domain of definition, which poses two major problems:

- the definition of the interpolation scheme for highly irregular grids may become ambiguous;
- the interpolation scheme has to be changed or reformulated near the boundaries.

### 3.5 INTRODUCTORY DISCUSSION ON ACCURACY AND STABILITY

The method has no direct stability limitations on the time step,  $\Delta t$ . For the advection equation, independence of stability on  $\Delta t$  is ensured by the fact that the concentration at the foot ( $P'$ , say) of each characteristic line is found by interpolation (centered on the element that contains  $P'$ ) rather than by extrapolation; we should note, however, that conditional stability (e.g., related to the dimensionless wavelength of dominant Fourier modes in the solution) may be associated with some of the interpolation schemes considered in Chapter 4. For the diffusion equation, unconditional stability is assured by the implicit time-discretization scheme that was adopted.

Such stability independence on  $\Delta t$  is a very significant achievement of ELM/C, and enhances their actual accuracy, as suggested by the following discussion.

Errors may arise in each of the three major components of the method: the splitting technique, the solution of the diffusion equation and the solution of the advection equation.

The error associated with the time-discretization and splitting of the full transport equation are of  $O(\Delta t)$ , as discussed in section 3.2.3.

The diffusion equation that results from the splitting is already in a time-discrete form. Errors inherent in the solution of this equation are therefore due only to spatial approximations, and are estimated to be of order  $O(\Delta x^2)$  or  $O(\Delta x^3)$ , respectively for linear and quadratic interpolation functions. This estimate is based on the theoretical bound of the mean-square error in 1-D

$$\|c - \hat{c}\| = \left\{ \int_{\mathcal{R}_e} (c - \hat{c})^2 dA \right\}^{1/2} \leq (\Delta x)^{p+1} \left\{ \int_{\mathcal{R}_e} \left( \frac{d^{p+1}c}{dx^{p+1}} \right)^2 dA \right\}^{1/2} \quad (3.58)$$

where  $p$  is the order of the interpolation function.

Errors inherent in the solution of the advection equation are associated with both time and space discretizations.

Time-discretization errors arise during the particle tracking, where the time-step for the solution of the hyperbolic equation,  $\Delta t$ , is broken into sub-steps,  $\delta t$ ; as a 4th order Runge-Kutta method is used, errors are estimated to be of order  $(\delta t^4)$ , and should be often negligible, as  $(\delta t^4)$  is small relative to  $\Delta t$ , and is adjusted as to satisfy an accuracy criterion selected by the user.

Errors per time step associated with the interpolation of the concentrations at the feet of the characteristic line, as given by Taylor-series analysis, are, for large Courant numbers, independent of  $\Delta t$ , i.e., a (scheme-specific) function of  $\Delta x$  alone - section 4.2.2. This implies that increasing  $\Delta t$ , i.e., reducing the number of time steps,  $N$ , may lead to improved accuracy in the solution of the advection equation.

Numerical experimentation and practice show (e.g. BAPTISTA 1984)

that interpolation errors in the advection step often dominate ELM/C solutions, suggesting that a strong effort should be put into formally understanding and into finding and actually implementing remedies for such errors.

CHAPTER 4

ACCURACY AND STABILITY ANALYSIS OF THE BACKWARDS  
METHOD OF CHARACTERISTICS





#### 4.1. INTRODUCTION

The advection step is critical for the accuracy of ELM/C solutions of advection-dominated transport, as suggested in Chapter 3. No significant accuracy loss is expected from the tracking step; indeed, the technique described in section 3.4.2 is virtually exact for any consistent flow field. The interpolation step, however, is a potential source of major errors.

The present chapter provides a detailed analysis of the accuracy of the interpolation step of the BMC, for a wide spectrum of alternative choices (some of which first proposed through this research) of the interpolation scheme used to find concentrations at the feet of the characteristic lines. Emphasis is placed on the formal understanding of the relevant error mechanisms, on the comparison of available interpolation schemes and on the search for improved alternatives.

Section 4.2 presents a systematic study (based on both formal analysis and numerical experimentation) of the BMC accuracy and stability, for 1-D uniform grids. Results provide significant insight on the general performance of the BMC and allow a first ranking of alternative interpolation schemes, as regards specially to accuracy, but also to convenience and cost.

Extension of the findings of section 4.2 to non-uniform and to 2-D grids, two cases often of more practical interest, is discussed in sections 4.3 and 4.4, respectively. In both cases, the analysis is mostly based in numerical experimentation (systematic formal analysis is, unfortunately, no longer feasible), and is carried out only for a restricted set of interpolation schemes. Although no interpolation scheme is found to be optimal, some schemes are recognized as inappropriate, and their use discouraged, while tentative scenarios are drawn for the most convenient use of the remaining ones.

## 4.2. CONSTANT ADVECTION IN ONE-DIMENSIONAL UNIFORM GRIDS

### 4.2.1. Introduction

In the next sections we will compare the performance of the BMC for several alternative interpolation schemes, all based on Lagrange and/or Hermite-type polynomials, and fitting into the following five general classes:

- LI schemes, using compact Lagrange interpolation polynomials (the word compact refers to the fact that the nodes that provide information for the interpolation function are all in the domain of validity of this function.)
- LR schemes, using non-compact Lagrange interpolation polynomials, with restricted domain of validity
- HI schemes, using compact Hermite interpolation polynomials
- HL schemes, using non-compact Hermite interpolation polynomials, with derivatives estimated from Lagrange polynomials
- PL schemes, using non-compact pseudo-Hermite interpolation polynomials, with derivatives estimated from Lagrange polynomials.

LI schemes were first used (e.g. LEITH 1965) and are still a very attractive option, because of their conceptual simplicity and practical convenience (e.g. BENQUE et al. 1980, BAPTISTA 1984). The other classes of schemes constitute attempts to improve the accuracy of LI schemes, at the expense of convenience and cost.

HI schemes (e.g. HOLLY and PREISSMAN 1977, HOLLY and POLATERA 1984) improve accuracy by introducing concentration derivatives as new dependent variables. This substantially increases computational costs, and poses conceptual problems at the boundaries. In turn, PL (e.g. HOLLY and KOMATSU 1984, KOMATSU et al. 1984), HL and LR schemes improve accuracy at the cost of losing compactness (nodes outside the domain of validity of the interpolation contribute to the definition of the interpolation), which poses conceptual and practical problems in multidimensional irregular grids, and near boundaries.

The individual interpolation schemes actually considered within the different classes are illustrated and defined (for 1-D uniform grids) in Fig. 4.1. In order to make their reference manageable, we will adopt throughout this work the general notation:

$$nP-XXm \quad (4.1)$$

where P denotes nodal points, and n, XX, m are variables, standing for

- n - the number of points that provide information (concentrations and/or concentrations derivatives) for interpolation

XX - the identification of the class of interpolation (LI, LR, HI, HL, PL)

m - the number of nodes of the core element (defined as the domain of validity for the interpolation)

While the full set of schemes considered at some point of this chapter includes

- 2P-LI2, 3P-LI3, 4P-LI4
- 4P-LR2, 5P-LR3, 6P-LR2, 8P-LR2
- 2P-HI2
- 4P-HL2, 5P-HL3, 7P-HL3
- 6P-PL2, 8P-PL2

our analysis will concentrate on schemes using linear and quadratic core elements (i.e. nP-XX2 and nP-XX3 schemes) and involving concentrations as single dependent variables (LI, LR, PL and HL schemes).

The 4P-LI4 is excluded from detailed analysis because of the early finding of its unstable characteristics, while the 2P-HI2, a potentially very accurate scheme, is excluded because of the need for derivatives as new dependent variables (which we want to avoid, given the formulation of our reference ELM). Both schemes are, however, used as sporadic terms of reference.

#### 4.2.2. Truncation errors

The numerical solution of any given PDE introduces truncation errors, which modify the actual form of the PDE. These errors are, in general, too complex to be evaluated; however, for schematic conditions (typically associated with constant coefficients and uniform grids) truncation errors can be assessed by expanding all terms of the algorithm of the numerical method in Taylor series, and rearranging so as to obtain the original equation plus a residual. Although a quantitative extension is often not possible, results are useful to a qualitative understanding of the performance of the numerical method for more complex problems.

This general procedure, first suggested by CYRUS AND FULTON 1967 and HIRT 1968, is easily applied to the BMC. We consider the solution of the constant advection equation

$$\frac{\partial c}{\partial t} + u \frac{\partial c}{\partial x} = 0 \quad (4.2)$$

in a uniform space-time grid, through a BMC with general algorithm

$$c_j^{n+1} = \sum_{m=P}^{P+Q} \phi_m c_{j-k+m}^n \quad (4.3)$$

(which applies to all considered schemes but the 2P-HI2 see Fig. 4.1.).

The expansion of  $c_j^{n+1}$  and  $c_{j-k+m}^n$  in Taylor series about the value of  $c_j^n$  leads, respectively, to

$$\begin{aligned} c_j^{n+1} = & c_j^n + \Delta t \frac{\partial c}{\partial t} + \frac{\Delta t^2}{2} \frac{\partial^2 c}{\partial t^2} + \frac{\Delta t^3}{6} \frac{\partial^3 c}{\partial t^3} + \frac{\Delta t^4}{24} \frac{\partial^4 c}{\partial t^4} + \\ & + \frac{\Delta t^5}{120} \frac{\partial^5 c}{\partial t^5} + \dots \end{aligned} \quad (4.4)$$

and

$$\begin{aligned} c_{j-k+m}^n = & c_j^n - (k-m) \Delta x \frac{\partial c}{\partial x} + \frac{(k-m)^2}{2} \Delta x^2 \frac{\partial^2 c}{\partial x^2} - \frac{(k-m)^3}{6} \Delta x^3 \frac{\partial^3 c}{\partial x^3} + \\ & + \frac{(k-m)^4}{24} \Delta x^4 \frac{\partial^4 c}{\partial x^4} - \frac{(k-m)^5}{120} \Delta x^5 \frac{\partial^5 c}{\partial x^5} + \dots \end{aligned} \quad (4.5)$$

where all derivatives are defined at  $(j,n)$ .

Quadratic and higher-order derivatives in time can be expressed in terms of spatial derivatives, by using Eq. 4.2 and the fact that  $u$  is a constant; indeed,

$$\frac{\partial^2 c}{\partial t^2} = -u \frac{\partial^2 c}{\partial t \partial x} = -u \frac{\partial}{\partial x} \left( \frac{\partial c}{\partial t} \right) = u^2 \frac{\partial^2 c}{\partial x^2}$$

$$\frac{\partial^3 c}{\partial t^3} = u^2 \frac{\partial^3 c}{\partial t \partial x^2} = u^2 \frac{\partial^2}{\partial x^2} \left( \frac{\partial c}{\partial t} \right) = -u^3 \frac{\partial^3 c}{\partial x^3}$$

⋮

$$\frac{\partial^r c}{\partial t^r} = (-1)^r u^r \frac{\partial^r c}{\partial x^r}$$

⋮

(4.6)

Replacing Eq.4.6 into Eq.4.4, gives

$$c_j^{n+1} = c_j^n + \Delta t \frac{\partial c}{\partial t} + \frac{u^2 \Delta t^2}{2} \frac{\partial^2 c}{\partial x^2} - \frac{u^3 \Delta t^3}{6} \frac{\partial^3 c}{\partial x^3} + \frac{u^4 \Delta t^4}{24} \frac{\partial^4 c}{\partial x^4} - \frac{u^5 \Delta t^5}{120} \frac{\partial^5 c}{\partial x^5} + \dots \quad (4.7)$$

and substitution of Eqs. 4.5 and 4.7 into the expression of the numerical algorithm, Eq. 4.3, leads finally to

$$\begin{aligned} \frac{\partial c}{\partial t} + u \frac{\partial c}{\partial x} = & \frac{1}{\Delta t} \left[ (1 - I_0) c_j^n + [u \Delta t - \Delta x (I_0 K + I_1)] \frac{\partial c}{\partial x} + \left[ -\frac{u^2 \Delta t^2}{2} + \frac{\Delta x^2}{2} (I_0 K^2 + 2 I_1 K + I_2) \right] \frac{\partial^2 c}{\partial x^2} + \right. \\ & + \left[ \frac{u^3 \Delta t^3}{6} - \frac{\Delta x^3}{6} (I_0 K^3 + 3 I_1 K^2 + 3 I_2 K + I_3) \right] \frac{\partial^3 c}{\partial x^3} + \\ & + \left[ -\frac{u^4 \Delta t^4}{24} + \frac{\Delta x^4}{24} (I_0 K^4 + 4 I_1 K^3 + 6 I_2 K^2 + 4 I_3 K + I_4) \right] \frac{\partial^4 c}{\partial x^4} + \\ & \left. + \left[ \frac{u^5 \Delta t^5}{120} - \frac{\Delta x^5}{120} (I_0 K^5 + 5 I_1 K^4 + 10 I_2 K^3 + 10 I_3 K^2 + 5 I_4 K + I_5) \right] \frac{\partial^5 c}{\partial x^5} + \dots \right. \end{aligned} \quad (4.8)$$

where

$$\begin{aligned} I_0 &= \sum_{m=P}^{P+Q} \phi_m(\alpha) \\ I_1 &= \sum_{m=P}^{P+Q} m \phi_m(\alpha) \\ &\vdots \\ I_r &= \sum_{m=P}^{P+Q} m^r \phi_m(\alpha) \\ &\vdots \end{aligned} \quad (4.9)$$

The right-hand side (RHS) of Eq. 4.8 represents the truncation error, which is scheme specific. The actual form of truncation error, for alternative interpolation schemes is presented in Tables 4.1 (general case) and 4.2 (for  $Cu \leq 1$ , i.e.,  $\alpha \cdot Cu = u\Delta t/\Delta x$ ).

A first striking finding is that truncation errors per time step (values in Tables 4.1 and 4.2 times  $\Delta t$ ) are not directly dependent on  $\Delta t$  (dependence is rather on the location of the foot of the characteristic line within the core element for interpolation) for  $Cu > 1$ , i.e., for large  $\Delta t$ , while they directly vary with  $\Delta t$  for  $Cu \leq 1$ , i.e., for small  $\Delta t$ .

Two major consequences may be identified:

- for a fixed total time, and in the zone of  $Cu > 1$ , accuracy should be improved by taking fewer (but larger) time steps (a both unusual and convenient feature);
- even so, consistency (in the precise mathematical sense of the original PDE being approached as  $\Delta x, \Delta t \rightarrow 0$ ) is not necessarily precluded, as truncation errors may still converge to zero as  $\Delta t \rightarrow 0$ .

Indeed, examination of table 4.2 indicates that all the considered schemes (but the 6P-PL2 and the 4P-LI4) are unconditionally consistent: for  $\Delta x, \Delta t \rightarrow 0$ , the expansion of the numerical algorithms in Taylor series approaches the original PDE, regardless of the relative rates of convergence of  $\Delta x$  and  $\Delta t$ . The 4P-LI4 is conditionally consistent (it depends on the relative convergence rate of  $\Delta x$  and  $\Delta t$ ), while the 6P-PL2 is not consistent.

The coefficients of all the truncation terms involving derivatives up to order M are null when the interpolation scheme adopted in the BMC is exact for functions up to degree M(1). The leading derivatives in the truncation errors for the different interpolation schemes (Tables 4.1 and 4.2) are therefore those expected from the conceptual generation procedure of each interpolation scheme, except in the case of the 6P-PL2.

This interpolation scheme would be expected to be exact for functions up to linear (we note that, although the basic interpolation function is a cubic Hermite polynomial, linear interpolations are used to estimate derivatives). However, the coefficients of both  $c_j^n$  and  $\partial c/\partial x$  are non-null.

Closer examination of the scheme proposed by KOMATSU et al. 1984 reveals that the authors indulged in unnecessary roundoff errors while estimating the actual interpolating coefficients; because of these roundoff errors, neither constant nor linear functions are exactly represented by the scheme, which explains not only the two anomalous behaviors already detected, but further deficiencies that will become apparent in the next sections,

-----  
(1) This can be shown by taking a generic function  $f(\alpha)$  of degree M, imposing  $f(\alpha) = \sum \phi_i f(\alpha_i)$  for all  $\alpha$ , and computing  $I_0, \dots, I_r$ ; we find  $I_r = \alpha^r$ , which, replaced in Eq. (4.8), gives the referred result.

such as:

- potential instability;
- systematic gain of mass;
- incorrect mean advection;

No general conclusions can, at this stage, be presented on the stability of the BMC. Hirt's criterion (which calls for the coefficient of  $\partial^2 c / \partial x^2$  - formally, a diffusivity - to be positive for stable schemes) suggests that the 2P-LI2 is unconditionally stable, while the 6P-PL2 is conditionally stable (it would be unconditionally stable if roundoff errors had not been introduced); however, this criterion should not be used for the other schemes, which have null artificial diffusivities. The issue of stability will be retaken in section 4.2.5.2.

### 4.2.3. Amplitude and phase errors

#### 4.2.3.1 General remarks

Numerical methods are known to artificially change the amplitudes and phases of the individual Fourier components of the true solution of the transport equation.

The formal analysis of amplitude and phase errors, through the expansion of numerical algorithms in complex Fourier series, was apparently first introduced by von Neuman, at Los Alamos, around 1939 (ROACHE 1976). Although originally applied to the study of stability (giving rise to the so-called von Neuman stability analysis), the idea has evolved to a powerful tool for accuracy analysis (e.g. GRAY and PINDER 1976, LAPIDUS and PINDER 1982).

The application of this tool to the analysis of the accuracy of the BMC is now described. This application has revealed an unexpected complexity for interpolation schemes with core elements higher than linear, the approach proposed for these cases being original.

#### 4.2.3.2 The case of interpolation schemes with linear core elements

##### 4.2.3.2.1 Theoretical framework

We consider a generic problem of 1-D constant advection, governed again by

$$\frac{\partial c}{\partial t} + v \frac{\partial c}{\partial x} = 0 \quad (4.10)$$

The general solution for this problem can be written (e.g. LAPIDUS and PINDER 1982) in the form of the complex Fourier series



$$c(x,t) = \sum_{m=-\infty}^{+\infty} c_m(x,t) \quad (4.11)$$

with

$$c_m(x,t) = A_m \exp \left\{ i \frac{2\pi}{L_m} (x-ut) \right\} \quad (4.12)$$

where  $A_m$  are problem-dependent coefficients (representing amplitudes of Fourier components),  $x-ut$  refers to the phase, and  $L_m$  is the wavelength of the  $m$ th component. As  $u$  is a constant, each individual Fourier component,  $c_m(x,t)$ , is easily recognized to be an elementary solution of Eq. 4.10.

In a uniform space-time grid, Eq. 4.12 becomes

$$c_m(j,n) = \sum_{m=-q}^q c_m(j,n) \quad (4.13)$$

where  $q$  corresponds to the integer number associated with the smallest wavelength that can be propagated by the numerical approximation ( $2\Delta x$ ), and

$$c_m(j,n) = A_m \exp \left\{ i \lambda_m (j-n\beta) \right\} \quad (4.14)$$

where  $\lambda_m = 2\pi\Delta x/L_m$  is the dimensionless wavenumber (with  $L_m/\Delta x$  being the dimensionless wavelength),  $\beta = u\Delta t/\Delta x$  is the Courant number, and  $j=x/\Delta x$ ,  $n=t/\Delta t$ .

Interpolation schemes with linear core elements, not involving derivatives, lead to BMC algorithms of the form

$$f(j,n) = \sum_{p=P}^{P+Q} \phi_p(\alpha) \cdot f(j-k+p, n-1) \quad (4.15)$$

where  $f$  is the unknown,  $\phi_i$  are real interpolation functions,  $\alpha = \beta - k$  is the location of the foot of the characteristic line within the core element,  $k = \text{int}(\beta)$  and  $p = P, P+1, \dots, P+Q$  are the local coordinates of the intervening nodes (Fig. 4.1).

Solving Eq. 4.10 through the algorithm of Eq. 4.15, between times  $n-1$  and  $n$ , and taking the elementary solution Eq. 4.14, written for  $(n-1)$ , as initial condition, leads to

$$\begin{aligned} \tilde{c}_m(j,n) &= \sum_{p=P}^{P+Q} \phi_p(\alpha) A_m \exp \left\{ i \lambda_m [j-k+p-(n-1)\beta] \right\} = \\ &= A_m \exp [i \lambda_m (j-n\beta)] \cdot \exp(i \lambda_m \alpha) \sum_{p=P}^{P+Q} \phi_p(\alpha) \exp(i \lambda_m p) = \\ &= G_m(\alpha) c_m(j,n) \end{aligned} \quad (4.16)$$

with

$$G_m(\alpha) = \exp(i\lambda_m \alpha) \sum_{p=P}^{P+Q} \phi_p(\alpha) \exp(i\lambda_m p) \quad (4.17)$$

Hence, the first step of the numerical solution introduces to the  $m$ th Fourier component an error,  $G_m(\alpha)$ , which is typically complex, i.e., has amplitude and phase components.

Amplitude errors are appropriately described by the amplifying factor

$$|G_m(\alpha)| = \left\{ \left[ \operatorname{Re} \left( \sum_{p=P}^{P+Q} \phi_p(\alpha) \exp(i\lambda_m p) \right) \right]^2 + \left[ \operatorname{Im} \left( \sum_{p=P}^{P+Q} \phi_p(\alpha) \exp(i\lambda_m p) \right) \right]^2 \right\}^{1/2} \quad (4.18)$$

which should be unity for exact solutions. If  $|G_m| < 1$ , the energy (the term is loosely used in the sense of the 0th moment of the square of the concentration) of the  $m$ th Fourier component is reduced, the numerical solution being dissipative or damping with regard to that component; if  $|G_m| > 1$ , the energy is amplified, and the numerical solution is said to be unstable relative to the  $m$ th component. We note that a numerical solution may be dissipative with regard to some components, and unstable with regard to others, the overall behavior depending on which components are dominant.

Phase errors are described by

$$\arg \{G_m(\alpha)\} = \lambda_m \alpha + \operatorname{arctg} \left\{ \frac{\operatorname{Im} \left[ \sum_{p=P}^{P+Q} \phi_p(\alpha) \exp(i\lambda_m p) \right]}{\operatorname{Re} \left[ \sum_{p=P}^{P+Q} \phi_p(\alpha) \exp(i\lambda_m p) \right]} \right\} \quad (4.19)$$

where  $\arg G_m(\alpha)$  should be zero for exact propagation. A useful associated concept is that of celerity ratio,

$$r = 1 - \frac{\arg \{G_m(\alpha)\}}{\beta \lambda_m} \quad (4.20)$$

In an exact solution, this ratio should be unity for all components. In an actual numerical solution, the celerity ratio is not only different from unity but also wavelength dependent; this implies that different Fourier components propagate at different speeds, giving rise to the so-called numerical dispersion (detectable through the presence of parasitic oscillations, known as "wiggles").

Because the same  $\alpha$  is associated to all grid nodes (a consequence of both the uniformity of the grid and the flow, and of the linearity of the core element), it can be easily shown (BAPTISTA, unpublished work) that the exact same error occurs in each new time step. Hence, errors after  $N$  time steps are simply described by:

$$H_m(N, \alpha) = \{G_m(\alpha)\}^N \quad (4.21)$$

$$|H_m(N, \alpha)| = |G_m(\alpha)|^N \quad \text{amplifying factor} \quad (4.22)$$

$$\text{arg} \{H_m(N, \alpha)\} = N \text{arg} \{G_m(\alpha)\} \quad \text{phase error} \quad (4.23)$$

$$R = r \quad \text{celerity ratio} \quad (4.24)$$

which are well-known results.

So far, we have been concerned with amplitude and phase errors for individual components. However, we can invoke the linearity of Eq. 4.2 (and the fact that no cause exterior to the equation - e.g., a uniform flow or grid - promote interaction between Fourier modes), to state that

$$\tilde{c}(j, n) \cong \sum_{m=-q}^q \tilde{c}_m(j, n) = \sum_{m=-q}^q H_m(N, \alpha) c_m(j, n) \quad (4.25)$$

Eq. 4.25 suggests that, for advection problems involving constant flow and uniform grids, a pseudo-numerical solution may be obtained by convolution of the exact solution with the known response function of the numerical algorithm. This will be put to rather useful use in the next sections.

#### 4.2.3.2.2. Characteristics of errors per time step

Particular forms of the formula describing the errors per time step of the BMC were derived for each of the considered interpolation schemes with linear core elements (except 2P-HI2), and are presented in Table 4.3. Figs. 4.2, 4.3 and 4.4 show the amplifying factors, the phases errors and the celerity ratios, respectively, as a function of both  $\alpha$  and  $L_m/\Delta x$ ; Fig. 4.5 shows statistics with regard to  $\alpha$  of the amplitude errors, as a function of  $L_m/\Delta x$ .

Amplitude errors depend only on  $L_m/\Delta x$  (a measure of the grid refinement), and on  $\alpha$  (the location of the foot of the characteristic line inside the core element). In particular, no direct dependence exists on the integer part of the Courant number, which indicates a very weak dependence on  $\Delta t$  for  $\beta > 1$ . This constitutes a major advantage of ELM, because large time steps can be taken without compromising stability (as we would do with explicit EM) or accuracy (as we would do with implicit EM).

Typically, amplifying factors converge to 1 (i.e. to the condition of no amplitude error) as  $L_m/\Delta x \rightarrow \infty$ . This is easily shown by taking

$$\begin{aligned} \lim_{L_m/\Delta x \rightarrow \infty} &= \lim_{\lambda_m \rightarrow 0} \left\{ \exp(i\lambda_m) \cdot \sum_{p=P}^{P+Q} \phi_p(\alpha) \exp(ip\lambda_m) \right\} = \\ &= \sum_{p=P}^{P+Q} \phi_p(\alpha) \end{aligned} \quad (4.26)$$

and recognizing that, for interpolation schemes that fit exactly constant functions, we have (see section 4.2.2),

$$\sum_{p=0}^{P-1} \phi_p(\alpha) = 1 \quad (4.27)$$

All considered schemes, but the 6P-PL2 (because of indulged round-off errors), obey this trivial condition, and, therefore, propagate the zero-frequency exactly. We note, in passing, that phase errors make no sense for the zero-frequency Fourier component, which is consistent with Eq. 4.26 (note that  $\phi_p$  are real functions).

The way the amplifying factor converges to 1 is of strong significance for the accuracy of the numerical solution; in general, a fast, monotonical, convergence, starting from values below 1, is desirable.

Examination of Figs. 4.2 and 4.3 suggests that convergence is monotonical, from values below 1, for all considered schemes but the 6P-PL2 and the 8P-PL2. For these two schemes, amplifying factors above 1 occur for some combinations of  $\alpha$ ,  $L_m/\Delta x$ , suggesting possible instability (see section 4.2.5.2).

For  $\alpha=0$  and  $\alpha=1$ , amplifying factors equal unity regardless of  $L_m/\Delta x$  (except for the 6P-PL2, because of unnecessary inconsistency), in a direct consequence of the fact that interpolation is exact at the grid nodes. The practical usefulness of this singularity is unfortunately small, because flows of interest are most often non-uniform, and, therefore, associating integer  $\alpha$  to all characteristic lines is not feasible. An interesting exception is the case of flows of the form  $u(y,z)$ , for which grids may be set up in such a way that  $\alpha$  is always an integer.

For intermediate values of  $\alpha$ , and fixed  $L_m/\Delta x$ , amplitude errors are typically symmetrical relative to  $\alpha=0.5$  (the 6P-PL2 is again an unnecessary exception), where they have maxima. The dependence of the amplifying factors on  $\alpha$ , although decreasing as  $L_m/\Delta x$  increases, is significant over a range of dimensionless wavelengths that are most often important for the solution of practical problems; in non-uniform flows and/or grids this may be in the origin of aliasing, as it shall be discussed later.

Like amplitude errors, phase errors per time step depend only on  $L_m/\Delta x$  and on  $\alpha$ . This implies, in particular, that the artificial celerity ratio decreases as  $\text{int}(\beta)$  increases (Fig. 4.4), and indicates that, for the same total time, the BMC will be more accurate (less dispersive) for a smaller than for a larger number of time steps.

Phase errors (and, as a consequence artificial celerity ratios) vanish as  $L_m/\Delta x \rightarrow \infty$  (see earlier discussion based on Eq. 4.26). Convergence form and rate are scheme dependent (e.g. Fig. 4.3(a)-(g)). As a rule, convergence is monotonical for LI and LR schemes, and non-monotonical for HL and PL schemes.

Phase errors are null for  $\alpha=0$ , 0.5 and 1, and are anti-

symmetrical relative to  $\alpha=0.5$  (with the usual exception of the 6P-PL2). Similarly to what happens with amplifying factors, the dependence of phase errors on  $\alpha$  decreases as  $L_m/\Delta x$  increases, but is significant over a range of wavelengths that may be non-negligible for practical applications.

#### 4.2.3.2.3. Characteristics of errors after N time steps

For schemes with linear core elements, as the ones under analysis, errors repeat time step after time step, and therefore, the qualitative discussion in the previous section directly extends to errors after N time steps.

This section provides a complementary quantitative illustration of the range of dimensionless wavelengths that are affected by amplitude errors as t increases.

Figs. 4.6 through 4.8 show profiles of the amplifying factor as a function of  $L_m/\Delta x$  (in an extended range, relative to Fig. 4.2), after 10, 100, 1000 and 10000 time steps, for selected constant  $\alpha$  (0.5, 0.25 and 0.625). We note, in particular, that:

- the 2P-LI2 is extremely damping, significantly affecting dimensionless wavelengths over 70 for N in the common range of 100 to 1000; this should be considered a very strong argument against using linear interpolations;

- for  $\alpha$  close to 0 or 1, the amplification factors for the 8P-PL2 blow up, when N gets large, for a progressively large (but bounded) range of  $L_m/\Delta x$ ; although this is an indication of potential instability, the effect is rather localized (recall Fig. 4.2), and should not lead to actual instability in most practical applications involving non-uniform or unsteady flows or irregular grids (i.e., a variety of  $\alpha$ 's)

- the 6P-PL2, with the interpolating coefficients computed by KOMATSU et al. 1984, blows up for a wide range of wavelengths as N increases; the elimination of unnecessary roundoff errors in the calculation of these coefficients would lead to a behavior similar to that described for the 8P-PL2 (although less performing); we note that tests reported by Komatsu and co-workers have been for time steps up to 100, i.e. in a range of N for which the deficiencies of the technique are not yet apparent.

- HL and LR schemes are typically well-behaved, with degrees of damping that are consistent with the order of their interpolation polynomials.

Fig. 4.9 provides brief insight on how time-varying  $\alpha$  (e.g. as a consequence of a uniform but unsteady carrying flow) may affect accuracy. Indeed, the  $|G_m|$  versus  $L_m/\Delta x$  profiles presented in this figure (for N=100, 1000 and 10000) correspond to sequences of  $\alpha$  that were randomly generated (uniform probability of occurrence of  $\alpha$ 's between 0 and 1). Results mask localized bad behaviors, and illustrate "average" performance. We note, in particular, that the 8P-PL2 shows no signs of instability, while the 6P-PL2 keeps showing strong deficiencies.

#### 4.2.3.3. Interpolation schemes with quadratic or higher order core elements.

##### 4.2.3.3.1. Theoretical framework

We consider now the BMC general algorithm for interpolation schemes with quadratic core elements

$$f(j,n) = \sum_{p=P}^{P+Q} \phi_p(\alpha) \cdot f(j-K+p, n-1) \quad (4.28)$$

where, again,  $f$  is the unknown,  $\phi_p$  are real interpolation functions,  $\alpha = \beta - k$  is the location of the foot of the characteristic line within the core element,  $k$  denotes the reference node of the core element, and  $p=P, P+1, \dots, P+Q$  are the nodes that provide information for the interpolation. We note, however, that  $k$  is now different for odd and for even nodes; indeed,

$$k = \begin{cases} \text{int}(\beta) + 1 & \text{if } \text{int}(\beta) \text{ even} \\ \text{int}(\beta) & \text{if } \text{int}(\beta) \text{ odd} \end{cases} \quad (4.29)$$

Hence, solving Eq. 4.18 through the algorithm of Eq. 4.28, between  $n-1$  and  $n$ , and taking Eq. 4.14 - written for  $n-1$  - as initial condition, leads to

$$\zeta_m(j,n) = G_m(\alpha, j) C_m(j, n) \quad (4.30)$$

with

$$G_m(\alpha, j) = \exp(i\lambda_m \alpha) \sum_{p=P}^{P+Q} \phi_p(\alpha) \exp(i\lambda_m p) \quad (4.31)$$

where the error introduced to the  $m$ th Fourier component is now a function of both  $\alpha$  and the type (odd or even) of the starting node  $j$ .

Loosely speaking, the first step of the numerical solution gives rise to two 'families' of Fourier components (one defined over odd nodes and the other over even nodes), each with specific propagation characteristics. The actual Fourier representation of the numerical solution does not coincide with any of these families, but represents their combination. We note that such combination necessarily implies energy exchange between Fourier components, and, therefore, depends on the specific problem under analysis.

The amplitude and phase errors for each of the "odd" and "even" modes of an original individual Fourier component are independent of the other Fourier components, both at the first time step and at later times. Therefore, propagation of each of these modes is independent of the specific problem under analysis.

However, the "odd" and "even" modes interact with each other in their propagation; therefore, amplitude and phase errors change in each time step, and Eq. 4.21 does not apply any more. This

feature (apparently singular, although intuitive reasoning suggests that it may have an as yet unreported equivalence in other numerical methods) led to one of the most challenging specific problems of this research work.

The problem was to find a workable general expression for the propagation of amplitude and phase errors for BMC with quadratic core elements, that could be used to support a formal accuracy and stability analysis similar to that produced for the case of linear core elements.

The solution to this problem was derived by inductive reasoning and tedious algebraic work (BAPTISTA, unpublished notes). Selecting the 3P-LI3 as a reference, we took a corner node, at time  $n$ , and, through successive application of the reasoning that led to Eqs. 4.30-4.31, we explicitly found the errors that would have occurred in such node if the solution procedure had started at times  $n-1$ ,  $n-2$ ,  $n-3$ , ... (we note that to find the error at time  $n$ , in a corner node, for a solution started at time  $n-2$ , we need to know the errors at  $n-1$  for all corner and middle nodes that provide information for the step  $n-1$  to  $n$ ; and so forth). The procedure was then repeated for a middle node. Careful examination of the results showed that, although the error after  $N$  time steps could not be determined without the knowledge of the error after  $N-1$  time steps, a recurrence formula could be established. This formula was assumed to hold, with adjustments of some specific functions, to the other schemes based on quadratic core elements, and the assumption was checked by the same type of algebraic work (which provided also the specific functions required for each scheme). As a result, the following general propagation formulae were established:

$$H_m(N, a, j) = \left\{ p_m(N, a, j) G_m(a) + q_m(N, a, j) G_m(a+l) \right\} \cdot \exp(iN\alpha\lambda_m) \cdot \exp(ir\lambda_m) \quad (4.32)$$

with:

$$\begin{cases} p_m(N, a, j) = S_m(\alpha) \cdot p_m(N, a, j) \\ q_m(N, a, j) = Q_m(\alpha, j) \cdot p_m(N-1, a, j) + \bar{Q}_m(\alpha+l, j) q_m(N-1, a, j) \end{cases} \quad (4.33)$$

$$\begin{cases} p_m(1, a, j) = 1 - |r| \\ q_m(1, a, j) = |r| \end{cases} \quad (4.34)$$

$$s = \begin{cases} -1 & \text{if } \text{int}(\beta) \text{ odd} \\ +1 & \text{if } \text{int}(\beta) \text{ even} \end{cases} \quad (4.35)$$

$$r = \begin{cases} 0 & \text{for corner nodes} \\ s & \text{for middle nodes} \end{cases} \quad (4.36)$$

where  $G_m(\alpha)$ ,  $S_m(\alpha)$ ,  $Q_m(\alpha, j)$  depend on the specific interpolation scheme (see Tables 4.3 and 4.4). We note that  $j$  is relevant only to distinguish corner from middle nodes.

The full numerical solution can now be described in terms of a complex Fourier series as

$$c_m(j, n) = \sum_{m=-q}^q a_m \exp \{ i \lambda_m (j - n \beta) \} \quad (4.37)$$

where the coefficients  $a_m$  have to be obtained by Fourier analysis of the function

$$F(j, n) = \begin{cases} \sum_{m=-q}^q H_m(N, \alpha, 1) \cdot c_m(j, n) & \text{for corner nodes} \\ \sum_{m=-q}^q H_m(N, \alpha, 2) \cdot c_m(j, n) & \text{for middle nodes} \end{cases} \quad (4.38)$$

Eq. 4.38 provides, by itself, a useful way to cheaply simulate, at grid nodes, the numerical solution of simple test problems, as demonstrated in latter sections.

Eq. 4.37 is, however, interesting to stress the fact that, unlike its "odd" and "even" families of Fourier components, the full numerical solution inherently suffers from aliasing.

#### 4.2.3.3.2. Characteristics of errors in the first time step

As in section 4.2.3.2.2., particular forms of the formula describing the errors in the first time step were derived, now for BMC based on interpolation schemes with quadratic core elements, and are presented in Table 4.3. Figs. 4.2, 4.3 and 4.4 show, also for these schemes, the amplifying factors, the phase errors and the celerity ratios, respectively, as a function of both  $\alpha$  and  $L_m/\Delta x$ ; and Fig. 4.5 shows statistics with regard to  $\alpha$  of the amplitude errors, as a function of  $L_m/\Delta x$  (this figure also display results for the 4P-LI4, based on a cubic core element).

The discussion of section 4.2.3.2.2. on the general dependence of amplitude and phase errors on  $\alpha$  and on  $L_m/\Delta x$  remains valid. However, we note that, now, errors vanish identically (i.e. for



all  $L_m/\Delta x$ ) at  $\alpha = -1, 0,$  and  $1$  (i.e., at the new locations of the nodes, in local coordinates), and symmetry (for amplitudes) and anti-symmetry (for phases) is defined relative to the axis  $\alpha = 0$ .

As for the properties associated to specific schemes, we note that:

- LI and LR schemes show amplifying factors below 1, for all  $L_m/\Delta x$ .
- HL schemes show wide zones of  $\alpha$  and  $L_m/\Delta x$  where amplifying factors are above 1.
- The 7P-HL3 has a singular behavior at  $\alpha = 0$ , where amplitude errors are not null; this is a direct consequence of the fact that the interpolation scheme is not exact for the middle node, and will later be shown to affect the convergence of the method.
- The 4P-LI4 leads to a very significant amplification of short wavelengths, clearly suggesting strong instability (this, and other unpromising preliminary results - e.g. BAPTISTA et al. 1985 - have determined a minor concern towards this scheme throughout this work).

#### 4.2.3.3.3. Characteristics of errors after N time steps

For schemes with quadratic core elements, errors are not the same in successive time steps, and corner and middle nodes have errors that propagate differently. Fig. 4.10, which plots amplitude errors per time step as a function of the number of time steps (for a fixed value of the Courant number,  $Cu=0.24$ ), clearly illustrates the previous point. This figure further suggests that, except in the close vicinity of  $L_m/\Delta x=4$  (where some sort of resonance occurs), both families of amplifying factors converge, and converge to the same limit; this limit will, in particular, dictate the stability and long-term accuracy of the scheme; phase errors exhibit a similar behavior.

As a (empirical) rule, schemes for which amplification of Fourier modes does not occur in the first time step, will have a limiting behavior also without amplifications. Schemes that exhibit amplification for some range of  $\alpha$  and  $L_m/\Delta x$  will also be amplificative in the limit (although not necessarily for the same range of  $\alpha$  and  $L_m/\Delta x$ ).

Figs. 4.6 through 4.8 show profiles of the amplifying factor (for corner nodes) as a function of  $L_m/\Delta x$ , after 10, 100, 1000 and 10000 time steps, for selected constant values of  $\alpha$  (0.5, 0.25 and 0.625). We note, in particular, that, while LR schemes exhibit no amplification, HL schemes do amplify Fourier modes over a large range of  $L_m/\Delta x$ , for some  $\alpha$ 's. Both types of schemes keep dissipation restricted to a relatively narrow range of short wavelengths, even when N gets very large.

Fig. 4.9 shows similar profiles for sequences of 100, 1000 and 10000 randomly generated  $\alpha$ 's. The amplification of Fourier modes is masked for the case of the 7P-HL3, but not for the case of the

SP-HL3.

#### 4.2.4. Global accuracy

##### 4.2.4.1. General remarks

In the following sections we integrate the findings of the earlier formal analysis in a discussion of global accuracy, based on numerical experimentation.

To define and analyze the numerical experiments, we will take loose advantage of the reference problems and the accuracy measures described in Appendix A, that were proposed for a forum on the solution of the advection-dominated transport equation (Convection-Diffusion Forum), held during the VI International Conference on Finite Elements in Water Resources (LNEC, June 1-5, 1986).

The problem of the advection of a source (often a Gauss-hill) in an uniform flow and grid will be retained as a basis for the discussion, which will concentrate on the following key aspects

- mass preservation
- numerical dissipation and dispersion
- dependence of global accuracy on controlling parameters

We should note that several of the results presented in the next sections as "numerical solutions" were actually simulated through the application of Eqs. 4.25 or 4.38, as appropriate. This procedure was found to be virtually exact for the Gauss-hill problem (BAPTISTA et al. 1986) and, specially for large  $N$ , reduces CPU costs very significantly (runs are essentially "free" for schemes with linear core elements, regardless of  $N$ , and are at least ten times faster than actual numerical computations for the case of quadratic core elements). It should be emphasized, however, that the procedure is only valid when an accurate Fourier representation of the exact solution is possible (which, for instance, excludes the problem of an advancing front, due to the Gibbs phenomenon).

##### 4.2.4.2. Mass preservation

Mass is a quantity of extreme importance in most engineering problems requiring the solution of the transport equation (e.g., pollutant transport in natural waters). Even so, numerical methods often do not preserve mass.

Previous formal analysis of the propagation of the zero-frequency component and of aliasing provide interesting insight into this question.

While all Fourier components are associated to some energy, mass is, because of the periodic nature of the other components, all concentrated in the zero-frequency.

For consistent numerical methods, mass preservation (unlike accuracy in general) seems to depend only on aliasing. Indeed, if no aliasing occurs, the zero-frequency component is exactly propagated (see section 4.2.3.2.2, Eq.4.26), and, therefore, mass should be exactly preserved. If aliasing does occur, though, the zero-frequency component is disturbed in a more or less significant way, and mass is artificially lost or gained.

As an illustration, we consider the reference problem of uniform advection of a Gauss-hill in an uniform grid, where (except for marginal boundary effects) no causes of aliasing extraneous to the numerical algorithm are present. Mass should be exactly preserved in BMC solutions involving interpolation schemes with linear core elements (which are inherently non-aliasing), but some artificial loss or gain of mass should occur when schemes with quadratic or higher order core elements (which are inherently aliasing) are used.

Table 4.5 summarizes error measures (including the mass preservation indicator  $\mu_0$ ) for BMC solutions of this problem, for different  $\Delta_0$  and  $N$  (problems 1A, 1D, 1E, 1K and 1L of the Convection-Diffusion Forum). Results agree with the previous discussion.

All schemes with linear core elements, except the 6P-PL2, preserve mass exactly, even if other accuracy measures indicate rather different global performances. The exception of the 6P-PL2 (which systematically gains mass) simply recalls the fact that, as defined, this scheme is not consistent (section 4.2.2) and does not correctly propagate the zero-frequency.

For schemes with quadratic core elements mass is not exactly preserved, but errors are typically kept small, and can be reduced by increasing the dimensionless wavelength of the dominant Fourier components or (much less effectively) by decreasing  $N$ .

For more complex problems, involving non-uniform flows and/or grids, no interpolation scheme should inherently ensure mass preservation, because aliasing will always occur. Mass preservation can only be achieved by reducing aliasing, which will typically imply refining the grid. This issue will be retaken in section 4.3.3.

#### 4.2.4.3. Numerical dissipation and dispersion

The concepts of numerical dissipation (or numerical damping), numerical dispersion, and numerical diffusion are widely used (and not seldom misused) in the literature.

Numerical dissipation or damping, a concept very much associated to amplitude errors of Fourier components, refers to the loss (or, less appropriately, to the gain, for unstable methods) of the energy of a numerical solution. It shows up in the reduction of peaks and consequent smearing (for the sake of mass preservation) of concentration profiles.

Numerical dispersion refers to the effect of differential phase errors of the various Fourier modes of the solution, and shows up in the form of parasitic spatial oscillations, known as wiggles.

Numerical dispersion is too often mistakenly used in the sense of numerical diffusion, which is in itself a misleading concept. Indeed, numerical diffusion refers to the smearing of the numerical solution by an artificial diffusion-like truncation error; however, the term numerical diffusion has been used even for methods that produce smearing without involving second derivatives ("diffusion terms") in their truncation terms.

In this work, we will associate artificial smearing of numerical solutions with numerical dissipation, and use numerical diffusion only when such smearing is due to a diffusion-like truncation error.

Several numerical experiments, based on the reference problem of uniform advection of a Gauss-hill, were performed to assess the numerical dissipation and numerical dispersion of the BMC, for the alternative interpolation schemes under analysis. Results are partially reported in Figs. 4.11 through 4.26.

Examination of Fig. 4.11 (which shows, for different interpolation schemes, the actual numerical solution and numerical solutions from which either amplitude errors or phase errors were eliminated) suggests that amplitude errors typically play a more important role in most BMC than phase errors, and, indeed, act as a controlling factor for numerical dispersion.

The actual amount and the relative role of numerical dissipation and dispersion introduced by the BMC is strongly dependent on the selected interpolation scheme.

The 2P-LI2 is by far the most dissipative scheme, which is certainly associated to the fact that it introduces an actual numerical diffusion (Tables 4.1 and 4.2). As a consequence, this scheme is virtually free of numerical dispersion, although significant phase errors are present (Fig. 4.11).

Even if much less dissipative than the 2P-LI2, the 2P-HI2 exhibits almost no numerical dispersion, in a clear suggestion that the use of derivatives as additional dependent variables effectively reduces phase errors.

All the remaining schemes exhibit both numerical dissipation and numerical dispersion, in variable but non-negligible degrees. It is interesting to note that the PL and the 5P-HL3 schemes show less numerical dissipation than the 2P-HI2. This is apparently contra-natura, as the former schemes are approximations of the latter. The explanation is found by recalling (section 4.2.3) that the former schemes amplify certain Fourier modes, which partially compensates for the dissipation of other Fourier modes, and leads to an apparently better (but uncontrolled) accuracy.

#### 4.2.4.4. Dependence of the global accuracy on controlling parameters

As expected from the formal analysis of section 4.2.3, accuracy strongly depends on  $N$ , on  $\bar{C}_0/\Delta x$  and, for  $\beta < 1$ , on  $\alpha$ . The former two parameters provide forms of actually controlling numerical accuracy, not only for the simple test problem under analysis, but also for more practical problems.

Comparative examination of Figs. 4.12 and 4.24 through 4.26 illustrates the dependence on  $N$ , while Table 4.5 (problems 1A, 1K and 1L) provides complementary quantitative information. For a fixed total time, reducing  $N$  as to increase the integer part of the Courant number leads to improved accuracy; this improvement, which is often quite striking, results from the substantial reduction of the number of times where (similar) interpolation errors are introduced. For Courant numbers below 1, reducing  $N$  may or may not improve accuracy (e.g., see Table 4.5, and compare the mean square error norm,  $\phi$ , for problems 1A and 1L), because, in this range, errors per time step strongly depend on the Courant number itself.

The dependence of accuracy on the source size (expressed in this case through  $\bar{C}_0/\Delta x$ ) is illustrated by Table 4.5 (problems 1A, 1D and 1E), and by comparison of groups of figures showing concentration profiles for problems where all parameters but  $\bar{C}_0/\Delta x$  were kept constant (e.g. Figs. 4.12 to 4.14; Figs. 4.15 to 4.17; Figs. 4.18 to 4.20; Figs. 4.21 to 4.23). Accuracy is clearly improved by increasing  $\bar{C}_0/\Delta x$ , which is an immediate consequence of the fact that the importance of short dimensionless wavelengths (those that are more affected by amplitude and phase errors) is reduced.

Increasing the dimensionless wavelength of the dominant (or simply non-negligible for accuracy) Fourier components of any given problem should, in fact, be a priority concern for modellers. The cleanest way of doing this is to refine the computational grid "enough"; the problem is that "enough" is often "too much" for practical purposes. Figures in section 4.2.3 (showing the dependence of amplitude and phase errors on  $L/\Delta x$ , for different interpolation schemes) provide guidance on acceptable ranges of dominant wavelengths, and should assist, when necessary, in the set-up of complementary procedures to grid refinement.

For problems involving single or sequential instantaneous releases of mass, both the shape and the size of the source contribute to the Fourier representation of the problem (which is also constrained, in the long wavelength range, by the size of the computational domain); this is clearly illustrated by Table 4.6, which displays the amplitudes of the Fourier components that correspond to different types (Gauss-hill and triangle-hill) and sizes of sources. In problems where the exact shape of the source is not meaningful, choosing smooth shapes (e.g., the Gauss-hill) is naturally recommended (see Chapter 6 for the discussion of this issue in the context of a practical problem).

## 4.2.5. Consistency, stability and convergence

### 4.2.5.1. General remarks

Consistency, stability and convergence are important features for a numerical method.

Consistency requires the numerical algorithm to approach the original PDE (or, equivalently, the truncation error to approach 0) as  $\Delta x, \Delta t \rightarrow 0$ . The BMC was shown in section 4.2.2 to be unconditionally consistent for all interpolation schemes, except the 4P-LI4 (conditionally consistent) and the 6P-PL2 (unconditionally inconsistent, because of non-fundamental reasons).

Convergence (discussed for BMC in section 4.2.5.3) requires that an arbitrarily accurate approximation to the exact solution be obtained by appropriately refining the grid, i.e., that suitable error norms defined for any node of the numerical grid vanish as  $\Delta x, \Delta t \rightarrow 0$ .

Stability (discussed for BMC in section 4.2.5.2) refers to the unstable growth or stable decay of errors in the arithmetic operations needed to actually apply the numerical algorithm.

Consistency, stability and convergence may be related by Lax equivalence theorem, which states that, for a consistent numerical scheme, stability is a necessary and sufficient condition for convergence, for a linear system of equations (Lax theorem was originally established for parabolic equations and finite-difference schemes, but has been assumed to have wider application; ROACHE 1976 discusses the extension of this theorem).

### 4.2.5.2. Stability

The amplitude errors after  $N$  equal or randomly generated time steps, presented in Figs. 4.6 through 4.9, for alternative interpolation schemes, provide (together with the general discussion of section 4.2.3) conceptual support for the analysis of the stability of the BMC.

Clearly, stability depends on the selected interpolation scheme. Schemes for which the amplifying factors in the first time step are at most unity, for all  $\alpha$  and  $L_m/\Delta x$ , are unconditionally stable; this is the case of the 2P-LI2, 3P-LI3, 4P-LR2, 4P-HL2, 5P-LR3, 6P-LR2 and 8P-LR2. On the contrary, schemes for which the amplifying factors in the first time step exceed unity for some range of  $\alpha$ ,  $L_m/\Delta x$ , are, at the best, conditionally stable; this is the case of the 5P-HL3, 6P-PL2, 7P-HL3 and 8P-PL2.

Whether these latter schemes will or will not blow-up the solution of a given problem depends on several factors, which include the number of time steps actually used, the dominant dimensionless wavelengths of the problem, the predominant  $\alpha$ , and the presence or absence of aliasing.

For instance, Fig. 4.15 through 4.16 show that, for the reference problem of the uniform advection of a Gauss-hill in an uniform grid, only the 7P-HL3 blows up the solution, when 1000 time steps are taken to reach a total time of 9600 ( $u=0.5$ ). Explanation lies on the small value of  $\alpha$ , which corresponds to a more critical zone for stability for the 7P-HL3, than for the other schemes (Fig. 4.2). However, examination of Figs. 4.6 through 4.9 suggests that we could also easily set-up problems which solution would blow-up while using the 5P-HL3, 6P-PL2 and the 8P-PL2.

General practical stability criteria seem (given the variety of relevant parameters, and the fact that they often can not be controlled in complex problems), a hopeless task for these schemes, which use will therefore involve a risk for high N.

Based on Figs. 4.2 and 4.6 through 4.9, we roughly estimate that solutions using the 5P-HL3, 6P-PL2, 7P-HL3 and 8P-PL2 may start blowing up for N in the order of 1000, 10000, 100 and 10000; however, the accuracy of each of these schemes may deteriorate much sooner, specially in the case of complex flows and grids (see also section 4.3).

#### 4.2.5.3. Convergence

As discussed in earlier sections, the accuracy of BMC solutions of the advection equation improves by taking large time steps (Courant number above 1). This rather unusual behavior has been both celebrated as a practical advantage with regard to computational cost (e.g., BAPTISTA 1984), and feared as an indication of the divergence of the method as  $\Delta t \rightarrow 0$  (e.g., NEUMAN 1984).

Although Lax equivalence theorem suggests that the BMC is convergent for most interpolation schemes (e.g., 2P-LI2, 3P-LI3, 4P-HL2, 4P-LR2, 5P-LR3, 6P-LR2, 8P-LR2, which we showed to be both consistent and stable), further analysis is deemed appropriate in this area.

To support such analysis, we set-up a numerical experiment, involving the solution of a same problem of constant advection of a Gauss-hill, for different interpolation schemes and nodal spacings, and for different combinations of N,  $\Delta t$  (but with  $T=N*\Delta t$  kept fixed).

The mean square error norms for the different runs were taken as representative of the global accuracy, and plotted against N (Figs. 4.27 and 4.28 - we note that straight lines were used to link computed points only to simplify visualization; no functional dependence is implied). If we discard singular points near integer Cu (see earlier discussion on the behavior of the BMC for integer Cu in section 3.2.4), results show a tendency for BMC solutions to:

- improve their accuracy as N decreases, over an initial range of N (say, up to N around 1000);

- Keep an essentially constant accuracy, function of the adopted space discretization, for larger values of N.

The 7P-HL3 (plots not shown) constitutes an exception, with the the mean square error norm growing without bound; this is consistent with our discussion of the stability for the 7P-HL3 scheme, for  $\alpha$  near 0.

Further insight into the behavior just described for "typical" BMC is obtained by examination of the truncation errors of the Taylor series expansion of BMC algorithms.

We take as a reference the case of the 3P-LI3 scheme, for which the truncation error per time step is given by

$$\epsilon = (\alpha^3 - \alpha) \frac{\Delta x^3}{6} \frac{\partial^3 c}{\partial x^3} + \dots \quad (4.39)$$

or, in the particular case of  $\beta \leq 1$ , i.e.  $\alpha = \beta$ , by

$$\epsilon = \frac{1}{6} (v^3 \Delta t^3 - v \Delta x^2 \Delta t) \frac{\partial^3 c}{\partial x^3} + \dots \quad (4.40)$$

In the range of "small" N, such that  $\beta \gg 1$ ,  $\alpha$  is very weakly dependent on  $\Delta t$  (Eq.4.39), and essentially the same error is introduced per time step, regardless of  $\Delta t$ . Hence, decreasing N will, in this range, improve accuracy, simply because it corresponds to reducing the number of times where very similar errors are introduced.

However, when N becomes large enough so as to  $\beta \leq 1$ ,  $\alpha$  becomes a direct function of  $\Delta t$  ( $\alpha = v \Delta t / \Delta x$ ), and the truncation error per time step varies (Eq.4.40), to the leading order, as  $\Delta t$ , i.e., N-1. The total truncation error, after N time steps, is then, to the leading order, independent of the actual choice of N,  $\Delta t$ , being rather, for any given problem, a function of the adopted space discretization. Increasing or decreasing N, in this range, will have just a minor effect on accuracy.

To complete the analysis of convergence, we need now to examine the accuracy behavior as  $\Delta x \rightarrow 0$ . Figs. 4.29 and 4.30 illustrate such behavior for the reference problem under analysis. In a rather conventional way, the mean square error monotonically decreases as  $\Delta x$  decreases; an exception is the 6P-PL2 which reaches a minimum around  $\Delta x = 100$  (a consequence of inconsistency).

Hence, we can conclude that the BMC is unconditionally convergent for most of the considered interpolation schemes, although errors



do not necessarily decrease as  $\Delta t \rightarrow 0$ . Exceptions are the 7P-HL3 (which blows up the numerical solution as  $\Delta t \rightarrow 0$ ) and the 6P-PL2 (which does not approach the exact solution as  $\Delta x \rightarrow 0$ , because of inconsistency).

### 4.3. EXTENSIONS TO NON-UNIFORM ONE-DIMENSIONAL GRIDS

#### 4.3.1. General remarks

The effect of non-uniform grids on the accuracy and stability of numerical methods for the solution of the transport equation is poorly understood. Yet, these grids are extensively used in engineering practice.

This constitutes the basic motivation for the following discussion, which briefly addresses:

- the extension of the definitions of selected interpolation schemes to the case of 1-D non-uniform grids;
- the error mechanisms inherently associated to these grids.

Schemes selected for this discussion were the 3P-LI3 (our standard scheme), and the 5P-HL3 (as a representative of schemes that, being unstable, are apparently accurate when tested for uniform flows and grids).

#### 4.3.2. Extension of the definition of the interpolation schemes

To extend to 1-D non-uniform grids the interpolation schemes considered in section 4.2, we map the zone involving all nodes contributing to the interpolation into local coordinates, where we apply the same concepts that were used for the scheme generation in uniform grids. The mapping is based on the isoparametric transformation of the core element, all the remaining nodes being mapped according to such transformation.

Table 4.7 recalls standard isoparametric mappings for 1-D elements of up to 4 nodes, while Table 4.8 presents an improved isoparametric mapping for three-nodes 1-D elements, proposed by CELIA AND GRAY 1984. These two types of mapping will be compared in the next section, for the case of quadratic core elements.

#### 4.3.3. Set-up of a numerical experiment and analysis of results

To provide a basis for discussion, we defined a numerical experiment consisting in the solution of the reference problem of uniform advection of a Gauss-hill, for five different types of irregular grids. In all cases, grids were defined by 69 nodes in the interval  $x \in [0, 13600]$ , as follows:

Grids of type 1:

$$\begin{cases} x_i = x_{i-1} + \Delta x_b & \text{if } i \text{ odd} \\ x_i = x_{i-1} + \Delta x_a & \text{if } i \text{ even} \end{cases} \quad (4.41)$$

with  $\Delta x_b / \Delta x_a = S > 1$ ;  $x_1 = 0$

Grids of type 2:

$$\begin{cases} x_i = x_{i-1} + \Delta x_b & \text{if } i \geq (N_T - 1)/2 \\ x_i = x_{i-1} + \Delta x_a & \text{if } i < (N_T - 1)/2 \end{cases} \quad (4.42)$$

with  $\Delta x_b / \Delta x_a = S > 1$ ;  $x_1 = 0$ ;  $N_T = \text{number of nodes}$

Grids of type 3:

$$\begin{cases} x_i = x_{i-1} + s(x_{i-1} - x_{i-2}) \\ \text{with } x_1 = 0 \end{cases} \quad (4.43)$$

Grids of type 4:

$$\begin{cases} x_i - x_{i-1} = \Delta x_b & \text{in even elements} \\ x_i - x_{i-1} = \Delta x_a & \text{in odd elements} \\ \Delta x_b / \Delta x_a = s > 1; x_1 = 0 \end{cases} \quad (4.44)$$

Grids of type 5:

$$\begin{cases} x_i = x_{i-1} + \Delta x_a & \text{if } i \text{ odd} \\ x_i = x_{i-1} + \Delta x_b & \text{if } i \text{ even} \\ \text{with } \Delta x_b / \Delta x_a = s > 1; x_1 = 0 \end{cases} \quad (4.45)$$

The controlling parameter for each grid type,  $s$  (we note that the other parameters were systematically adjusted as to fit the specified length and number of nodes, for the specified  $s$ ), was varied from 1 (regular grid) to 10 (extremely distorted grid); Fig 4.31 illustrates the aspect of the grids for some considered values of  $s$ . Results of the calculations are shown in Figs. 4.32 through 4.42, in the form of concentration profiles, and in Table 4.9, in the form of different accuracy measures. These measures were taken from Appendix A, with the single exception of the "energy" ratio

$$e = \frac{\int_{\Omega} [c^{nu}(\alpha, t)]^2 dx}{\int_{\Omega} [c^{er}(\alpha, t)]^2 dx} \quad (4.46)$$

which is newly proposed as a measure for the stability of numerical solutions (it should be less than one for stability).

Fig. 4.32 confirms, in a very clear way, the claim by CELIA and GRAY 1984 on the superiority of their improved isoparametric mapping over the standard isoparametric mapping.

All the other results were therefore generated with the improved mapping. They indicate that, in particular:

- The grid non-uniformity has a definite influence on the performance of the BMC, and, in particular, on phase errors and aliasing.

- Errors due to grid non-uniformity may either add to or compensate for errors that would occur in an uniform grid; however, except for small  $s$  (say up to 1.5-2), the general tendency is for the degradation of accuracy.

- Numerical dispersion tends to become uncontrolled as  $s$  increases, and, as a consequence, solutions become strongly distorted by wiggles; aliasing also tends to increase, which, in particular, leads typically to a much smaller (or, at least, much less controlled) ability to preserve mass. Both these effects

are more significant when shorter (case of  $\sigma_0=264$ ) rather than larger (case of  $\sigma_0=400$ ) dimensionless wavelengths are present in the solution.

- Examination of the energy ratio,  $e$ , reveals that while the 3P-L13 is a dissipative scheme for all considered grids, the 5P-HL3 is clearly unstable for several of the grid choices, while it is dissipative for others. In general, while the 5P-HL3 performs better for regular and quasi-regular grids, it often leads to numerical garbage for large values of  $s$ .

While it is recognized that the considered grids have, most often, a regularity pattern that may constrain the general validity of the above comments, we strongly recommend, as a practical rule, that in the set-up of numerical grids, ratios between the characteristic sizes of adjacent elements be kept as low as possible, and, preferably, below 1.5.

## 4.4. EXTENSION TO TWO DIMENSIONS

### 4.4.1. The case of straight orthogonal grids

Extension to 2-D of the definition of the interpolation schemes considered in earlier sections is conceptually trivial for the case of straight orthogonal grids: indeed, in this case, the 2-D interpolation is simply constructed by successive use of the 1-D interpolation along  $n$  grid lines (as many as nodes defining the 1-D scheme) in one direction, and one final use in the perpendicular direction. This is illustrated in Fig. 4.43, for the case of a scheme involving five nodes in one-dimension (e.g., 5P-LR3, 5P-HL3).

The 2-D interpolation becomes  $(n+1)$  times more expensive than the 1-D interpolation, which, although non-negligible, represents just a linear increase of cost.

The formal analysis of amplitude and phase errors of section 4.2.3 is also easily extended: 2-D amplitude errors are for these grids the product of 1-D amplitude errors in each of two reference normal directions, while 2-D phase errors are described by the vectorial sum of 1-D phase errors in each of the space directions.

To illustrate the performance of the BMC for this type of two-dimensional grids, we considered the rather conventional problem of a source in rigid-body rotation (we should note that this problem also first introduces in this work a non-uniform flow). Appendix A, prepared for the Convection-Diffusion Forum of the VI FEWR, describes the problem and sets specific test parameters (from which we elected to solve here the cases 3A and 3B, which differ one from the other only in the type of the source: a Gauss-hill and a Cone-hill, respectively).

A uniform grid, based on 9-nodes quadrangular elements, with the nodal spacings specified in Appendix A, was used for the calculations. Interpolation schemes selected for alternative use were the standard 3P-LI3, and the 5P-LR3 and 5P-HL3 (we note that, for the sake of simplicity, we keep in 2-D the terminology adopted in 1-D).

Results after a complete tour ( $N=30$ ) of the source, are displayed in Figs. 4.44 and 4.45, in the form of concentration profiles along two radial axis of the exact solution (one along the local direction of the flow, and the other normal to it).

The following comments apply:

- The general accuracy of the BMC is, for all schemes, satisfactory; damping is low to moderate (typical peak reductions below 10-15%, except for the 3P-LI3), negative concentrations stay (typically well) below 5%, and introduced asymmetries are minor.

- The 5P-HL3 provides overall best results (even if, as discussed for the 1-D case, the accuracy of this scheme is somewhat fictitious, and due to the artificial amplification of some

Fourier modes - which implies the risk of instability), followed by the 5P-LR3 and the 3P-LI3.

- None of the considered schemes is able to preserve the sharpness of the Cone-hill, which becomes smoother near the corners; zones of negative concentrations are more important for the case of the Cone-hill than in the case of the Gauss-hill, in a natural consequence of the presence in the solution of smaller dimensionless wavelengths.

#### 4.4.2. The case of unstructured grids

Extension of the definitions of the considered interpolation schemes to 2-D unstructured grids (such as those of Figs. 6.3, 6.8 and 6.16) is made in a natural way only for the case of compact schemes (e.g., 2P-LI2, 3P-LI3).

Indeed, for compact schemes, there is no ambiguity as to the nodes that contribute to the interpolation (all nodes within the core element, and only those), and efficient and convenient normalized forms of the interpolation functions, written in local coordinates through appropriate mappings, can be used (e.g., Table 4.10). The choice of the shape of the element, of the actual number of its nodes, and of the type of elementary mapping (e.g., for quadratic elements, subparametric, standard isoparametric or improved isoparametric) has not been subject to systematic analysis in the context of the BMC; however, from our earlier 1-D analysis, the following should apply:

- Nine-nodes quadrangular elements (the direct equivalent to the 3P-LI3) are potentially those that lead to the best accuracy for the BMC. Four-nodes quadrangles (the direct equivalent to the 2P-LI2) and three-nodes triangles should be avoided, as they will introduce excessive damping. Six-nodes triangles and five to eight-nodes quadrangles provide intermediary accuracy, and should be used only if and when strictly necessary.

- If an isoparametric mapping is going to be used for quadratic elements, the improved mapping proposed by CELIA AND GRAY 1984, adapted to the selected type of elements, should be chosen. However, isoparametric mapping leads to a significant increase in the cost of the tracking scheme, specially (but not only) when curvilinear sides are involved, and subparametric mapping should be used as much as possible.

ELA, the transport model discussed in Chapter 6, uses six-nodes triangles (which was imposed by the companion circulation models TEA and TEANL), with subparametric mapping. BAPTISTA 1984 and, briefly, Chapter 6, discuss the accuracy of this approach.

Non-compact interpolation schemes are much harder to extend to two-dimensional unstructured grids. A first difficulty consists in identifying the grid nodes that will contribute to the interpolation; indeed, ambiguity can easily arise, as illustrated in Fig. 4.46, by means of the application of the 5P-LR3 scheme to a zone of one of the triangular grids used in Chapter 6.

This difficulty has to be overcome on a case-by-case basis, by the set-up of carefully designed grids, and constitutes a constraint to the use of non-compact schemes.

The second difficulty concerns efficient computation of the interpolated value. While for compact schemes normalized forms of the interpolation functions, applicable to all elements, could be used (keeping the computational effort at moderate levels), for non-compact schemes each element has to be dealt with individually, as no convenient general mapping between global and local coordinates can be established. Fig. 4.47 illustrates the point: using an isoparametric mapping for the core element, the local representation of the nodes involved in the interpolation is not any more general or easier to handle than the global representation.

The best approach is suggested to be performing the interpolation in global coordinates, by extension of the conceptual procedure in 1-D. For LR schemes, this involves the solution of a  $n \times n$  system of linear equations (e.g., see illustration in Fig. 4.48(a), for the 5P-LR3 scheme); for HL schemes, the solution of four slightly smaller systems, plus estimation of derivatives and average of results, will typically be required (e.g., see illustration in Fig. 4.48(b), for the 5P-HL3; note that a simpler procedure can be set for the 7P-HL3). PL schemes, because of their conceptual complexity, become unfeasible, in practice.

For both LR and HL schemes, a tradeoff between CPU and memory requirements has to be decided upon while developing the specific computer code. Also, one should be concerned with loss of accuracy due to irregular nodal spacing; section 4.3 provides only a first glance on error mechanisms that may become important.

#### 4.5 REMARKS ON THE SELECTION OF THE INTERPOLATION SCHEME

Taking as a reference the simplest interpolation scheme, 2P-LI2, which is very often unacceptably damping, we have considered improving the accuracy of the BMC by increasing the order or both the order and the class of the interpolation function.

To increase the order of the interpolation, we first used compact Lagrange polynomials, to find out that the quadratic interpolation, 3P-LI3, represents a potential best-choice within this class; indeed, higher-order interpolations (e.g. 4P-LI4) lead to very strong numerical dispersion and instability in the range of short wavelengths.

We then relaxed the constraint of compactness, and, keeping the core elements for interpolation linear or quadratic, resorted to progressively higher-order Lagrange polynomials (4P-LR2, 5P-LR3, 6P-LR2, 8P-LR2). Accuracy clearly increases with the order of the interpolation, but at the expense of additional cost and complexity (e.g. in the definition of the interpolation schemes in irregular grids, and in the handling of core elements adjacent to boundaries).

The use of compact Hermite polynomials had been explored by HOLLY and PREISSMAN 1977 and HOLLY and POLATERA 1984, who indicated that significant accuracy improvements can be achieved by this change of the class of the interpolation scheme (which our results, while non-systematic for this scheme, confirm). The problem is that derivatives are introduced as new dependent variables, increasing costs and forcing the set-up of unnatural boundary conditions.

In an attempt to keep the high accuracy of Hermite interpolations, while avoiding the need for derivatives as new dependent variables, HOLLY and KOMATSU 1984 and KOMATSU et al. 1984 explored the idea of estimating the derivatives based on information on concentrations from outside the core element for interpolation (6P-PL2, 8P-PL2); we kept this general idea to create a set of interpolation schemes simpler to use in a FE context, more robust (i.e. non-dependent on empirical optimization coefficients), and with the same type of accuracy properties (4P-HL2, 5P-HL3; also, the less robust 7P-HL3).

While accuracy for several simple test cases is apparently very good, our Fourier analysis reveals that HL and PL schemes amplify the amplitude of Fourier modes in some range of  $\omega$ ,  $L/\lambda$ ; the BMC becomes unstable, in a way difficult to control, and therefore, its use becomes unreliable (as revealed by the extension of the 5P-HL3 scheme for non-uniform grids. An exception is the 4P-HL2, which is, however, a relatively uninteresting scheme, due to a very close similitude with the accuracy of the conceptually simpler 4P-LR2). Being non-compact, PL and HL schemes share with LR schemes the complexity of the extension to unstructured grids (which they indeed aggravate) and of the handling of zones near boundaries.

A singular set of inconvenient characteristics (including formal



inconsistency, divergence as  $\Delta x \rightarrow 0$ , systematic mass gain, etc.) is associated specifically with one of these schemes, the 6P-PL2; unnecessary roundoff errors introduced by KOMATSU et al. 1984 in the evaluation of the interpolation coefficients (an easily solvable problem) is found to be the reason.

Given the above, it should be clear that no optimal scheme exists, and the choice among the different alternatives involves a often subjective tradeoff involving accuracy, convenience and cost.

Results reported in earlier sections should be helpful in guiding one such choice. Our reading of such information suggests that several of the considered schemes will not constitute, in general, attractive alternatives; namely

- the 2P-LI2, because it is excessively damping;
- the 4P-LI4, because it is unstable and highly dispersive;
- the 4P-HL2, because it has an accuracy very similar to that of the 4P-LR2, but involves significant additional conceptual complexity (which, in particular, translates in higher costs and less controlled accuracy for multi-dimensional unstructured grids);
- all the remaining HL and PL schemes, because of their instability;
- the 6P-LR2 and 8P-LR2, because of the excessive number of nodes involved, which, for multi-dimensions, will often pose conceptual problems (e.g., definition of the algorithm, choice of intervening nodes, and handling of zones near boundary conditions), and lead to unfeasible costs;

From the remaining schemes, we want to avoid the use of Hermite polynomials, as they would imply the introduction of derivatives as new dependent variables, both for diffusion and for advection. Our choice is, therefore, restricted to the 3P-LI3, 4P-LR2 and the 5P-LR3.

For a same grid, the 5P-LR3 is clearly the most accurate of these schemes (and is quite close to the accuracy of the 2P-HI2); the 4P-LR2 and the 3P-LI3 constitute progressively less accurate options. However, costs for each of these schemes will vary in the opposite way (see Table 4.13, for reference), and, depending on the specific problem, it may be cost-effective to use a more accurate scheme with a less refined grid, or, on the contrary, a less accurate scheme with a more refined grid.

It should be intuitive that harder problems, and more strict requirements on accuracy will make inherently more accurate schemes (e.g., the 5P-LR3) more attractive relative to less accurate ones (3P-LI3). Fig. 4.29 (which is relative to the 1-D advection of a Gauss-hill) can be used to illustrate the point.

We take as a reference solutions for both the 3P-LI3 and the 5P-LR3, and assume that  $\Delta x = 400$ ; the 5P-LR3 performs better, but reducing  $\Delta x$  to 200 (i.e, doubling the number of elements) for the

3P-LI3 alone, will even out accuracies. Now, we start out at  $\Delta x=40$  for both schemes (a much more refined solution); again the 5P-LR3 performs better; now, however, doubling the number of the elements used in the 3P-LI3 solution will be clearly insufficient to provide an accuracy comparable to that of the 5P-LR3 for  $\Delta x=40$  (much more elements would be required for that). As the ratio (5P-LR3 cost)/(3P-LI3 cost) has not increased (the opposite will typically happen, because the interpolation step is only a part - and, often, for actual problems, a relatively small part - of the total cost), the 5P-LR3 is now much more cost-effective than before.

We note that there is an essentially unexplored potential in the combination of compatible (i.e., sharing a common core element) interpolation schemes. While explicit mention has not been made to it, we used such combination to handle the problem of zones near boundaries, for non-compact schemes, in the numerical experiments of earlier sections (a compact scheme would be used in such zones); however, as discussed in Chapter 6, such combination may prove a general "optimal" procedure in a cost-effectiveness sense.



CHAPTER 5

GENERAL PROPERTIES OF EULERIAN-LAGRANGIAN METHODS



## 5.1. INTRODUCTION

In Chapter 4 we analyzed in detail the interpolation procedure associated with the solution of the advection equation, which had previously (section 3.5) been identified as critical for the accuracy of our reference ELM. In particular, we explored several highly performing interpolation schemes, which significantly improve our ability to solve the advection equation.

We now retake the full transport equation and briefly discuss general features of ELM solutions. Discussion is based on the 1-D case, and the solution of diffusion is obtained using the 1-D version of the Galerkin FEM described in section 3.3. FEM interpolation functions are either quadratic or linear Lagrange polynomials, as to allow consistency with the interpolation scheme adopted for advection; i.e., when the core element for the interpolation step in the advection solution is linear (quadratic), a FEM linear (quadratic) interpolation function is used.

The discussion concentrates first (section 5.2) on the dependence of accuracy on the relative importance of advection and diffusion. The motivation is two-folded: first, to compare, at the light of more performing interpolation schemes, errors introduced by the solution of advection and by the solution of diffusion; second, to reassess the relative merits of the alternative interpolation functions analysed in Chapter 4 for a (in principle) easier, but often more realistic problem.

Section 5.3, in turn, concentrates on the analysis of the optimal (in a cost-effectiveness sense) time step for ELM, an area that had earlier been identified as requiring further research (BAPTISTA 1984). While an ultimate goal is to reach a practically useful criterion for the selection of cost-efficient time steps, in this work we simply motivate, both conceptually and quantitatively, the issue.

## 5.2. DEPENDENCE OF ACCURACY ON THE RELATIVE IMPORTANCE OF ADVECTION AND DIFFUSION

Physical diffusion progressively transfers energy from short to long wavelengths. From section 4.2.3, it should be clear that, as a consequence, the solution of the advection part of the transport problem becomes progressively easier.

However, while for pure advection, errors come essentially from the interpolation step of the BMC, the solution of the full transport equation involves in addition splitting errors and errors in the solution of the diffusion equation.

Hence, although experience shows that physical diffusion typically makes the solution of the full transport equation easier, the argument can be made that problems involving a very high, but not infinite, Peclet number ( $u\Delta x/D$ ), are potentially harder to solve than purely advective ones (this was, indeed, a major point of debate in the Convection-Diffusion Forum held during the recent VI international Conference on Finite Elements in Water Resources - Lisbon, LNEC, June 1-5, 1986). Apparent strength is given to this general argument by the fact that the very accurate ELM/CP used by CADY and NEUMAN 1986 to solve the reference problems of the Forum effectively performed less well for the case involving the highest finite Peclet number ( $Pe=50$ ) than for pure advection.

On the other hand, if diffusion simplifies the solution of the transport equation in at least a wide range of Peclet numbers, the solution strategy for practical problems involving non-negligible physical diffusion should, for the sake of efficiency, be able to take advantage of this fact (e.g., by selecting cheaper interpolation schemes for the solution of advection).

With the previous aspects in mind, we solved a reference problem of advection-diffusion of a Gauss-hill in an uniform flow, for Peclet numbers ranging from small to infinity ( $Pe=2, 20, 200, \infty$ ), using four alternative interpolation schemes (3P-LI3, 5P-LR3, 5P-HL3 and 8P-PL2). Results are presented in Fig. 5.1, in the form of concentration profiles, and in Table 5.1, in the form of selected accuracy measures.

We observe a systematic improvement of accuracy (as represented by the mean square error,  $\phi$ , and its discrete equivalent,  $\phi_d$ ) as the Peclet number decreases; in particular, accuracy is better for the case of  $Pe=200$  (i.e., very high, but finite), than for the case of  $Pe=\infty$ . These conclusions apply to computations involving any of the considered interpolation schemes.

While, as suggested by Chapter 4, no general conclusions should be derived from non-systematic numerical experiments, results just presented support the idea that the reference ELM/C of Chapter 3 does improve accuracy when (even very small) diffusion is present; i.e. the limiting case of pure advection should be a worst-case condition. Hence, the behavior of the ELM/CP proposed by NEUMAN 1984, which seems to result from the adopted splitting procedure (NEUMAN and SOREK 1982), may be misleading as to "typical" ELM behavior.

A question mark remains, however, concerning early time steps of the numerical solution, for which damping due to physical diffusion is of little significance.

The actual choice of the interpolation scheme for advection becomes progressively less important as the Peclet number decreases, in a natural consequence of the physical damping of short wavelengths. The relative ranking of the considered interpolation schemes is not significantly changed with regard to pure advection problems, but the actual accuracy differences are substantially reduced as progressively higher dimensionless wavelengths dominate the exact solution (which is consistent with the analysis of Chapter 4).

In particular, for  $Pe=2$ , essentially no difference is found between the different schemes, each of them leading to virtually exact solutions. However, very often, practical applications are performed for  $Pe$  in much higher ranges (e.g, around  $Pe=20$ ), because of cost constraints on the spatial discretization. In this case, the differences between the performance of different interpolation schemes are significant, and the discussion of Chapter 4 on the choice of the most effective scheme should hold as a reference.



### 5.3. ON THE CHOICE OF THE TIME STEP

We now consider the problem of the selection of the time step,  $\Delta t$ , to be used for the solution of a given problem between times 0 and T.

For a conventional Eulerian method, and except for roundoff errors, both accuracy and cost increase monotonically as  $\Delta t$  decreases; hence, improving accuracy by refining the time discretization always implies an increase in cost.

For the reference ELM/C of Chapter 3 (and other ELM/C), though, the tradeoff between accuracy and cost is more complex, as suggested by BAPTISTA 1984: reducing  $\Delta t$ , while typically increasing the cost, may or may not lead simultaneously to improved accuracy. Indeed, reducing  $\Delta t$  will often reduce accuracy for pure advection problems (see Chapter 4), while (except for roundoff errors in the limit of small  $\Delta t$ ) it will increase accuracy for pure diffusion problems. For problems involving both advection and diffusion, optimal accuracy should therefore be achieved for some finite value of N, which will strongly depend on the relative importance of advection and diffusion (as quantified by the Peclet number).

To detail and provide quantitative support to the previous arguments, we solved again the reference test problem of the advection-diffusion of a Gauss-hill, for different Peclet numbers, different N (hence, different Courant numbers and Diffusion numbers ( $Di=u\Delta x/D$ )), and different interpolation schemes (3P-LI3, 5P-LR3, 5P-HL3, 8P-PL2). Figs. 5.2 through 5.5 graphically display the obtained concentration profiles, while the values of selected accuracy measures are presented in Tables 5.2 through 5.5 and in Fig. 5.6.

This latter figure, which shows the dependence of the discrete mean square error norm,  $\phi_0$ , on N, is particularly interesting for illustration of the optimal (in an accuracy sense) time step (Note: actually computed values of  $\phi_0$  are connected by straight lines only to facilitate visualization; no functional dependence should be assumed).

For each interpolation scheme, this optimal time step is seen to depend on Pe, and, while specific criteria can not be issued from this single experiment, the following comments loosely apply:

- For low Pe, the optimal time step will progressively decrease as the interpolation scheme for advection becomes more accurate. For instance, for Pe=2, optimal N is around 50 for the 3P-LI3 and around 500 for the 5P-LR3, while no minima is detected up to N=10000 for the 5P-HL3; the 8P-PL2 has, in this regard, an uncharacteristic behavior (optimal N around 50), which may be related to a strong effect of roundoff errors in the solution of the diffusion (we recall that linear interpolations are used for diffusion, in this case).

- For moderately high Pe (e.g. Pe=20), leading errors are clearly associated with the advection solution, and the optimal step will

always approach T.

In a practical view point, we are not so much interested in an optimal time step in the strict sense of accuracy, but rather in a cost-efficient time step that provides either best accuracy at a specified maximum cost, or minimum cost at a specified minimum accuracy.

For this, we need to define both an accuracy function (such as in Fig. 5.6) and a cost function. For simplicity, we will assume that such cost function is directly related to the CPU time (often a reasonable assumption).

The CPU time required, in a VAX 11-780, to solve the reference problem used in this section in a grid with 69 nodes and N varying from 10 to 10000, is shown in Table 5.6, for the different interpolation schemes and for the pure-advection, pure-diffusion and advection-diffusion cases.

Values in this table are strongly misleading with regard to the cost of the tracking step, because of the oversimplification of the tracking procedure in 1-D steady uniform flows. These values do suggest, though, that

- the costs of both the interpolation step and the solution of diffusion vary in an essentially linear way with the number of time steps required to reach a fixed final time;
- the cost of the interpolation step strongly depends on the adopted scheme; even in 1-D (ratios will aggravate in 2-D), the 8P-PL2 is about three times more expensive than the 3P-LI3;
- while the solution of diffusion is more expensive than the interpolation step for the 3P-LI3 (a ratio of little less than three), this tendency will tend to invert as more complex interpolation schemes are considered for advection.

According to our experience with ELA, the pollutant transport model for coastal waters described in Chapter 6, a realistic qualitative cost function for the 2-D reference ELM, while using a standard 3P-LI3, is characterized by (Fig. 5.7):

- an important background component, associated with the tracking step, and quasi-independent of N,  $\Delta t$  (it depends essentially on the total particle-tracking time);
- a often secondary but non-negligible component, associated with the solution of the diffusion equation, and varying in an approximately linear way with N;
- a typically minor component associated with the interpolation step, varying again in an approximately linear way with N.

The use of interpolation schemes both more accurate and more expensive than the 3P-LI3 will tend to increase the cost of the interpolation step, and to bring it closer to that of the diffusion solution. The cost of the solution of the full transport equation will grow faster with increasing N, making it even more attractive to take advantage of the ELM ability to

accomodate large time steps.

The qualitative combination of accuracy and cost functions (Fig. 5.8) suggests that:

- for high  $Pe$ , taking the largest  $\Delta t$  still compatible with the physics of the problem and with the needs for intercalar observation of the progression of the numerical solution, will very often correspond to a very cost-effective choice, close to both minimum cost and maximum accuracy;

- for low and moderate  $Pe$ , optimal accuracy will often require high cost, and may prove unfeasible; however, errors are in this case typically smaller than in the case of high  $Pe$  numbers, and it may be less important to stay close to optimal accuracy; i.e., the time step may be set based on a maximum desired cost, and changed only if obtained accuracy is not satisfactory (empiricism will certainly be involved on deciding whether accuracy is satisfactory).

In problems involving time-varying  $Pe$  (e.g., in consequence of the variation of the velocity of tidal currents), it may be effective to consider variable time steps: shorter when  $Pe$  is smaller, and larger when  $Pe$  is high.

CHAPTER 6

THE NUMERICAL MODELING OF POLLUTANT TRANSPORT IN  
COASTAL WATERS REVISITED



## 6.1. INTRODUCTION

LNEC was first seriously faced with the need for systematic modeling of effluent disposal and pollutant transport in coastal waters(1) in late 1978, when Electricidade de Portugal, E.P. (EDP) asked this National Laboratory to perform studies of recirculation and thermal impact, in connection with EDP program for the construction of thermal power plants along the Portuguese coast.

Following this request, LNEC 1979 established a general (yet flexible) conceptual framework for the development of studies of thermal impact in coastal zones, which includes mathematical, numerical and physical modeling of near-field, intermediate-field and far-field phenomena; Fig. 6.1 provides clarification on some of the terms used. This framework can be particularized to the study of purely hydrodynamic problems, or extended in a natural way to accommodate the modeling of other types of pollutants, suspended sediments, tracers, etc. Through research and development work, and making extensive use of open-literature knowledge and of the experience of fellow research institutions (e.g., Laboratoire National d'Hydraulique, in France, and Massachusetts Institute of Technology, in USA), several of the tools required by the defined framework were developed, and expertise was gained in the respective use.

Simplified mathematical models for the analysis of thermal jets (BAPTISTA 1981) and for the analysis of heat transport in schematic receiving water bodies (BAPTISTA 1981, LNEC 1984b) were implemented, tested, and used for preliminary analysis concerning different power plants and power plant sites (LNEC 1984a, LNEC 1984b and LNEC 1986), providing quick useful information at relatively low cost.

A modern, highly automatized, experimental set-up for scale modeling of thermal jets and consequent heat transport in the intermediate field was built, equipped and used to assist the design of the discharge structure of the Sines Power Plant (now in the early phases of industrial production) - BAPTISTA 1981, LNEC 1983a, LNEC 1984a. This experimental set-up remains a powerful tool for the detailed modeling of the near and intermediate fields of thermal effluents, its use being planned for other EDP power plants.

Two-dimensional (depth-averaged) finite element models for circulation - TEA (WESTERINK et al. 1984) and TEANL (WESTERINK et al. 1985) - and for passive transport - ELA (BAPTISTA 1984) -, developed at Massachusetts Institute of Technology by a research team joined by the author, became available at LNEC, where they were assembled in a coherent computational structure.

---

(1) The term "coastal waters" is used throughout this work in a broad sense, so as to include estuaries, lagoons, etc.

An alternative circulation model was meanwhile developed at LNEC - MHD2 (VIEIRA 1984). While both TEA and TEANL (which differ from each other by the fact that the former is linear while the latter is nonlinear) resort to frequency-domain formulations (Appendix B), MHD2 uses a more conventional time-domain formulation; these three models have a large potential for complementary use, which is yet essentially unexplored.

Several applications of the above numerical models have been reported by MIT and LNEC, involving either just circulation (VIEIRA 1983, WESTERINK et al. 1985) or both circulation and passive transport (BAPTISTA et al. 1984, KOSSIK 1986). However, most of these applications have to be considered illustrative or (because of shortage of field data) tentative.

Planned applications of TEA, TEANL and ELA to the study of the thermal impact of a power plant at Lavos, Portugal, and of MHD2 to the study of the circulation of Rio de la Plata, Uruguay, will certainly enhance general expertise of the involved researchers on the use of these models, as extensive field data should be available in both cases.

Field data collection and processing has been an early concern, both at the pre- and post-operational stages of the engineering works under analysis. In particular, a number of extensive field surveys, involving the measurement of currents, tides, wind, air and water temperatures, salinities, etc, were performed by Instituto Hidrográfico, based on specifications issued by LNEC, and often under an EDP contract (e.g. LNEC 1981, LNEC 1984c). This information complements that already available, from which we emphasize long-term tidal records that Instituto Hidrográfico routinely collects in several points of the Portuguese coast.

Providing that reliability can be demonstrated, data collected for Sines, Setúbal and Lavos are, to our knowledge, among the most comprehensive data sets available worldwide, and contain information that is precious for both research and engineering practice. While a first processing (consisting mainly on elimination of spurious measurements, graphical display of data, and general interpretation of results) was, in all cases, done by Instituto Hidrográfico, it has been found that additional processing, specifically adapted to the needs of a particular application or even a particular run, must necessarily be done by the modeller, specially in what concerns tides and tidal currents. For that sake, a set of codes for digital data processing (e.g. sinusoidal least square analysis of tidal and tidal current constituents, elimination of spurious data, filtering of tidal constituents) were developed or adapted at LNEC (unpublished work by CAPITÃO and BAPTISTA), and their use has been initiated for the data available on the Lavos coast, in connection with ongoing thermal impact studies.

While the set of tools mentioned above is powerful and incorporates some of the most recent technology, several "grey areas" (in the wording of IAHR Section for the Use of Computers in Hydraulics, see quotation in the front page of this work) remain associated to a part of such tools.

These areas include, but are clearly not restricted to:

- collecting, processing and interpreting field data (specially on currents), in a way compatible with the needs of numerical models;

- defining well the physical problem, for either circulation or transport, including proper, in both mathematical and physical senses, choice of governing equations and boundary conditions; the dimensionality of the models to use, the closure of turbulence, and the actual specification of boundary conditions in open regions are often particularly challenging issues;

- solving accurately (in some range of practical interest) the mathematically defined physical problem, within prevailing constraints.

A part of this latter area, concerning the accurate numerical solution of the transport equation, was analysed in the previous chapters in a very fundamental, purely numerical, way, unrestricted to particular applications.

Results described in earlier chapters will now be related to the main motivation for such numerical investigation: the improvement of the current ability to simulate pollutant transport in coastal waters. Our attention will focus on the modeling of far-field transport of passive scalars by a pre-computed carrying flow.



## 6.2. OUTLINE OF THE TRANSPORT PROBLEM

We consider an unsteady, pre-computed (e.g., by a numerical circulation model) flow, which is assumed to be representative of the circulation in a coastal zone(1). Our goal is to predict the fate of a passive scalar discharged into and transported by such flow.

Depending on our engineering goal and on the nature of the scalar (which may be conservative or undergo physical, chemical or biological transformation), we may be interested in simulating the transport for just a few hours (often the case of problems involving coliforms), or for several days or weeks (e.g. for heat disposed from power plants). Also, we may want considerable spatial detail (e.g. if we are concerned with thermal recirculation), or simply general indication on the location and extent of the plume of the scalar (e.g. to identify residence time in semi-enclosed water bodies). Very often, land boundaries are irregularly shaped, and the level of required discretization is unevenly distributed throughout the zone under study.

The source of the scalar may be a single point (e.g., an outfall pipe), distributed over a limited area (e.g., from a multi-port diffuser, or from an oil spill), distributed over a large area (as in surface runoff), or any combination of the former cases. Such source may be accidental (as in spills) or intentional (as in cooling water systems), and may be continuous, instantaneous or intermittent; also, it may (e.g., a thermal discharge from a power plant) or may not (e.g., an oil spill) have significant initial momentum.

Ambient currents may range from weak (some cm/s) to strong (order of 1 m/s), and may be considerably symmetrical over the tidal cycle, or on the opposite, be characterized by a strong net drift; characteristics of the currents (together with decay properties of the scalar) will determine the spatial extent of the area of interest for the transport study. For instance, thermal impact from a nuclear power plant often concerns areas of several tens of square kilometers, although significant heating (say, above 3°C) affects only much smaller areas.

The relative importance of advection and diffusion depends on the ability of the adopted flow representation to capture the relevant scales of time and space, as discussed in Chapter 2. For 2-D numerical models, diffusion results mainly from the neglecting of vertical shear and of sub-grid horizontal shear. A tentative representative range of values for diffusion coefficients is 1 to 5 m<sup>2</sup>/s, but further work needs to be done in this issue. If we scale the intensity of currents by 0.5m/s (a reasonable value), and scale dispersion by 5 m<sup>2</sup>/s, we get a representative Peclet number of  $0.1\Delta x$ . This immediately implies

-----

(1) It should be emphasized that the definition of the carrying flow may be, and often is, a very challenging problem in itself.

that grids with nodal spacings above a few tens of meters will lead to advection-dominated transport problems, at least during a part of the tidal cycle; experience has shown that nodal spacings are more often, because of practical constraints (CPU and memory requirements), rather in the range of a few hundred meters, which aggravates the dominance of advection.

## 6.3. REVIEW OF THE TRANSPORT MODEL ELA

### 6.3.1. Motivation

The transport model ELA (Eulerian-Lagrangian Analysis of Pollutant Transport) was developed between 1983 and 1984 (BAPTISTA et al. 1984), with the objective of overcoming the severe limitations of DISPER, a still very popular finite element Eulerian model developed in the middle seventies (LEIMKUEHLER 1974).

DISPER limitations are mostly a direct consequence of the constraints that must be satisfied for stable and wiggle-free solutions, namely (LEIMKUEHLER 1974):

$$\frac{D\Delta t}{\Delta x^2} < 0.1 \quad (6.1)$$

$$\frac{U\Delta t}{\Delta x} < 0.1 \quad (6.2)$$

$$\frac{U\Delta x}{D} < 2 \quad (6.3)$$

To satisfy these constraints, DISPER users have often been forced, for current applications in coastal waters, to use time steps of less than one minute and artificially high diffusivities of some tens (or even a few hundred) m<sup>2</sup>/s, but even so they have not always been successful in preventing spurious spatial oscillations (e.g. KAUFMAN and ADAMS 1981).

Because of such small time steps, CPU costs were high (1 hour of CPU for each 4 prototype hours of simulation, in a Honeywell HISI 68/DPS, is a representative order-of-magnitude value for several practical runs). Also, results were excessively damped relative to reality, in consequence of the large artificial diffusion.

It is worthwhile noting that the companion circulation model CAFE (WANG and CONNOR 1975) would require about 6 times more CPU time than DISPER; hence, many users considered the lack of accuracy of DISPER a much stronger shortcoming than its cost (computing circulation was the most significant cost constraint, anyway). With the development of TEA and TEANL, the companion frequency-domain circulation models for ELA, which substantially reduce required CPU time, the issue of the cost of the transport model becomes of much greater relevance.

Eulerian FE transport models alternative to, and sometimes more efficient than, DISPER, were developed in more recent years (e.g., ONISHI 1981). However, none has avoided the need for artificially high diffusivities, either self-generated by the numerical scheme (as in Petrov-Galerkin schemes) or introduced by the user, as a (false) remedy for wiggles. Also, none has achieved order-of-magnitude savings in CPU time relative to DISPER, which, together with the cost of conventional circulation models, have strongly inhibited the simulation of phenomena involving large time scales (indeed, practical simulations have

most often been carried out for just one or a very few tidal cycles).

### 6.3.2. Formulation

ELA is based on the ELM described in Chapter 3. It solves the 2-D (depth averaged) transport equation at the nodes of an unstructured finite element grid of subparametric 6-nodes triangles; the solution involves the splitting of advection and diffusion, the former being solved by a Backwards Method of Characteristics (with quadratic Lagrange interpolations), and the latter by a Galerkin FEM.

ELA is unconditionally stable, and its accuracy typically increases with the time step. Time steps of above one hour have been used apparently with good results.

Information on circulation is given to ELA by either TEA or TEANL; such information is provided at the corner nodes of each element, in the form of the amplitudes and phases of the periodic (plus a zero-frequency) components of velocities and elevations.

A recent extension of the original code (KOSSIK et al. 1986) incorporated to ELA a specialized treatment of sources, which reduces the need for extreme local grid refinements; this treatment, based on the forward tracking of a series of Gaussian puffs, is described in Appendix C. The ability to simulate transformation processes (such as volatilization) for multiple components was also incorporated (KOSSIK 1986).

## 6.4. REVIEW OF SELECTED APPLICATIONS

### 6.4.1. Sludge dumping in Massachusetts Bay

This application, reported by BAPTISTA 1984, concerns a preliminary (and mostly illustrative) study of the dispersal of sludge dumped in a large bay (Massachusetts Bay, in the Northeast coast of the United States). Sludge is produced at the Wastewater Treatment Plants of Deer Island and Nut Island, in the Boston Harbor, and, among other alternatives, dumping from a barge and discharge from a submerged offshore outfall were being considered at the time.

For our calculations, Massachusetts Bay was discretized by means of the grid shown in Fig. 6.2. The grid has 360 triangular elements, with 215 corner nodes, out of a total of 789 corner plus mid-side nodes. A constant depth of 10m, was considered over the whole bay, which was realistic enough for the purpose of the application.

The circulation was considered to be driven simply by a steady coastal current and by a tidal forcing, and was computed by TEA in the corner nodes of the grid. The tidal forcing was specified by prescribing elevations at the ocean nodes, and driving the system at a single frequency (M2); tidal elevations were varied linearly from Cape Ann to Cape Cod and no phase shifts were applied. The steady coastal current was simulated by imposing a linear elevation gradient along the ocean boundary, and driving the system at zero frequency. Calibration was brief, and based only on tidal elevation available at Boston, Cape Ann and Cape Cod (WESTERINK and BAPTISTA 1984). We note the rather inconvenient location of the ocean boundary, imposed by the expected zone of influence of the sludge plume.

Resulting circulation patterns (e.g., Fig. 6.3 and 6.4) are qualitatively reasonable, from what is known from field data and previous numerical studies, but no claim of quantitative reliability should be made (in particular, due to the oversimplification of the boundary forcings and of the tidal phenomenon).

Sludge concentrations were computed by ELA in the mid-side and corner nodes of the grid. Two alternative sites were considered for the disposal of the sludge: site 1 just outside Boston Harbor, and site 2 further offshore but still within Massachusetts Bay. The simulations emphasized the long-term transport, trying to assess general tendencies of the movement of the sludge plume (in particular its time of residence in the Bay).

Consistently with our objective, we considered, for both sites, instantaneous sludge sources, released at the beginning of the ebb tide, and followed through 6 tidal cycles. Each source was described as a Gaussian-hill, characterized by standard deviations  $\sigma_x$  and  $\sigma_y$ , and total mass  $M$ ; for any given calculation, the source may be thought as the result of near-field, short term, dilution of the sludge discharged continuously for a few hours, which is consistent with barge dumping

procedures. For site 2, we set  $\sigma_x = 2\sigma_y = 8400$  m, assuming the barge to describe a long zig-zag trajectory along a main axis; for site 1, we set  $\sigma_x = \sigma_y = 2000$  m, assuming the barge to describe a shorter, more circular, motion.

Results of the transport model, using the generated driving flow, are partially shown in Figs. 6.5 and 6.6 (where concentrations are expressed in percentage of the maximum source concentration). We note that, for site 2, alternative runs were made with  $E_x = E_y = 0$  and  $E_x = E_y = 30$  m<sup>2</sup>/s, the latter being in the highest range of diffusivities expected for the bay (CHRISTODOULOU et al. 1974); for site 1, pure advection was considered. Computations were carried out for 75 hours, with a time step of 1 hour; typically, representative Courant numbers were below 1, while representative Peclet numbers were above 30 ( $\infty$ , for  $E_x = E_y = 0$ ),

For the purposes of the present work, it is particularly interesting to note that:

- No generalized spurious spatial oscillations occur; however, for pure advection, a small spot of non-negligible negative concentrations - up to 2% in magnitude - was typically detected, in the immediate wake of the plume (this is unfortunately not shown in the figures, as isoline 0% was not plotted).

- Numerical dissipation is kept low or moderate, as seen by the examination of the evolution of the horizontal areas associated to each isoline (for pure advection, such areas should remain unchanged). Dissipation is superior in the case of dumping at site 1 than in the case of site 2, which derives in a natural way from the smaller dimensionless source size adopted in the former case.

- Numerical diffusion does not significantly contribute to the observed numerical dissipation, as revealed by the non-smoothed contour of the sludge plume, for site 2; this contour also suggests the dominance, for this problem, of physical advection over physical diffusion.

- Mass was preserved within a range of  $\pm 3\%$  (these are upper ranges; the dependence of the actual mass transformation on  $E_x, E_y$  was not assessed).

- Each simulation of sludge transport took, for 75 hours of prototype, 56 (for pure advection, in which case the code skips the diffusion step) or 68 (for advection and diffusion) minutes of CPU time, in a VAX 11-780. TEA calculations took 2 minutes of CPU.

#### 6.4.2. Heat disposal from the Brayton Point Generating Station

This application, reported by BAPTISTA et al. 1984, concerns the simulation of the dispersal of heat discharged with non-negligible initial momentum in a relatively small embayment (Brayton Point Generating Station, Mount Hope Bay, in the Northeast coast of USA - Fig. 6.7).

The fact that the source is not passive with regard to the

ambient flow, which will be locally disturbed, constitutes a significant difference relative to the previous application, and, due to the large variation of scales involved, represents a major difficulty.

KAUFMAN and ADAMS 1981, who were primarily interested in the resolution of induced velocities and temperatures in the intermediate field, proposed the following approach to solve the dilemma of scales:

- a transition region, corresponding to the near field, is carved out and used to define an inner boundary for the intermediate and far fields, which are simulated through depth-averaged numerical models;

- the location and size of the transition region, the near-field dilution of the effluent, the vertical and lateral entrainment rates, and the depth of the far-field layer affected by the effluent are computed from analytical formulae describing the near field mixing of surface discharges (e.g., STOLZENBACH and HARLEMAN 1971) and given to the numerical model in the form of water and heat fluxes along the inner boundary.

While relatively successful in producing 2-D descriptions of velocity and temperature fields, for two different nuclear power plants, this approach was strongly limited by the need for artificial high diffusivities and by excessive computer costs of the circulation and transport models, CAFE and DISPER, then available at MIT (KAUFFMAN and ADAMS 1981). In particular, as a strong grid refinement is required near the inner boundary, time step constraints were enormous, typically imposing  $\Delta t$  in the order of a few seconds.

BAPTISTA et al. 1984 retook, for the case of the Brayton Point Generating Station, the inner boundary approach, now implemented by means of the alternative numerical models TEA and ELA.

The computational grid for circulation (Fig. 6.7) contains 684 triangular elements, with 411 corner nodes, while the computational grid for transport (Fig. 6.12), which keeps just 468 elements of the previous grid, has 1037 nodes (both corner and mid-side). We note that reducing the number of grid elements for the transport calculations was, in this case, a necessary strategy to be able to fit ELA in the memory of the used VAX 11-780; however, the procedure is recommended whenever, as in this case, extense regions that must be modeled in the circulation phase to allow a proper set-up of boundary conditions, are not relevant for the transport process.

Ambient circulation was assumed to be driven by a tidal forcing and by an inflow from the Taunton river, located northeast of the power plant site. The tidal forcing was specified by prescribing elevations at the ocean nodes, and driving the system at a single frequency, M2 (as in the previous application, an oversimplification of the tidal mechanisms; this does not correspond to a limitation of TEA, simply no further effort was deemed necessary for the sake of the specific application); the inflow from the Taunton River was simulated as a constant flux normal to the river boundary.

Circulation induced by the power plant discharge was generated by prescribing inflow and outflow fluxes along the transition zone; the former represent the original discharge flow rate corrected (increased) as to account for near field volumetric dilution, while the latter represent the horizontal entrainment induced by the discharge. The intake flow rate was also simulated, as a normal flux along the east side of the discharge peninsula. Fig. 6.8 illustrates these forcings, while BAPTISTA et al. 1984 should be read for further details.

A general circulation pattern is shown in Fig. 6.9, and approximations to the Brayton Point zone are provided in Figs. 6.10 and 6.11. While the general circulation is qualitatively reasonable, the jet-like behavior at the edge of the near field is not fully simulated, as too much spreading occurs; this is an expected limitation of TEA, which, being based on the linearized shallow water equations, does not include the non-linear momentum needed to simulate jet behavior (TEA drives the discharge only by elevation gradients).

As the non-linear model TEANL was unavailable by the time, the illustrative application of ELA was carried out on the basis of the circulation computed by TEA, although stressing the limitations of this procedure.

Excess temperatures were computed for one tidal cycle, and are partially shown in Fig. 6.13, in the form of maps of isolines for the two tidal phases corresponding to the velocities plotted in Figs. 6.10 and 6.11. Alternative values of diffusivities ( $E_x=E_y=0$  and  $E_x=E_y=10\text{m}^2/\text{s}$ ) were considered. We note that KAUFMAN and ADAMS 1981 suggest that actual diffusivities, while varying throughout the domain, are typically less than  $1\text{m}^2/\text{s}$  (i.e., close to the pure advection case), but that DISPER requires at least  $10\text{m}^2/\text{s}$  to reduce wiggles to a manageable level.

For the purposes of the present work, it is particularly interesting to note that:

- Generalized spatial spurious oscillations are not present, even for the pure advection case (although, in this case, a localized spot of small negative concentrations is detected near the plume edge).

- Numerical dissipation is kept low, as seen by comparing the pure advection and the advection-diffusion problems (the latter leading to a much stronger dissipation and smearing of the plume).

- Because of the characteristics of the considered source, strong initial concentration gradients are induced and the role of diffusion may be easily overemphasized by the specification of unrealistic high diffusivities.

- Mass is preserved within the 4-5% range (again, these are upper values, the functional dependence on  $E_x, E_y$  having not been examined).

- In a VAX 11-780, and with a time step of 30 minutes, ELA



simulated 12.4 prototype hours in 34 minutes (pure-advection) or 44 minutes (advection-diffusion) of CPU. TEA calculations took 4 minutes of CPU.

#### 6.4.3. Sludge disposal in Boston Harbor

This application, reported by KOSSIK 1986, concerns the same general area of the application described in section 6.4.1, but emphasizes the analysis of the transport and volatilization of volatile halogenated organic compounds (VHOC) in the interior of the Boston Harbor, for the present situation of contamination (major sources of pollution are identified, although not characterized, in Fig. 6.14). While the objective of the application was rather involved (including the analysis of volatilization processes in the harbor), we concentrate only in the aspects relevant to this work.

We note the complex geometry of the physical system (e.g., Fig. 6.17), and the wide range of spatial scales that will be relevant for the solution of the problem: from below one hundred meters, for pollutant transport analysis within the harbor, to over an hundred kilometers, for circulation analysis in Massachusetts Bay.

The computational grid for circulation includes elements with characteristic length scales ranging from a few hundred meters in the harbor to 10 km in the outer bay; the grid contains a total of 888 triangular elements, and 552 corner nodes. The bathymetry of the harbor and the bay was reproduced through linear interpolation within each element.

The transport grid is much smaller in extension, and involves only 694 of the original elements; a total of 1575 nodes (corner and mid-side) are used in the transport calculations. Sources of pollution are characterized by variable, but moderate, flow rates, inducing no significant initial horizontal momentum, and very small near field zones. Only the two main sources (the Deer Island and the Nut Island sewage outfalls) were considered by KOSSIK 1986 in his analysis.

Circulation was assumed to be driven by a single tidal frequency (M2) and a zero-frequency component, and calculations were carried out by the linear model TEA. These options clearly involve significant approximations for a problem where, from simple examination of the geometry, we should expect nonlinearities to play an important role, and to generate strong energy transfer among tidal components. Hence, computed circulation patterns should be considered a first approximation to the problem (see Fig. 6.17), but the complementary use of the nonlinear model TEANL, taking into account all the significant tidal components, would be strongly recommended.

Transport calculations were performed for several tidal cycles (so as to achieve dynamic equilibrium, which can take from a few hours to 60 tidal cycles, depending on the decay rate of the considered component). Fig. 6.18 presents a sample output. The following aspects of the application are of particular interest to the present work:

- Sources were treated by the "puff"-tracking technique described by ADAMS et al. 1986 (and reproduced in Appendix C), in an attempt to avoid the need for further local grid refinement.
- Time steps between 2 and 12.4 hours were used, without apparent malfunction of the model (we note, however, that accuracy can not be controlled in a fully satisfactory way).
- Small but apparent artificial mass transformation, with a periodic-like behavior, is consistently detected (e.g., Fig. 6.19).
- CPU costs per tidal cycle were as follows: tracking step - 66 minutes; solution of diffusion and interpolation step - 4 minutes for  $\Delta t=2.1$  h and 2/3 minutes for  $\Delta t=12.4$  h. Support runs by TEA took 20 minutes of CPU.

## 6.5. DISCUSSION OF THE GENERAL PERFORMANCE AND FURTHER IMPROVEMENTS FOR ELA.

The applications described in earlier sections, indicate that ELA is a flexible engineering tool for the analysis of the transport of passive pollutants in coastal shallow waters. In particular, ELA can accomodate:

- complex geometries and ambient circulation;
- different source types, ranging from the simple case of an instantaneous mass release in large areas (as in sludge dumping from barges, or oil spills) to the more complex cases of spatially localized continuous discharges with or without significant initial momentum (as in heat discharges from power plants, and in sewage discharges, respectively); sources may be single or multiple, and may be of the point or non-point type.
- single or multiple scalars, either conservative or undergoing non-uniform linear transformation.

ELA formulation constitutes, in almost every single account, a net improvement over that of DISPER and other Eulerian methods, allowing, in particular:

- the use of any arbitrarily low range of values of diffusivities (specification of large diffusivities are not required to avoid wiggles, and the numerical technique introduces no numerical diffusion, although it can not fully avoid artificial dissipation);
- the use of large time steps; the time step does not constrain stability, and increasing  $\Delta t$  will typically improve accuracy when advection is dominant;
- the simulation of long-term transport at affordable cost, as a consequence of the freedom in the selection of the time step, and of the frequency-domain formulation of the companion circulation models TEA and TEANL;
- the accurate tracking of individual fluid parcels, through an inherent procedure (results not shown).

However, the performance of ELA can still be improved in a number of ways, which may represent modifications in the formulation, or simply the establishment of criteria for more effective use. Major objectives of such modifications would be:

- reduction of the cost of the tracking step, while keeping a satisfactory high level of accuracy;
- improvement of the general accuracy, in particular of the ability to handle short dimensionless wavelengths (e.g., generated near sharp fronts or near sources), and of mass preservation characteristics.
- incorporation of a physically realistic formulation for internal computation of diffusivities.

The cost of the tracking step has been shown to be the major component of costs in all considered applications, while accuracy in this step is most often nearly perfect. This suggests that attempts to further reduce costs of ELA simulations should concentrate in the tracking. Review of the formulation suggests that savings can be achieved either by re-stating the initial value problem to be solved or by simplifying the solution strategy.

The former approach could be taken by using, whenever possible, the standard splitting of advection and diffusion of section 3.2.1, and adopting the modified approach of section 3.2.2, now routinely used, only for special cases (with strong pseudo-velocities associated to diffusion). In this way, the initial value problem to be solved could be substantially simplified in many situations of practical interest, and inherent costs reduced; while this would imply an increase of the cost of the diffusion equation, the overall balance is expected to correspond to considerable savings.

As for the simplification of the current tracking strategy, the replacement of the fourth-order Runge-Kutta scheme used to solve the tracking, by a cheaper technique (e.g., a 2nd-order Runge-Kutta scheme), should be explored, together with the relaxation of the internal back-checking and/or accuracy criteria for the set-up of the R-K time step (see section 3.4.2). We note that, while no systematic analysis was performed, only sporadically was the back-checking found to lead to a modification of the R-K time step, which clearly suggests a potential for savings (either by skipping the back-checking, or by start-out with higher R-K time steps).

For the improvement of the general accuracy, one should concentrate again in the solution of advection (as suggested by Chapter 5), but now in the interpolation step. Chapter 4 provides theoretical support for the outline of improvements.

An immediate improvement, at modest extra cost and complexity, should be obtained by replacing the 6-nodes sub-parametric triangles currently used by ELA by 8- or 9-nodes subparametric rectangles, which provide higher order interpolation within the safety of a 3P-LI3 scheme. We note, however, that the restriction to subparametric elements is extremely important for the cost of the tracking step, which increases dramatically if the geometry of the element itself is described by quadratic or higher order functions (in which case transformation of generic global coordinates into local coordinates, a frequently required operation, must be handled iteratively).

Further improvements can be achieved by using more accurate interpolation schemes. However, this will typically lead to an increased cost of the interpolation step within the solution of advection (see section 5.3), and to an increased complexity in the handling of zones near boundary conditions.

The strategy that is being adopted in the transformation of ELA is to allow the grid elements to be either 6-nodes subparametric triangles or 9-nodes subparametric rectangles, and defining alternatively over each element either a 3P-LI3 or a more

accurate 5P-LR3 interpolation scheme; selection of which interpolation scheme is to be used is made in an automatic, time-dependent basis. The former interpolation will be used throughout most of the domain, and, in particular, near the boundaries (so as to avoid the need for artificial boundary conditions); the latter will be used only for the elements where sharp gradients are expected (or are detected) to occur.

The choice of the 5P-LR3 rather than an alternative higher-accuracy scheme represents a tradeoff, where we privileged compatibility (using the core elements used by 3P-LI3 was a requirement), reliability (e.g., we eliminated the 5P-HL3 because of the potential instability) and simplicity and cost (e.g., for irregular grids, 5P-LR3 is easier to define than HL or PL schemes, and should be cheaper - see section 4.4).

Because in most intended applications the zones in space where high gradients may occur are confined (e.g., around sources), the 5P-LR3 (or, conceptually, other scheme more complex but more accurate than the 3P-LI3) will be applied as an exception, not as a rule, and costs should therefore be kept low. Also, the zones of potential applicability may be specially prepared (e.g. by keeping the grid fairly regular), as to allow an unambiguous definition of the interpolation scheme, and to enhance its accuracy.

While the above approach should constitute a cost-effective contribution to improved accuracy (through a more correct handling of a larger range of short wavelengths), it will often not preclude the complementary use of the strategy for source representation described by ADAMS et al. 1986, or alternative strategies (e.g. NEUMAN 1984). We recall, in this context, that no numerical method can handle wavelengths smaller than  $2\Delta x$  (where, in an irregular grid,  $\Delta x$  is scaled by the largest nodal spacing, in some relevant zone), and that even the most performing interpolation schemes considered in Chapter 4 introduce significant distortion to Fourier modes with  $L_m/\Delta x < 5$  or so.

Transformation (successive loss and gain) of mass within the small but non-negligible range of up to  $\pm 5\%$ , was detected in the applications of ELA. On the basis of the argument that numerical experimentation for reference test problems with mass preserving flows revealed nearly perfect mass preservation for the ELM used by ELA, BAPTISTA 1984 attributed the detected mass transformation to minor inter-elementary leakage and to leakage through the boundaries, that TEA could not fully avoid (for the latter, we note that boundary fluxes are handled by TEA as natural, rather than essential, boundary conditions).

While leakage due to TEA may contribute to mass transformation, Chapter 4 suggests that aliasing in the ELM solution could also be playing a non-negligible role specially due to abrupt changes in characteristic sizes of adjacent elements. Tests to check the relative importance of the two potential mass loss mechanisms are a priority task, and they should take advantage of the fact that increasing the source size will reduce eventual mass losses due to aliasing, but not those due to leakage in TEA.

The incorporation of a physically realistic formulation for the internal computation of diffusivities, in a way that relates to the local average flow and to the space dimensionality and discretization, was, for conventional Eulerian models, an unnecessary complication: much higher artificial diffusivities would, anyway, be introduced through the numerical solution procedure. The situation has considerably changed with the use of ELM, and a serious effort to provide ELA with such realistic formulation (which is trivial to handle mathematically, but may assume high conceptual complexity - see ADAMS and BAPTISTA 1986) should be undertaken.



CHAPTER 7  
CONCLUSIONS





## 7.1. NUMERICAL SOLUTION OF THE TRANSPORT EQUATION BY EULERIAN-LAGRANGIAN METHODS

This work presents a systematic analysis of the stability and accuracy of a reference Eulerian-Lagrangian method, with emphasis on the Backwards Method of Characteristics used to solve the advection equation. Both formal analysis and numerical experimentation are extensively used; results are presented in a way that, while supporting our own analysis, should also be able to provide, in several points (e.g., amplitude and phase errors), reference information of general interest.

The BMC is shown to be, for proper choices of the associated interpolation scheme, consistent, stable and convergent. However, other choices of the interpolation schemes (e.g., a cubic Lagrange interpolation defined over a cubic core element, or a cubic Hermite interpolation with derivatives estimated from information outside the core element) lead to instability; also, roundoff errors in the evaluation of the interpolation coefficients may lead to inconsistency (e.g., as in the scheme proposed by KOMATSU et al. 1984).

With regard to accuracy, the BMC is potentially very powerful, but actual performance strongly depends on the choice of the interpolation scheme and on the adopted space and time discretizations. Such performance results, in all cases, from a balance between numerical dissipation, numerical dispersion and aliasing.

The choice of the most appropriate interpolation scheme is a difficult problem. While compact Lagrange interpolation schemes are the most convenient to formulate and allow a clean treatment of the boundaries and nearby zones, they provide a worse compromise between numerical dissipation and dispersion than alternative interpolation schemes (e.g. based on non-compact Lagrange polynomials, and on compact or non-compact Hermite or pseudo-Hermite polynomials). For a specific problem, optimized cost-efficiency seems to be possible through the use of a compact Lagrange interpolation (e.g., quadratic, which is shown to be optimal within the class) as a standard, and of a compatible non-compact interpolation (which we recommend to be based also in Lagrange polynomials) in the zones of time and space where sharp gradients have to be solved; this approach should be explored in a systematic way, and may constitute one of the goals for future work.

A most unusual and convenient property of the BMC is its ability to, as a rule, perform progressively better as the number of time steps required to reach a fixed final time is reduced, i.e., as  $\Delta t$  is increased. This property, which is a consequence of the fact that major errors in the solution come from the interpolation step, can be used for extensive savings in computational effort, and (unlike feared by some authors) does not imply the divergence of the method.

The spatial discretization plays a decisive role in the accuracy of the BMC, whatever the choice of the interpolation scheme is. Indeed, no scheme can reproduce exactly the propagation

characteristics (amplitude and phase) of "short" dimensionless wavelengths, and one should be concerned, in any specific problem, in assuring that the spatial discretization is fine enough to avoid that dominant Fourier modes fit the adopted scheme concept of "short".

A tradeoff necessarily exists between refining the spatial discretization, or selecting a more accurate but, in general, more complex, interpolation scheme. A potentially cost-effective procedure, for cases where the spatial discretization is a limiting factor for accuracy, is the following:

- Set-up a grid that is fine enough to provide, over most of the domain, satisfactory accuracy through the use of a relatively simple interpolation scheme (e.g., based on compact Lagrange quadratic polynomials), but is too coarse to allow such scheme to resolve sharp gradients in localized regions.
- Use the simple scheme as a standard, but, over the regions that so require, either (a) resort to a more elaborated (but compatible) interpolation scheme, or (b) replace locally the BMC solution by a forward particle of "puff" tracking procedure. Combining (a) and (b) may often prove attractive.

Non-uniform grids affect the accuracy of the BMC in a double way: by modifying the accuracy of each specific interpolation, and by introducing aliasing (this latter effect being common to all other sources of non-uniformities, non-uniform circulation included). While our analysis is not systematic enough in this regard, and should be extended in future work, results clearly show that the transition between the characteristic sizes of adjacent elements should be kept as smooth as possible, with the ratio of 1.5 being suggested as a tentative upper bound.

An additional effect of non-uniform grids is to complicate the extension of non-compact interpolation schemes to dimensions higher than one: costs are significantly higher for non-uniform than for uniform grids (an exception being non-uniform but straight orthogonal grids), and conceptual and practical problems may arise in the definition and implementation of the interpolation (this is particularly so for non-compact Hermite or pseudo-Hermite schemes, and for grids of triangular elements). Significant effort has still to be put on cost-effective extension of non-compact interpolation schemes to generic multidimensional grids.

When both advection and diffusion (rather than only advection) are considered, the performance of the BMC in the solution of the advection step is improved, in consequence of the progressive increase of the wavelength of dominant Fourier modes. Because the solution of the advection is critical for the overall accuracy, the reference ELM consistently improves its accuracy as the role of diffusion becomes more important; we stress, however, that the performance of the method is very satisfactory in the whole range between pure advection and pure diffusion.

## 7.2. NUMERICAL MODELING OF POLLUTANT TRANSPORT IN COASTAL WATERS

The present work contributes to a more effective modeling of pollutant transport in coastal waters by improving our ability to solve numerically the advection-dominated transport equation, and our understanding and ability to control the deficiencies of such solution.

Among the significant features of Eulerian-Lagrangian pollutant transport models (e.g. ELA), we emphasize:

- The ability to use very large time steps. This, in particular, allows long-term simulations at moderate cost, which is a significant practical achievement relative to more conventional Eulerian models.
- The need for no artificial diffusion as a remedy for numerical dispersion or instability, and the introduction of only a moderate (and not diffusion-like) numerical dissipation. This allows a much more accurate (as compared to Eulerian models) treatment of sharp gradients, and motivates further research on the relative importance of advection and diffusion (and, in particular, in the careful evaluation of the diffusivities, in a way consistent with the adopted representation of the carrying flow).

The hybrid use of alternative interpolation schemes (a standard scheme for most of the domain and an improved one for zones of sharp gradients) is recommended as a further improvement, and implementation of this strategy on ELA is on the way.

A specific area requiring priority further work is the set-up of practical criteria guiding the definition of non-uniform grids; indeed, it seems of strong importance to assure relatively smooth transitions between the characteristic size of adjacent elements; otherwise, numerical dispersion may be overly increased and significant artificial mass transformation may occur.

A phase of intense application of ELA and its companion circulation models TEA and TEANL to environmental and engineering problems is now planned at LNEC, taking as a starting point ongoing studies of recirculation and thermal impact of Portuguese power plants.

Each application is an integrated work, involving activity in field data processing, circulation modeling and transport modeling, and taking into account the objectives and constraints of the specific project. While significant common ground exists, each application will challenge the body of knowledge and the tools now available at LNEC in specific different ways, helping, as in the past, in the identification of priority research and development areas.

It is anticipated that a general area requiring a concentration of efforts in the near future is that of field data processing, oriented towards the needs of numerical models. Technical exchange and active collaboration among the organisms that, in Portugal, have interest and experience in this area is highly

recommended. Earlier collaboration of Instituto Hidrográfico and LNEC, for coastal sites related to EDP power plants, should, in particular, be continued and enhanced.

Lisboa, Laboratório Nacional de Engenharia Civil, Junho de 1986

O Assistente de Investigação

António EMBaptista

António Eugénio de Melo Baptista

REFERENCES



Adams, E.E. and A.M. Baptista - "Ocean Dispersion Modeling", in Encyclopedia of Fluid mechanics, Vol. 6: Complex Flows (N. Chermisinoff, Ed.), to be published.

Adams, E.E., D.R.F. Harleman, G.H. Jirka and K.D. Stolzenbach - "Heat Disposal in the Water Environment", Lecture Notes, R.M. Parsons Laboratory for Water Resources and Hydrodynamics, M.I.T., 1981.

Adams, E.E., R. Kossick and A.M. Baptista - "Source representation in a numerical transport model", in Finite Elements in Water Resources. Proceedings of the 6th International Conference (Sá da Costa et al., Ed.), Springer-Verlag, 1986.

Adams, E.E., K.D. Stolzenbach and D.R.F. Harleman - "Near and Far Field Analysis of Buoyant Surface Discharges into Large Bodies of Water", Report No. 205, R.M. Parsons Laboratory for Water Resources and Hydrodynamics, M.I.T., 1975.

Baptista, A.M. - "Introdução aos Estudos de Recirculação e Impacto Térmico de Centrais Térmicas Refrigeradas em Circuito Aberto para o Mar", in Simpósio sobre a Utilização da Água na Produção de Energia, APRH, Lisboa, 1980.

Baptista, A.M. - "Sines Power Plant: A Case in Study", in Course on Engineering Aspects of Heat Disposal in the Water Environment, LNEC, Lisboa, 1981.

Baptista, A.M. - "Eulerian-Lagrangian Analysis of Pollutant Transport in Shallow Waters", M.Sc. Thesis, M.I.T., 1984.

Baptista, A.M. - "On the Solution of the Transport Equation", in Seminário sobre Gestão e Modelação Matemática da Qualidade da Água em Rios, LNEC, Lisboa, 1985a.

Baptista, A.M. - "An Efficient Computational Structure for the Simulation of Tidal Circulation and Pollutant Transport in Shallow Water", in Seminário sobre Gestão e Modelação Matemática da Qualidade da Água em Rios, LNEC, Lisboa, 1985b.

Baptista, A.M. - "Reference Problems for the Convection-Diffusion Forum, VI International Conference on Finite Elements in Water Resources", LNEC, Lisboa, 1985c.

Baptista, A.M., E.E. Adams and K.D. Stolzenbach - "The 2-D Unsteady Transport Equation Solved by the Combined Use of the Finite Element Method and the Method of Characteristics", in 5th Int. Conf. on Finite Elements in Water Resources, Burlington, Vermont, 1984a.

Baptista, A.M., E.E. Adams and K.D. Stolzenbach - "Eulerian-Lagrangian Analysis of Pollutant Transport in Shallow Water". MIT R.M. Parsons Laboratory, Technical Report 296, 1984b (extended version of BAPTISTA 1984).



- Baptista, A.M., E.E. Adams and K.D. Stolzenbach - "Comparison of Several Eulerian-Lagrangian Models to Solve the Advection-Diffusion Equation", in Int. Symp. on Refined Flow Modeling and Turbulence Measurements, U. Iowa, USA, 1985.
- Baptista, A.M., E.E. Adams and K.D. Stolzenbach - "Accuracy Analysis of the Backwards Method of Characteristics", in Finite Elements in Water Resources. Proceedings of the 6th International Conference (Sá da Costa et al., Ed.), Springer-Verlag, 1986.
- Baptista, A.M., K.D. Stolzenbach, J.J. Westerink and E.E. Adams - "Near Field/ Far Field Interaction of Thermal Plumes from Power Plants", Progress Report, Energy Laboratory/R.M. Parsons Laboratory, M.I.T., 1983.
- Bathe, K.-J. - "Finite Element Procedures in Engineering Analysis", Prentice-Hall Inc., 1982.
- Benque, J.P., G. Labadie and G. Ibler - "A Finite Element Method for Navier-Stokes Equations", in 3rd Conf. on Fin. Elem. in Flow Problems, 1980.
- Book, D.L., J.P. Boris and K. Hain - "Flux-Corrected Transport II: Generalization of the Method", in J. of Comp. Phys., Vol. 18, 248-283, 1975.
- Brooks, N.H. - "Diffuser of Sewage Effluent in an Ocean Current", in Proc. 1st International Conf. on Waste Disposal in the Marine Environment, Pergamon Press, 246-267, 1960.
- Brutsaert, W. and G.H. Jirka (Eds.) - "Gas Transfer at Water Surfaces", D. Reidel Publishing Company, 1984.
- Cady, R. and S.P. Neuman - "Solutions of the Reference Test Problems", Convection-Diffusion Forum, VI FEWR, LNEC, Lisboa, 1986.
- Celia, M.A. and W.G. Gray - "An Improved Isoparametric Transformation for Finite Element Analysis", in International Journal for Numerical Methods in Engineering, Vol. 20, pp. 1443-1459, 1984.
- Cheng, R.T., V. Casulli and S. Milford - "Eulerian-Lagrangian Solution of the Convection-Diffusion Equation in Natural Coordinates", in Water Resources Research, Vol. 20, No. 7, pp. 944-952, 1984.
- Chin, A.D. and P.J. Roberts - "A Model of Dispersion in Coastal Waters", in Journal of Hydr. Engrg., ASCE, 1984.
- Christie, I., D.F. Griffiths, A.R. Mitchell and O.C. Zienkiewicz - "Finite Element Methods for Second Order Differential Equations with Significant First Derivatives", in Int. J. Num. Meth. Engrg., Vol. 10, 1389-1396, 1976.
- Christodoulou, G.C., J.J. Connor and B.K. Pearce - "Mathematical Modeling of Dispersion in Stratified Waters", Report No. 219,

R.M. Parsons Laboratory for Water Resources and Hydrodynamics, M.I.T., 1976.

Christodoulou, G.C., W.F. Leimkuhler and A.T. Ippen - "Mathematical Models of the Massachusetts Bay. Part III: A Mathematical Model for the Dispersion of Suspended Sediments in Coastal Waters", Report No. 179, R.M. Parsons Laboratory for Water Resources and Hydrodynamics, M.I.T., 1974.

Csanady, G.T. - "Turbulent Diffusion in the Environment", D. Reidel Publishing Co., 1973.

Csanady, G.T. - "Dispersion by Randomly Varying Currents", in J. Fluid Mech., Vol. 132, 375-394, 1983.

Cyrus, N.J., and R.E. Fulton - "Accuracy Study of Finite Difference Methods", NASA TN D-4372, National Aeronautics and Space Administration, Langley Research Center, Langley Station, Hampton, Virginia, 1967.

Deardorff, J.W. - "On the Magnitude of the Sub-Grid Scale Eddy Coefficient", in J. Computational Physics, Vol. 7, Part 1, 1971.

Dronkers, J.J. - "Tidal Computations in Rivers and Coastal Waters", North Holland Publishing Company, Amsterdam, 1964.

Emmons, H.W. - in Annu. Rev. Fluid. Mech., vol. 2, pp. 15-36, 1970

Ferreira, J.P.C.L. - "A Dispersão de Poluentes em Aguas Subterrâneas", LNEC, 1986.

Figueira, P.M. - "Numerical Simulation of the Tidal Flow in Homogeneous Estuaries", LNEC, 1981.

Fisher, H.B. (Ed.) - "Transport Models for Inland and Coastal Waters, Proceedings of a Symposium on Predictive Ability", Academic Press, 1981.

Fisher, H.B., E.J. List, R.C.Y. Koh, J. Imberger and N.H. Brooks - "Mixing in Inland and Coastal Waters", Academic Press, 1979.

Glass, J. and W. Rodi - "A Higher Order Numerical Scheme for Scalar Transport", in Comp. Math. in Appl. Mech. and Eng., Vol. 31, 337-358, 1982.

Gray, W.G. - "Do Finite Element Models Simulate Surface Flow", in 3rd Conf. on F.E. in Water Resources, Hannover, 1980.

Gray, W.G. and I.P. Kinnmark - "Evolution of Two-Dimensional Finite Element Wave Equation Models", in Proc. of the VI

- International Conference on Finite Elements in Water Resources, LNEC, Lisboa, 1986.
- Gray, W.G. and G.F. Pinder - "An Analysis of the Numerical Solution of the Transport Equation", in *Water Resources Res.*, 12, p. 547, 1976.
- Hanna, S.R. - in *J. Appl. Meteor.*, 18, 518, 1979.
- Hasbani, Y., E. Livne and M. Bercovier - "Finite Elements and Characteristics Applied to Advection-Diffusion Equations", in *Computer and Fluids*, Vol. 11, No. 2, 71-83, 1983.
- Heinrich, J.C., P.S. Huyakorn, O.C. Zienkiewicz and A.R. Mitchell - "An 'Upwind' Finite Element Scheme for Two-Dimensional Convective-Transport Equation", in *Int. J. Num. Meth. Engrg.*, Vol. 11, 131-143, 1977.
- Heinrich, J.C. and O.C. Zienkiewicz - "Quadratic Finite Element Schemes for Two-Dimensional Convective Transport Problems", in *Int. J. Num. Meth. Engrg.*, Vol. 11, 1831-1844, 1977.
- Hirt, C.W. - "Heuristic Stability Theory for Finite-Difference Equations", in *J. of Computational Physics*, Vol. 2, pp. 39-355, 1968.
- Holly Jr., F.M. - "Two-dimensional Mass Dispersion in Rivers", *Hydrology Papers*, Colorado State University, 1975.
- Holly Jr., F.M. and T. Komatsu - "Derivative Approximations in the Two-Point Fourth-Order Method for Pollutant Transport", in *Proceedings of the Conference on Frontiers in Hydraulic Engineering*, ASCE, M.I.T., 1984.
- Holly Jr., F.M. and J.M. Polatera - "Dispersion Simulation in 2-D Tidal Flow", in *Journal Hydr. Engrg.*, ASCE, 1984.
- Holly Jr., F.M. and A. Preissmann - "Accurate Calculation of Transport in Two Dimensions", in *Journal of the Hydraulics Division*, ASCE, Vol. 103, No. HY11, 1259-1278, Nov. 1977.
- Hughes, T.R. - "A Simple Scheme for Developing Upwind Finite Elements", in *Int. J. Num. Meth. Engrg.*, Vol. 12, 1359-1365, 1979.
- Hughes, T.R. and A. Brooks - "A Multi-Dimensional Upwind Scheme with no Crosswind Diffusion", in *Proc. A.S.M.E. Speciality Conference*, New York, 1979.
- Huyakorn, P.S. - "Techniques for Making Finite Elements Competitive in Modeling Three Dimensional Flow and Transport", in *Proceedings of the 5th International Conference on Finite Elements in Water Resources*, Burlington, Vermont, USA, 1984.
- Jeffrey, A. - "Quasilinear Hyperbolic Systems and Waves",

Research Notes in Mathematic, Pitman, 1976.

Kaufman, J.T. and E.E. Adams - "Coupled Near and Far Field Thermal Plume Analysis Using Finite Element Techniques", Report No. MIT-EL 81-036, Energy Laboratory, M.I.T., 1981.

Kelly, D.W., S. Nakazawa, O.C. Zienkiewicz and J.C. Heinrich - "A Note on Upwinding and Anisotropic-Balancing Dissipation in Finite Element Approximations to Convective Diffusion Problems", in Int. J. Num. Meth. Engrg., Vol.15, 1705-1711, 1980.

Koh, R.C.Y. and C. Chang - "Mathematical Model for Barged Ocean Disposal of Wastes", Report No. 660-2-73-029, U.S. Environmental Protection Agency, 1973.

Komatsu, T., F.M. Holly Jr. and N. Nakashiki - "Numerical Calculation of Pollutant Transport in Rivers and Coastlines", in 4th Congress, Asian and Pacific Division, IAHR, Chiang Mai, Thailand, 1984.

Komatsu, T., F.M. Holly Jr., N. Nakashiki and K. Ohgushi - "Numerical Calculation of Pollutant Transport in One and Two Dimensions", in Journal of Hydroscience and Hydraulic Engineering, Vol. 3, No. 2, pp. 15-30, 1985.

Kossik, R.F. - "Tracing and Modeling Pollutant Transport in Boston Harbor", M.Sc. thesis, MIT, 1984.

Kossik, R.F. et al. - "Users Manual for ELA, a Two-dimensional Eulerian-Lagrangian Transport Model", R.M. Parsons Laboratory, M.I.T., in preparation.

Laible, J.P. - "A Modified Wave Equation Model for 3-D Flow in Shallow Bodies of Water", in Proceedings of the 5th International Conference on Finite Elements in Water Resources, Burlington, Vermont, USA, 1984.

Lange, R. - in J. Appl. Meteor., 17,320,1978.

Lapidus, L. and G.F. Pinder - "Numerical Solution of Partial Differential Equation in Science and Engineering", J. Wiley & Sons, 1982.

Leendertse, J.J. - "Aspects of a Computational Model for Long-Period Water-Wave Propagation", Report RM-5294-PR, The Rand Corporation, 1967.

Leimkuhler, W.F. - "A Two-Dimensional Finite Element Dispersion Model", Civil Engineer Thesis, M.I.T., 1974.

Leith, C.E. - "Numerical Simulation of the Earth's Atmosphere", in Methods in Computational Physics, 4, 1-28, 1965.

LNEC - "Participação do LNEC em Estudos de Recirculação e Impacto Térmico de Centrais Termoeléctricas Refrigeradas em Circuito.

Aberto para o Mar - Proposta", LNEC, 1979.

LNEC - "Estudos de Observação da Central Termoeléctrica de Setúbal. Especificação dos Trabalhos de Campo", 1981.

LNEC - "Central Termoeléctrica de Sines. Estudo Preliminar da Capacidade de Diluição Térmica no Campo Próximo", 1982.

LNEC - "Central Termoeléctrica de Sines. Estudos de Recirculação e Impacto Térmico no Campo Próximo. Análise de uma Solução Alternativa de Rejeição", 1983a.

LNEC - "ISOVAT - Um Programa para Tratamento Gráfico e Processamento de Dados de Modelos Matemáticos por Elementos Finitos", 1983b.

LNEC - "Central Termoeléctrica de Sines. Estudos de Recirculação e Impacto Térmico no Campo Próximo", 1984a.

LNEC - "Estudo Comparativo da Capacidade de Refrigeração dos Sítios de Lavos e da Amorosa", 1984b.

LNEC - "Sítio de Lavos. Especificação da Campanha Oceanográfica de Apoio aos Estudos de Dispersão dos Efluentes de uma Central Termoeléctrica", 1984c.

LNEC - "Central Termoeléctrica de Sines. Necessidade de Estudos Adicionais de Recirculação e Impacto térmico", 1984d.

LNEC - "On the Numerical Solution of the Transport Equation ", in Seminário sobre Gestão e Modelação Matemática da Qualidade da Água em Rios, Lisboa, 1985.

LNEC - "Nova Central a Carvão. Estudo Preliminar de Impacto Térmico para um Sítio entre Lavos e Guia", in preparation.

Lynch, D.R. and F.E. Werner - "Three-Dimensional Harmonic Model for Linearized Tidal Circulation", in Proc. of the VI International Conference on Finite Elements in Water Resources, LNEC, Lisboa, 1986.

Neuman, S.P. - "An Eulerian-Lagrangian Scheme for the Dispersion Convection Equation Using Conjugate Space-Time Grids", in Journal of Comp. Phys., Vol. 41, 270-279, 1981.

Neuman, S.P. - "Adaptive Eulerian-Lagrangian Finite Element Method For Advection-Dispersion", in Int. Journal For Numerical Methods In Engineering, Vol. 20, pp. 321-337, 1984.

Neuman, S.P. and S. Sorek - "Eulerian-Lagrangian Methods for Advection-Dispersion", in Finite Elements in Water Resources, (Mole, K.P. et al. Ed.) Vol. 4, 14.41-14.68, 1982.

Noronha and Baker - "Solutions of the Reference Test Problems", Convection-Diffusion Forum, VI FEWR, LNEC, Lisboa, 1986.

- Okubo, A. - "Oceanic Diffusion Diagrams", in **Deep Sea Research**, Vol. 18, 789-802, 1971.
- Okubo, A. and M.J. Karweit - "Diffusion from a Continuous Source in a Uniform Shear Flow", in **Limnology and Oceanography**, Vol. 14, 514-520, 1969.
- O'Neill, K. and D.R. Lynch - in **Proc. 3rd Int. Conf. on Fin. Elem. in Wat. Res.**, Vol. 1, 367-376, Univ. of Mississippi, Oxford, 1980.
- Onishi, Y. - "Sediment-Contaminant Transport Model", in **Journal of the Hydraulics Division**, ASCE, Vol. 107, HY79, 1089-1107, 1981.
- Pingree R.D. and D.K. Griffiths - "Sand Transport Paths Around the British Isles Resulting from M2 and M4 Tidal Interactions". in **Jour. Mar. Biol. Ass.**, vol. 59, pp. 497-513, 1979.
- Prickett, T.A. et al. - "A Random-walk Solute Transport Model for Selected Groundwater Quality Evaluations", in **Bull.** 65, Champaign, Illinois State Water Survey, 1981.
- Roache, P. - "Computational Fluid Dynamics", Hermosa Publishers, 1982.
- Rodi, W. - "Turbulence Models and Their Application in Hydraulics", International Association for Hydraulic Research, 1980.
- Stolzenbach, K.D. and D.R.F. Harleman - "An Analytical and Experimental Investigation of Surface Discharges of Heated Water", **Technical Report No. 135**, R.M. Parsons Laboratory for Water Resources and Hydrodynamics, MIT, 1971.
- Vanoni, V.A. (Ed.) - "Sedimentary Engineering", ASCE Manuals and Reports On Engineering Practice, No. 55, New York, 1977.
- Varoglu, E. and W.L. Finn - "Space-Time Finite Elements Incorporating Characteristics for the Burgers Equation", in **Int. J. Num. Meth. Engrg.**, Vol. 16, 171-184, 1980.
- Vieira, J.R. - "Marchica à Nador. Etude sur Modèle Mathématique du Régime Hydrodynamique", LNEC, 1983.
- Vieira, J.R. - "Mathematical Modeling of Hydrodynamic and Transport Processes in Coastal Regions", LNEC, 1984.
- Wang, J.D. and J.J. Connor - "Mathematical Modeling of Near-

Coastal Circulation", Report No. 200, R.M. Parsons Laboratory for Water Resources and Hydrodynamics, M.I.T., 1975.

Werner, F.E. and D.R. Lynch - "Field Studies with the Wave Equation Formulation", in Proc. of the VI International Conference on Finite Elements in Water Resources, LNEC, Lisboa, 1986.

Westerink, J.J., J.J. Connor, K.D. Stolzenbach, E.E. Adams and A.M. Baptista - "TEA: A Linear Frequency Domain Finite Element Model for Tidal Embayment Analysis", Energy Laboratory and R.M. Parsons Laboratory for Water Resources and Hydrodynamics, M.I.T., 1984.

Westerink J.J., K.D. Stolzenbach and J.J. Connor - "A Frequency Domain Finite Element Model for Tidal Circulation". R.M. Parsons Laboratory for Water Resources and Hydrodynamics, M.I.T., 1985.

Wnek, W.J. and E.G. Fochtman - "Mathematical Model for Fate of Pollutants in Near-Shore Water", in *Envir. Science and Technology*, Vol. 6, No. 4, 331-337, 1972.

White, F.M. - "Viscous Fluid Flow", McGraw Hill, 1974.

Yudelson, J.M. - "A Survey of Ocean Diffusion Studies and Data", Tech. Memo No. 67-2, W.M. Keck Laboratory of Hydraulics and Water Resources, California Institute of Technology, 1967.

Zanetti, P. - "New Monte Carlo Scheme for Simulating Lagrangian Particle Diffusion with Wind Shear Effects", in *Appl. Math. Modeling*, Vol. 8, June 1984.

**FIGURES**





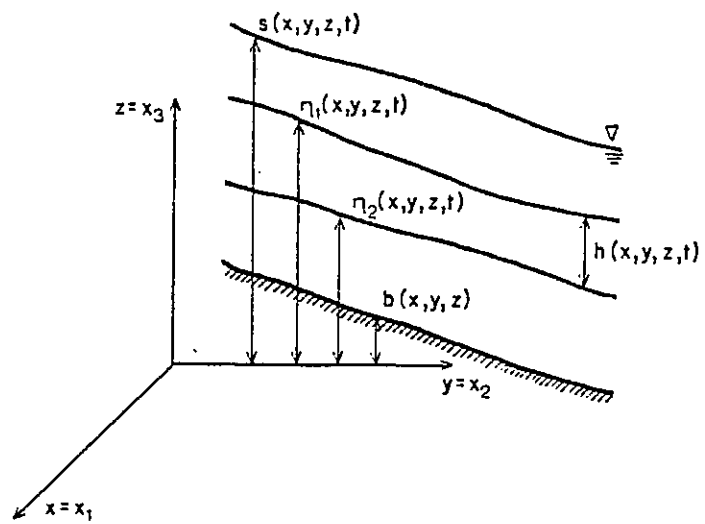
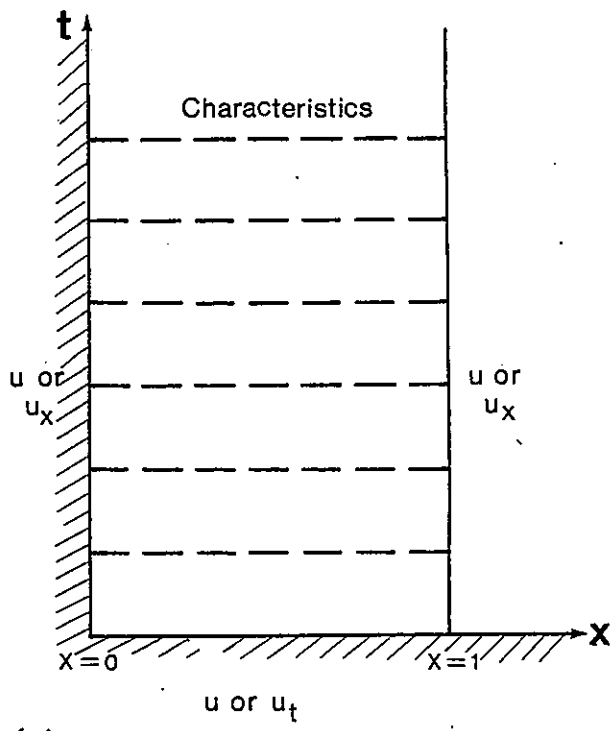
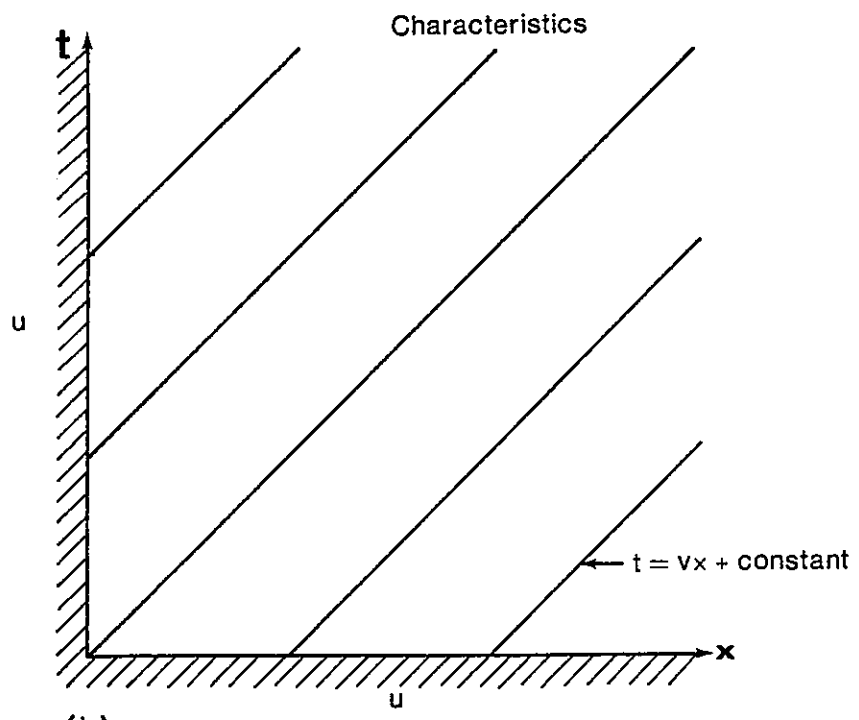


Fig. 2.1. Definition sketch for a 2-D quasi-horizontal flow



(a) parabolic equation



(b) hyperbolic equation

Fig. 2.2. Diagrammatic representation of hyperbolic and parabolic partial differential equations

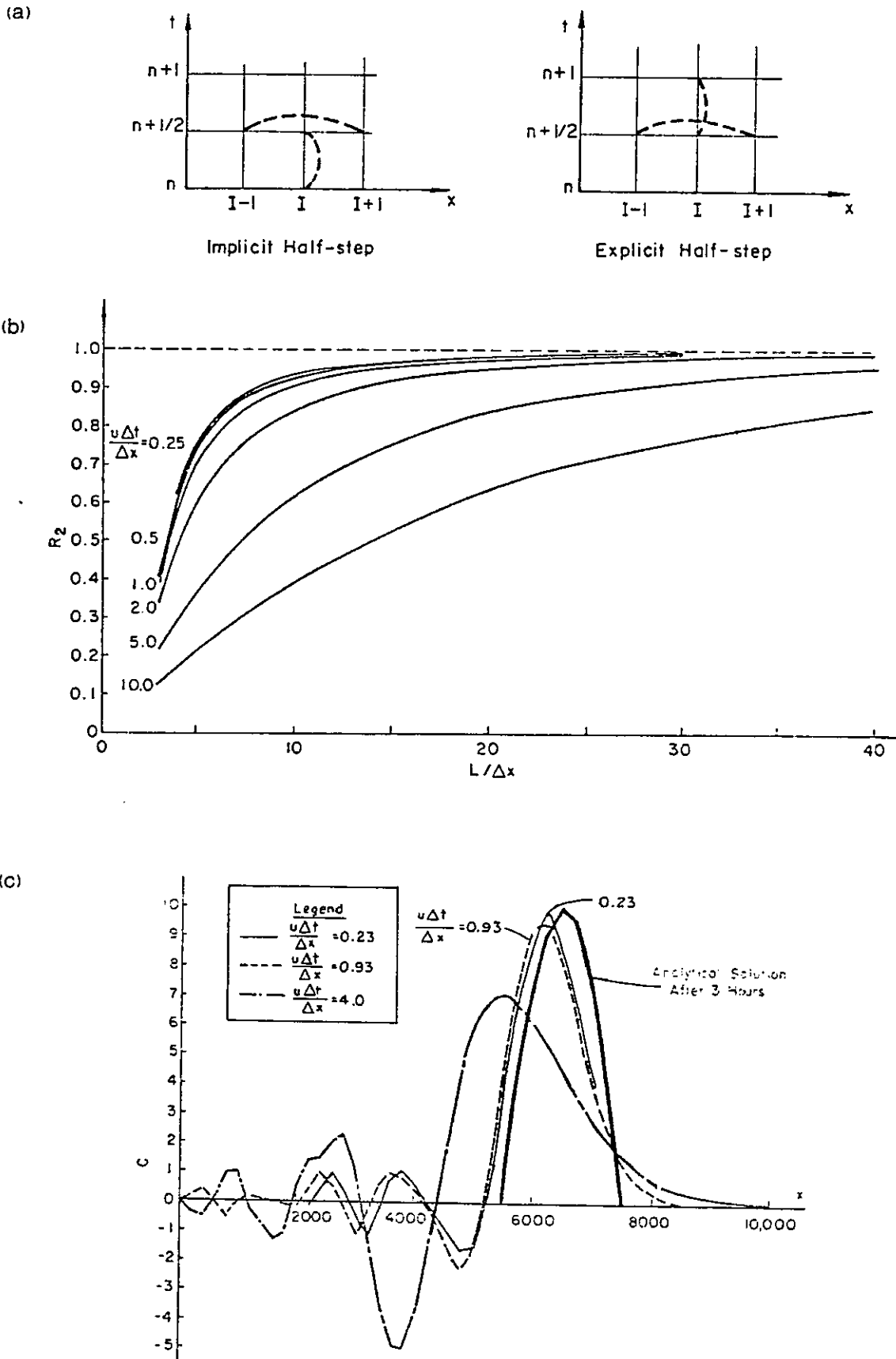


Fig. 2.3. The double-step, implicit-explicit second order scheme: (a) Finite-difference discretization; (b) Numerical dispersion characteristics (the method has no amplitude errors); (c) Application to the advection of a cosine-hill

[from HOLLY 1975]



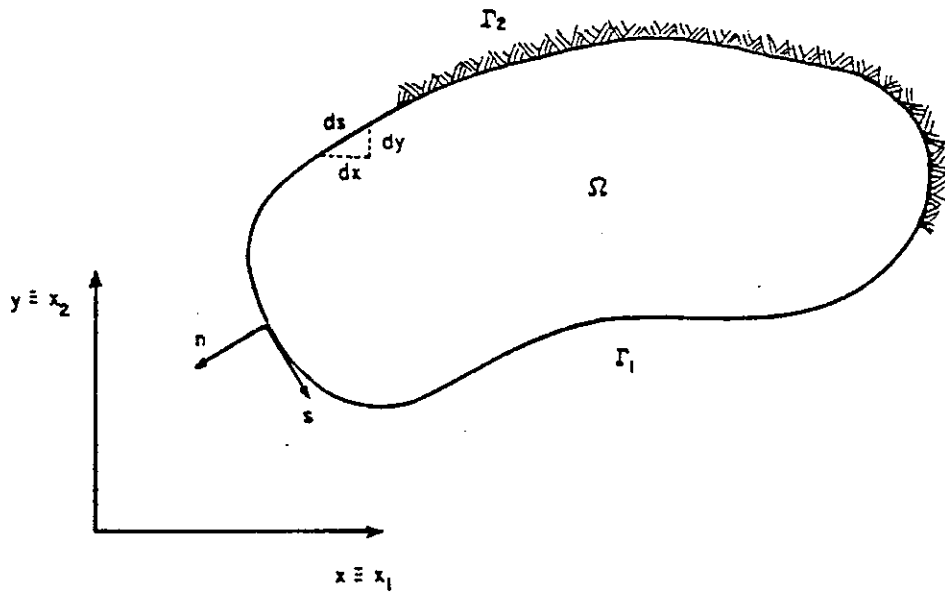
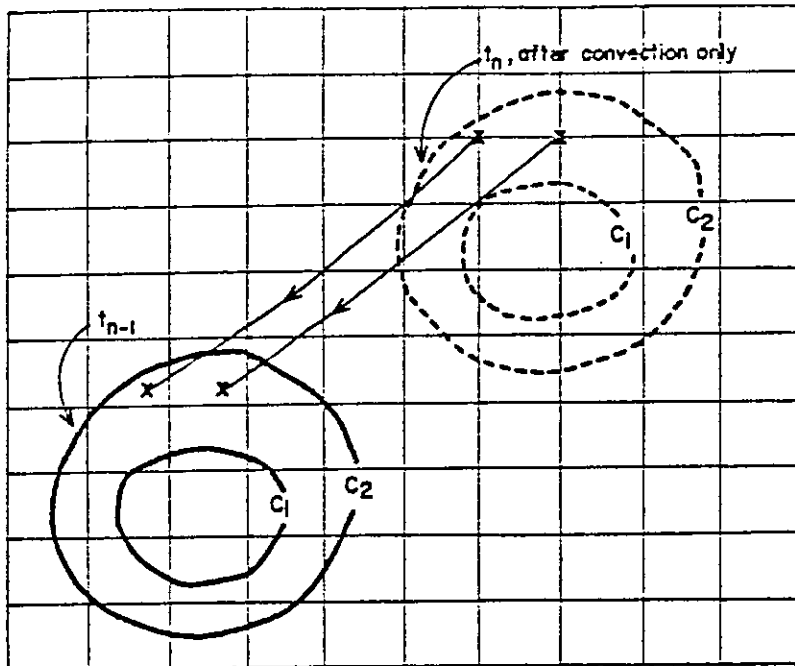
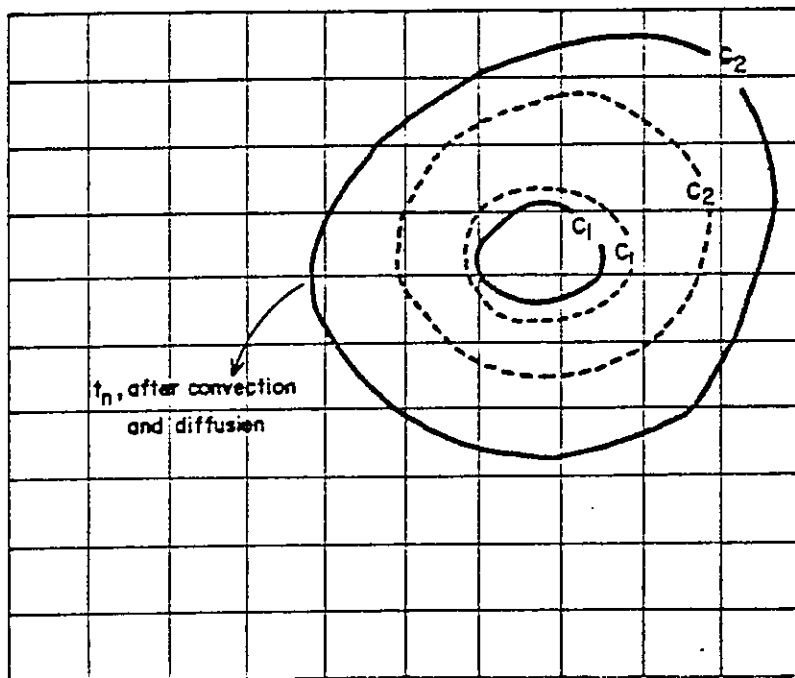


Fig. 3.1. Statement of the 2-D transport problem. Definition sketch



(a)



(b)

Fig. 3.2. General solution procedure for the reference Eulerian-Lagrangian method. Illustrative sketch

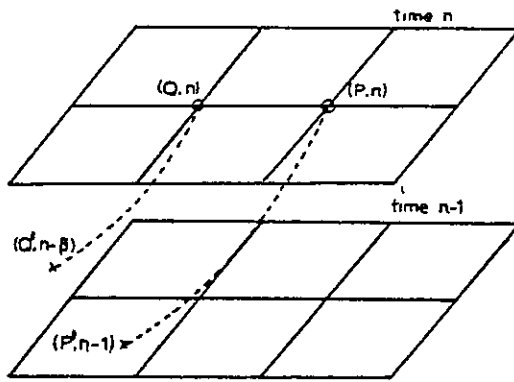


Fig. 3.3. Solution of the advection equation. Illustrative sketch

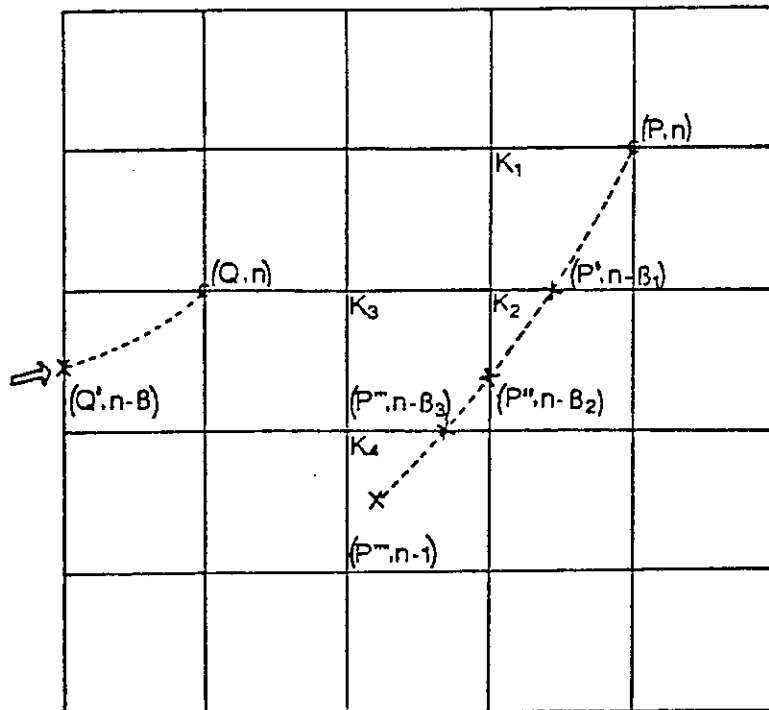


Fig. 3.4. Particle tracking. Illustrative sketch





Type of core element	Illustrative sketch
<p>Linear</p> <p>(2P-LI2, 2P-HI2, 4P-LR2, 6P-LR2, 8P-LR2, 4P-HL2, 6P-HL2, 8P-HL2)</p>	<p style="text-align: center;">Characteristic line</p> <p style="text-align: center;"> <math>\langle \text{core ele.} \rangle</math>  <math>\beta = Cu = u \cdot \Delta t / \Delta x</math>  <math>k = \text{int}(\beta)</math>  <math>\alpha</math> </p>
<p>Quadratic</p> <p>(3P-LI3, 5P-LR3, 5P-HL3, 7P-HL3)</p>	<p style="text-align: center;"> <math>\langle \text{core element} \rangle</math>  <math>\beta = Cu = u \cdot \Delta t / \Delta x</math>  <math>k = \text{int}(\beta) \text{ or } \text{int}(\beta) + 1</math>  <math>\alpha</math> </p>
<p>Cubic</p> <p>(4P-LI4)</p>	<p style="text-align: center;"> <math>\langle \text{core element} \rangle</math>  <math>\beta = Cu = u \cdot \Delta t / \Delta x</math>  <math>k = \text{int}(\beta)</math>  <math>\alpha = \frac{2}{3}(\beta - k - \frac{3}{2})</math> </p>

(a) General elementary mappings

Fig. 4.1. Definition of alternative interpolation schemes for the Backwards Method of Characteristics

Scheme	Reference sketch	Definition
2P-LI2		$f(\alpha) = \sum_{p=0}^1 \phi_p(\alpha) \cdot f_p$ $\phi_0(\alpha) = 1 - \alpha$ $\phi_1(\alpha) = \alpha$
3P-LI3		$f(\alpha) = \sum_{p=-1}^2 \phi_p(\alpha) \cdot f_p$ $\phi_{-1}(\alpha) = \frac{1}{2}(\alpha^2 - \alpha)$ $\phi_0(\alpha) = 1 - \alpha^2$ $\phi_1(\alpha) = \frac{1}{2}(\alpha^2 + \alpha)$
4P-LI4		$f(\alpha) = \sum_{p=-1}^3 \phi_p(\alpha) \cdot f_p$ $\phi_{-1}(\alpha) = \frac{1}{16}(-9\alpha^3 + 9\alpha^2 + \alpha - 1)$ $\phi_{1/3}(\alpha) = \frac{1}{16}(27\alpha^3 - 9\alpha^2 - 27\alpha + 9)$ $\phi_{-1/3}(\alpha) = \frac{1}{16}(-27\alpha^3 - 9\alpha^2 + 27\alpha + 9)$ $\phi_1(\alpha) = \frac{1}{16}(9\alpha^3 + 9\alpha^2 - \alpha - 1)$

(b) Definition of the interpolation schemes

Fig. 4.1 Cont.

Scheme	Reference sketch	Definition
4P-LR2		$f(\alpha) = \sum_{p=-1}^2 \phi_p(\alpha) \cdot f_p$ $\phi_{-1}(\alpha) = -\frac{1}{6}(\alpha^3 - 3\alpha^2 + 2\alpha)$ $\phi_0(\alpha) = \frac{1}{6}(3\alpha^3 - 6\alpha^2 - 3\alpha + 6)$ $\phi_1(\alpha) = -\frac{1}{6}(3\alpha^3 - 3\alpha^2 - 6\alpha)$ $\phi_2(\alpha) = \frac{1}{6}(\alpha^3 - \alpha)$
5P-LR3		$f(\alpha) = \sum_{p=-2}^2 \phi_p(\alpha) \cdot f_p$ $\phi_{-2}(\alpha) = \frac{1}{24}(\alpha^4 - 2\alpha^3 - \alpha^2 + 2\alpha)$ $\phi_{-1}(\alpha) = -\frac{1}{6}(\alpha^4 - \alpha^3 - 4\alpha^2 + 4\alpha)$ $\phi_0(\alpha) = \frac{1}{4}(\alpha^4 - 5\alpha^2 + 4)$ $\phi_1(\alpha) = -\frac{1}{6}(\alpha^4 + \alpha^3 - 4\alpha^2 - 4\alpha)$ $\phi_2(\alpha) = \frac{1}{24}(\alpha^4 + 2\alpha^3 - \alpha^2 - 2\alpha)$
6P-LR2		$f(\alpha) = \sum_{p=-2}^3 \phi_p(\alpha) \cdot f_p$ $\phi_{-2}(\alpha) = -\frac{1}{120} \alpha(\alpha^2-1)(\alpha-2)(\alpha-3)$ $\phi_{-1}(\alpha) = \frac{1}{24} \alpha(\alpha-1)(\alpha^2-4)(\alpha-3)$ $\phi_0(\alpha) = -\frac{1}{12} (\alpha^2-1)(\alpha^2-4)(\alpha-3)$ $\phi_1(\alpha) = \frac{1}{12} \alpha(\alpha+1)(\alpha^2-4)(\alpha-3)$ $\phi_2(\alpha) = -\frac{1}{24} \alpha(\alpha^2-1)(\alpha+2)(\alpha-3)$ $\phi_3(\alpha) = \frac{1}{120} \alpha(\alpha^2-1)(\alpha^2-4)$

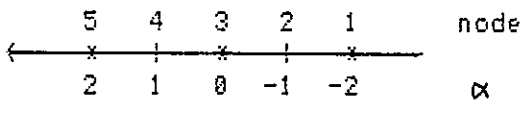
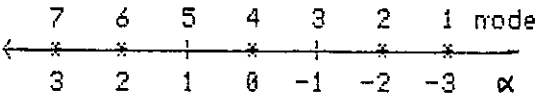
(b) Definition of the interpolation schemes (cont.)

Fig. 4.1 Cont.

Scheme	Reference sketch	Definition
8P-LR2		$f(\alpha) = \sum_{p=-3}^4 \phi_p(\alpha) \cdot f_p$ $\phi_{-3}(\alpha) = -\frac{\alpha(\alpha^2-1)(\alpha^2-4)(\alpha-3)(\alpha-4)}{5040}$ $\phi_{-2}(\alpha) = \frac{\alpha(\alpha^2-1)(\alpha-2)(\alpha^2-9)(\alpha-4)}{720}$ $\phi_{-1}(\alpha) = -\frac{\alpha(\alpha-1)(\alpha^2-4)(\alpha^2-9)(\alpha-4)}{240}$ $\phi_0(\alpha) = \frac{(\alpha^2-1)(\alpha^2-4)(\alpha^2-9)(\alpha-4)}{144}$ $\phi_1(\alpha) = \frac{\alpha(\alpha+1)(\alpha^2-4)(\alpha^2-9)(\alpha-4)}{144}$ $\phi_2(\alpha) = \frac{\alpha(\alpha^2-1)(\alpha+2)(\alpha^2-9)(\alpha-4)}{240}$ $\phi_3(\alpha) = -\frac{\alpha(\alpha^2-1)(\alpha^2-4)(\alpha+3)(\alpha-4)}{720}$ $\phi_4(\alpha) = \frac{\alpha(\alpha^2-1)(\alpha^2-4)(\alpha^2-9)}{5040}$
2P-HI2		$f(\alpha) = \sum_{p=0}^1 \phi_p(\alpha) \cdot f_p + \psi_p(\alpha) \cdot \left. \frac{\partial f}{\partial \alpha} \right _p$ $\phi_0(\alpha) = \frac{1}{4}(\alpha^3 - 3\alpha + 2)$ $\phi_1(\alpha) = \frac{1}{4}(-\alpha^3 + 3\alpha + 2)$ $\psi_0(\alpha) = \frac{1}{4}(\alpha^3 - \alpha^2 - \alpha + 1)$ $\psi_1(\alpha) = \frac{1}{4}(\alpha^3 + \alpha^2 - \alpha - 1)$
4P-HL2		$f(\alpha) = \sum_{p=-1}^2 \phi_p(\alpha) \cdot f_p$ $\phi_{-1}(\alpha) = \frac{1}{4}(\alpha^2 - \alpha)$ $\phi_0(\alpha) = -\frac{1}{4}(\alpha^2 + 3\alpha - 4)$ $\phi_1(\alpha) = -\frac{1}{4}(\alpha^2 - 5\alpha)$ $\phi_2(\alpha) = \frac{1}{4}(\alpha^2 - \alpha)$

(b) Definition of the interpolation schemes (cont.)

Fig. 4.1 Cont.

Scheme	Reference sketch	Definition
5P-HL3		$f(\alpha) = \sum_{p=-2}^2 \phi_p(\alpha) \cdot f_p$ $\phi_2(\alpha) = -\frac{1}{12} \alpha(\alpha^2 - 1)$ $\phi_{-1}(\alpha) = \frac{1}{6} (\alpha^3 + 3\alpha^2 - 4\alpha)$ $\phi_0(\alpha) = 1 - \alpha^2$ $\phi_1(\alpha) = -\frac{1}{6} (\alpha^3 - 3\alpha^2 + 4\alpha)$ $\phi_2(\alpha) = \frac{1}{12} \alpha(\alpha^2 - 1)$
7P-HL3	 <p data-bbox="399 1377 798 1444"><math>\tau = 0.91</math> was used, after empirical optimization</p>	$f(\alpha) = \sum_{p=-3}^3 \phi_p(\alpha) \cdot f_p$ $\phi_3(\alpha) = \frac{\tau-1}{8} (\alpha^3 - \alpha^2 - \alpha + 1)$ $\phi_2(\alpha) = \frac{1-\tau}{2} (\alpha^3 - \alpha^2 - \alpha + 1)$ $\phi_{-1}(\alpha) = \frac{1}{8} \{ 5(1-\tau)\alpha^3 + (7\tau-3)\alpha^2 + (5\tau-9)\alpha + 7(1-\tau) \}$ $\phi_0(\alpha) = \tau(1 - \alpha^2)$ $\phi_1(\alpha) = \frac{1}{8} \{ 5(\tau-1)\alpha^3 + (7\tau-3)\alpha^2 + (9-5\tau)\alpha + 7(1-\tau) \}$ $\phi_2(\alpha) = \frac{\tau-1}{2} (\alpha^3 + \alpha^2 - \alpha - 1)$ $\phi_3(\alpha) = -\frac{1-\tau}{8} (\alpha^3 + \alpha^2 - \alpha - 1)$

(b) Definition of the interpolation schemes (cont.)

Fig. 4.1 Cont.

Scheme	Reference sketch	Definition
6P-PL2		$f(\alpha) = \sum_{p=-2}^3 \phi_p(\alpha) \cdot f_p$ $\phi_2(x) = 0.01806 x^3 - 0.09245 x^2 + 0.07439 x$ $\phi_1(x) = -0.2570 x^3 + 0.8236 x^2 - 0.5667 x$ $\phi_0(x) = 0.6806 x^3 - 1.394 x^2 - 0.2869 x + 1$ $\phi_{-1}(x) = -0.6806 x^3 + 0.6480 x^2 + 1.033 x$ $\phi_{-2}(x) = 0.2570 x^3 + 0.05276 x^2 - 0.3097 x$ $\phi_{-3}(x) = -0.01806 x^3 - 0.03828 x^2 + 0.05633 x$
8P-PL2		$f(\alpha) = \sum_{p=-3}^4 \phi_p(\alpha) \cdot f_p$ $\phi_{-3}(x) = \phi_4'(x) = \frac{1}{66} x^2 - \frac{1}{66} x$ $\phi_{-2}(x) = \frac{1}{54} x^3 - \frac{115}{792} x^2 + \frac{301}{2376} x$ $\phi_{-1}(x) = -\frac{7}{27} x^3 + \frac{713}{792} x^2 - \frac{1523}{2376} x$ $\phi_0(x) = \frac{37}{54} x^3 - \frac{569}{396} x^2 - \frac{295}{1188} x + 1$ $\phi_1(x) = -\frac{37}{54} x^3 + \frac{245}{396} x^2 + \frac{1267}{1188} x$ $\phi_2(x) = \frac{7}{27} x^3 + \frac{97}{792} x^2 - \frac{907}{2376} x$ $\phi_3(x) = -\frac{1}{54} x^3 - \frac{71}{792} x^2 + \frac{257}{2376} x$

(b) Definition of the interpolation schemes (cont.)

Fig. 4.1 Cont.

Scheme	Generation procedure
4P-HL2	<p data-bbox="539 369 925 403"><u>Basic Hermite polynomial</u></p> $c_j^{n+1} = r(\alpha) c_{j-k}^n + r(\alpha) c_{j-k-1}^n + s(\alpha) \left. \frac{dc}{dx} \right _{j-k}^n + s(\alpha) \left. \frac{dc}{dx} \right _{j-k-1}^n$ <p data-bbox="550 593 630 627">with:</p> $r(\alpha) = 2\alpha^3 - 3\alpha^2 + 1$ $r(\alpha) = -2\alpha^3 + 3\alpha^2$ $s(\alpha) = \alpha^3 - 2\alpha^2 + \alpha$ $s(\alpha) = \alpha^3 - \alpha^2$ <p data-bbox="539 907 949 940"><u>Estimation of derivatives</u></p> $\left. \frac{dc}{dx} \right _{j-k}^n = \frac{1}{2} \left\{ \left. \frac{dP_1(\alpha)}{d\alpha} \right _{z=0} + \left. \frac{dP_2(\alpha)}{d\alpha} \right _{z=0} \right\}$ $\left. \frac{dc}{dx} \right _{j-k-1}^n = \frac{1}{2} \left\{ \left. \frac{dP_1(\alpha)}{d\alpha} \right _{z=1} + \left. \frac{dP_2(\alpha)}{d\alpha} \right _{z=1} \right\}$ <p data-bbox="550 1288 646 1321">where,</p> $P_1(\alpha) = \frac{1}{2} (\alpha^2 + \alpha) c_{j-k-1}^n + (1 - \alpha^2) c_{j-k}^n + \frac{1}{2} (\alpha^2 - \alpha) c_{j-k+1}^n$ $P_2(\alpha) = \frac{1}{2} \alpha (\alpha - 1) c_{j-k-2}^n - \alpha (\alpha - 2) c_{j-k-1}^n + \frac{1}{2} (\alpha - 1) (\alpha - 2) c_{j-k}^n$

(c) Generation procedure for HL schemes

Fig. 4.1 Cont.



Scheme	Generation procedure
SP-HL3	<p data-bbox="494 414 885 448">Basic Hermite polynomial</p> $c_j^{n+1} = r_{-1}(\alpha) c_{j-k+1}^n + r_1(\alpha) c_{j-k-1}^n + s_{-1}(\alpha) \left. \frac{dc}{d\alpha} \right _{j-k+1}^n + s_1(\alpha) \left. \frac{dc}{d\alpha} \right _{j-k-1}^n$ <p data-bbox="494 638 590 672">with:</p> $r_{-1}(\alpha) = 0.25 (\alpha^3 - 3\alpha + 2)$ $r_1(\alpha) = 0.25 (-\alpha^3 + 3\alpha + 2)$ $s_{-1}(\alpha) = 0.25 (\alpha^3 - \alpha^2 - \alpha + 1)$ $s_1(\alpha) = 0.25 (\alpha^3 + \alpha^2 - \alpha - 1)$ <p data-bbox="494 952 901 985">Estimation of derivatives</p> $\left. \frac{dc}{d\alpha} \right _{j-k+1}^n = \frac{1}{2} \left\{ \left. \frac{dP_1(\alpha)}{d\alpha} \right _{\alpha=-1} + \left. \frac{dP_2(\alpha)}{d\alpha} \right _{\alpha=-1} \right\}$ $\left. \frac{dc}{d\alpha} \right _{j-k-1}^n = \frac{1}{2} \left\{ \left. \frac{dP_1(\alpha)}{d\alpha} \right _{\alpha=1} + \left. \frac{dP_2(\alpha)}{d\alpha} \right _{\alpha=1} \right\}$ <p data-bbox="494 1332 606 1366">where,</p> $P_1(\alpha) = -\frac{1}{6} (\alpha^3 - 3\alpha^2 + 2\alpha) c_{j-k+1} + \frac{1}{2} (\alpha^3 - 2\alpha^2 - \alpha + 2) c_{j-k} - \frac{1}{2} (\alpha^3 - \alpha^2 - 2\alpha) c_{j-k-1} + \frac{1}{6} (\alpha^3 - \alpha) c_{j-k-2}$ $P_2(\alpha) = -\frac{1}{6} (\alpha^3 - \alpha) c_{j-k+2} + \frac{1}{2} (\alpha^3 + \alpha^2 - 2\alpha) c_{j-k+1} + \frac{1}{2} (-\alpha^3 - 2\alpha^2 + \alpha + 2) c_{j-k} + \frac{1}{6} (\alpha^3 + 3\alpha^2 + 2\alpha) c_{j-k-1}$

(c) Generation procedure for HL schemes (cont.)

Fig. 4.1 Cont.

Scheme	Generation procedure
7P-HL3	<p data-bbox="517 443 906 477">Basic Hermite polynomial</p> $c_j^{n+1} = r_{-1}(\alpha) c_{j-k+1}^n + r_1(\alpha) c_{j-k-1}^n + s_{-1}(\alpha) \left. \frac{dc}{dx} \right _{z=-1}^{j-k+1} + s_1(\alpha) \left. \frac{dc}{dx} \right _{z=-1}^{j-k-1}$ <p data-bbox="528 667 612 696">with:</p> $r_1(\alpha) = 0.25 (\alpha^3 - 3\alpha + 2)$ $r_2(\alpha) = 0.25 (-\alpha^3 + 3\alpha + 2)$ $s_1(\alpha) = 0.25 (\alpha^3 - \alpha^2 - \alpha + 1)$ $s_2(\alpha) = 0.25 (\alpha^3 + \alpha^2 - \alpha - 1)$ <p data-bbox="512 987 922 1021">Estimation of derivatives</p> $\left. \frac{dc}{dx} \right _{z=-1}^{j-k+1} = \tau \left. \frac{dP_2(\alpha)}{d\alpha} \right _{z=-1} + (1-\tau) \left. \frac{dP_1(\alpha)}{d\alpha} \right _{z=-1}$ $\left. \frac{dc}{dx} \right _{z=-1}^{j-k-1} = \tau \left. \frac{dP_2(\alpha)}{d\alpha} \right _{z=1} + (1-\tau) \left. \frac{dP_3(\alpha)}{d\alpha} \right _{z=1}$ <p data-bbox="523 1368 624 1402">where,</p> $P_1(\alpha) = \frac{(\alpha+2)(\alpha+1)}{2} c_{j-k+3} - (\alpha+3)(\alpha+1) c_{j-k+2} + \frac{(\alpha+3)(\alpha+2)}{2} c_{j-k+1}$ $P_2(\alpha) = \frac{\alpha(\alpha-1)}{2} c_{j-k+1} - (\alpha+1)(\alpha-1) c_{j-k} + \frac{\alpha(\alpha+1)}{2} c_{j-k-1}$ $P_3(\alpha) = \frac{(\alpha-2)(\alpha-3)}{2} c_{j-k-1} - (\alpha-1)(\alpha-3) c_{j-k-2} + \frac{(\alpha-1)(\alpha-2)}{2} c_{j-k-3}$

(c) Generation procedure for HL schemes (cont.)

Fig. 4.1 Cont.



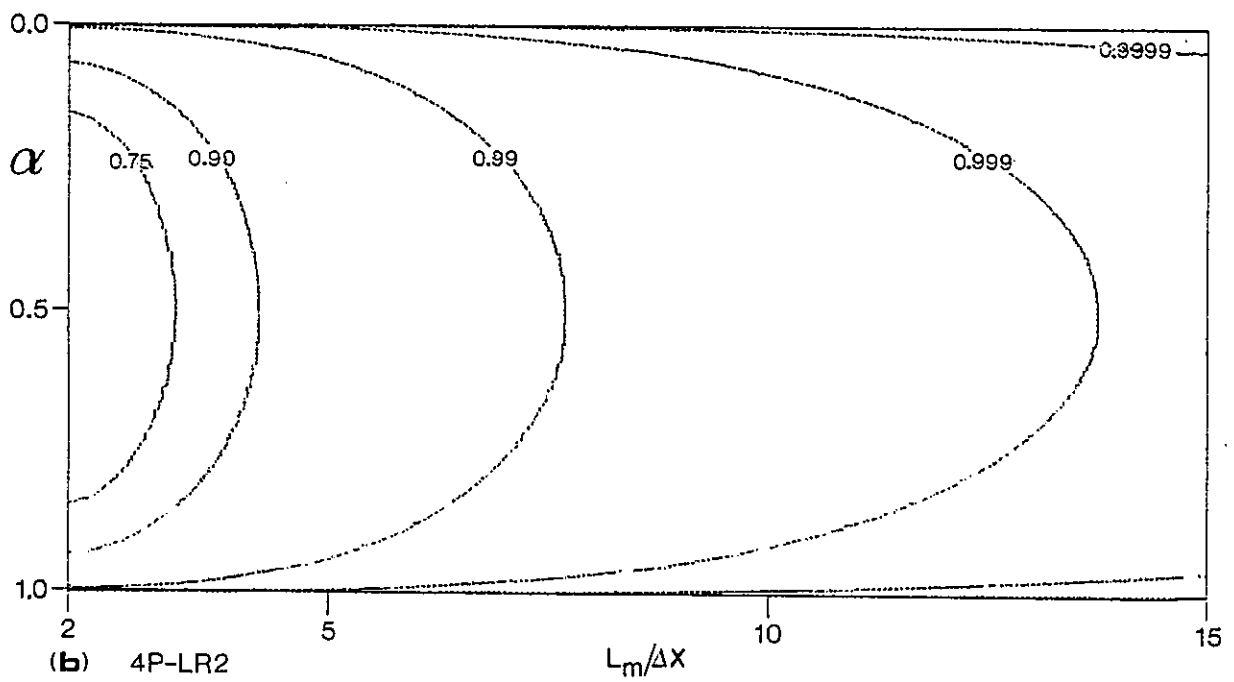
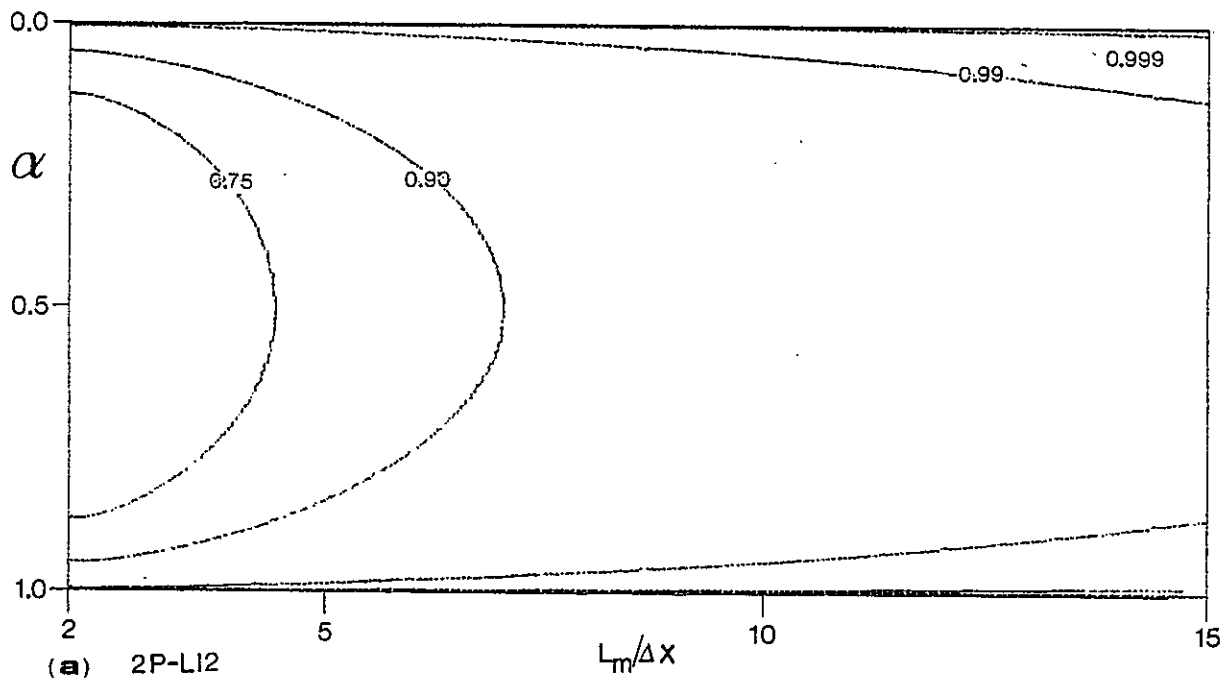


Fig. 4.2. Amplifying factors as a function of  $\alpha$  and  $L_m/\Delta x$  (first time step)

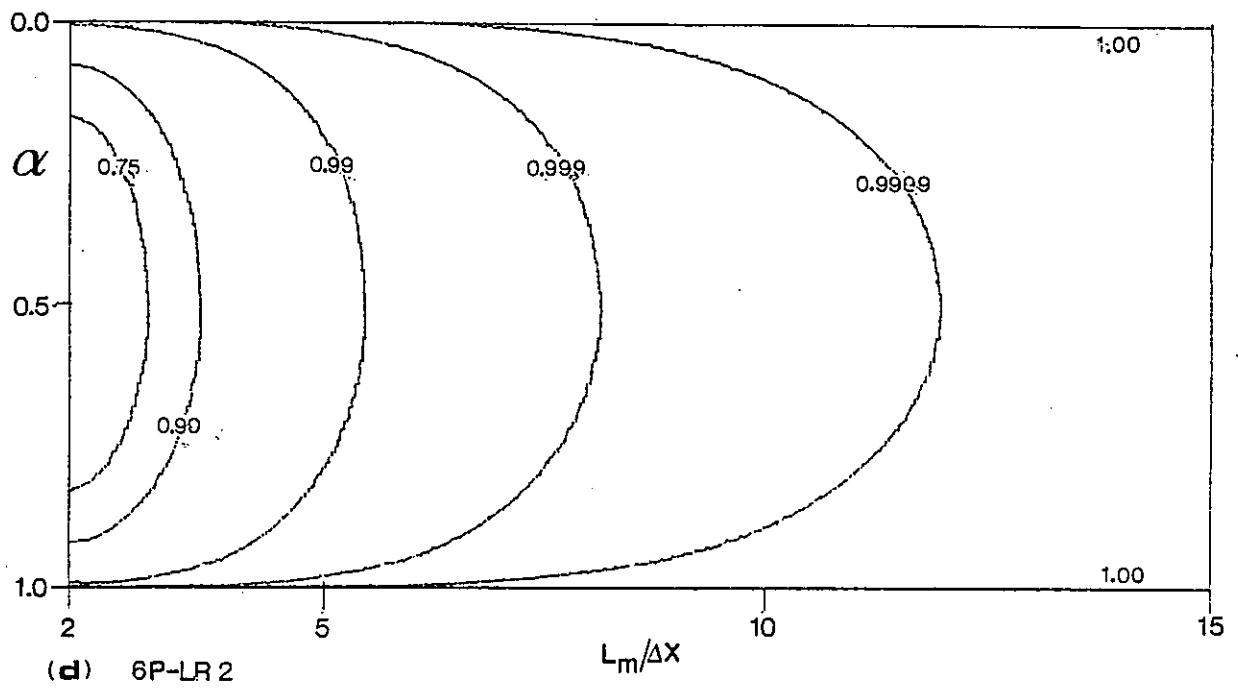
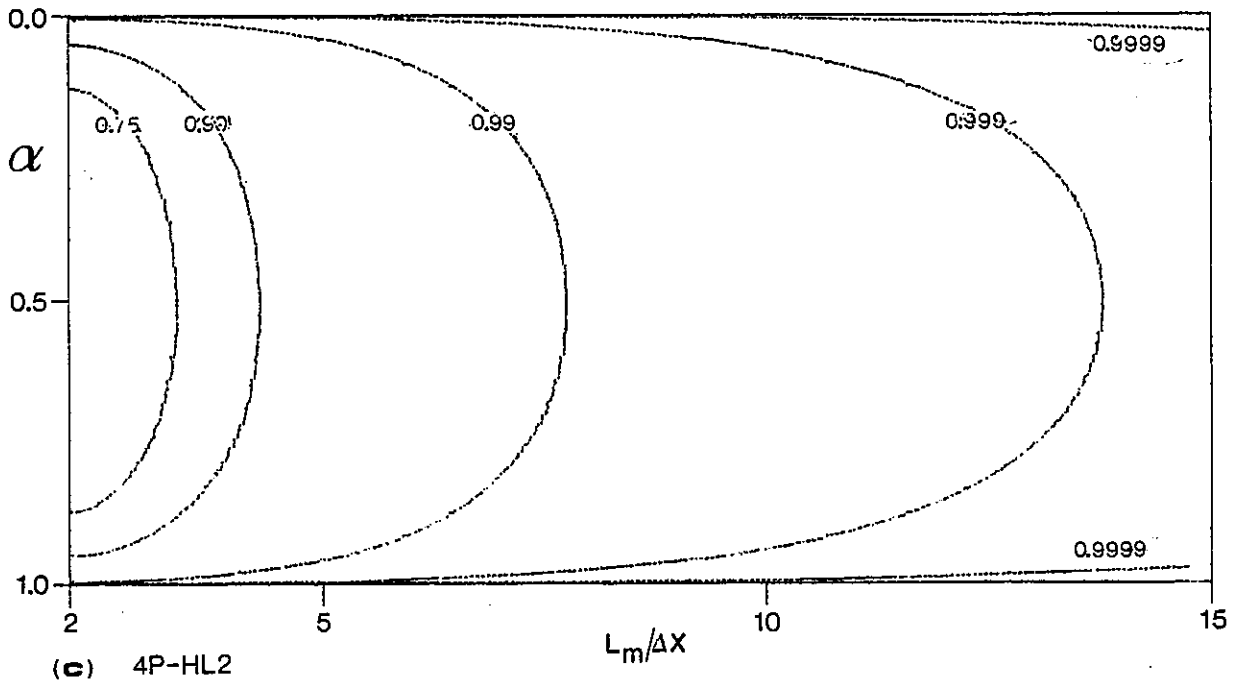


Fig. 4.2. Cont.

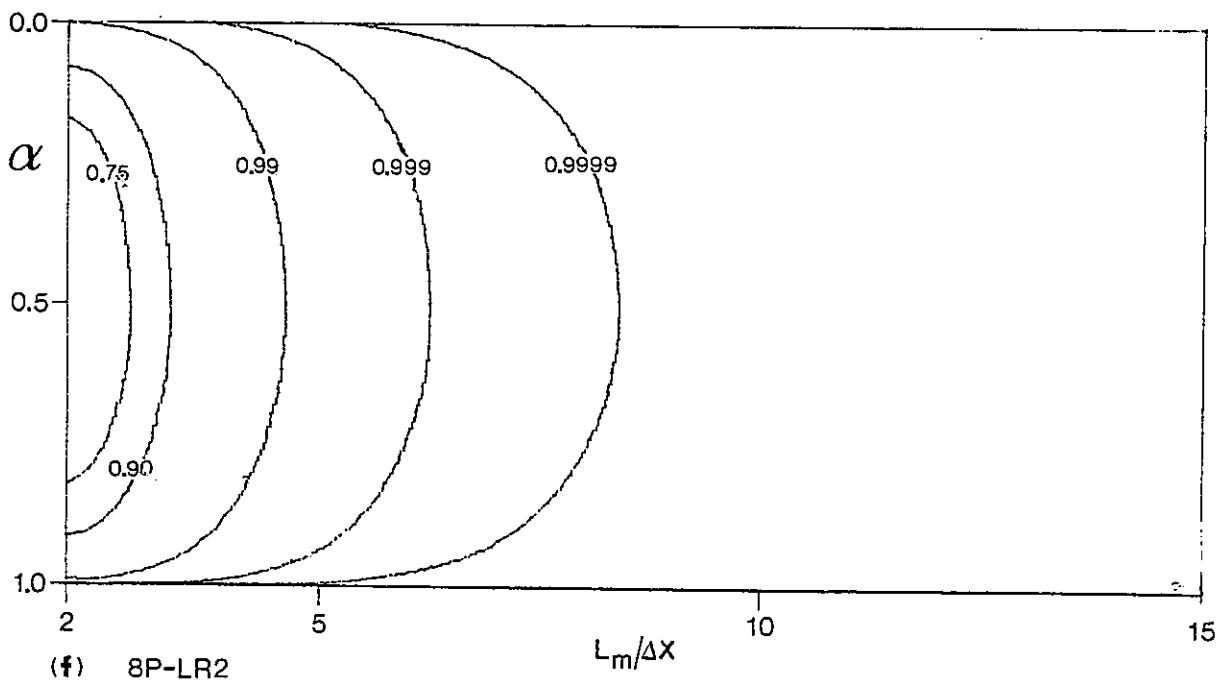
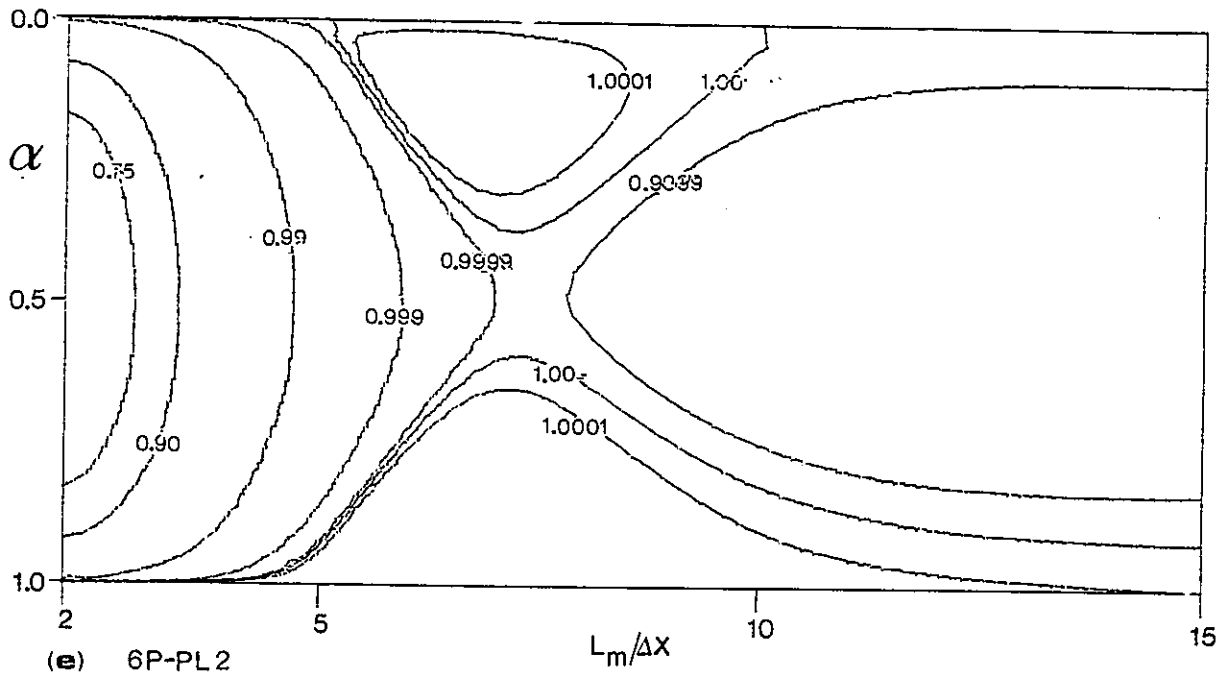


Fig. 4.2. Cont.

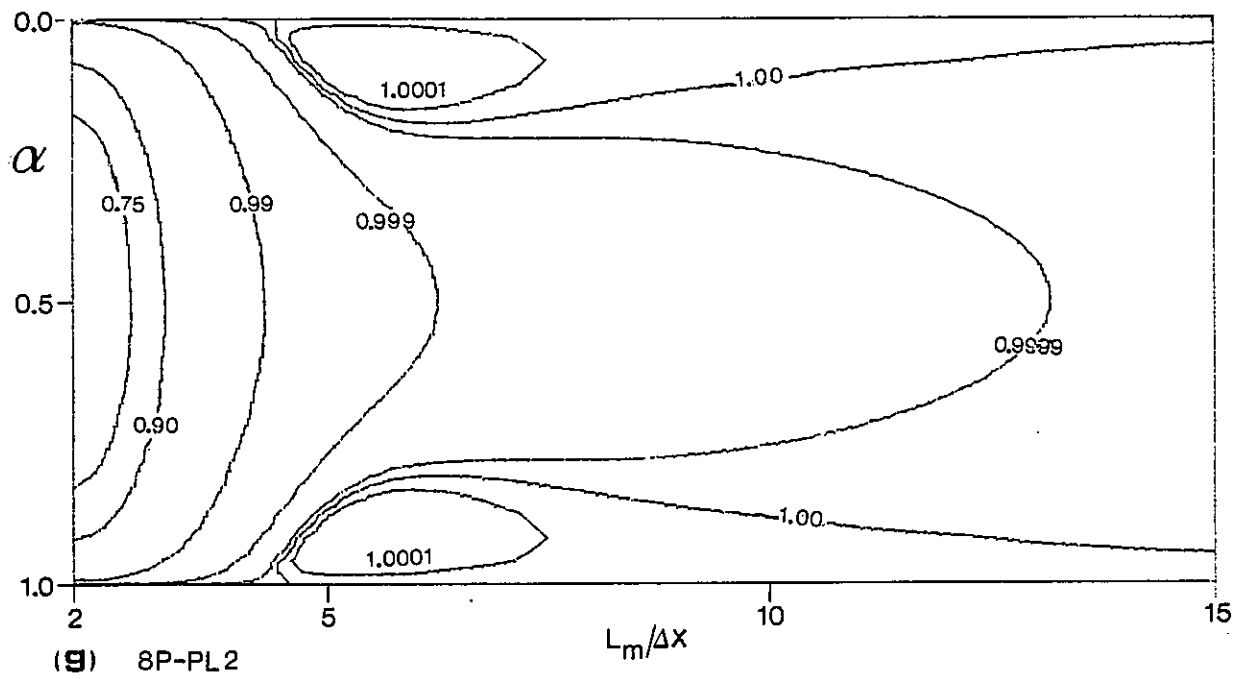


Fig. 4.2. Cont.

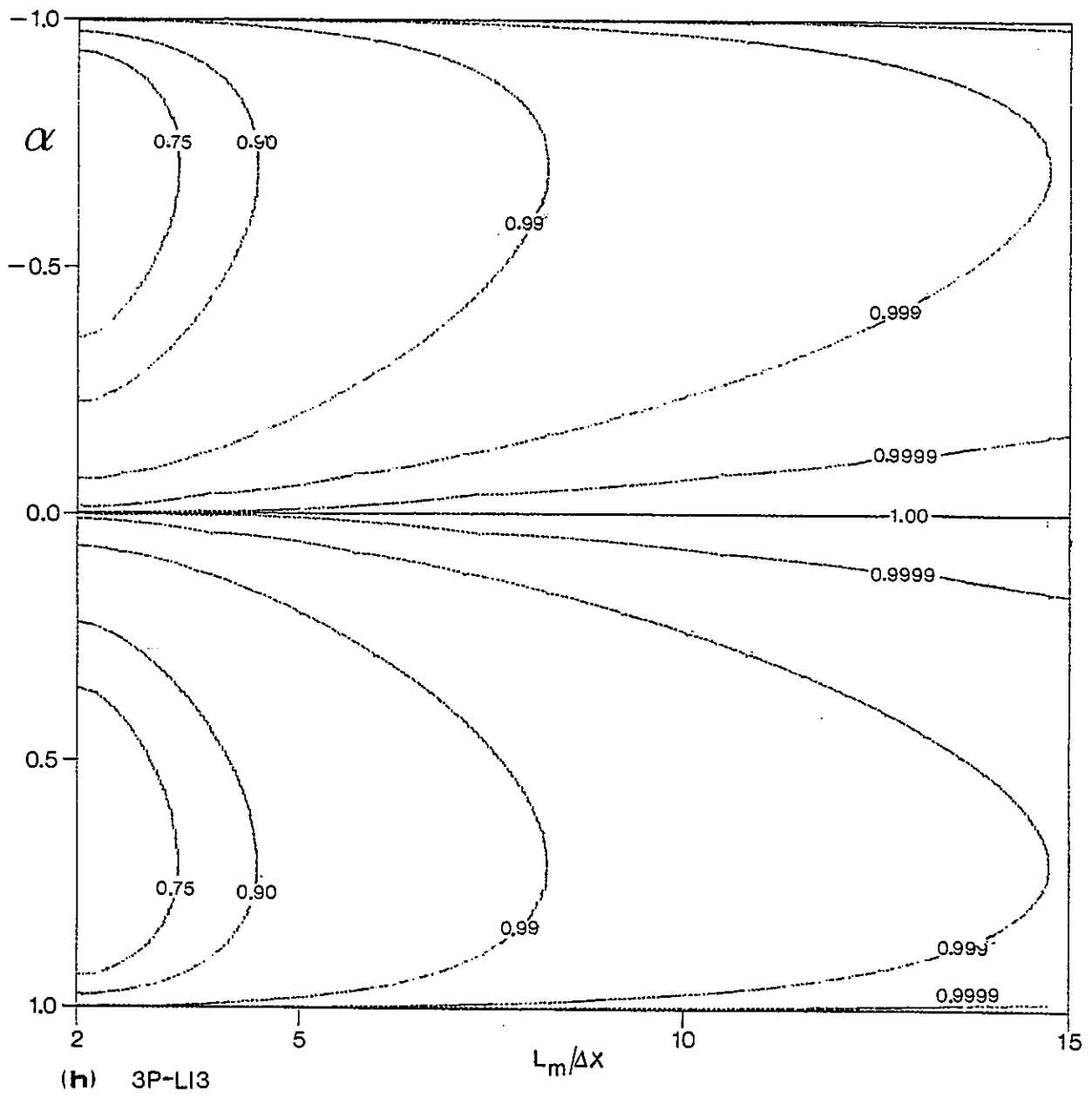


Fig. 4.2. Cont.



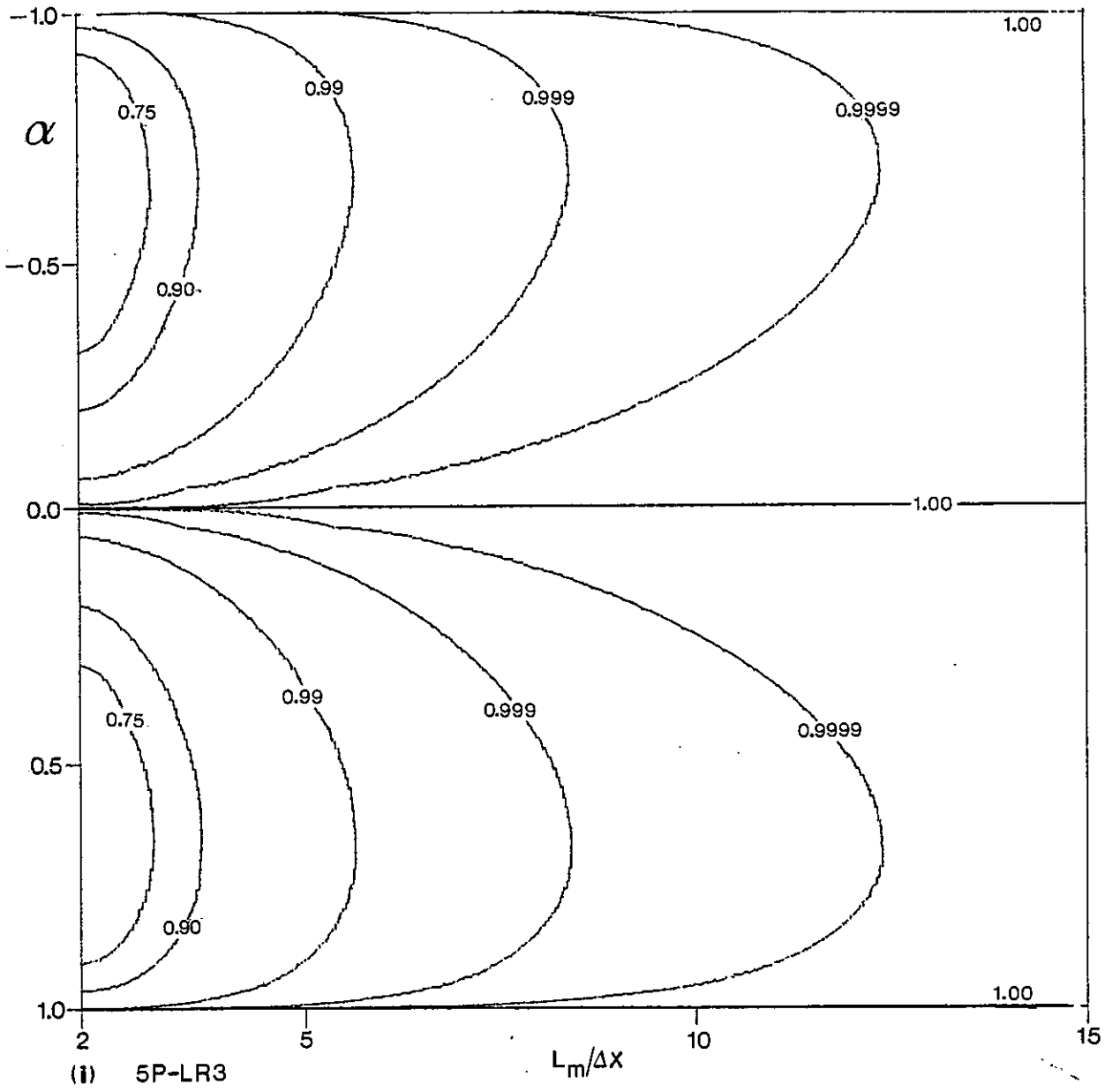


Fig. 4.2. Cont.

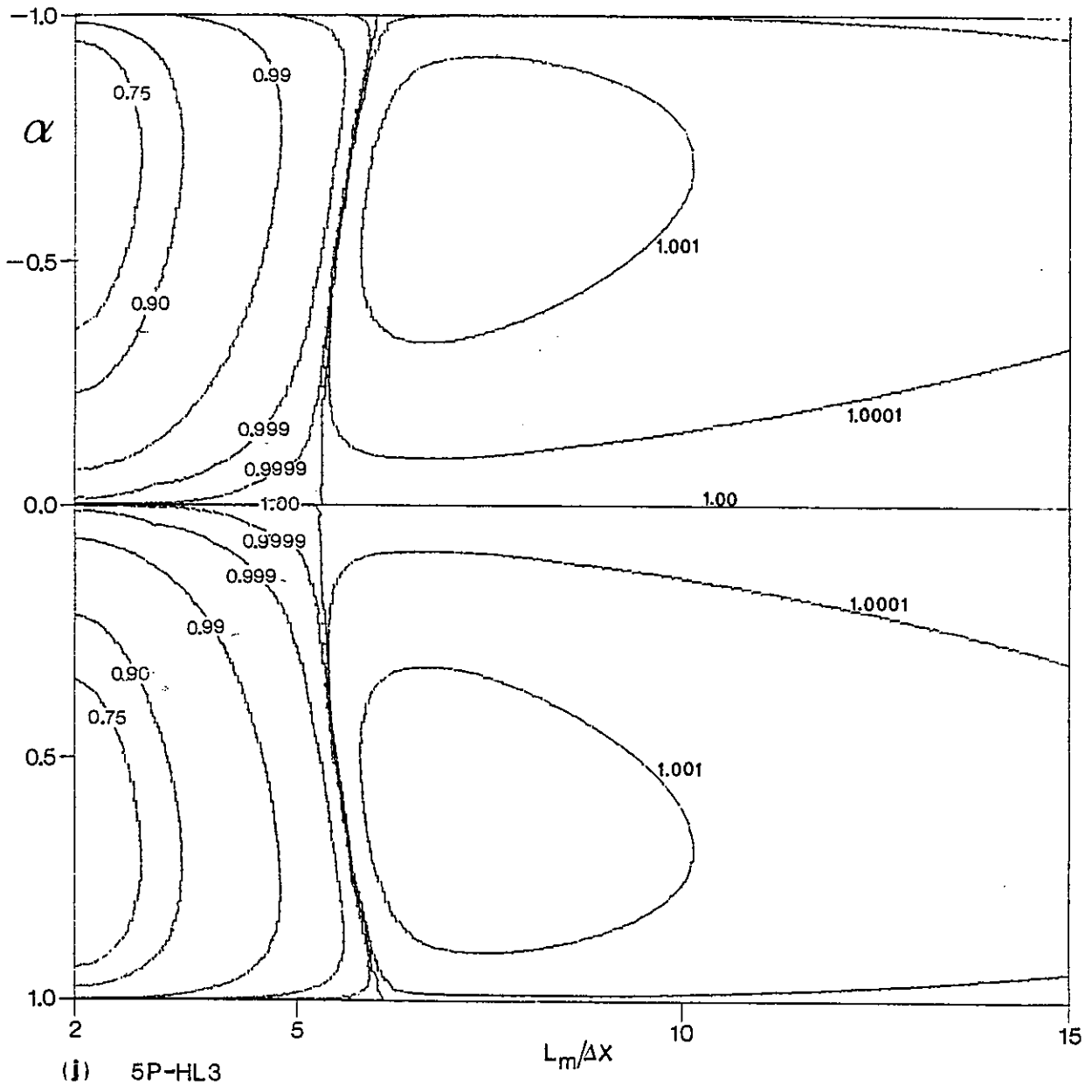


Fig. 4.2. Cont.

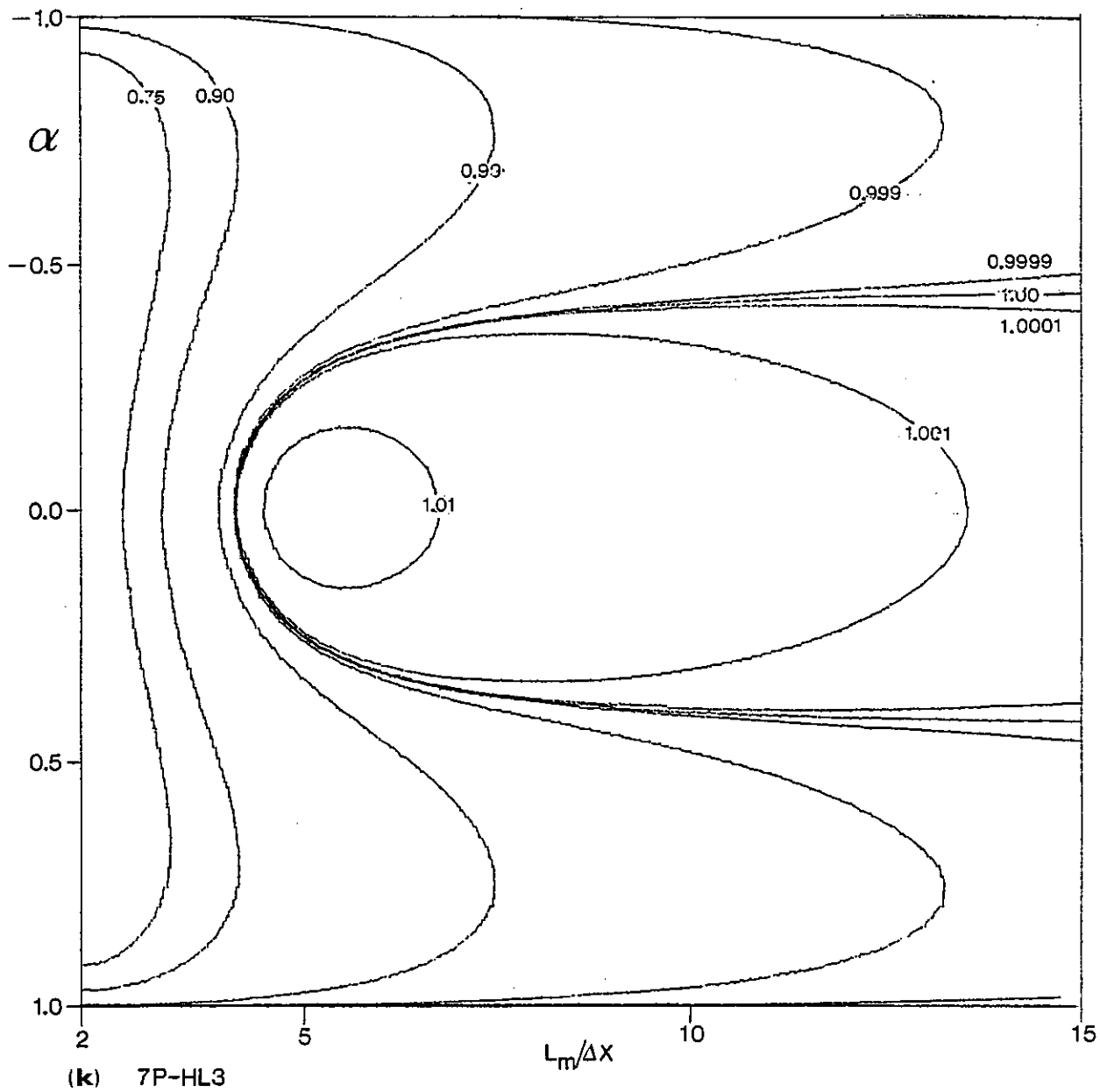


Fig. 4.2. Cont.

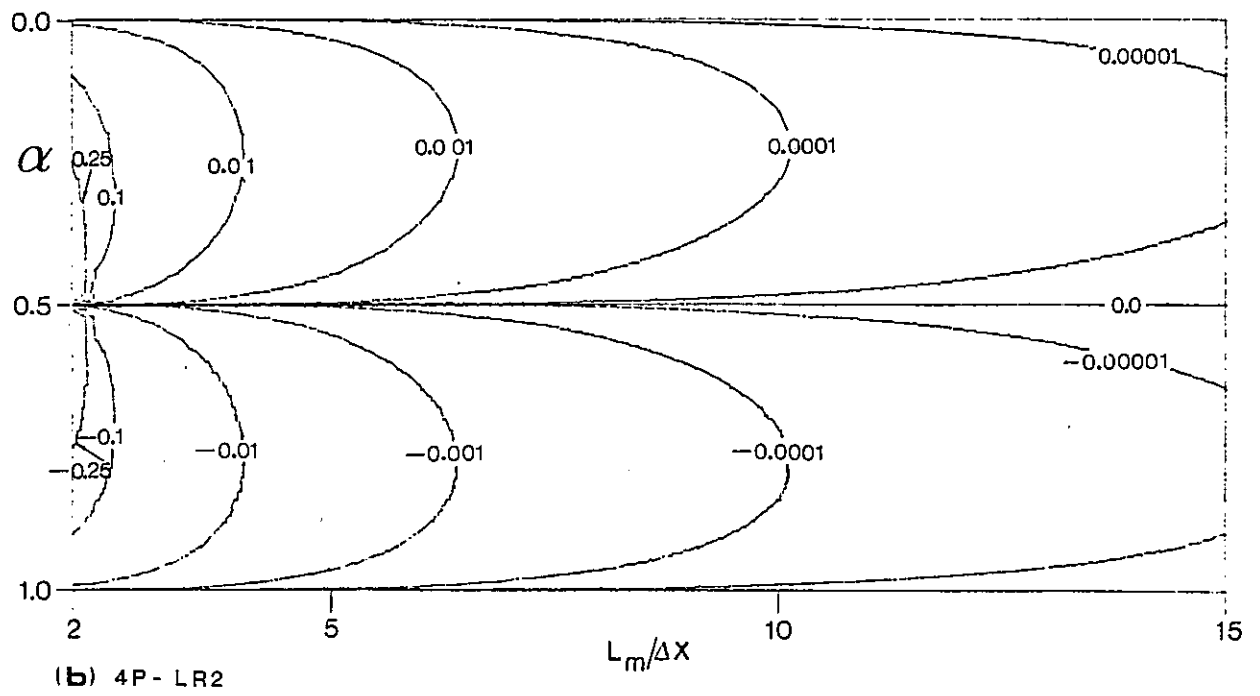
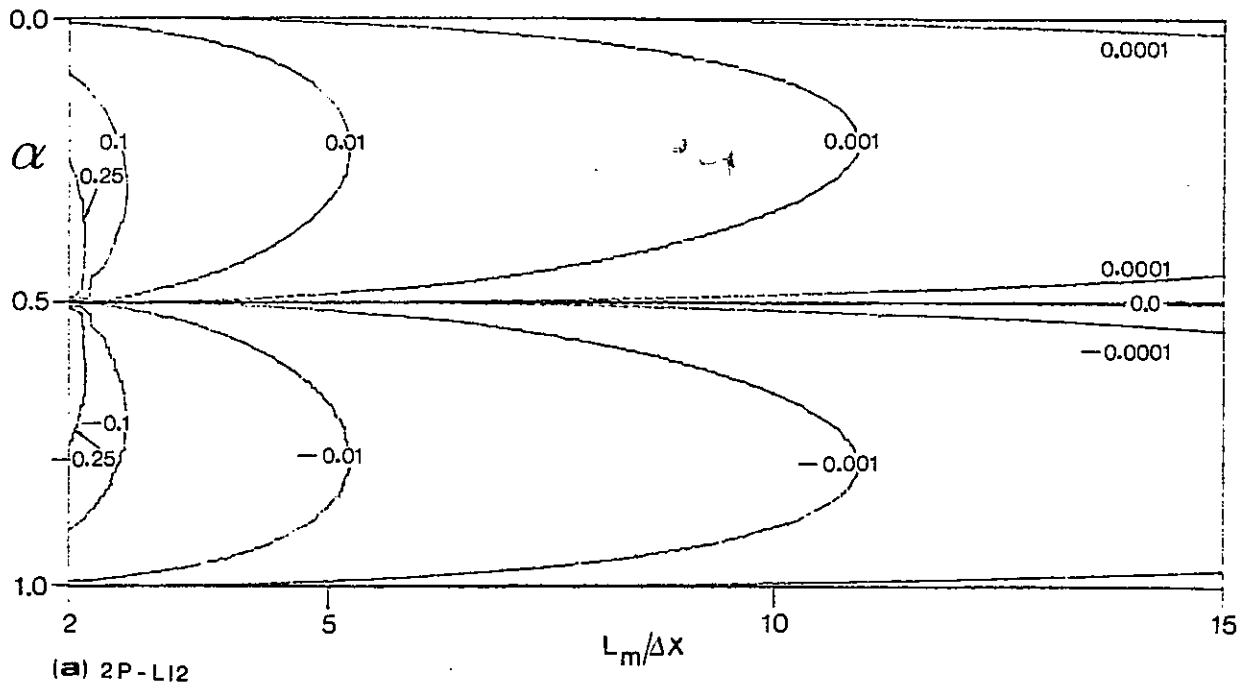


Fig. 4.3. Phase errors as a function of  $\alpha$  and  $L_m/\Delta x$  (first time step)

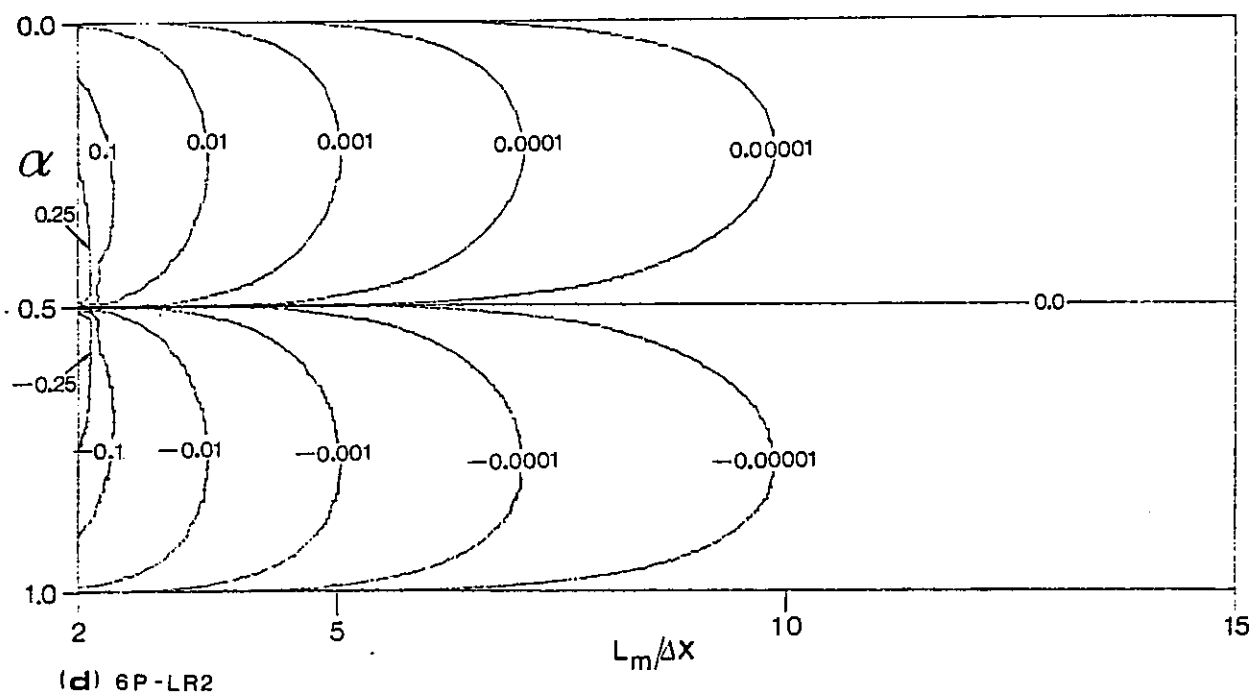
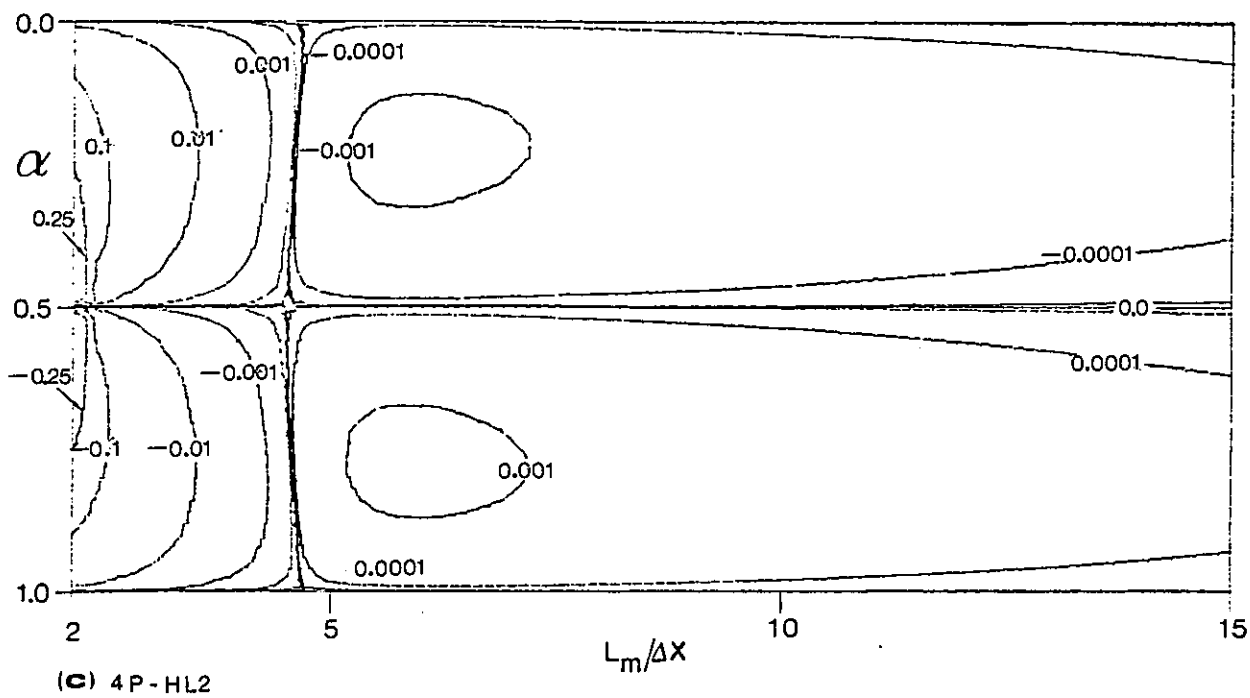


Fig. 4.3. Cont.

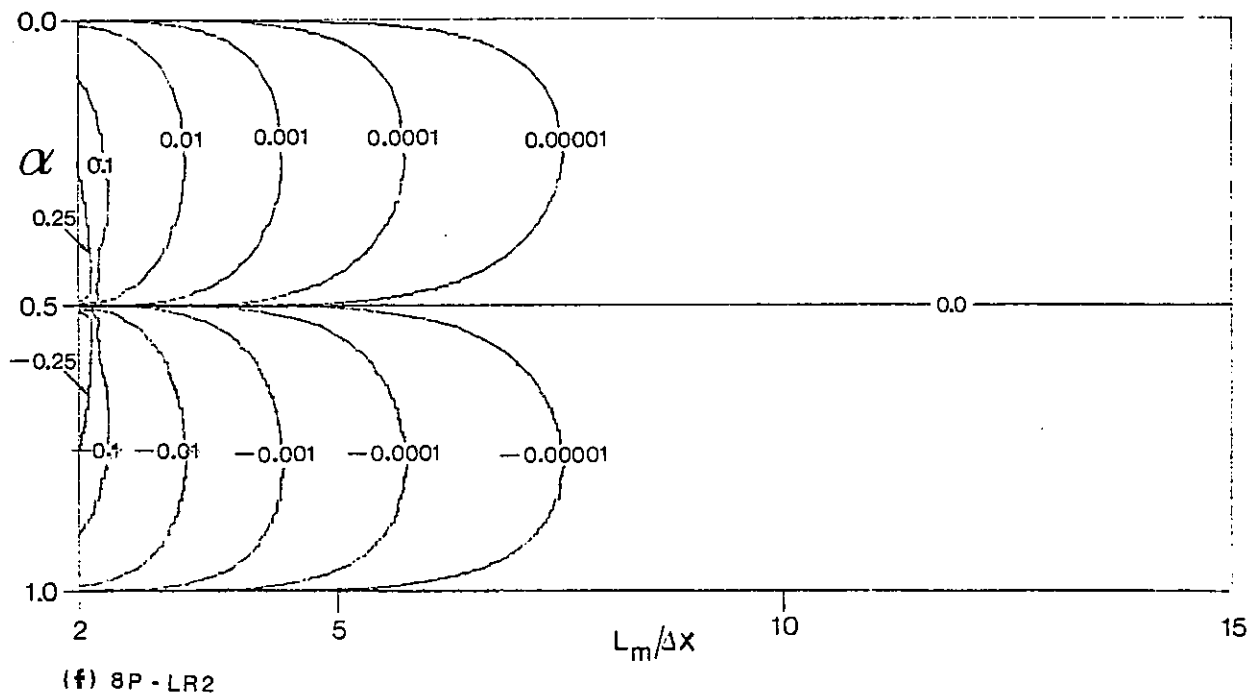
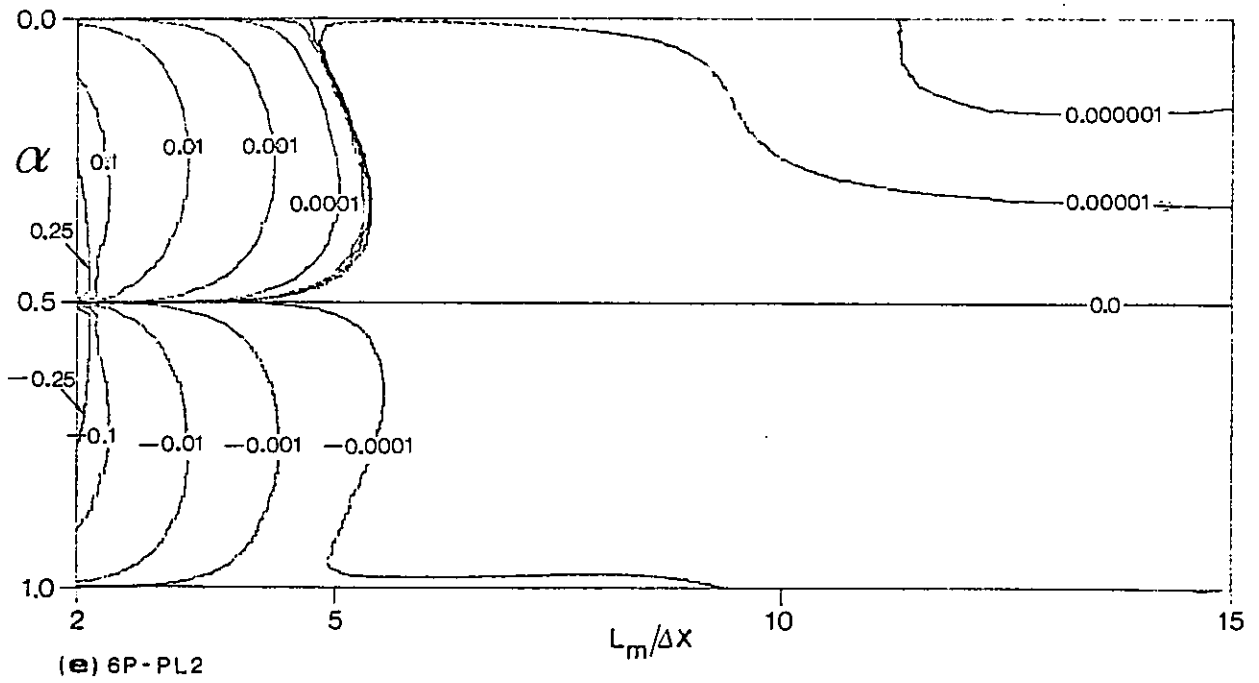


Fig. 4.3. Cont.

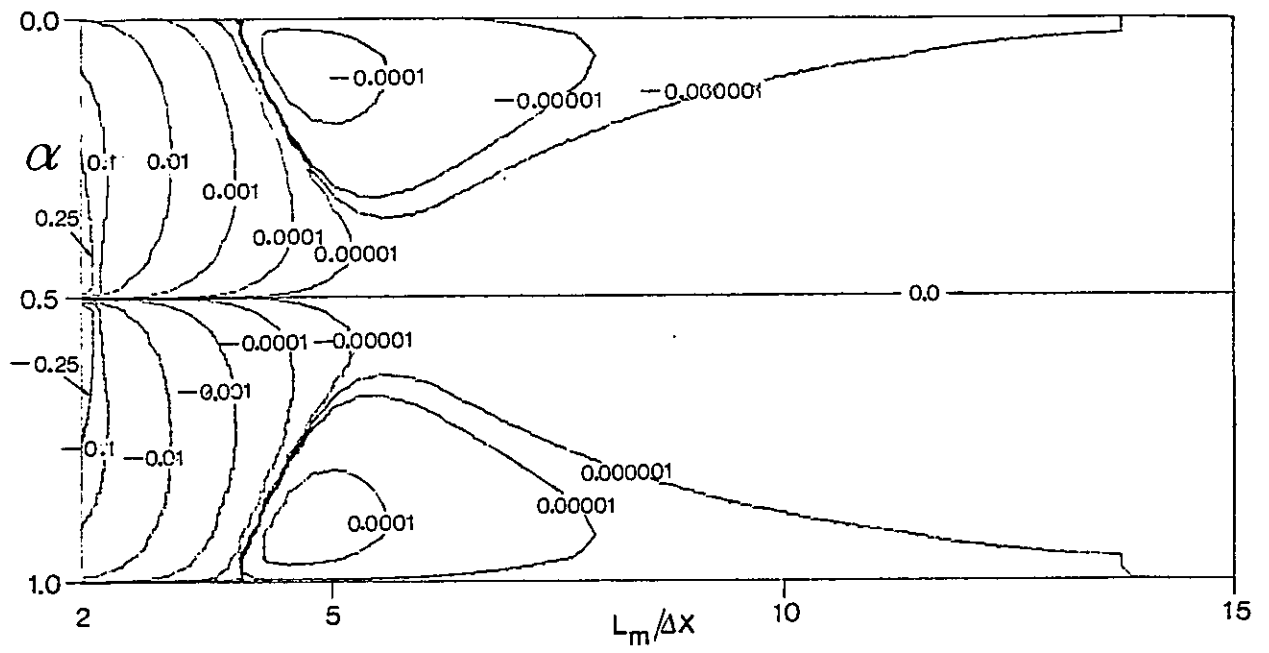


Fig. 4.3. Cont.

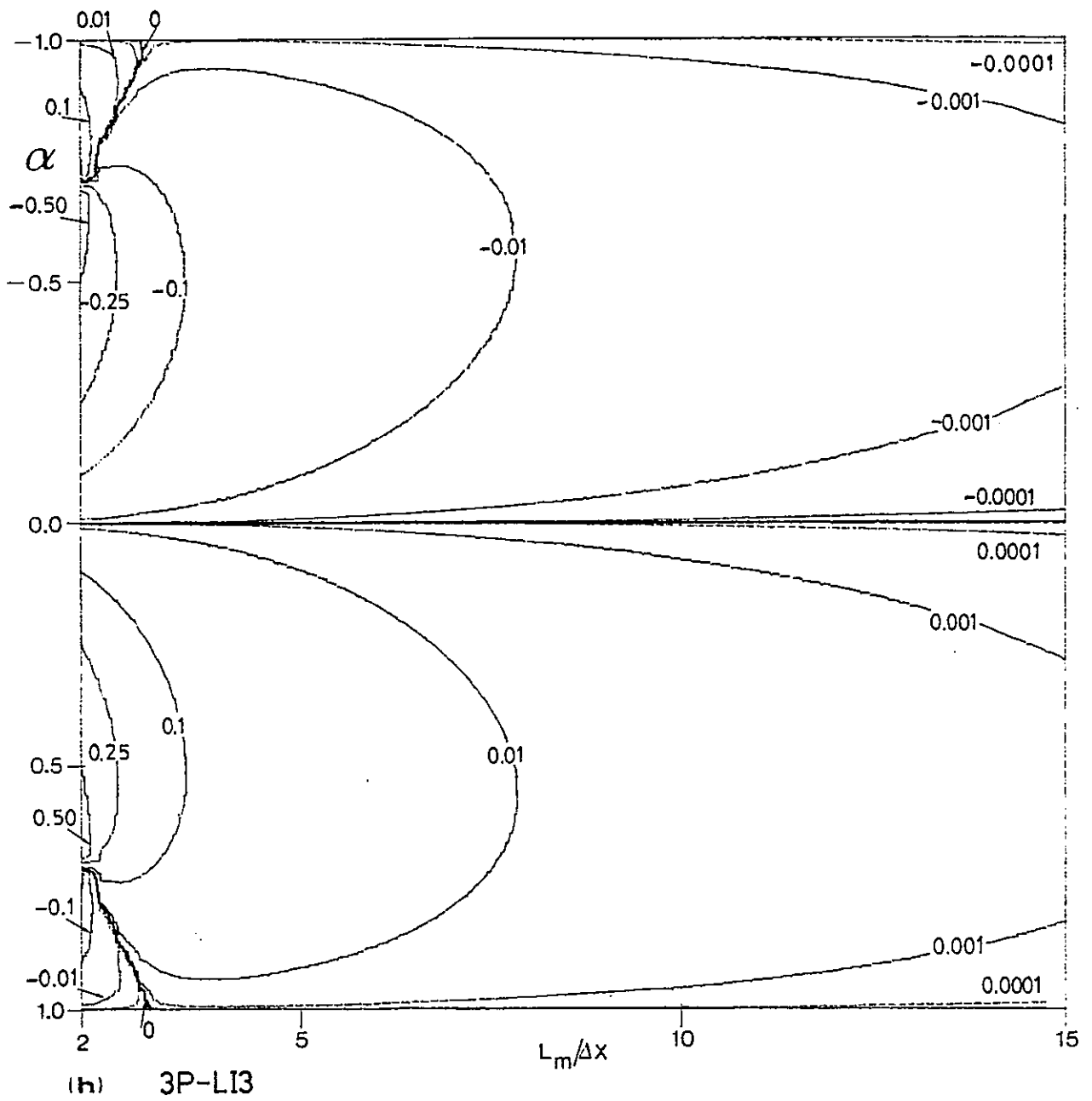


Fig. 4.3. Cont.



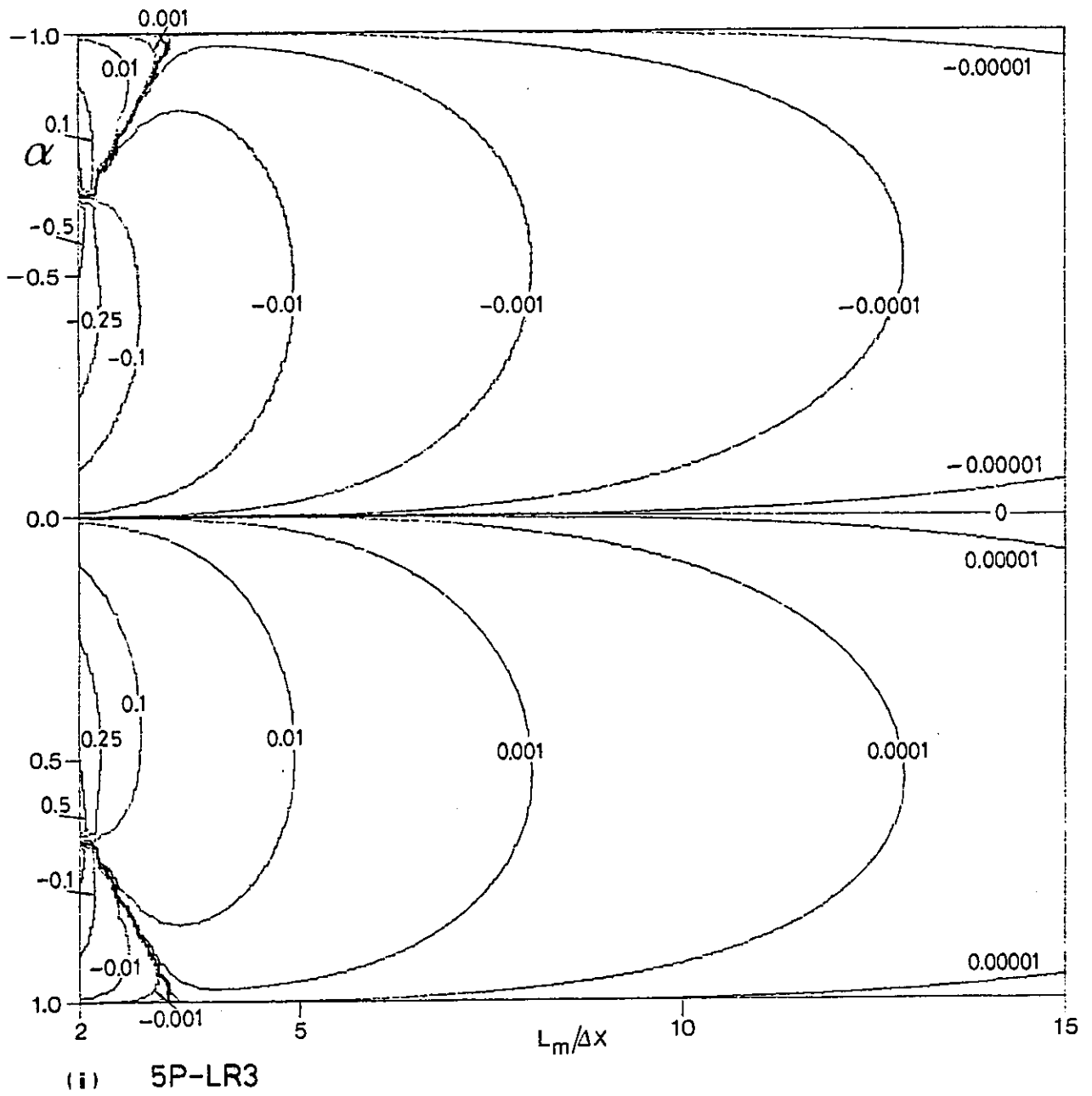
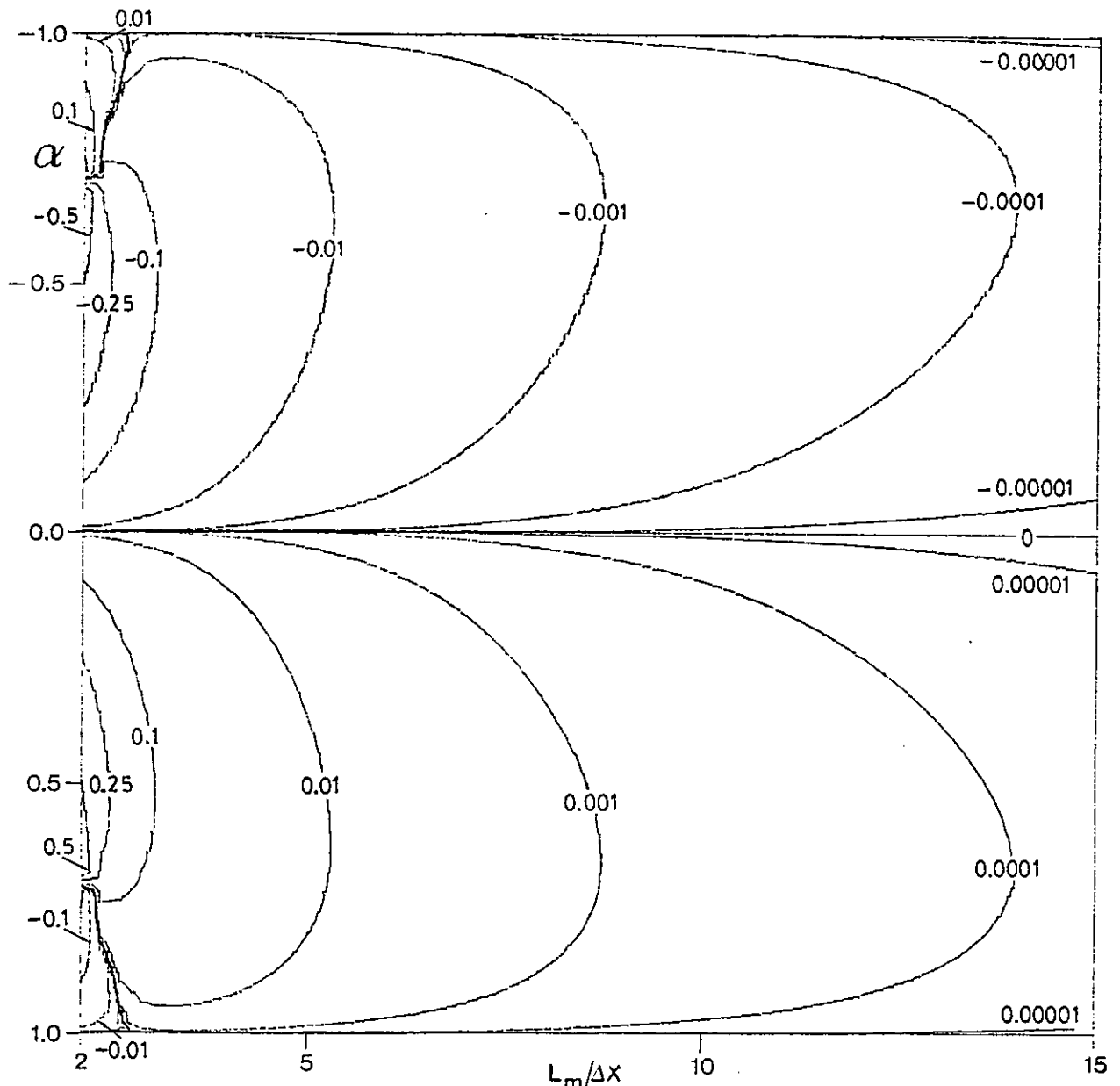


Fig. 4.3. Cont.



(j) 5P-HL3

Fig. 4.3. Cont.

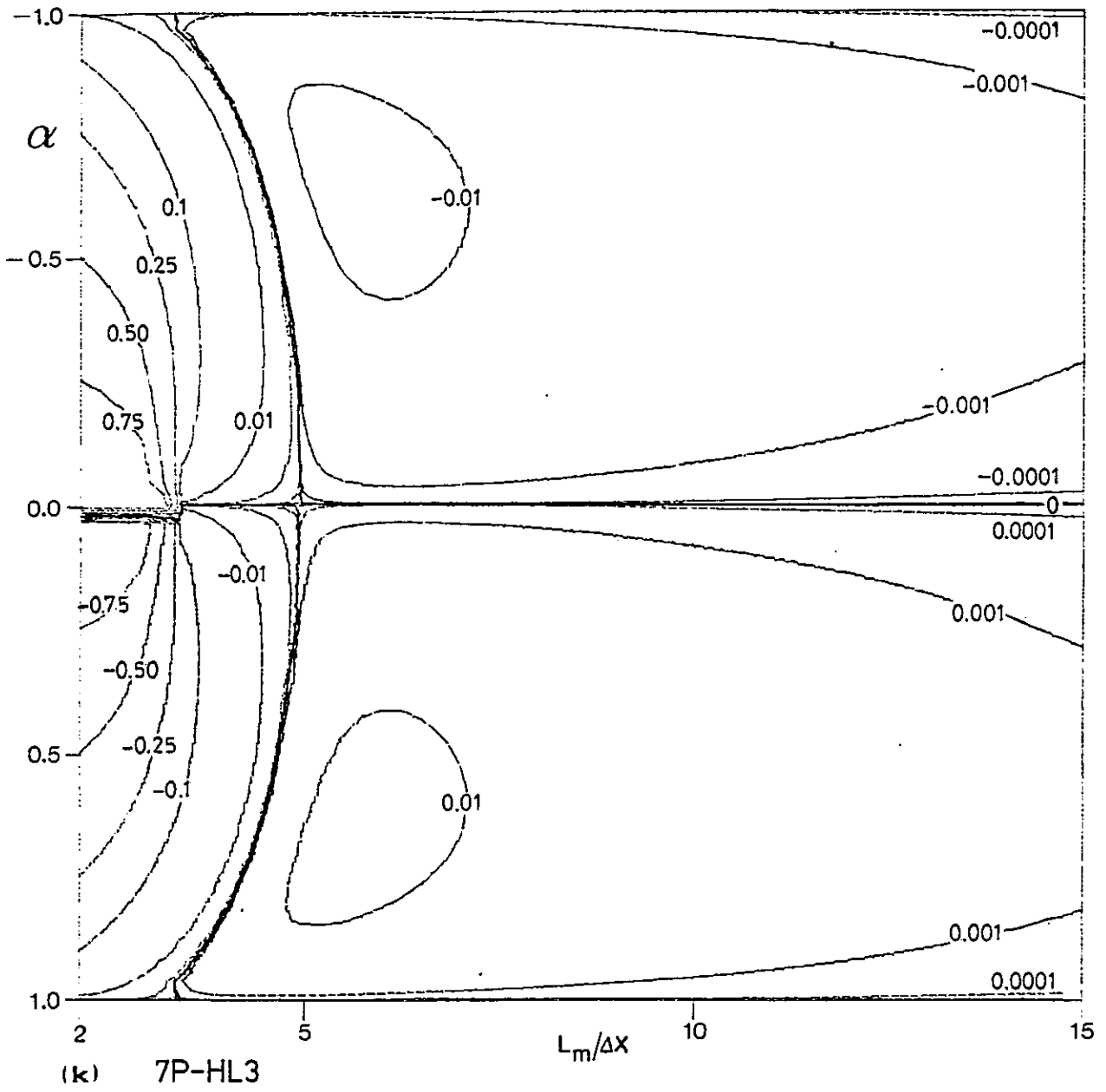


Fig. 4.3. Cont.

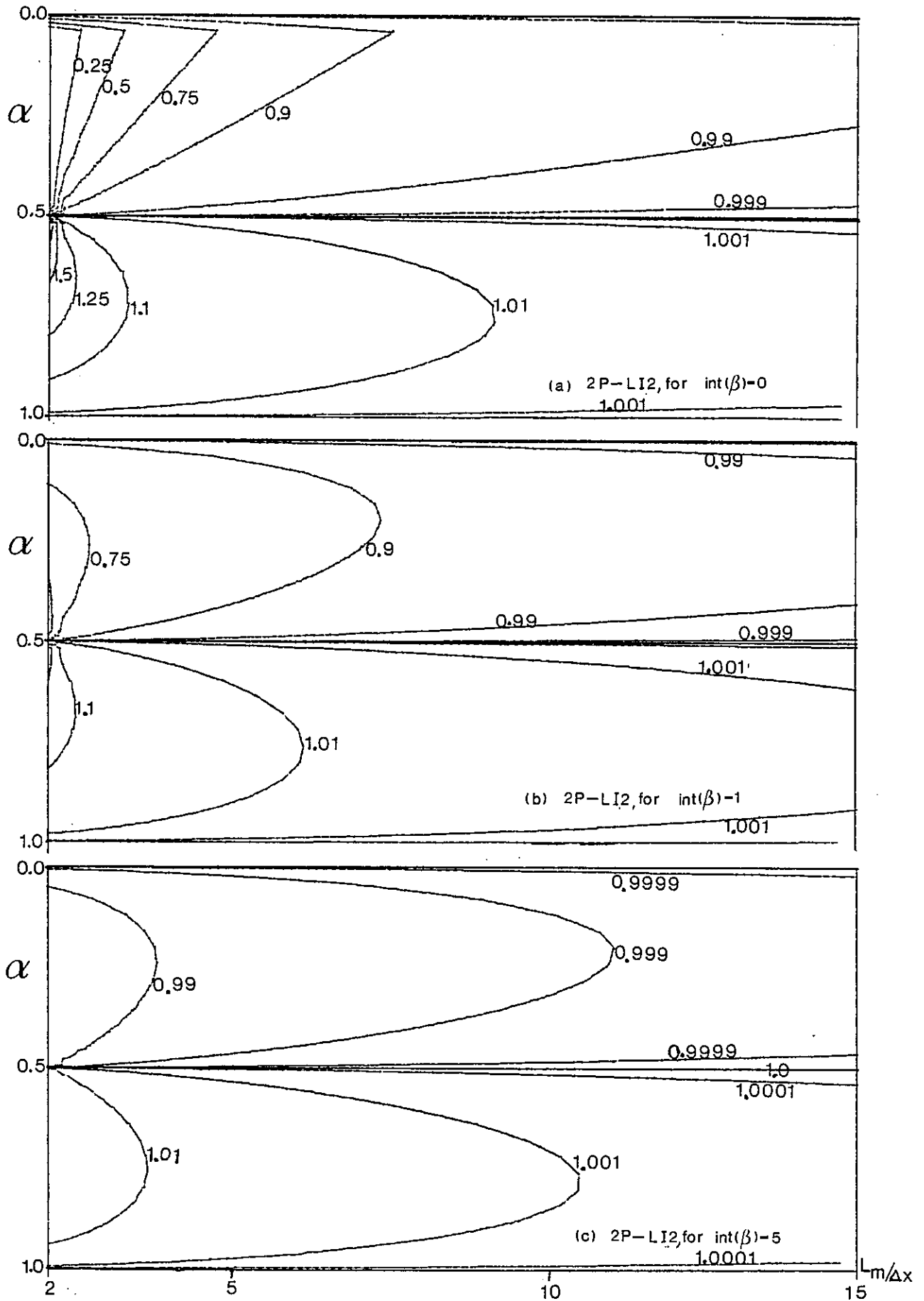
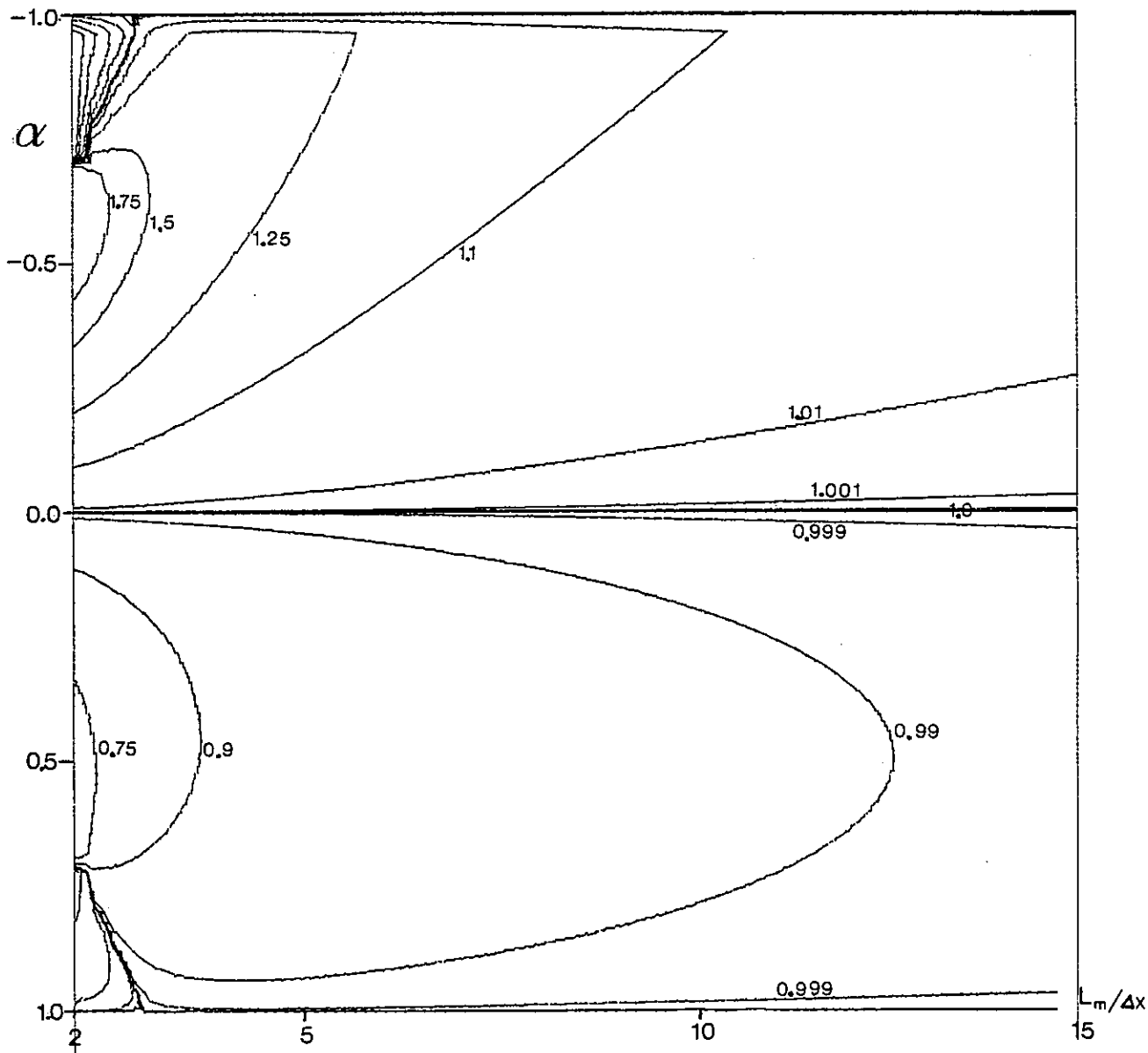
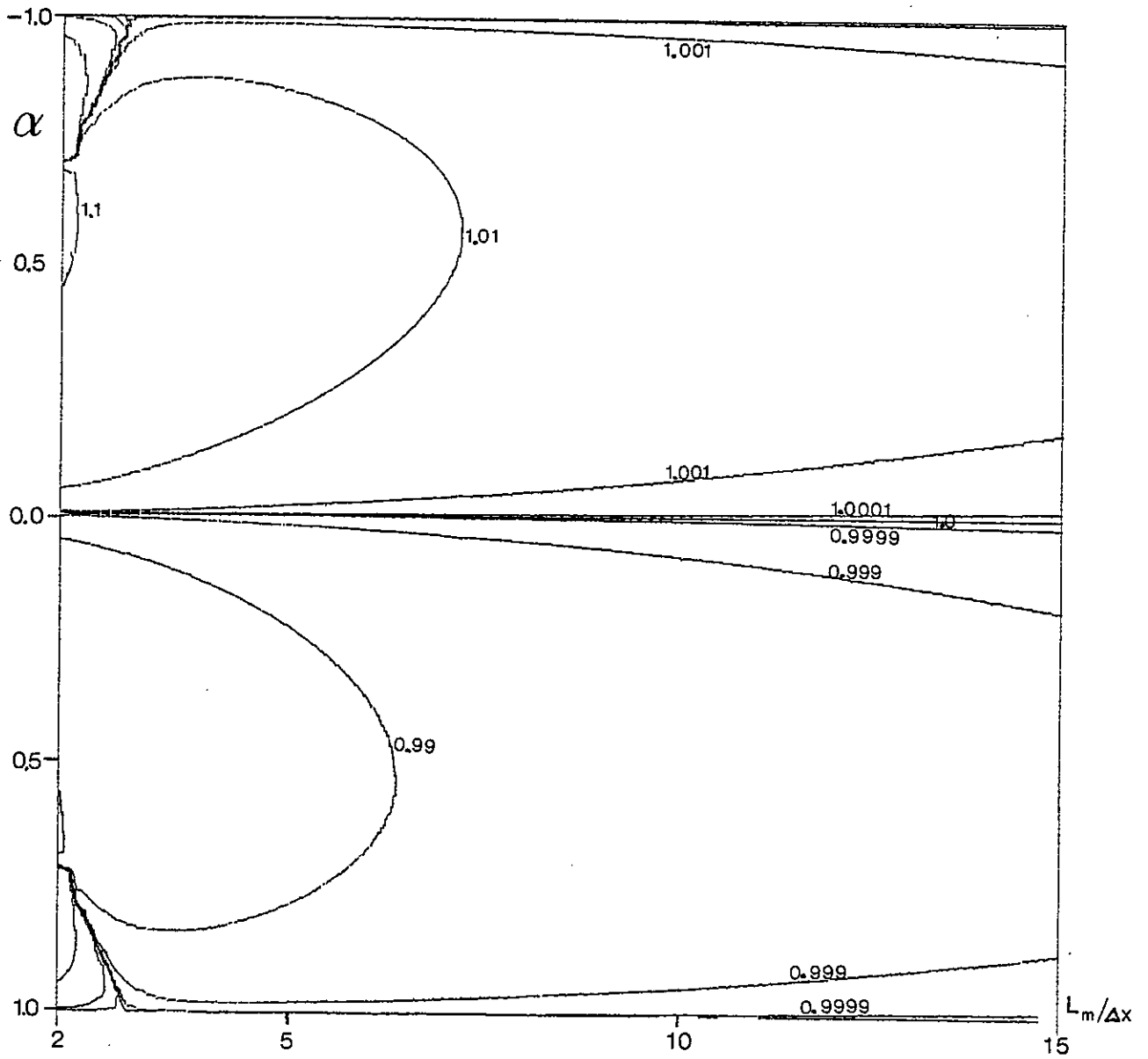


Fig. 4.4. Celerity ratios as a function of  $\alpha$  and  $L_m/\Delta x$  (first time step)



(d) 3P-L13, for  $\text{int}(\beta) = 1$

Fig. 4.4. Cont.



(e) 3P-LI 3, for  $\text{Int}(\beta) = 5$

Fig. 4.4. Cont.

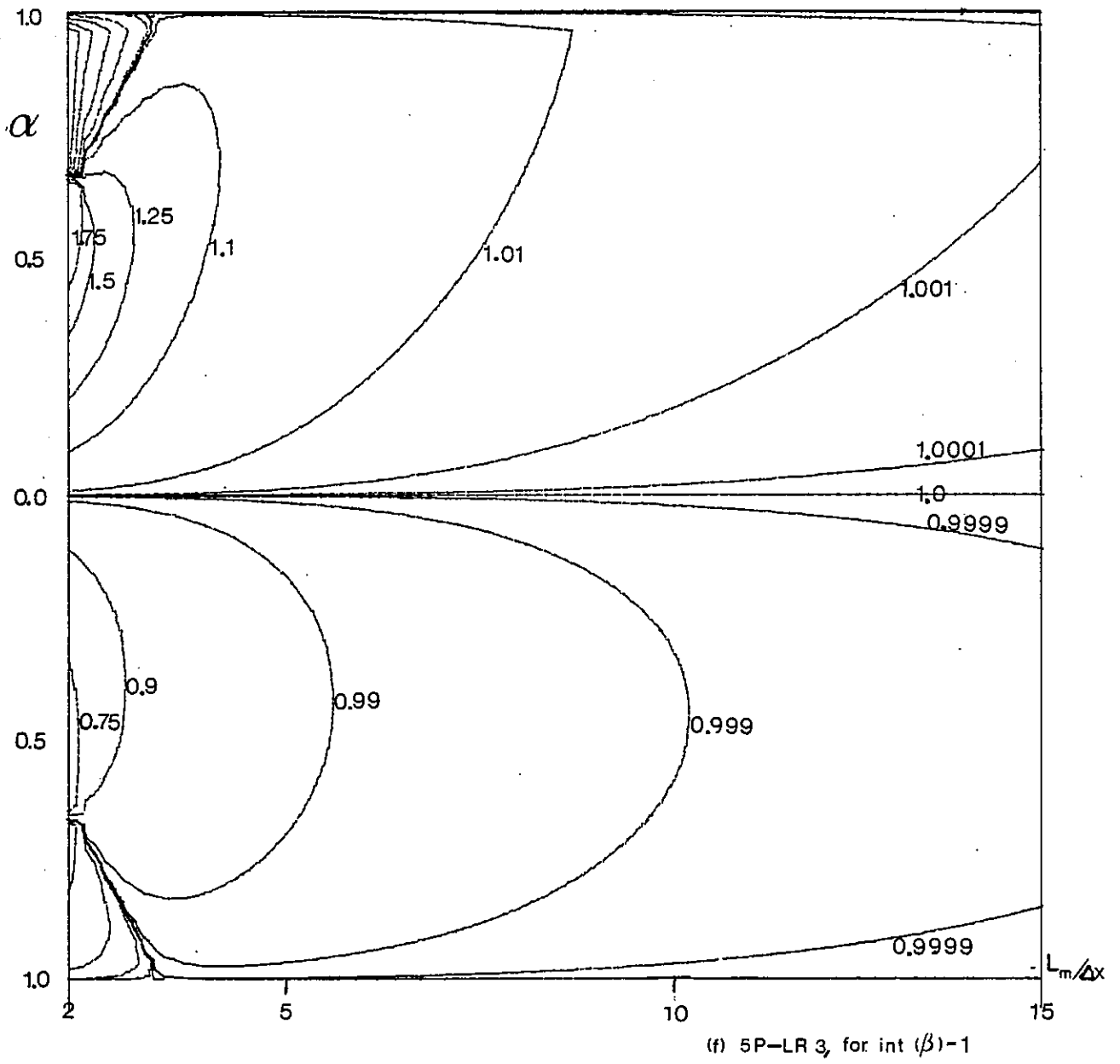


Fig. 4.4. Cont.

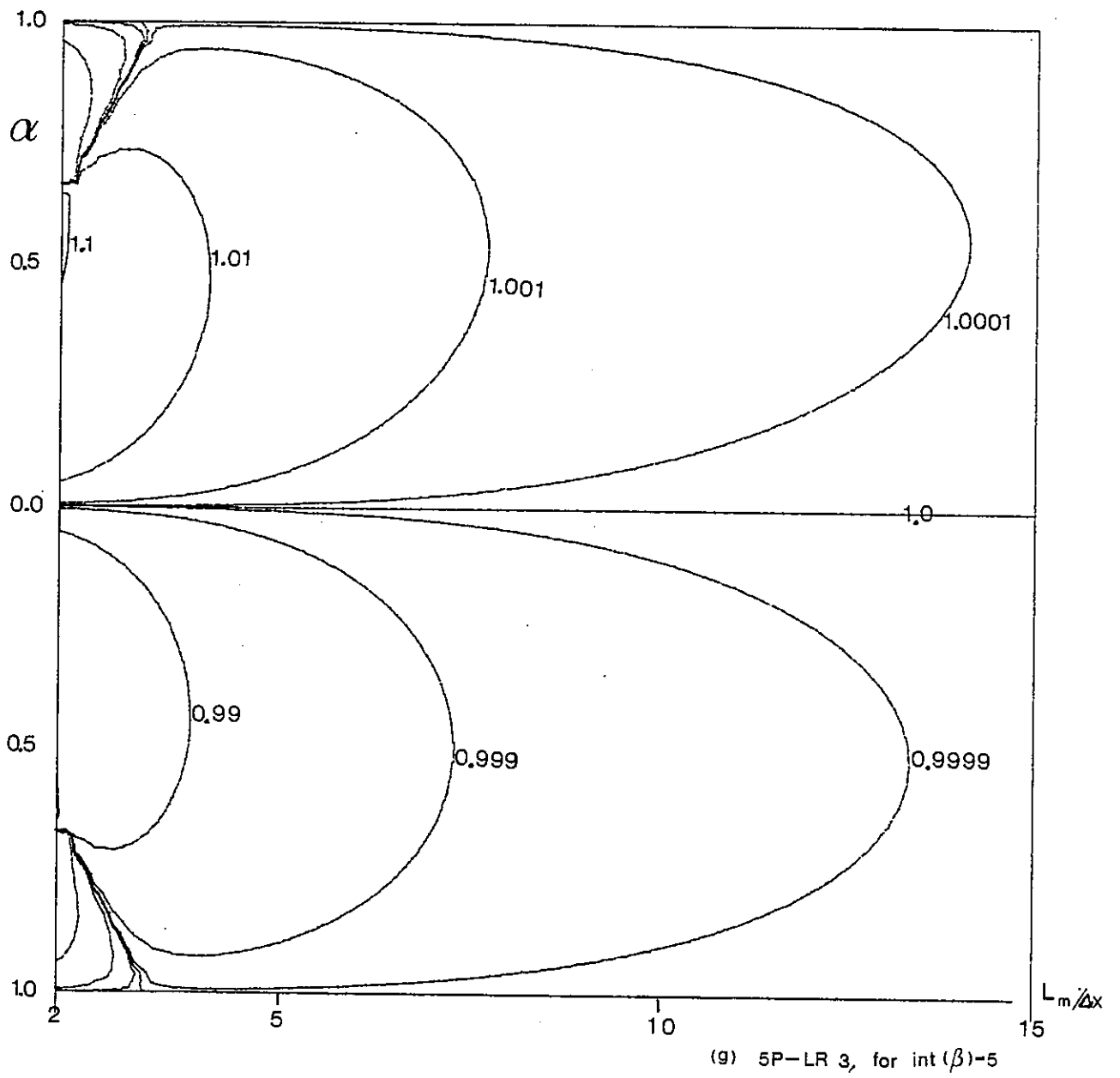


Fig. 4.4. Cont.





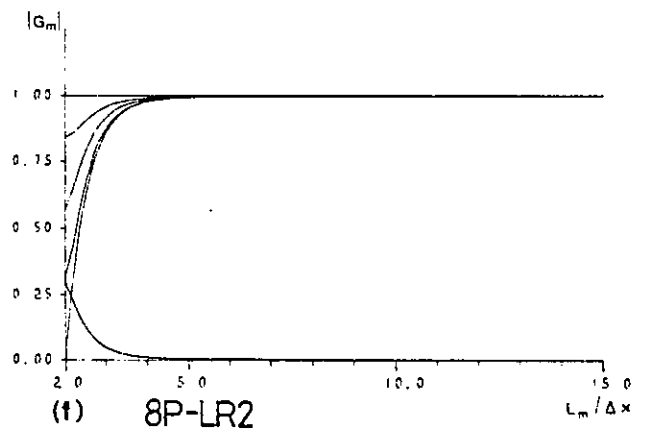
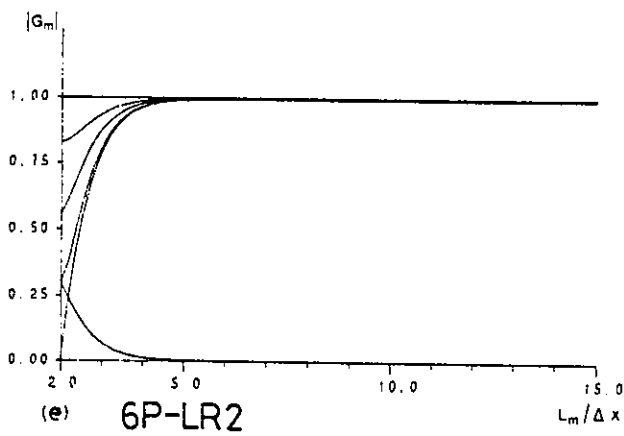
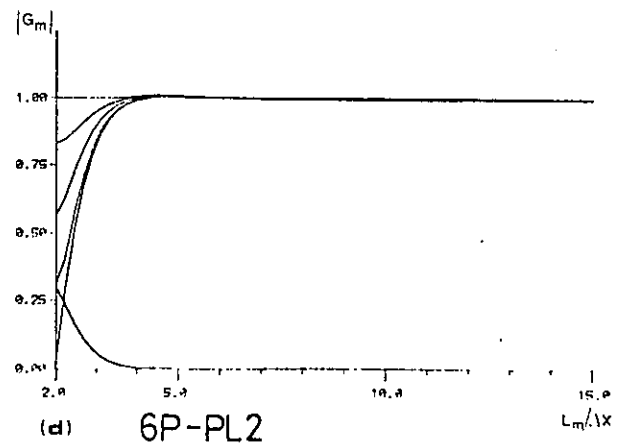
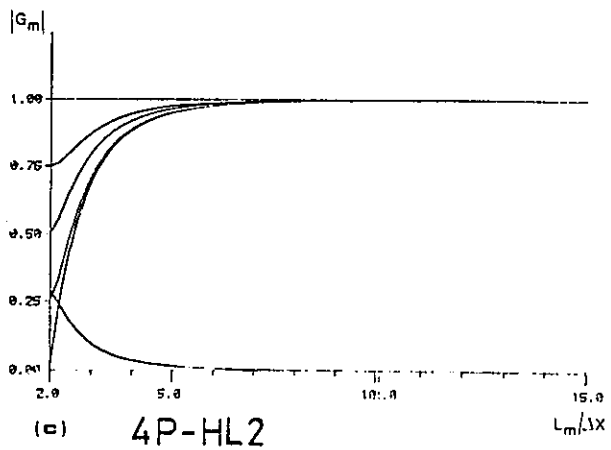
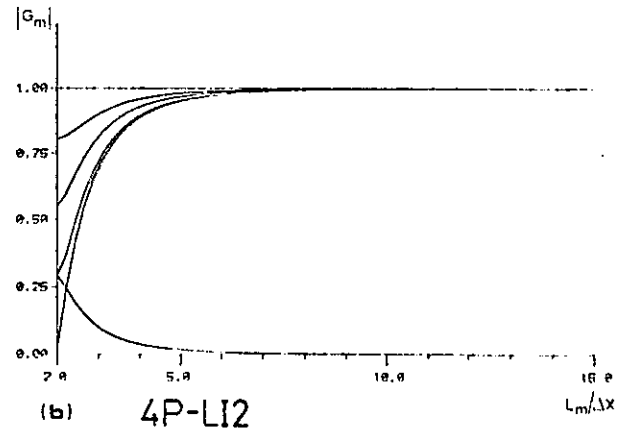
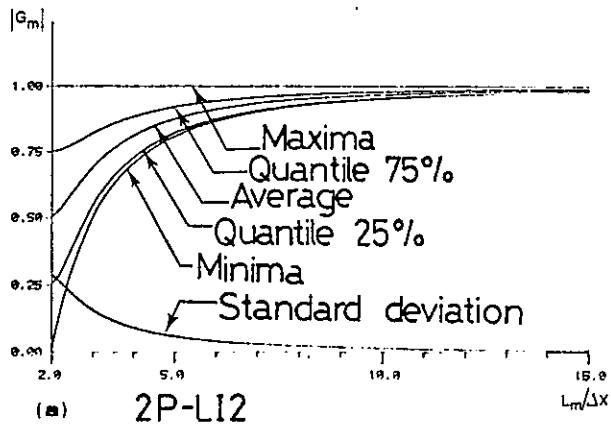


Fig 4.5. Statistics of the amplifying factors as a function of  $L_m/\Delta x$  (first time step)

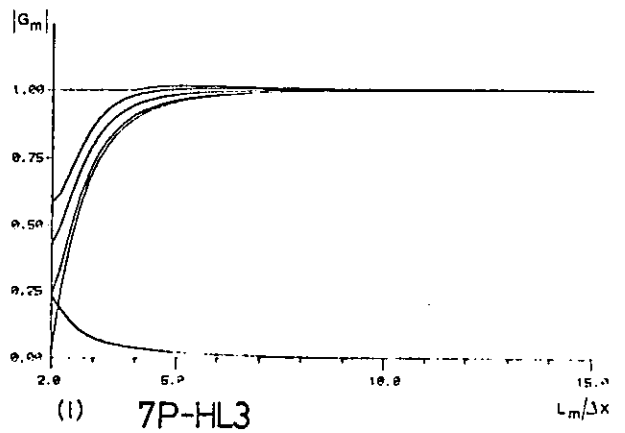
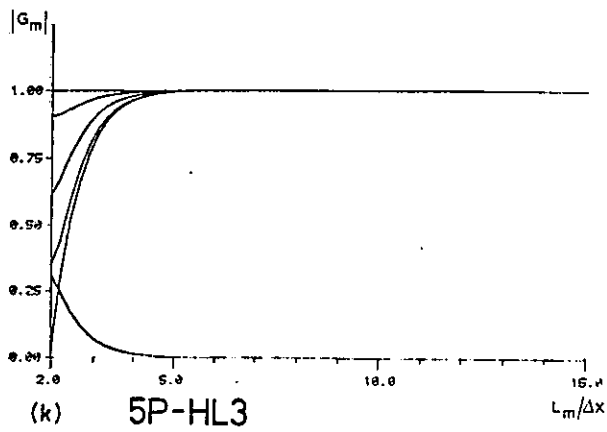
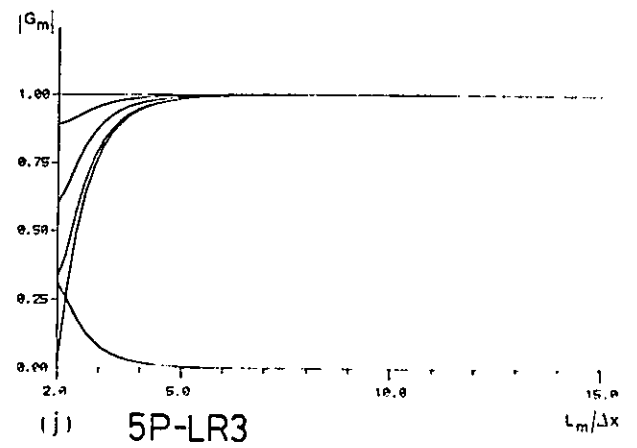
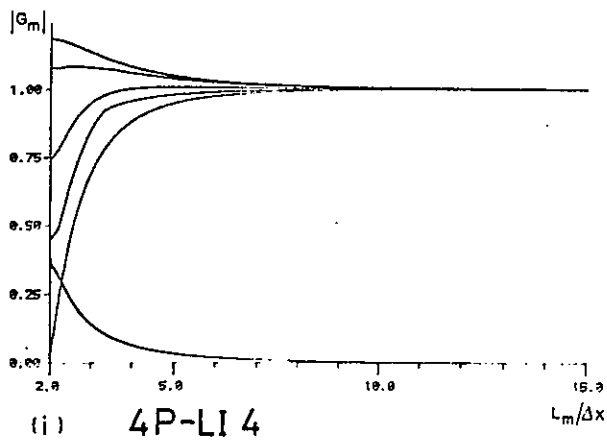
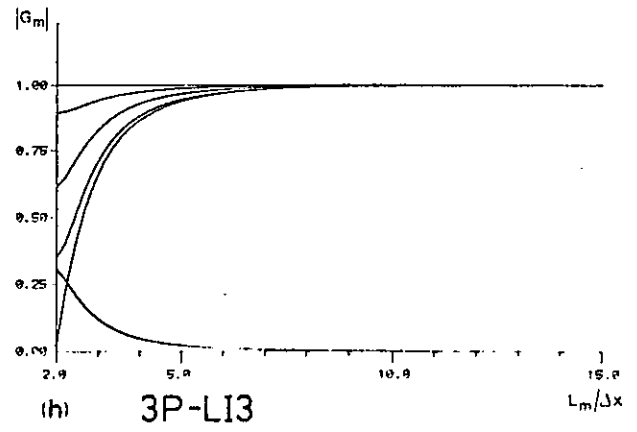
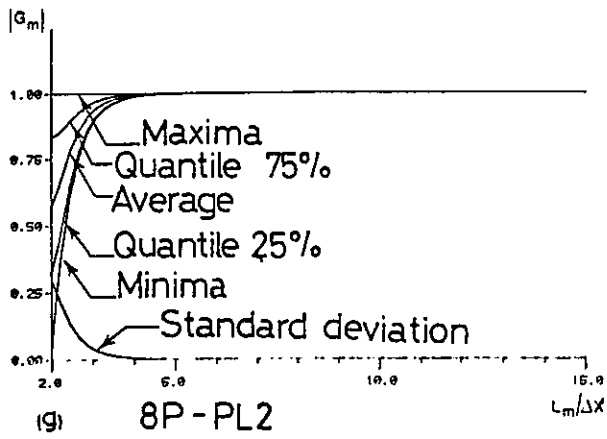


Fig. 4.5. Cont.

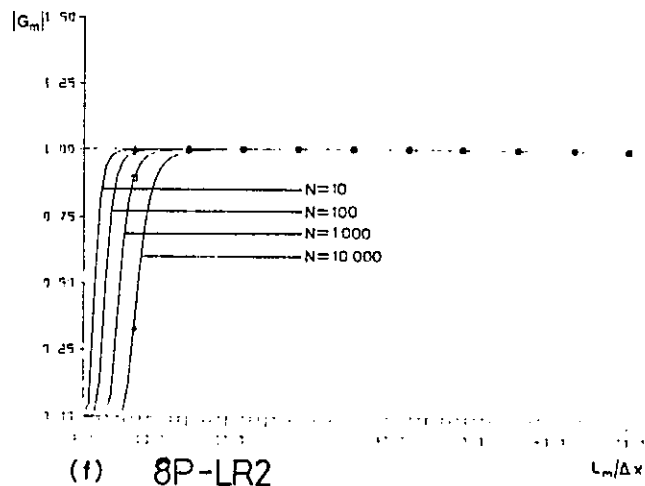
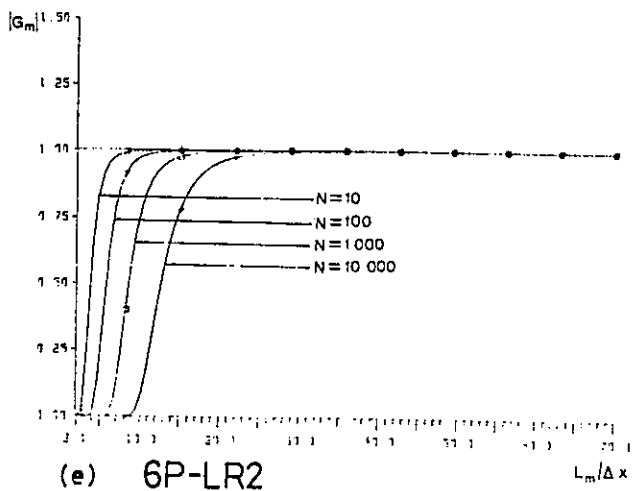
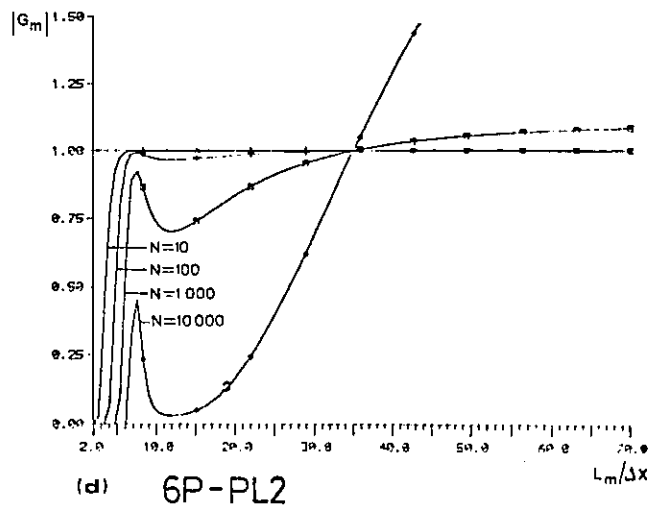
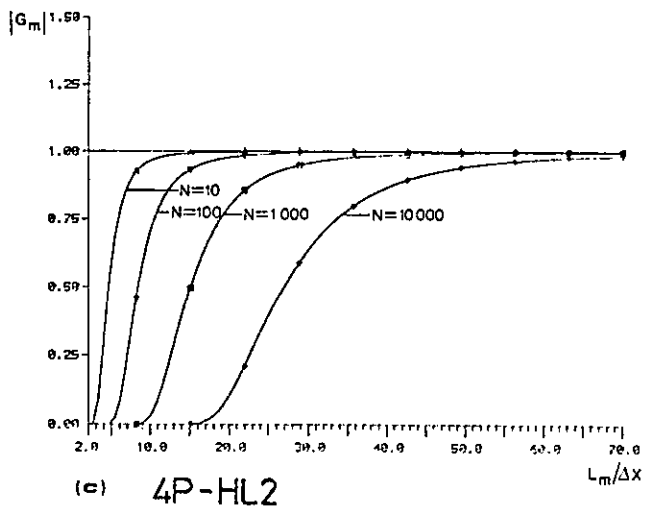
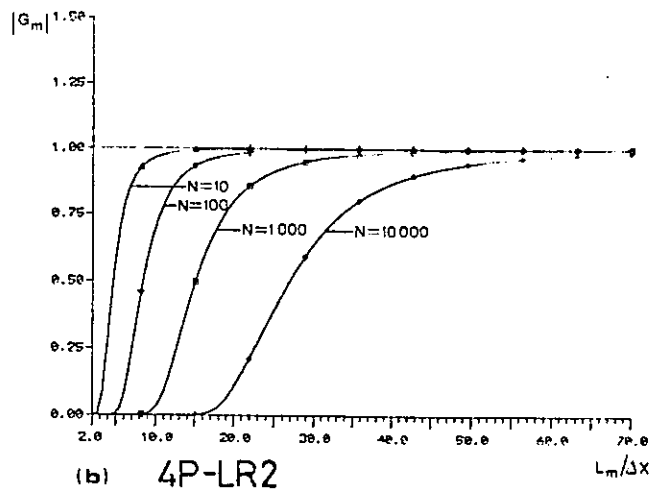
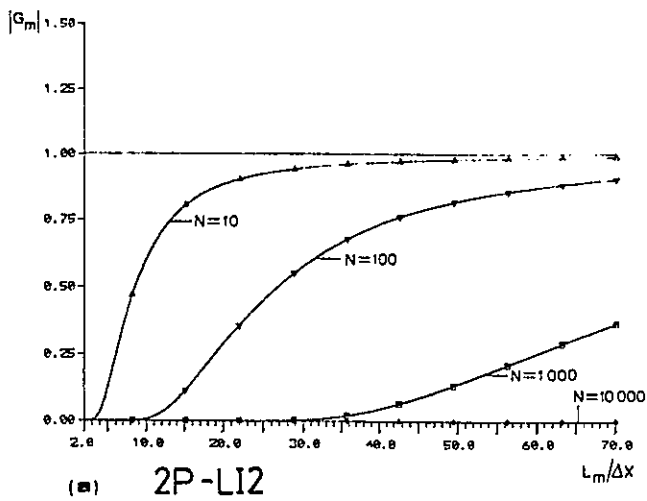


Fig. 4.6. Amplifying factors as a function of  $L_m/\Delta x$  ( $\alpha=0.5$ ), after  $N$  time steps ( $N=10, 100, 1000, 10000$ )

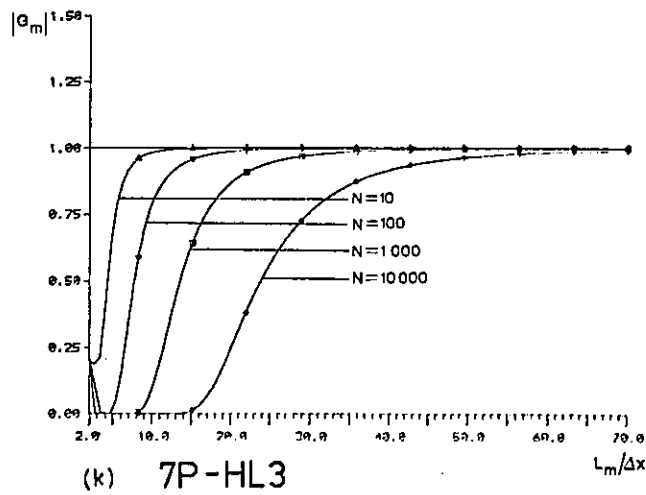
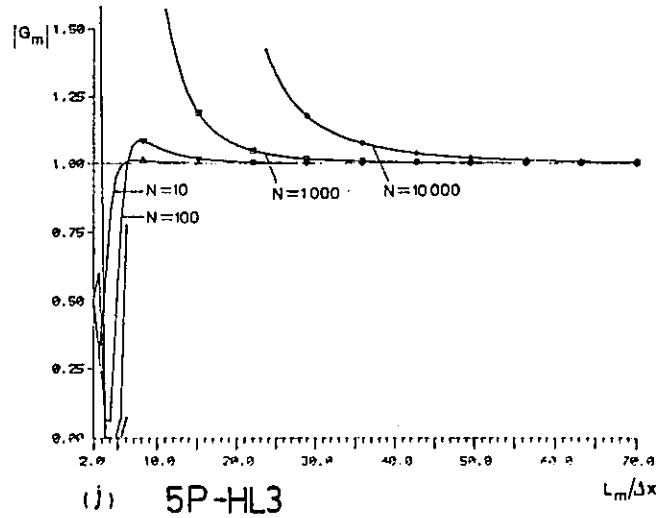
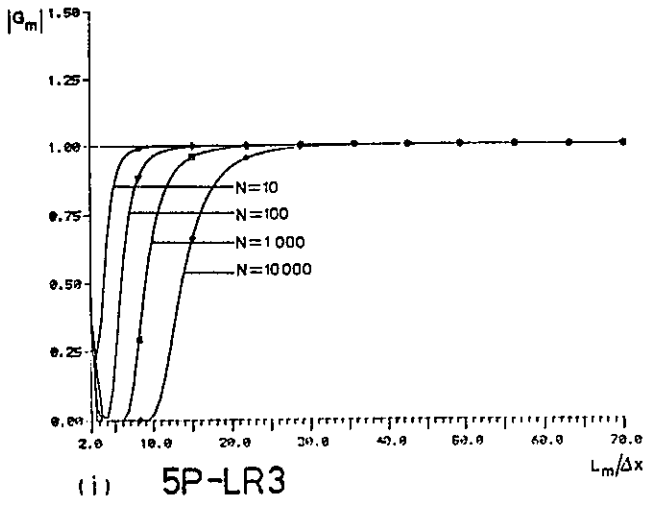
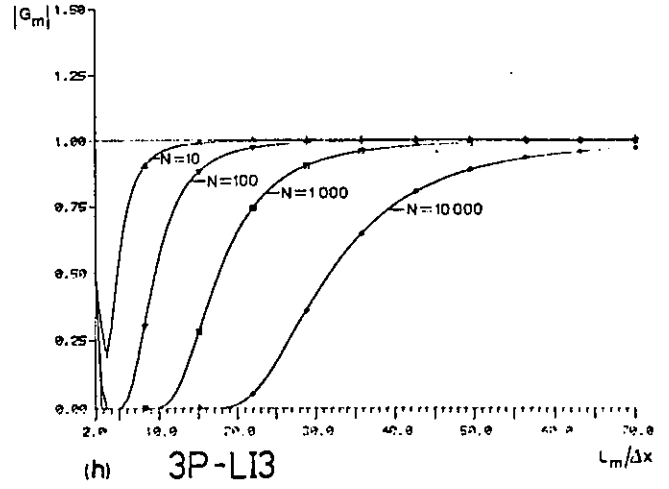
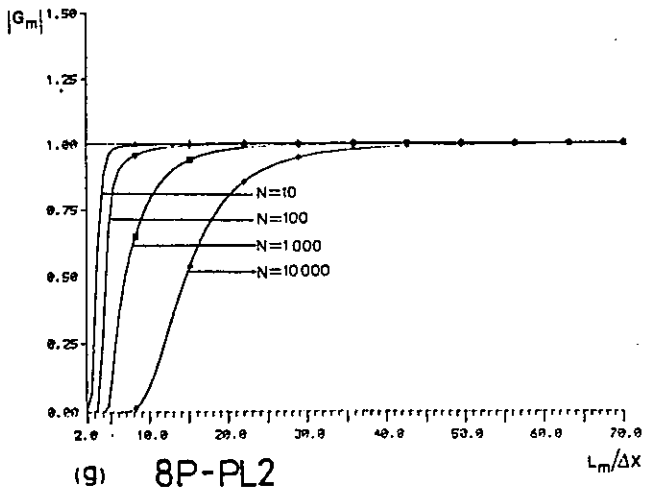


Fig. 4.6. Cont.

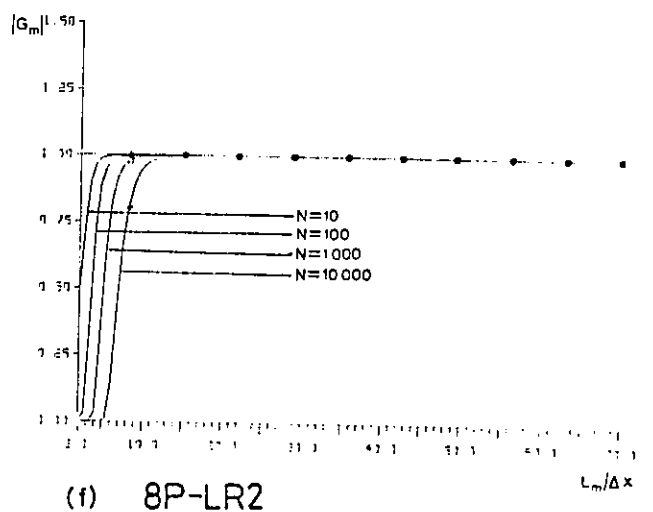
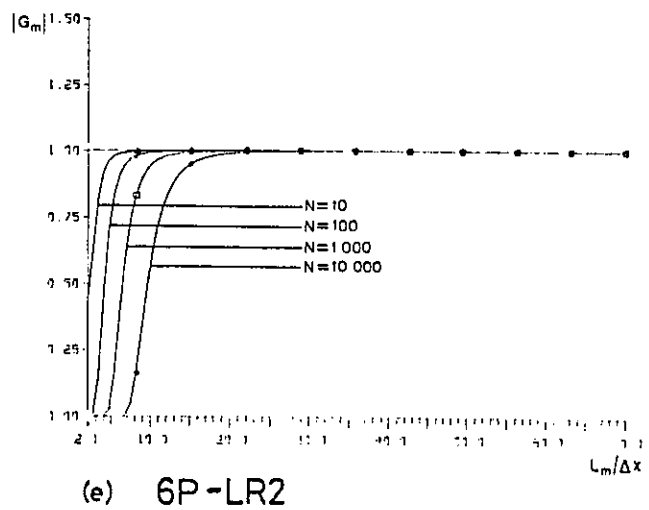
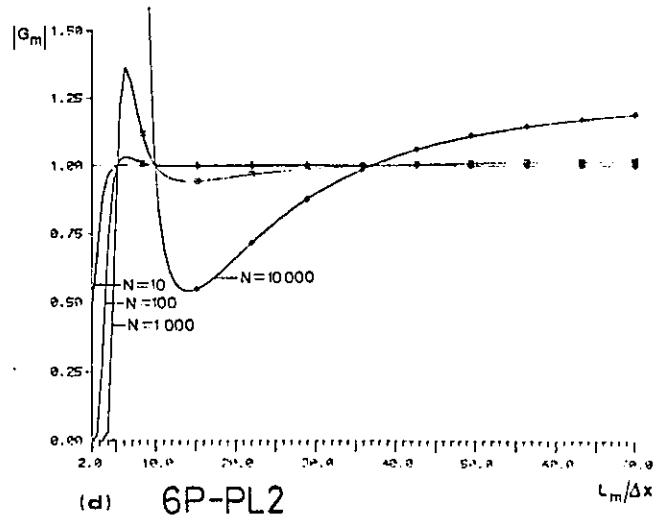
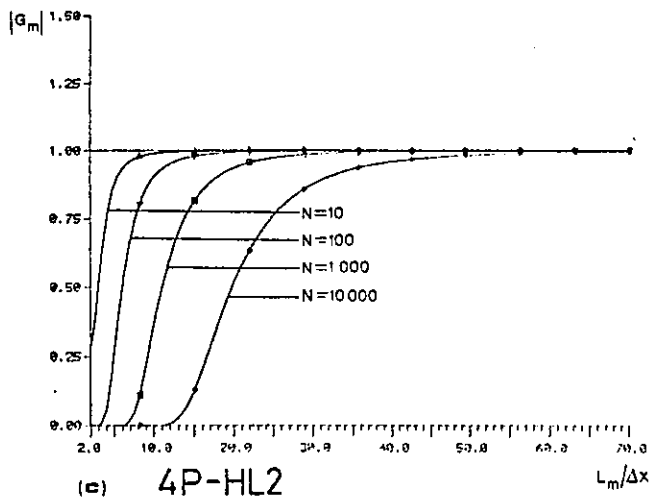
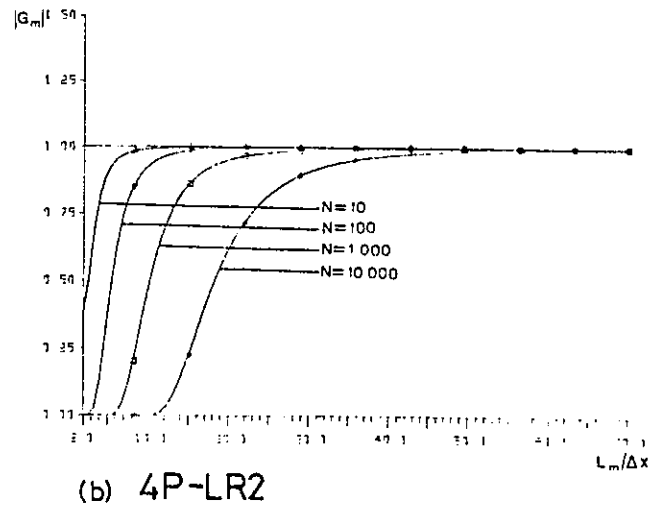
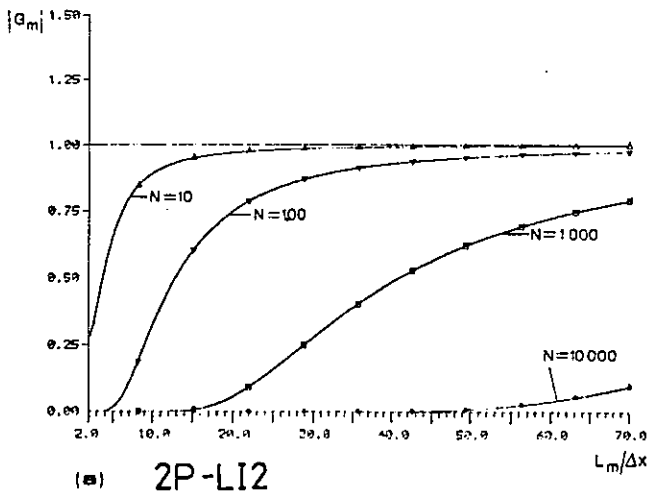


Fig. 4.7. Amplifying factors as a function of  $L_m/\Delta x$  ( $\alpha=0.0625$ ), after  $N$  time steps ( $N=10, 100, 1000, 10000$ )

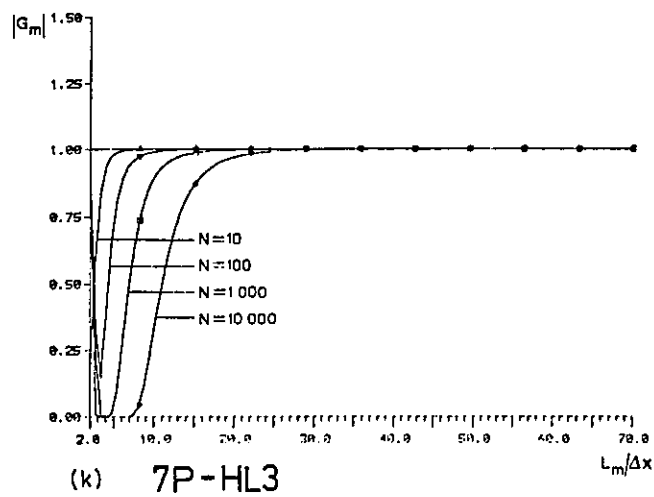
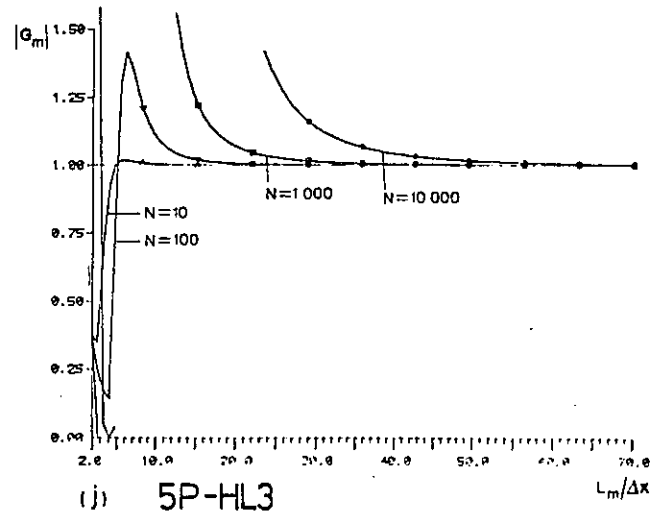
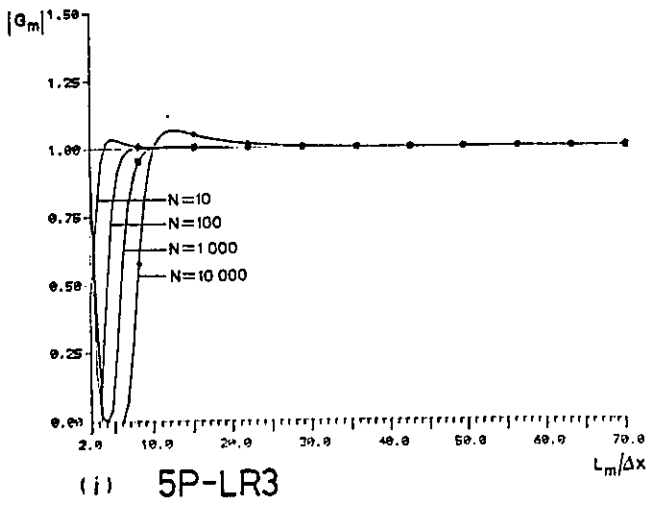
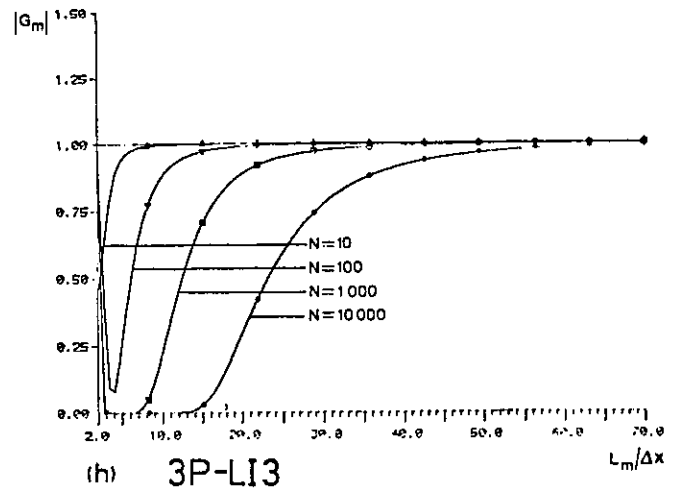
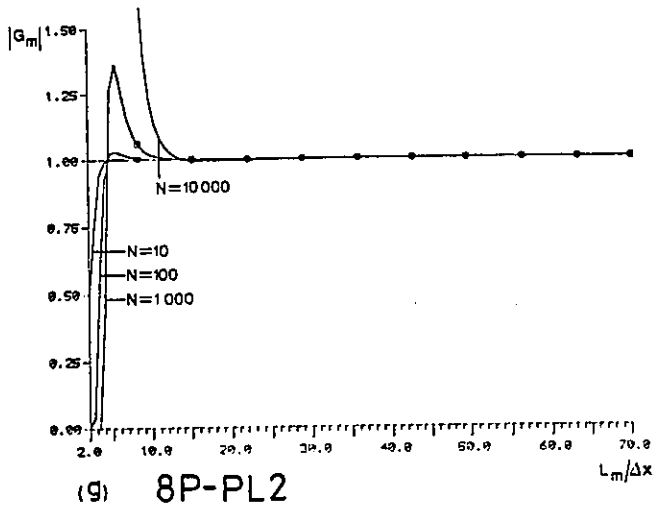


Fig. 4.7. Cont.

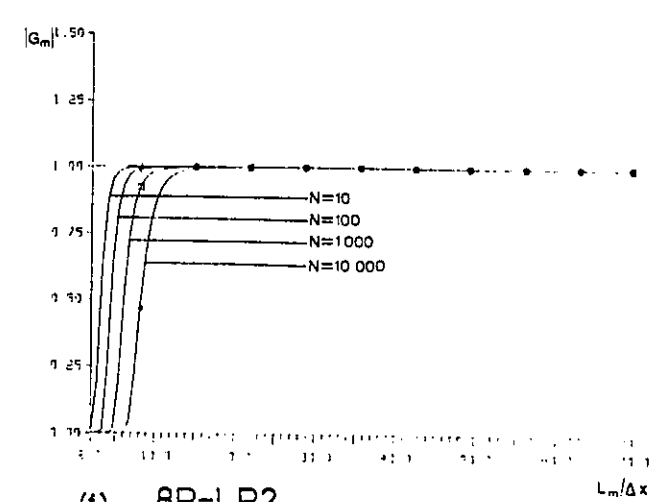
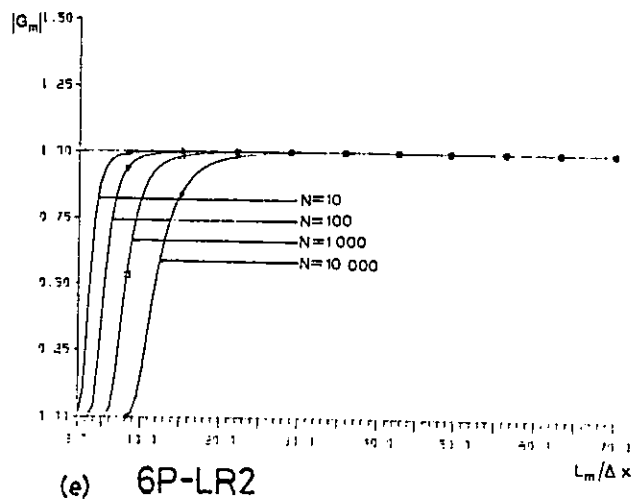
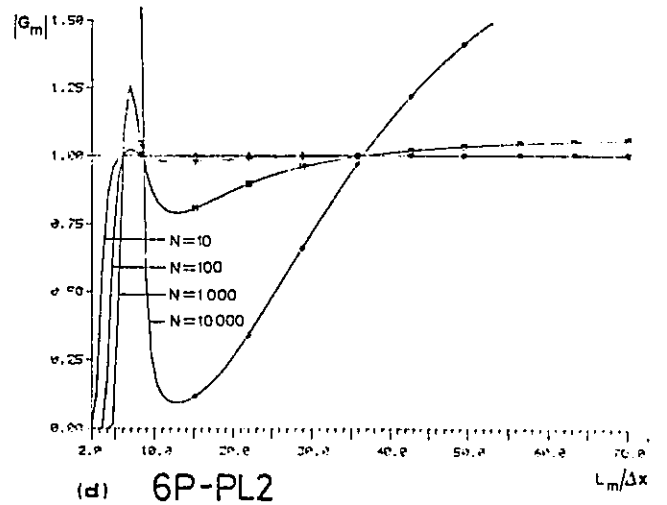
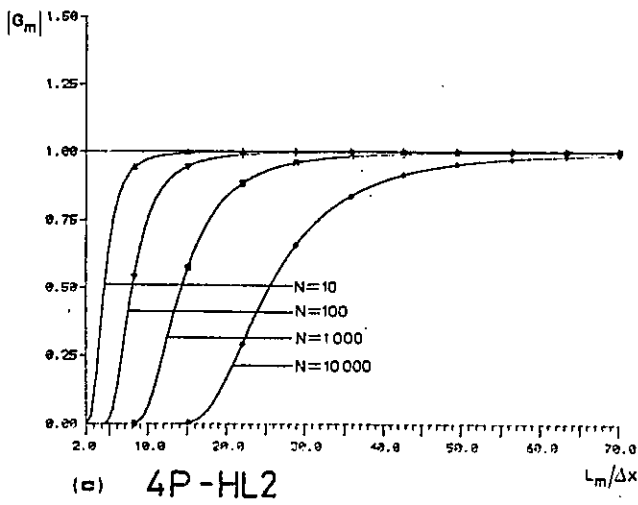
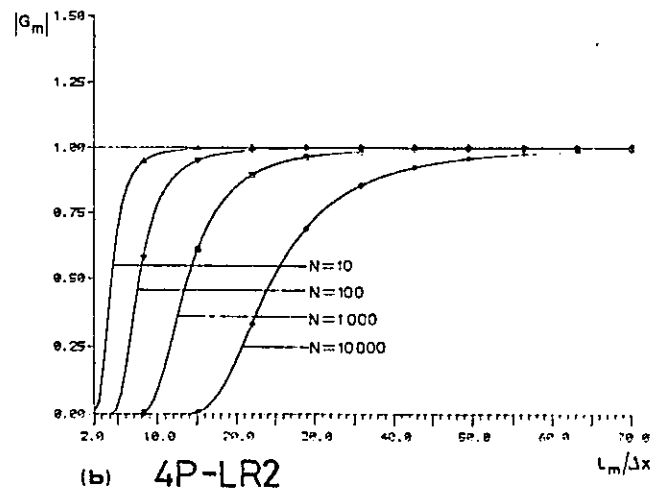
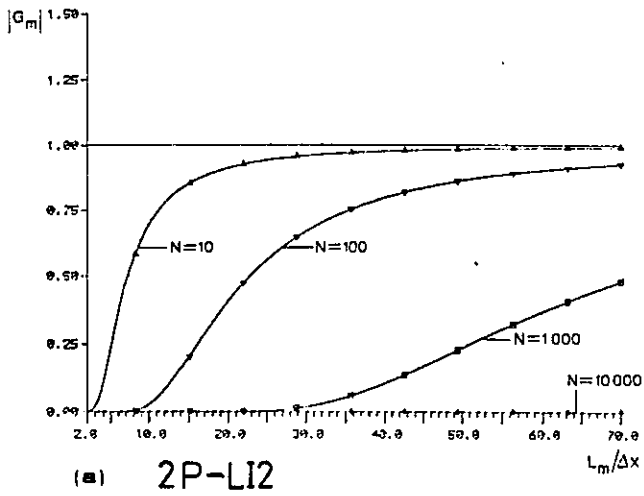


Fig. 4.8. Amplifying factors as a function of  $L_m/\Delta x$  ( $\alpha=0.24$ ), after  $N$  time steps ( $N=10, 100, 1000, 10000$ )



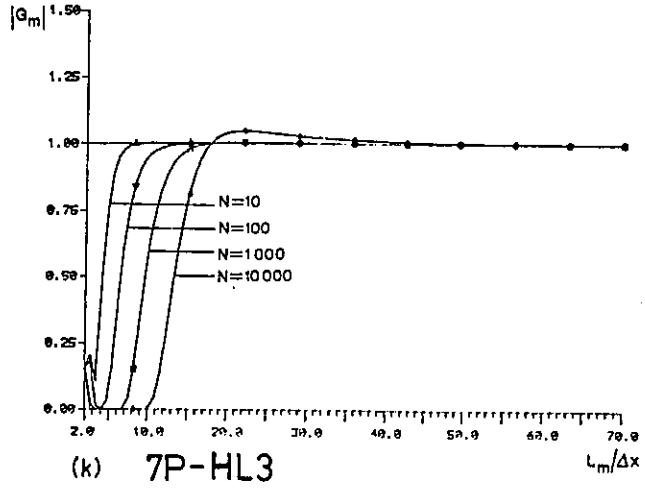
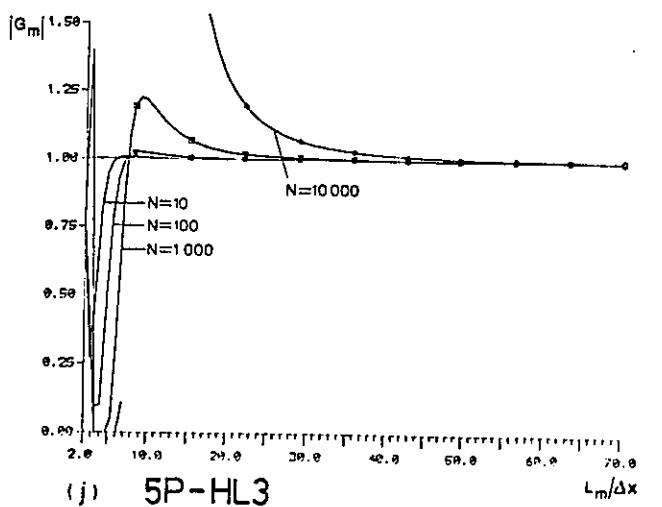
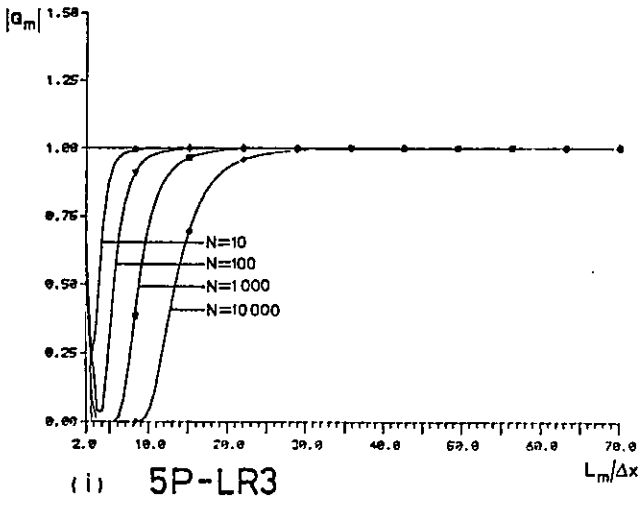
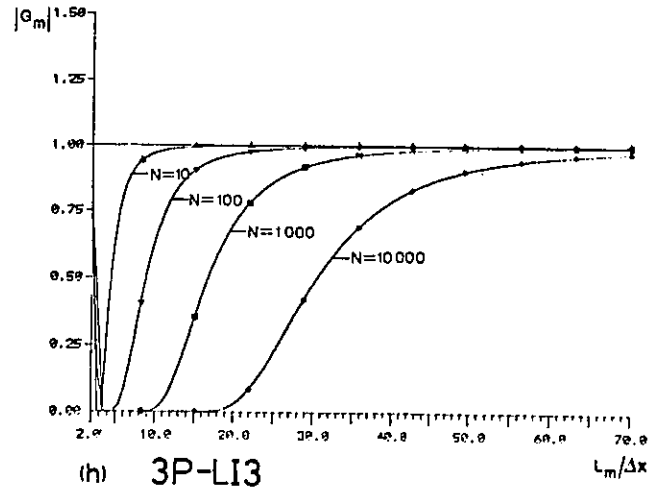
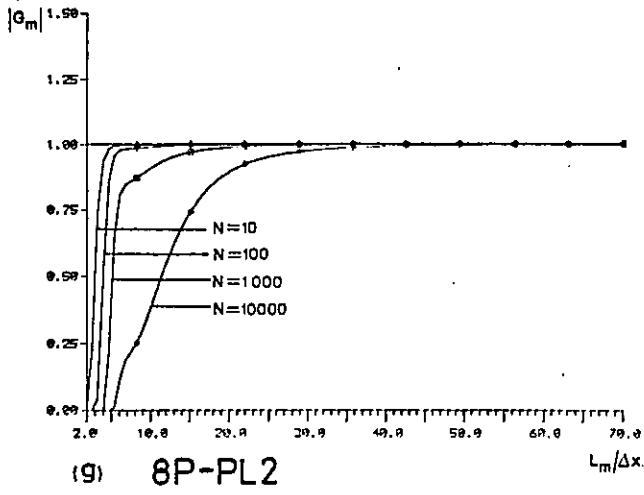


Fig. 4.8. Cont.

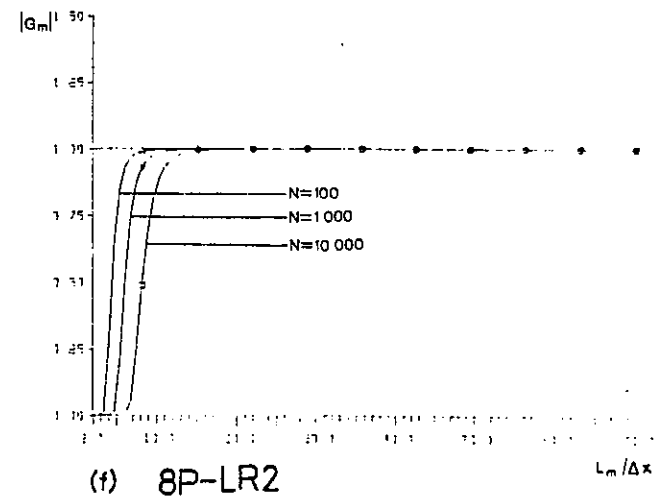
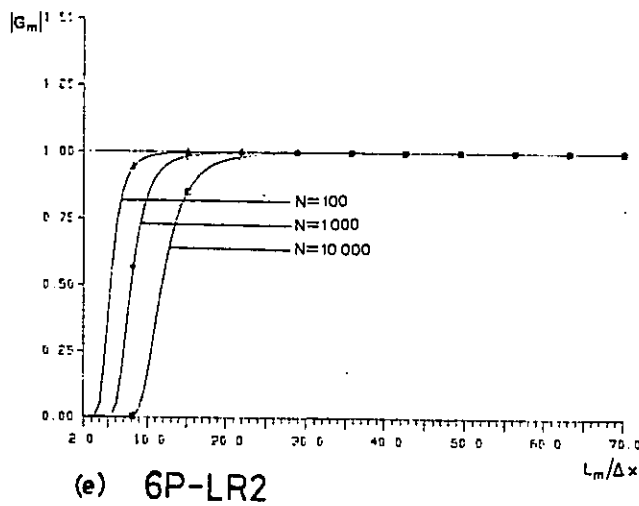
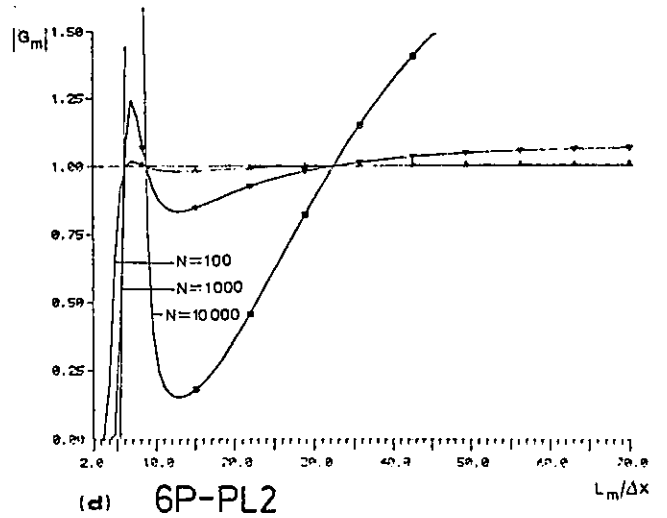
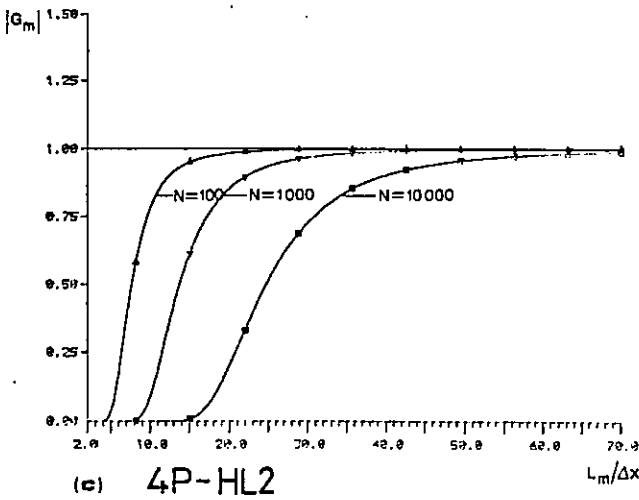
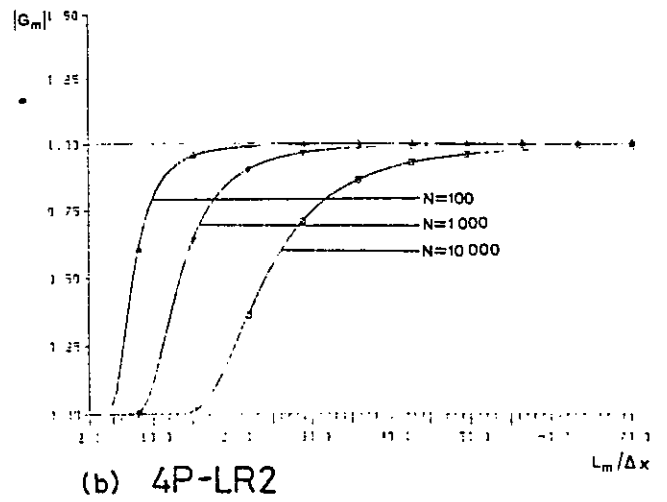
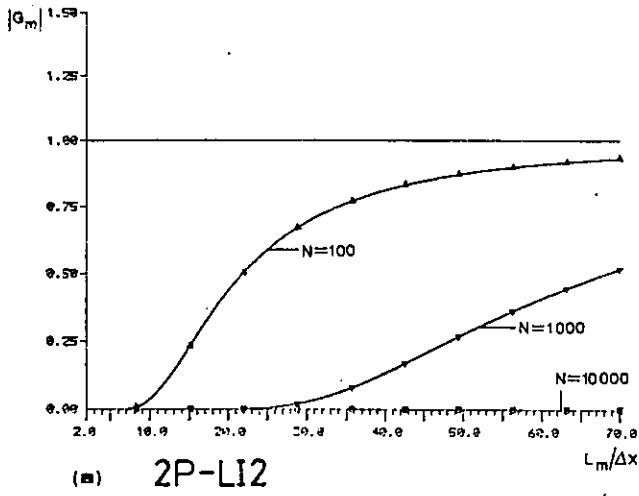


Fig. 4.9. Amplifying factors as a function of  $L_m/\Delta x$ , after a sequence of  $N$  randomly generated time steps ( $N=100, 1000, 10000$ )

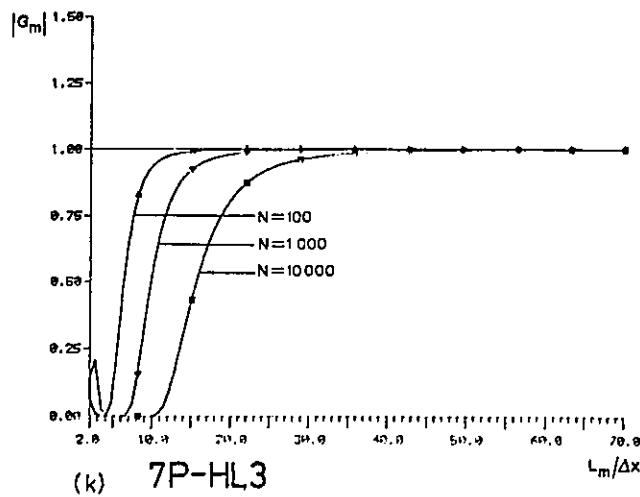
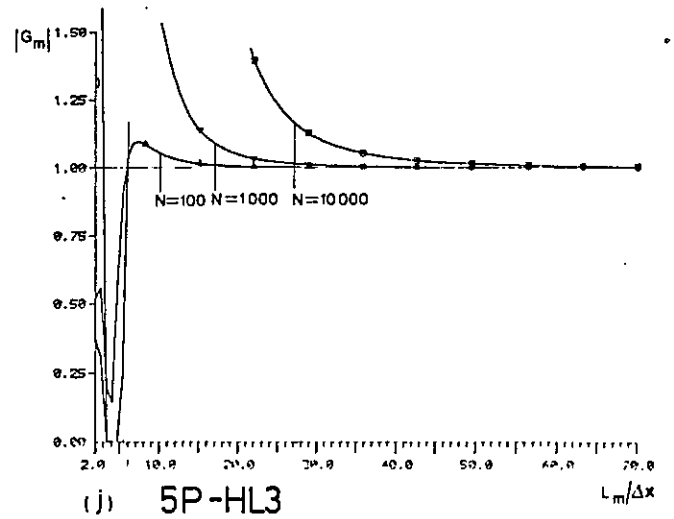
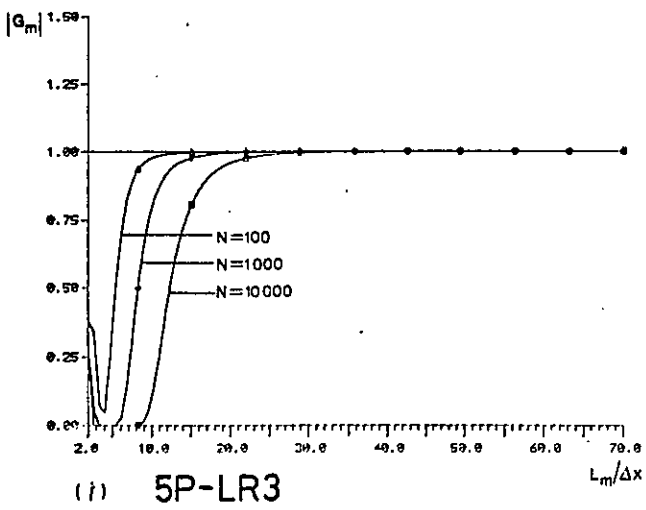
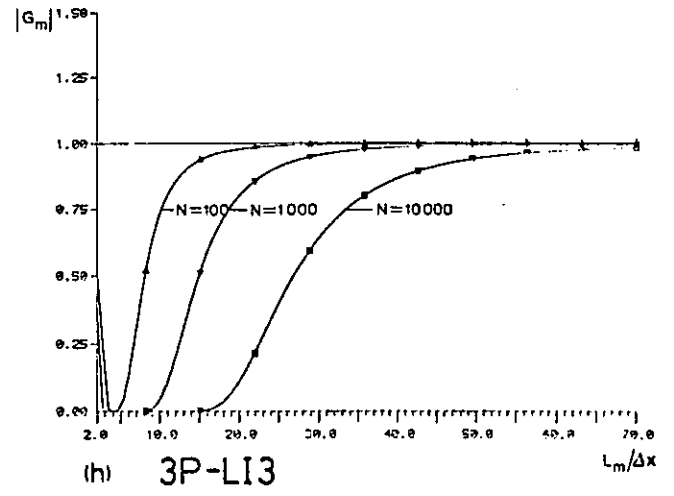
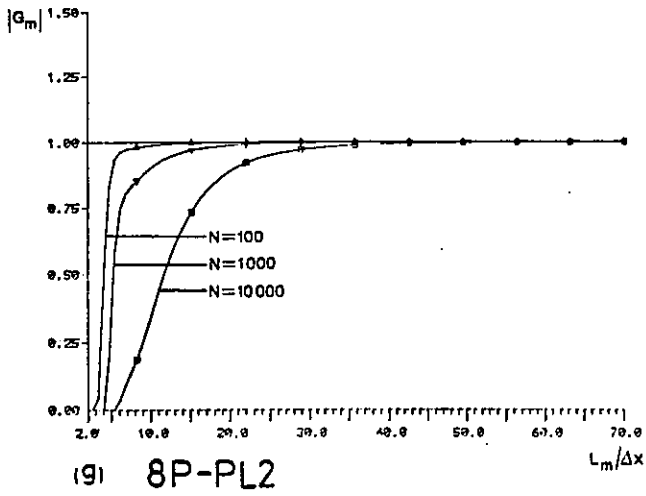
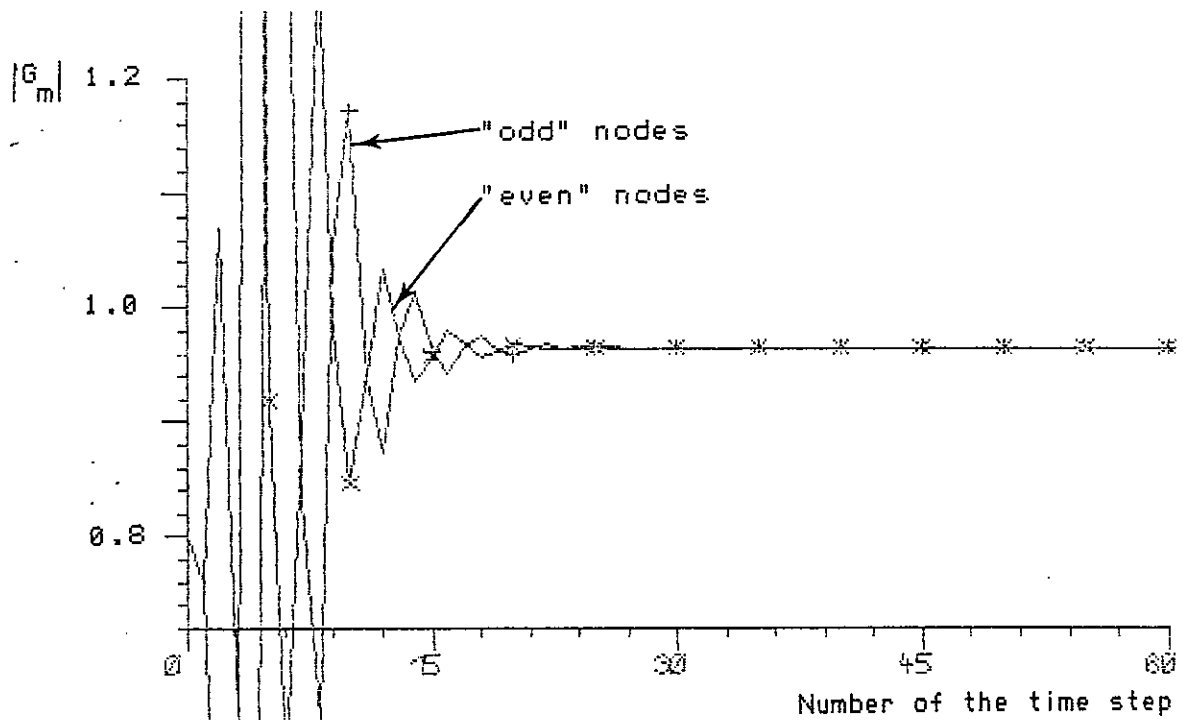
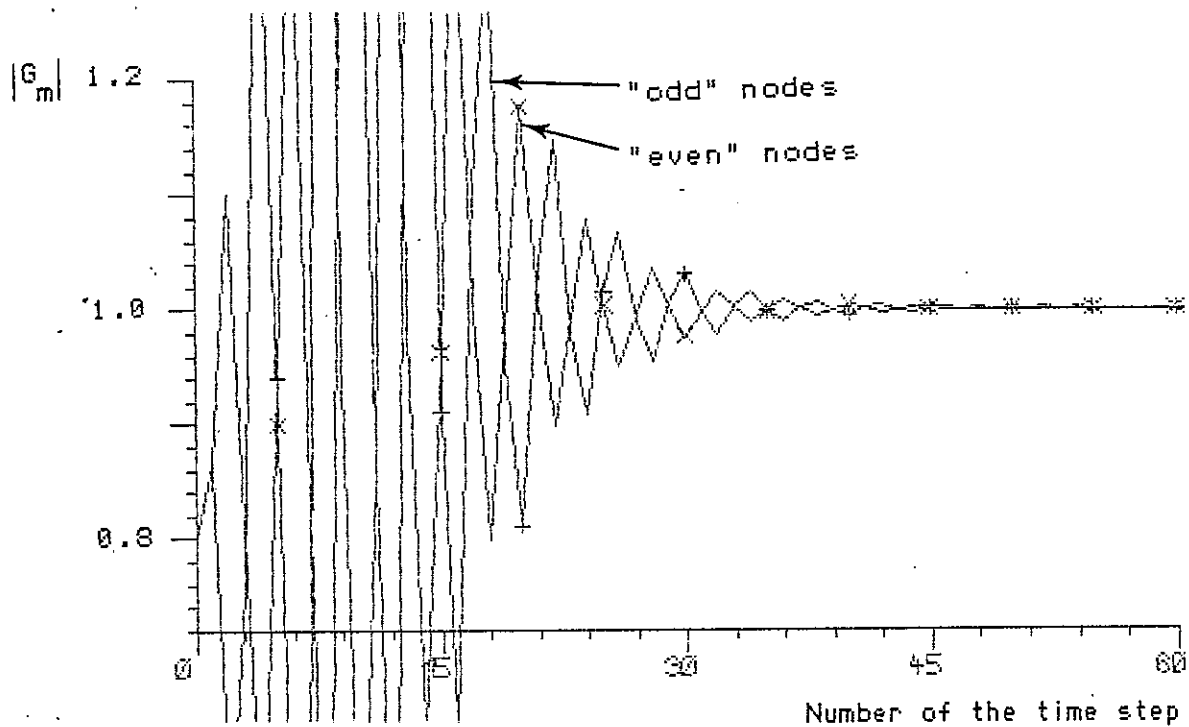


Fig. 4.9. Cont.

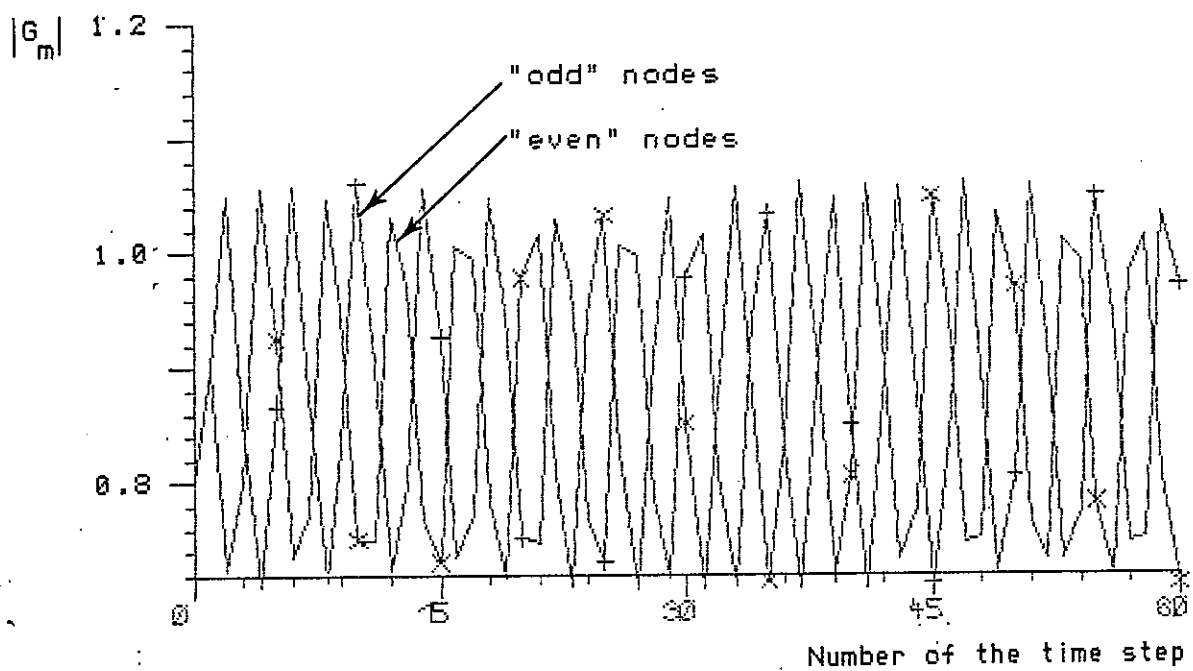


(a) 3P-LI3,  $L_m/\Delta x=3$

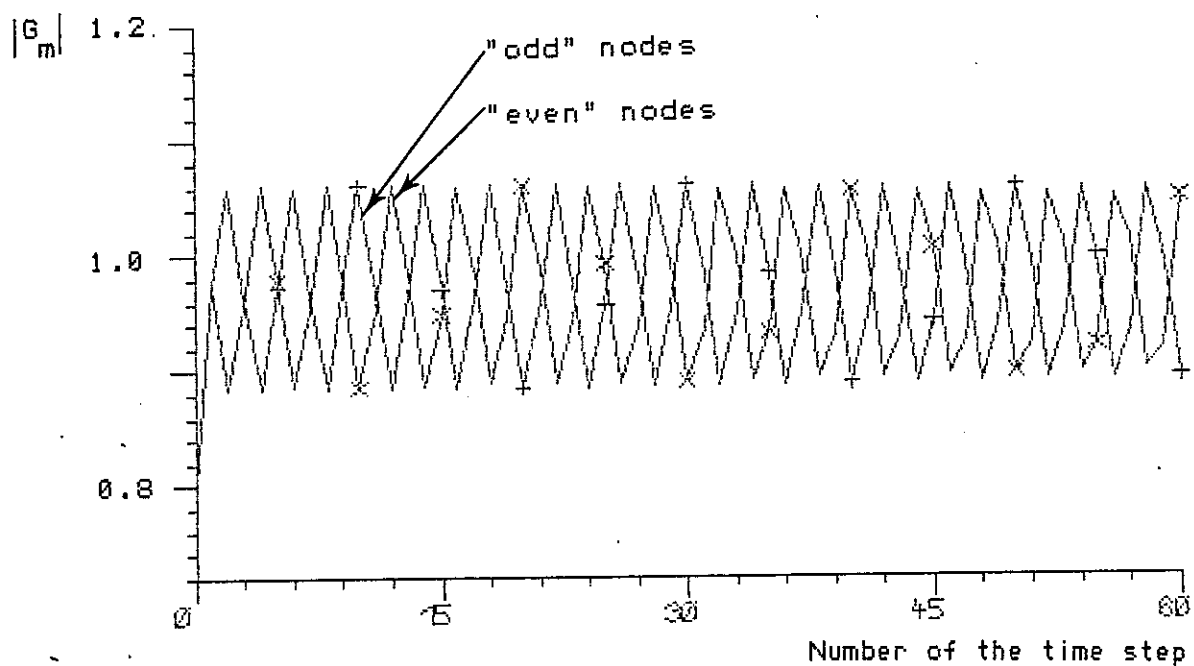


(b) 5P-LR3,  $L_m/\Delta x=3$

Fig. 4.10. Amplifying factors per time step ( $L_m/\Delta x=3, 4, 5$ ), as a function of the number of the time steps, for interpolation schemes with quadratic core elements

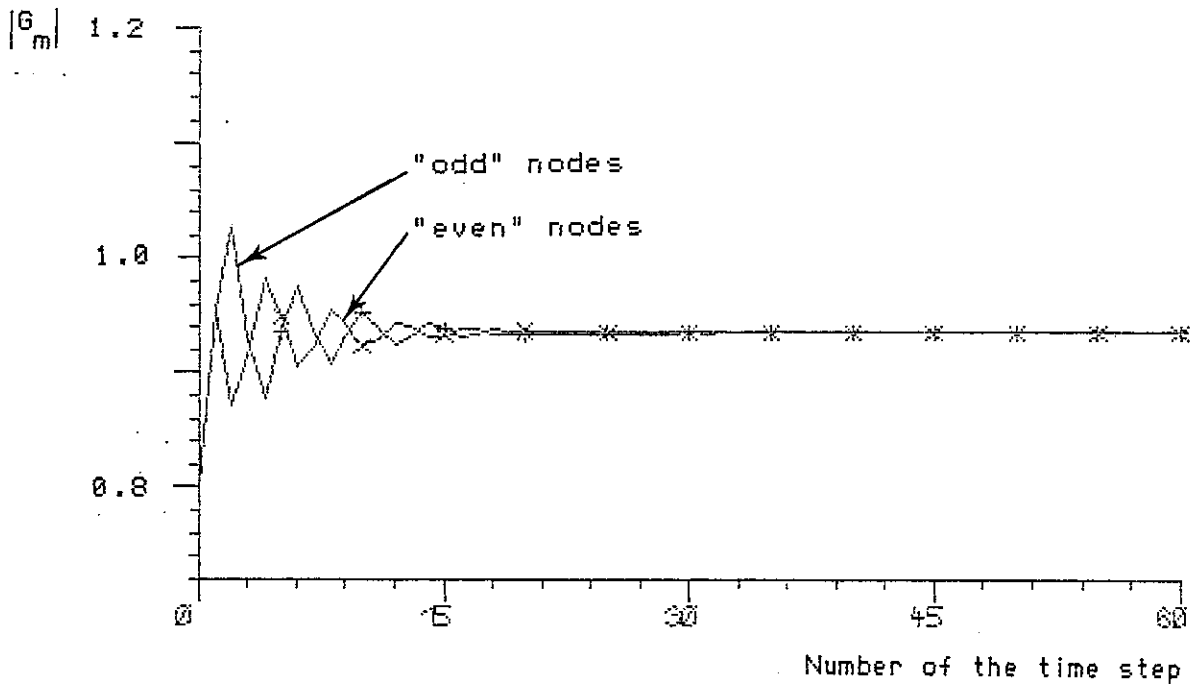


(c) 3P-LI3,  $L_m/\Delta x=4$

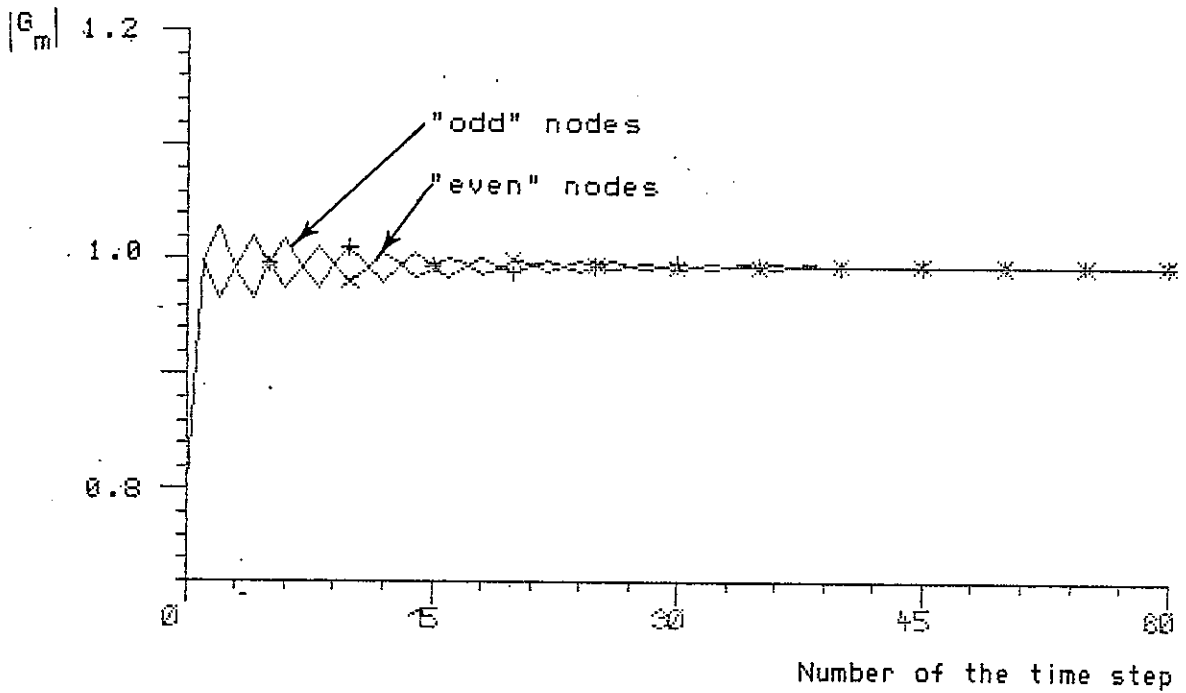


(d) 5P-LR3,  $L_m/\Delta x=4$

Fig. 4.10. Cont.



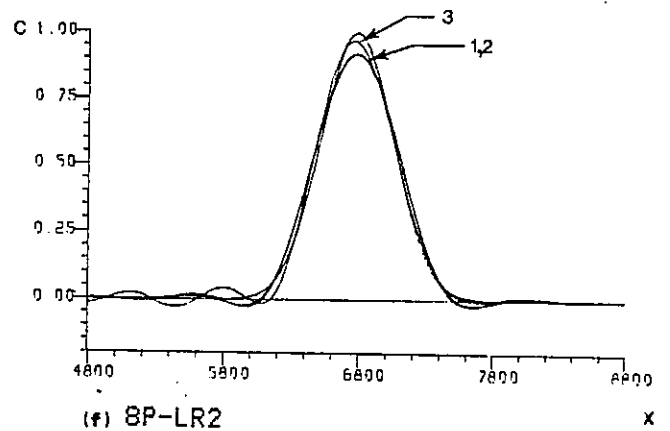
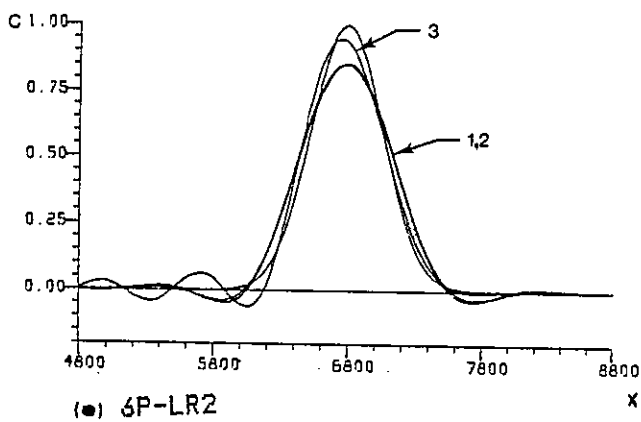
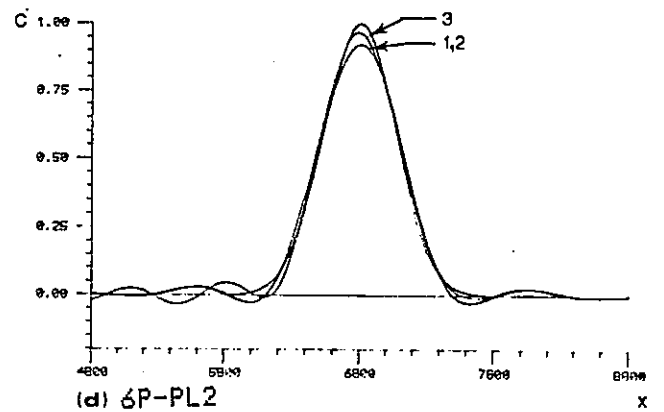
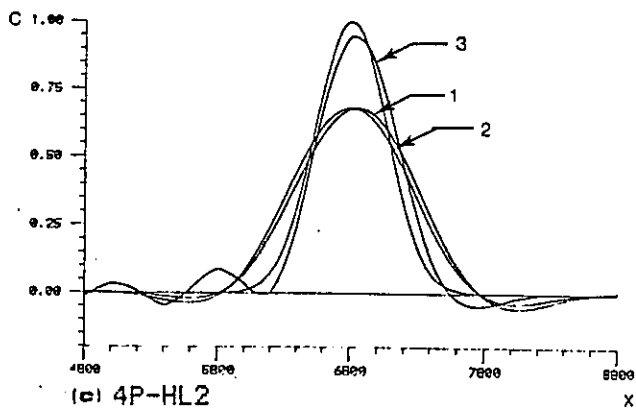
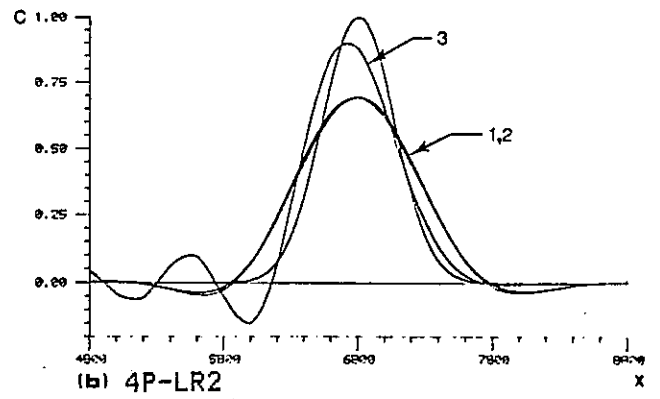
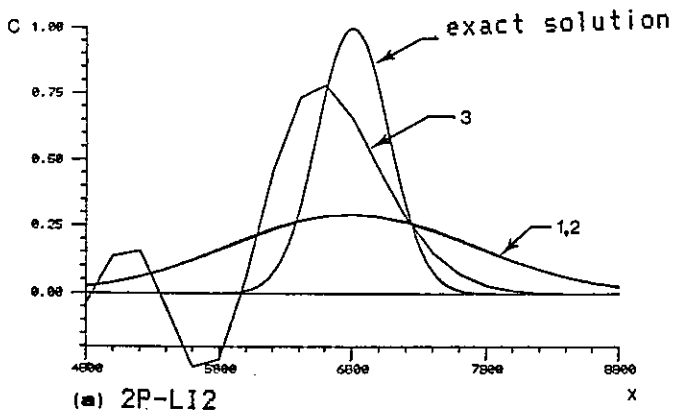
(e) 3P-L13,  $L_m/\Delta x=5$



(f) 5P-LR3,  $L_m/\Delta x=5$

Fig. 4.10. Cont.

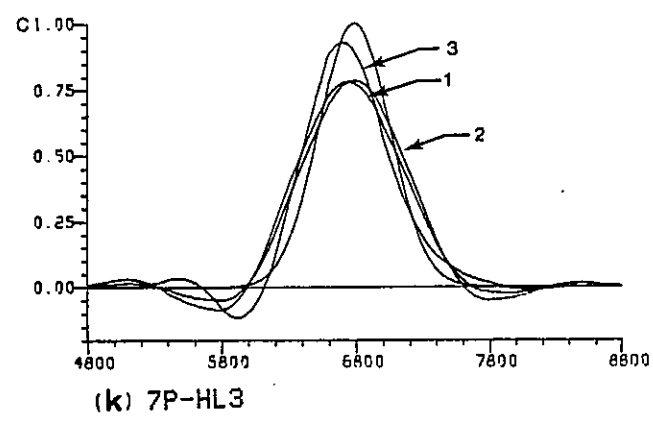
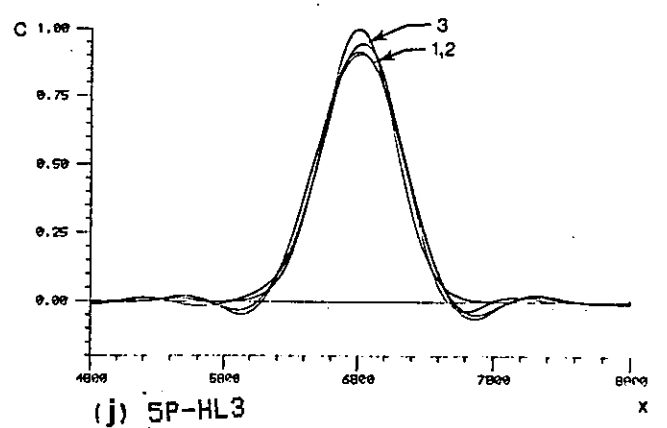
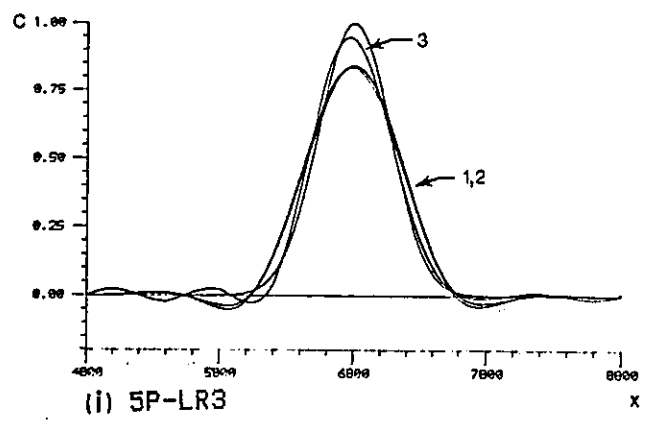
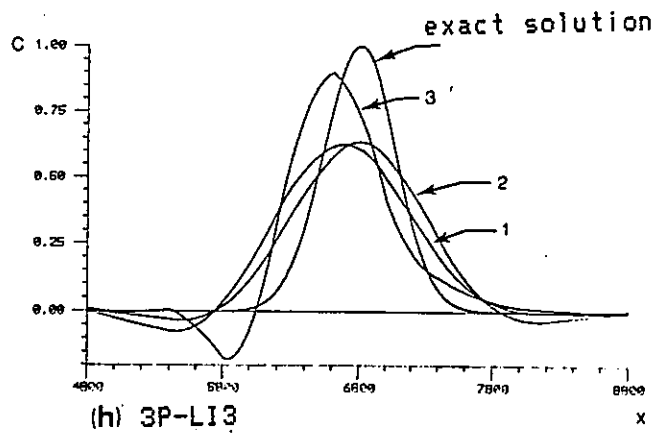
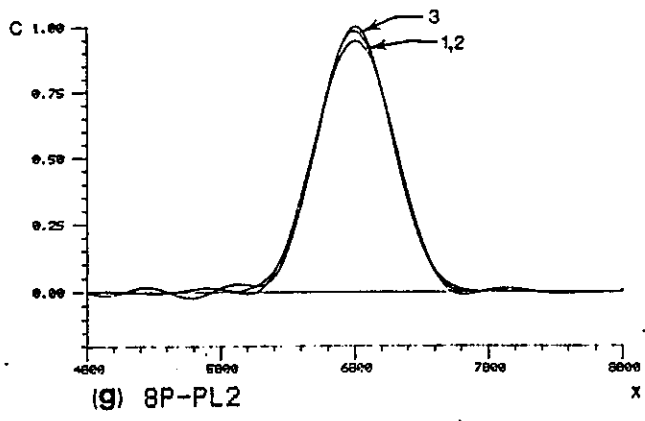




- 1 - Numerical solution
- 2 - Numerical solution purged from phase errors
- 3 - Numerical solution purged from amplitude errors

Fig. 4.11. Amplitude and phase errors in BMC solutions of the uniform advection of a Gauss-hill ( $Cu=0.24$ ;  $N=100$ ;  $\sigma_0/\Delta x=1.32$ ;  $t=T=9600$ )





- 1 - Numerical solution
- 2 - Numerical solution purged from phase errors
- 3 - Numerical solution purged from amplitude errors

Fig. 4.11. Cont.

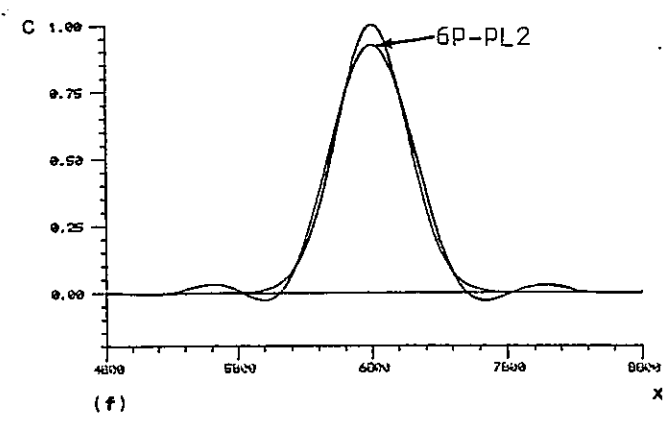
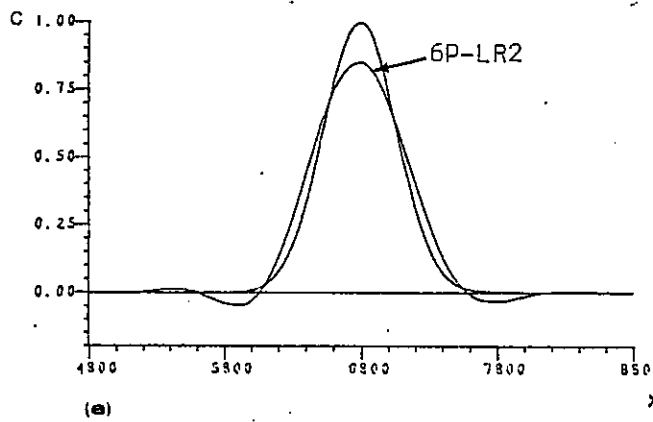
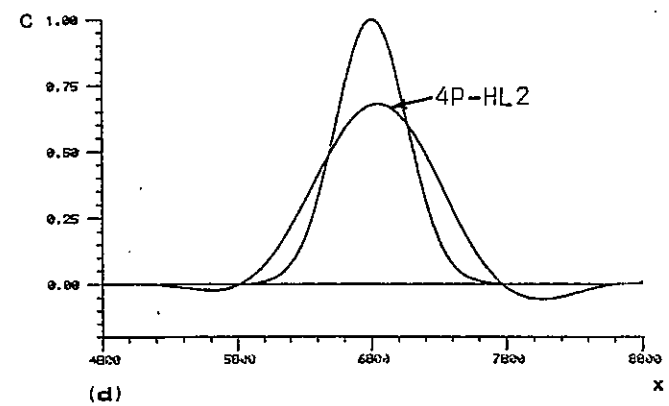
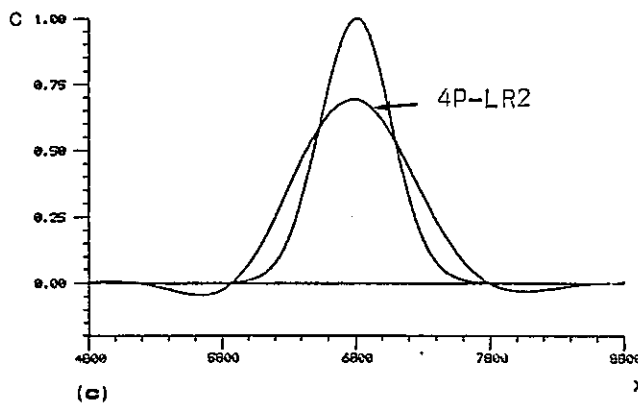
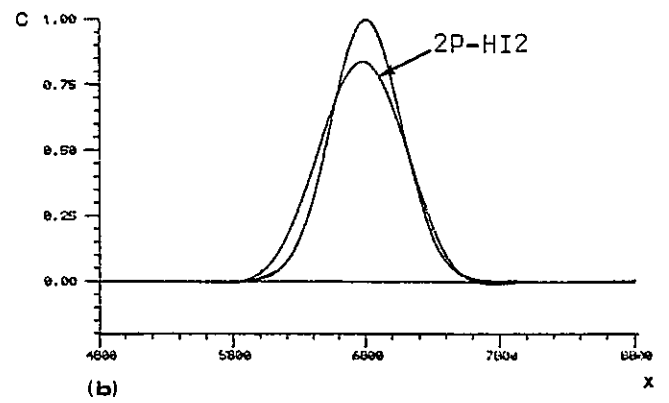
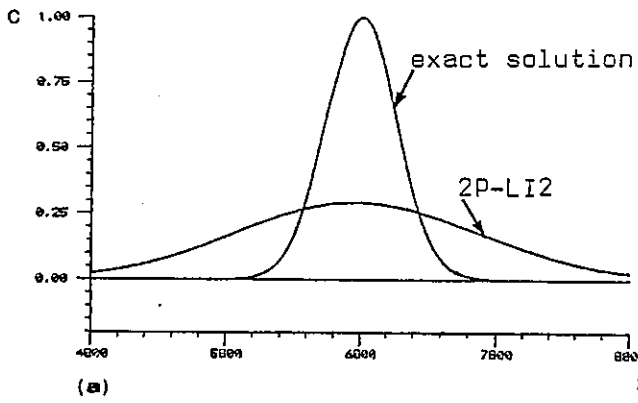


Fig. 4.12. BMC solutions for the uniform advection of a Gauss-hill ( $C_0=0.24$ ;  $N=100$ ;  $C_0/\Delta x=1.32$ ;  $t=T=9600$ )

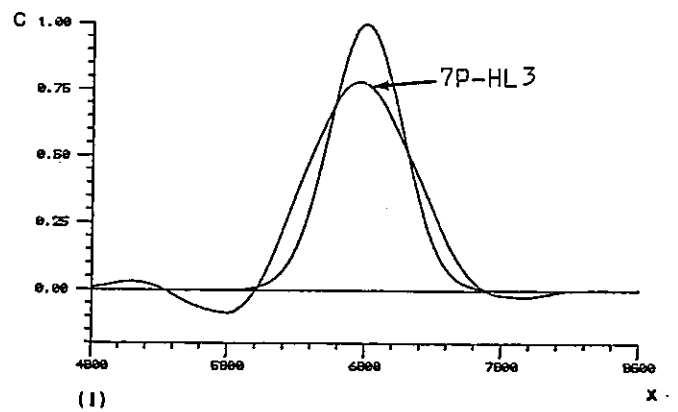
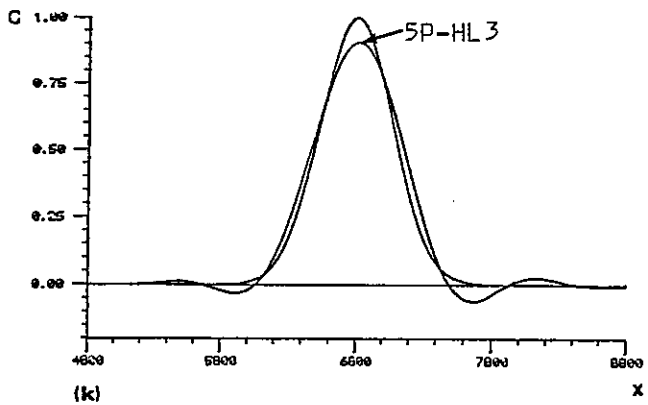
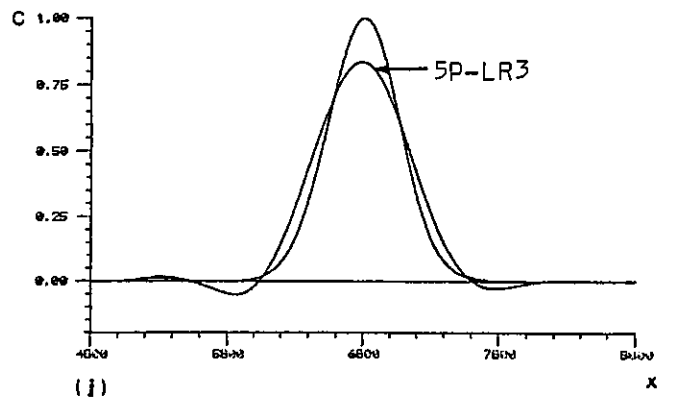
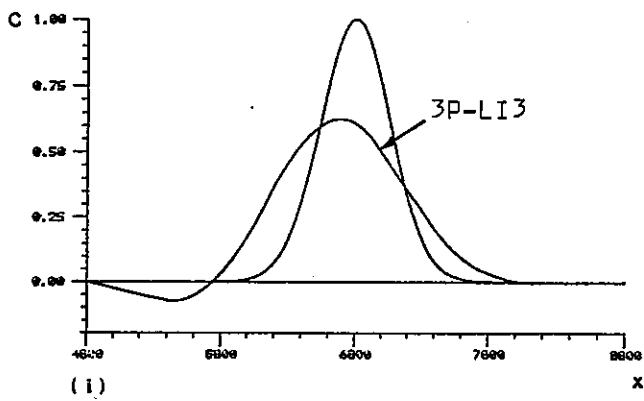
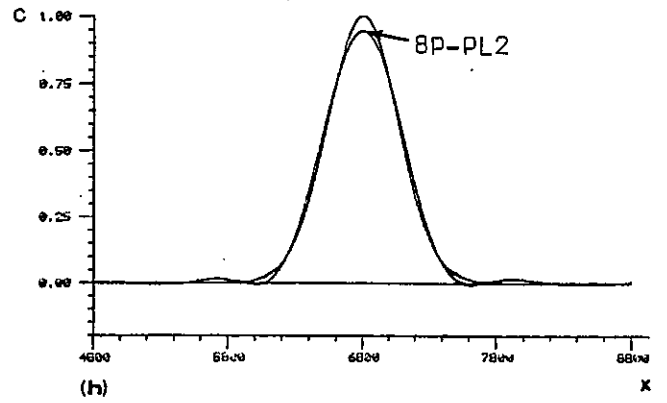
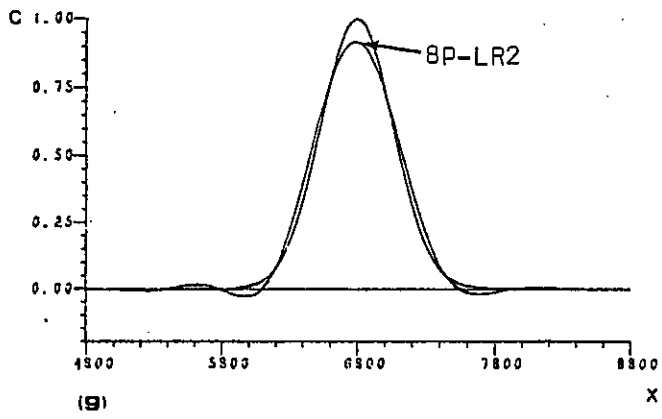


Fig. 4.12. Cont.

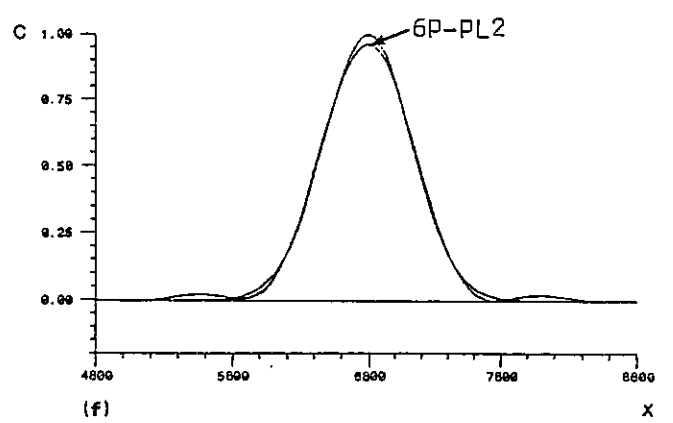
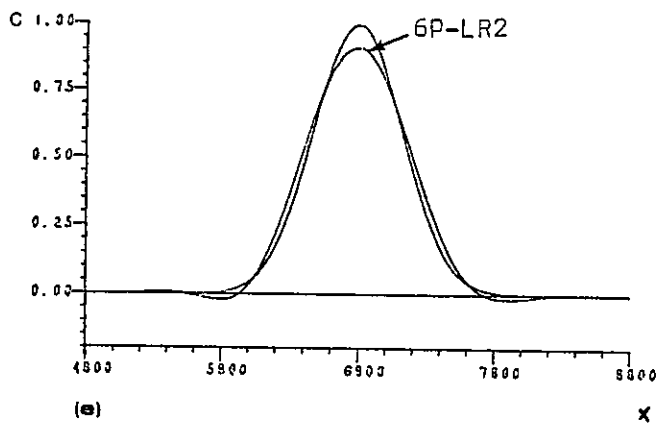
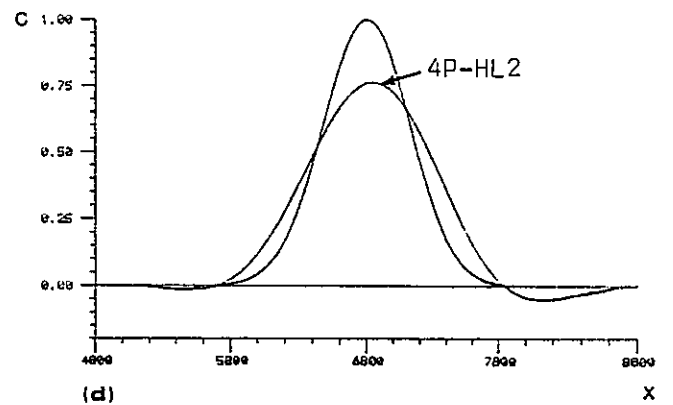
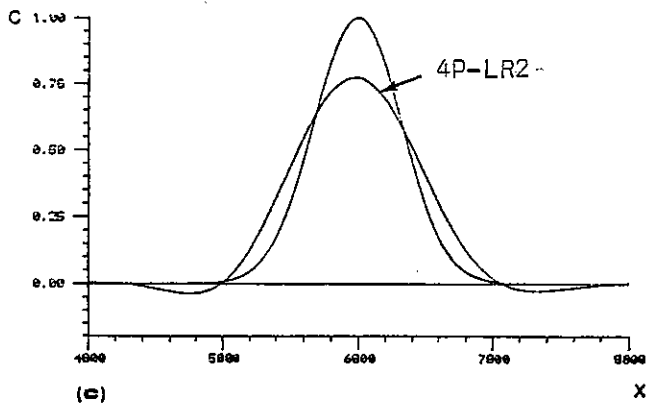
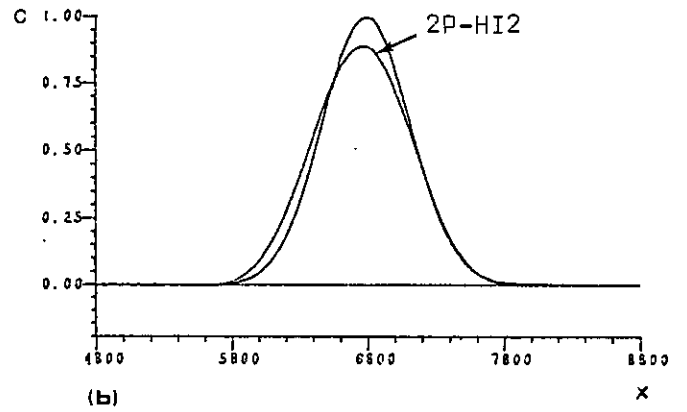
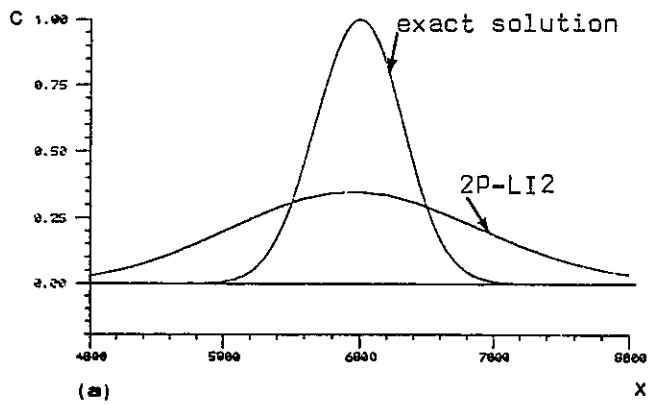


Fig. 4.13. BMC solutions for the uniform advection of a Gauss-hill ( $Cu=0.24$ ;  $N=100$ ;  $\sigma_0/\Delta x=1.6$ ;  $t=T=9600$ )

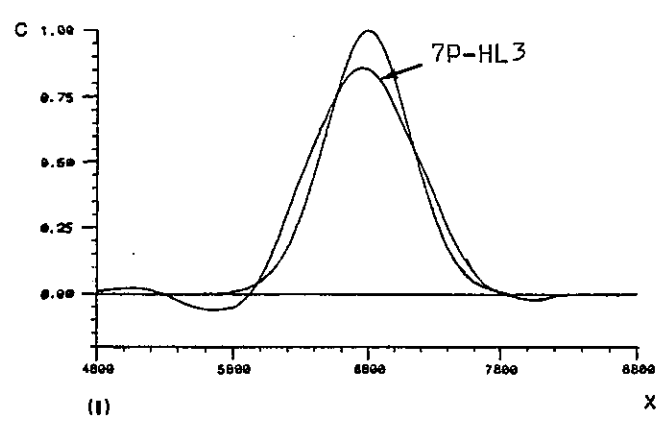
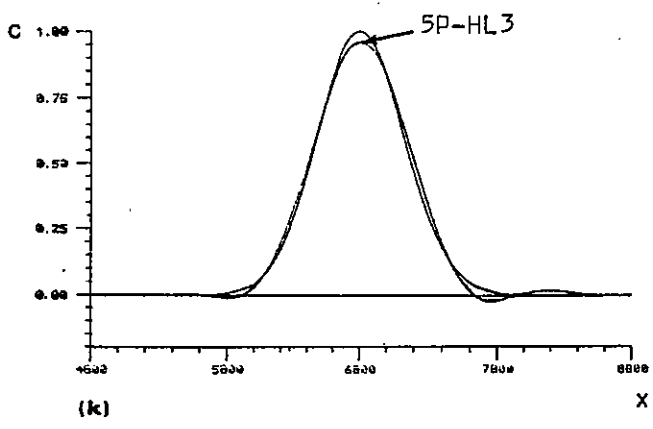
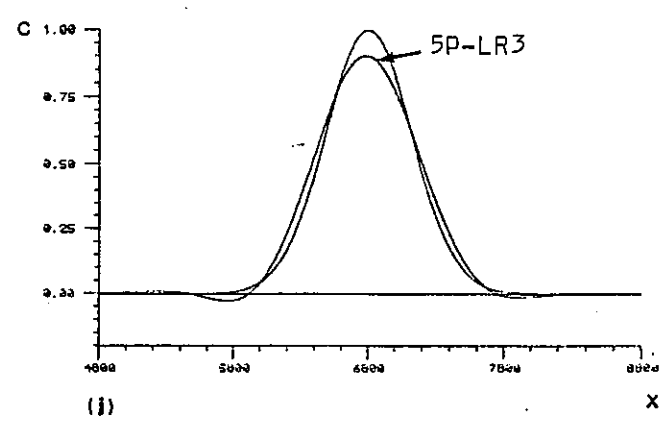
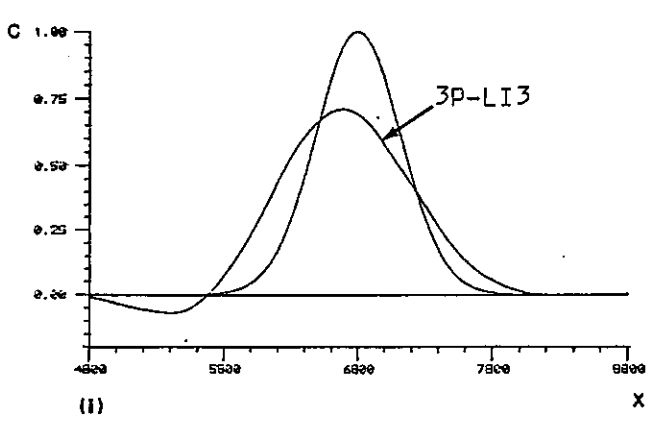
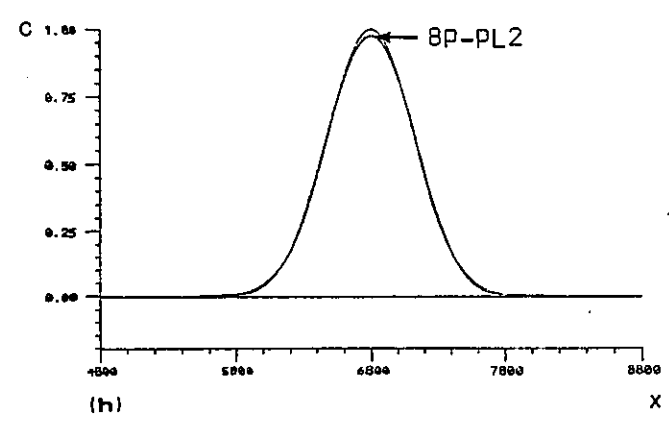
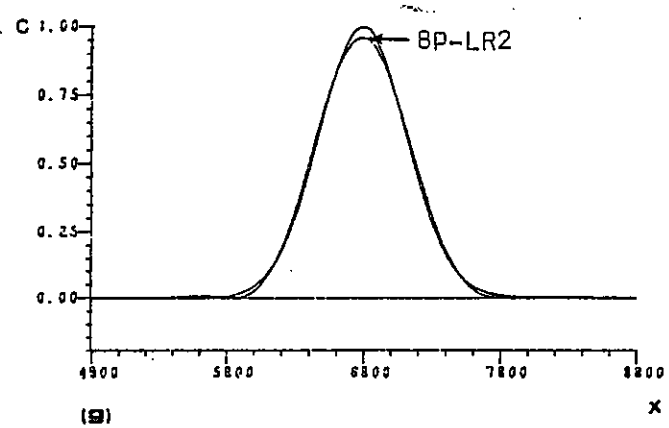


Fig. 4.13. Cont.

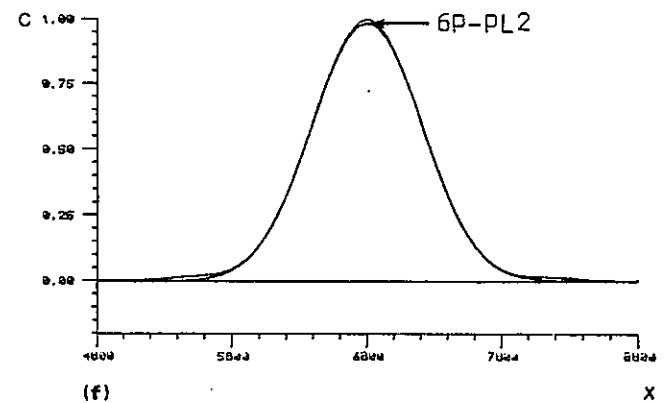
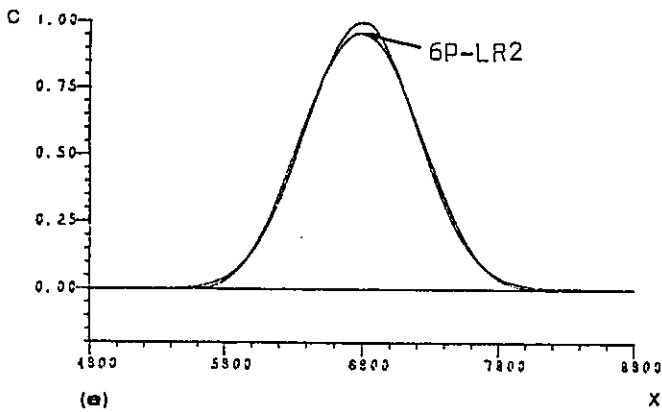
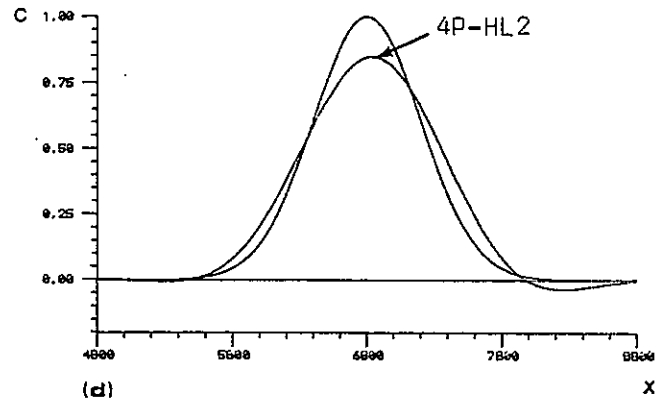
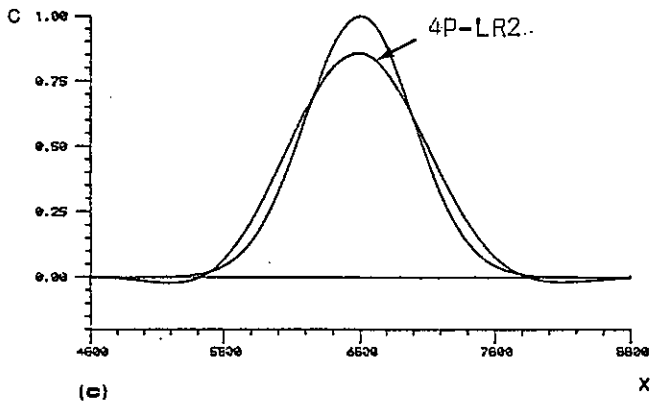
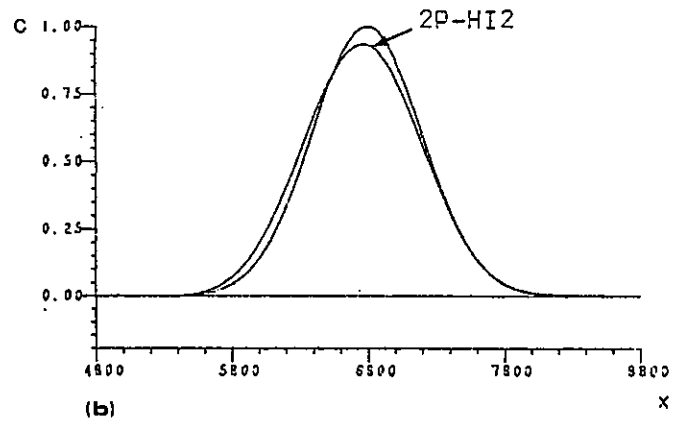
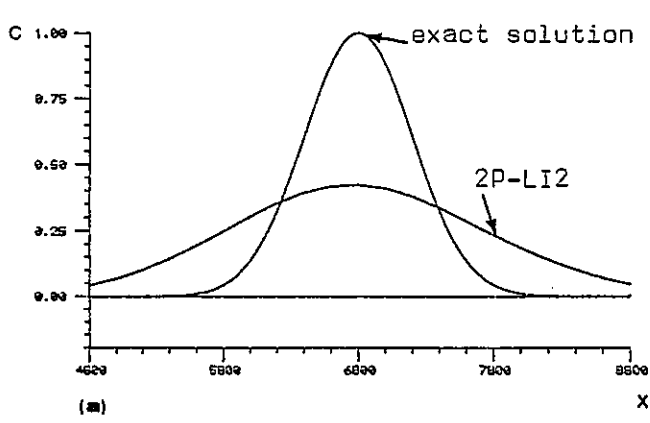


Fig. 4.14. BMC solutions for the uniform advection of a Gauss-hill ( $Cu=0.24$ ;  $N=100$ ;  $\sigma_0/\Delta x=2.0$ ;  $t=T=9600$ )

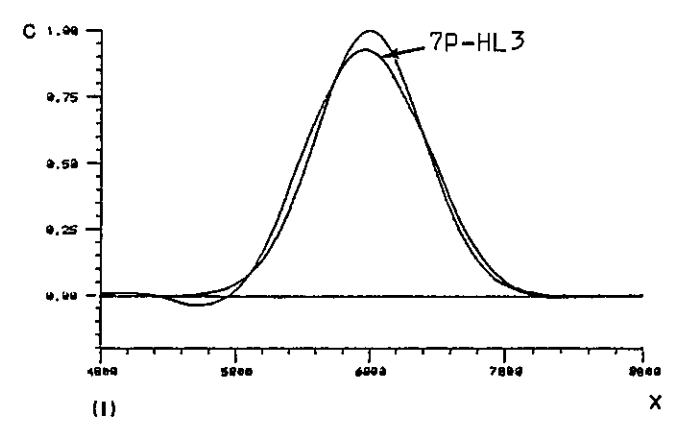
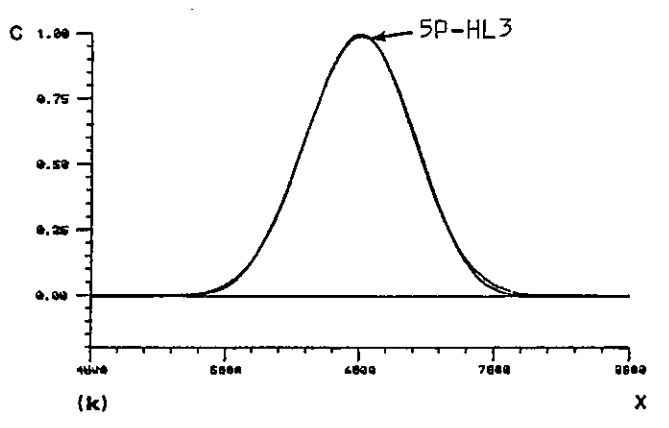
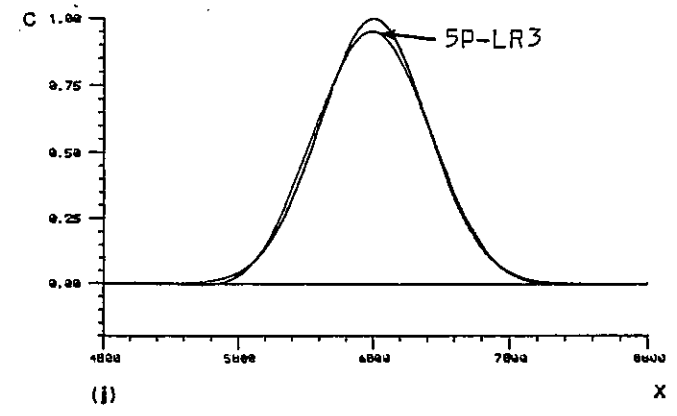
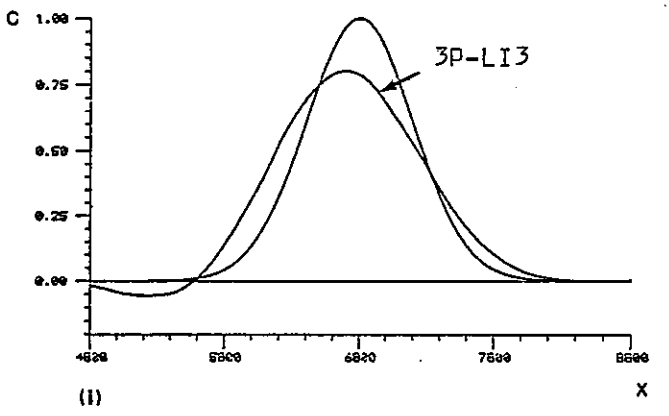
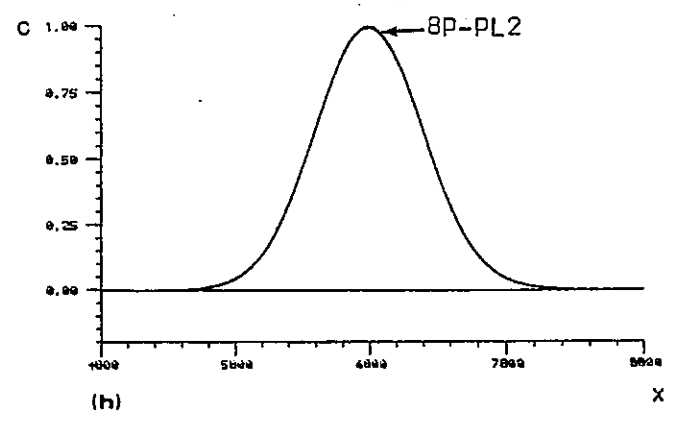
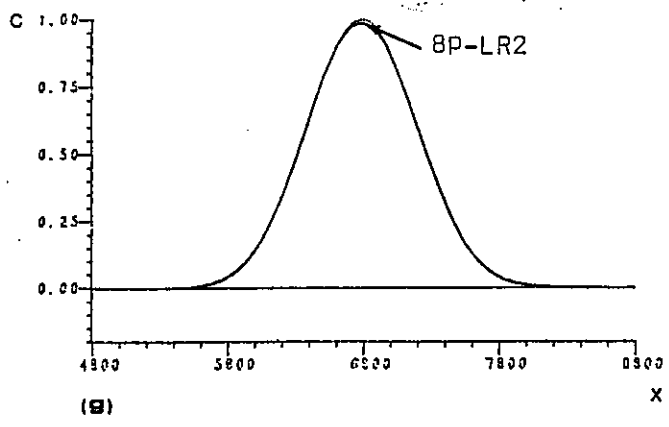


Fig. 4.14. Cont.

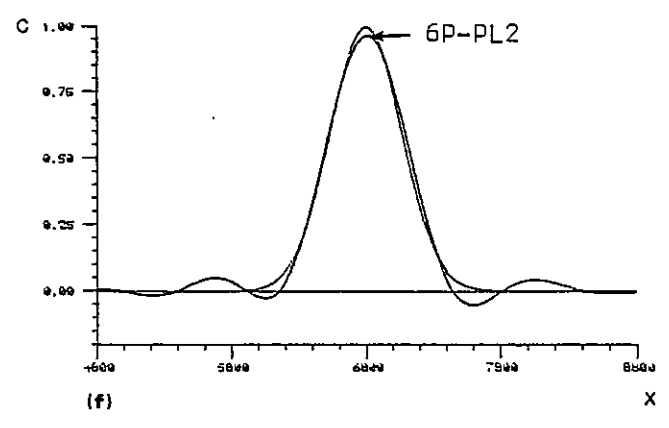
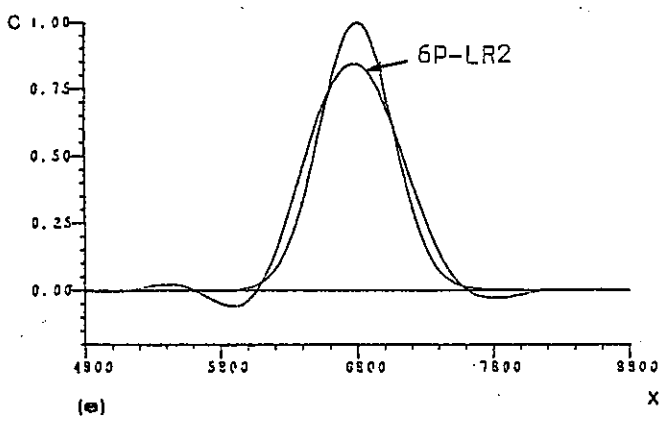
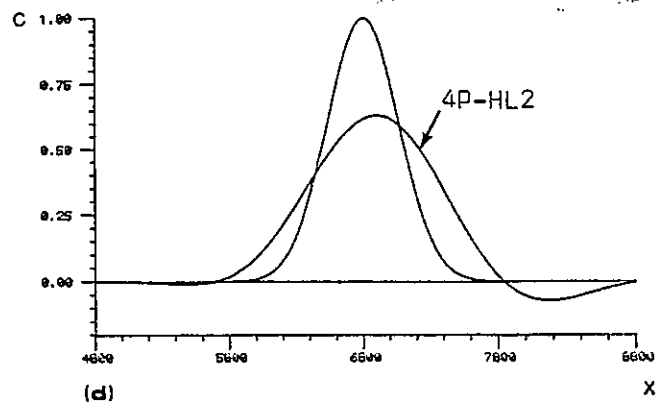
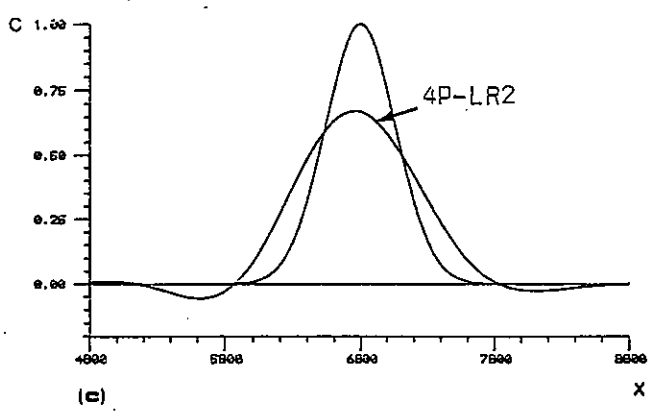
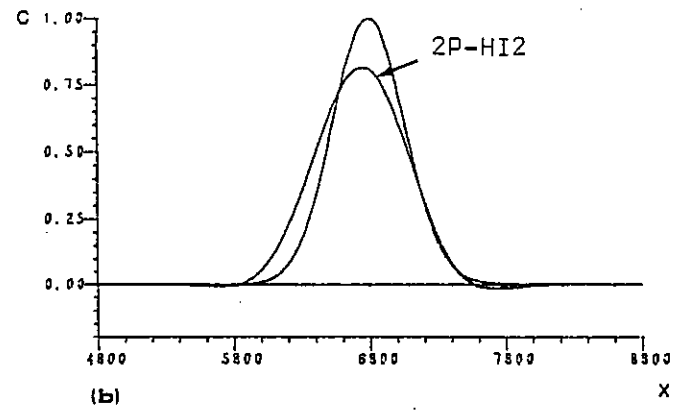
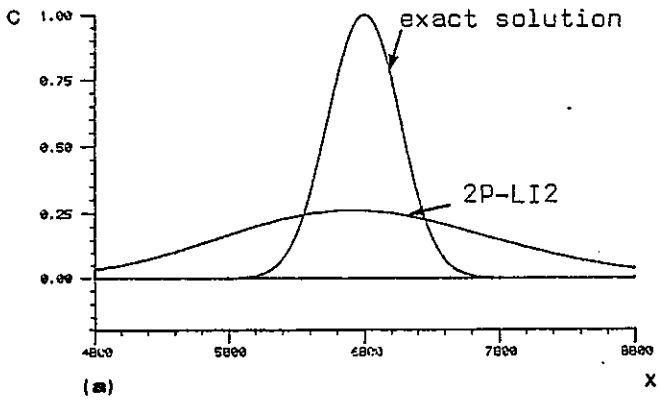


Fig. 4.15. BMC solutions for the uniform advection of a Gauss-hill ( $Cu=0.024$ ;  $N=1000$ ;  $\sigma_0/\Delta x=1.32$ ;  $t=T=9600$ )



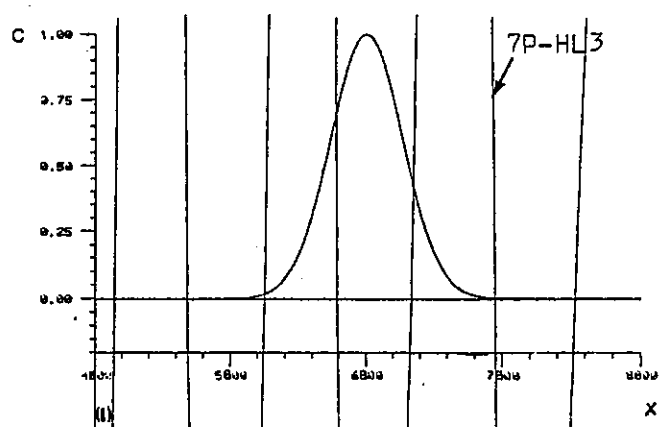
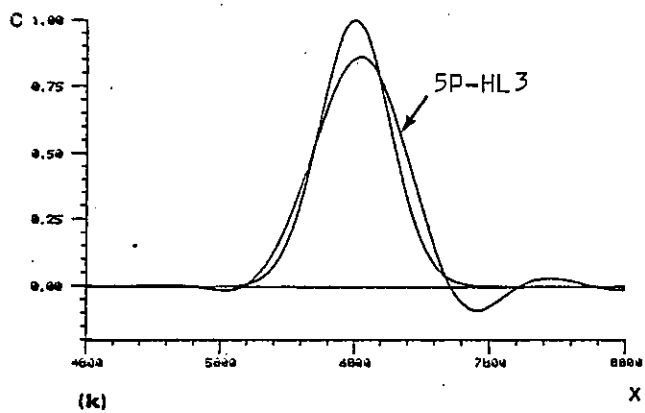
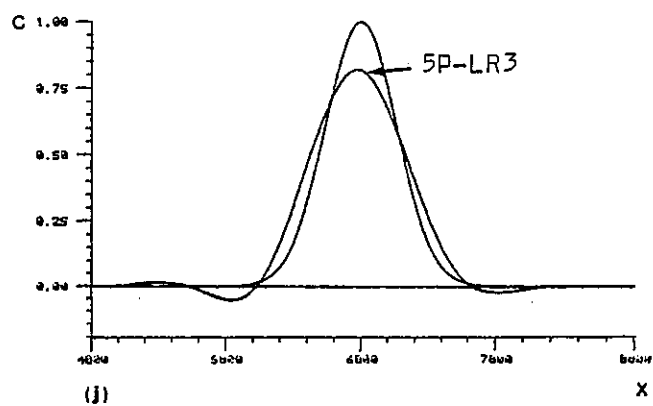
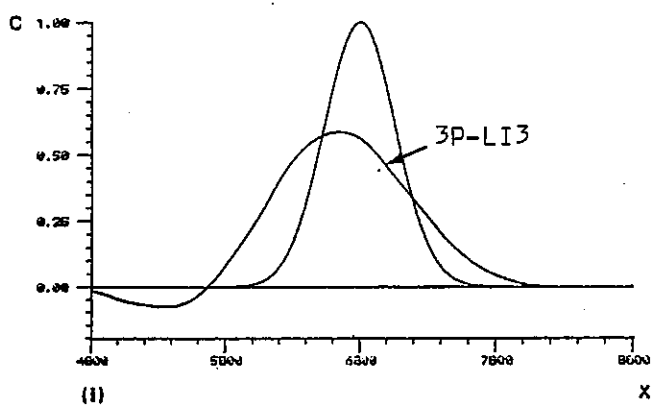
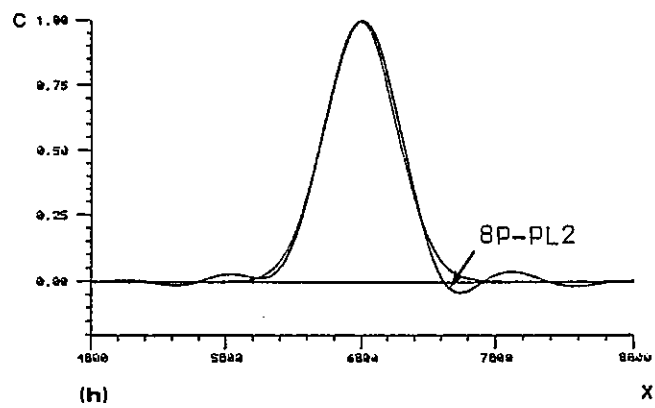
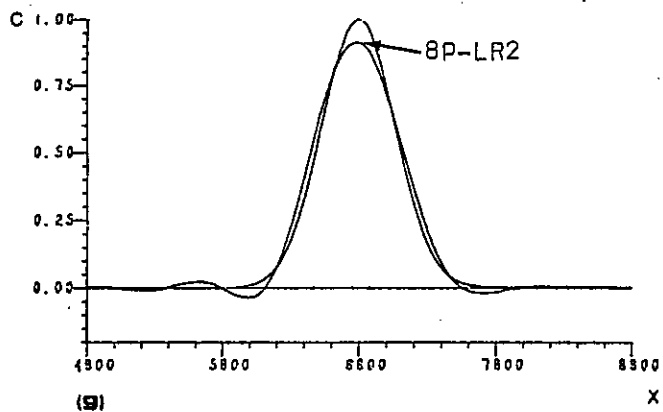


Fig. 4.15. Cont.

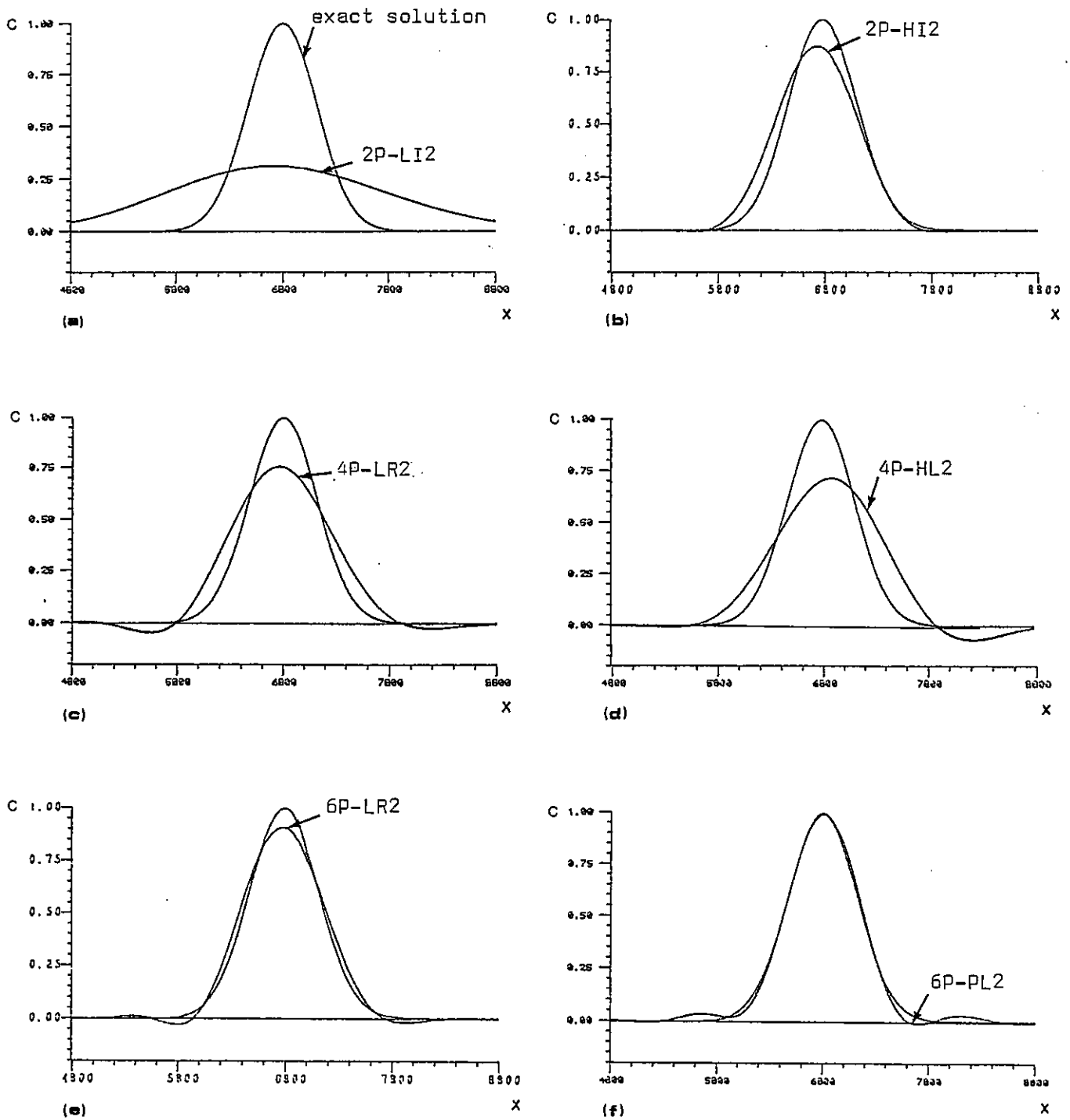


Fig. 4.16. BMC solutions for the uniform advection of a Gauss-hill ( $C_0=0.024$ ;  $N=1000$ ;  $C_0/\Delta x=1.6$ ;  $t=T=9600$ )

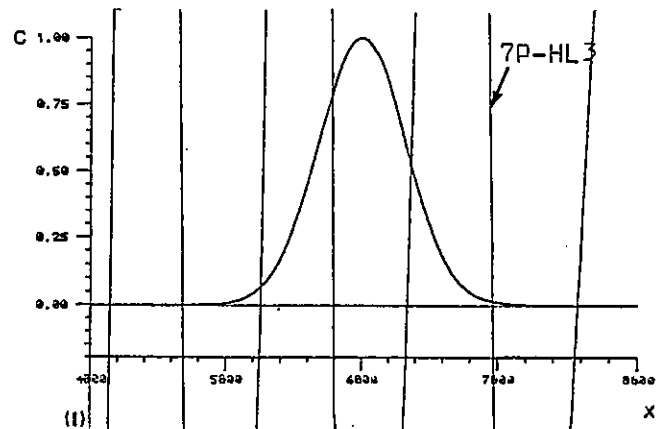
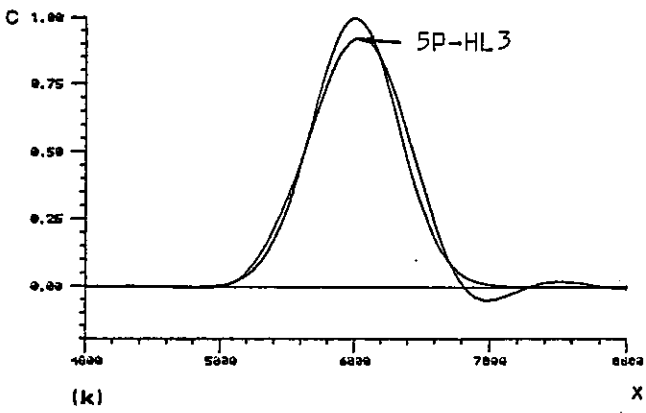
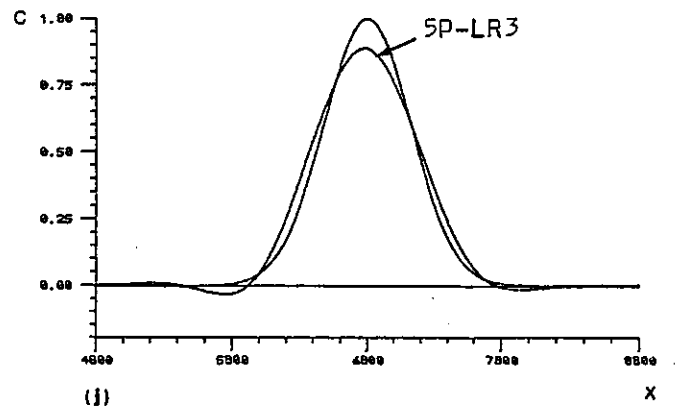
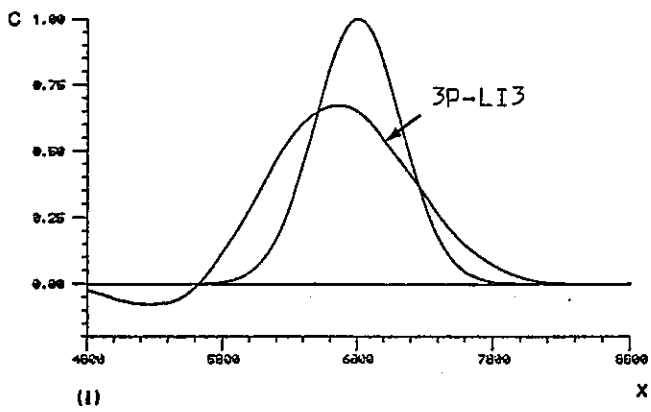
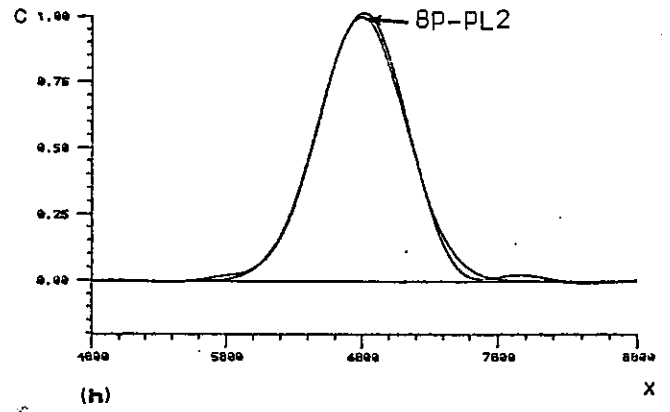
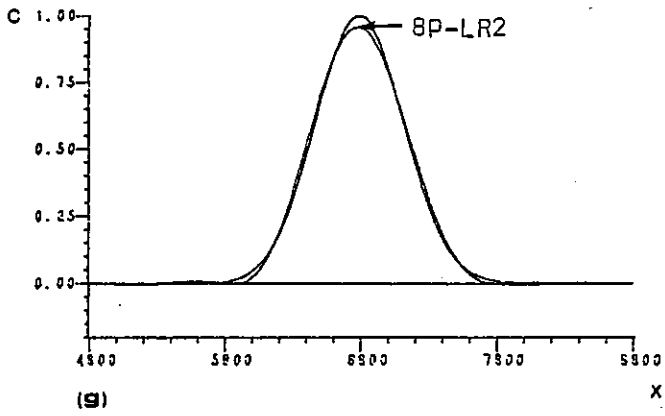


Fig. 4.16. Cont.

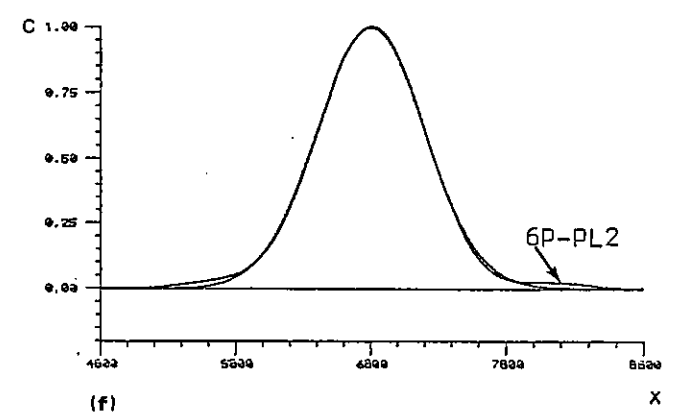
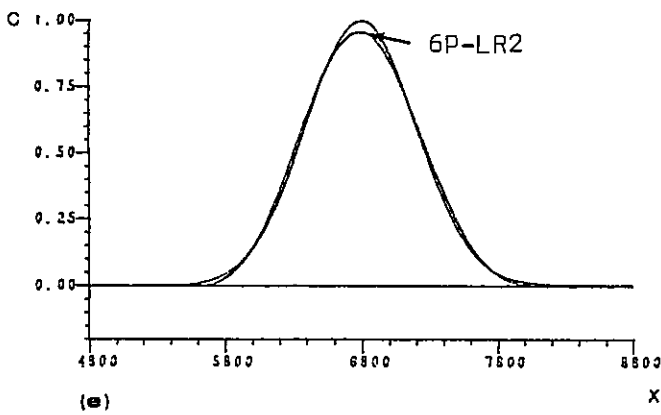
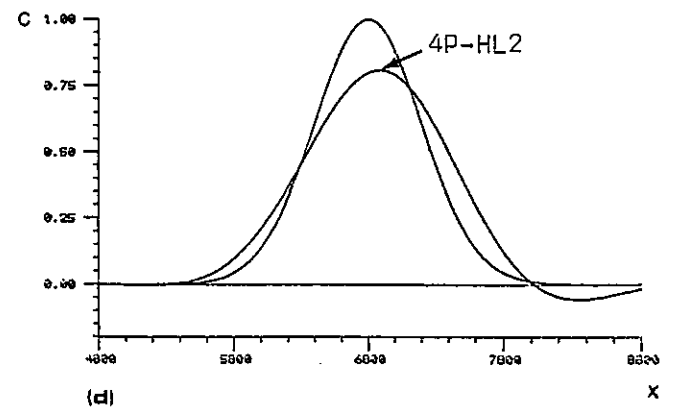
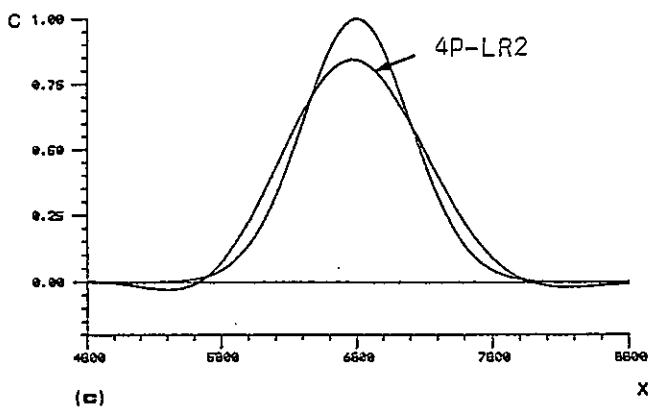
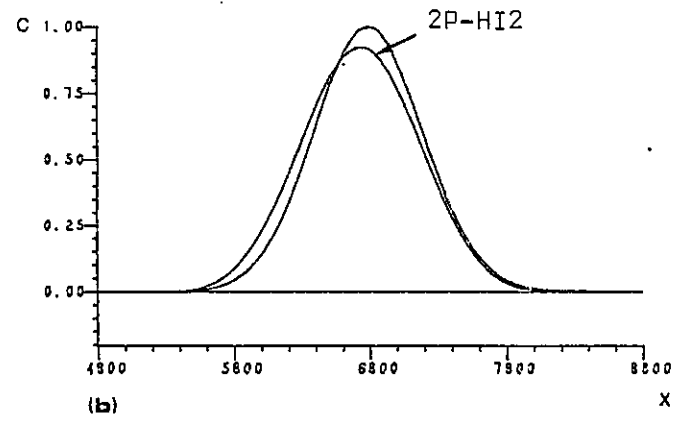
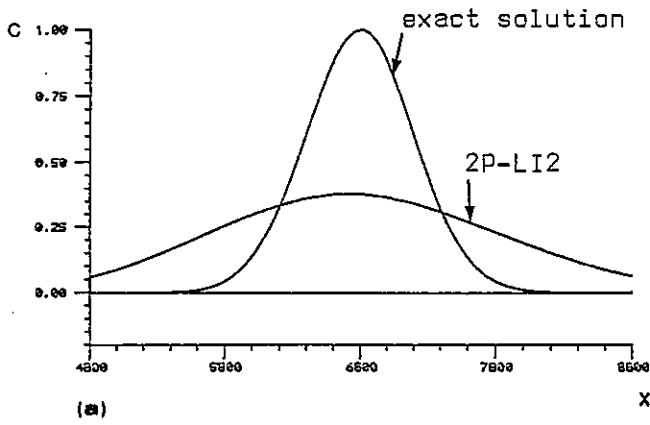


Fig. 4.17 BMC solutions for the uniform advection of a Gauss-hill ( $Cu=0.024$ ;  $N=1000$ ;  $C_0/\Delta x=2.0$ ;  $t=T=9600$ )

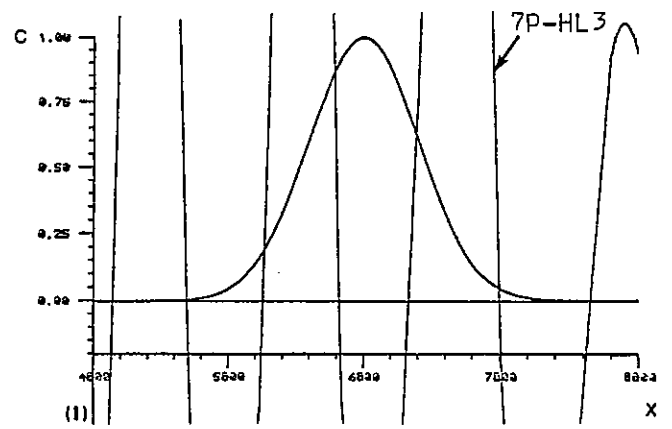
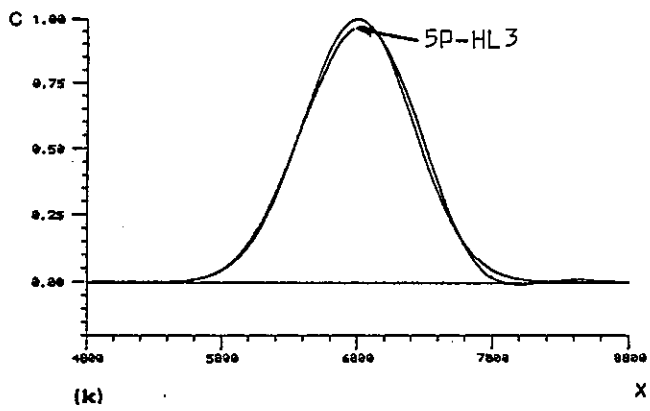
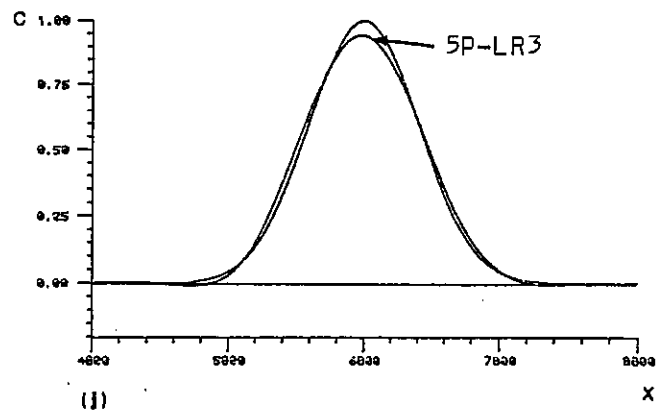
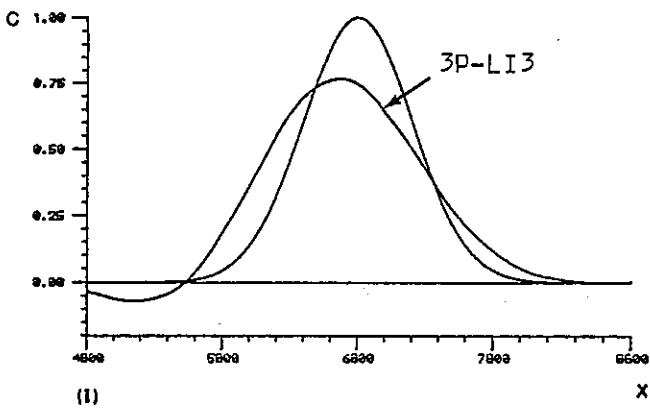
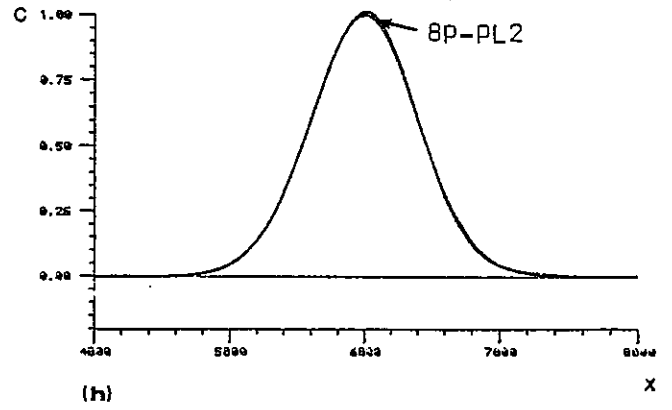
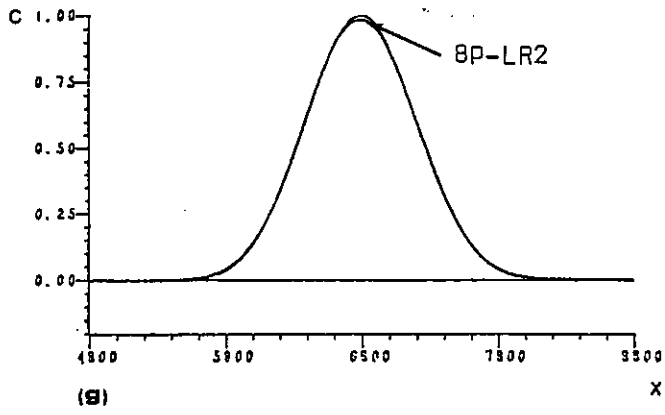


Fig. 4.17. Cont.

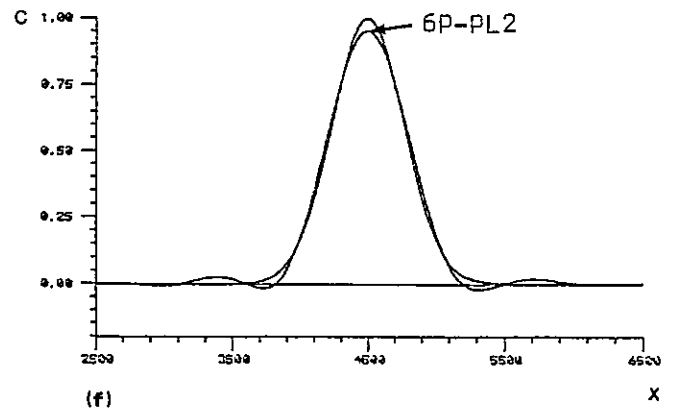
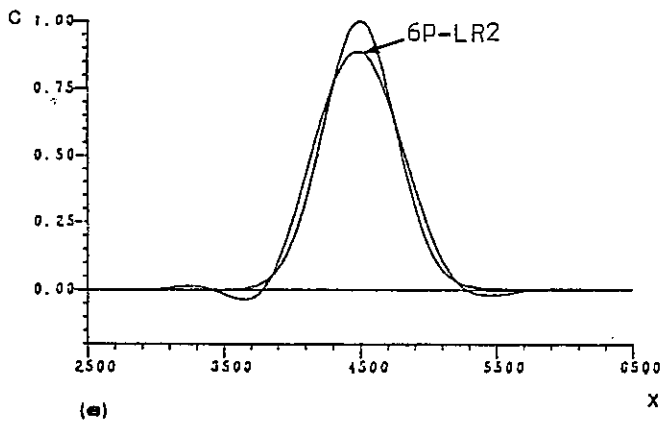
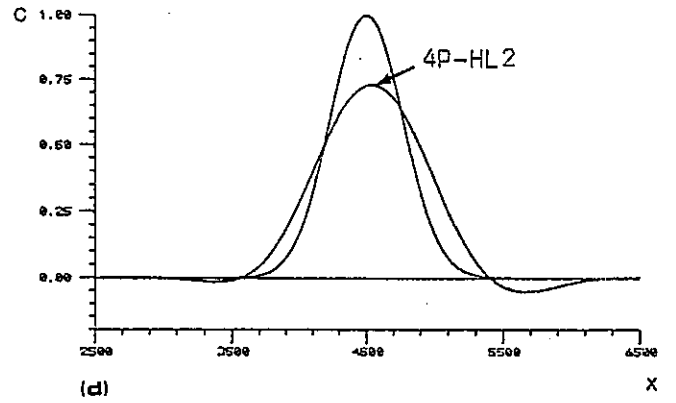
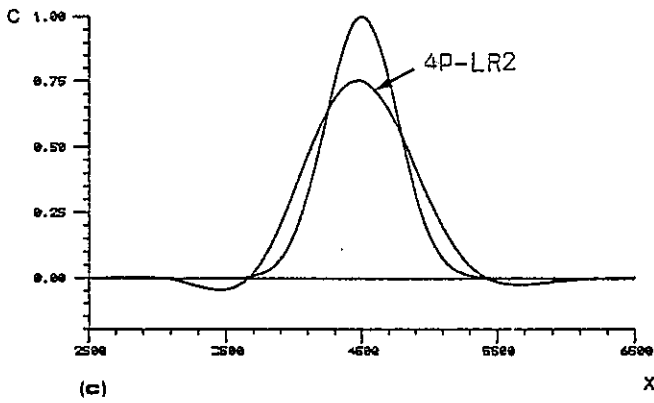
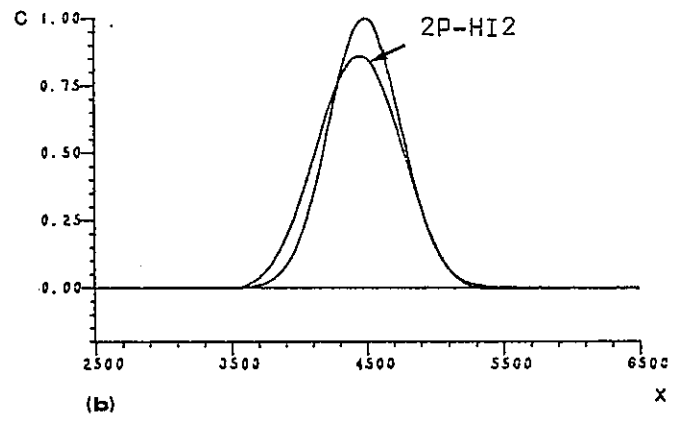
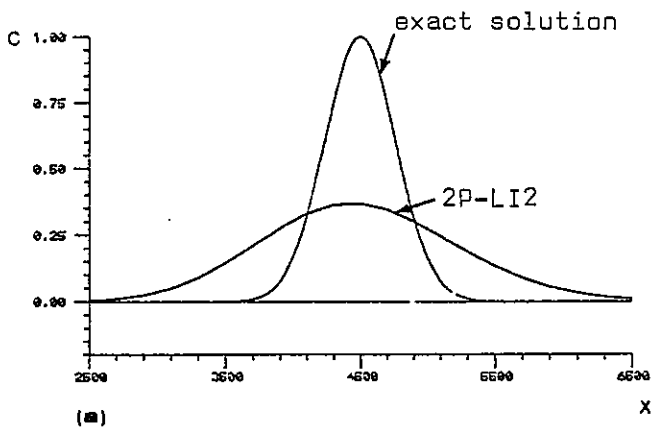


Fig. 4.18. BMC solutions for the uniform advection of a Gauss-hill ( $Cu=0.125$ ;  $N=100$ ;  $\sigma_0/\Delta x=1.32$ ;  $t=T=5000$ )

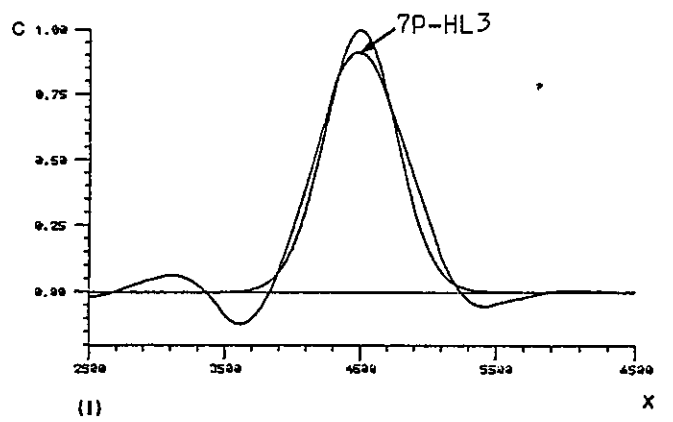
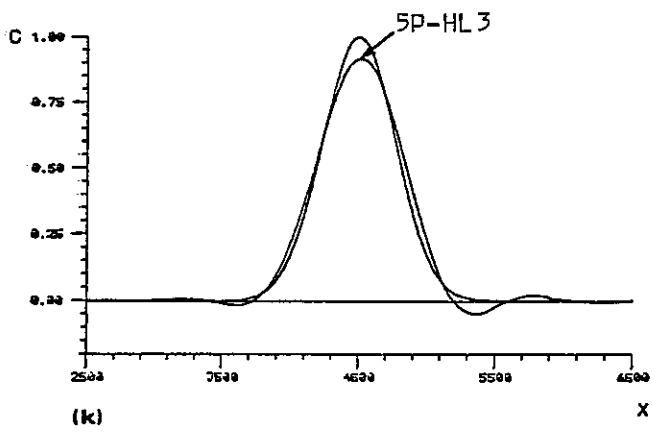
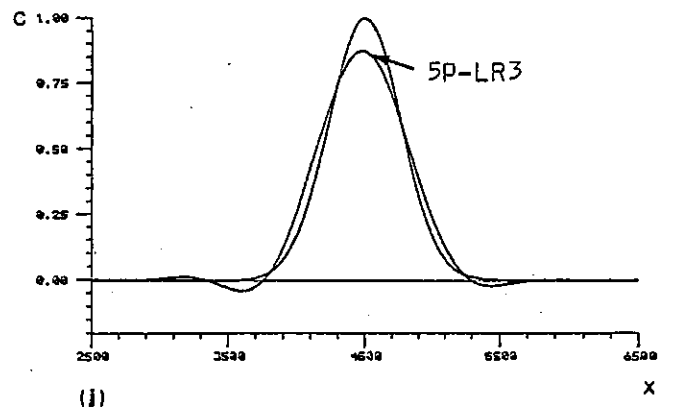
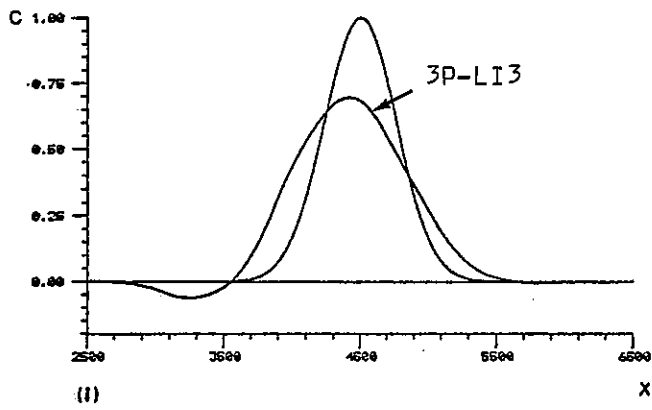
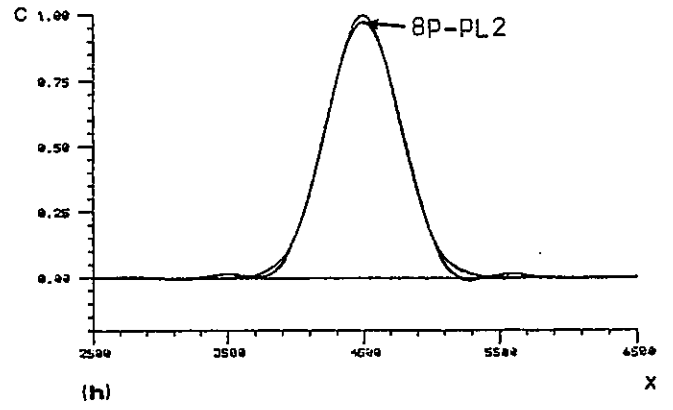
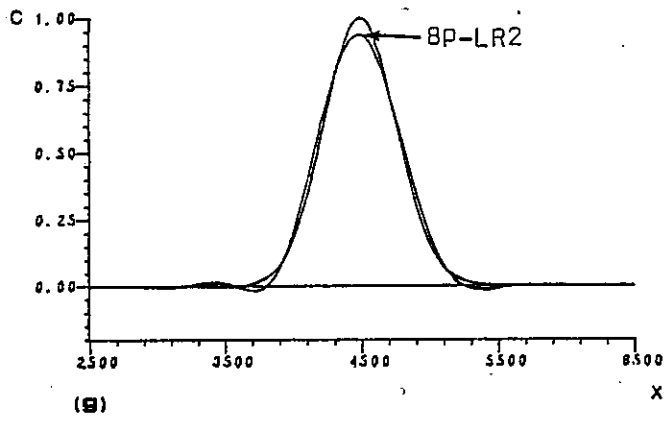


Fig. 4.18. Cont.

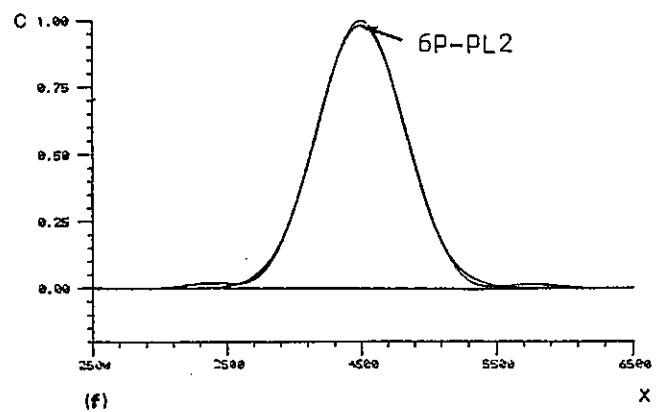
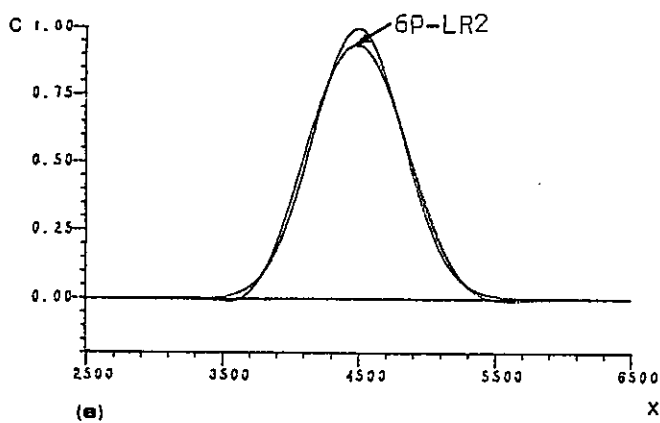
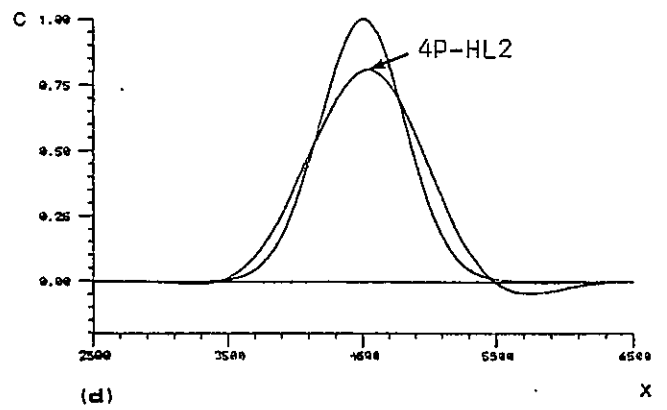
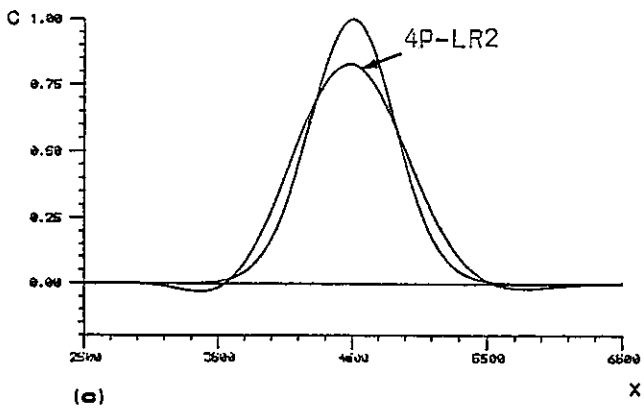
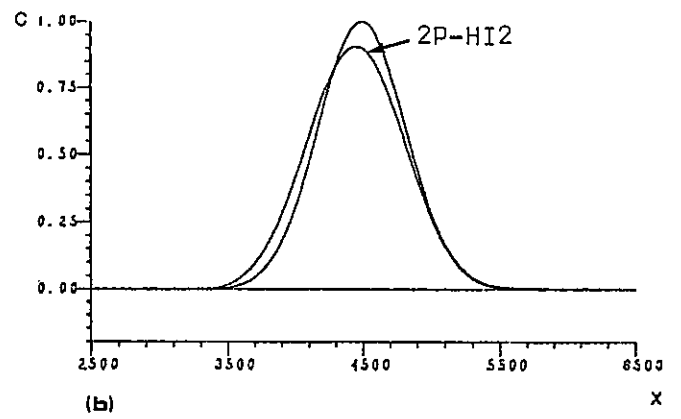
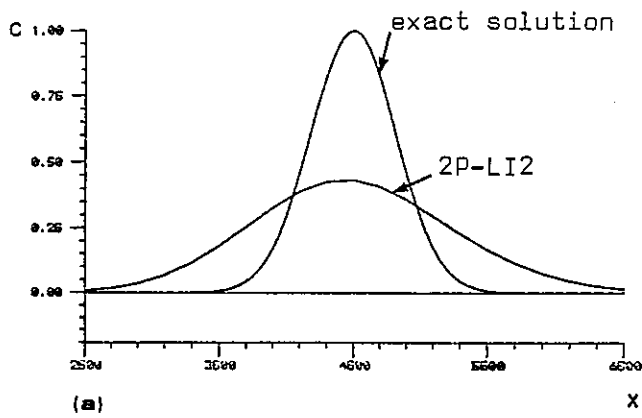


Fig. 4.19. BMC solutions for the uniform advection of a Gauss-hill ( $Cu=0.125$ ;  $N=100$ ;  $\sigma_0/\Delta x=1.6$ ;  $t=T=5000$ )



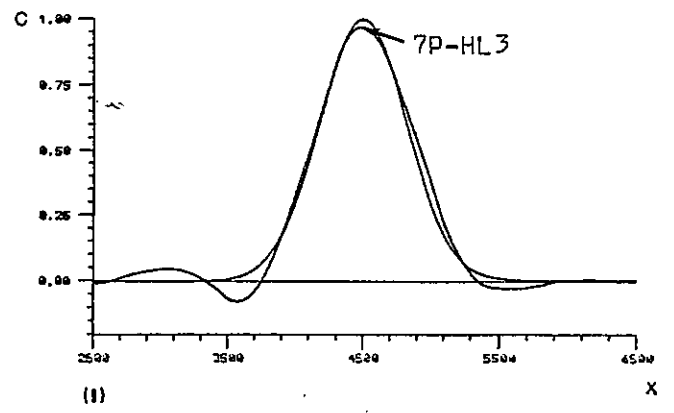
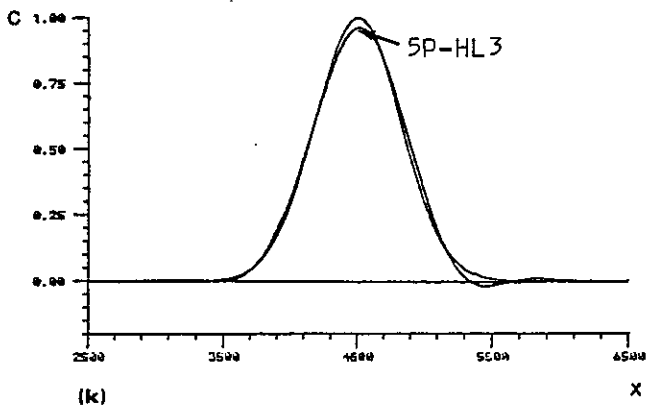
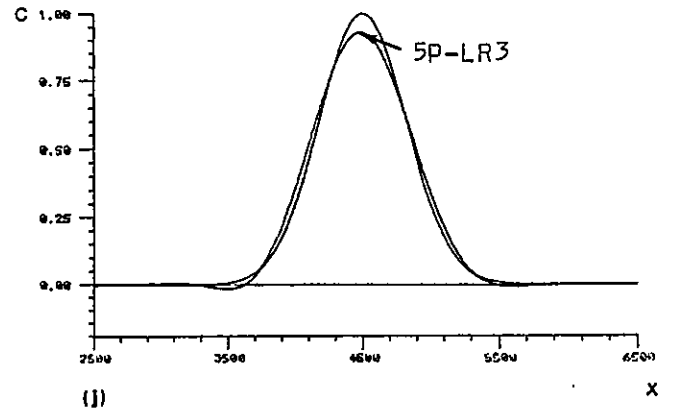
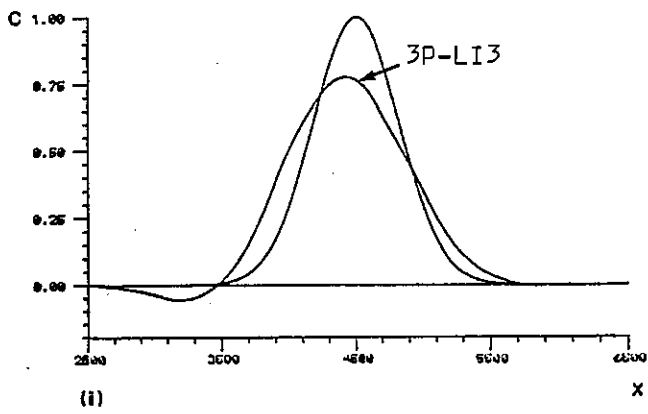
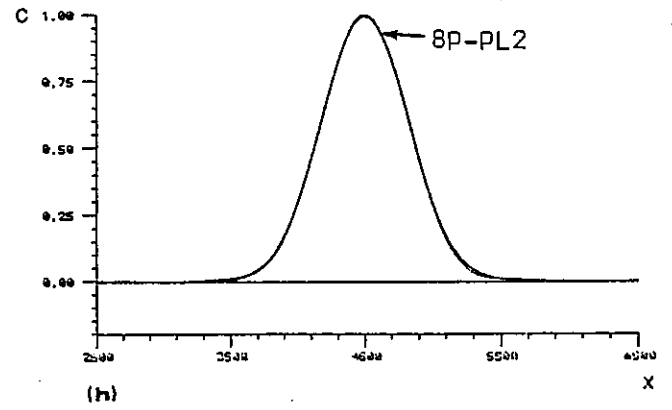
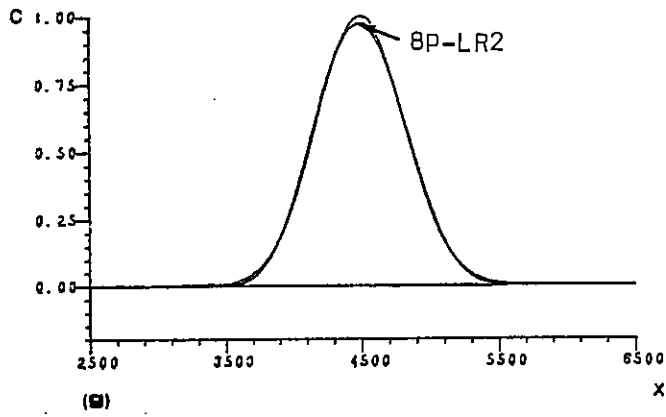


Fig. 4.19. Cont.

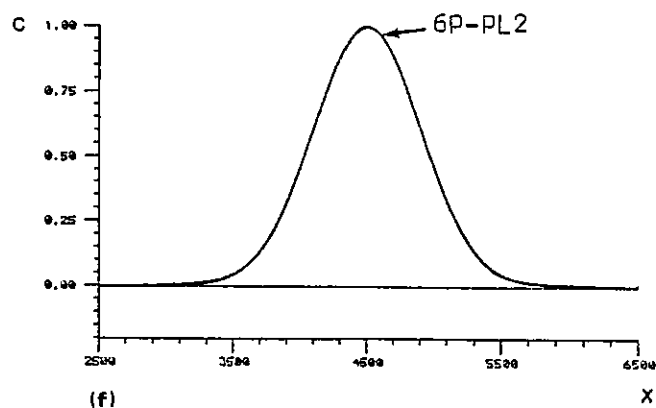
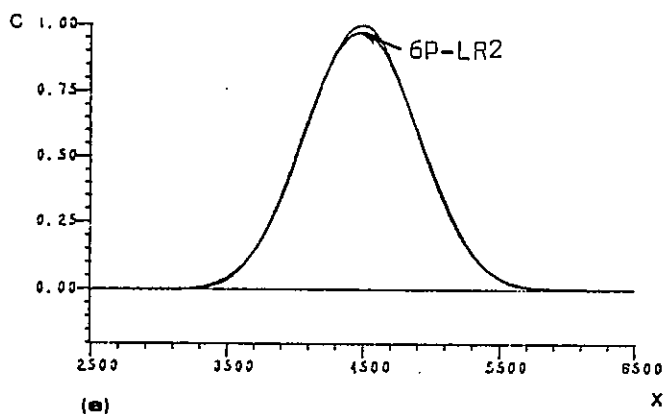
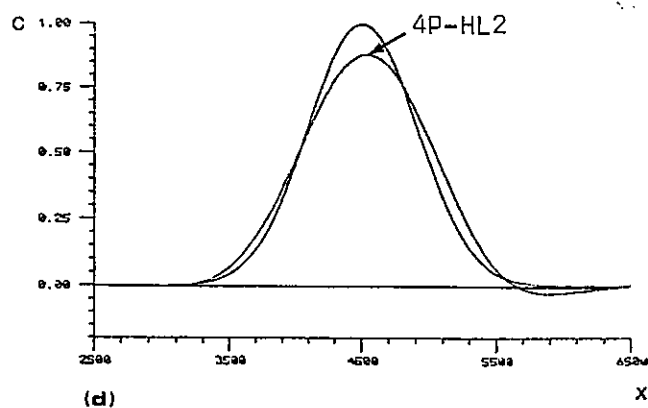
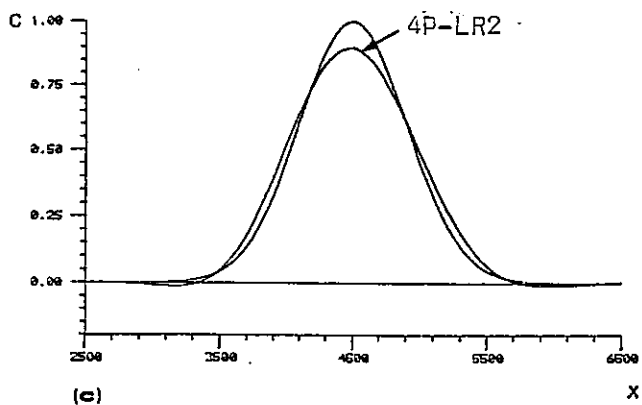
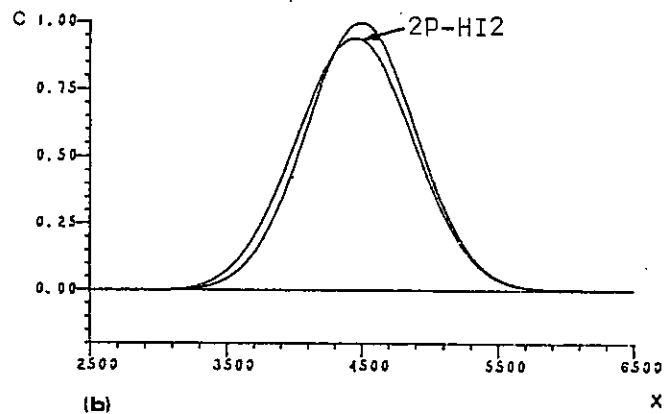
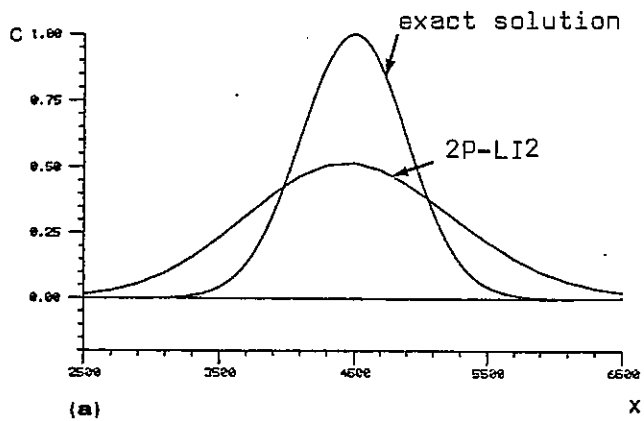


Fig. 4.20. BMC solutions for the uniform advection of a Gauss-hill ( $C_0=0.125$ ;  $N=100$ ;  $\sigma_0/\Delta x=2.0$ ;  $t=T=5000$ )

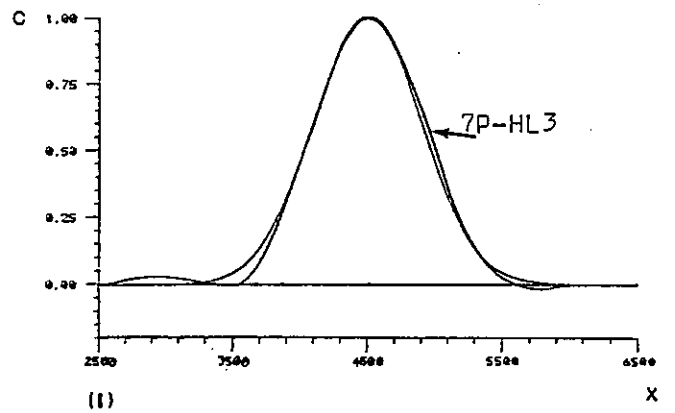
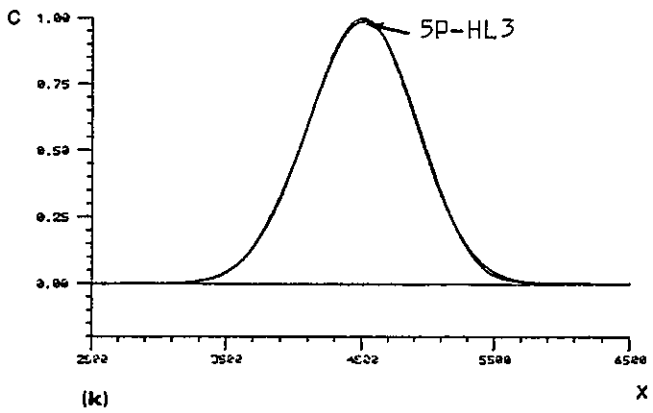
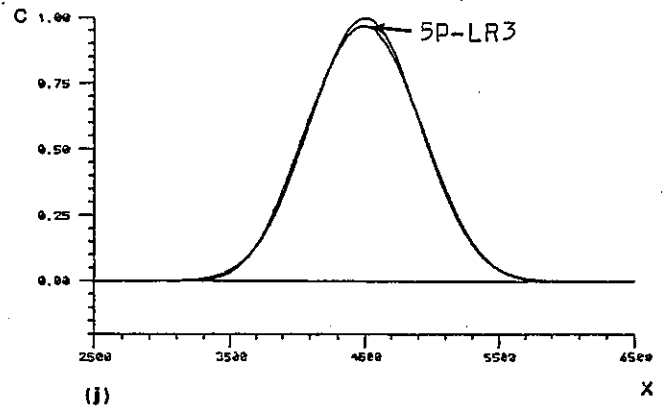
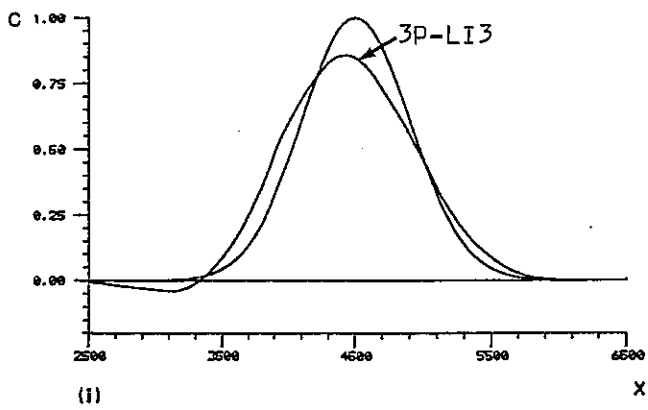
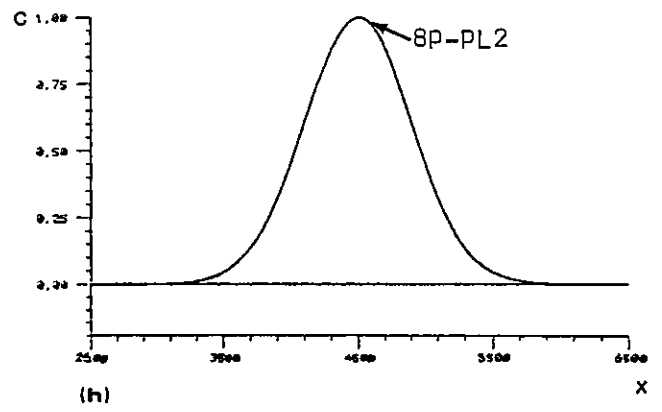
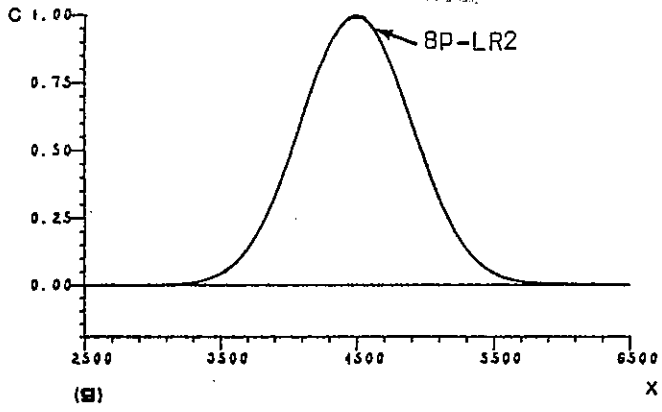


Fig. 4.20. Cont.

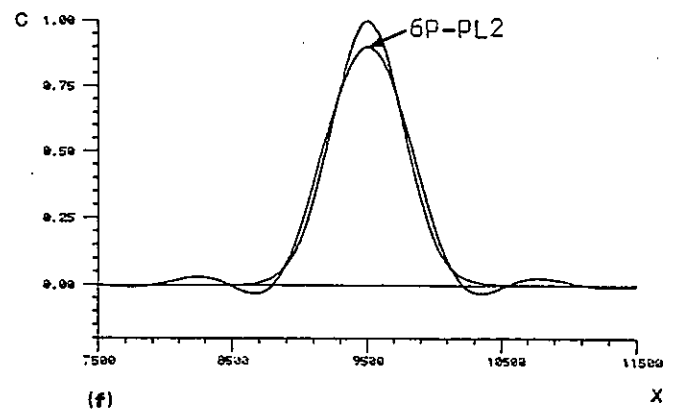
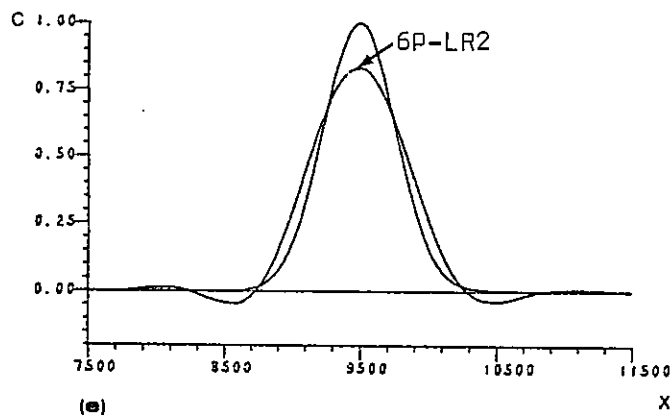
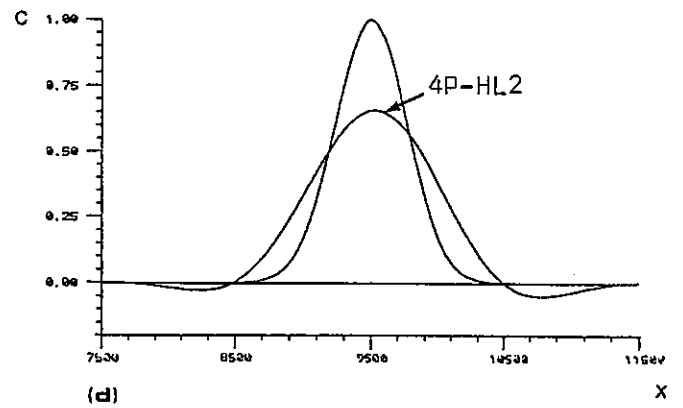
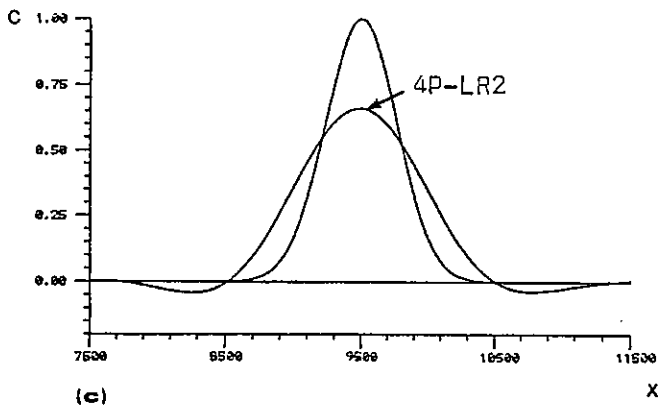
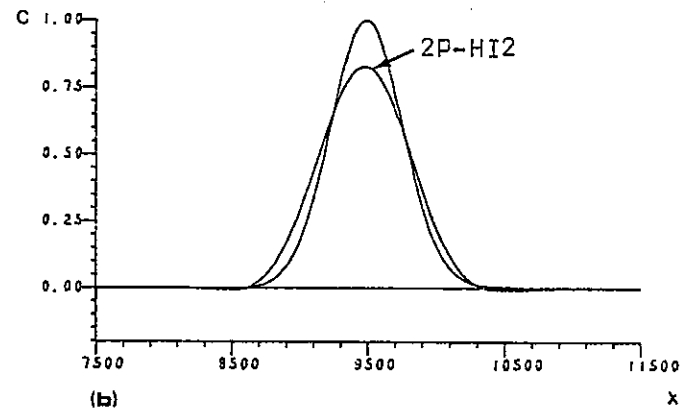
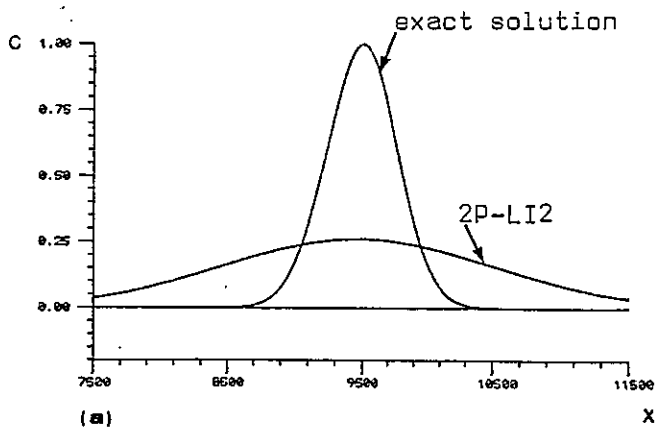


Fig. 4.21. BMC solutions for the uniform advection of a Gauss-hill ( $Cu=0.375$ ;  $N=100$ ;  $\sigma_0/\Delta x=1.32$ ;  $t=T=15000$ )

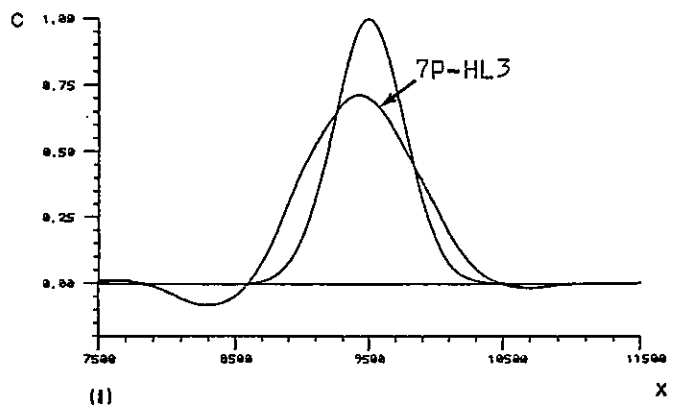
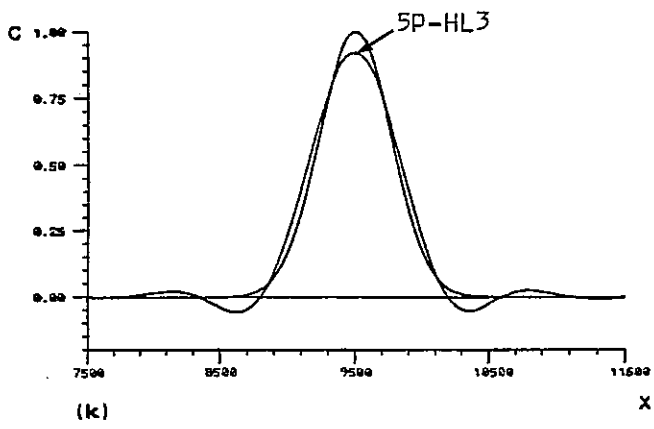
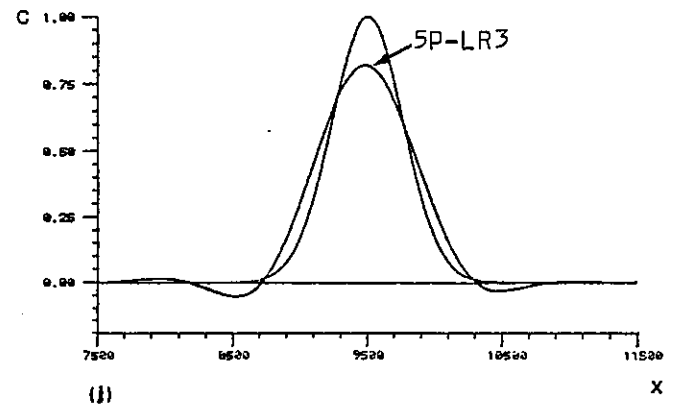
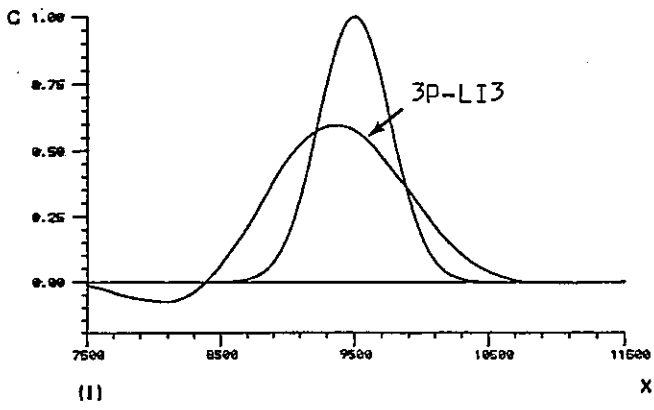
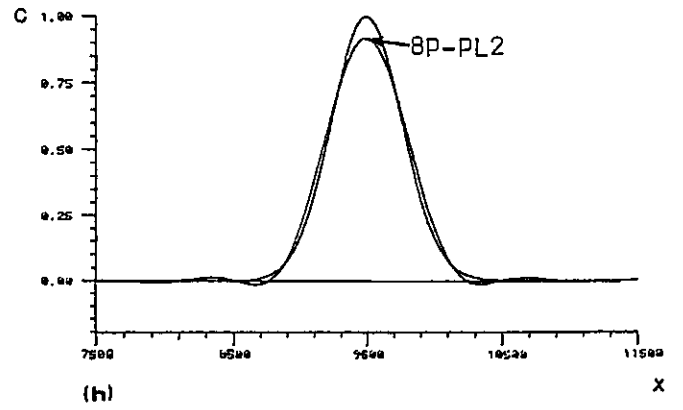
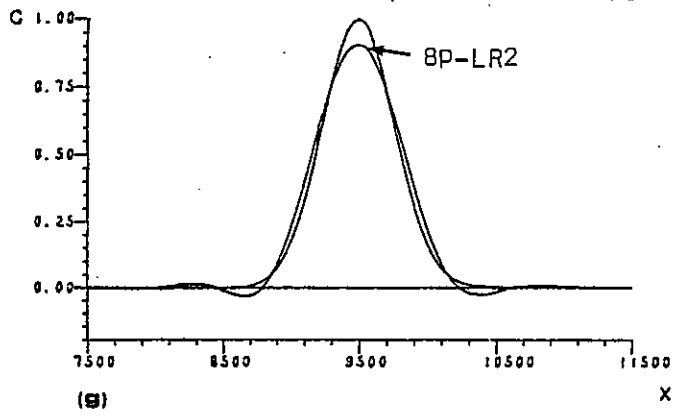


Fig. 4.21. Cont.

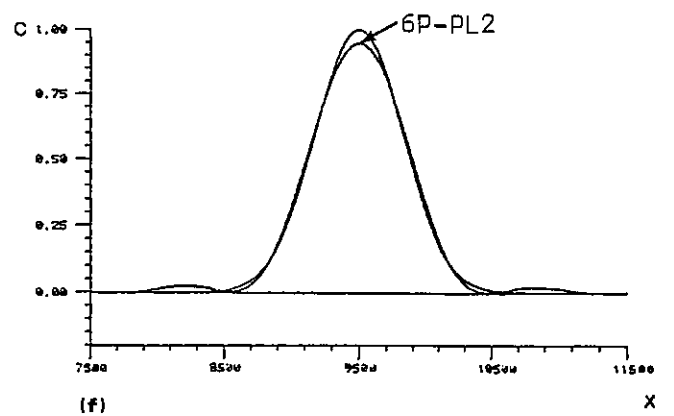
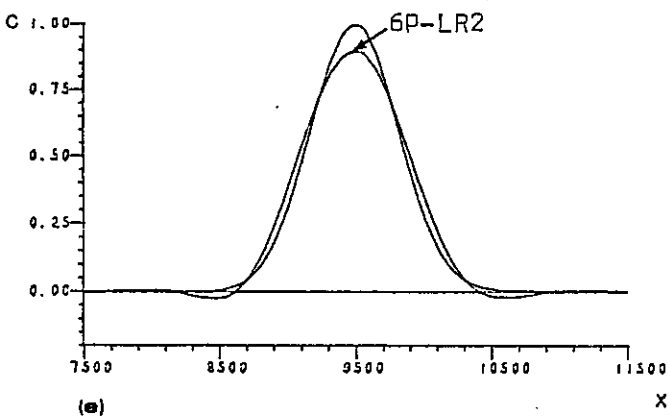
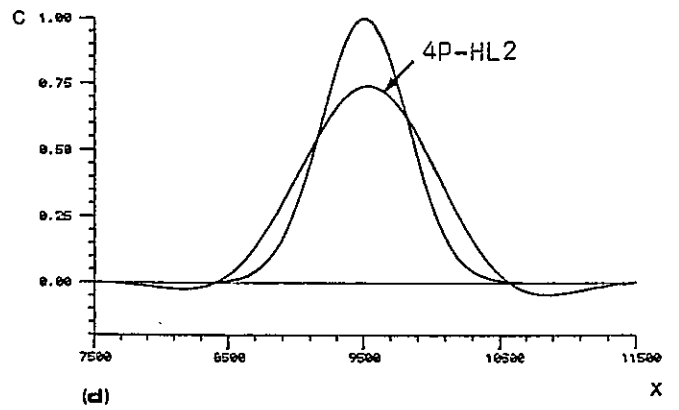
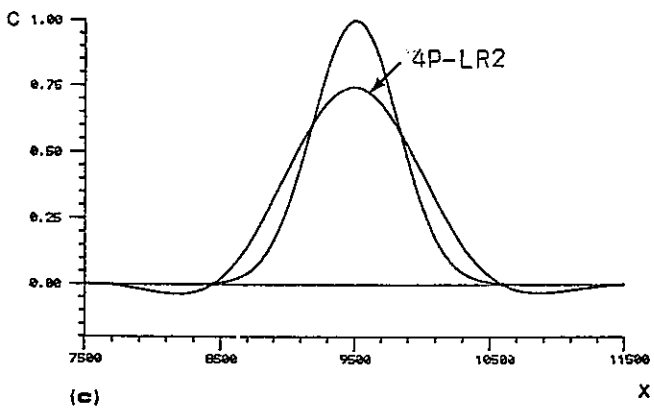
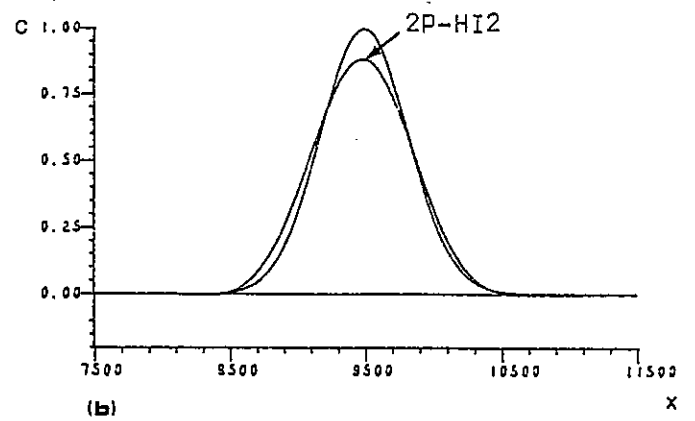
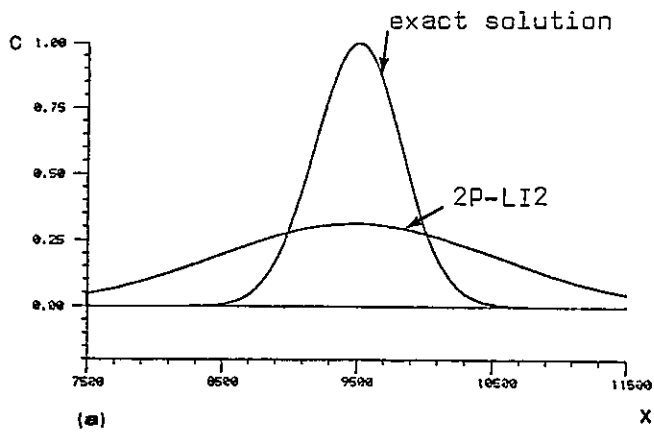


Fig. 4.22. BMC solutions for the uniform advection of a Gauss-hill ( $Cu=0.375$ ;  $N=100$ ;  $\sigma_0/\Delta x=1.6$ ;  $t=T=15000$ )

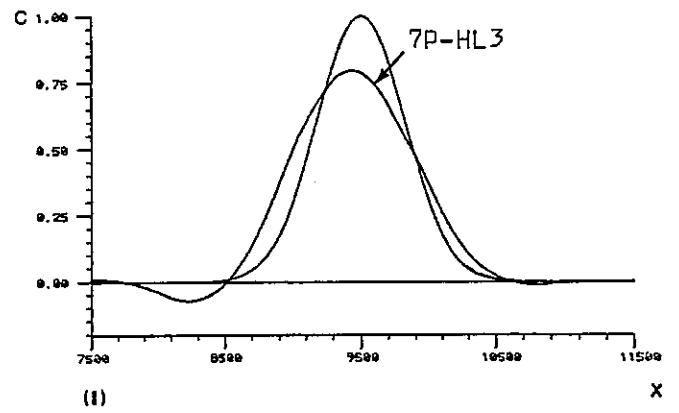
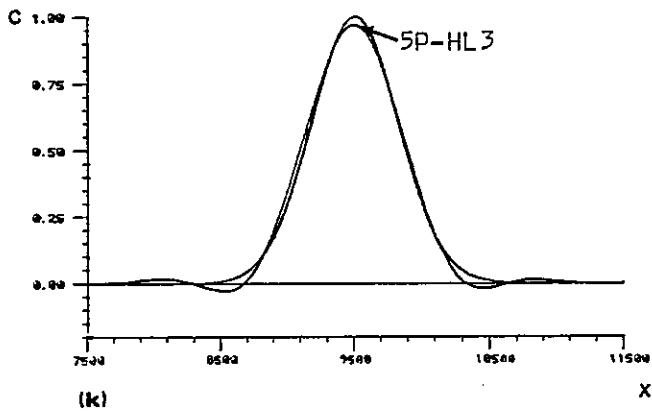
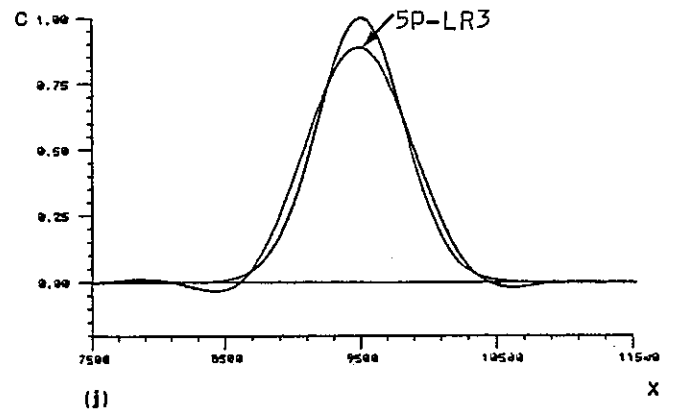
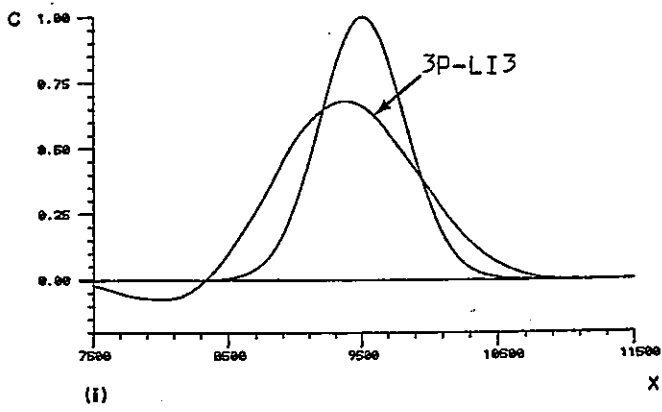
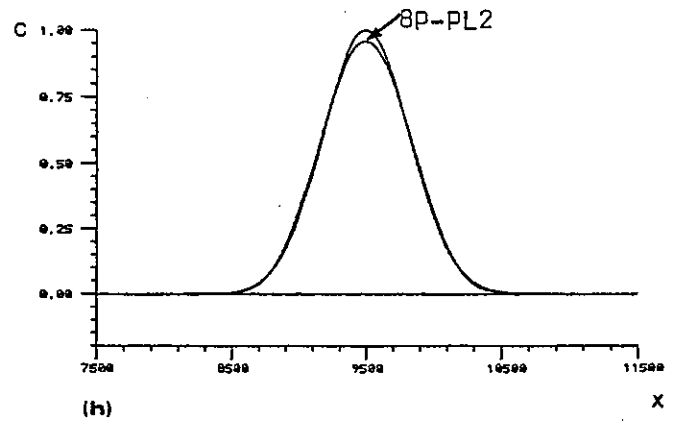
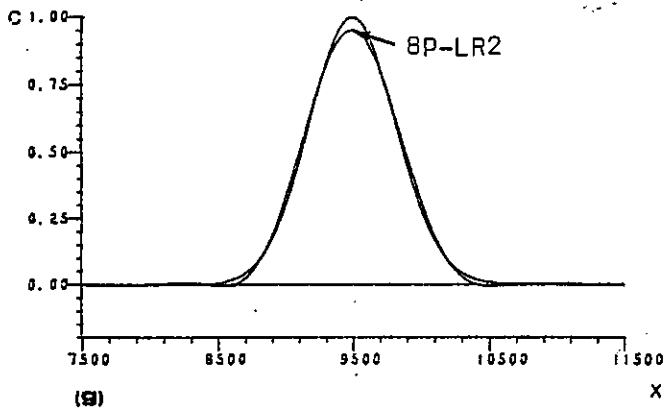


Fig. 4.22. Cont.

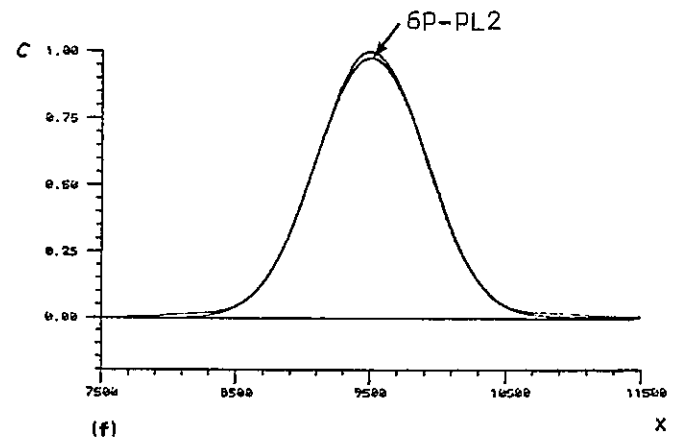
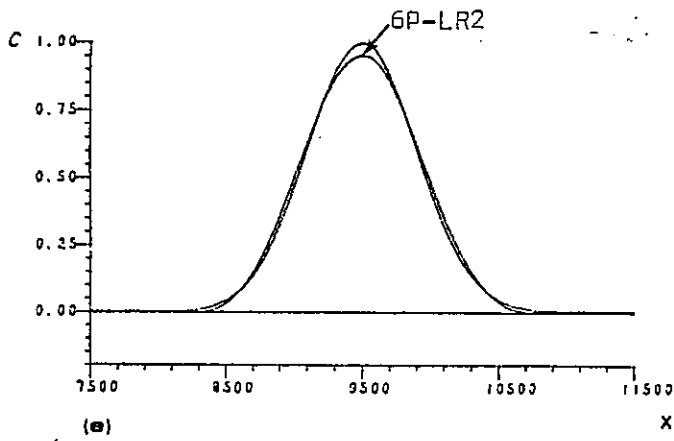
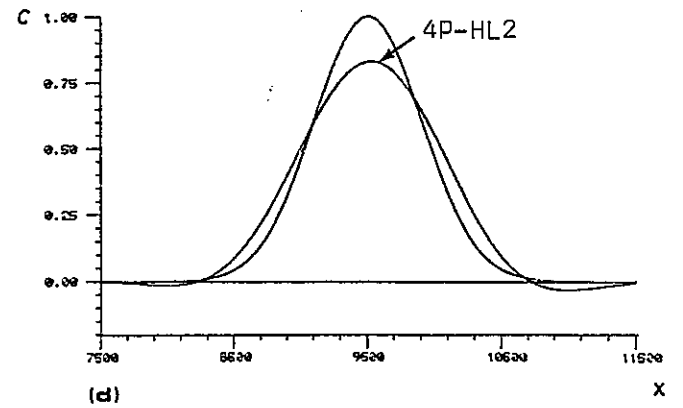
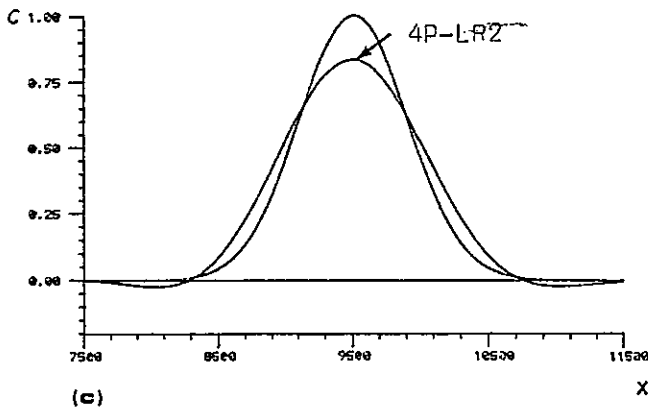
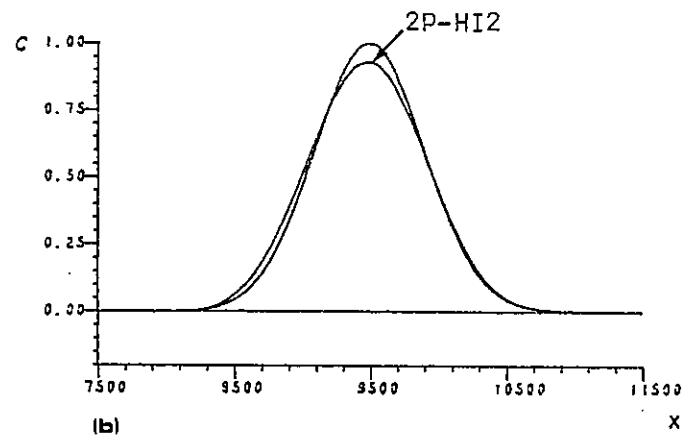
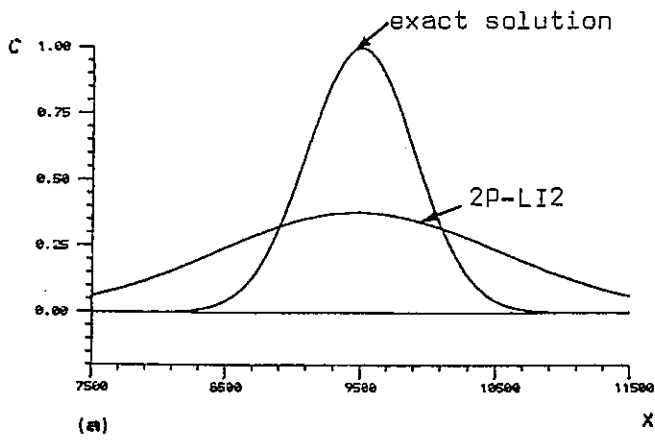


Fig. 4.23. BMC solutions for the uniform advection of a Gauss-hill ( $Cu=0.375$ ;  $N=100$ ;  $\sigma_0/\Delta x=2.0$ ;  $t=T=15000$ )



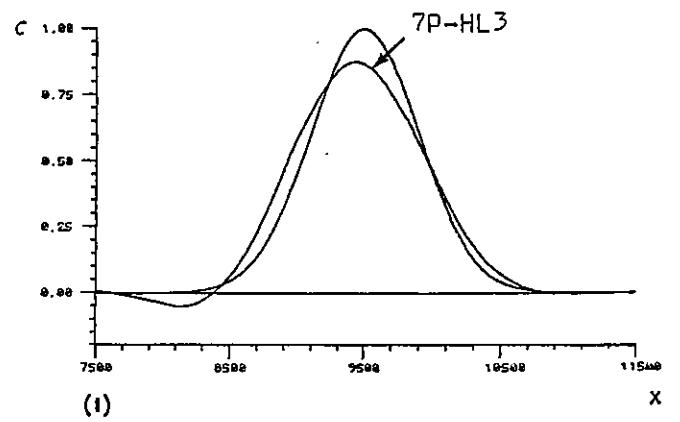
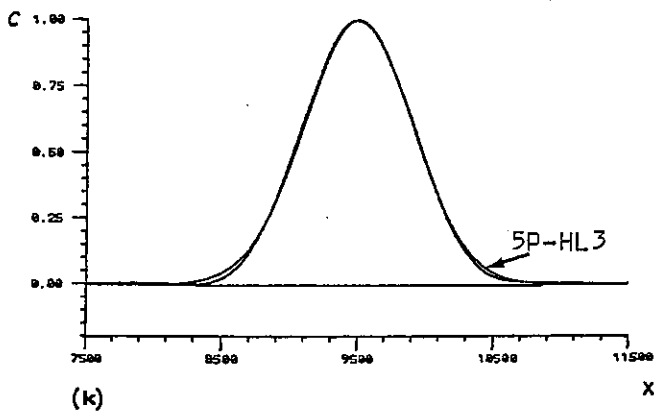
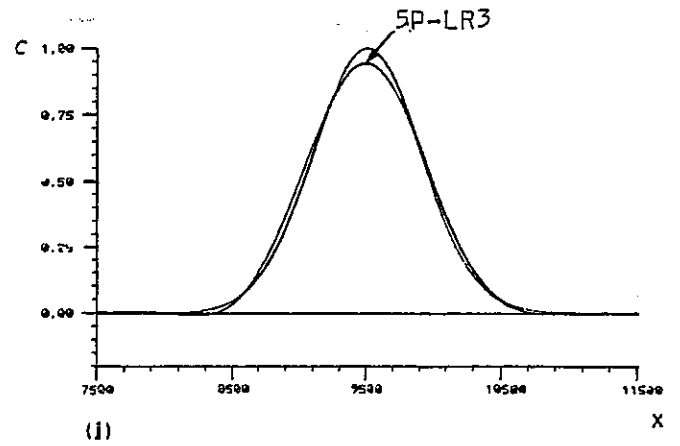
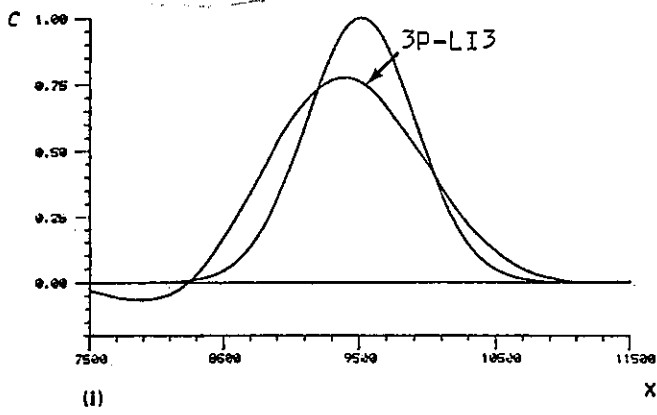
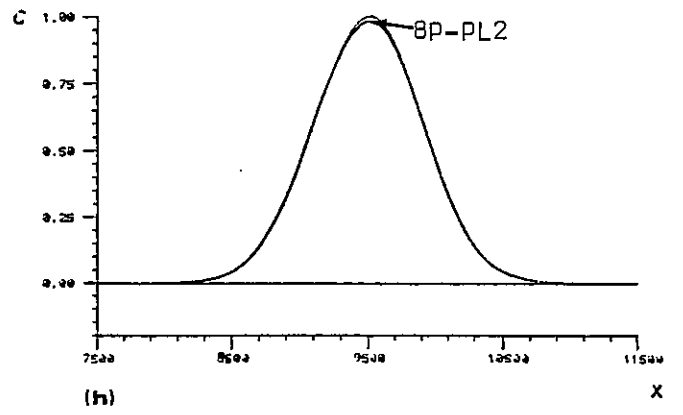
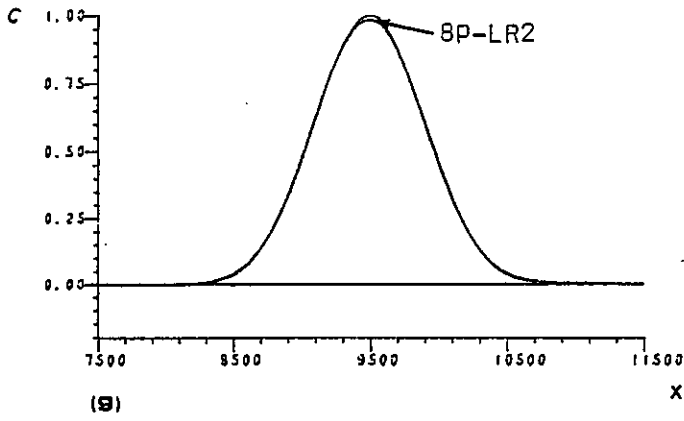


Fig. 4.23. Cont.

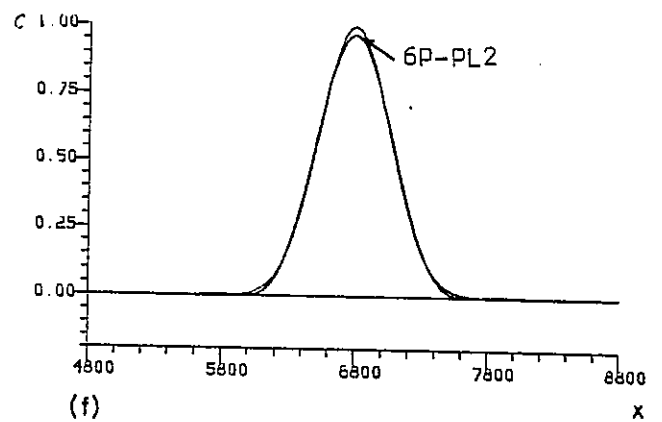
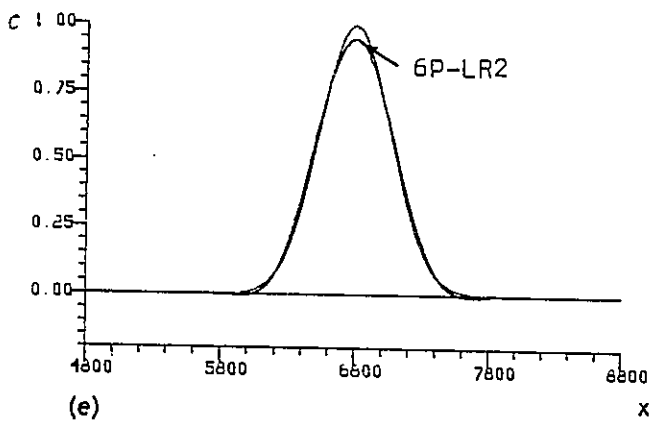
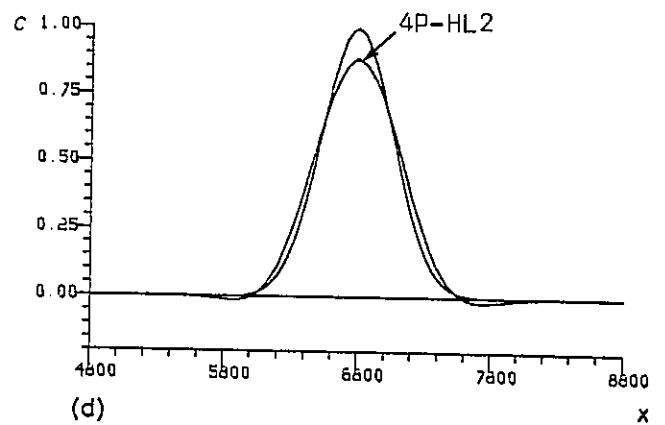
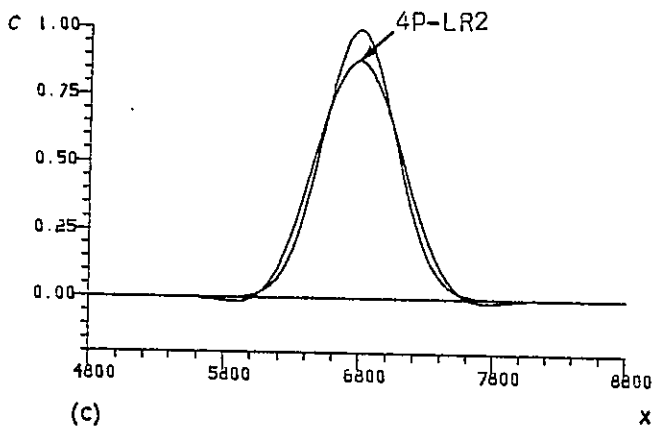
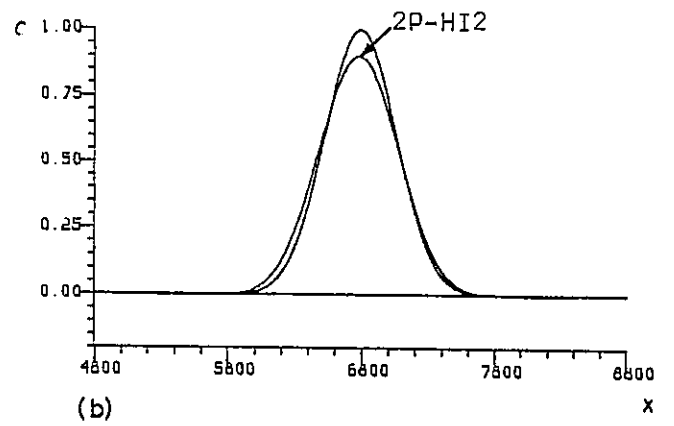
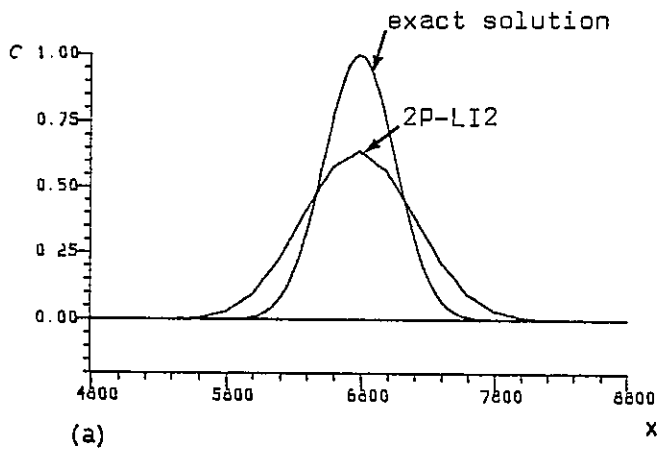


Fig. 4.24. BMC solutions for the uniform advection of a Gauss-hill ( $Cu=1.2$ ;  $N=20$ ;  $\sigma_0/\Delta x=1.32$ ;  $t=T=9600$ )

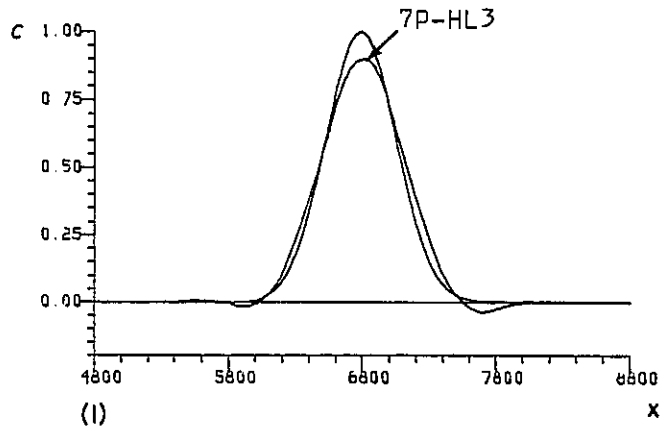
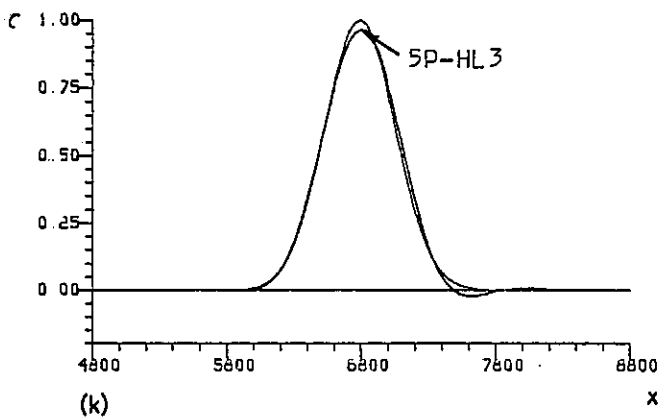
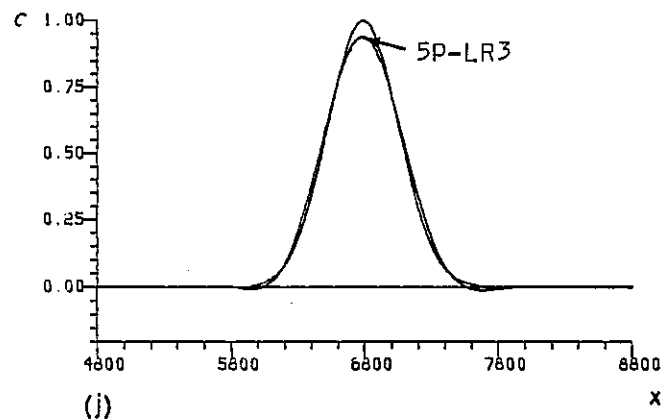
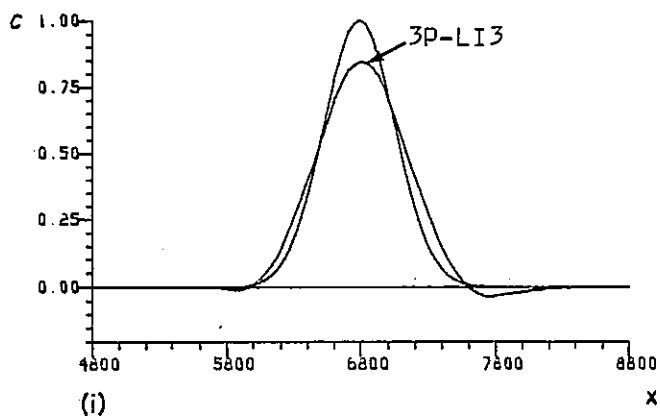
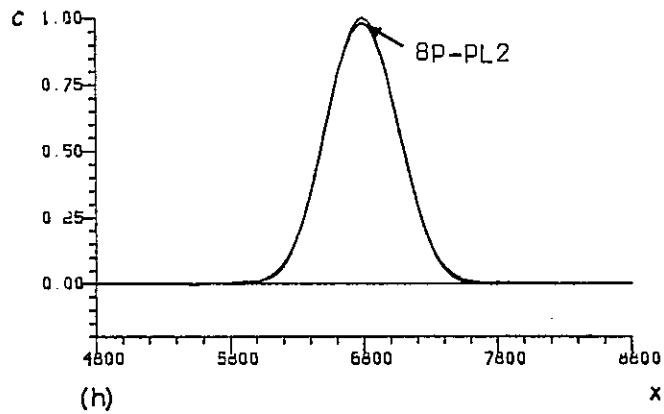
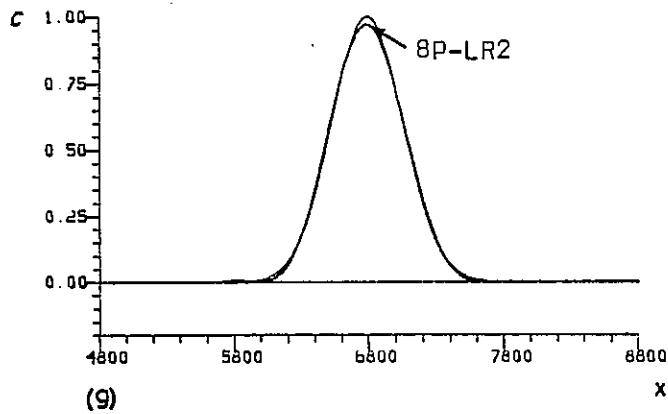


Fig. 4.24. Cont.

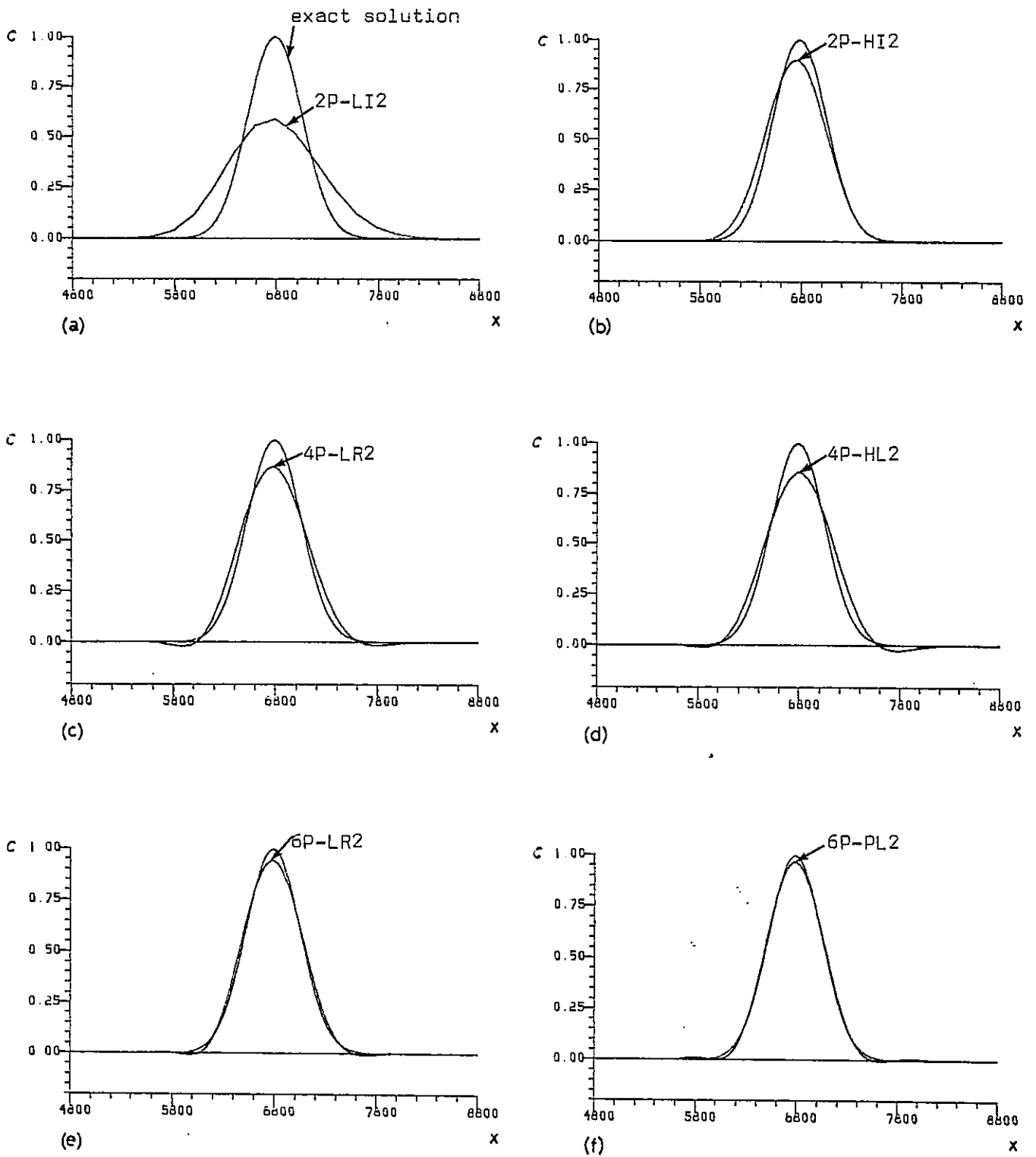


Fig. 4.25. BMC solutions for the uniform advection of a Gauss-hill ( $Cu=2.4$ ;  $N=10$ ;  $\sigma_0/\Delta x=1.32$ ;  $t=T=9600$ )

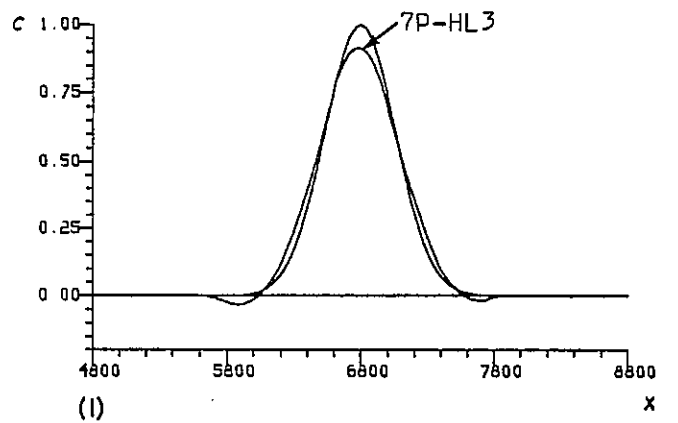
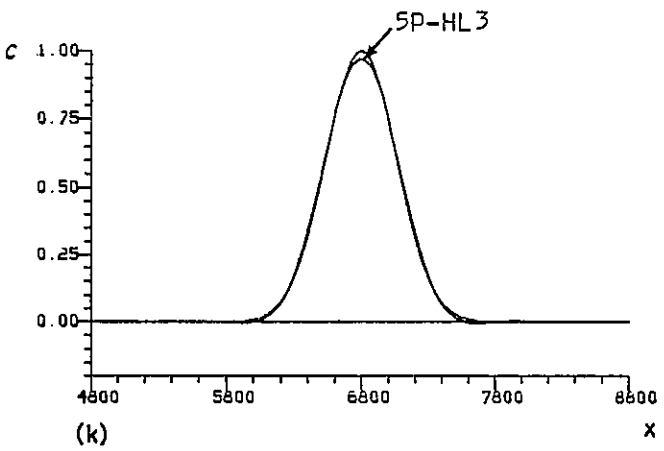
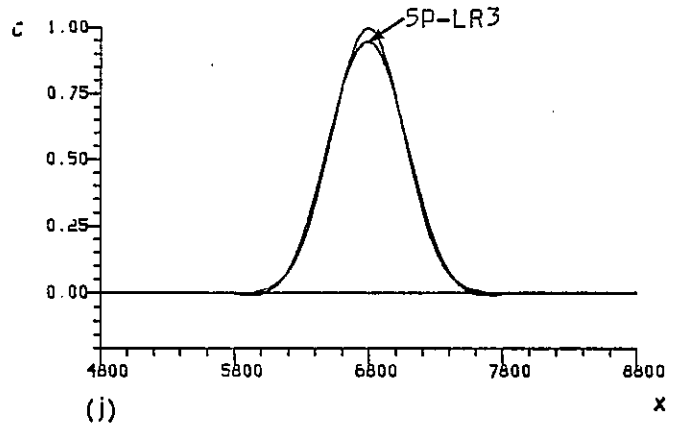
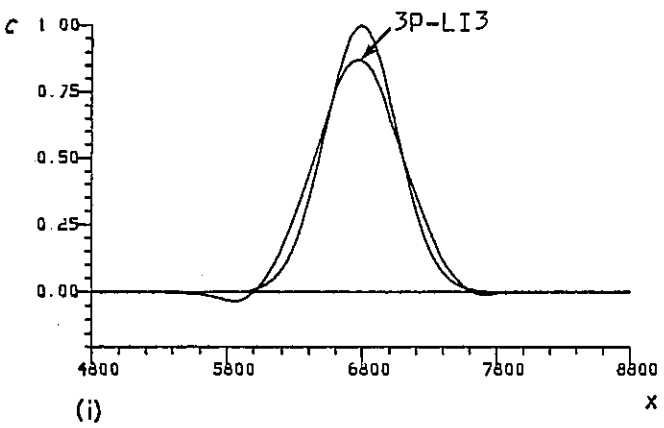
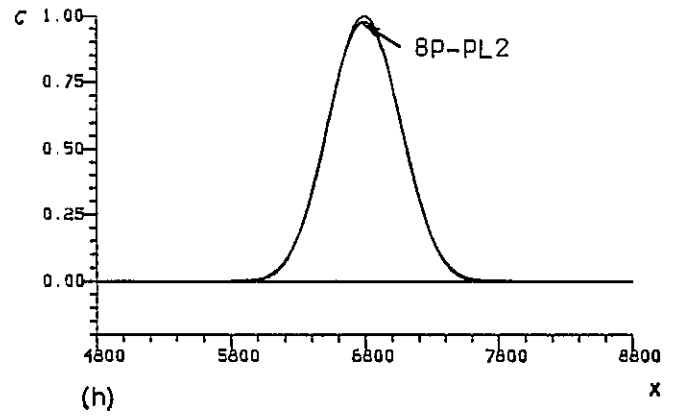
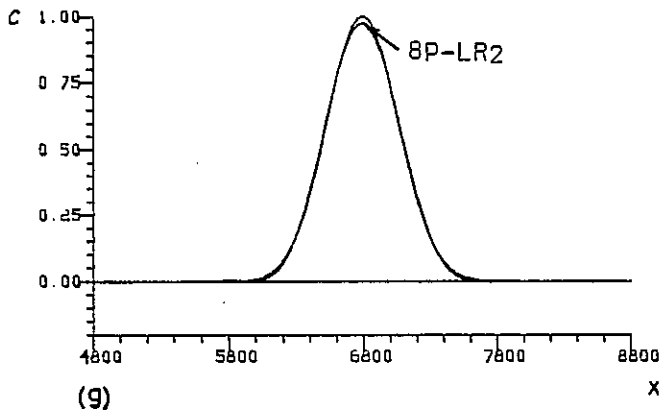


Fig. 4.25. Cont.

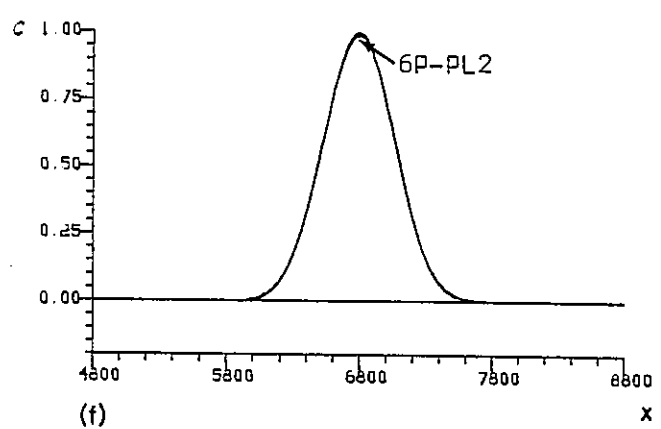
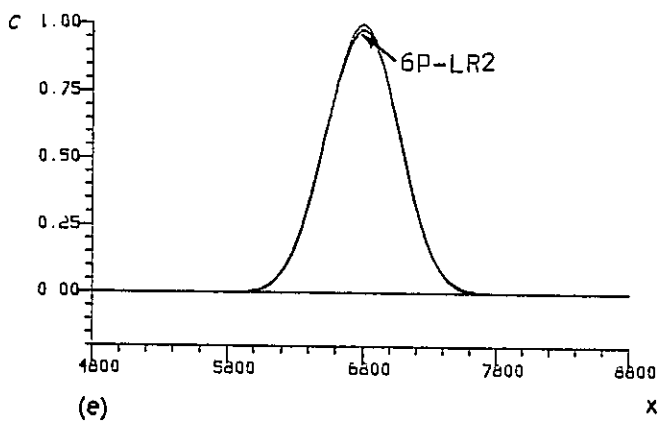
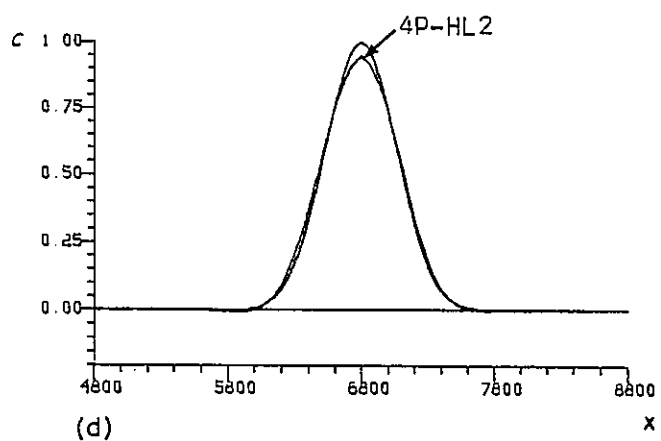
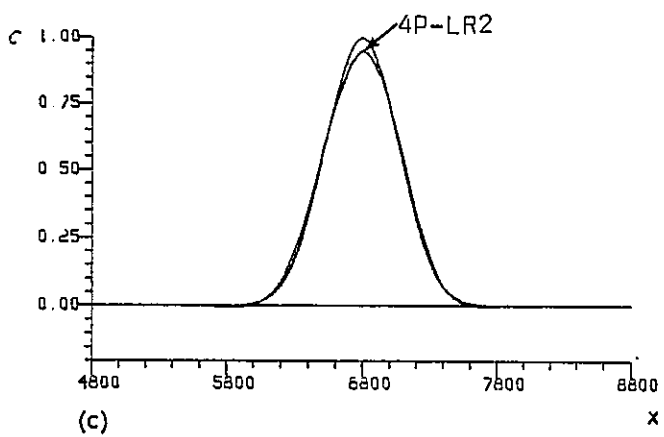
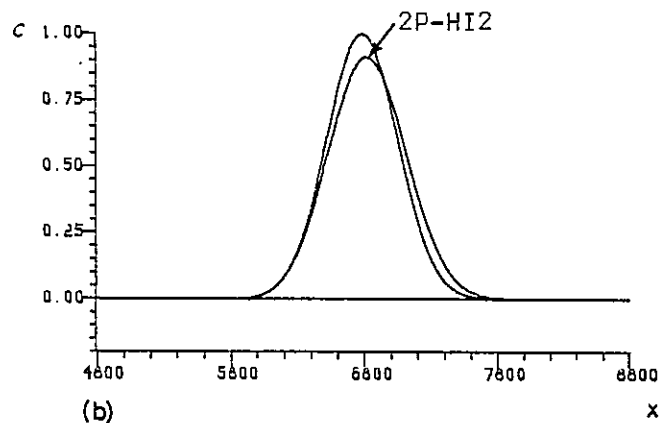
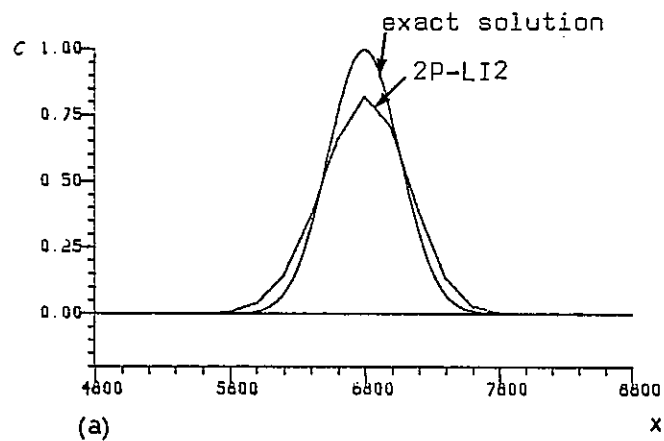


Fig. 4.26. BMC solutions for the uniform advection of a Gauss-hill ( $Cu=4.8$ ;  $N=5$ ;  $\sigma_0/\Delta x=1.32$ ;  $t=T=9600$ )

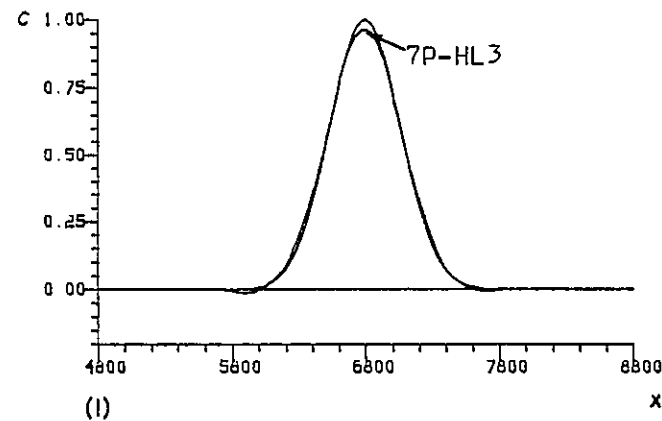
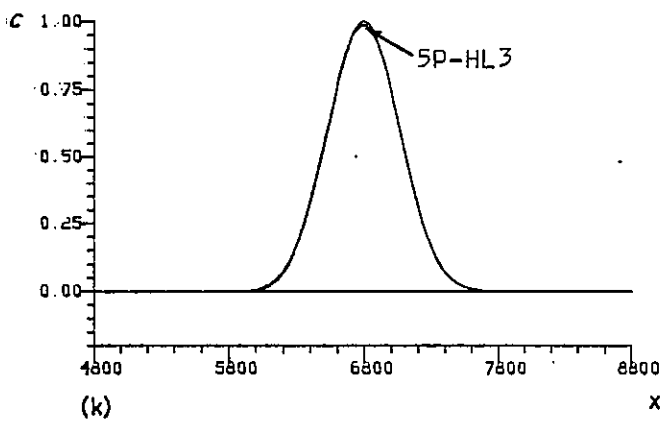
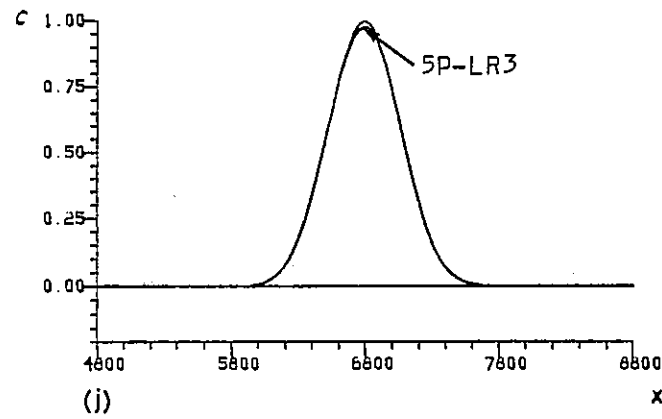
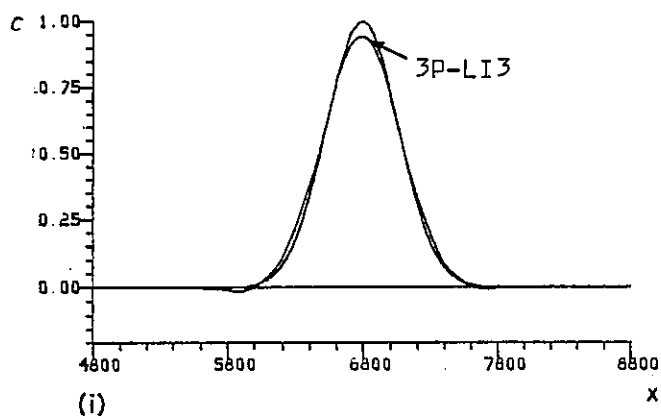
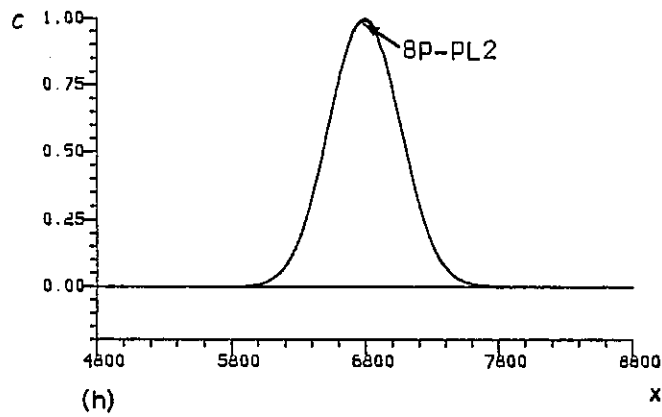
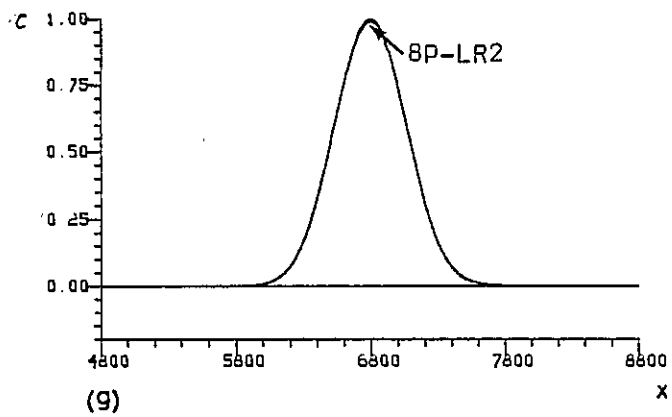


Fig. 4.26. Cont.

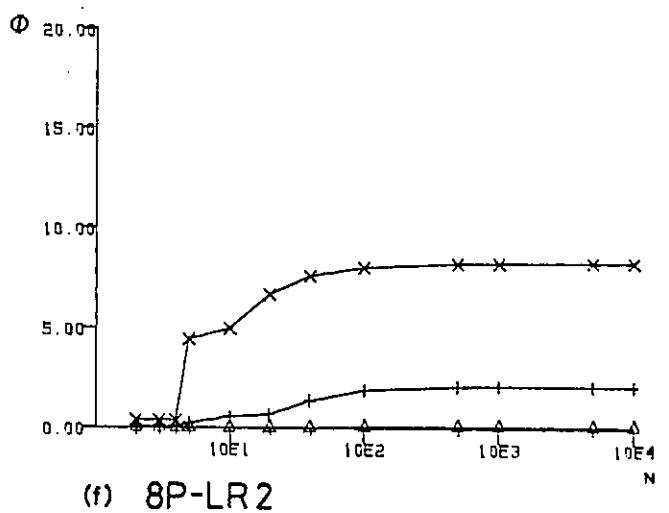
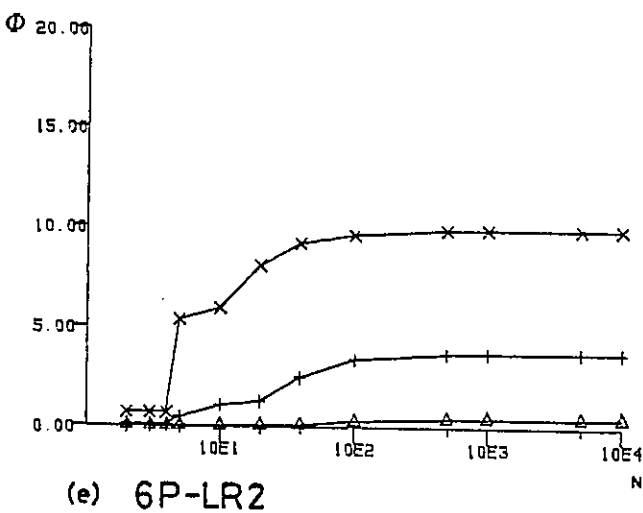
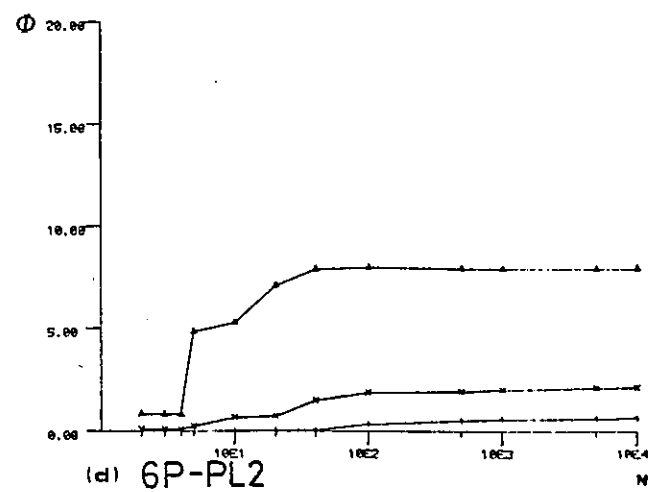
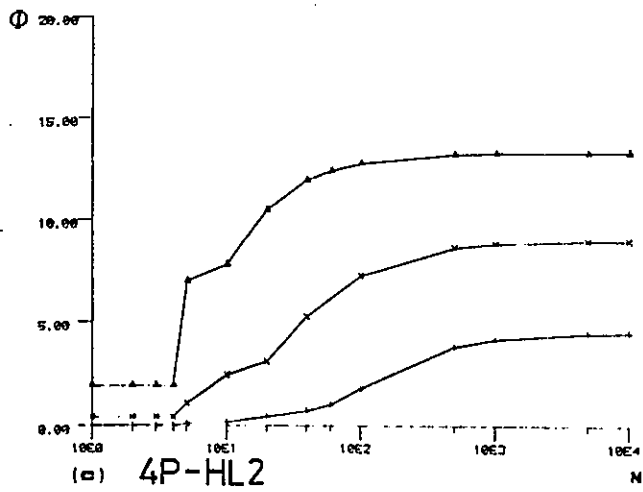
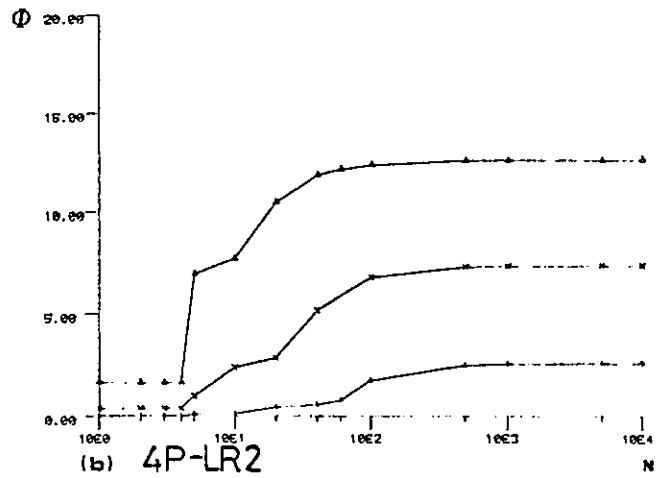
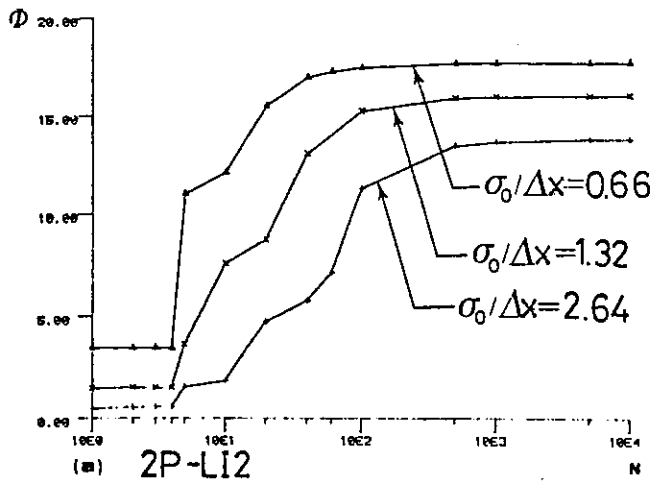


Fig. 4.27. Mean square error as a function of the number of time steps required to reach a fixed total time ( $Cu=24/N$ ,  $t=T=9600$ )



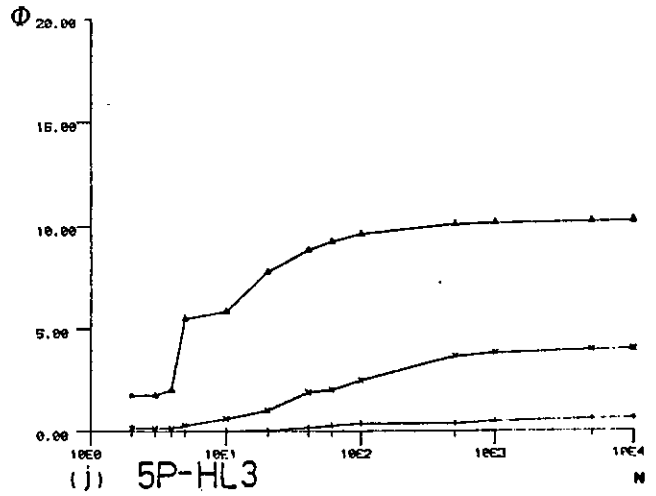
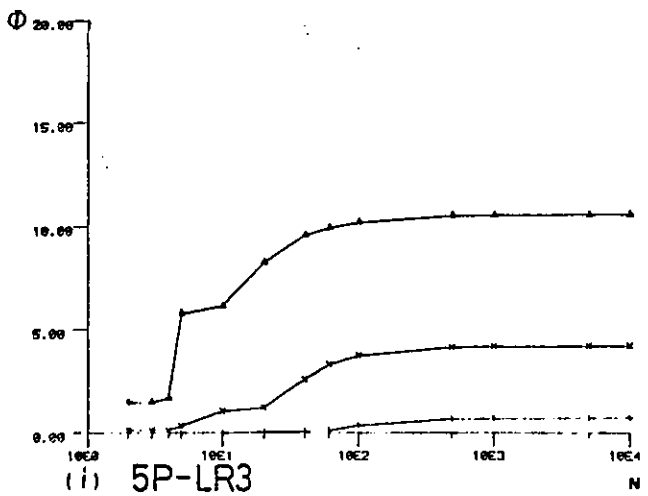
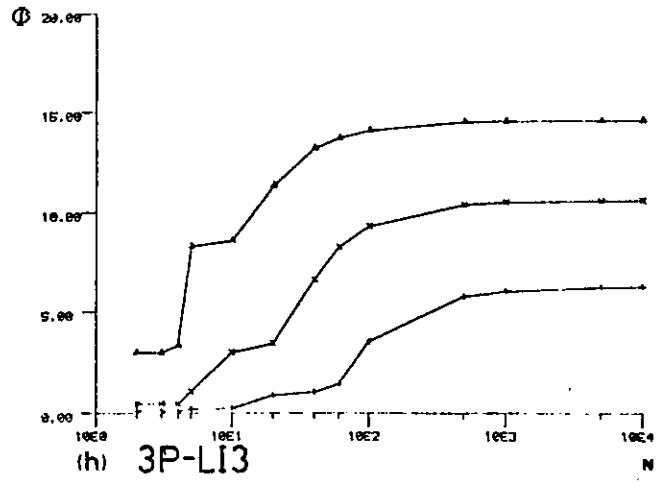
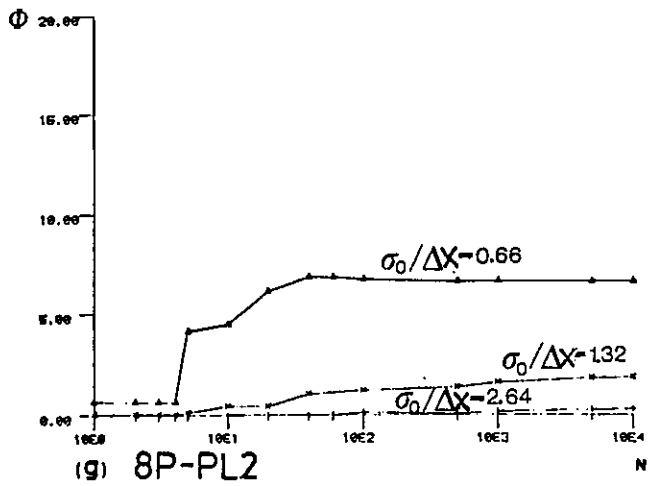


Fig. 4.27. Cont.

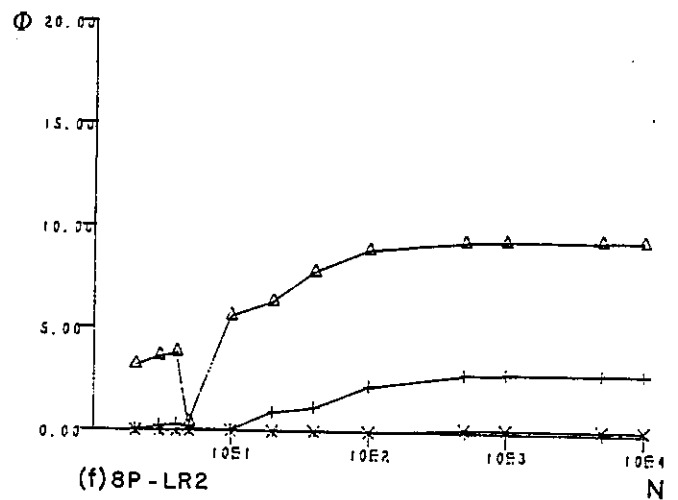
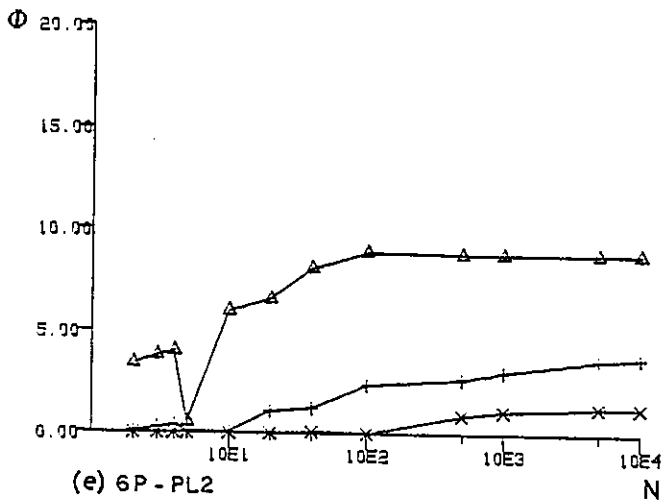
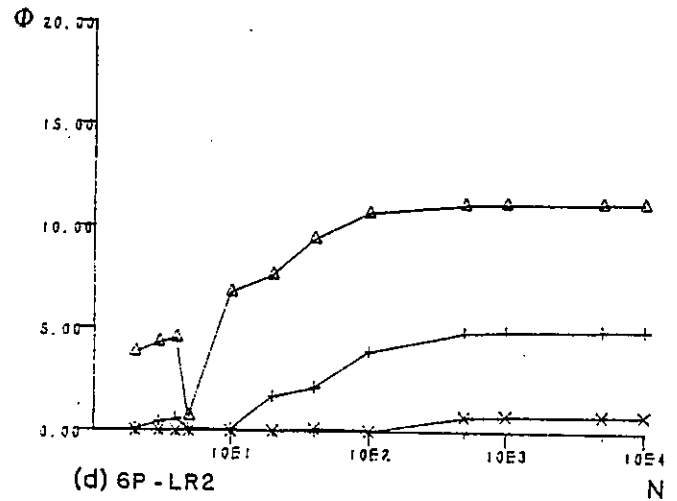
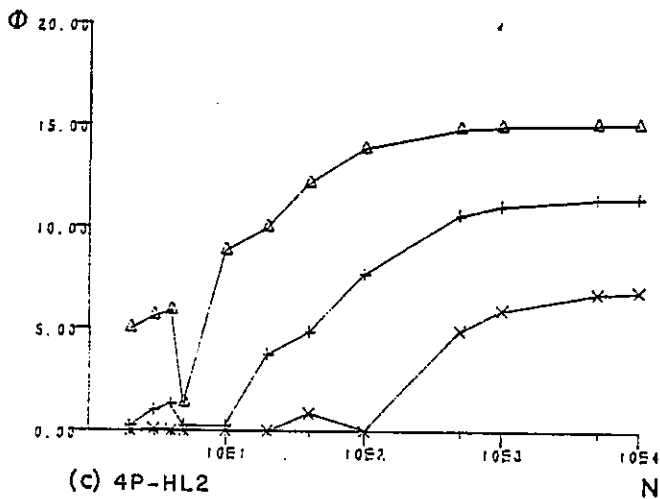
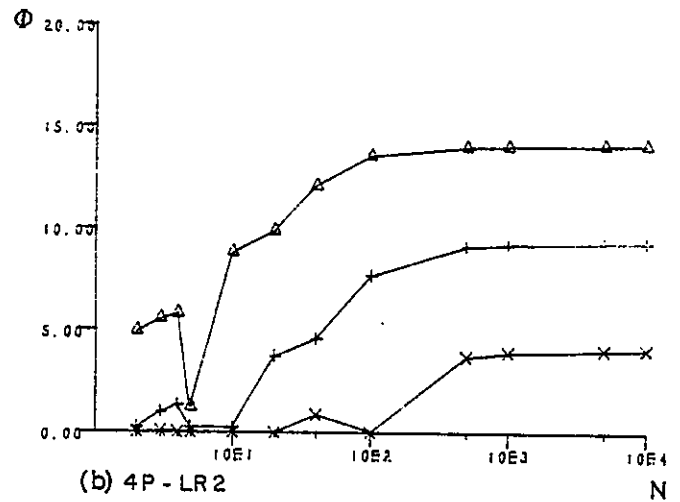
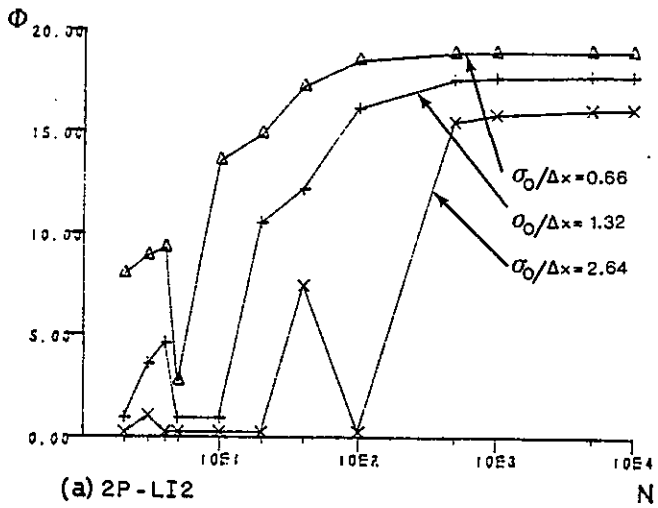


Fig. 4.28. Mean square error as a function of the number of time steps required to reach a fixed total time ( $Cu=50/N$ ,  $t=T=20000$ )

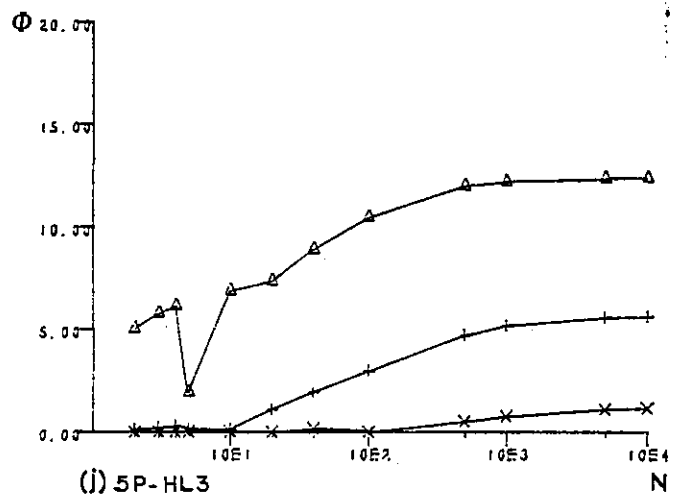
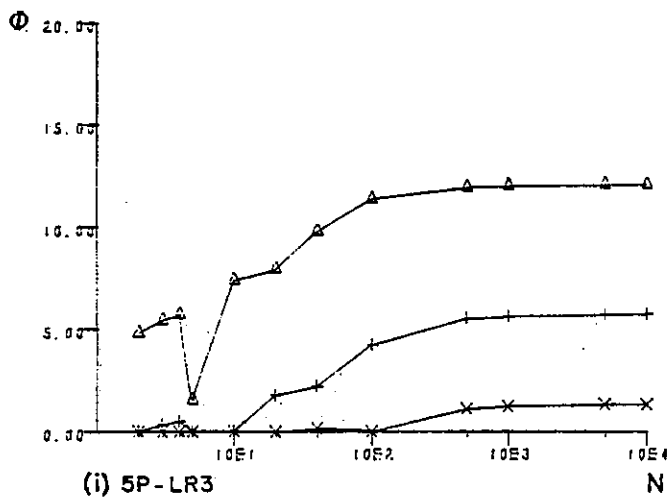
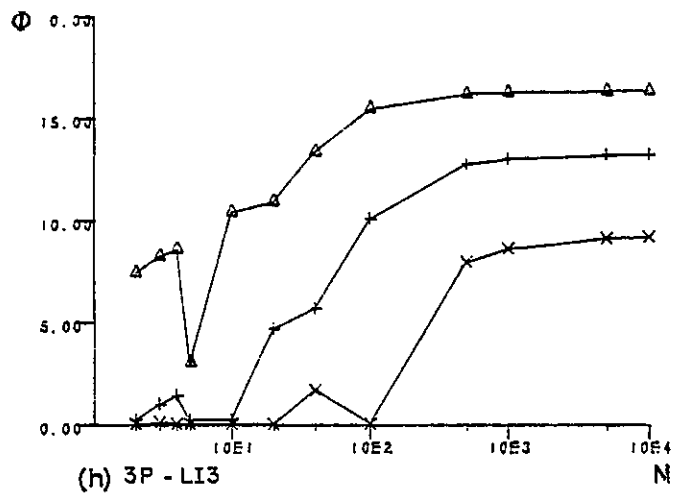
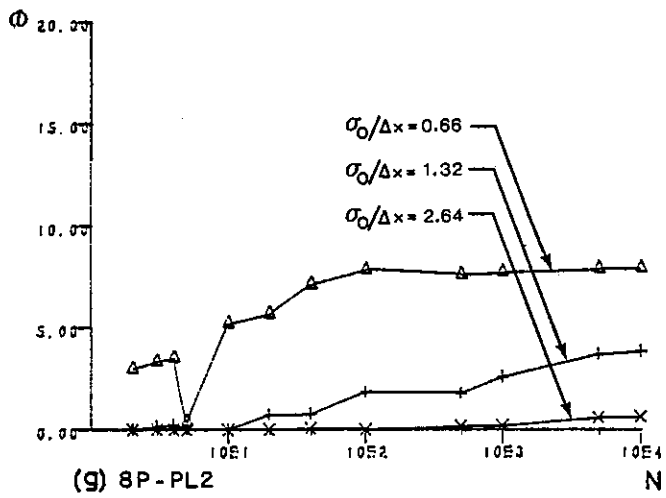


Fig. 4.28. Cont.

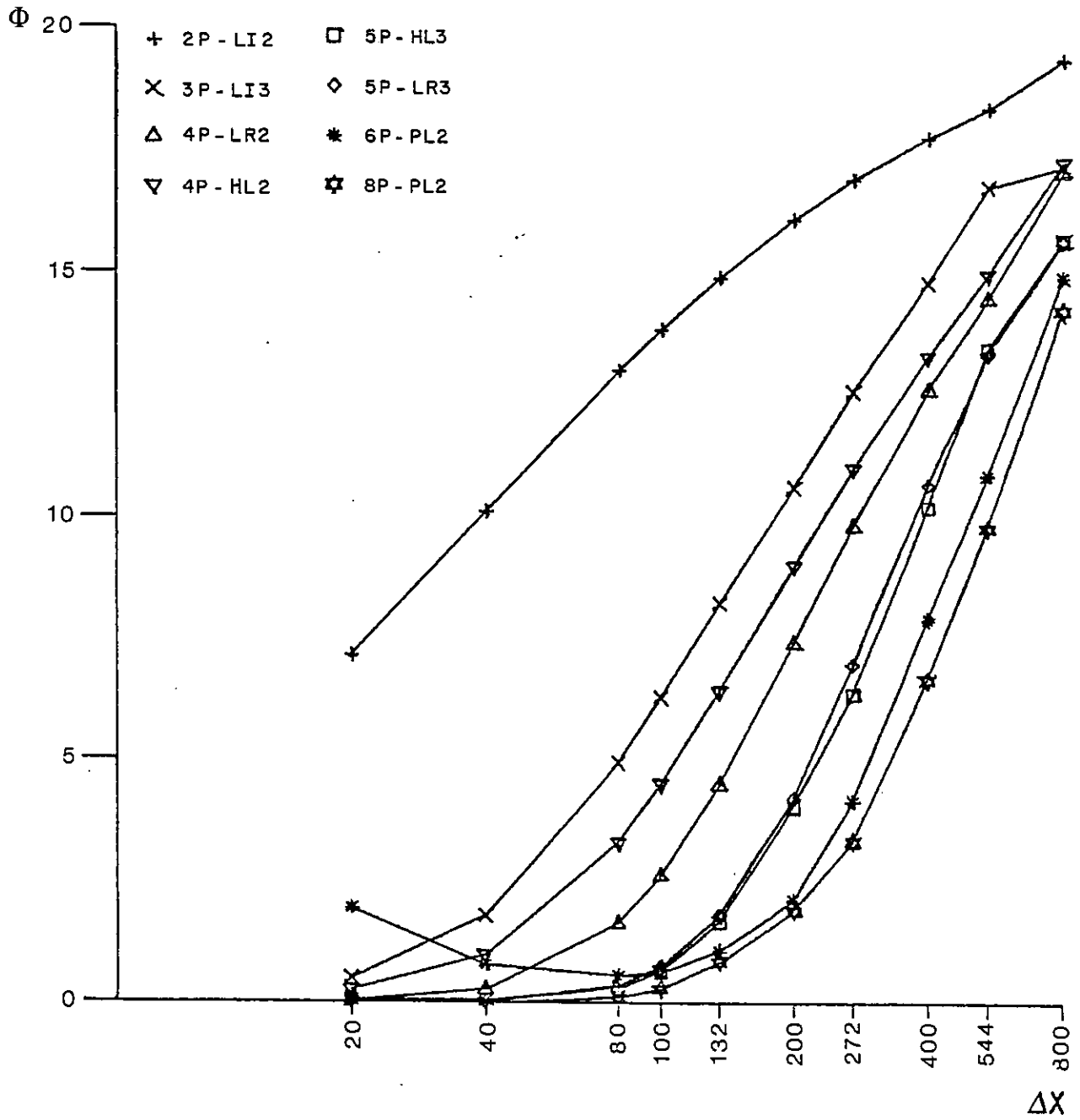


Fig. 4.29. Mean square error as a function of the grid discretization ( $Cu=0.096/\Delta x$ ;  $N=50000$ ;  $t=T=9600$ ;  $\sigma_0=264$ )

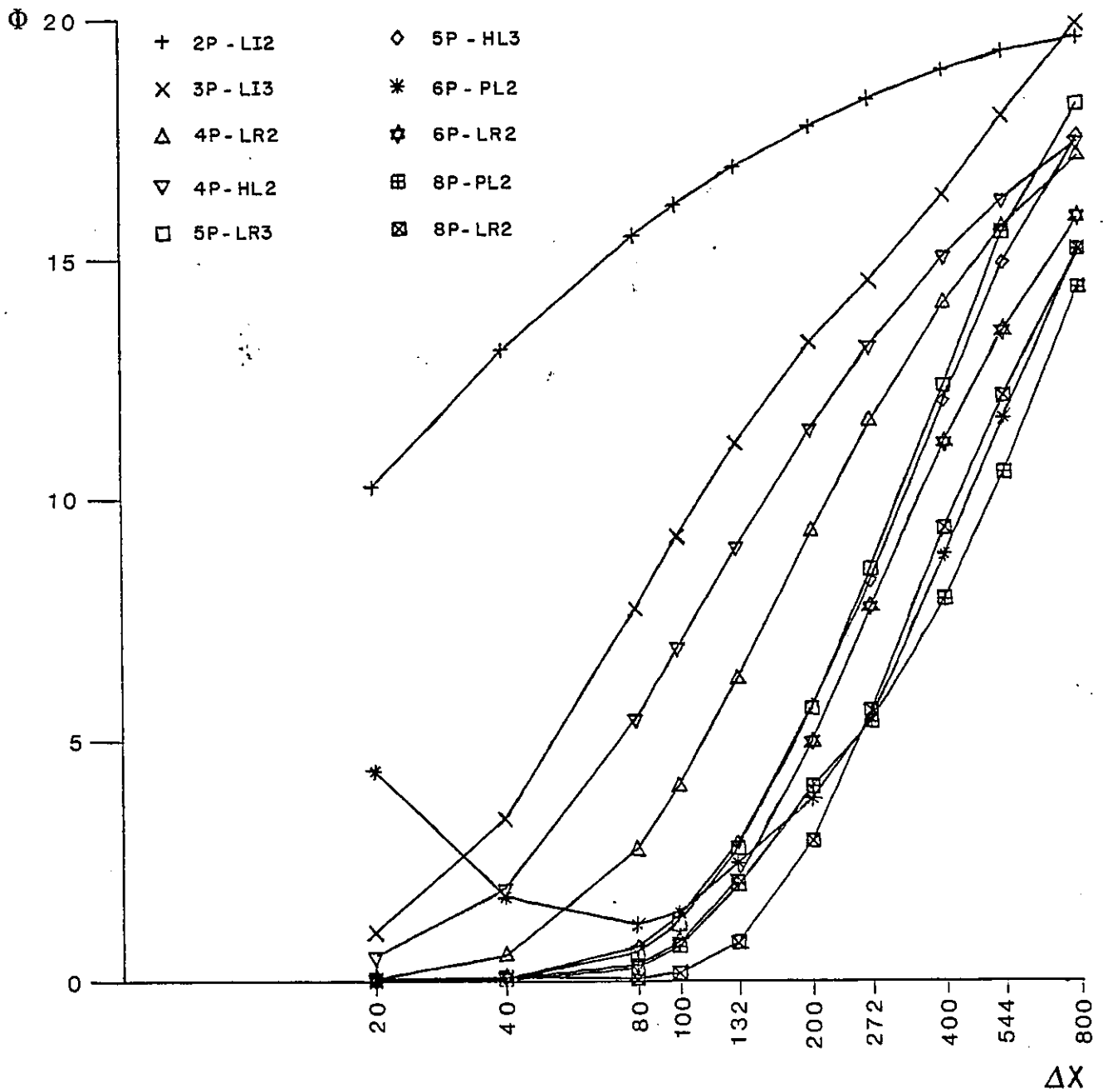
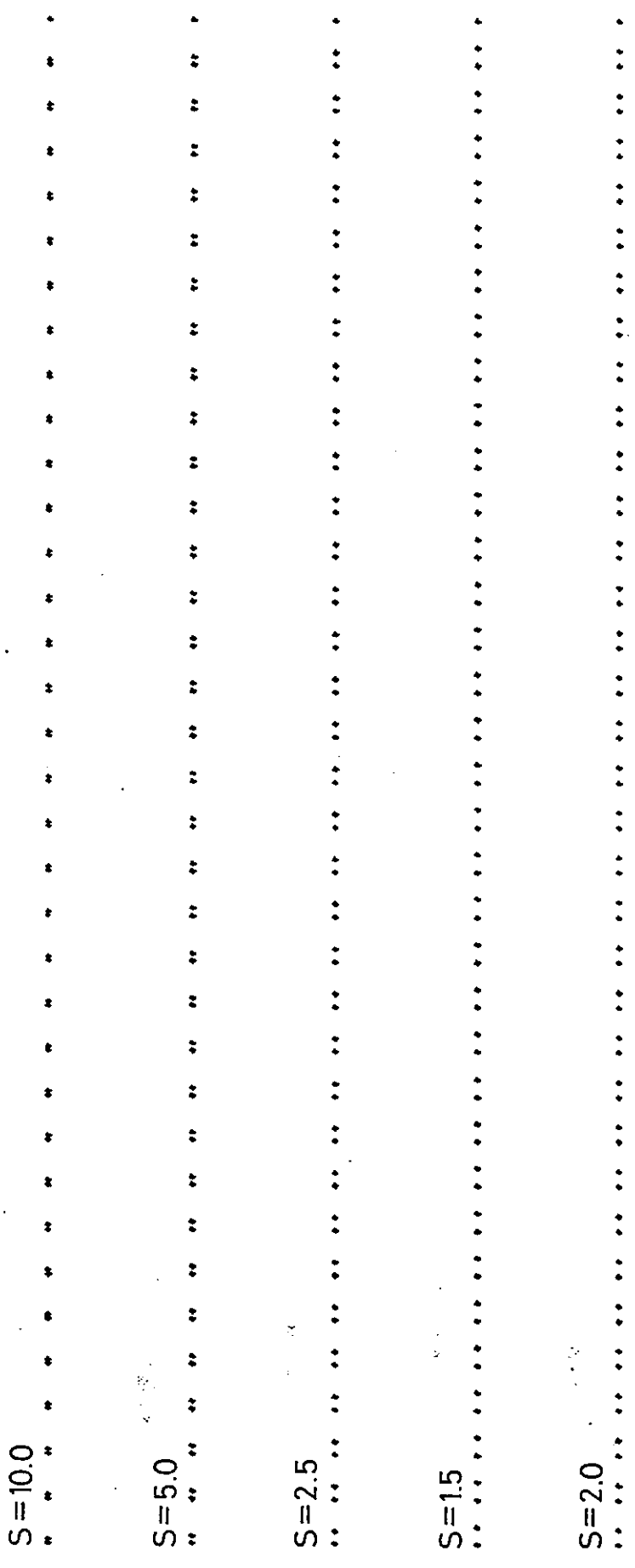



Fig. 4.30. Mean square error as a function of the grid discretization ( $Cu=0.2/\Delta x$ ;  $N=50000$ ;  $t=T=20000$ ;  $\sigma_c=264$ )




(a) Grids of type 1

Fig. 4.31. Definition of the non-uniform grids considered in section 4.3

S=10.0 

S=5.0 

S=2.5 

S=1.5 

S=2.0 

(b) Grids of type 2

Fig. 4.31. Cont.

S=1.01



S=1.02



S=1.03



(c) Grids of type 3

Fig. 4.31. Cont.



S=10.0  
.....

S=5.0  
.....

S=2.5  
.....

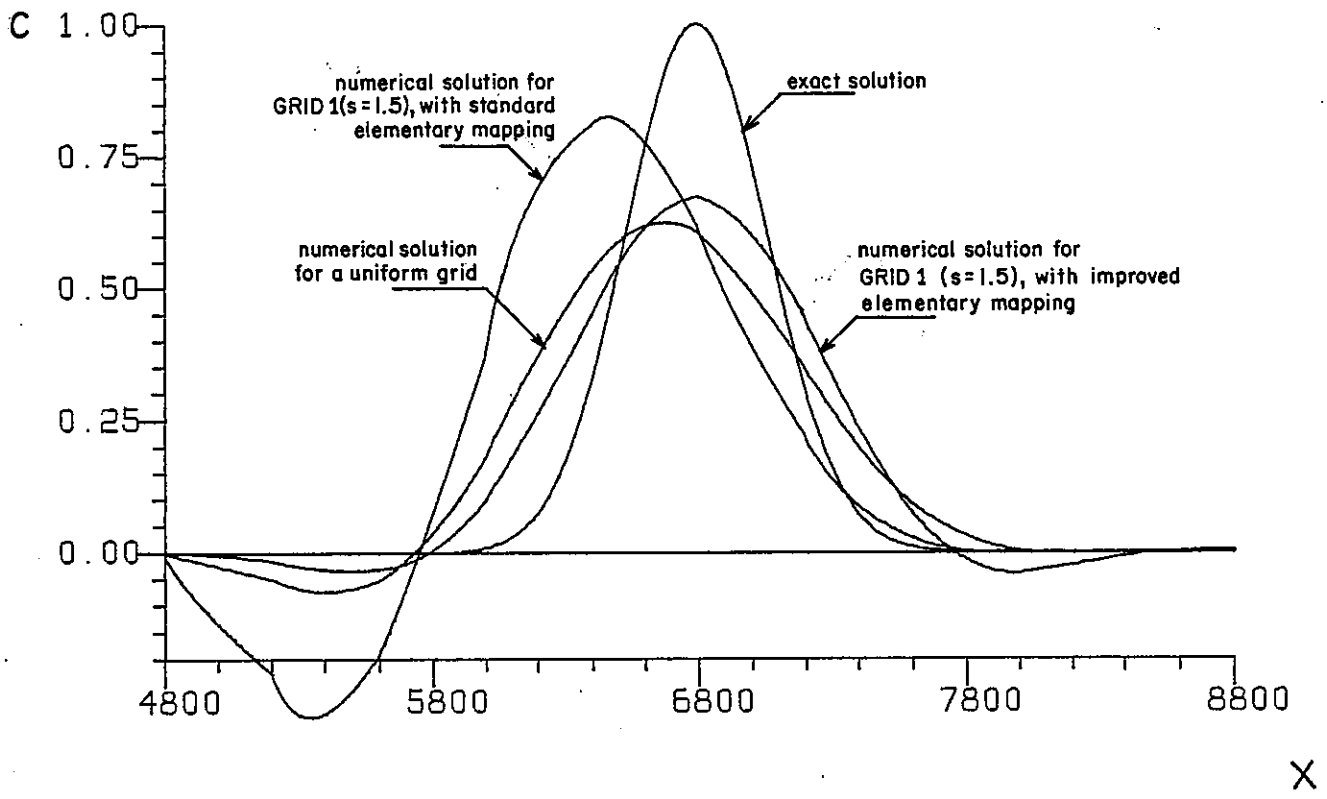
S=1.5  
.....

S=2.0  
.....

(d) Grids of type 4

Fig. 4.31. Cont.





3P-L13

Fig. 4.32. Effect of different elementary mappings in the accuracy of BMC solutions for non-uniform grids.

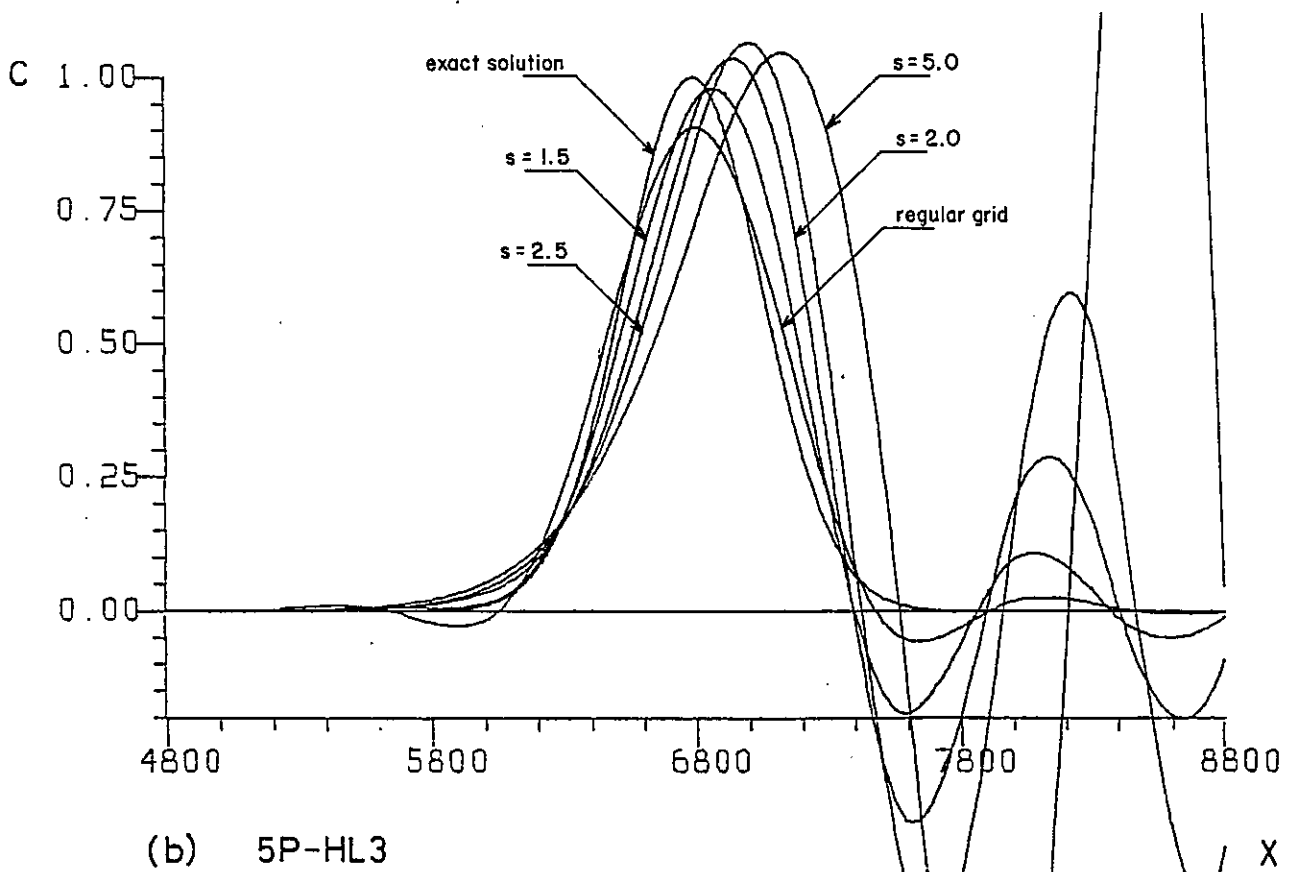
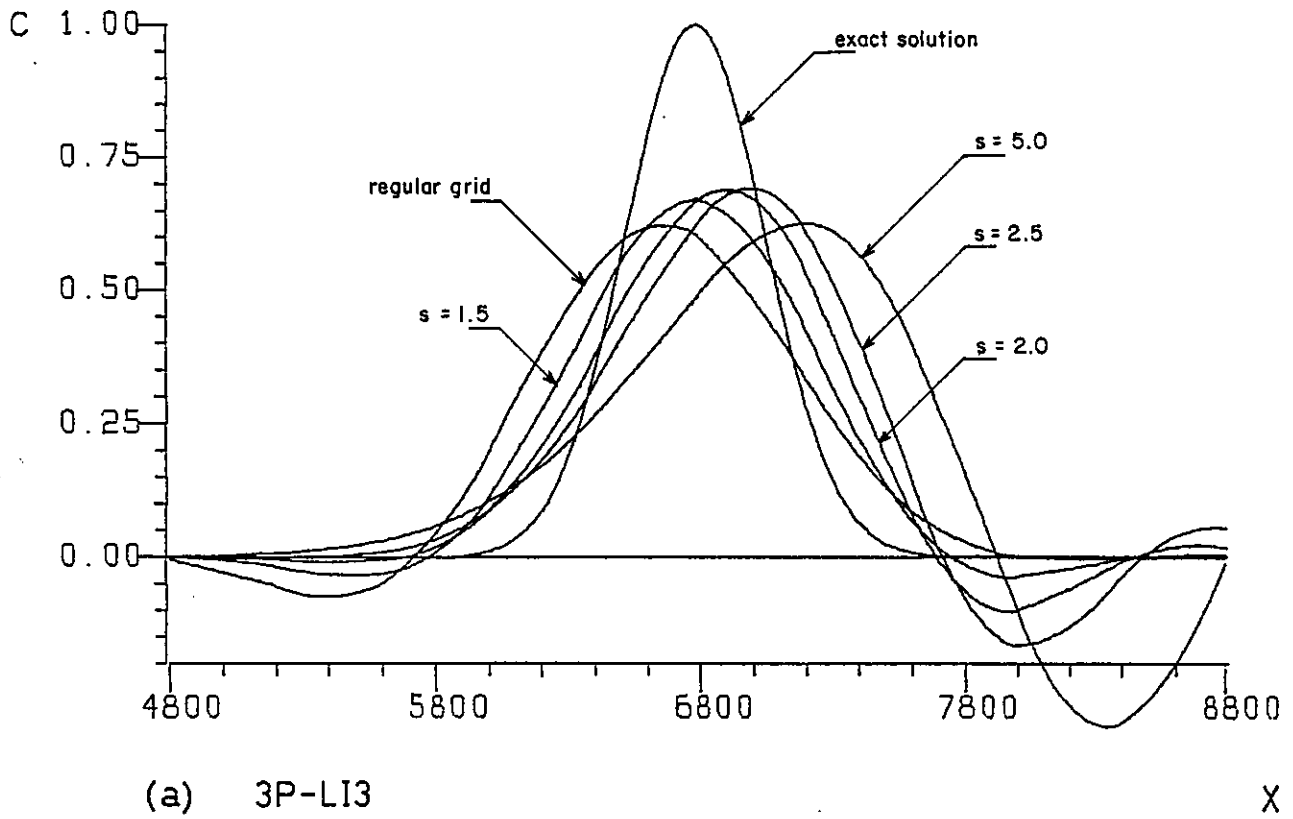


Fig. 4.33. BMC solutions for the uniform advection of a Gauss-hill in grids of type 1 ( $N=100$ ;  $t=T=9600$ ;  $\sigma_0=264$ ;  $u=0.5$ )

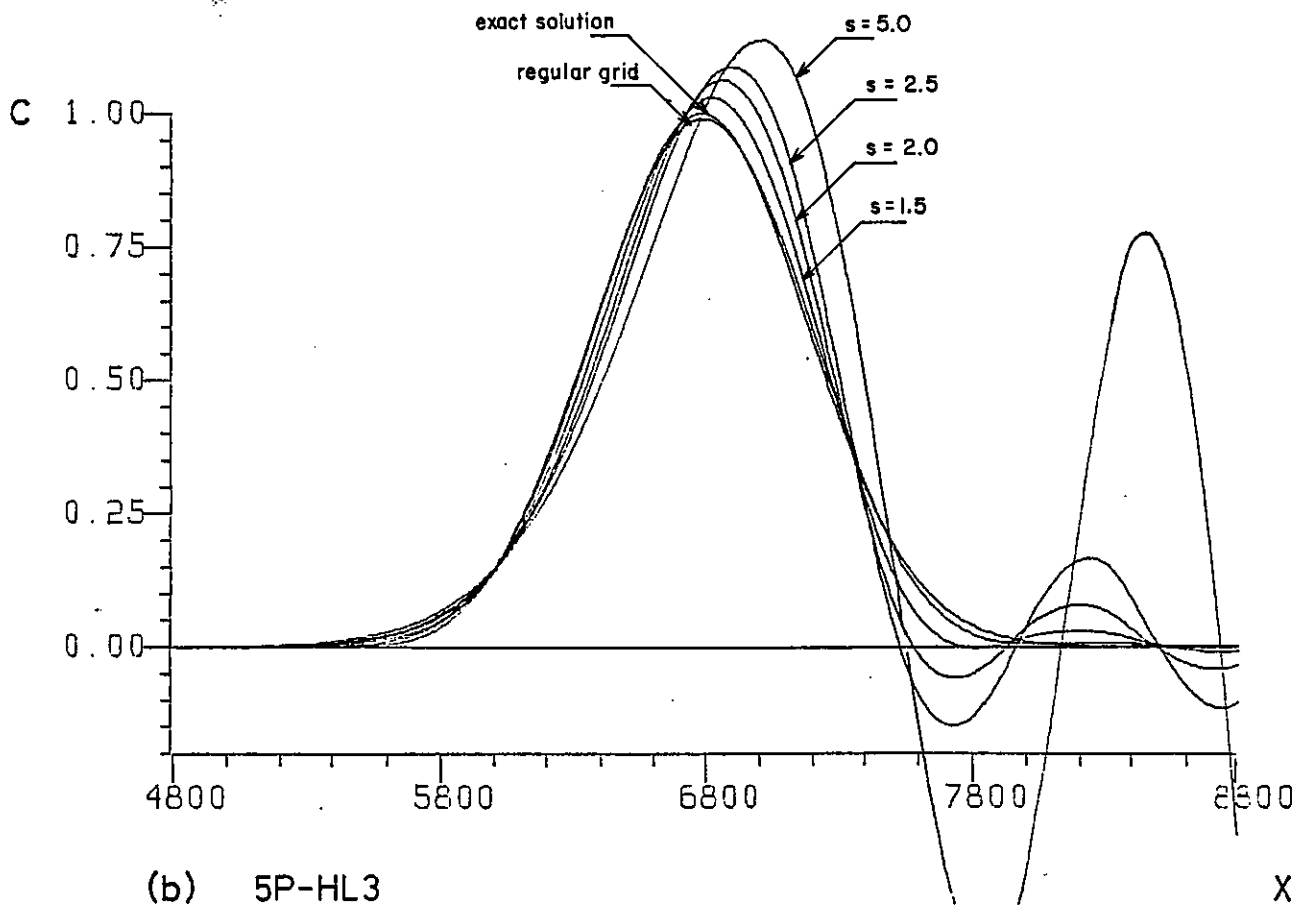
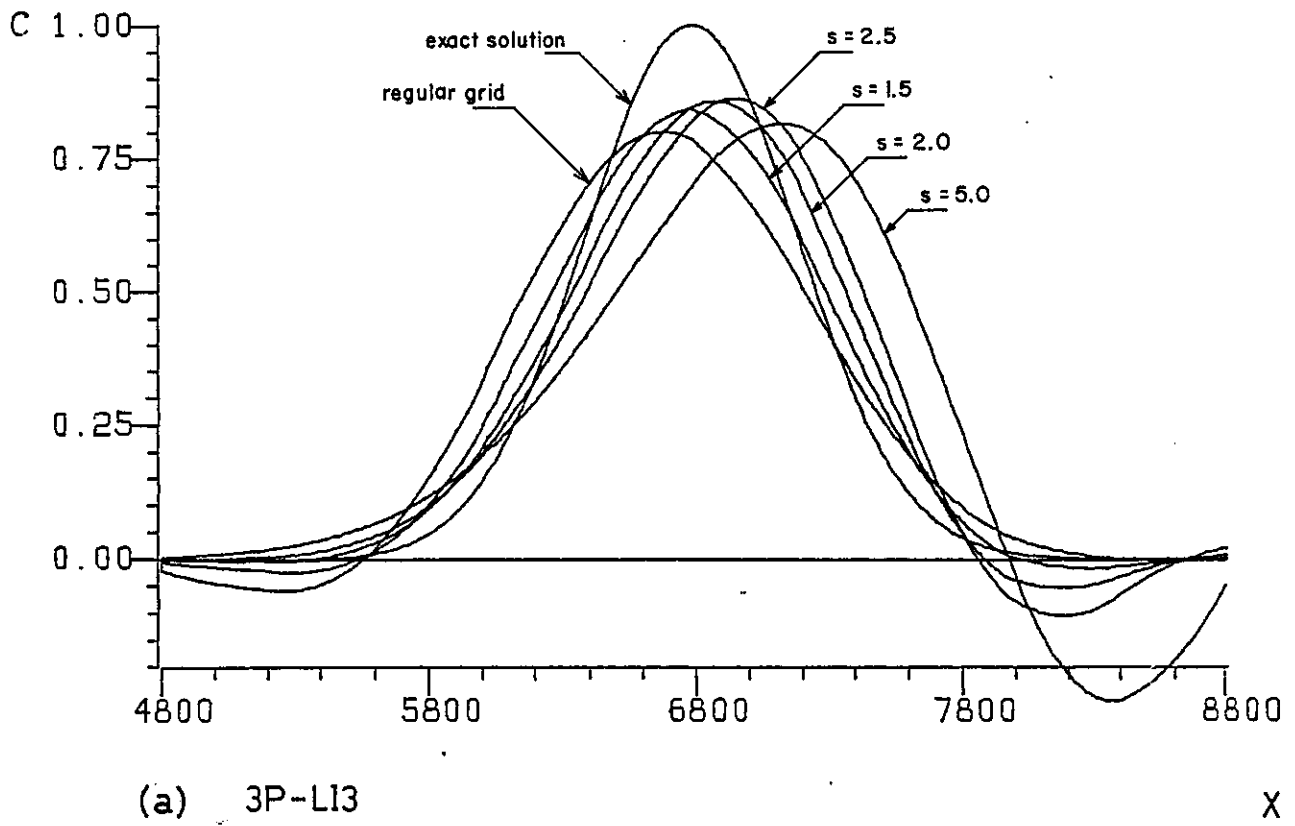


Fig. 4.34. BMC solutions for the uniform advection of a Gauss-hill in grids of type 1 ( $N=100$ ;  $t=T=9600$ ;  $\sigma_0=400$ ;  $u=0.5$ )

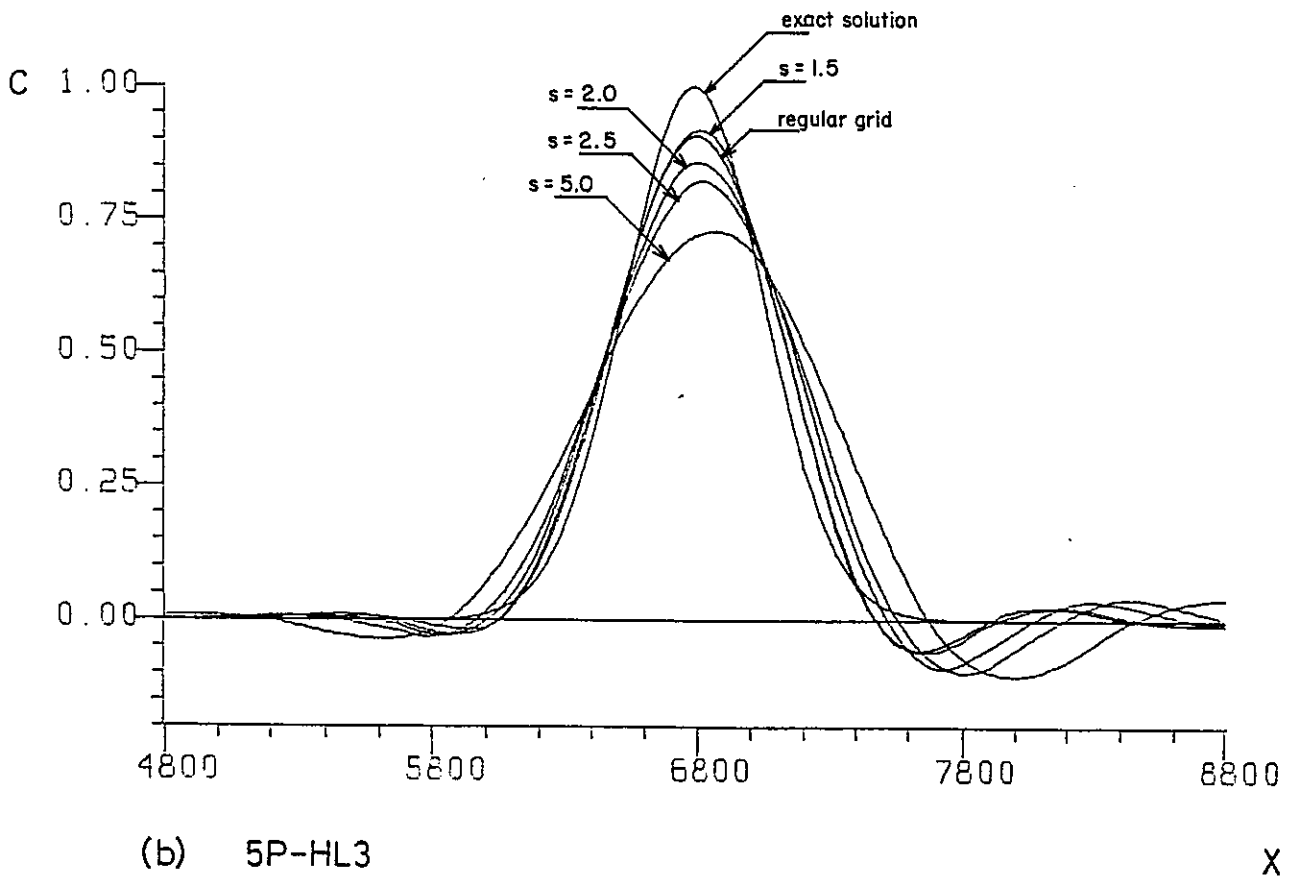
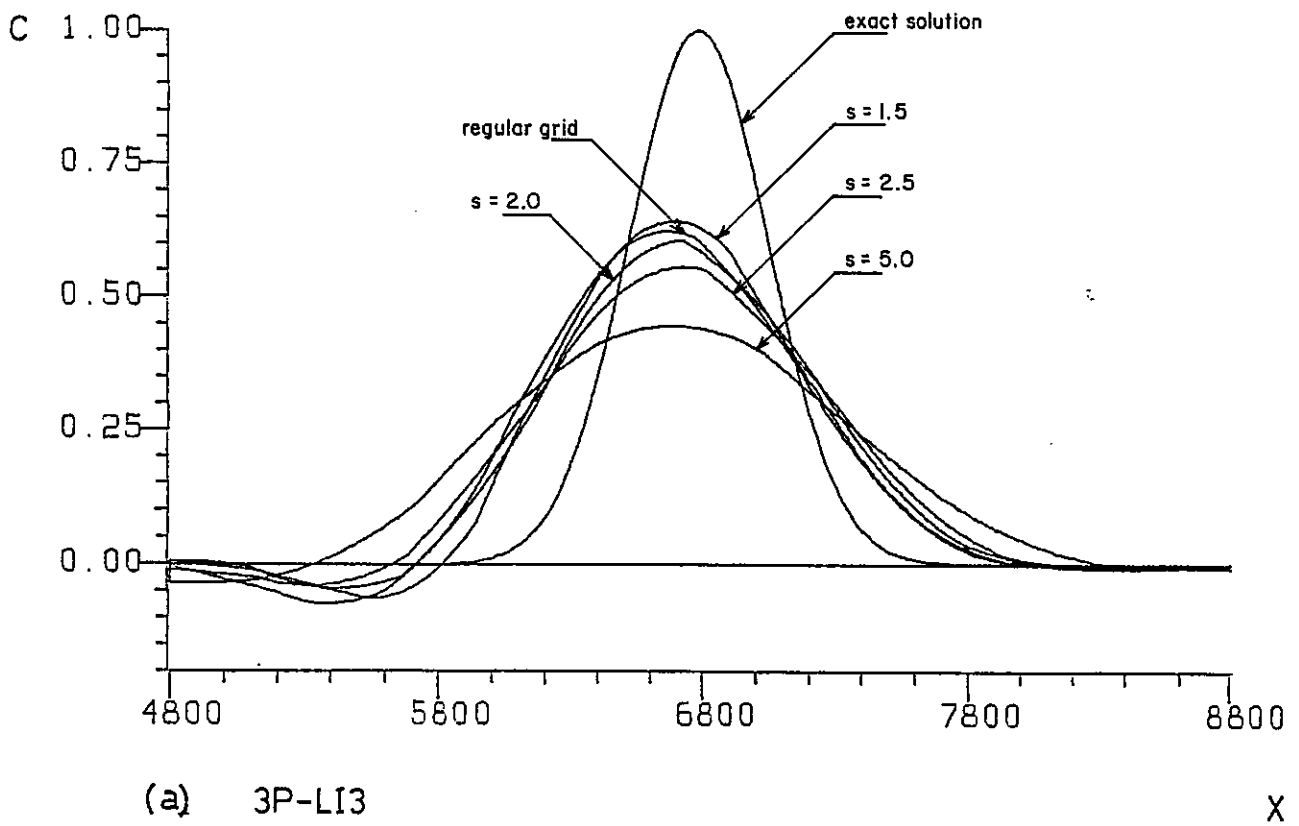


Fig. 4.35. BMC solutions for the uniform advection of a Gauss-hill in grids of type 2 ( $N=100$ ;  $t=T=9600$ ;  $\sigma_0=264$ ;  $u=0.5$ )

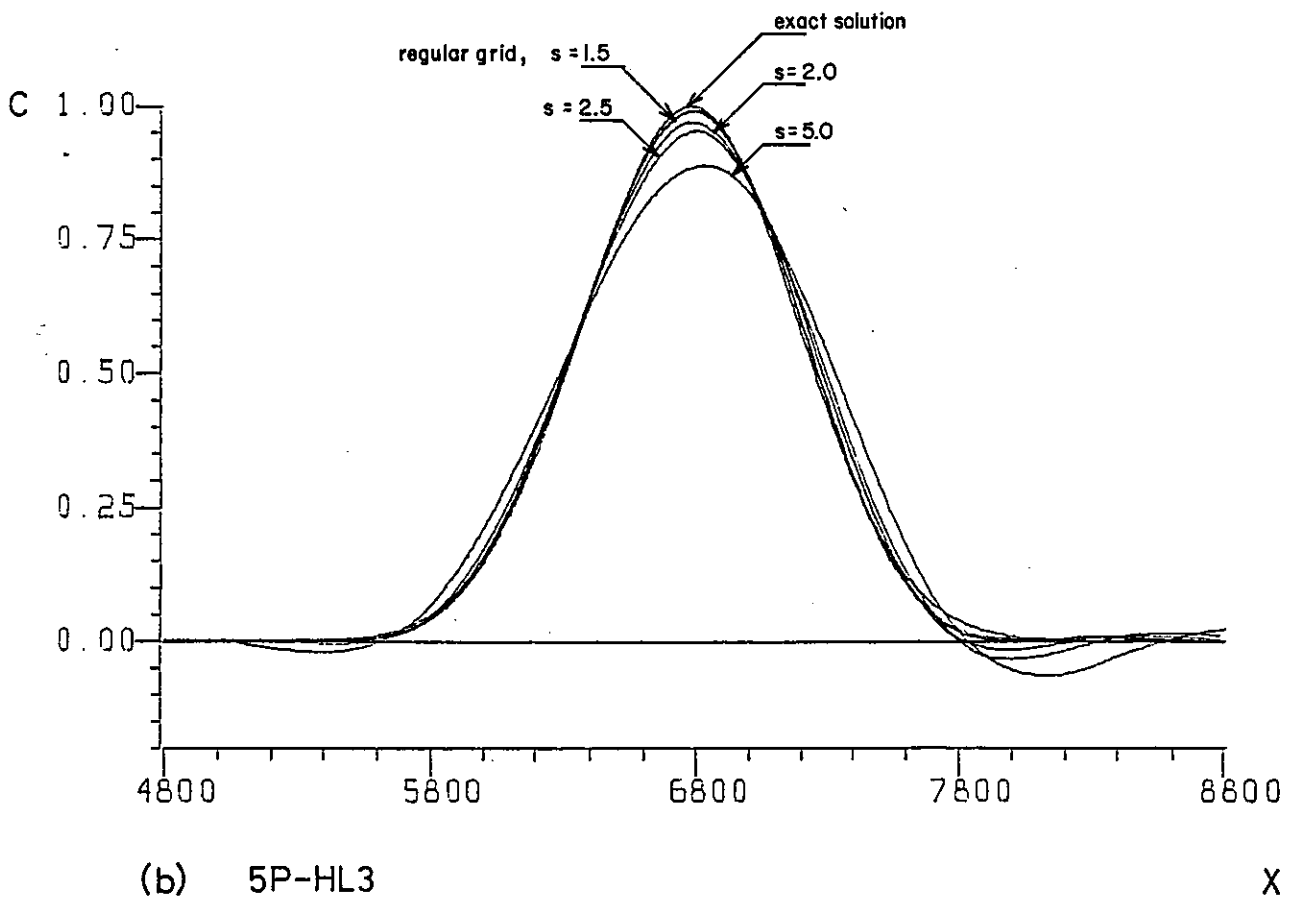
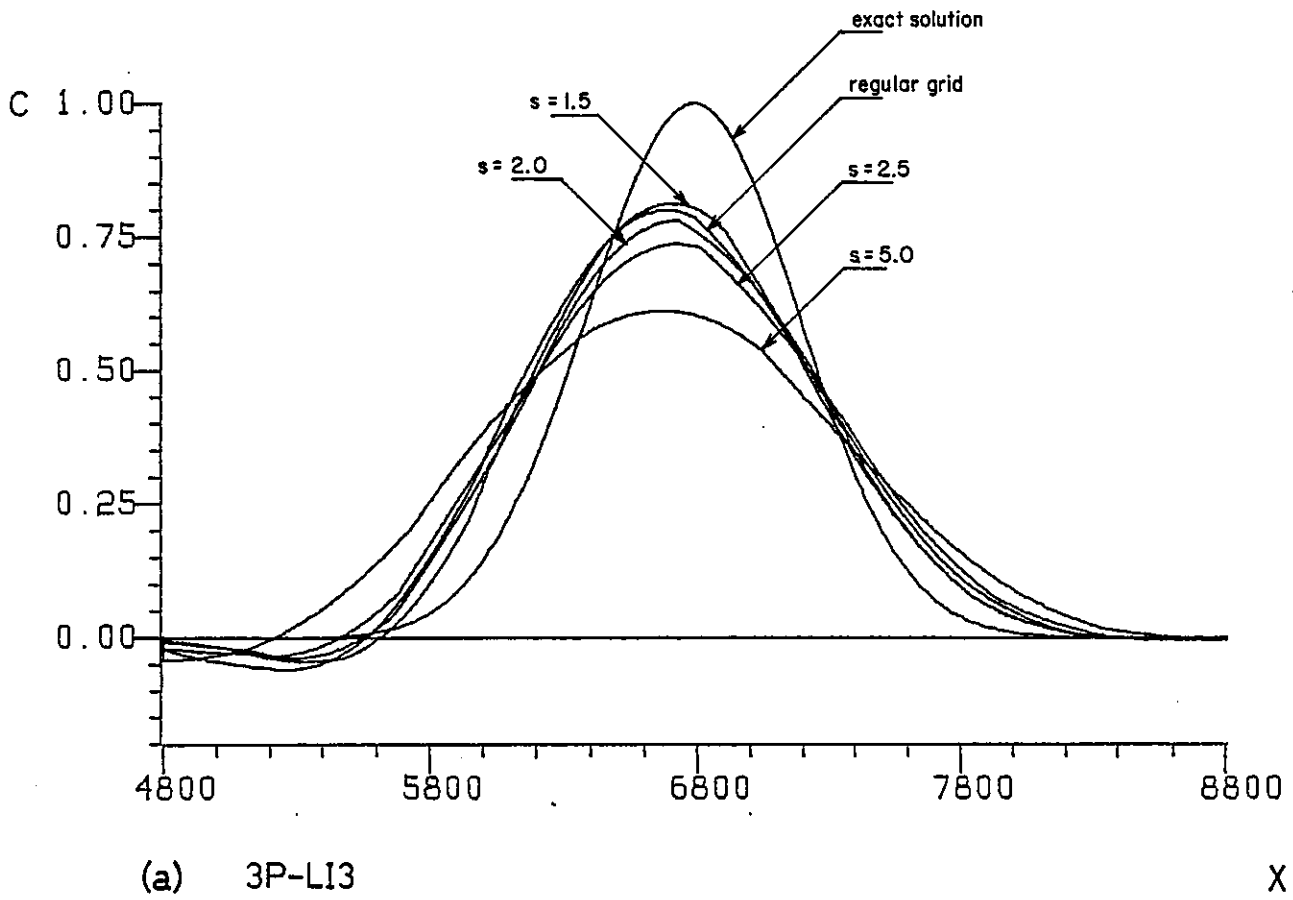


Fig. 4.36. BMC solutions for the uniform advection of a Gauss-hill in grids of type 2 ( $N=100$ ;  $t=T=9600$ ;  $\sigma_0=400$ ;  $u=0.5$ )

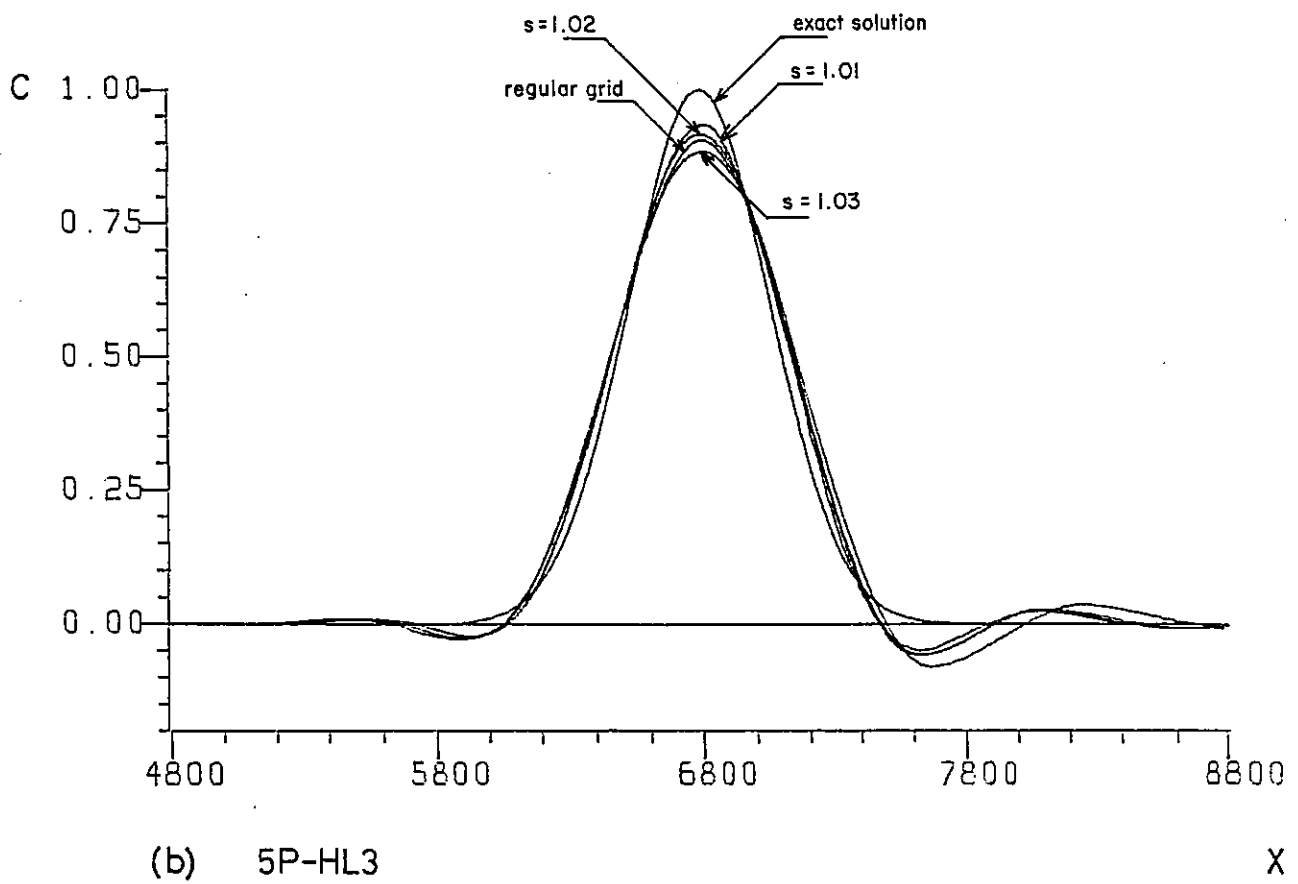
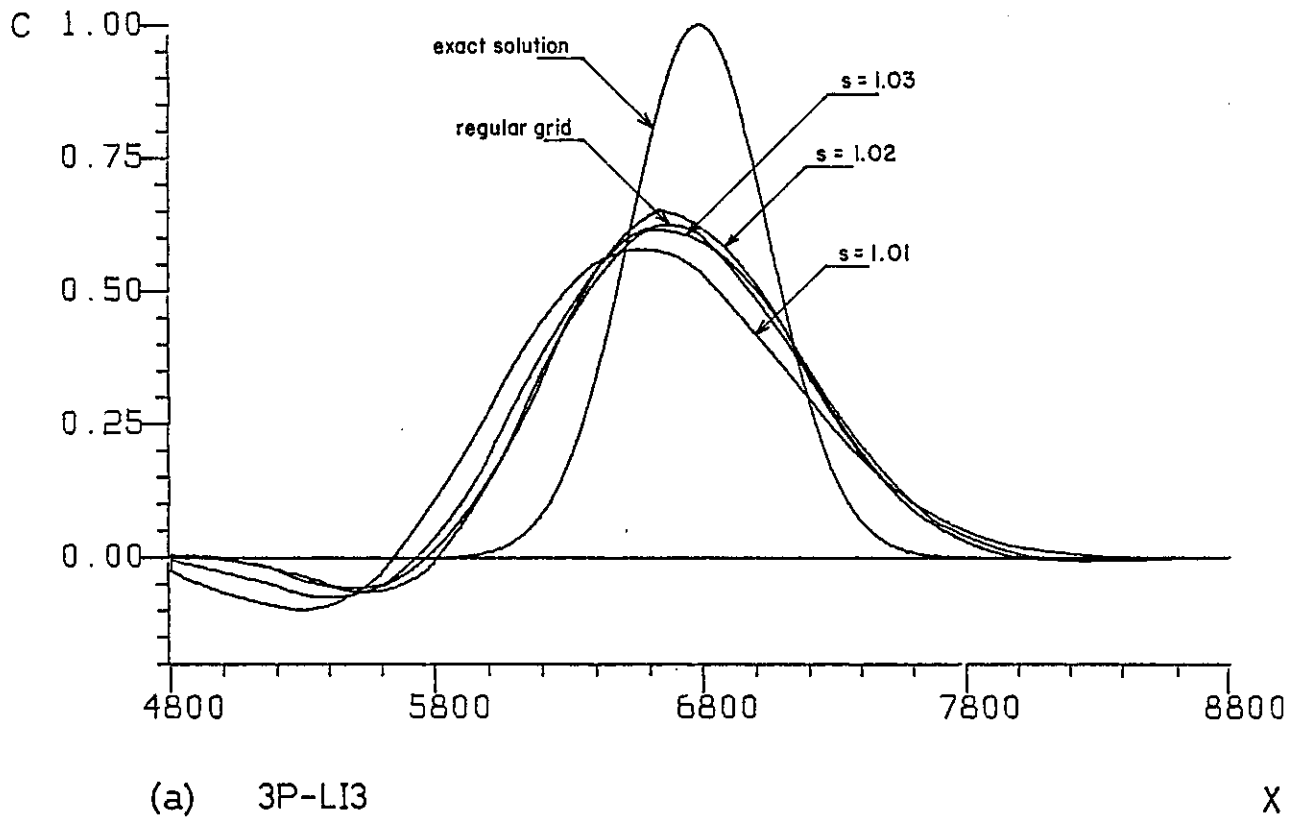


Fig. 4.37. BMC solutions for the uniform advection of a Gauss-hill in grids of type 3 ( $N=100$ ;  $t=T=9600$ ;  $\sigma_0=264$ ;  $u=0.5$ )



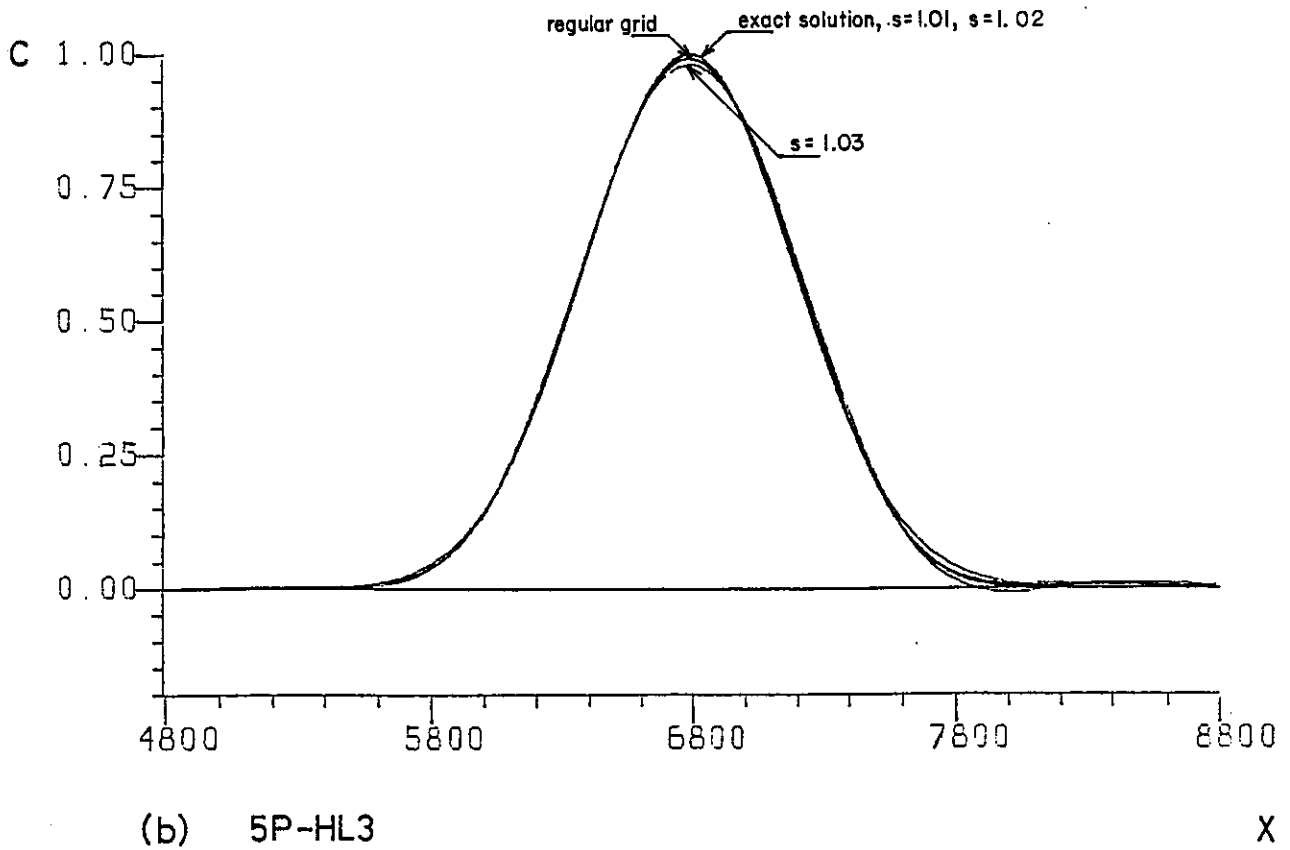
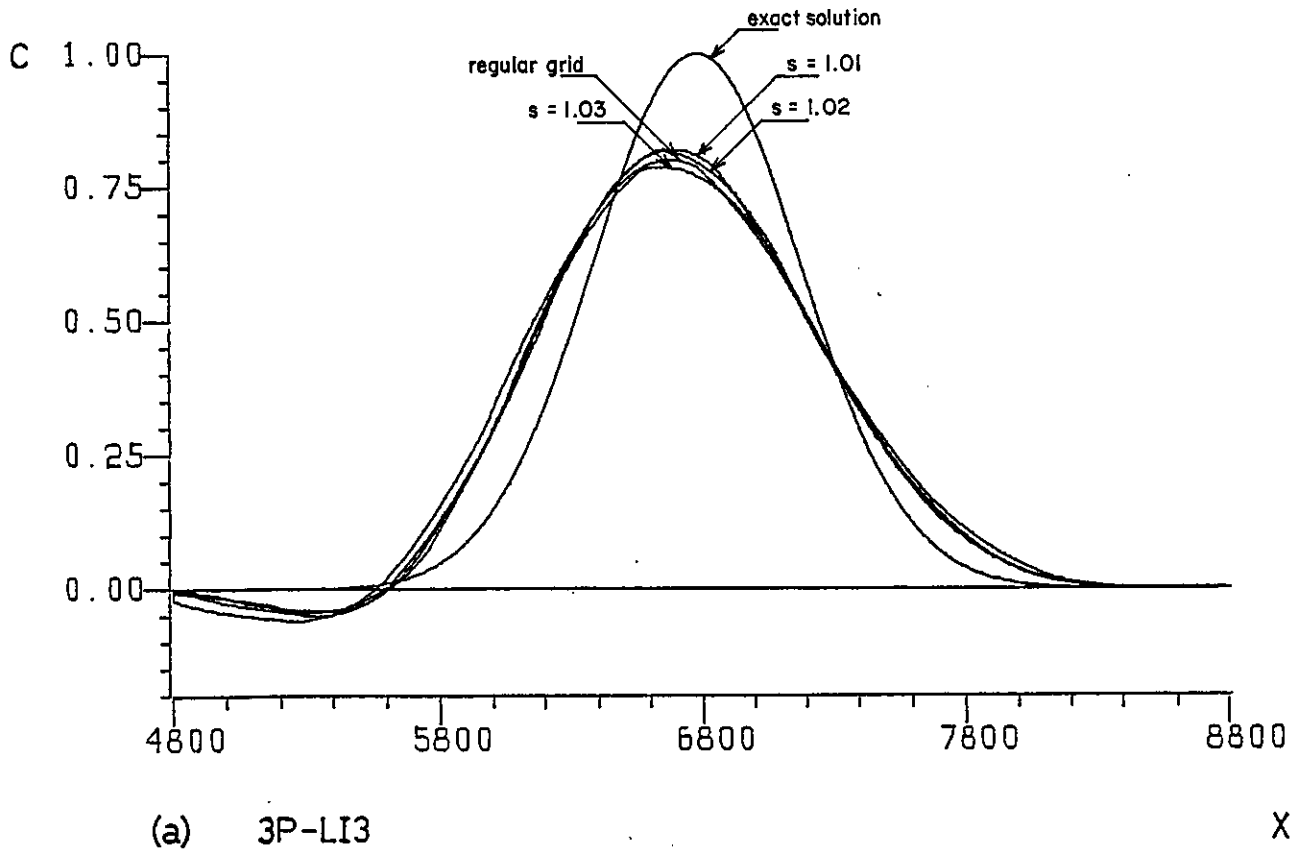
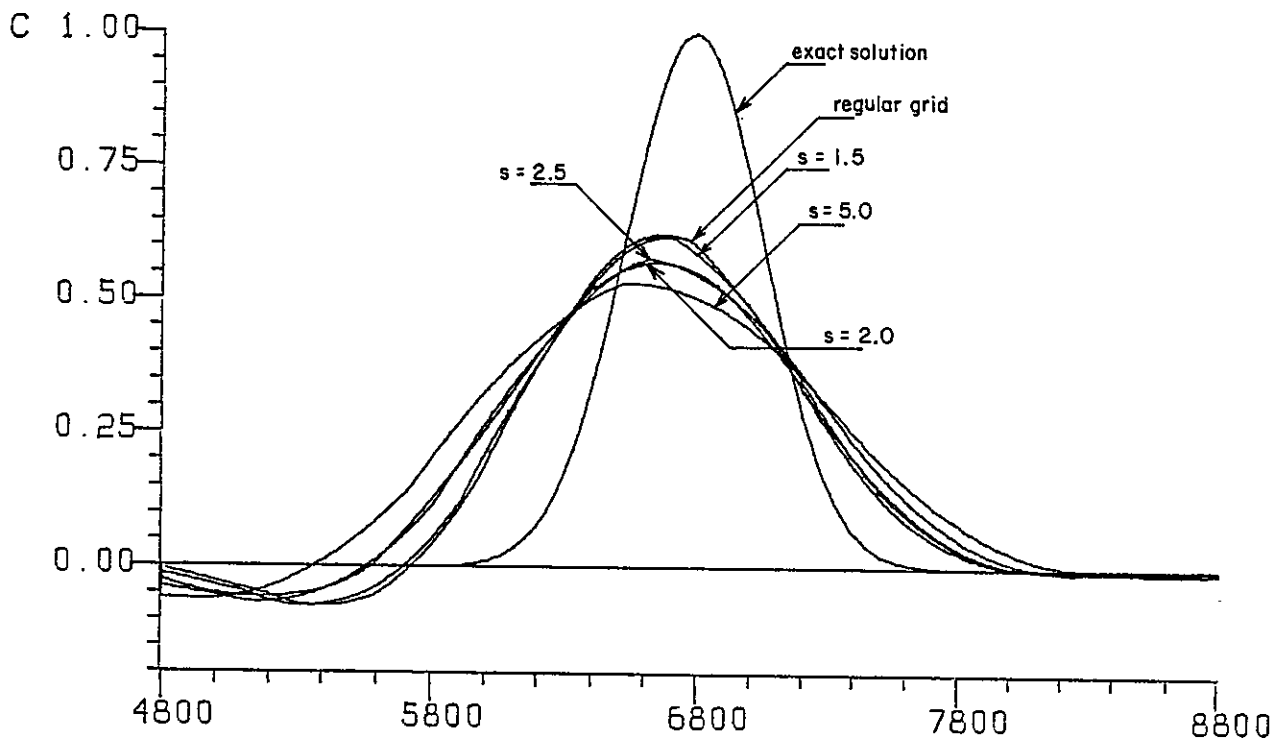
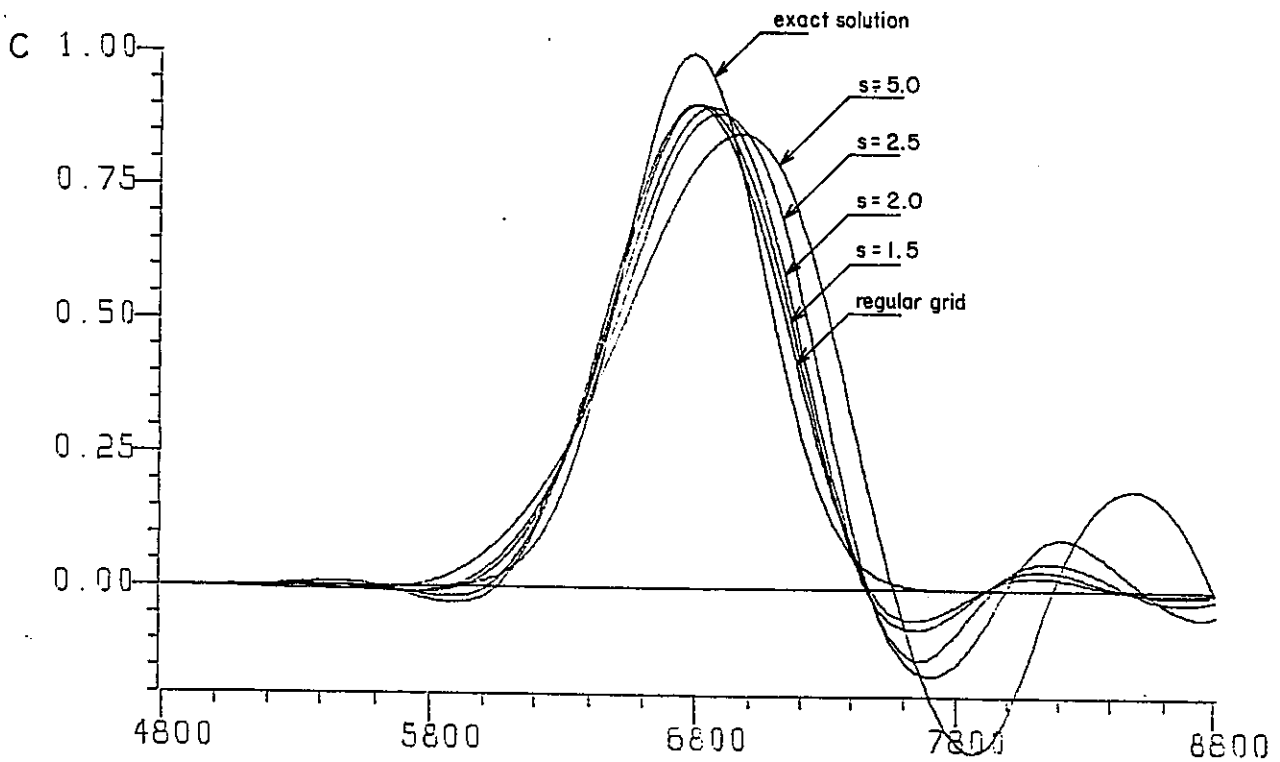


Fig. 4.38. BMC solutions for the uniform advection of a Gauss-hill in grids of type 3 ( $N=100$ ;  $t=T=9600$ ;  $\sigma_0=400$ ;  $u=0.5$ )



(a) 3P-LI3

X



(b) 5P-HL3

X

Fig. 4.39. BMC solutions for the uniform advection of a Gauss-hill in grids of type 4 ( $N=100$ ;  $t=T=9600$ ;  $\Delta\sigma=264$ ;  $u=0.5$ )

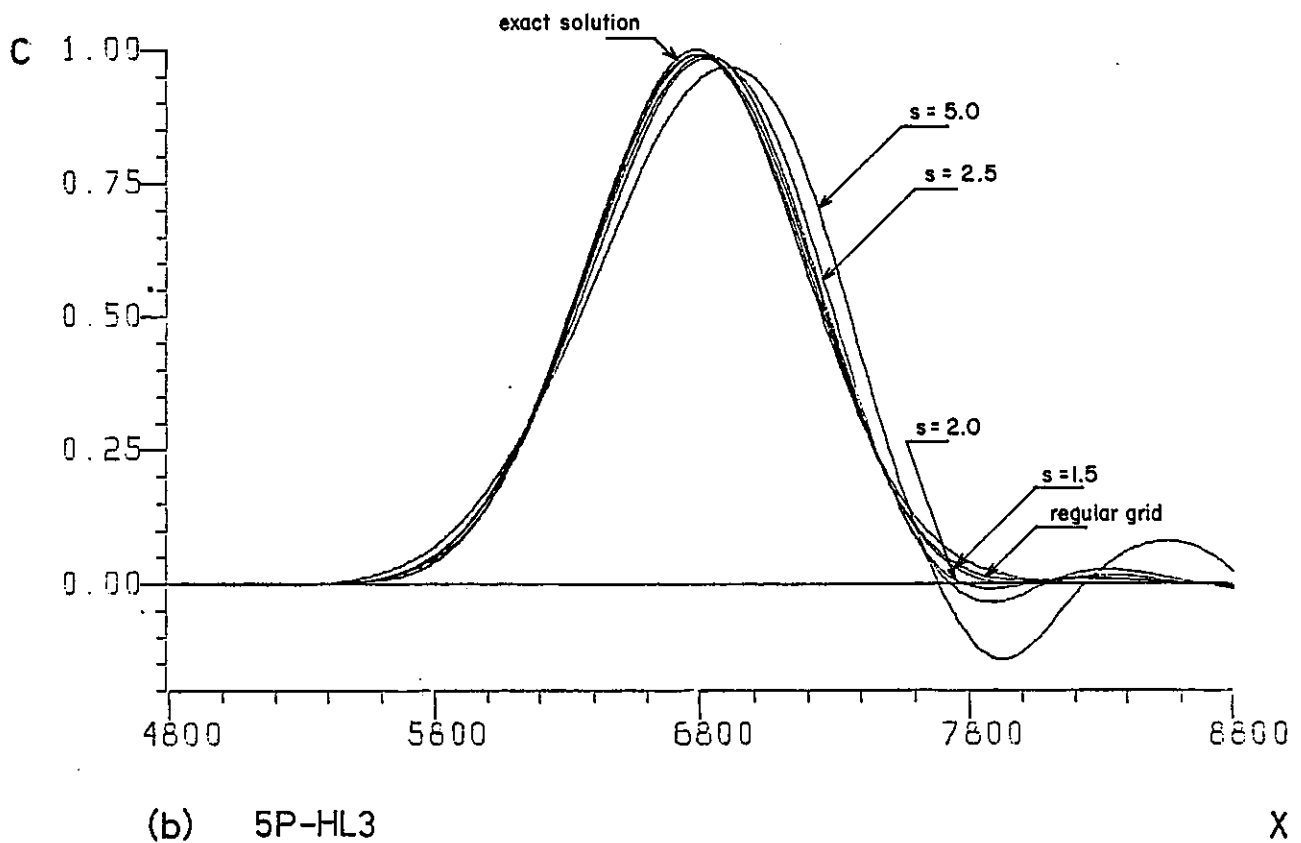
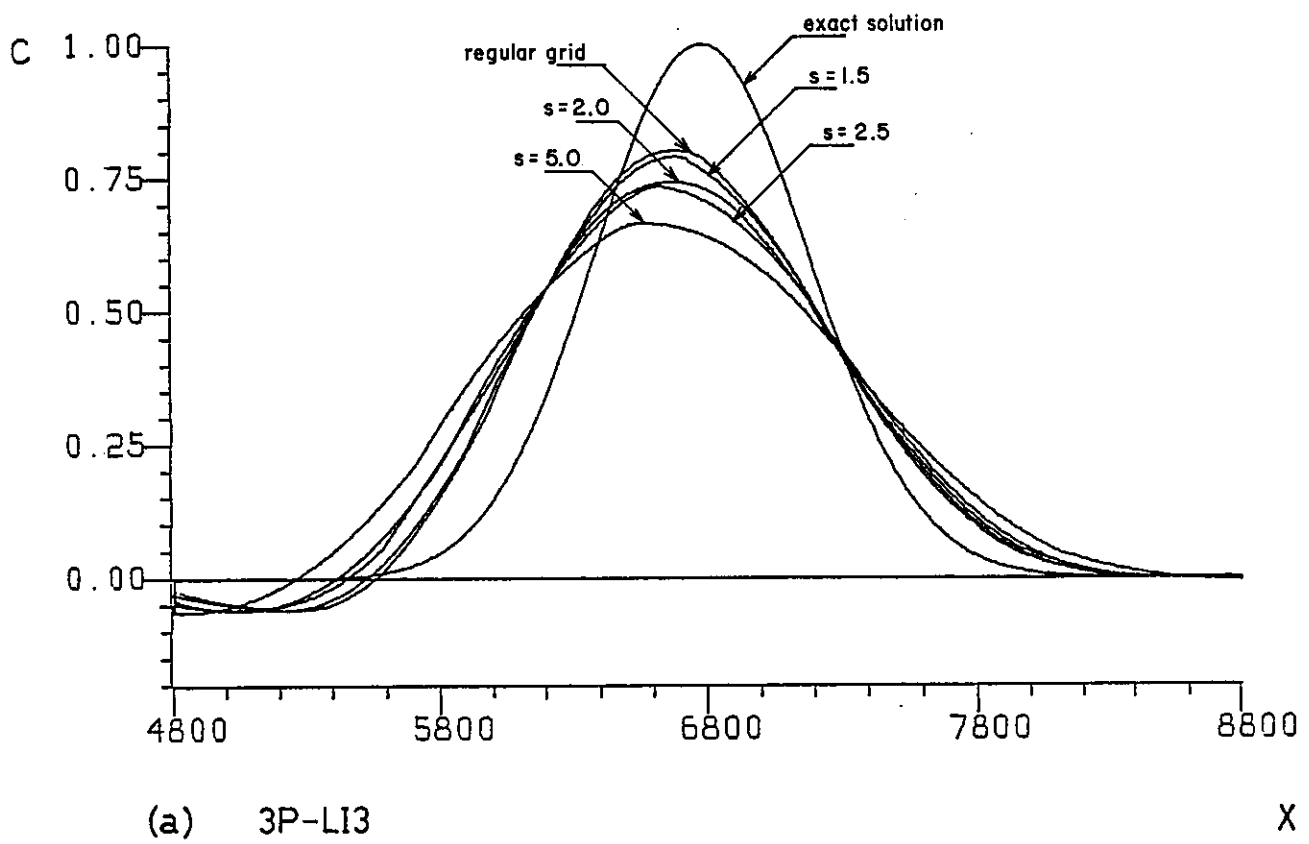


Fig. 4.40. BMC solutions for the uniform advection of a Gauss-hill in grids of type 4 ( $N=100$ ;  $t=T=9600$ ;  $\sigma_0=400$ ;  $u=0.5$ )

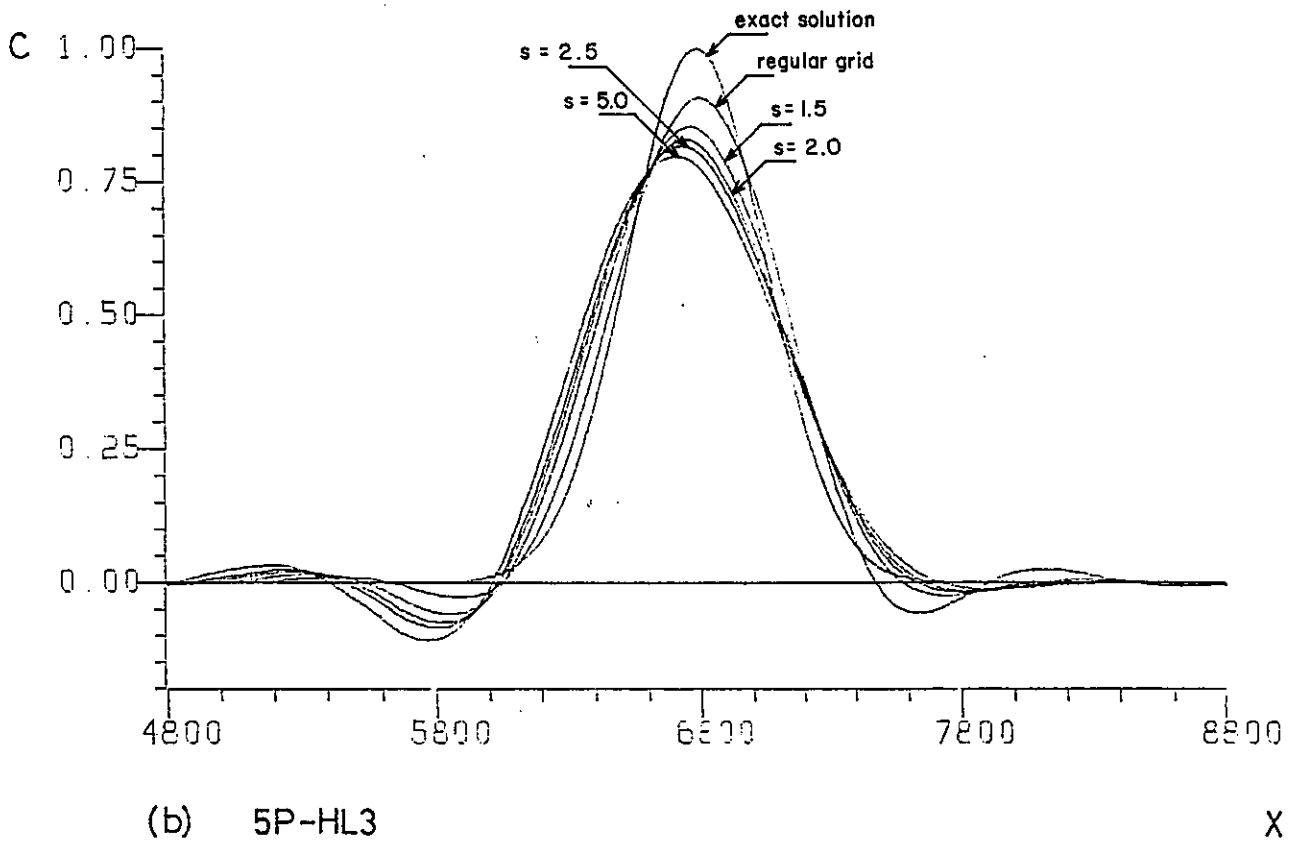
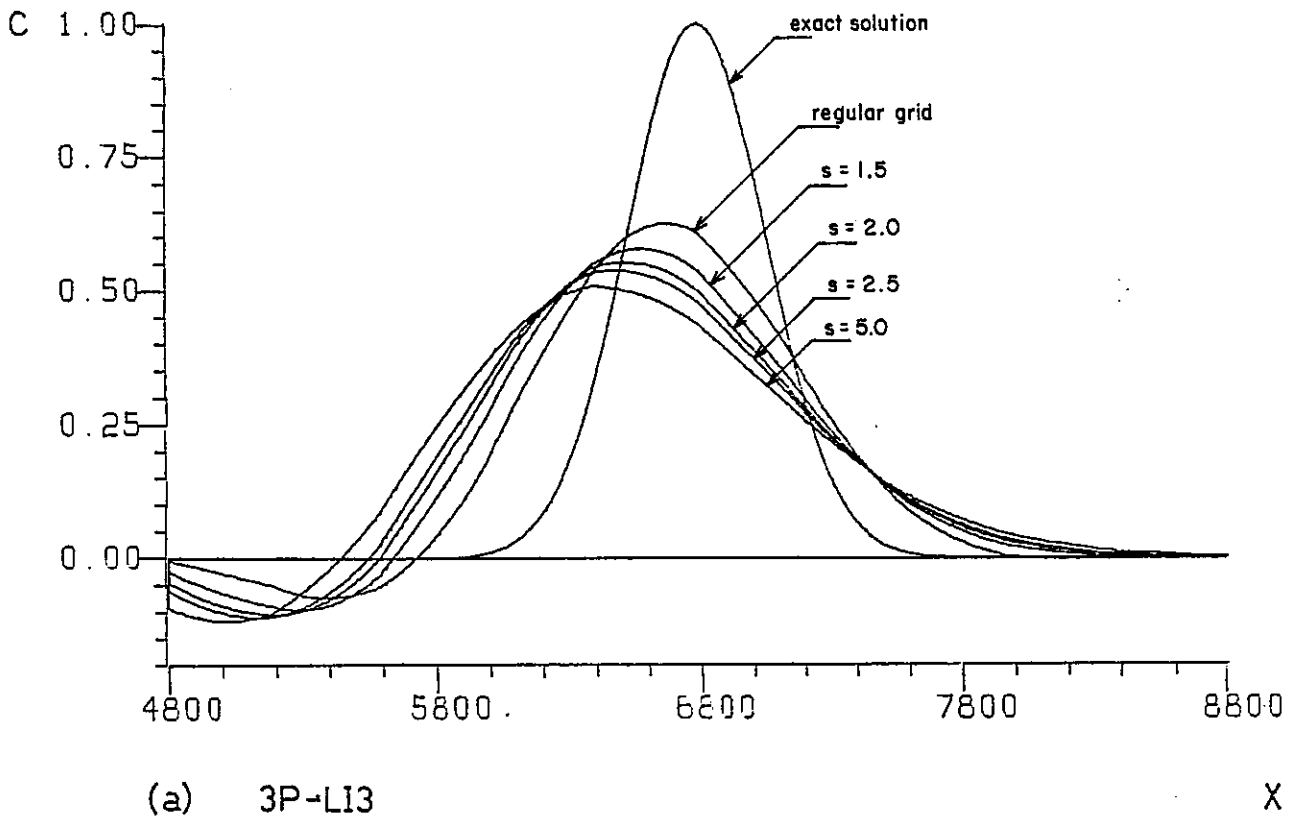


Fig. 4.41. BMC solutions for the uniform advection of a Gauss-hill in grids of type 5 ( $N=100$ ;  $t=T=9600$ ;  $\sigma_0=264$ ;  $u=0.5$ )

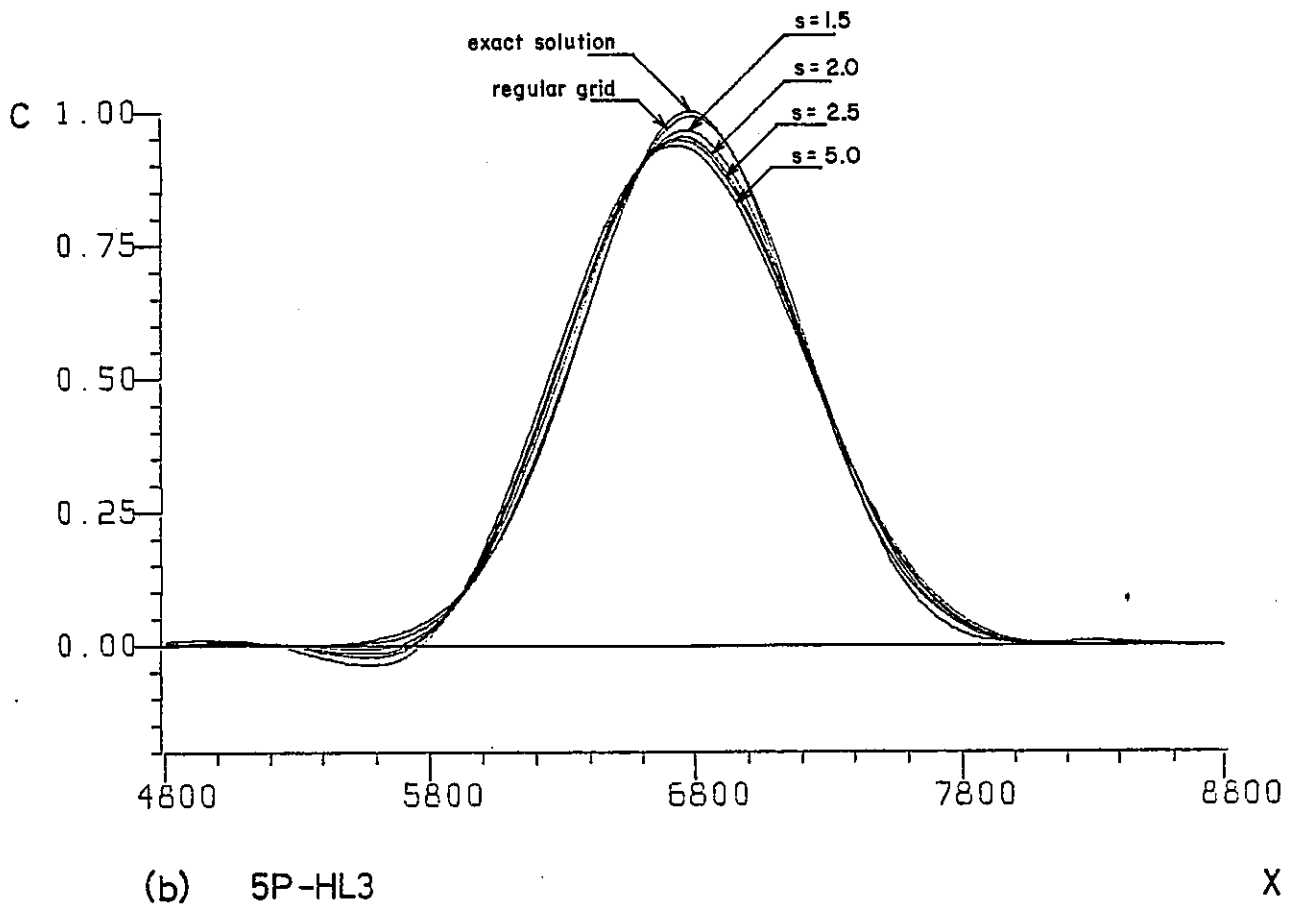
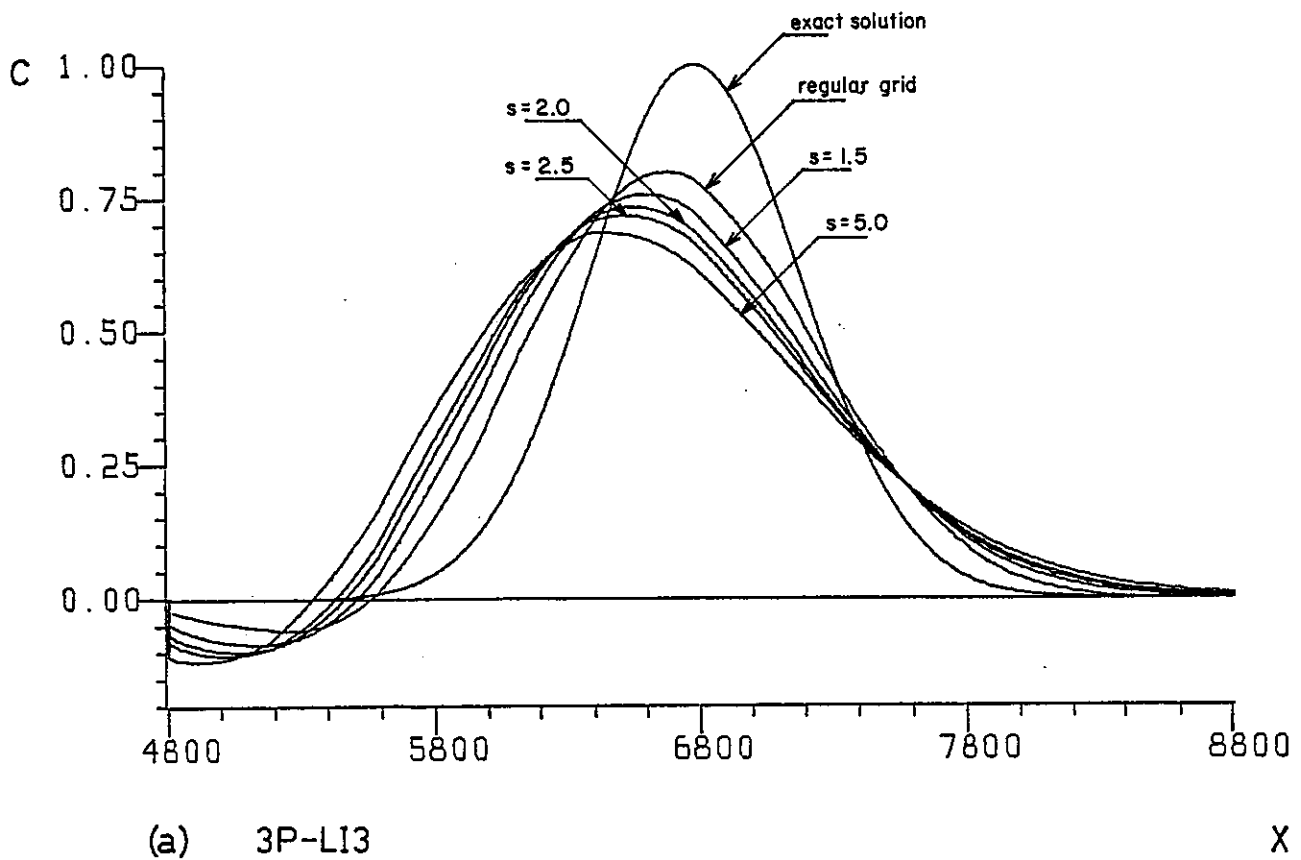
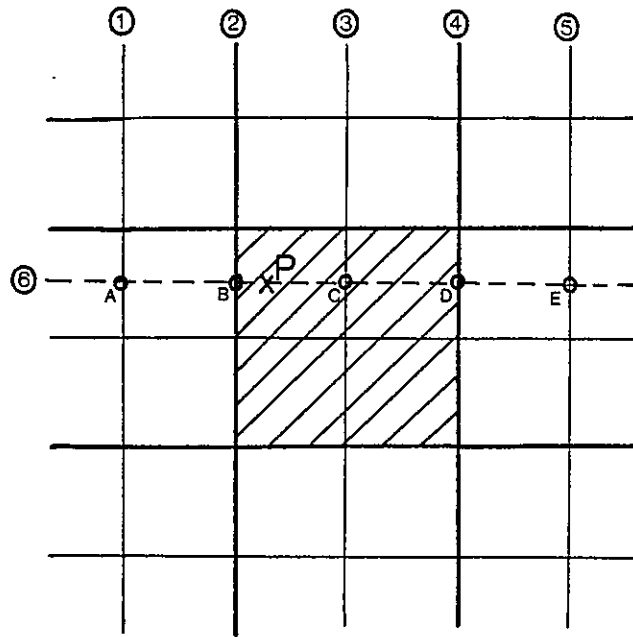


Fig. 4.42. BMC solutions for the uniform advection of a Gauss-hill in grids of type 5 ( $N=100$ ;  $t=T=9600$ ;  $\sigma_0=400$ ;  $u=0.5$ )

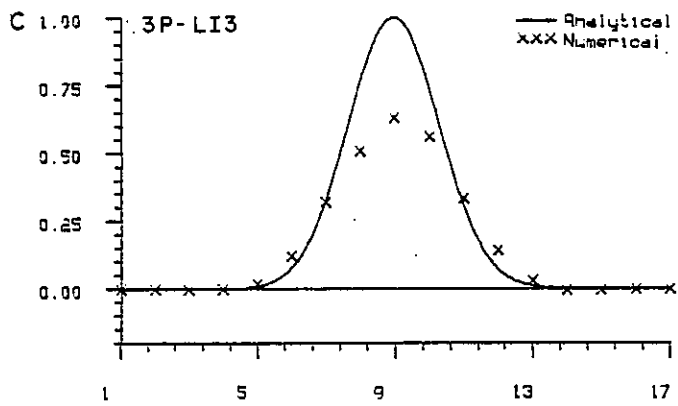


PROBLEM: Find concentrations at point P, given concentrations at all grid nodes

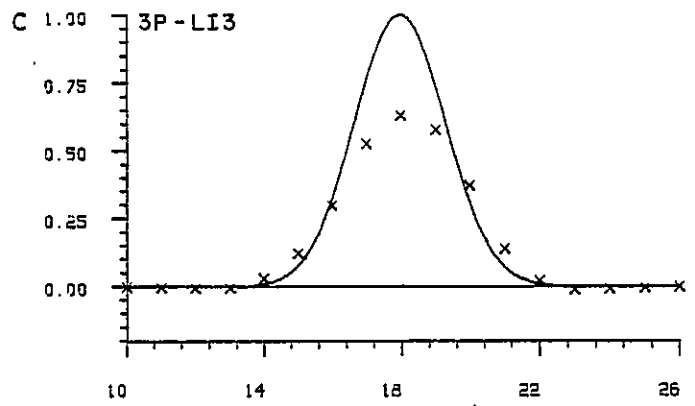
PROCEDURE: (a) Find concentrations at points A through E, by using the 1-D interpolation scheme, defined successively along axis 1 to 5

(b) Find concentration at point P, by using the 1-D interpolation scheme, defined along axis 6

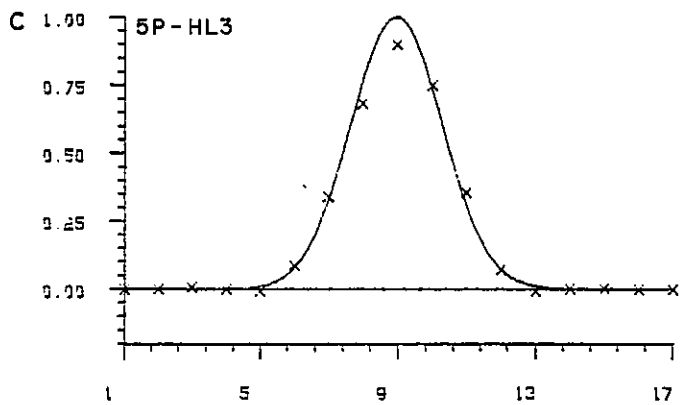
Fig. 4.43. Interpolation in 2-D straight orthogonal grids. Illustrative sketch



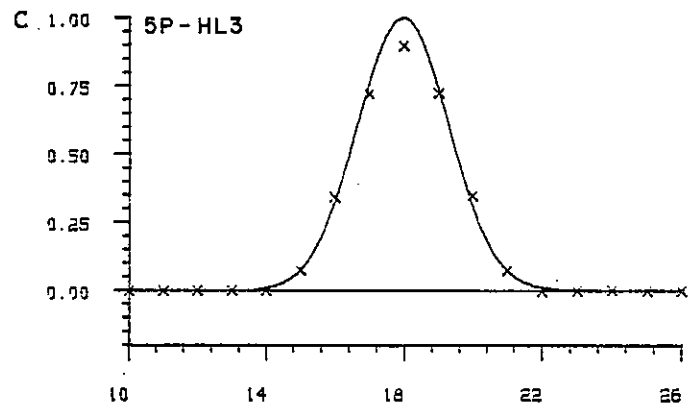
(a) normal to the flow



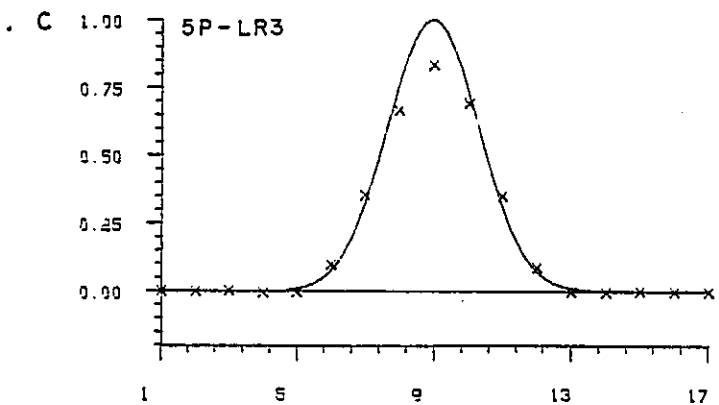
(b) along the flow



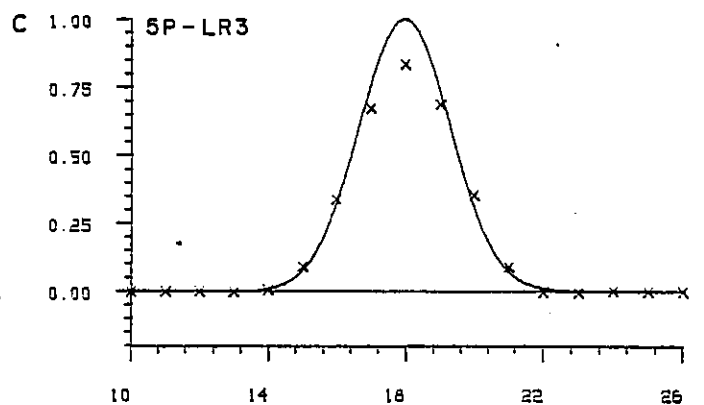
(c) normal to the flow



(d) along the flow



(e) normal to the flow



(f) along the flow

Fig. 4.44. BMC solutions for the 2-D advection of a Gauss-hill in a flow field in rigid-body rotation. Concentration profiles after one revolution ( $w=2\pi/3000$ ;  $N=30$ ;  $\sigma_x=\sigma_y=264$ )

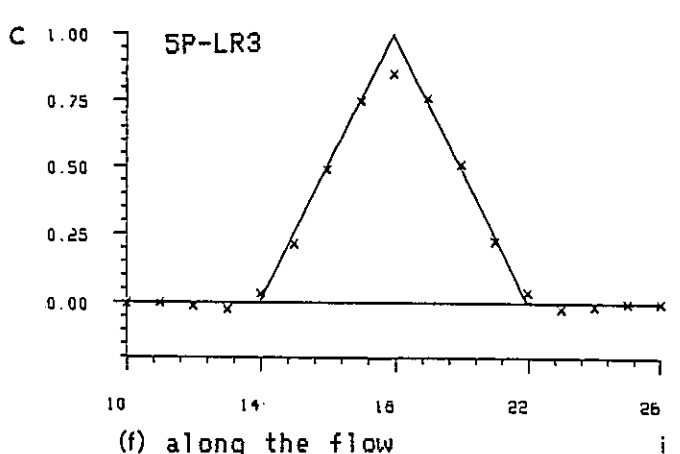
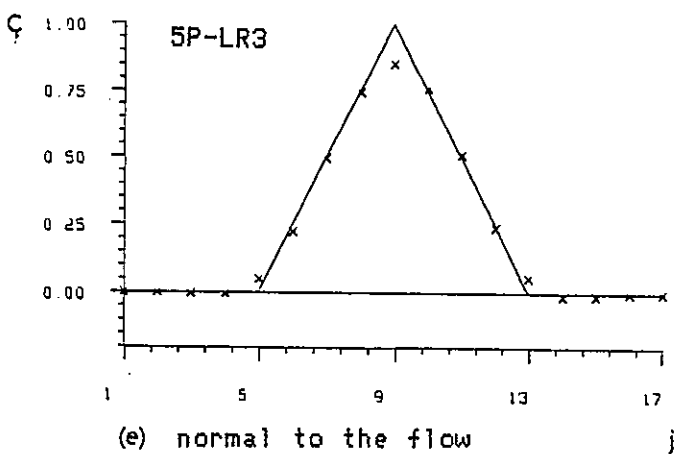
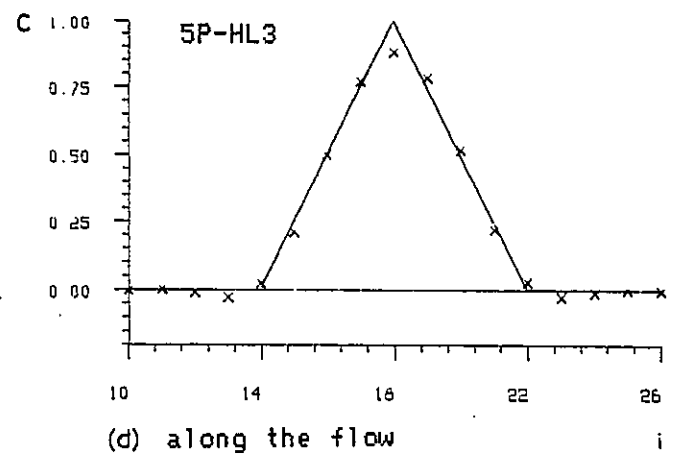
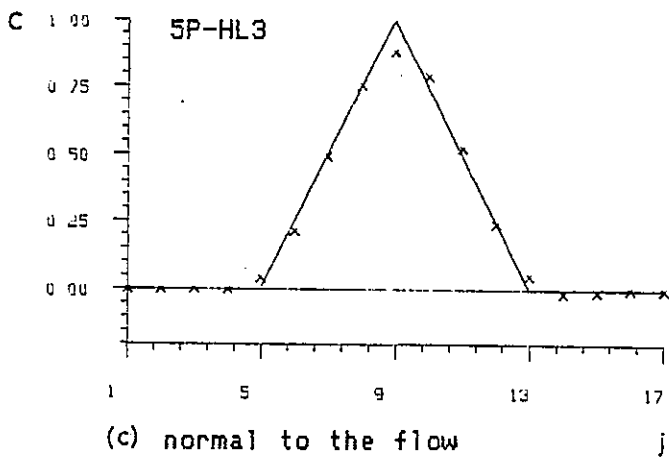
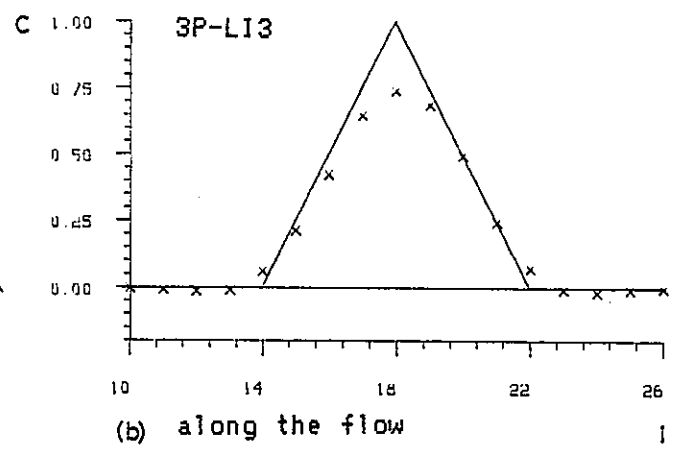
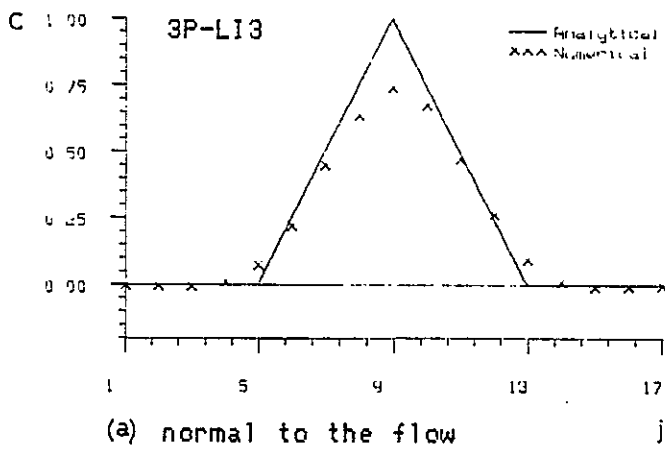
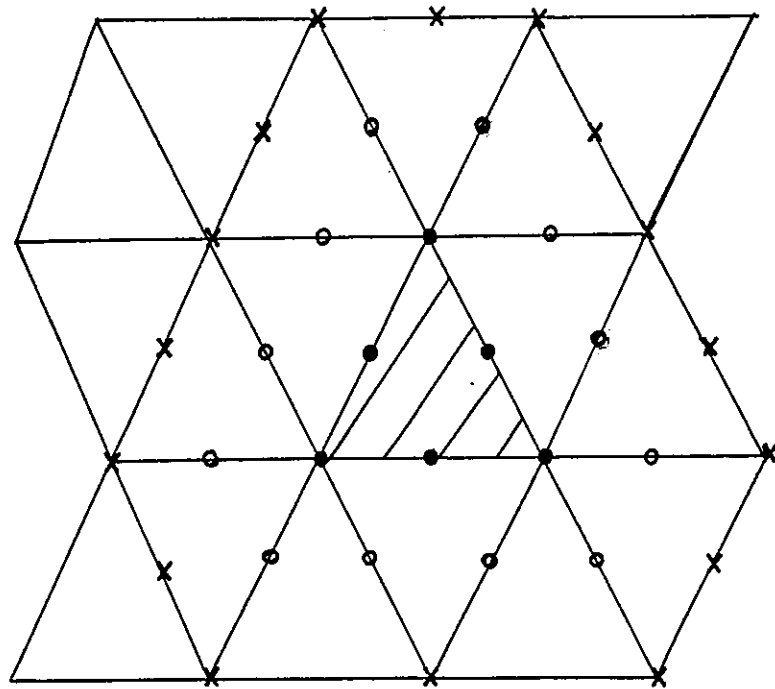


Fig. 4.45. BMC solutions for the 2-D advection of a Cone-hill in a flow field in rigid-body rotation. Concentration profiles after one revolution ( $\omega=2\pi/3000$ ;  $N=30$ ;  $l=800$ )

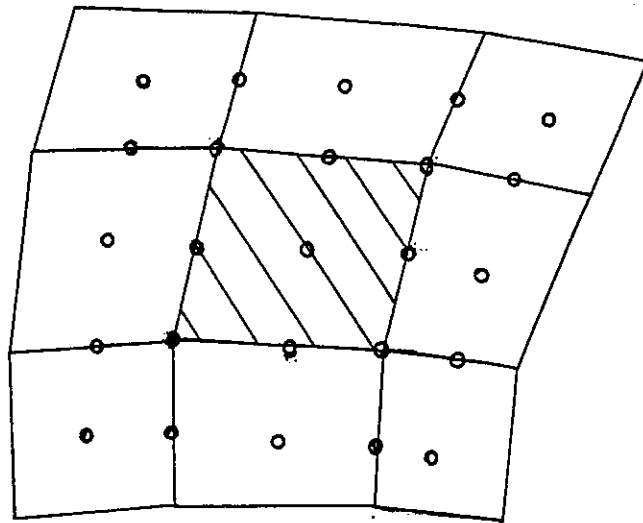




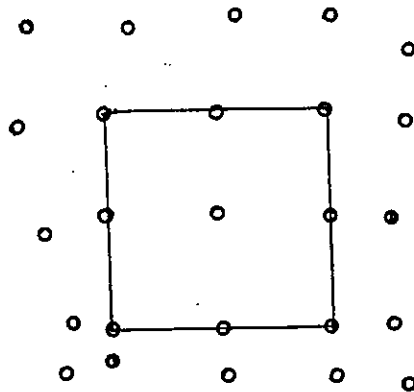
PROBLEM: Select points that will contribute to define a 5P-LR3 interpolation.

AMBIGUITY: While nodes marked with  $\bullet$  and  $\circ$  are unambiguously appropriate, we only need 7 of the 13 nodes marked with  $\times$  to define the interpolation.

Fig. 4.46. Extension of non-compact interpolation schemes to 2-D unstructured grids. Illustration of a possible ambiguity in the identification of nodes contributing to the interpolation

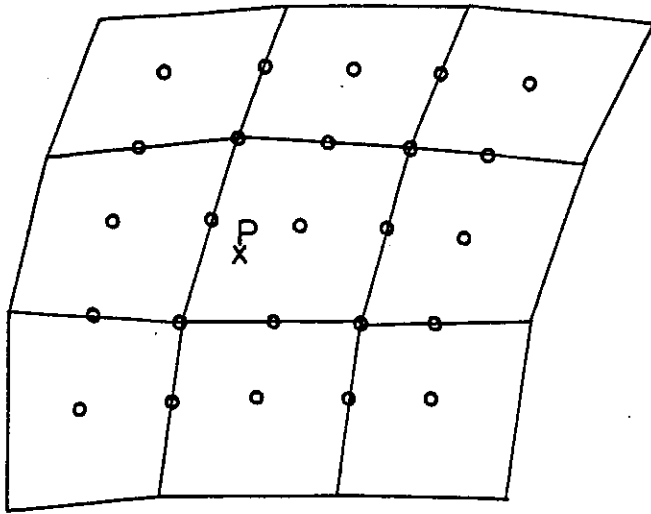


(a) Global coordinates



(b) Local coordinates (qualitative sketch)

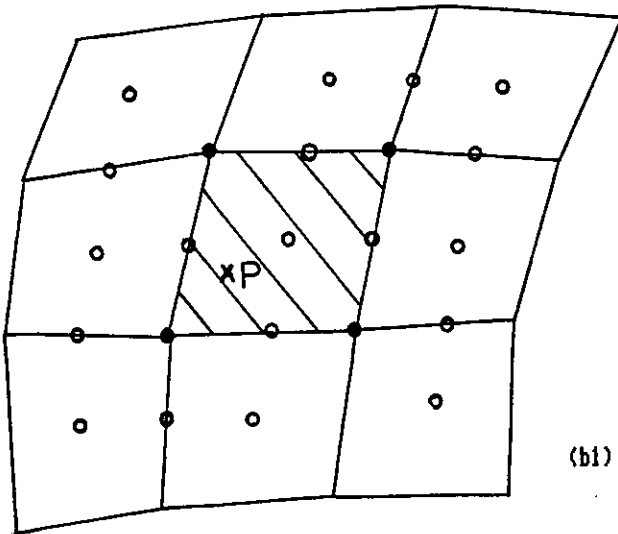
Fig. 4.47. Extension of non-compact interpolation schemes to 2-D unstructured grids. Illustration of difficulties in mapping global into local coordinates.



(a) PROCEDURE FOR 5P-LR3

1- Define a bi-4th order polynomial by fitting the concentrations at the 25 nodes marked with  $\circ$  (this requires the solution of a system of 25 linear equations).

2- Find concentration at P by substitution.



(b1)

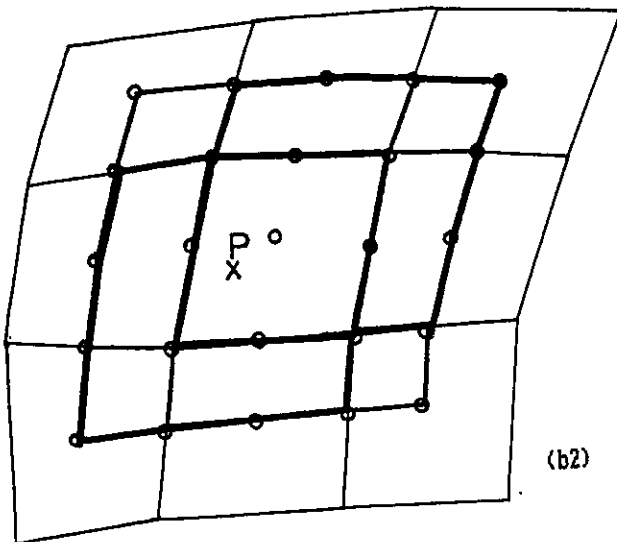
(b) PROCEDURE FOR 5P-HL3

1- Define bi-cubic interpolation polynomials over each of the four zones marked in (b2), by fitting concentrations at the respective nodes (this requires the solution of a system of 16 linear equations, per zone).

2- Estimate derivatives ( $\partial/\partial x$ ,  $\partial/\partial y$ ,  $\partial^2/\partial x \partial y$ ) in the corner nodes of the core element, by simple average of the contributions from the four polynomials.

3- Define a bi-cubic Hermite polynomial over the core element, by fitting concentrations and concentration derivatives at the corner nodes (this requires the solution of a system of 16 linear equations).

4- Find the concentration at P by substitution.



(b2)

Fig. 4.48. Extension of non-compact interpolation schemes to 2-D unstructured grids. Illustration of the interpolation procedure in global coordinates

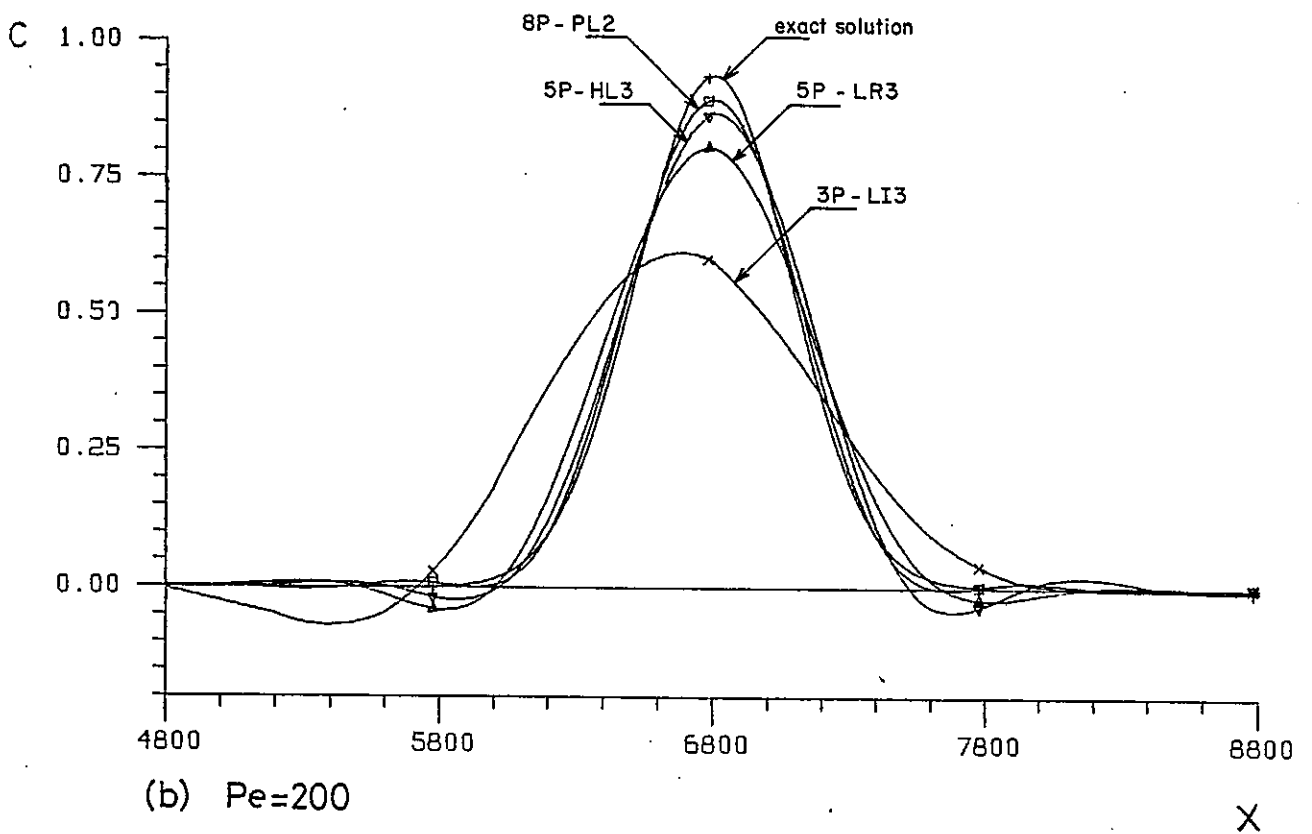
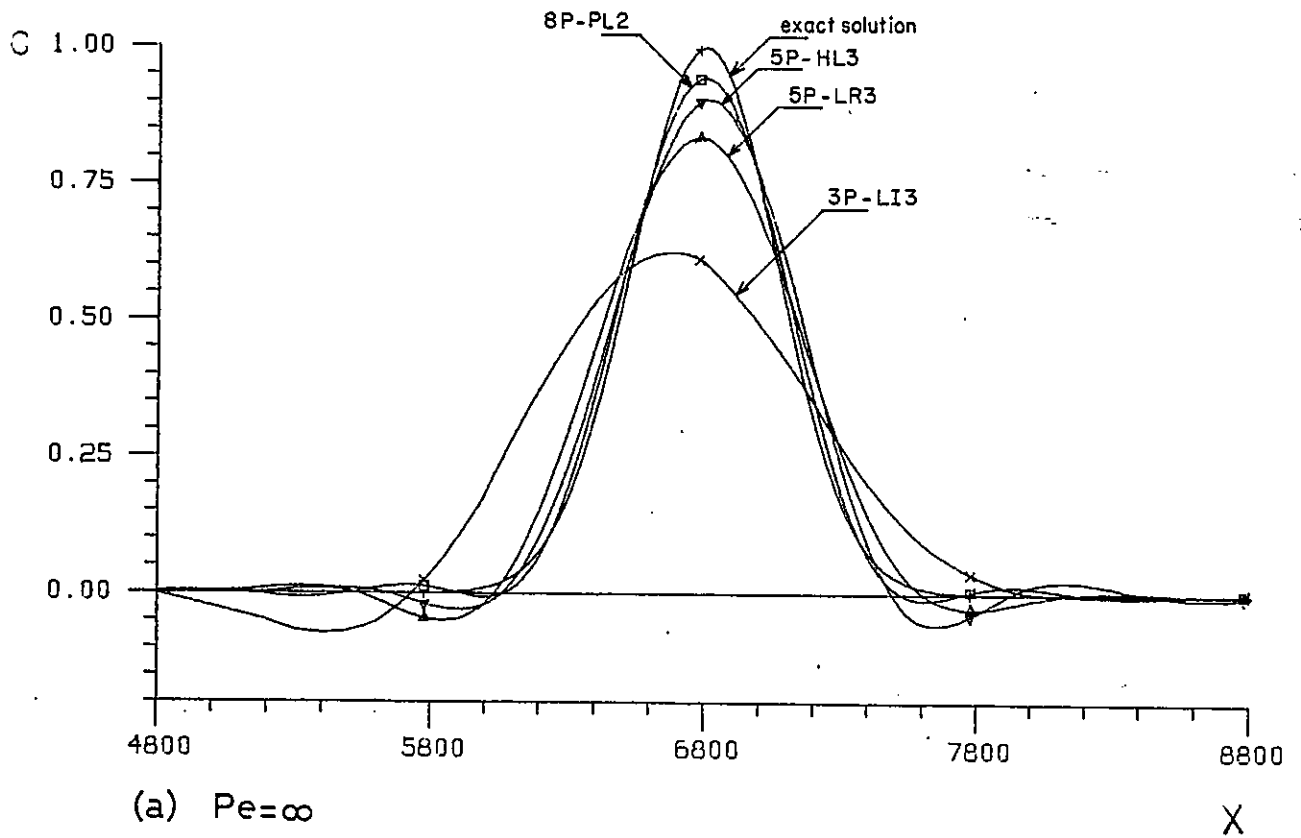


Fig. 5.1. ELM solutions for the transport of a Gauss-hill in a uniform flow. An illustration of the accuracy dependence on  $Pe$  ( $Cu=0.24$ ;  $N=100$ ;  $\sigma_0/\Delta x=1.32$ ;  $t=T=9600$ )

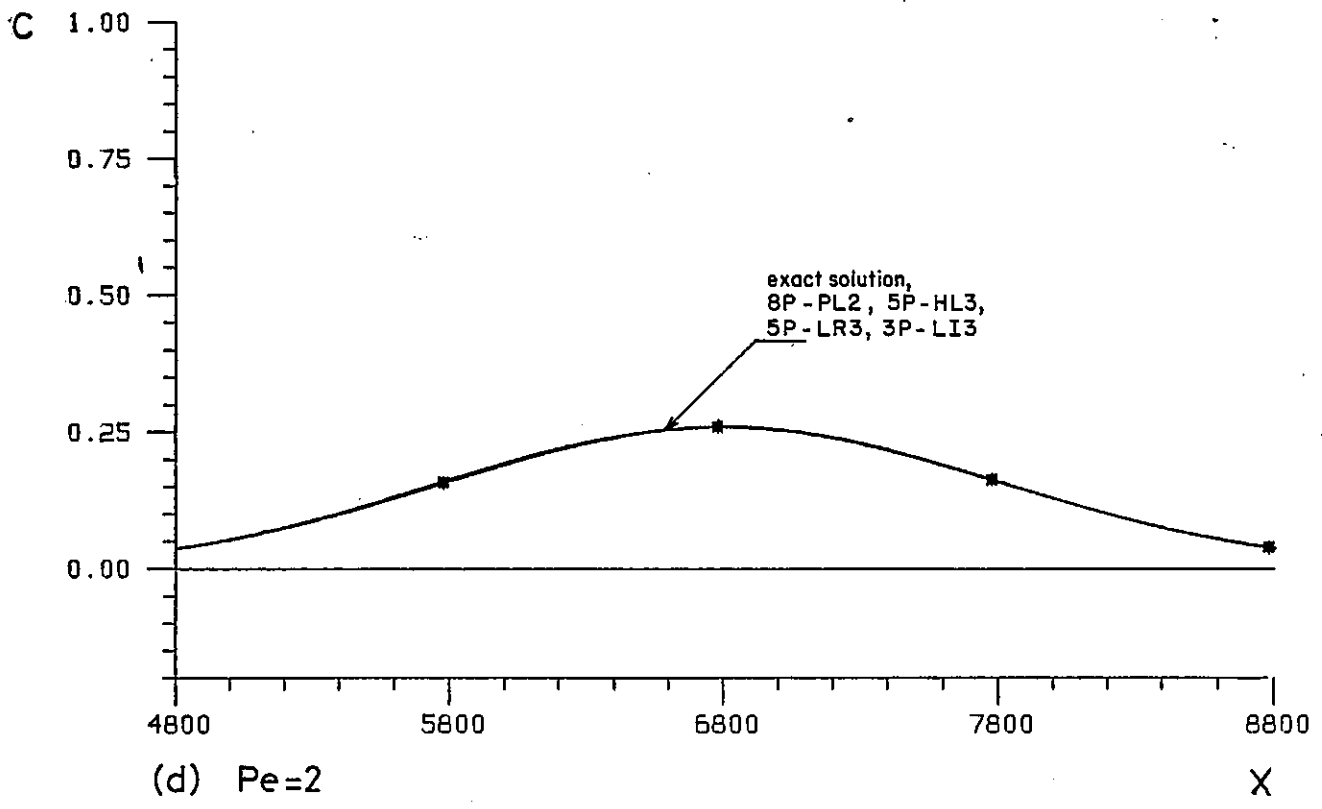
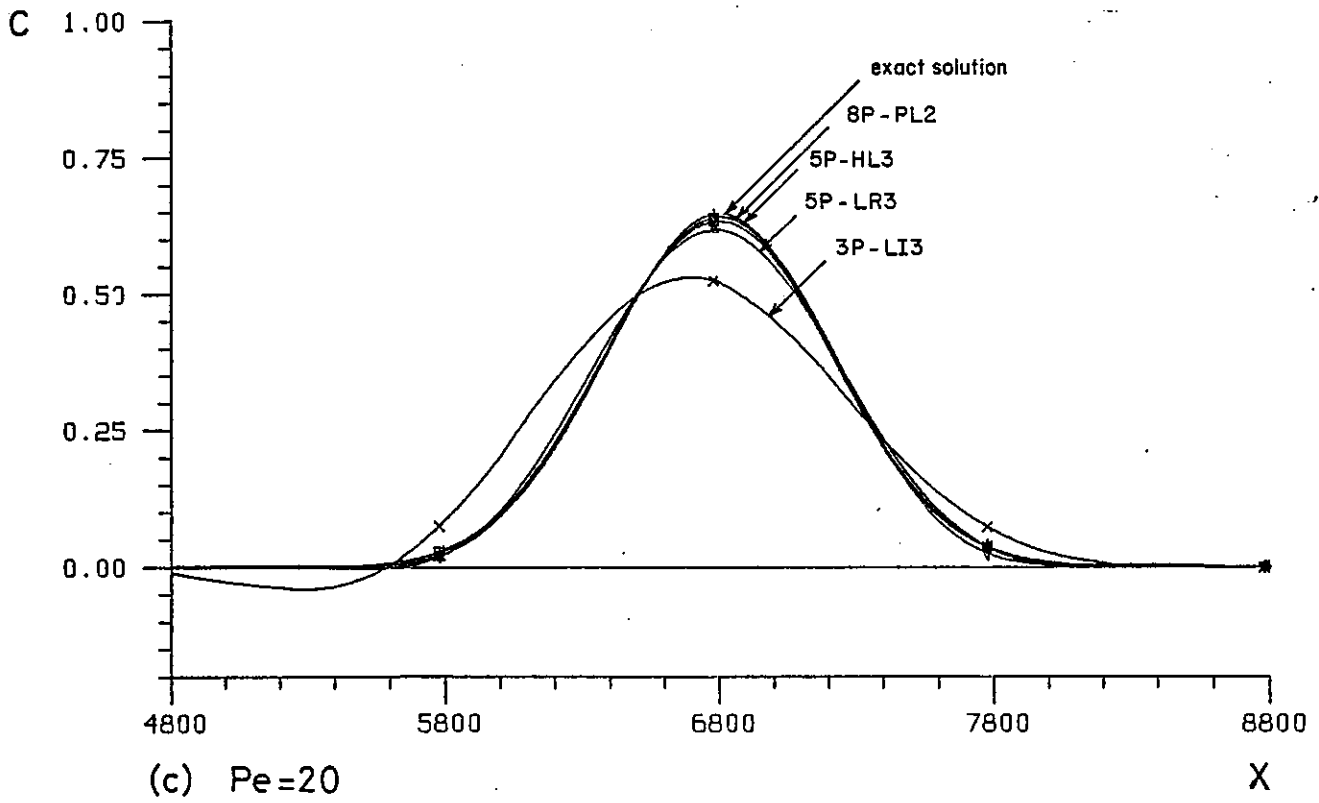


Fig. 5.1. Cont.

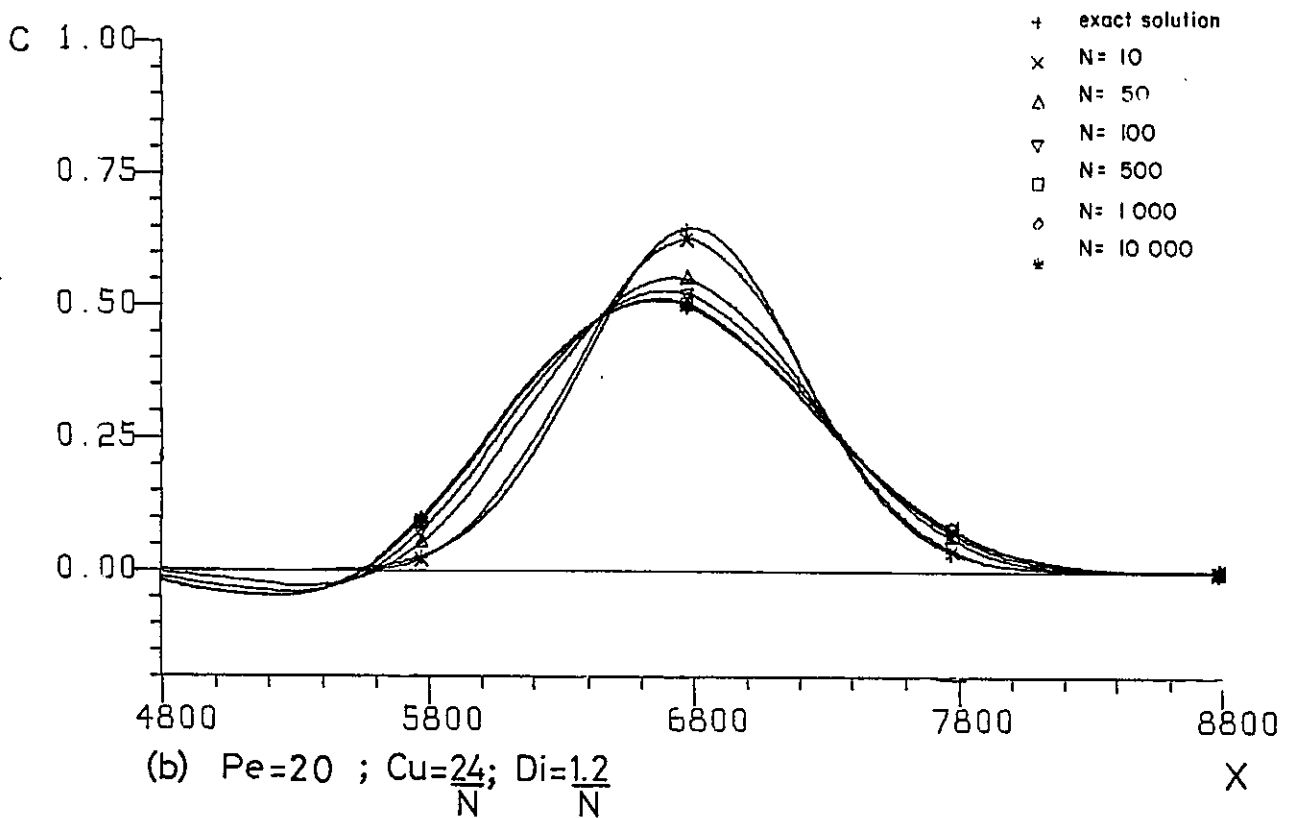
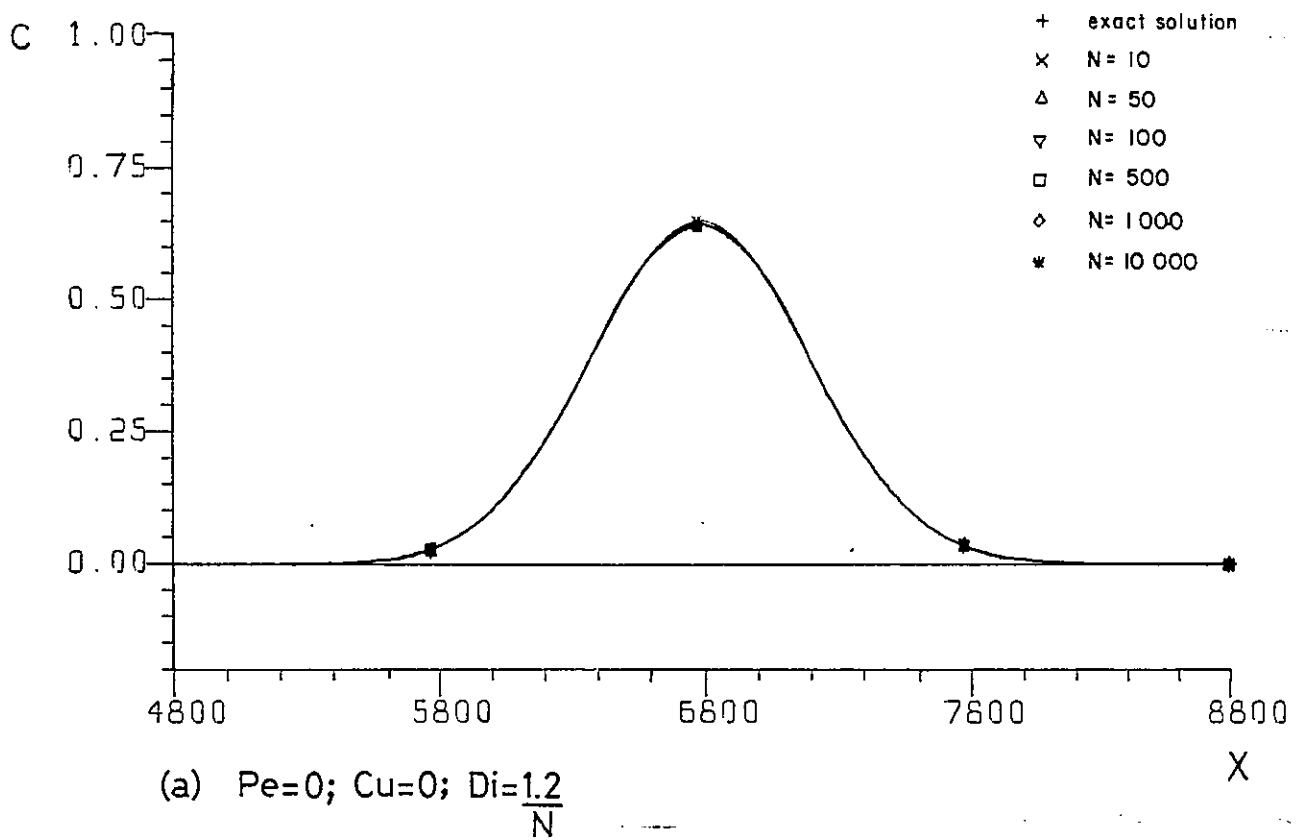


Fig. 5.2. ELM solutions for the transport of a Gauss-hill in a uniform flow, using the 3P-LI3. An illustration of the accuracy dependence on  $N$ , for different  $Pe$ ,  $Cu$ ,  $Di$  ( $\sigma_0/\Delta x=1.32$ ;  $t=T=9600$ )

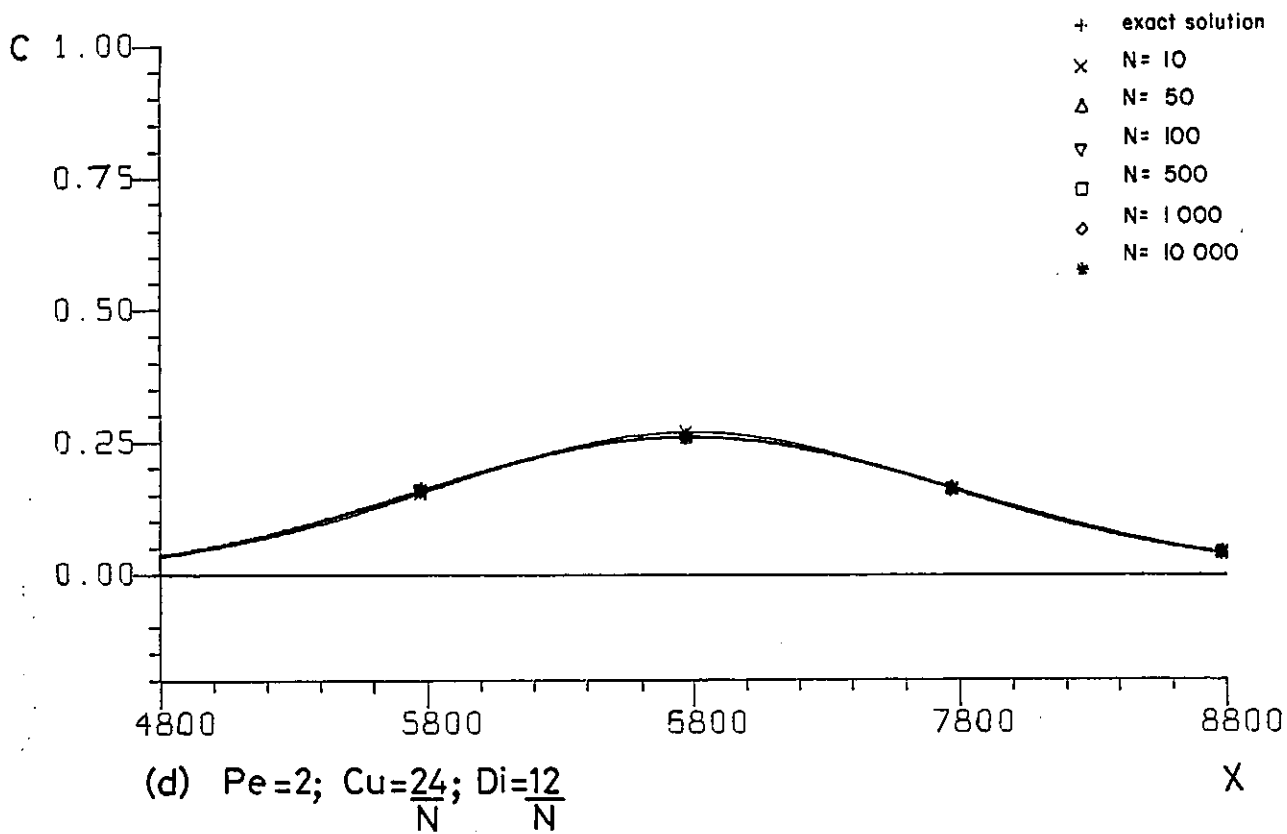
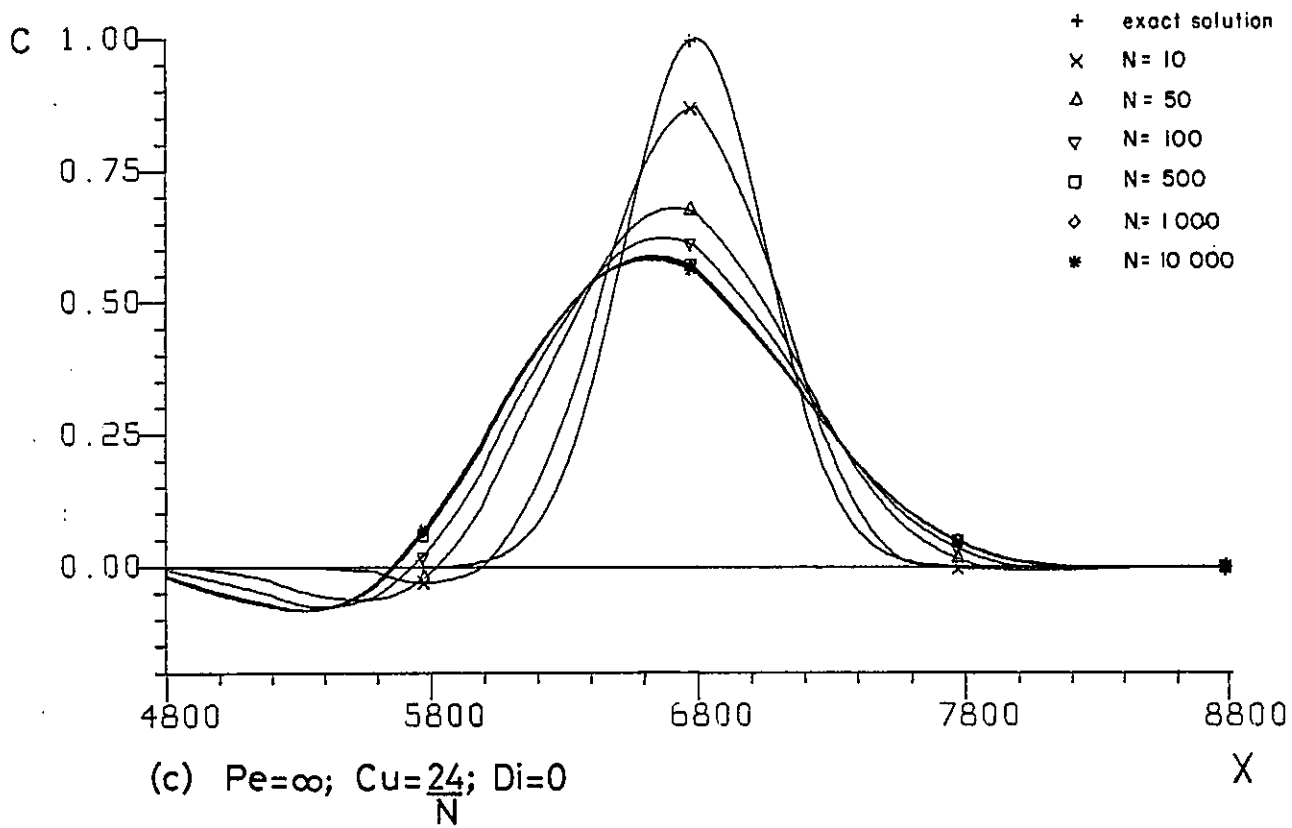


Fig. 5.2. Cont.

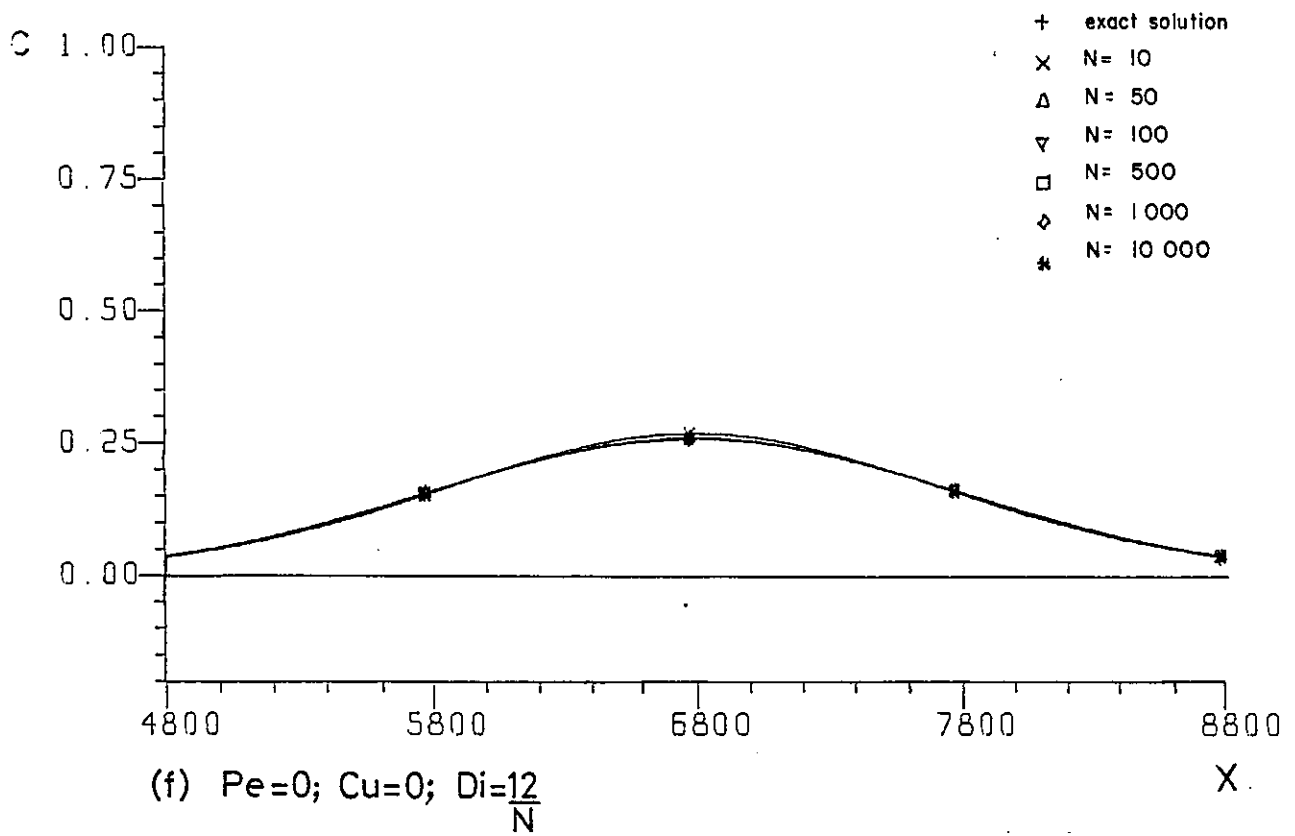
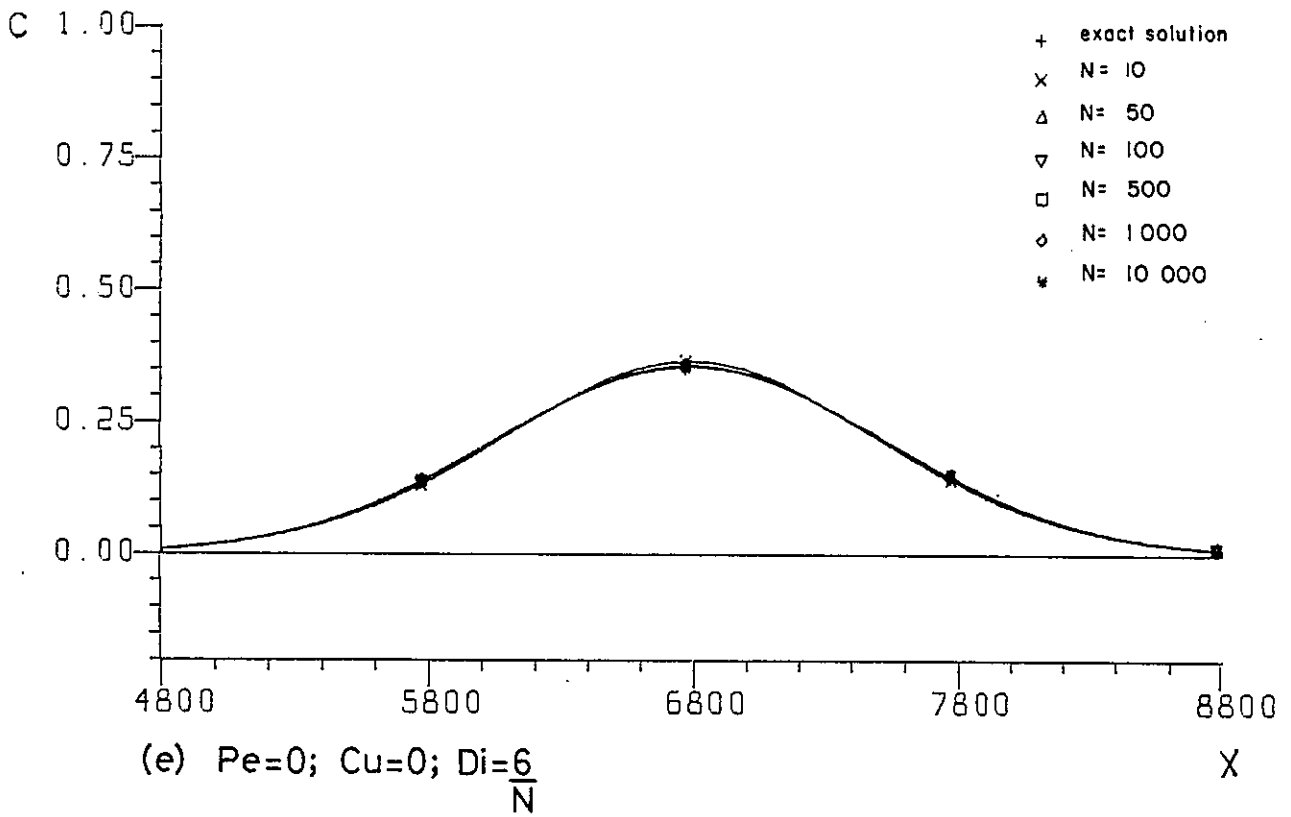


Fig. 5.2. Cont.



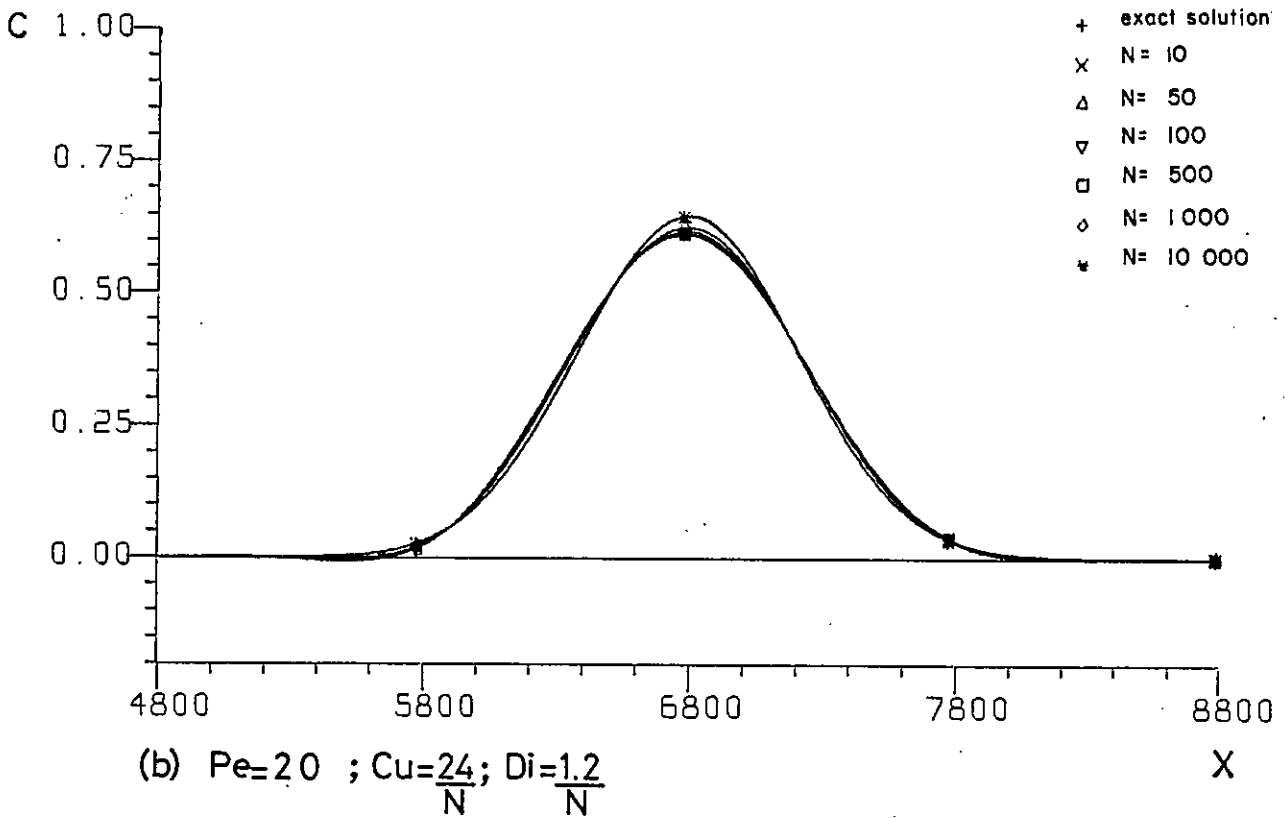
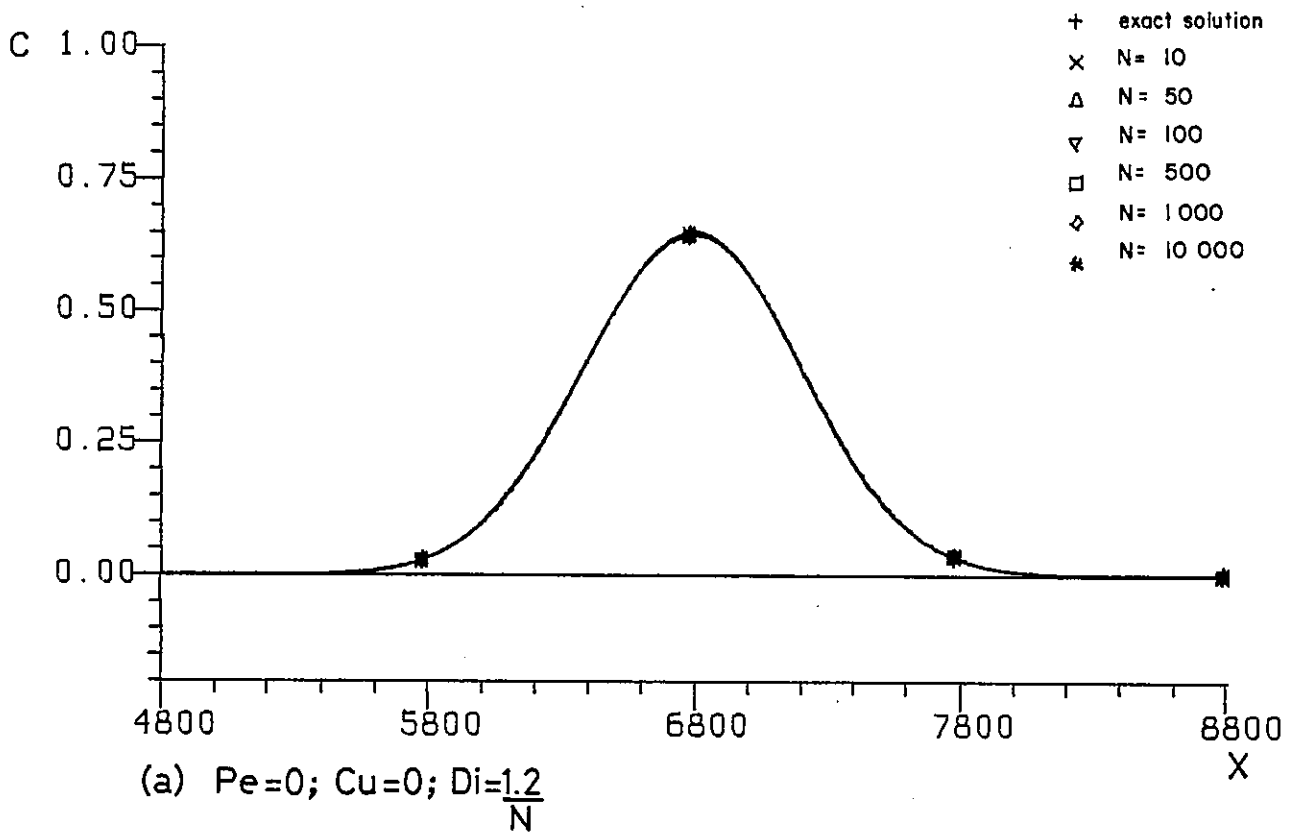


Fig. 5.3. ELM solutions for the transport of a Gauss-hill in a uniform flow, using the 5P-LR3. An illustration of the accuracy dependence on  $N$ , for different  $Pe, Cu, Di$  ( $\sigma_0/\Delta x=1.32; t=T=9600$ )

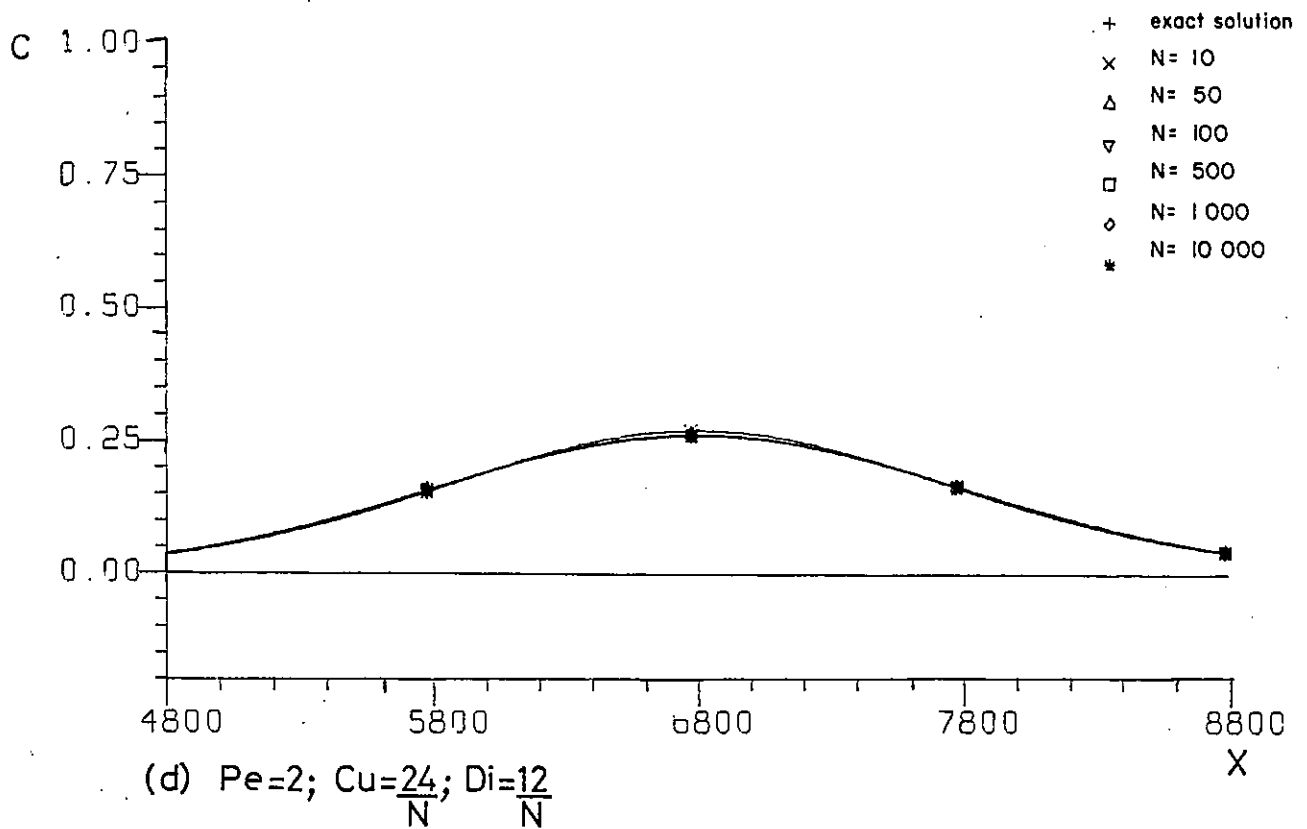
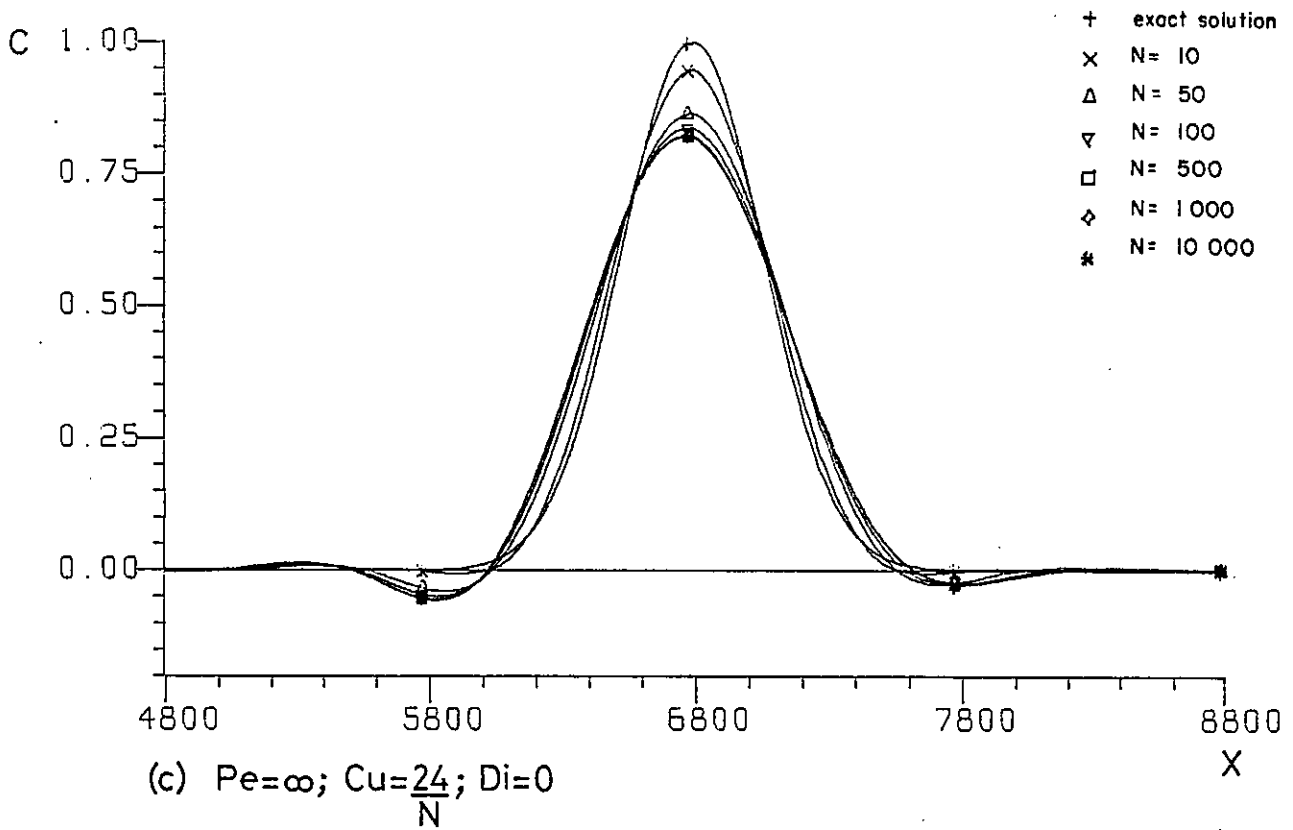


Fig. 5.3. Cont.

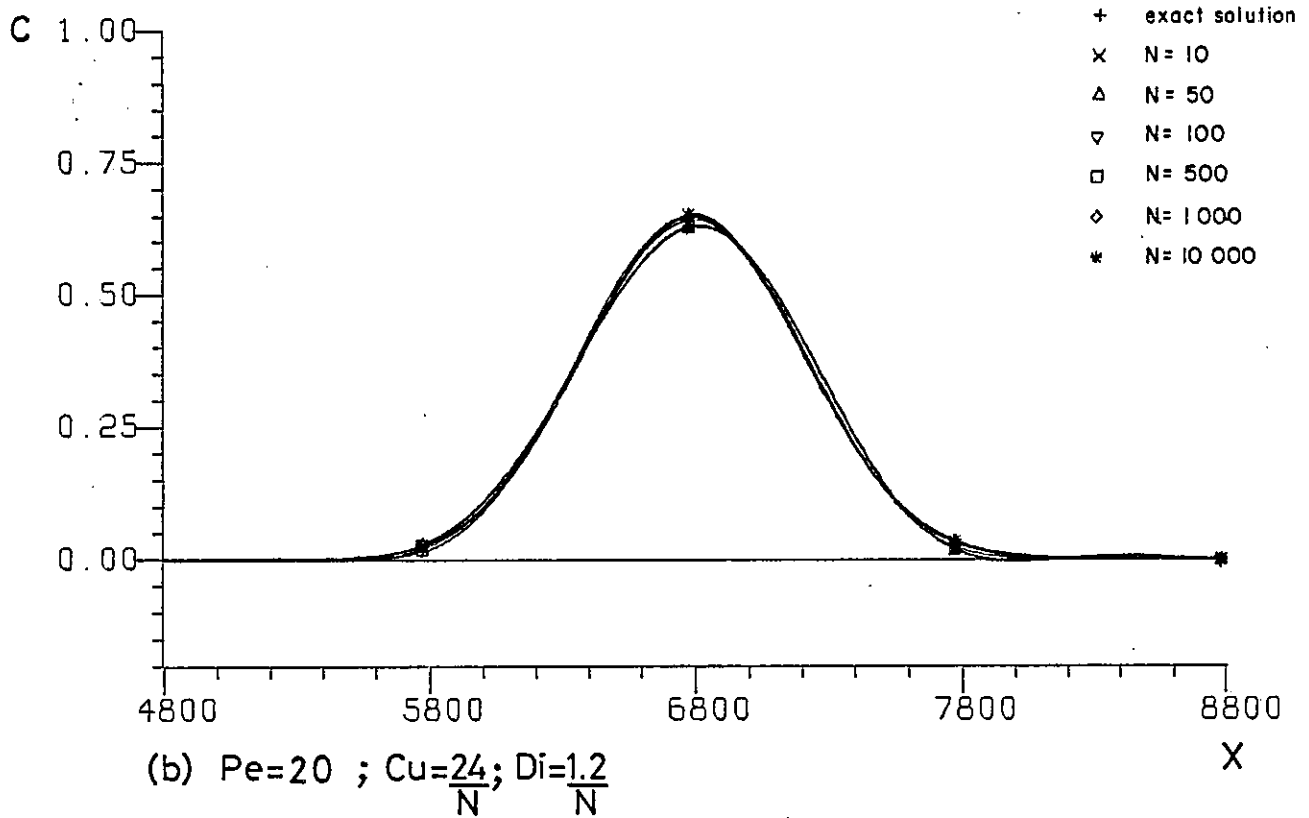
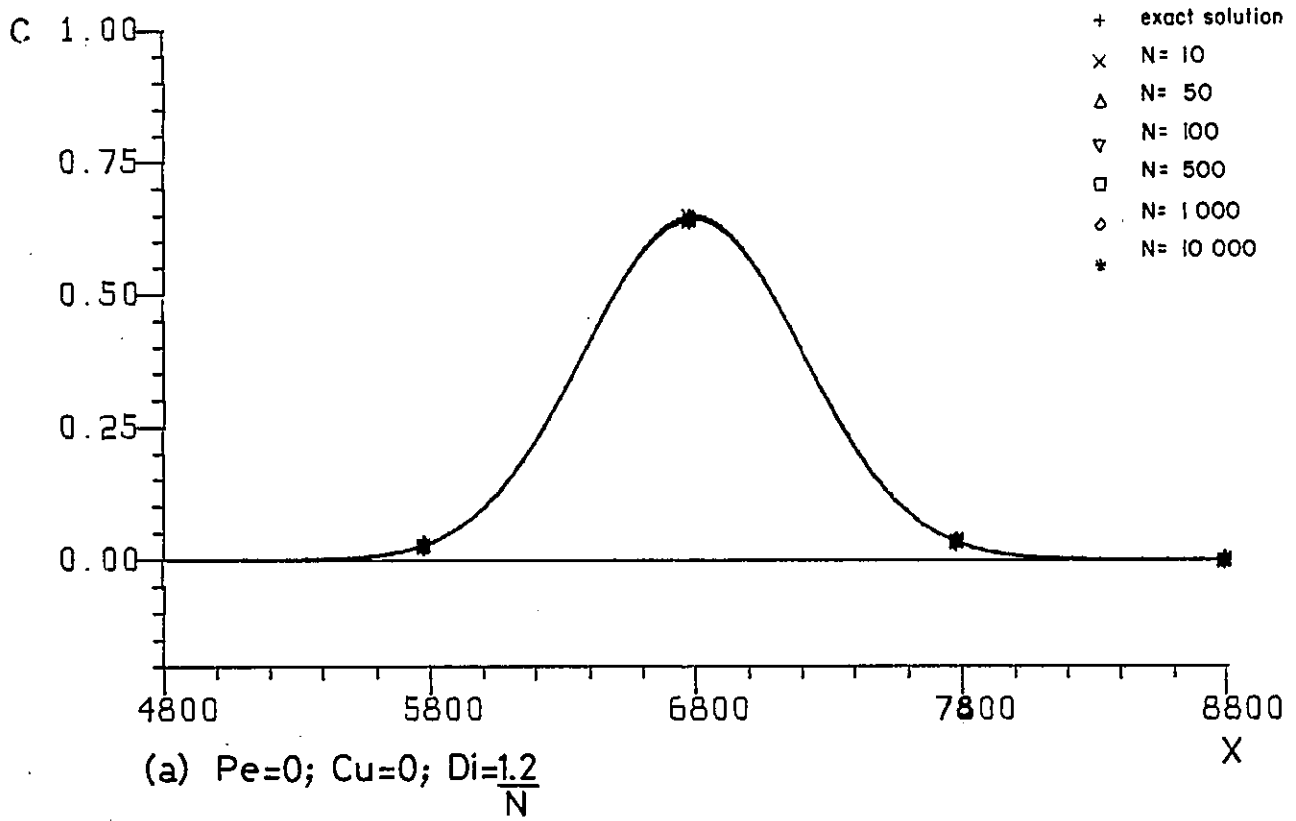


Fig. 5.4. ELM solutions for the transport of a Gauss-hill in a uniform flow, using the SP-HL3. An illustration of the accuracy dependence on  $N$ , for different  $Pe$ ,  $Cu$ ,  $Di$  ( $\sigma_0/\Delta x=1.32$ ;  $t=T=9600$ )

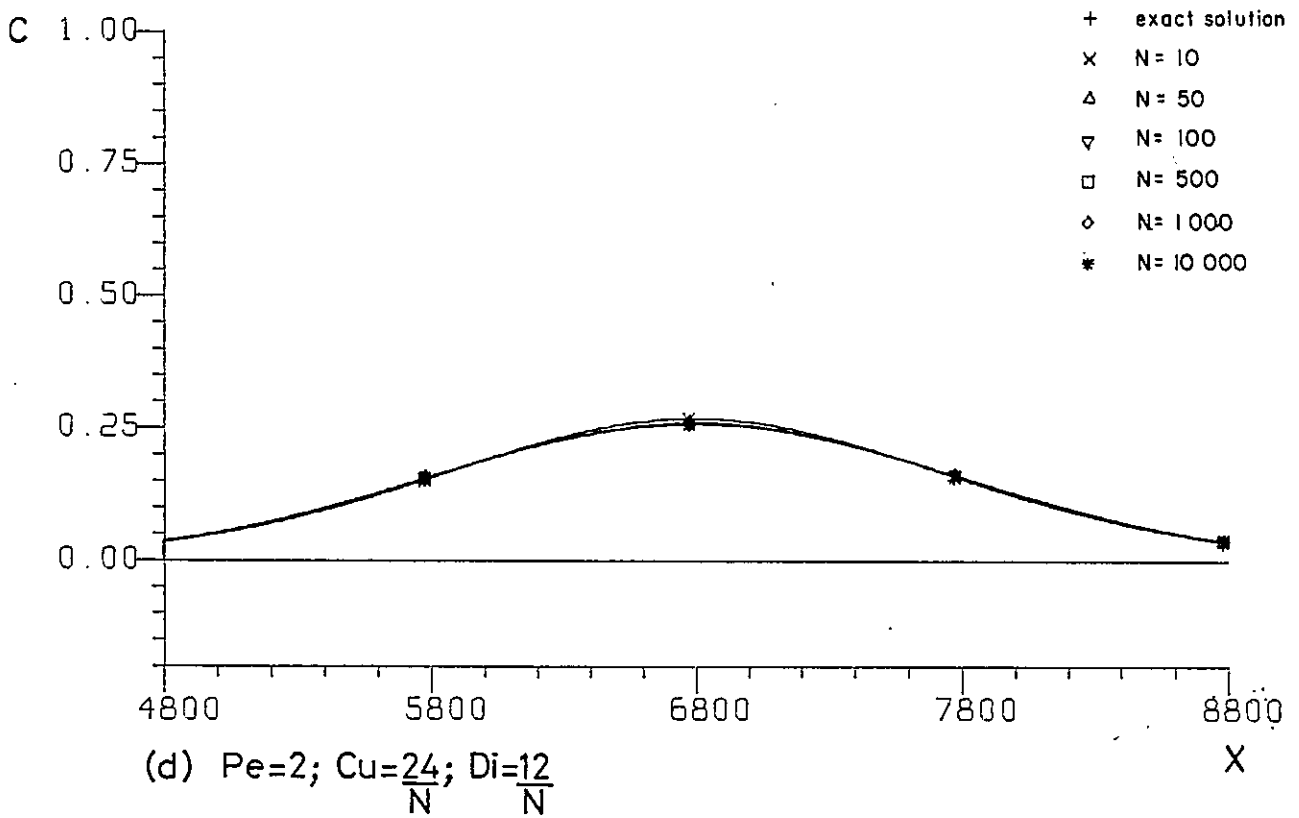
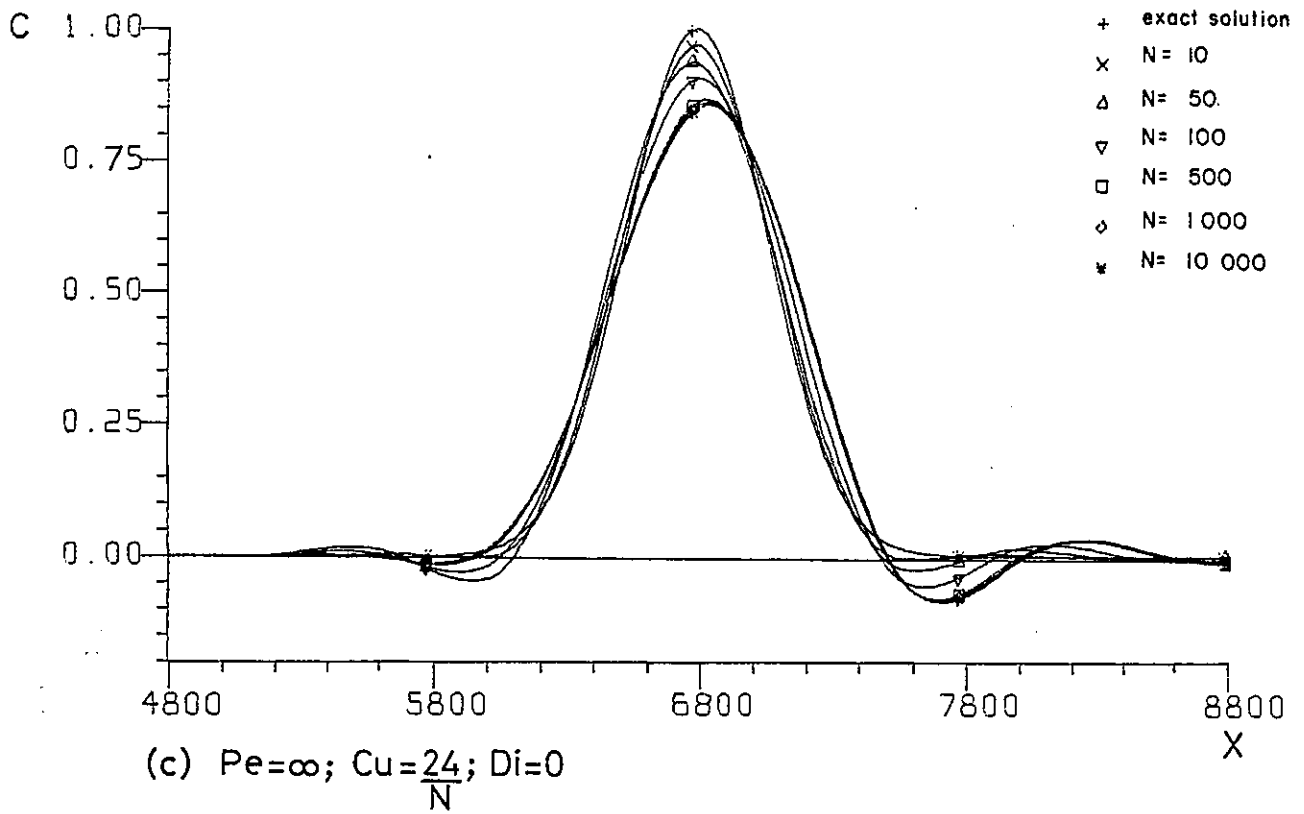


Fig. 5.4. Cont.

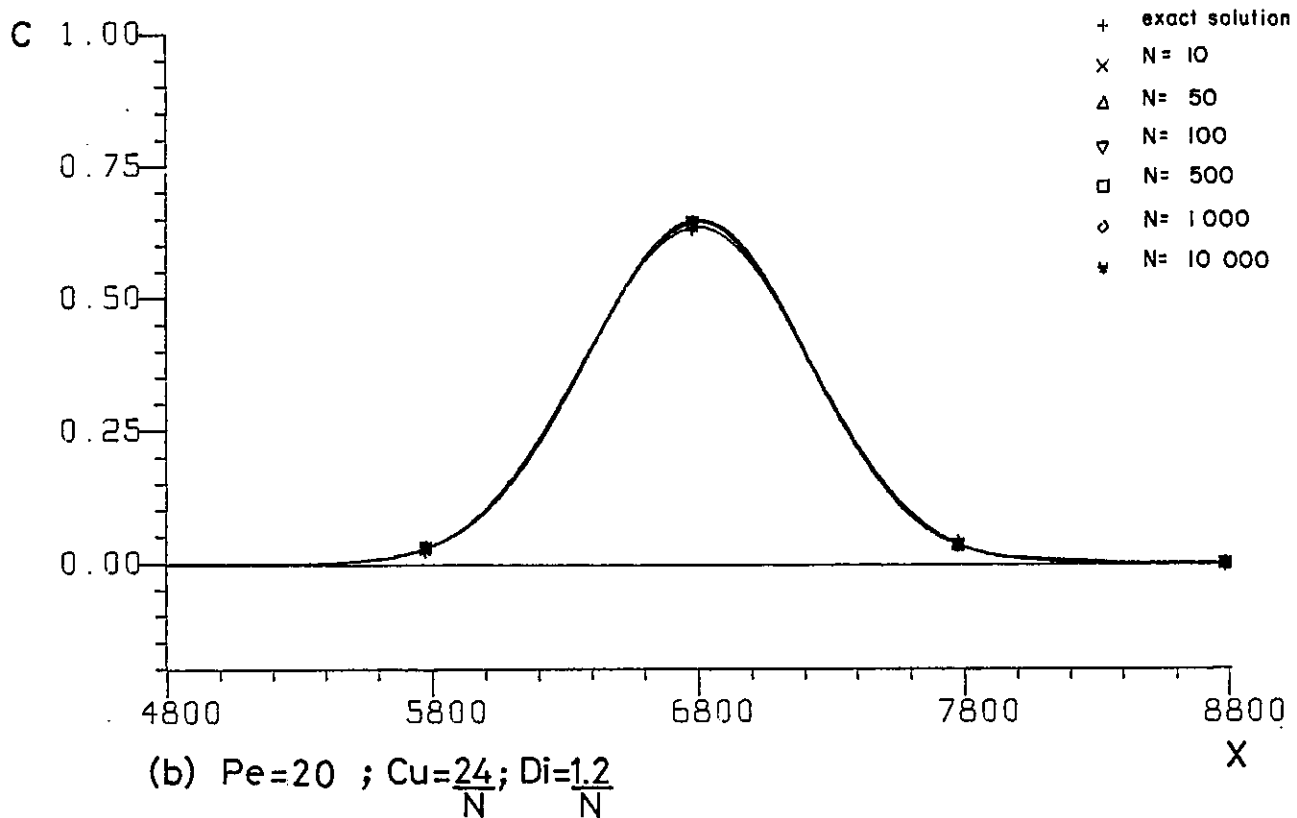
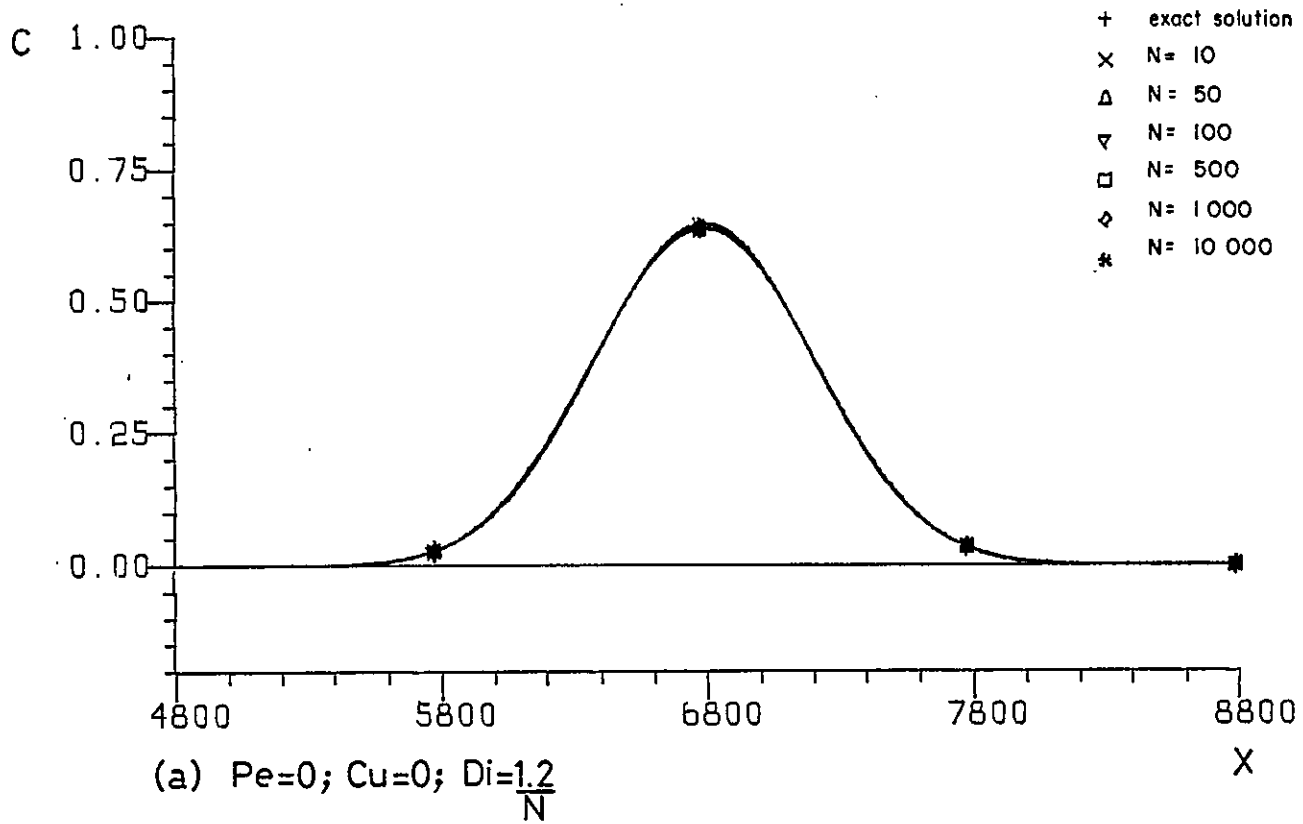


Fig. 5.5. ELM solutions for the transport of a Gauss-hill in a uniform flow, using the 8P-PL2. An illustration of the accuracy dependence on  $N$ , for different  $Pe$ ,  $Cu$ ,  $Di$  ( $\sigma_0/\Delta x=1.32$ ;  $t=T=9600$ )

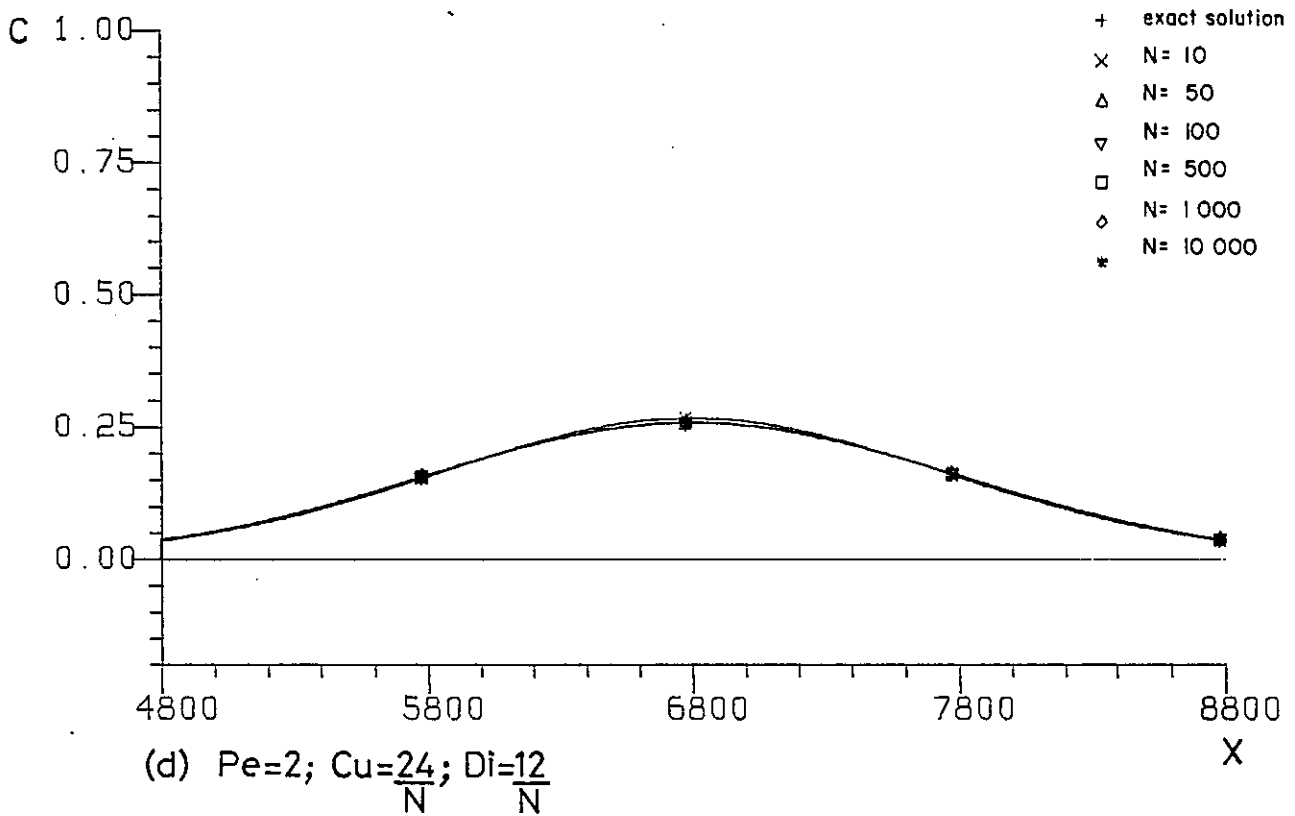
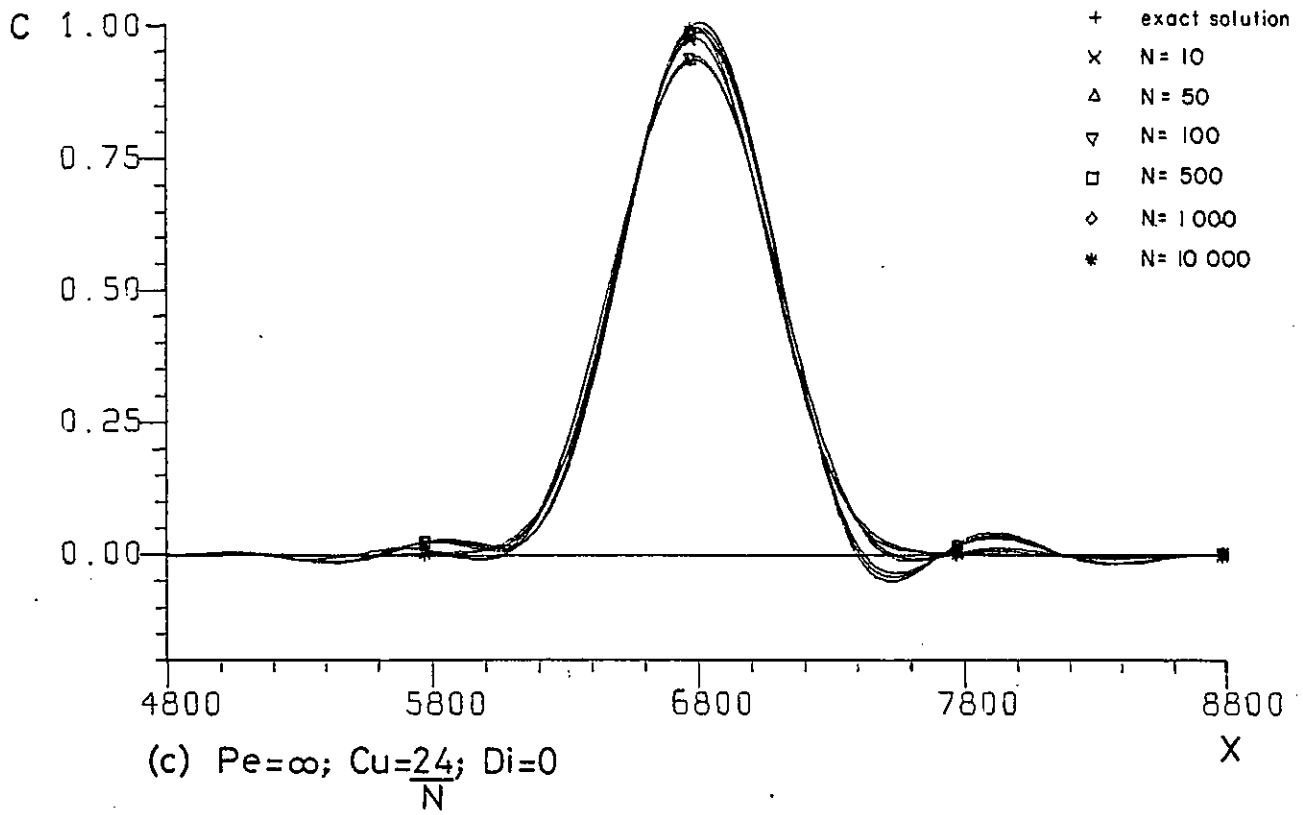


Fig. 5.5. Cont.

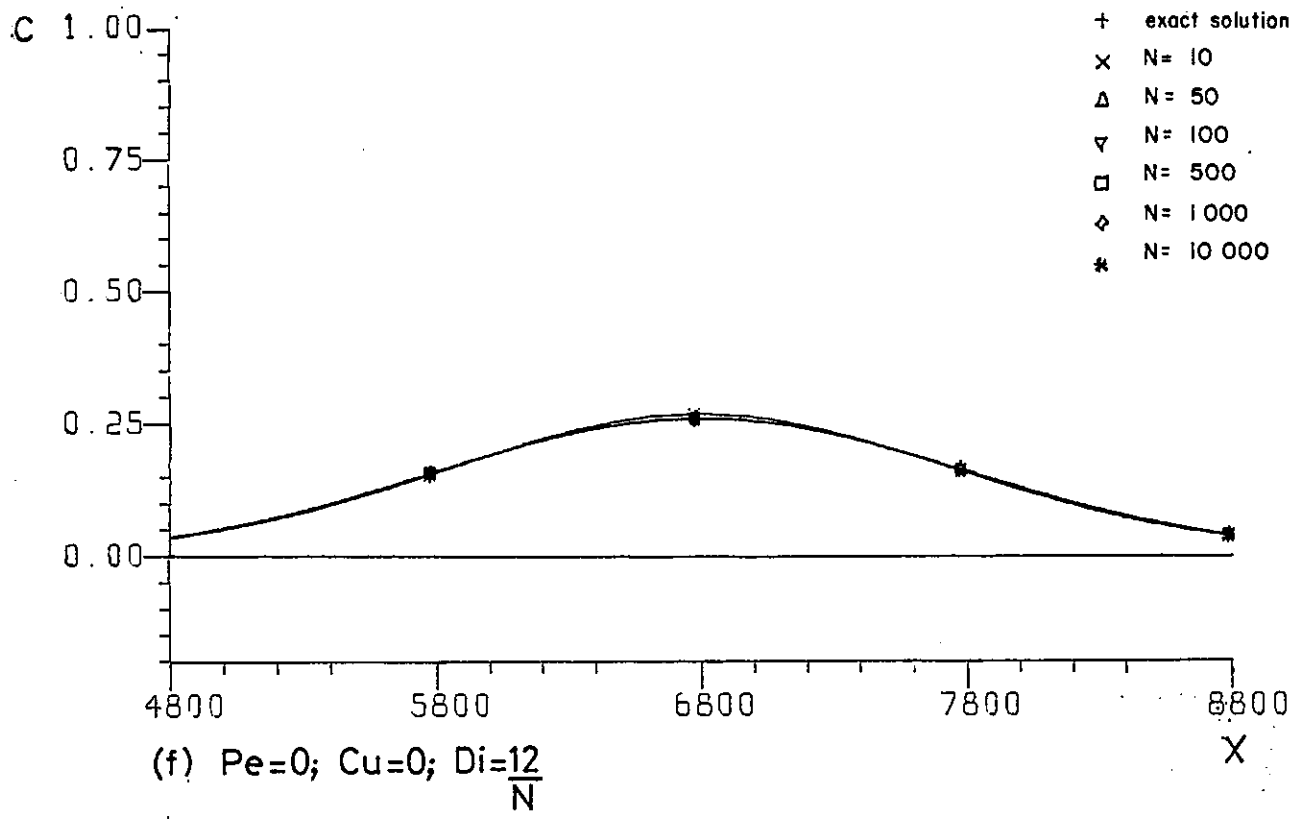
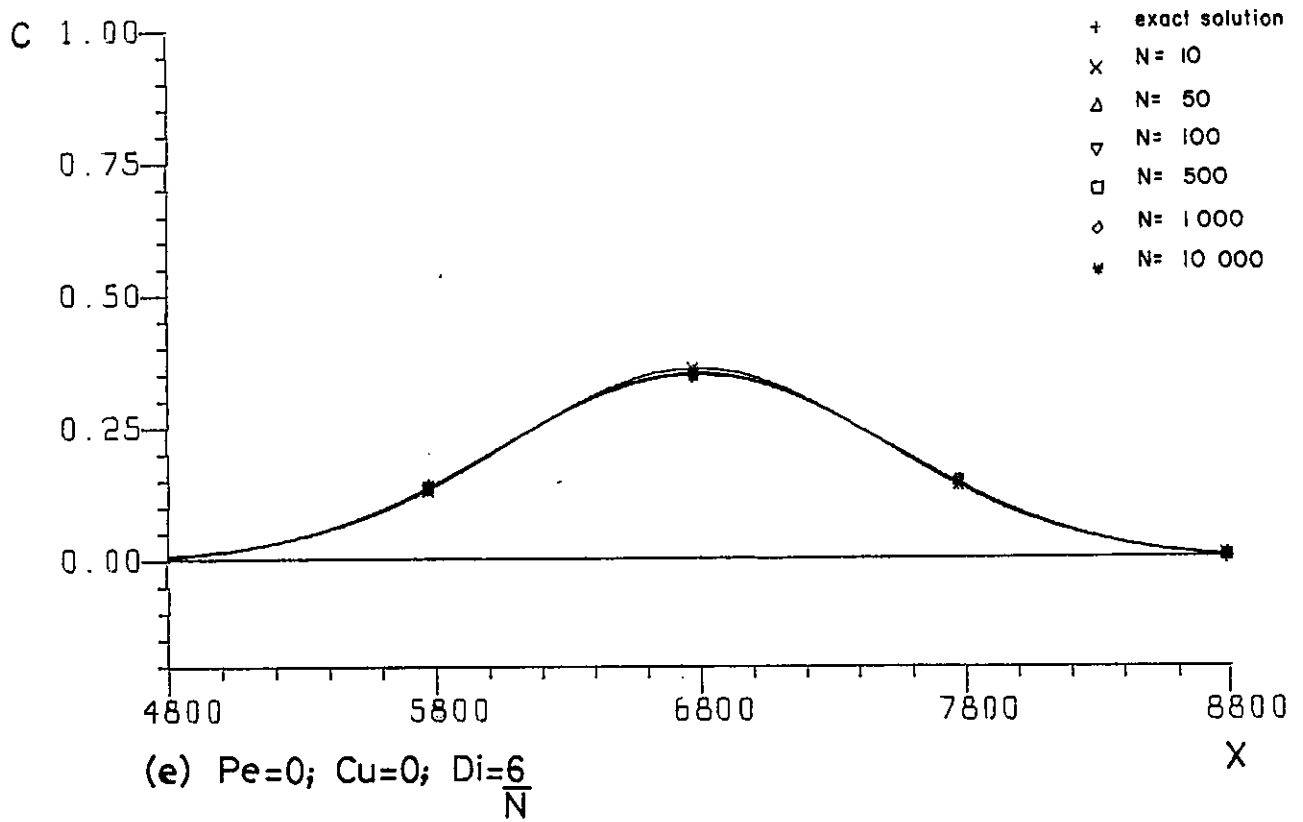


Fig. 5.5. Cont.

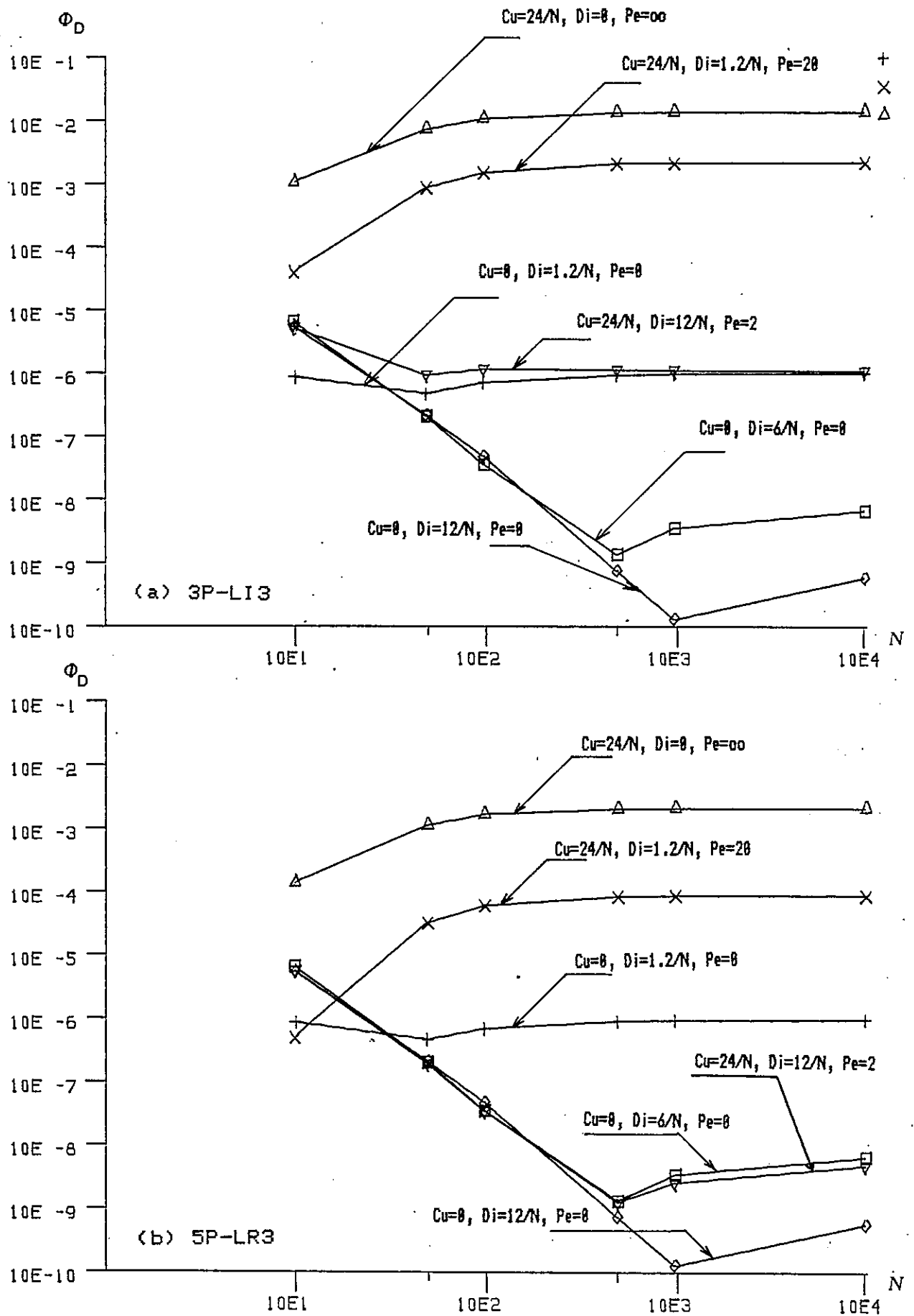


Fig. 5.6. Mean square error as a function of the number of time steps required to reach a fixed total time ( $\sigma_0/\Delta x=1.32$ ;  $t=T=9600$ )



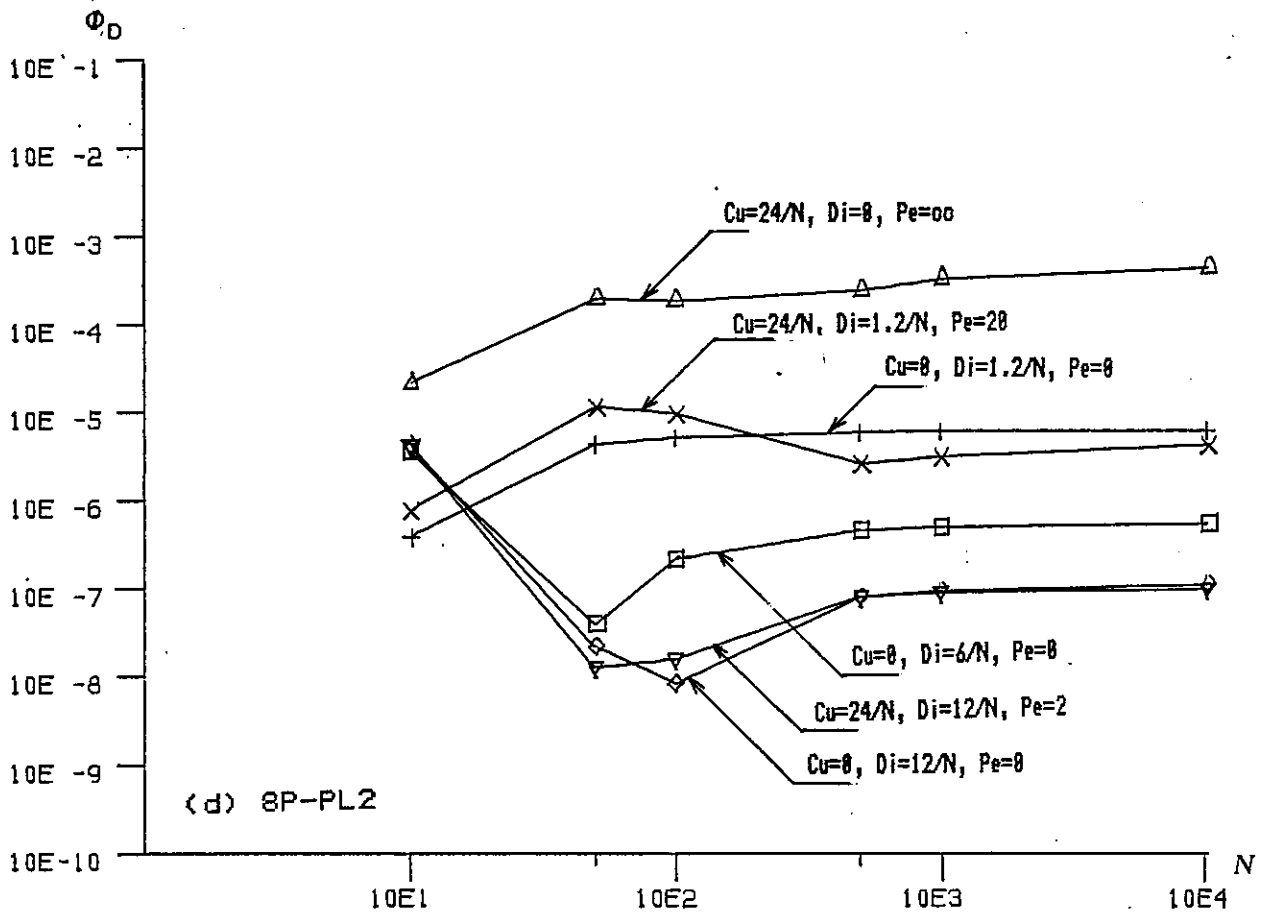
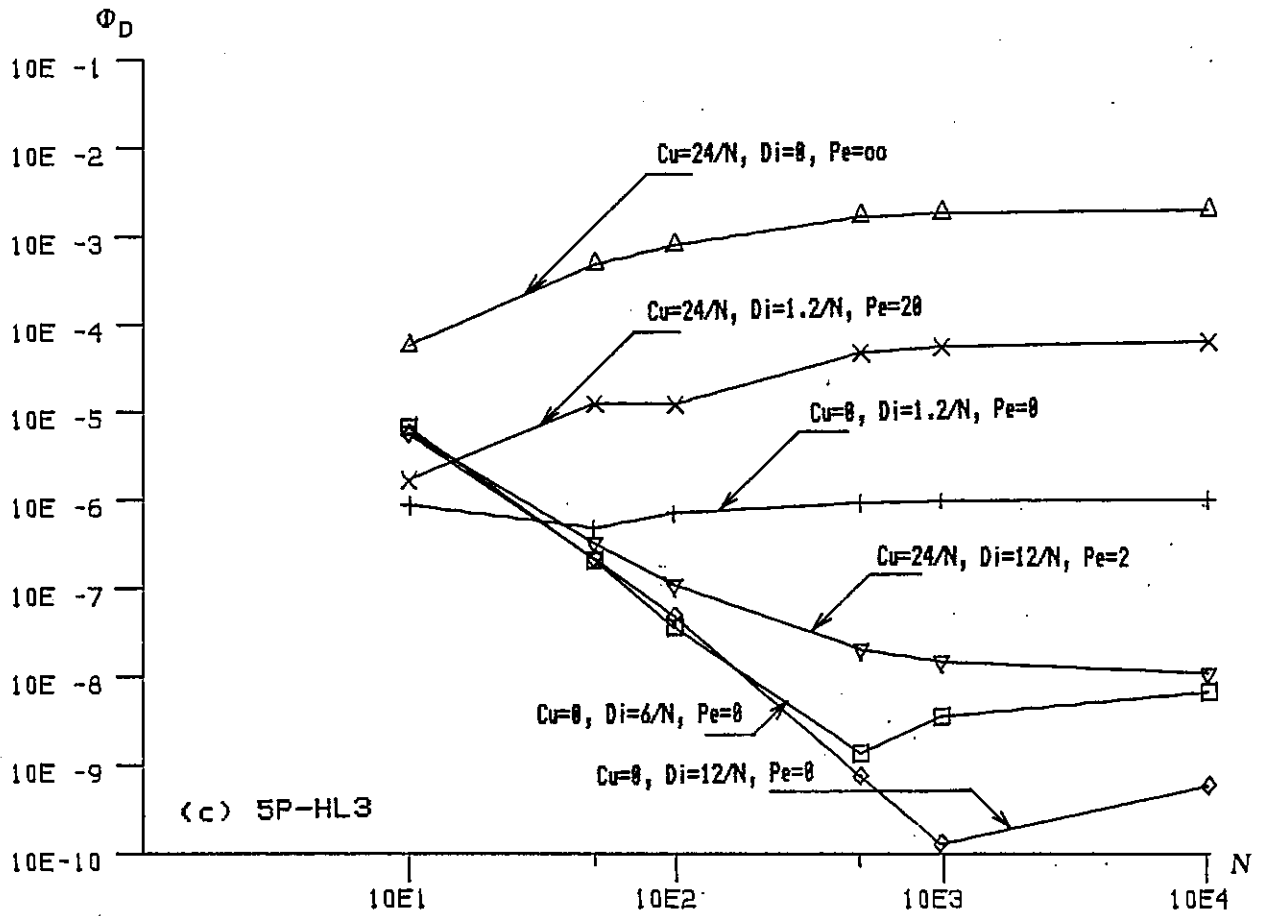


Fig. 5.6. Cont.

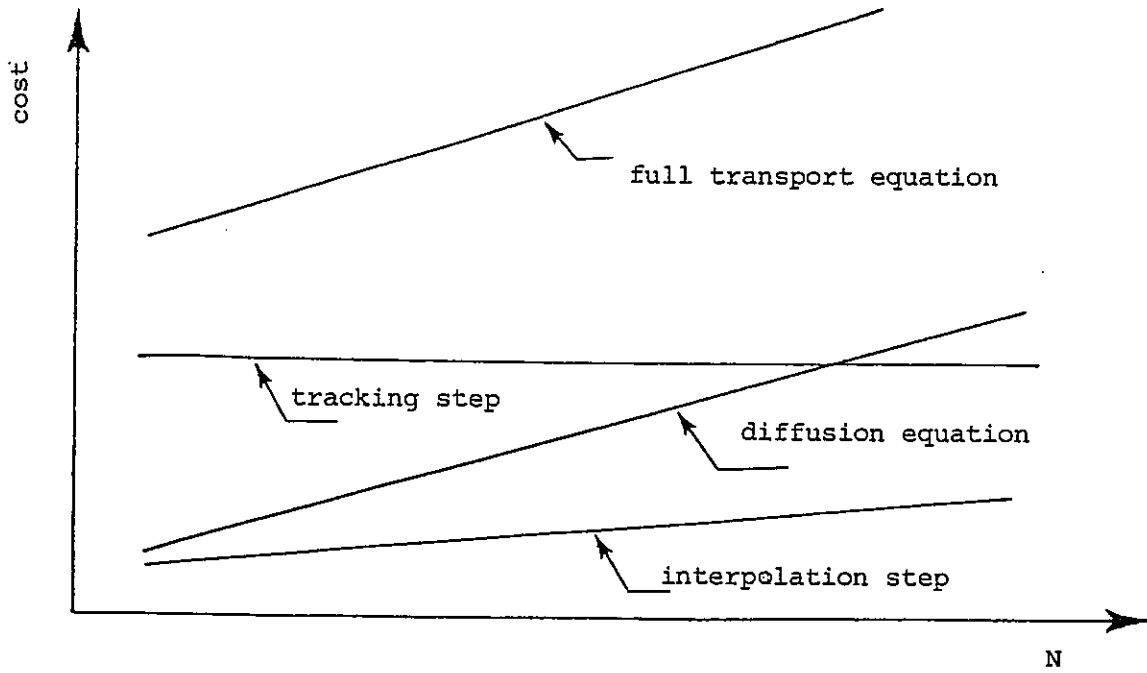


Fig. 5.7. Qualitative cost function for the reference ELM

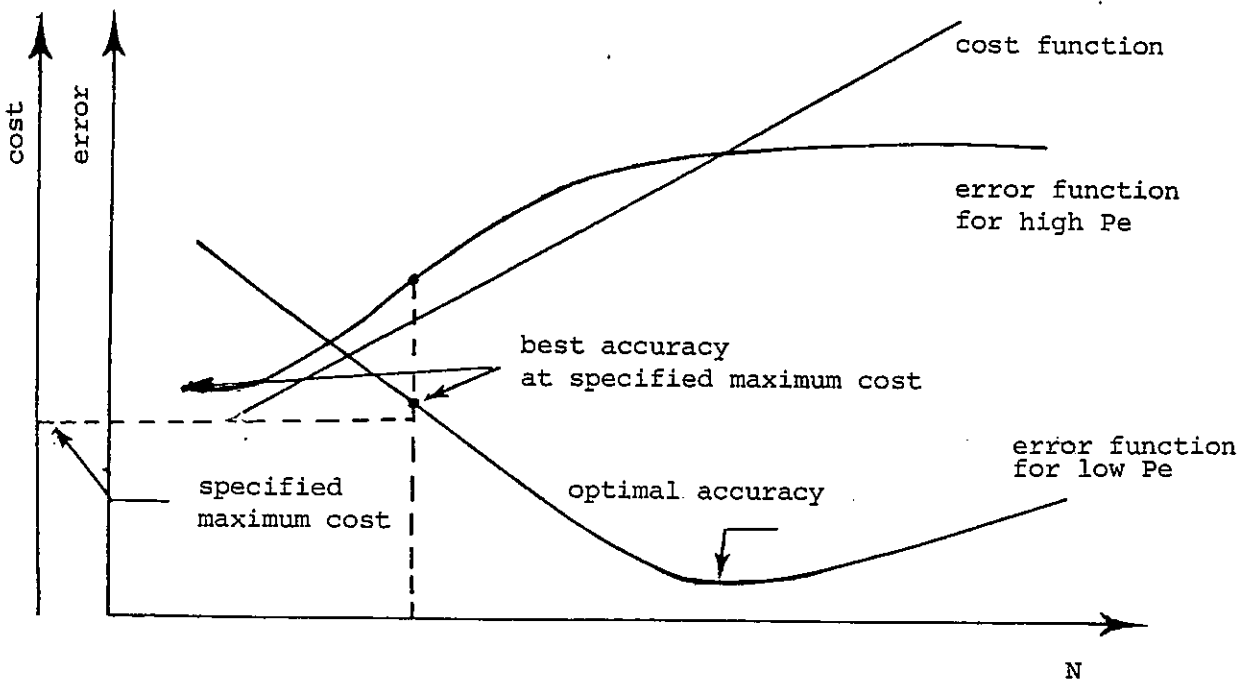


Fig. 5.8. Qualitative cost and accuracy functions, for the reference ELM

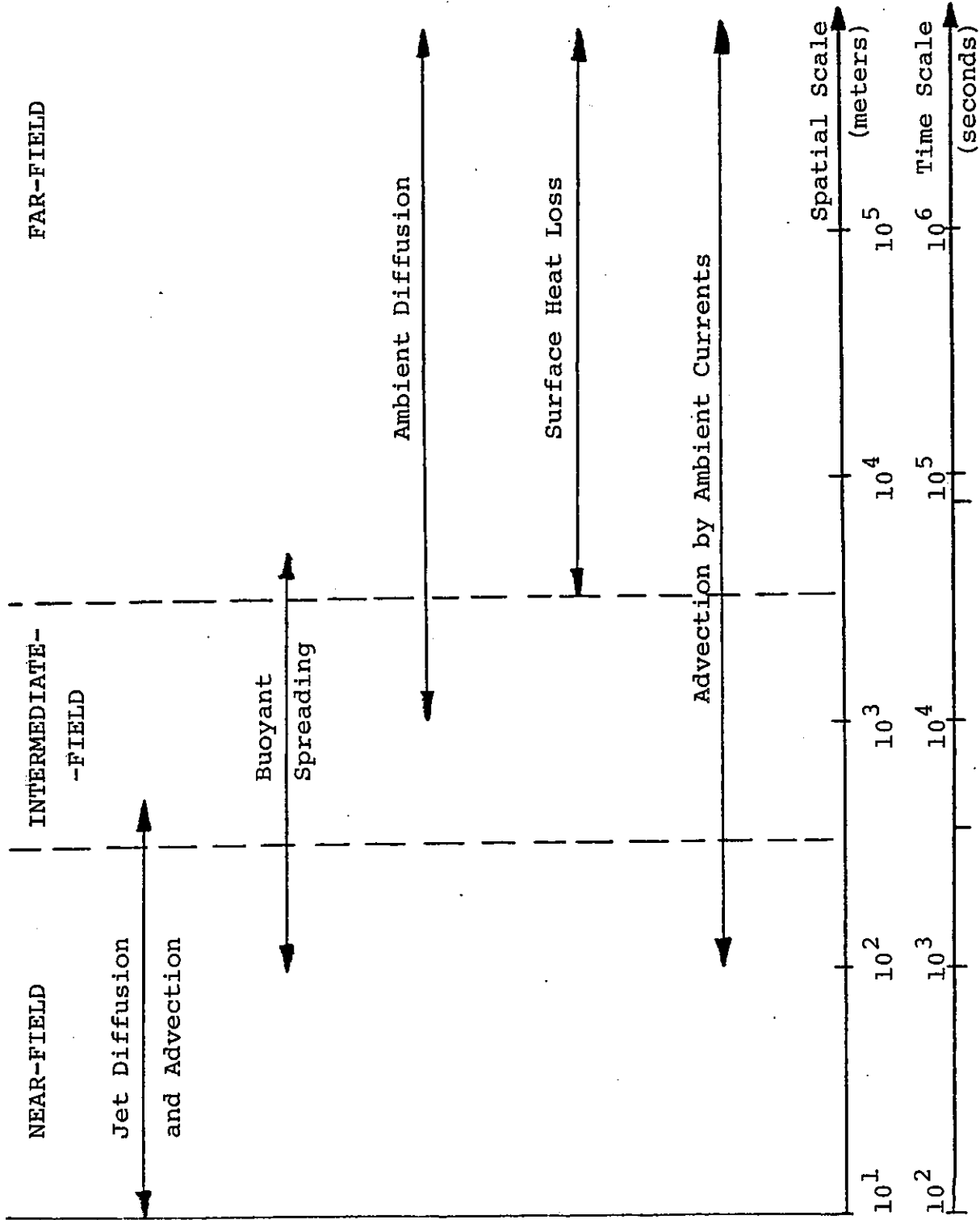


Fig. 6.1. Heat dispersion in the water environment. Identification of zones of analysis and of transport processes

[from ADAMS et al., 1981]

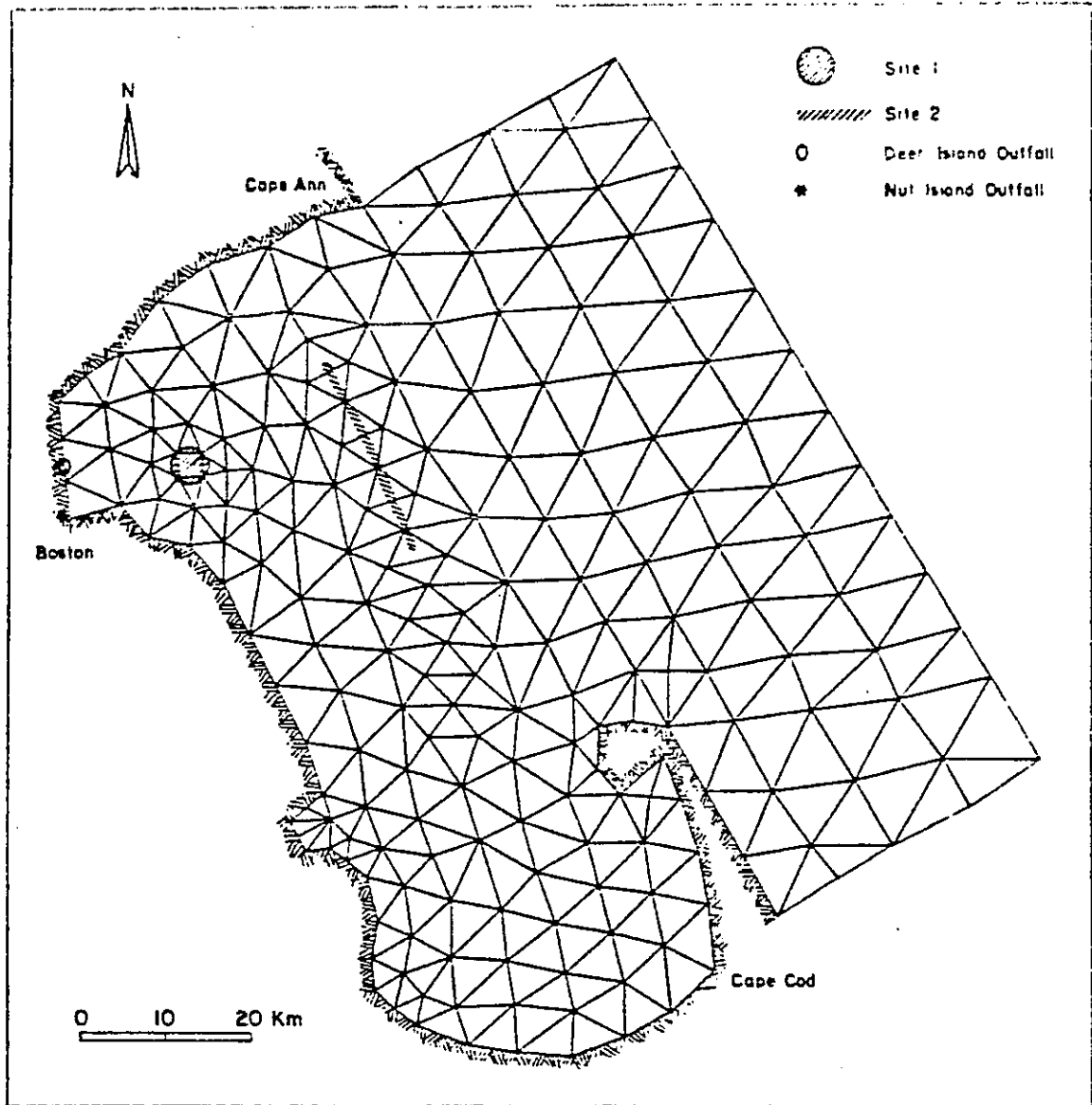


Fig. 6.2. Massachusetts Bay. Finite element grid

[from BAPTISTA 1984]

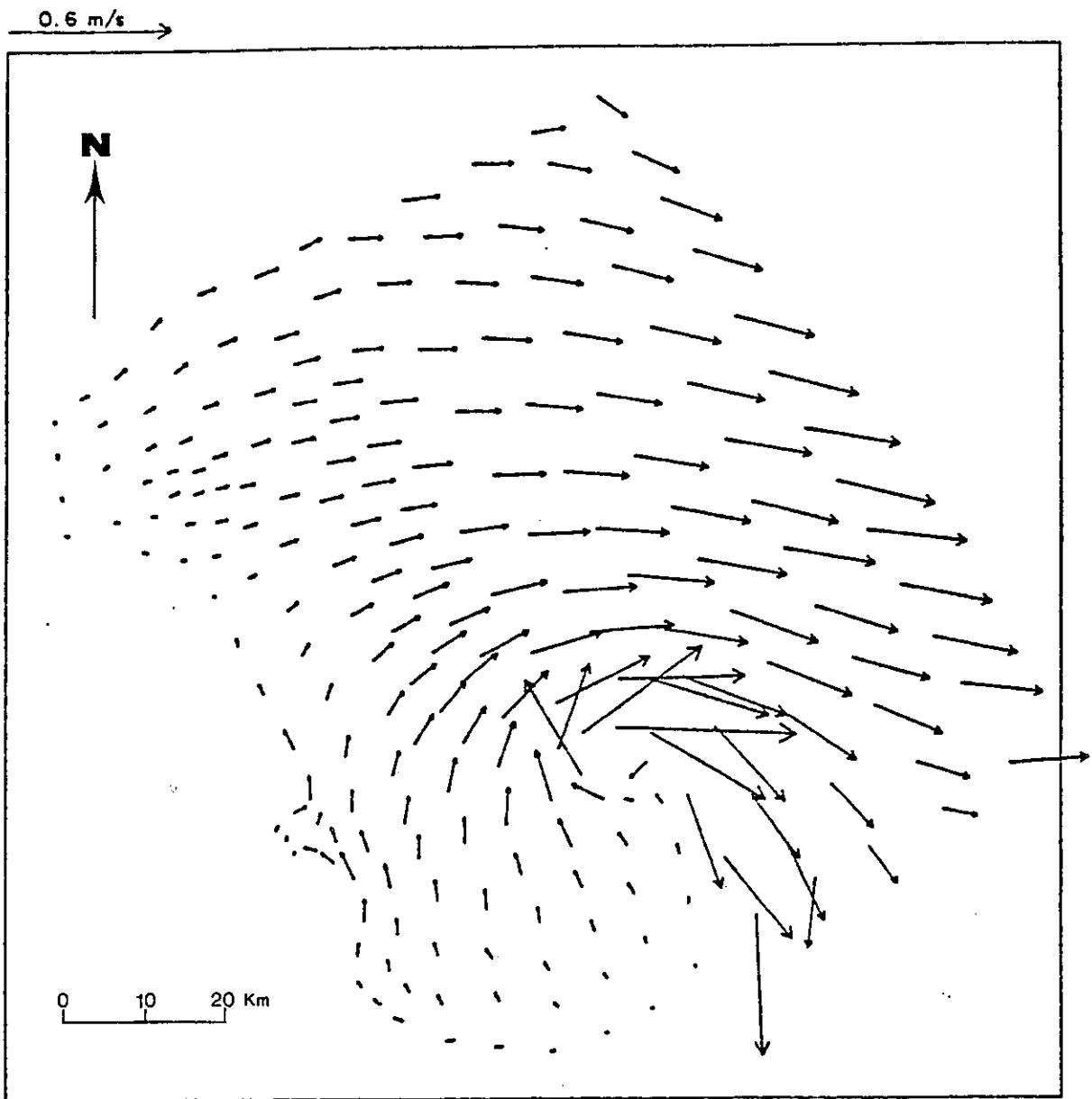


Fig. 6.3. Massachusetts Bay. Flow field at maximum ebb

[from BAPTISTA, 1984]

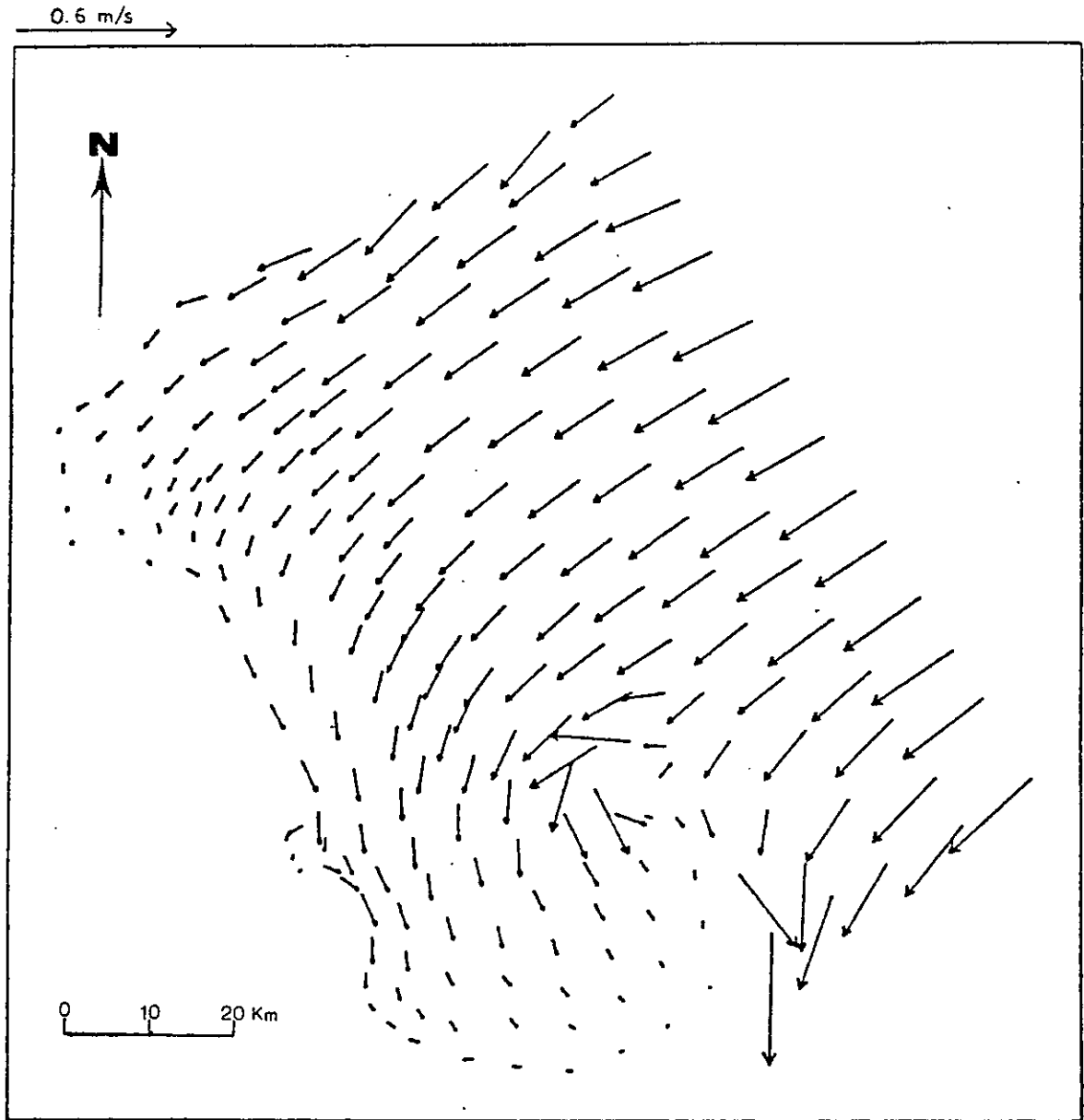
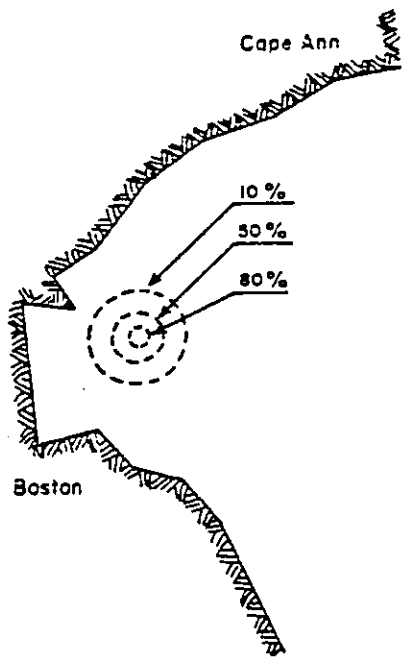
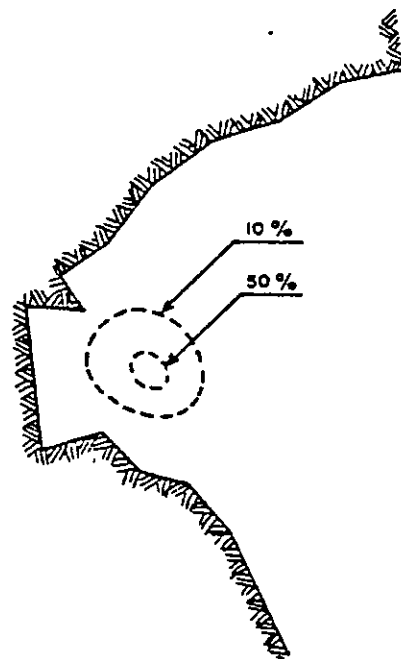


Fig. 6.4. Massachusetts Bay. Flow field at maximum flood

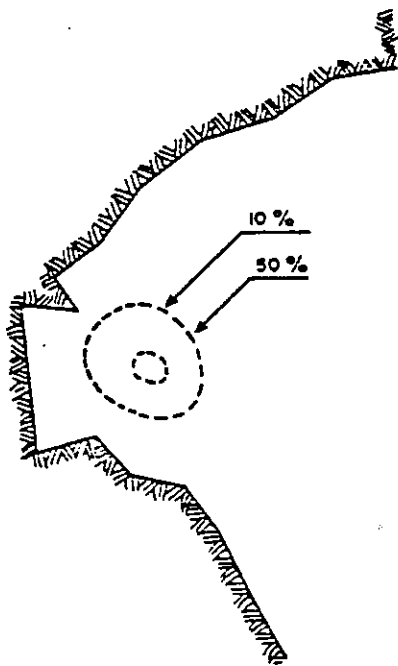
[from BAPTISTA 1984]



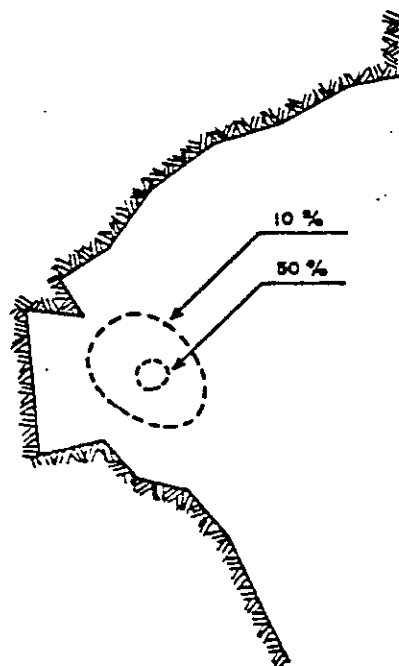
(a) Instant of discharge



(b) After 62 hours



(c) After 68 hours



(d) After 75 hours

Fig. 6.5. Massachusetts Bay. Sludge plumes for dumping at Site 1

[from BAPTISTA 1984]

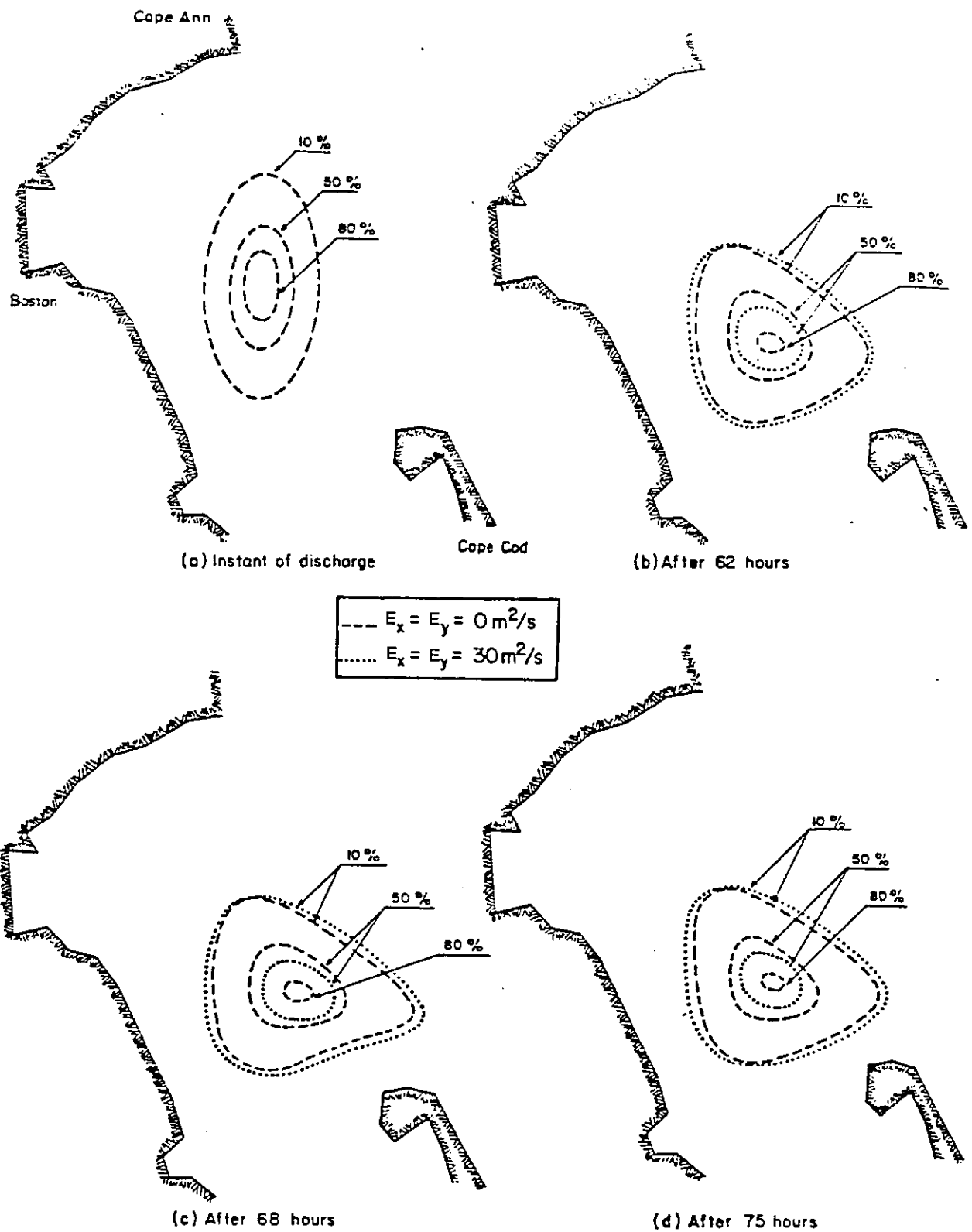


Fig. 6.6. Massachusetts Bay. Sludge plumes for dumping at Site 2

[from BAPTISTA 1984]



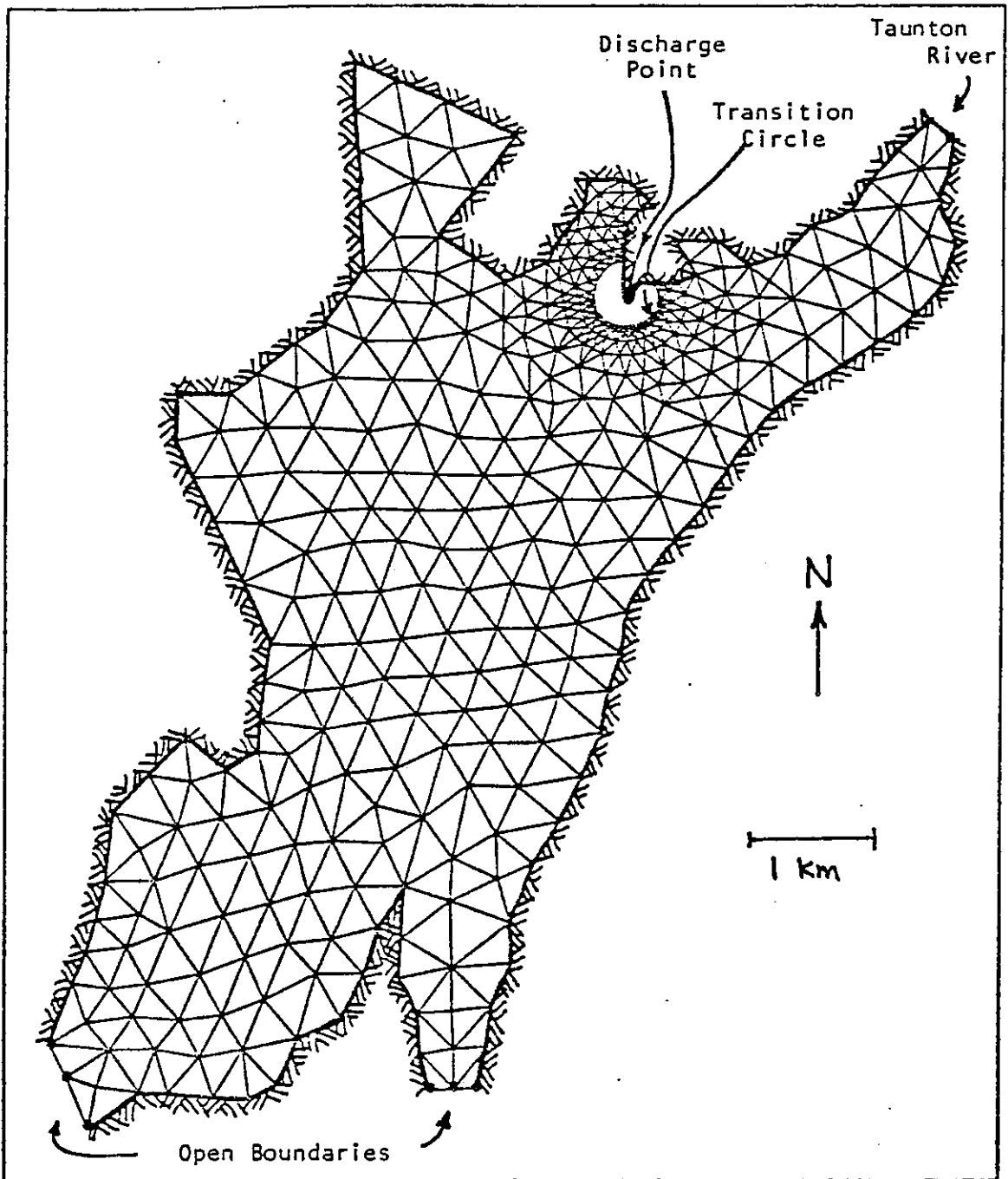
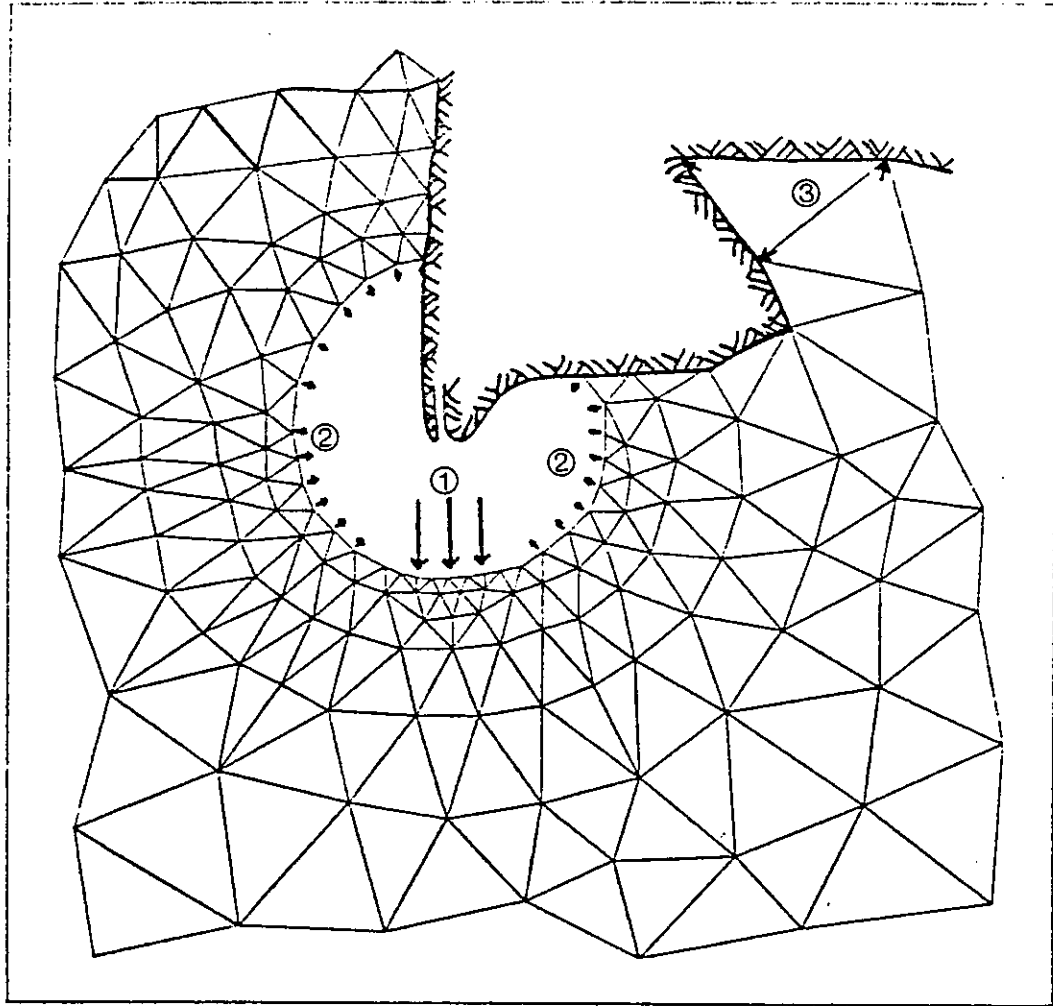


Fig. 6.7. Brayton Point. Complete finite element grid for Mt. Hope Bay  
[from BAPTISTA et al. 1984]



- ① discharge flow corrected by near field dilution
- ② reentrainment
- ③ intake

Fig. 6.8. Brayton Point. Detail of the finite element grid near the discharge

[from BAPTISTA et al. 1984]

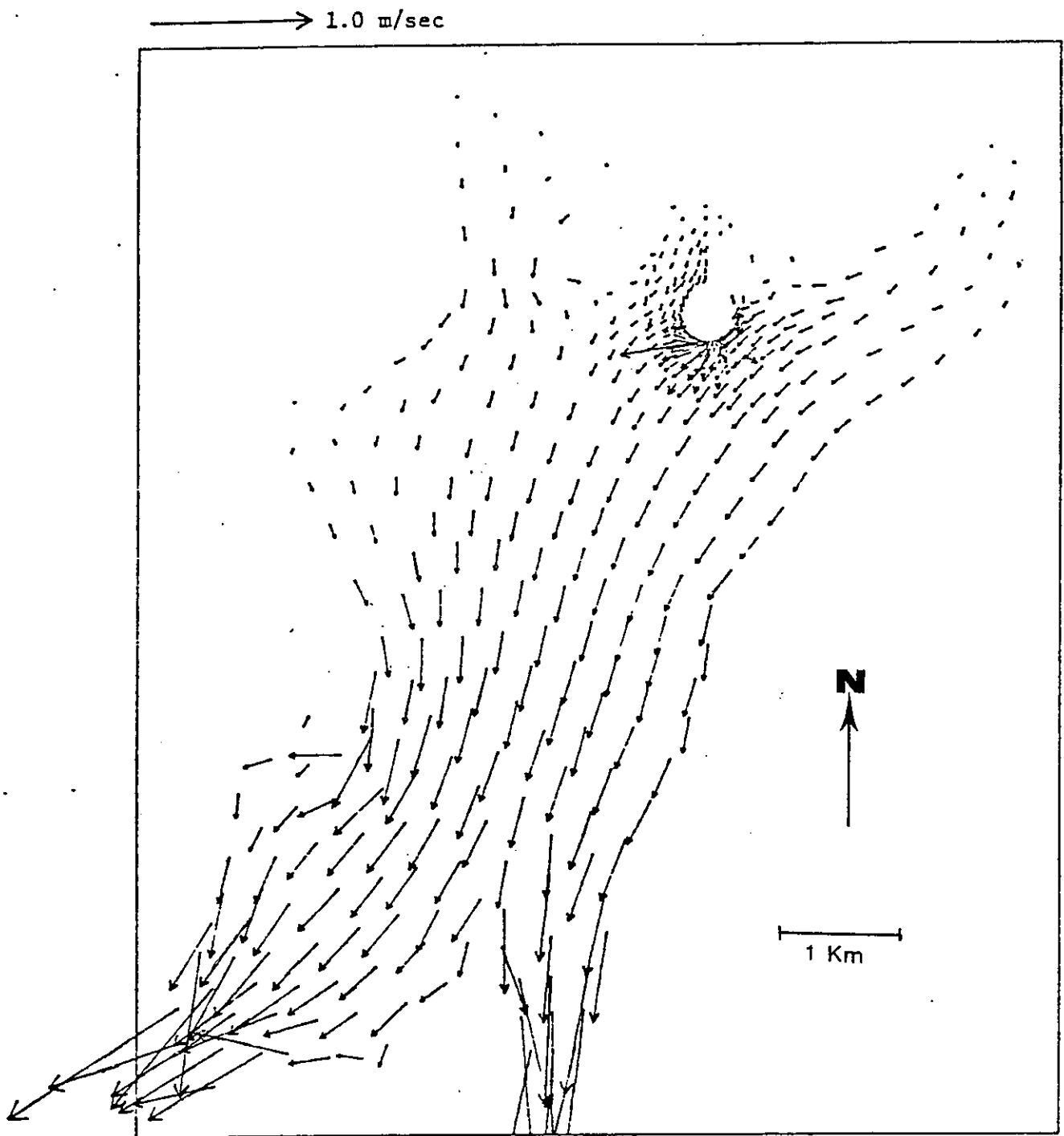


Fig. 6.9. Brayton Point. Circulation computed by TEA at maximum ebb

[from BAPTISTA et al. 1984]

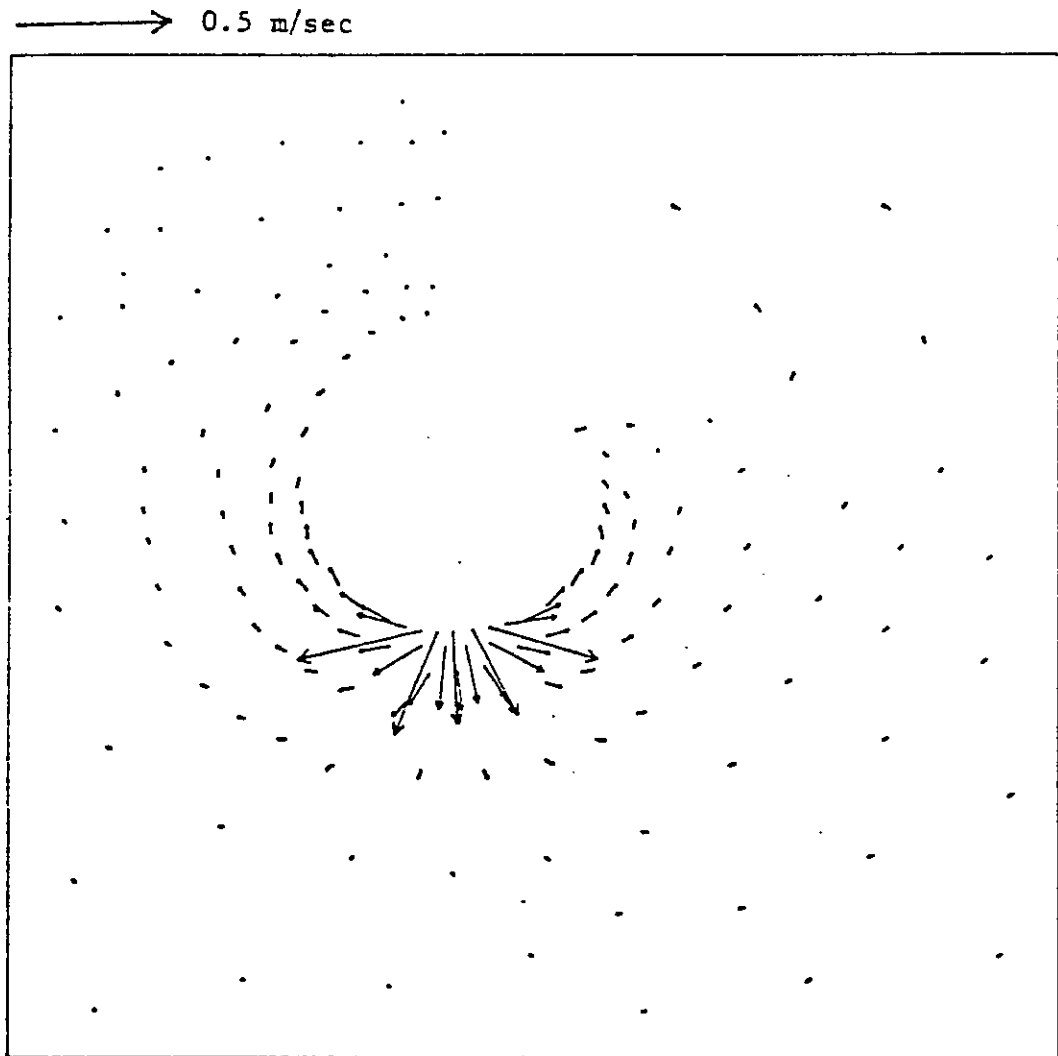


Fig. 6.10. Brayton Point. Detail of circulation computed by TEA at high tide

[from BAPTISTA et al. 1984]



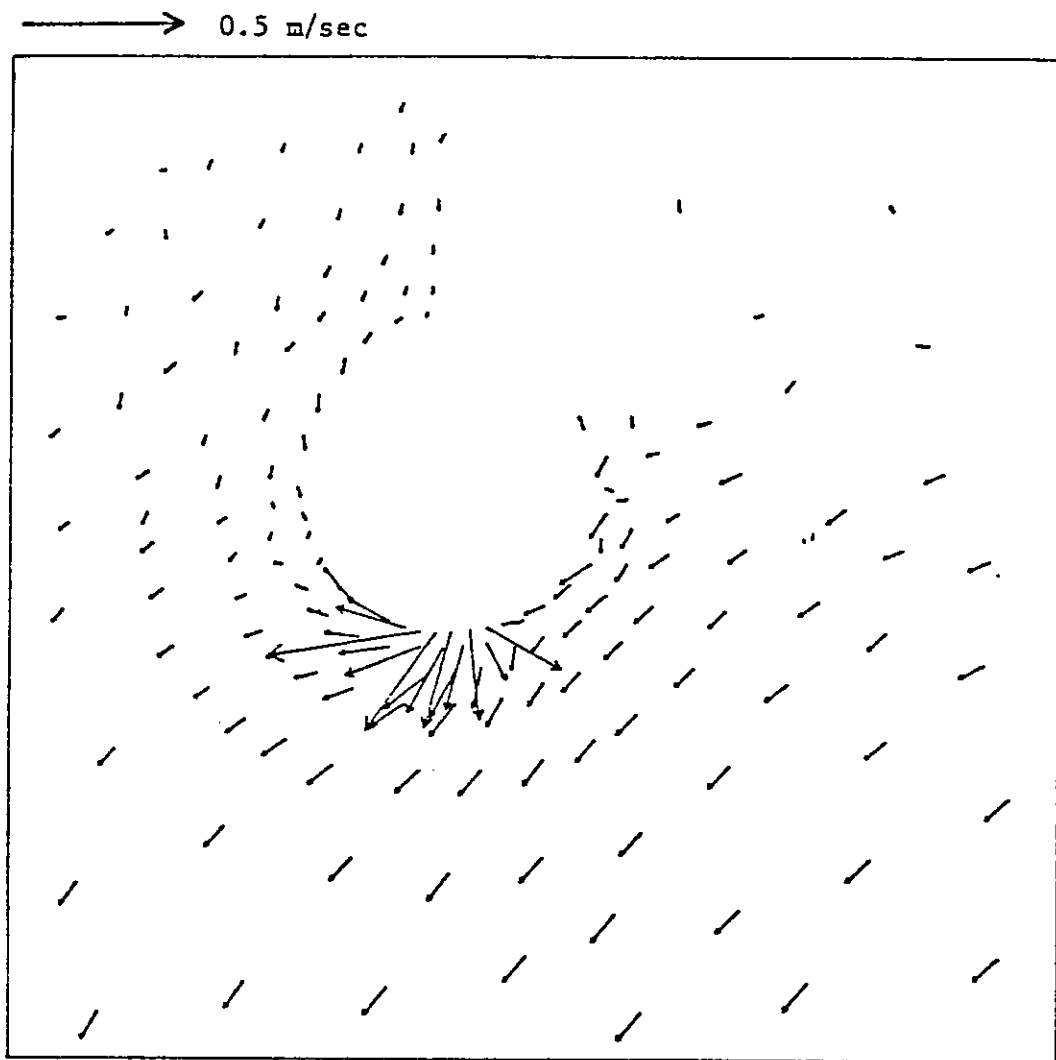


Fig. 6.11. Brayton Point. Detail of circulation computed by TEA at maximum ebb

[from BAPTISTA et al. 1984]



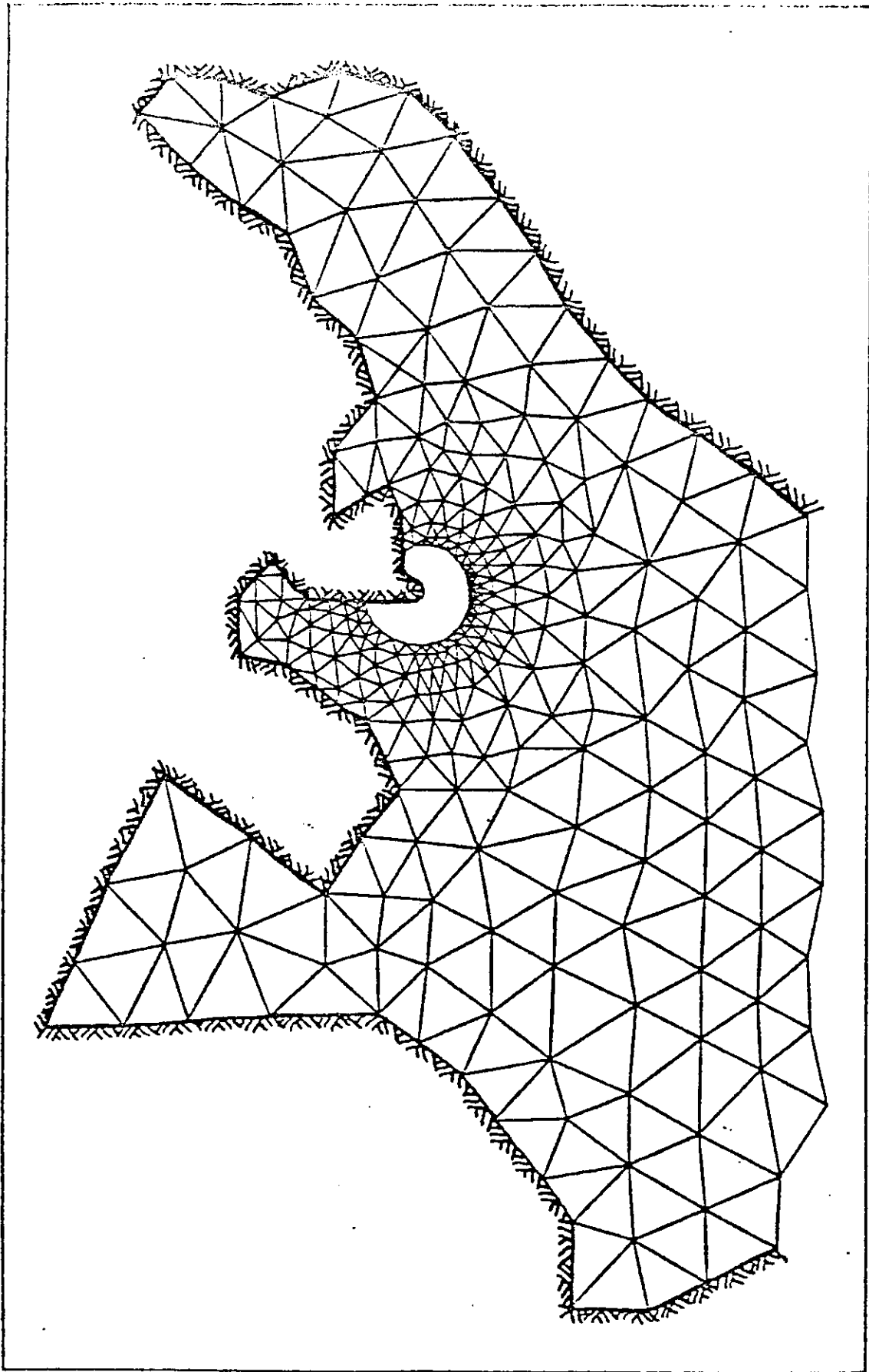
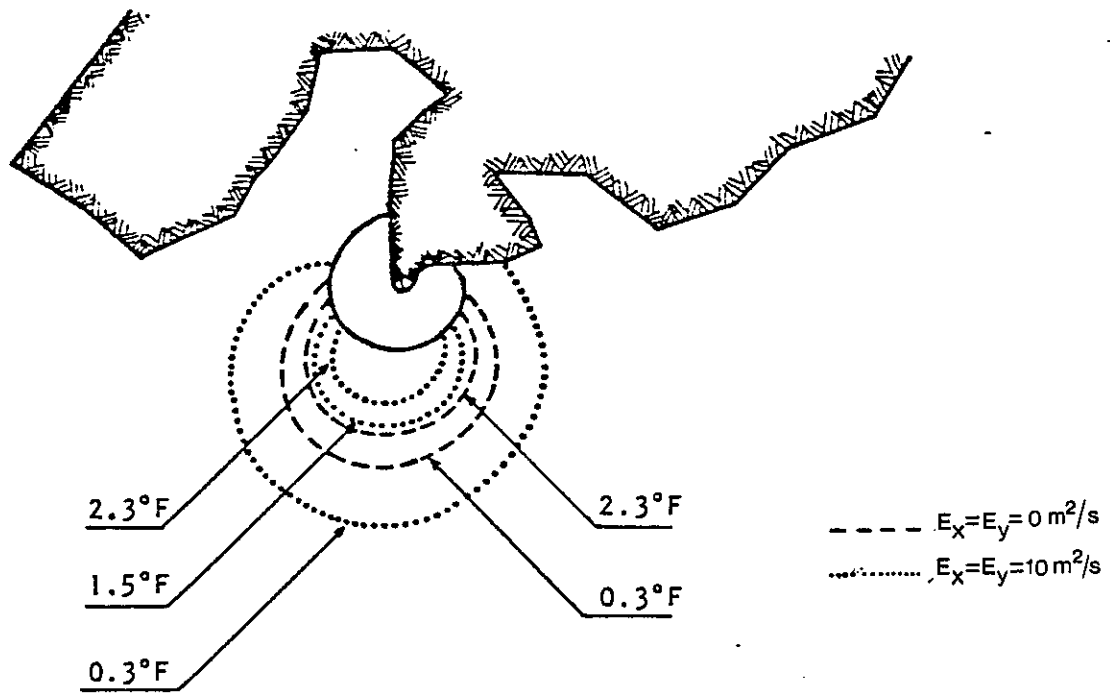


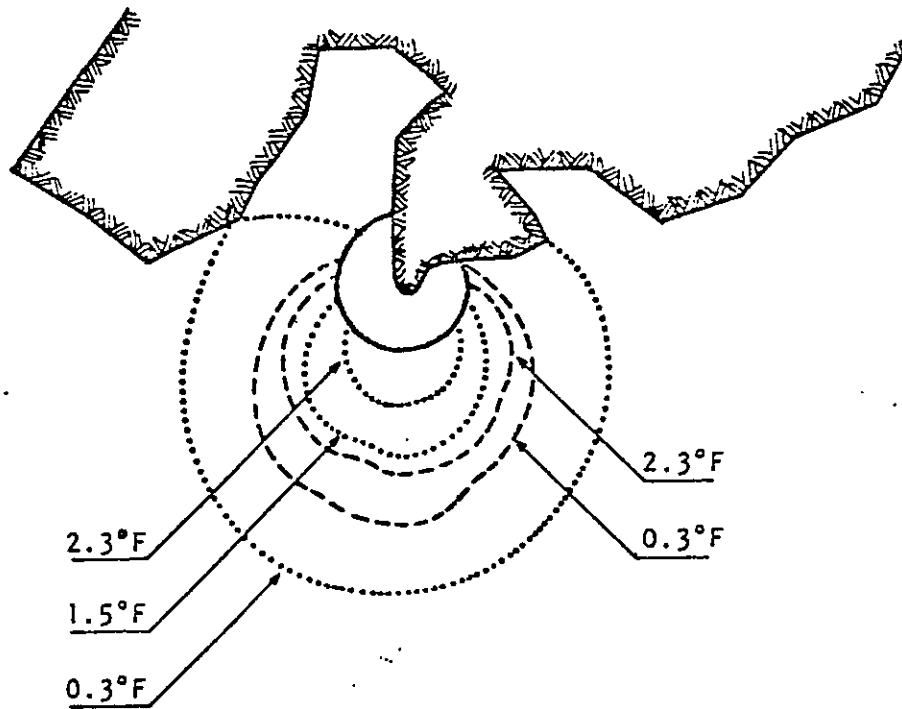
Fig. 6.12. Brayton Point. Finite element grid for transport calculations.

[from BAPTISTA et al. 1984]





(a) 3 hours after maximum flood (approximately high tide)



(b) 6 hours after maximum flood (approximately maximum ebb)

Fig. 6.13. Brayton Point. Excess temperature at high tide and maximum ebb.

[from BAPTISTA et al. 1984]

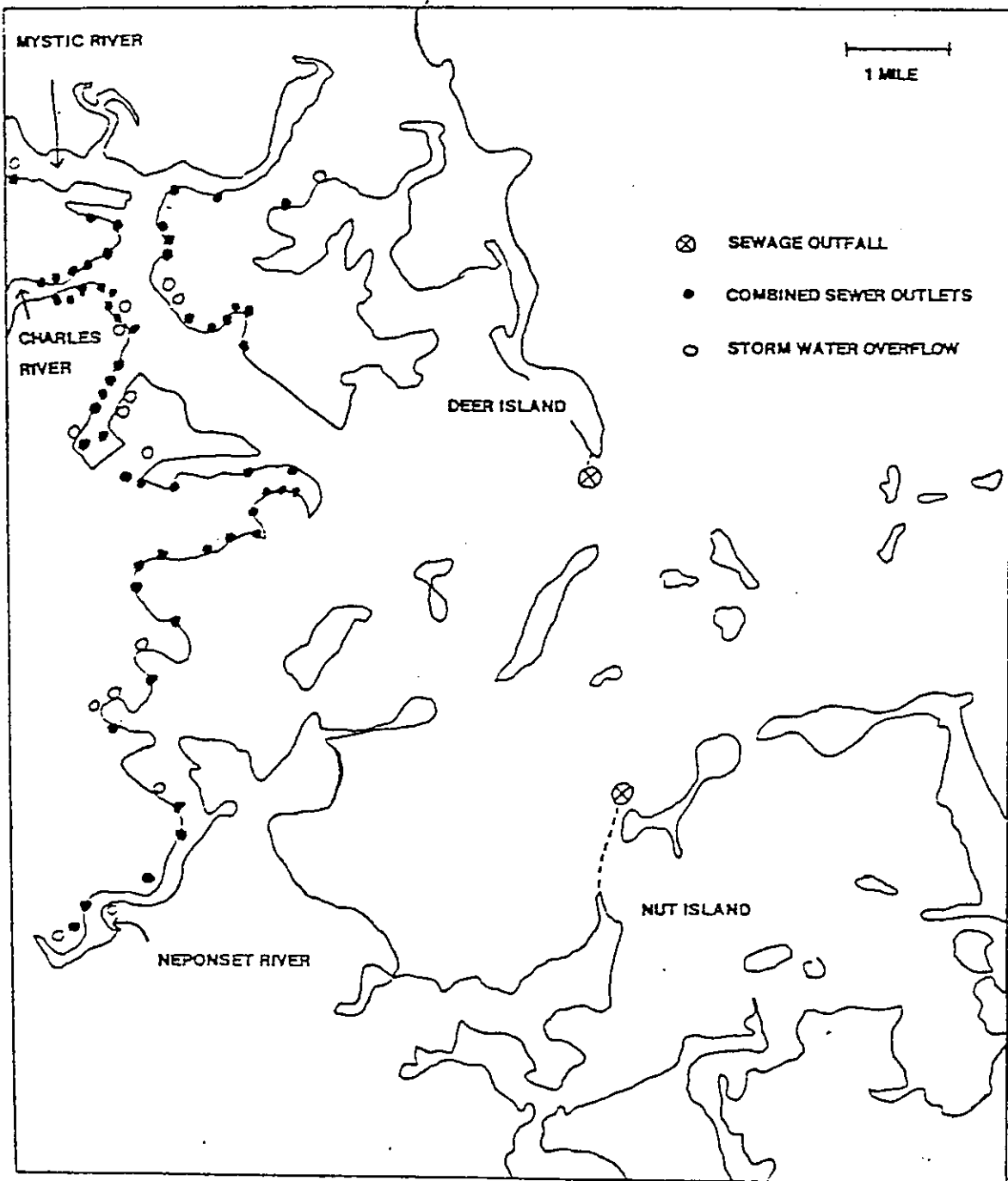


Fig. 6.14. Major sources of pollution to Boston Harbor

[from KOSSIK 1986]

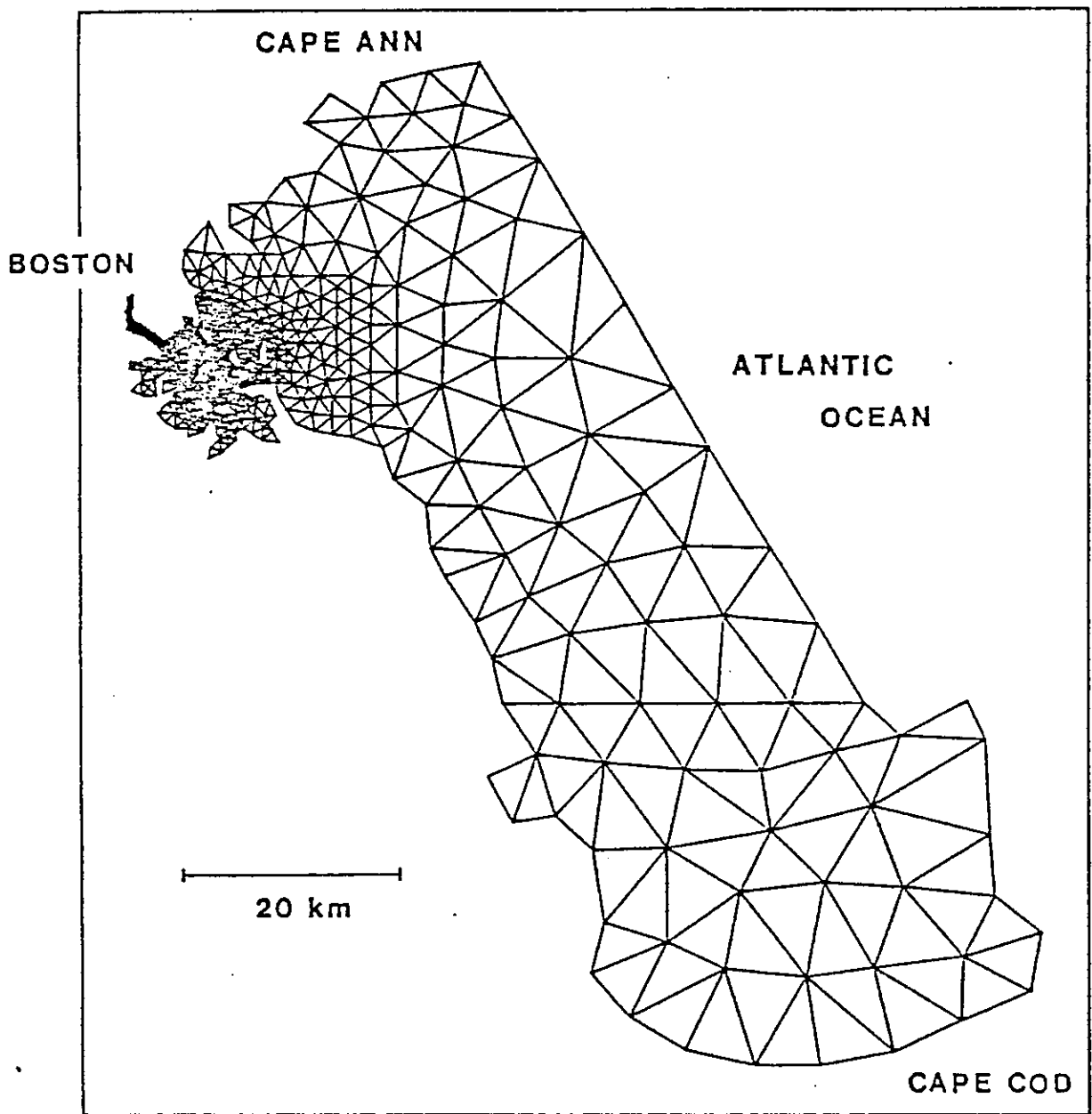


Fig. 6.15. Boston Harbor application. Finite element grid for Massachusetts Bay

[from KOSSIK 1986]

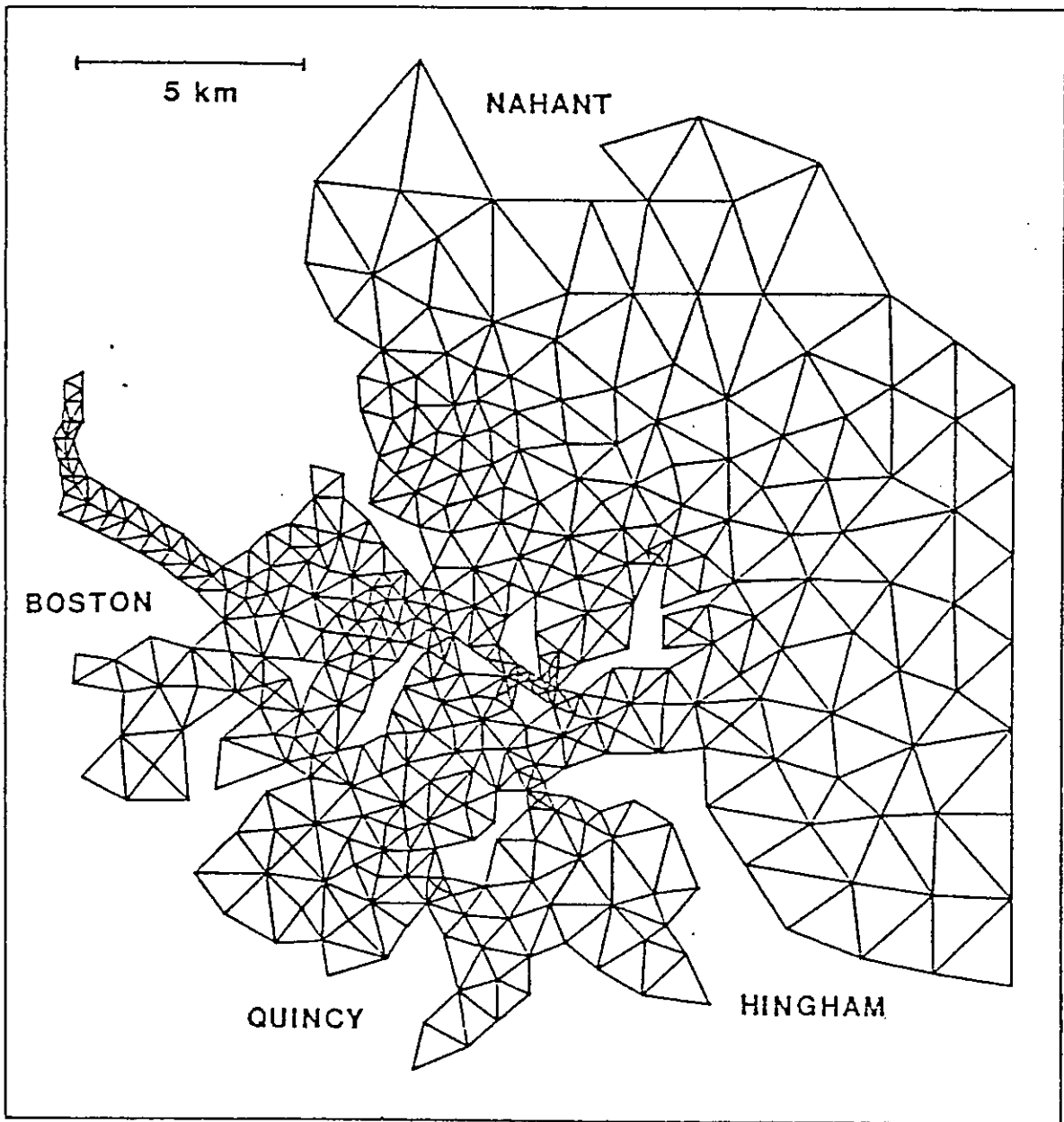
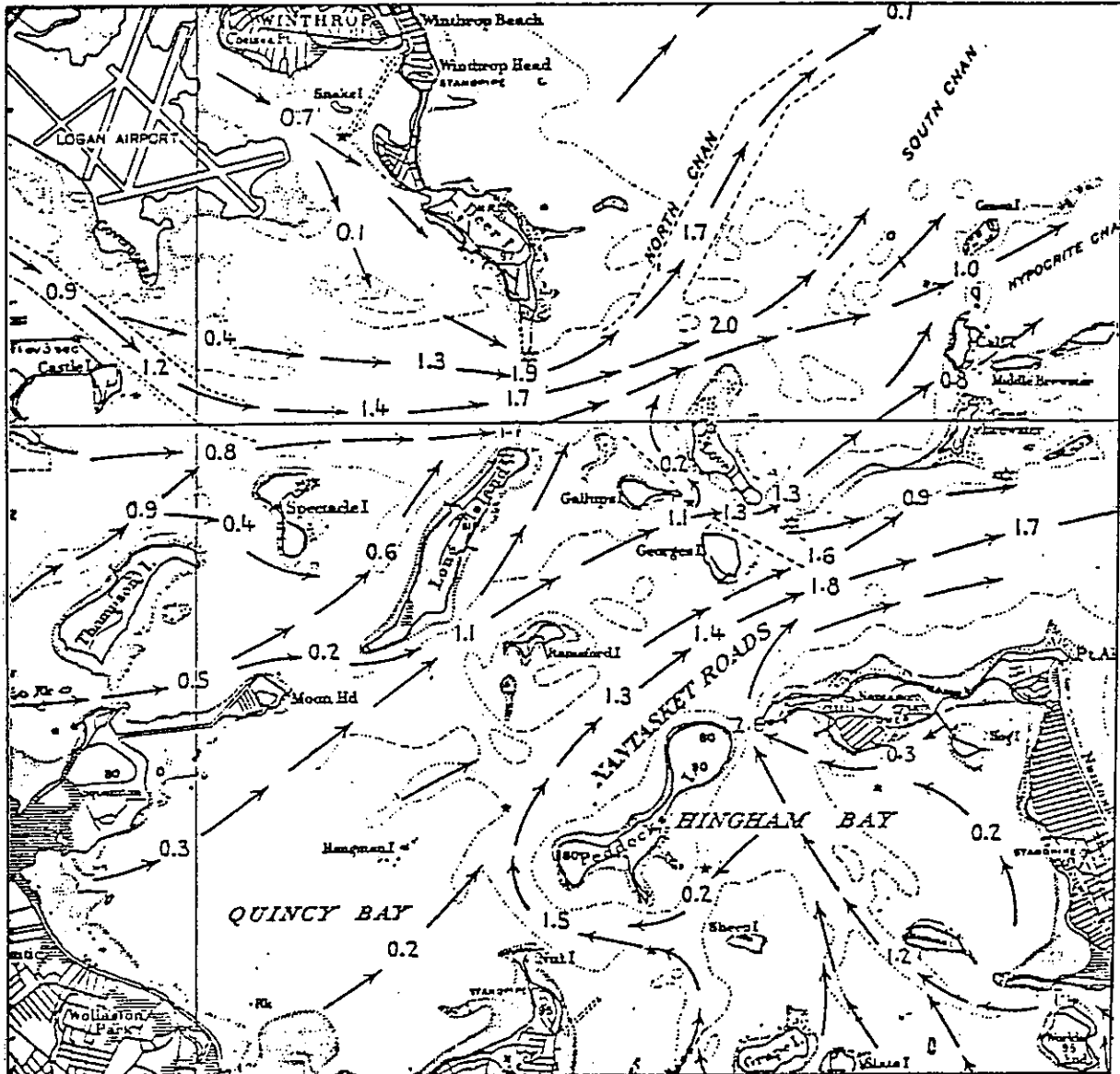


Fig. 6.16. Boston Harbor application. Detail of the finite element grid in the zone of the Harbor

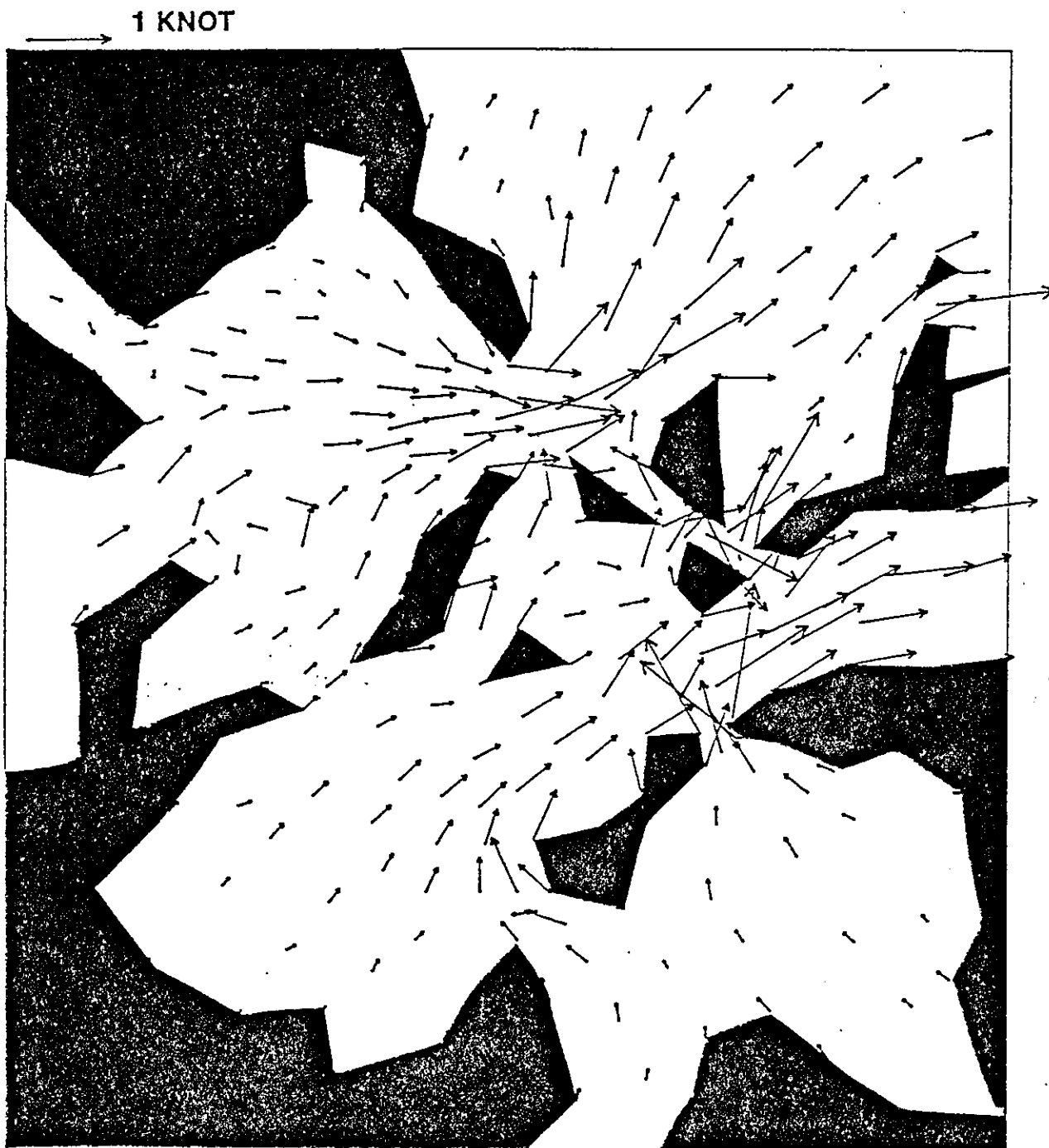
[from KOSSIK 1986]



(a) from NOAA tidal currents charts

Fig. 6.17. Current velocities in the Boston Harbor 4 1/2 hours after low tide

[from KOSSIK 1986]



(b) calculated by TEA

Fig. 6.17. Cont.

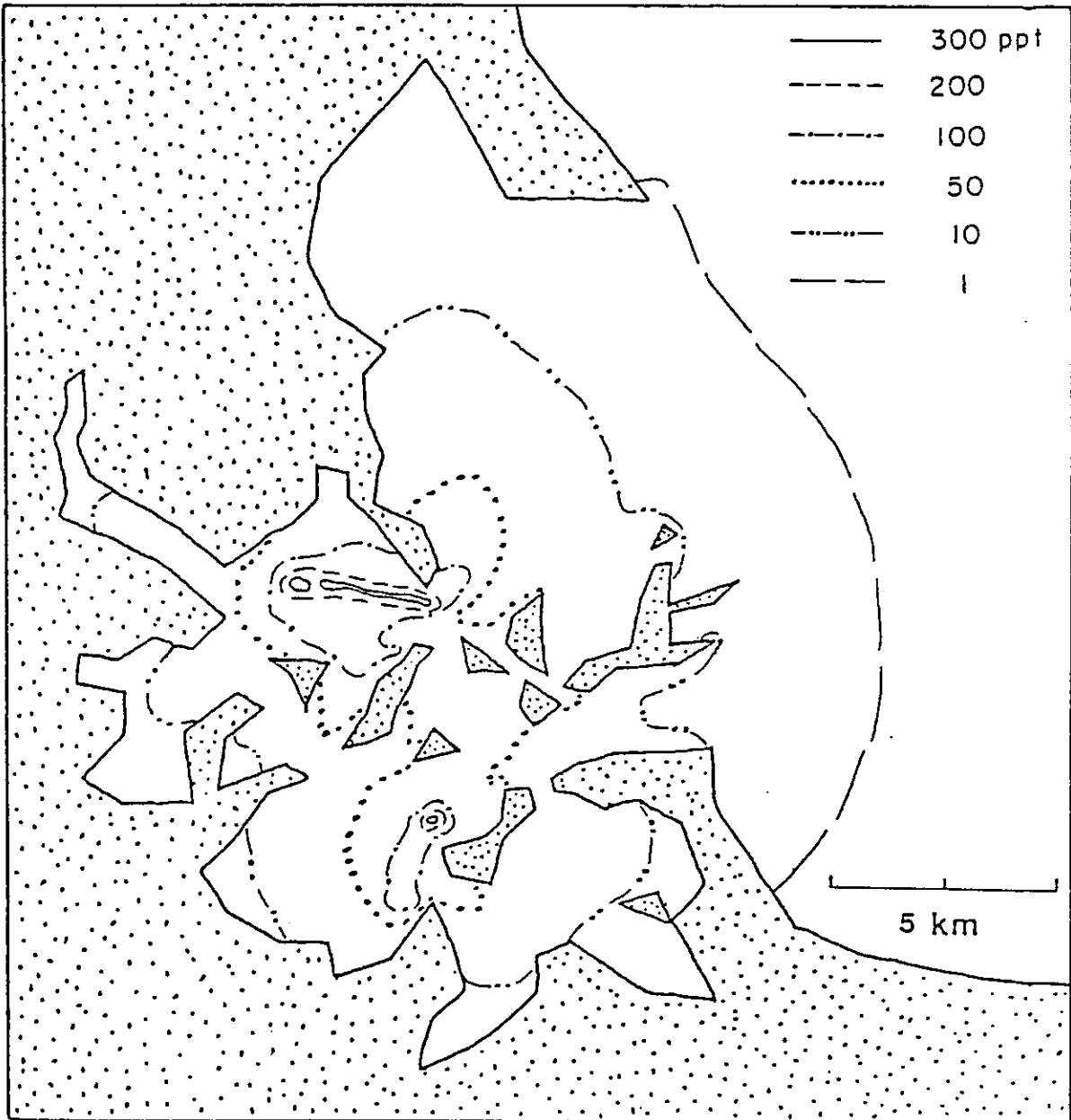


Fig. 6.18. Simulated concentrations (parts-per-trillion) in Boston Harbor at high water slack ( $E_x=E_y=10\text{m}^2/\text{sec}$ ;  $K=10\text{ cm/hr}$ ; variable source strength)

[from KOSSIK, 1986]

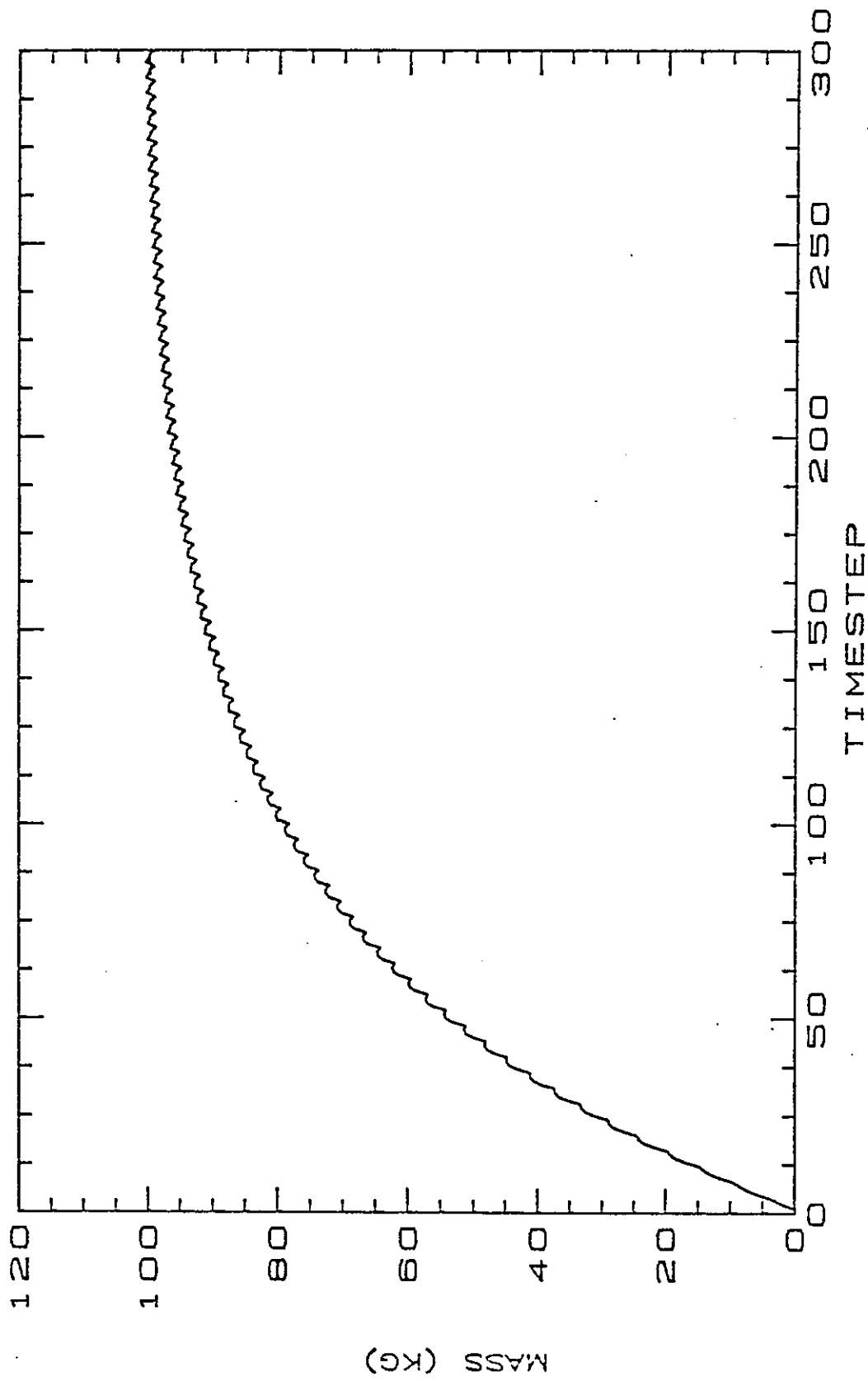


Fig. 6.19. Boston Harbor application. Total mass in the domain versus number of time steps ( $\Delta t=3.1$  hrs;  $E_x=E_y=60\text{m}^2/\text{s}$ ;  $K=1\text{cm/hr}$ ;  $\text{CoQo}=13.4$  Kg/day)

[from KOSSIK 1986]





TABLES



Scheme	Truncation error
2P-LI2	$\alpha(1-\alpha) \frac{\Delta x^2}{2\Delta t} \frac{\partial^2 c}{\partial x^2} + \text{higher order derivatives (H.O.D.)}$
3P-LI3	$\alpha(\alpha^2-1) \frac{\Delta x^3}{6\Delta t} \frac{\partial^3 c}{\partial x^3} + \text{H.O.D.}$
4P-LI4	$-\frac{3}{128} (9\alpha^4 + 10\alpha^2 - 1) \frac{\Delta x^4}{\Delta t} \frac{\partial^4 c}{\partial x^4} + \text{H.O.D.}$
4P-LR2	$\alpha(\alpha-2)(\alpha^2+1) \frac{\Delta x^4}{24\Delta t} \frac{\partial^4 c}{\partial x^4} + \text{H.O.D.}$
5P-LR3	$-\alpha(\alpha^2-1)(\alpha^2-4) \frac{\Delta x^5}{120\Delta t} \frac{\partial^5 c}{\partial x^5} + \text{H.O.D.}$
6P-LR2	$(\dots) \frac{\Delta x^6}{\Delta t} \frac{\partial^6 c}{\partial x^6} + \text{H.O.D.}$
8P-LR2	$(\dots) \frac{\Delta x^8}{\Delta t} \frac{\partial^8 c}{\partial x^8} + \text{H.O.D.}$
2P-HI2	$(\alpha^2-\alpha)^2 \frac{\Delta x^4}{24\Delta t} \frac{\partial^4 c}{\partial x^4} + \text{H.O.D.}$
4P-HL2	$-\alpha(\alpha-1)(2\alpha-1) \frac{\Delta x^3}{12\Delta t} \frac{\partial^3 c}{\partial x^3} + \text{H.O.D.}$
5P-HL3	$-\alpha^2(\alpha^2+1) \frac{\Delta x^4}{24\Delta t} \frac{\partial^4 c}{\partial x^4} + \text{H.O.D.}$
7P-HL3	$-\alpha(1-\alpha^2) \frac{\Delta x^3}{6\Delta t} \frac{\partial^3 c}{\partial x^3} + \text{H.O.D.}$
6P-PL2	$(3.7\alpha - 4.2)\alpha \cdot 10^{-4} c + \frac{\Delta x}{\Delta t} [\alpha^2 + (3.7K + 3.5)\alpha + (0.9 - 4.2K)] \alpha \cdot 10^{-4} \frac{\partial c}{\partial x} +$ $+ \frac{\Delta x^2}{2\Delta t} [\alpha^2(2K - 1443.8) + \alpha(3.7K^2 + 7K + 320.1) + (-4.2K^2 + 12K - 314.3)] \alpha \cdot 10^{-4} \frac{\partial^2 c}{\partial x^2} + \text{H.O.D.}$
8P-PL2	$(\alpha^2-\alpha)^2 \frac{\Delta x^4}{24\Delta t} \frac{\partial^4 c}{\partial x^4} + \text{H.O.D.}$

Table 4.1 Truncation errors for alternative interpolation schemes (general case)

Scheme	Truncation error
2P-LI2	$\frac{u}{2} (\Delta x - u \Delta t) \frac{\partial^2 c}{\partial x^2} + \text{higher order derivatives (H.O.D.)}$
3P-LI3	$\frac{u}{6} (u^2 \Delta t^2 - \Delta x^2) \frac{\partial^3 c}{\partial x^3} + \text{H.O.D.}$
4P-LI4	$-\frac{3}{128} \left( 9u^4 \Delta t^3 + 10u^2 \Delta t \Delta x^2 - \frac{\Delta x^4}{\Delta t} \right) \frac{\partial^4 c}{\partial x^4} + \text{H.O.D.}$
4P-LR2	$\frac{u}{24} (u^3 \Delta t^3 - 2u^2 \Delta t^2 \Delta x - u \Delta t \Delta x^2 + 2 \Delta x^3) \frac{\partial^4 c}{\partial x^4} + \text{H.O.D.}$
5P-LR3	$-\frac{u}{120} (u^4 \Delta t^4 - 5u^2 \Delta t^2 \Delta x^2 - 4 \Delta x^4) \frac{\partial^5 c}{\partial x^5} + \text{H.O.D.}$
6P-LR2	$(\dots) \frac{\partial^6 c}{\partial x^6} + \text{H.O.D.}$
8P-LR2	$(\dots) \frac{\partial^8 c}{\partial x^8} + \text{H.O.D.}$
2P-HI2	$-\frac{u}{24} (u^2 \Delta t^3 - 2u \Delta t^2 \Delta x + \Delta t \Delta x^2) \frac{\partial^4 c}{\partial x^4} + \text{H.O.D.}$
4P-HL2	$\frac{u}{12} (2u^2 \Delta t^2 - 3u \Delta t \Delta x + \Delta x^2) \frac{\partial^3 c}{\partial x^3} + \text{H.O.D.}$
5P-HL3	$-\frac{u}{24} (u^2 \Delta t^3 + \Delta x^2 \Delta t) \frac{\partial^4 c}{\partial x^4} + \text{H.O.D.}$
7P-HL3	$\frac{u}{6} (u^2 \Delta t^2 - \Delta x^2) \frac{\partial^3 c}{\partial x^3} + \text{H.O.D.}$
6P-PL2	$(\dots) c + (\dots) \frac{\partial c}{\partial x} + (\dots) \frac{\partial^2 c}{\partial x^2} + \text{H.O.D.}$
8P-PL2	$-\frac{u}{24} (u^2 \Delta t^3 - 2u \Delta t^2 \Delta x + \Delta t \Delta x^3) \frac{\partial^4 c}{\partial x^4} + \text{H.O.D.}$

Table 4.2 Truncation errors for alternative interpolation schemes (case of  $\beta < 1$ , i.e.,  $\beta = u \Delta t / \Delta x$ )

Scheme	Errors
2P-LI2	$G_m(\alpha) = \exp(i\alpha\lambda_m) \{ 1 - \alpha(1 - \cos\lambda_m) - i\alpha \sin\lambda_m \}$ $ G_m(\alpha)  = \{ 1 - 2\alpha(1 - \alpha) [1 - \cos(\lambda_m)] \}^{1/2}$ $\arg\{G_m(\alpha)\} = \alpha\lambda_m + \arctg\left\{ \frac{-\alpha \sin(\lambda_m)}{1 - \alpha(1 - \cos\lambda_m)} \right\}$
3P-LI3	$G_m(\alpha) = \exp(i\lambda_m) \{ [1 - \alpha^2(1 - \cos\lambda_m)] - i\alpha \sin\lambda_m \}$ $ G_m(\alpha)  = \{ 1 - \alpha^2(1 - \alpha^2)(1 - \cos\lambda_m)^2 \}^{1/2}$ $\arg\{G_m(\alpha)\} = \lambda_m + \arctg\left\{ \frac{-\alpha \sin\lambda_m}{1 - \alpha^2(1 - \cos\lambda_m)} \right\}$
4P-LI4	$G_m(\alpha) = \exp\left\{ \frac{i\lambda_m}{2}(3\alpha+1) \right\} \{ \phi_1(\alpha) \exp(i\lambda_m) + \phi_2(\alpha) + \phi_3(\alpha) \exp(-i\lambda_m) + \phi_4(\alpha) \exp(-i2\lambda_m) \}$ $ G_m(\alpha)  = \left\{ 1 - \frac{3}{16}(9\alpha^4 - 10\alpha^2 + 1)(1 - \cos\lambda_m)^2 + \frac{1}{32}(81\alpha^6 - 99\alpha^4 + 19\alpha^2 - 1)(1 - \cos\lambda_m)^3 \right\}^{1/2}$ $\arg\{G_m(\alpha)\} = (3\alpha+1)\frac{\lambda_m}{2} + \arctg\left\{ \frac{[\phi_1(\alpha) - \phi_3(\alpha)] \sin\lambda_m - \phi_4(\alpha) \sin(2\lambda_m)}{\phi_2(\alpha) + [\phi_1(\alpha) + \phi_3(\alpha)] \cos\lambda_m + \phi_4(\alpha) \cos(2\lambda_m)} \right\}$
4P-LR2	$G_m(\alpha) = \exp(i\alpha\lambda_m) \{ \phi_1(\alpha) \exp(i\lambda_m) + \phi_2(\alpha) + \phi_3(\alpha) \exp(-i\lambda_m) + \phi_4(\alpha) \exp(-i2\lambda_m) \}$ $ G_m(\alpha)  = \{ A_R^2 + A_I^2 \}^{1/2}$ $\arg\{G_m(\alpha)\} = \alpha\lambda_m + \arctg\left\{ \frac{A_I}{A_R} \right\}$ <p style="text-align: right;">with <math>\begin{cases} A_R = \phi_2(\alpha) + [\phi_1(\alpha) + \phi_3(\alpha)] \cos\lambda_m + \phi_4(\alpha) \cos(2\lambda_m) \\ A_I = [\phi_1(\alpha) - \phi_3(\alpha)] \sin\lambda_m - \phi_4(\alpha) \sin(2\lambda_m) \end{cases}</math></p>
5P-LR3	$G_m(\alpha) = \exp(i\alpha\lambda_m) \{ \phi_1(\alpha) \exp(i2\lambda_m) + \phi_2(\alpha) \exp(i\lambda_m) + \phi_3(\alpha) + \phi_4(\alpha) \exp(-i\lambda_m) + \phi_5(\alpha) \exp(-i2\lambda_m) \}$ $ G_m(\alpha)  = \{ A_R^2 + A_I^2 \}^{1/2}$ $\arg\{G_m(\alpha)\} = \alpha\lambda_m + \arctg\left\{ \frac{A_I}{A_R} \right\}$ <p style="text-align: right;">with <math>\begin{cases} A_R = [\phi_1(\alpha) + \phi_5(\alpha)] \cos(2\lambda_m) + [\phi_2(\alpha) + \phi_4(\alpha)] \cos\lambda_m + \phi_3(\alpha) \\ A_I = [\phi_1(\alpha) - \phi_5(\alpha)] \sin(2\lambda_m) + [\phi_2(\alpha) - \phi_4(\alpha)] \sin\lambda_m \end{cases}</math></p>
6P-LR2	$G_m(\alpha) = \exp(i\alpha\lambda_m) \{ \phi_1(\alpha) \exp(i2\lambda_m) + \phi_2(\alpha) \exp(i\lambda_m) + \phi_3(\alpha) + \phi_4(\alpha) \exp(-i\lambda_m) + \phi_5(\alpha) \exp(-i2\lambda_m) + \phi_6(\alpha) \exp(-i3\lambda_m) \}$ $ G_m(\alpha)  = \{ A_R^2 + A_I^2 \}^{1/2}$ $\arg\{G_m(\alpha)\} = \alpha\lambda_m + \arctg\left\{ \frac{A_I}{A_R} \right\}$ <p style="text-align: right;">with <math>\begin{cases} A_R = \phi_3(\alpha) + [\phi_2(\alpha) + \phi_4(\alpha)] \cos\lambda_m + [\phi_1(\alpha) + \phi_5(\alpha)] \cos(2\lambda_m) + \phi_6(\alpha) \cos(3\lambda_m) \\ A_I = -\phi_6(\alpha) \sin(3\lambda_m) + [\phi_1 - \phi_5] \sin(2\lambda_m) + [\phi_2(\alpha) - \phi_4(\alpha)] \sin\lambda_m \end{cases}</math></p>
8P-LR2	$G_m(\alpha) = \exp(i\alpha\lambda_m) \{ \phi_1(\alpha) \exp(i3\lambda_m) + \phi_2(\alpha) \exp(i2\lambda_m) + \phi_3(\alpha) \exp(i\lambda_m) + \phi_4(\alpha) + \phi_5(\alpha) \exp(-i\lambda_m) + \phi_6(\alpha) \exp(-i2\lambda_m) + \phi_7(\alpha) \exp(-i3\lambda_m) + \phi_8(\alpha) \exp(-i4\lambda_m) \}$ $ G_m(\alpha)  = \{ A_R^2 + A_I^2 \}^{1/2}; \arg\{G_m(\alpha)\} = \alpha\lambda_m + \arctg\{A_I/A_R\};$ <p style="text-align: right;">with: <math>\begin{cases} A_R = \phi_4(\alpha) + [\phi_3(\alpha) + \phi_5(\alpha)] \cos\lambda_m + [\phi_2(\alpha) + \phi_6(\alpha)] \cos(2\lambda_m) + [\phi_1(\alpha) + \phi_7(\alpha)] \cos(3\lambda_m) + \phi_8(\alpha) \cos(4\lambda_m) \\ A_I = [\phi_3(\alpha) - \phi_5(\alpha)] \sin\lambda_m + [\phi_2(\alpha) - \phi_6(\alpha)] \sin(2\lambda_m) + [\phi_1(\alpha) - \phi_7(\alpha)] \sin(3\lambda_m) - \phi_8(\alpha) \sin(4\lambda_m) \end{cases}</math></p>

Note: See Fig. 4.1 for the definition of the functions  $\phi_i(\alpha)$ , for each scheme

Table 4.3. Amplitude and phase errors of the BMC for alternative interpolation schemes (first time step)

Scheme	Errors
4P-HL2	$G_m(\alpha) = \exp(i\alpha\lambda_m) \{ \phi_1(\alpha) \exp(i\lambda_m) + \phi_2(\alpha) + \phi_3(\alpha) \exp(-i\lambda_m) + \phi_4(\alpha) \exp(-iz\lambda_m) \}$ $ G_m(\alpha)  = \{ A_E^2 + A_I^2 \}^{1/2}; \arg \{ G_m(\alpha) \} = \alpha\lambda_m + \arctg \{ A_I / A_E \}; \text{ with}$ $A_E = \phi_2(\alpha) + \{ \phi_1(\alpha) + \phi_3(\alpha) \} \cos \lambda_m + \phi_4(\alpha) \cos(z\lambda_m)$ $A_I = [\phi_1(\alpha) - \phi_3(\alpha)] \sin \lambda_m - \phi_4(\alpha) \sin(z\lambda_m)$
5P-HL3	$G_m(\alpha) = \exp(i\alpha\lambda_m) \{ \phi_1(\alpha) \exp(iz\lambda_m) + \phi_2(\alpha) \exp(i\lambda_m) + \phi_3(\alpha) + \phi_4(\alpha) \exp(-i\lambda_m) + \phi_5(\alpha) \exp(-iz\lambda_m) \}$ $ G_m(\alpha)  = \{ [1 - \alpha^2(1 - \cos \lambda_m)]^2 + [-\frac{1}{6} \alpha(\alpha^2 - 1) \sin(z\lambda_m) + \frac{1}{3} \alpha(\alpha^2 - 4) \sin \lambda_m]^2 \}^{1/2}$ $\arg \{ G_m(\alpha) \} = \alpha\lambda_m + \arctg \left\{ \frac{1 - \alpha^2(1 - \cos \lambda_m)}{\frac{1}{3} \alpha(\alpha^2 - 4) \sin \lambda_m - \frac{1}{6} \alpha(\alpha^2 - 1) \sin(z\lambda_m)} \right\}$
7P-HL3	$G_m(\alpha) = \exp(i\alpha\lambda_m) \{ \phi_1(\alpha) \exp(i3\lambda_m) + \phi_2(\alpha) \exp(iz\lambda_m) + \phi_3(\alpha) \exp(i\lambda_m) + \phi_4(\alpha) + \phi_5(\alpha) \exp(-i\lambda_m) + \phi_6(\alpha) \exp(-iz\lambda_m) + \phi_7(\alpha) \exp(-i3\lambda_m) \}$ $ G_m(\alpha)  = \{ A_E^2 + A_I^2 \}^{1/2}; \arg \{ G_m(\alpha) \} = \alpha\lambda_m + \arctg \{ A_I / A_E \}; \text{ with}$ $A_E = [\phi_1(\alpha) + \phi_7(\alpha)] \cos(3\lambda_m) + [\phi_2(\alpha) + \phi_6(\alpha)] \cos(z\lambda_m) + [\phi_3(\alpha) + \phi_5(\alpha)] \cos \lambda_m + \phi_4(\alpha)$ $A_I = [\phi_1(\alpha) - \phi_7(\alpha)] \sin(3\lambda_m) + [\phi_2(\alpha) - \phi_6(\alpha)] \sin(z\lambda_m) + [\phi_3(\alpha) - \phi_5(\alpha)] \sin \lambda_m$
6P-PL2	$G_m(\alpha) = \exp(i\alpha\lambda_m) \{ \phi_1(\alpha) \exp(iz\lambda_m) + \phi_2(\alpha) \exp(i\lambda_m) + \phi_3(\alpha) + \phi_4(\alpha) \exp(-i\lambda_m) + \phi_5(\alpha) \exp(-iz\lambda_m) + \phi_6(\alpha) \exp(-i3\lambda_m) \}$ $ G_m(\alpha)  = \{ A_E^2 + A_I^2 \}^{1/2}; \arg \{ G_m(\alpha) \} = \alpha\lambda_m + \arctg \{ A_I / A_E \}; \text{ with}$ $A_E = \phi_3(\alpha) + [\phi_2(\alpha) + \phi_4(\alpha)] \cos \lambda_m + [\phi_1(\alpha) + \phi_5(\alpha)] \cos(z\lambda_m) + \phi_6 \cos(3\lambda_m)$ $A_I = [\phi_2(\alpha) - \phi_4(\alpha)] \sin \lambda_m + [\phi_1(\alpha) - \phi_5(\alpha)] \sin(z\lambda_m)$
8P-PL2	$G_m(\alpha) = \exp(i\alpha\lambda_m) \{ \phi_1(\alpha) \exp(iz\lambda_m) + \phi_2(\alpha) \exp(i2\lambda_m) + \phi_3(\alpha) \exp(i\lambda_m) + \phi_4(\alpha) + \phi_5(\alpha) \exp(-i\lambda_m) + \phi_6(\alpha) \exp(-iz\lambda_m) + \phi_7(\alpha) \exp(-i3\lambda_m) + \phi_8(\alpha) \exp(-i4\lambda_m) \}$ $ G_m(\alpha)  = \{ A_E^2 + A_I^2 \}^{1/2}; \arg \{ G_m(\alpha) \} = \alpha\lambda_m + \arctg \{ A_I / A_E \}; \text{ with}$ $A_E = \phi_4(\alpha) + [\phi_3(\alpha) + \phi_5(\alpha)] \cos \lambda_m + [\phi_2(\alpha) + \phi_6(\alpha)] \cos(z\lambda_m) + [\phi_1(\alpha) + \phi_7(\alpha)] \cos(3\lambda_m) + \phi_8(\alpha) \cos(4\lambda_m)$ $A_I = [\phi_3(\alpha) - \phi_5(\alpha)] \sin \lambda_m + [\phi_2(\alpha) - \phi_6(\alpha)] \sin(z\lambda_m) + [\phi_1(\alpha) - \phi_7(\alpha)] \sin(3\lambda_m) - \phi_8(\alpha) \sin(4\lambda_m)$

Note: See Fig. 4.1 for the definition of the functions  $\phi_i(\alpha)$ , for each scheme

Table 4.3. Cont.

Scheme	Functions $Q_m(\alpha, j)$ and $S_m(\alpha)$
3P-LI3	$Q_m(\alpha) = \begin{cases} \phi_0(\alpha) \exp(i\lambda_m) \\ \phi_0(\alpha) \exp(-i\lambda_m) \end{cases}$ $S_m(\alpha) = \phi_{-1}(\alpha) \exp(i\lambda_m) + \phi_1(\alpha) \exp(-i\lambda_m)$
5P-LR3 and 5P-HL3	$Q_m(\alpha) = \begin{cases} [\phi_{-2}(\alpha) + \phi_0(\alpha)] \exp(i\lambda_m) + \phi_2(\alpha) \exp(i3\lambda_m) \\ \phi_{-2}(\alpha) \exp(i\lambda_m) + \phi_0(\alpha) \exp(-i\lambda_m) + \phi_2(\alpha) \exp(-i3\lambda_m) \end{cases}$ $S_m(\alpha) = \phi_{-1}(\alpha) \exp(i\lambda_m) + \phi_1(\alpha) \exp(-i\lambda_m)$
7P-HL3	$Q_m(\alpha) = \begin{cases} \phi_{-2}(\alpha) \exp(i3\lambda_m) + [\phi_0(\alpha) + \phi_2(\alpha)] \exp(i\lambda_m) \\ \phi_{-2}(\alpha) \exp(i3\lambda_m) + \phi_0(\alpha) \exp(i\lambda_m) + \phi_2(\alpha) \exp(-i\lambda_m) \end{cases}$ $S_m(\alpha) = [\phi_{-3}(\alpha) + \phi_3(\alpha)] \exp(i3\lambda_m) + [\phi_{-1}(\alpha) + \phi_1(\alpha)] \exp(i\lambda_m)$

Note: see Fig. 4.1 for the definition of functions  $\phi_i(\alpha)$

Table 4.4. Complementary functions for the propagation of amplitude and phase errors for interpolation schemes with quadratic core elements

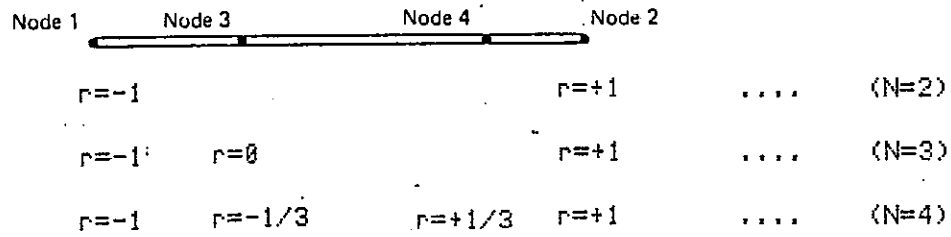


Problem	Scheme	$\phi_m$	$\mu_0$	$\mu_x$	$\mu_{xx}$
1A N = 100 $\sigma_0 = 264$ Cu = 0.24	2P-LI2	15.27	1.0000	.0000	11.5960
	3P-LI3	9.32	.9997	.0004	1.0050
	4P-HL2	6.82	1.0000	.0000	1.0004
	5P-HL3	2.53	.9997	.0004	1.0040
	6P-PL2	1.89	1.0001	-.0006	-.2125
	7P-HL3	5.60	.9999	.0001	.9996
	8P-PL2	1.24	1.0000	.0000	1.0016
	1D N = 100 $\sigma_0 = 320$ Cu = 0.24	2P-LI2	15.41	1.0000	.0000
3P-LI3		8.13	1.0000	.0000	1.0010
4P-HL2		5.39	1.0000	.0000	1.0002
5P-HL3		1.39	1.0000	.0000	1.0000
6P-PL2		.94	1.0001	-.0006	.1772
7P-HL3		4.09	1.0000	-.0000	.9990
8P-PL2		.53	1.0000	.0000	1.0010
1E N = 100 $\sigma_0 = 400$ Cu = 0.24		2P-LI2	15.15	1.0000	.0000
	3P-LI3	6.44	1.0000	.0000	1.0000
	4P-HL2	3.69	1.0000	.0000	1.0002
	5P-HL3	.56	1.0000	.0000	1.0000
	6P-PL2	.43	1.0001	-.0006	.4763
	7P-HL3	2.45	1.0000	.0000	.9993
	8P-PL2	.18	1.0000	.0000	1.0006
	1K N = 50 $\sigma_0 = 264$ Cu = 0.48	2P-LI2	14.04	1.0000	.0000
3P-LI3		7.68	.9998	.0003	1.0030
4P-HL2		5.88	1.0000	.0000	.9998
5P-HL3		1.95	.9998	.0003	1.0030
6P-PL2		1.76	1.0001	-.0006	.0952
7P-HL3		5.59	.9999	.0001	1.0010
8P-PL2		1.27	1.0000	.0000	1.0000
1L N = 10 $\sigma_0 = 264$ Cu = 2.40		2P-LI2	7.56	1.0000	.0000
	3P-LI3	2.92	.9998	.0003	1.0040
	4P-HL2	2.40	1.0000	.0000	1.0002
	5P-HL3	.62	.9998	.0003	1.0030
	6P-PL2	.68	1.0001	-.0002	.8351
	7P-HL3	1.97	.9999	.0001	1.0010
	8P-PL2	.44	1.0000	.0000	.9998

Table 4.5 Accuracy measures for the BMC solution of the uniform advection of a Gauss-hill (problems of the Convection-Diffusion Forum).

L m	Amplitudes					
	Gauss-hill			Triangle-hill		
	$\sigma=264$	$\sigma=320$	$\sigma=400$	$l=800$	$l=1000$	$l=1200$
Infinity	0.04859	0.05889	0.07362	0.02937	0.05874	0.08811
13600.000	0.04823	0.05825	0.07237	0.02929	0.05807	0.08568
6800.000	0.04717	0.05638	0.06877	0.02904	0.05612	0.07947
4533.333	0.04545	0.05339	0.06316	0.02863	0.05298	0.06963
3400.000	0.04315	0.04947	0.05606	0.02806	0.04882	0.05751
2720.000	0.04036	0.04485	0.04810	0.02735	0.04386	0.04442
2266.667	0.03720	0.03978	0.03988	0.02650	0.03834	0.03169
1942.857	0.03378	0.03453	0.03196	0.02551	0.03254	0.02046
1700.000	0.03023	0.02932	0.02476	0.02442	0.02672	0.01150
1511.111	0.02665	0.02436	0.01854	0.02322	0.02114	0.00521
1360.000	0.02314	0.01981	0.01341	0.02194	0.01599	0.00153
1236.364	0.01981	0.01576	0.00938	0.02059	0.01147	0.00009
1133.333	0.01670	0.01226	0.00634	0.01919	0.00767	0.00026
1046.154	0.01387	0.00934	0.00414	0.01775	0.00467	0.00132
971.429	0.01136	0.00696	0.00262	0.01629	0.00247	0.00263
906.667	0.00916	0.00507	0.00160	0.01483	0.00102	0.00367
850.000	0.00728	0.00362	0.00094	0.01338	0.00024	0.00415
800.000	0.00570	0.00253	0.00054	0.01196	0.00000	0.00399
755.556	0.00440	0.00173	0.00030	0.01059	0.00017	0.00330
715.789	0.00334	0.00115	0.00016	0.00927	0.00061	0.00233
680.000	0.00250	0.00075	0.00008	0.00801	0.00118	0.00133
647.619	0.00185	0.00048	0.00004	0.00684	0.00176	0.00054
618.182	0.00134	0.00030	0.00002	0.00575	0.00226	0.00009
591.304	0.00096	0.00018	0.00001	0.00475	0.00261	0.00002
566.667	0.00068	0.00011	0.00000	0.00385	0.00277	0.00025
544.000	0.00047	0.00006	0.00000	0.00305	0.00275	0.00065
523.077	0.00032	0.00004	0.00000	0.00235	0.00255	0.00107
503.704	0.00022	0.00002	0.00000	0.00174	0.00221	0.00137
485.714	0.00015	0.00001	0.00000	0.00124	0.00179	0.00146
468.966	0.00010	0.00001	0.00000	0.00083	0.00133	0.00133
453.333	0.00006	0.00000	0.00000	0.00051	0.00089	0.00104
438.710	0.00004	0.00000	0.00000	0.00028	0.00051	0.00067
425.000	0.00002	0.00000	0.00000	0.00012	0.00023	0.00033
412.121	0.00002	0.00000	0.00000	0.00003	0.00006	0.00009
400.000	0.00001	0.00000	0.00000	0.00000	0.00000	0.00000
388.571	0.00001	0.00000	0.00000	0.00002	0.00004	0.00006
377.778	0.00000	0.00000	0.00000	0.00009	0.00017	0.00024
367.568	0.00000	0.00000	0.00000	0.00018	0.00034	0.00045
357.895	0.00000	0.00000	0.00000	0.00031	0.00054	0.00063
348.718	0.00000	0.00000	0.00000	0.00045	0.00072	0.00073
340.000	0.00000	0.00000	0.00000	0.00059	0.00086	0.00072
331.707	0.00000	0.00000	0.00000	0.00074	0.00095	0.00061
323.810	0.00000	0.00000	0.00000	0.00089	0.00098	0.00043
316.279	0.00000	0.00000	0.00000	0.00102	0.00094	0.00024
309.091	0.00000	0.00000	0.00000	0.00114	0.00084	0.00009
302.222	0.00000	0.00000	0.00000	0.00124	0.00070	0.00001
295.652	0.00000	0.00000	0.00000	0.00132	0.00054	0.00002
289.362	0.00000	0.00000	0.00000	0.00137	0.00037	0.00010
283.333	0.00000	0.00000	0.00000	0.00140	0.00022	0.00022
277.551	0.00000	0.00000	0.00000	0.00141	0.00010	0.00034
272.000	0.00000	0.00000	0.00000	0.00139	0.00003	0.00043
266.667	0.00000	0.00000	0.00000	0.00135	0.00000	0.00045
261.538	0.00000	0.00000	0.00000	0.00129	0.00002	0.00041
256.604	0.00000	0.00000	0.00000	0.00121	0.00008	0.00031
251.852	0.00000	0.00000	0.00000	0.00112	0.00016	0.00019
247.273	0.00000	0.00000	0.00000	0.00102	0.00026	0.00008
242.857	0.00000	0.00000	0.00000	0.00091	0.00035	0.00002
238.596	0.00000	0.00000	0.00000	0.00079	0.00043	0.00000
234.483	0.00000	0.00000	0.00000	0.00068	0.00048	0.00004
230.508	0.00000	0.00000	0.00000	0.00056	0.00050	0.00012
226.667	0.00000	0.00000	0.00000	0.00045	0.00049	0.00020
222.951	0.00000	0.00000	0.00000	0.00035	0.00044	0.00027
219.355	0.00000	0.00000	0.00000	0.00026	0.00038	0.00030
215.873	0.00000	0.00000	0.00000	0.00018	0.00029	0.00029
212.500	0.00000	0.00000	0.00000	0.00012	0.00020	0.00024
209.231	0.00000	0.00000	0.00000	0.00007	0.00012	0.00016
206.061	0.00000	0.00000	0.00000	0.00003	0.00006	0.00008
202.985	0.00000	0.00000	0.00000	0.00001	0.00002	0.00002
200.000	0.00000	0.00000	0.00000	0.00000	0.00000	0.00000

Table 4.6 Fourier representation of different instantaneous sources, in the domain  $x \in [0, 13600]$ .



(a) Reference sketch

	Include only if node 3 is present	Include only if nodes 3 and 4 are present
$h_1 = \frac{1}{2}(1-r)$ .....	$-\frac{1}{2}(1-r^2)$ .....	$+\frac{1}{16}(-9r^3+r^2+9r-1)$
$h_2 = \frac{1}{2}(1+r)$ .....	$-\frac{1}{2}(1-r^2)$ .....	$+\frac{1}{16}(9r^3+r^2-9r-1)$
$h_3 = (1-r^2)$ .....		$+\frac{1}{16}(27r^3+7r^2-27r-7)$
$h_4 = \frac{1}{16}(-27r^3-9r^2+27r+9)$		

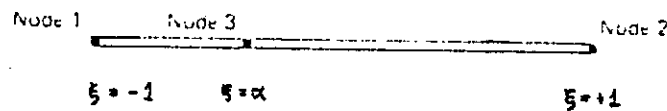
(b) Interpolation functions

$$f(r) = \sum_{i=1}^N h_i f_i \quad (N=\text{number of nodes})$$

(c) Interpolation formula

Table 4.7. Standard interpolation functions and isoparametric mappings for 1-D elements

[adapted from BATHE 1982]



(a) Reference sketch

$$\phi_1(\xi) = \frac{(\xi-1)(\xi-\alpha)}{2(1+\alpha)}$$

with:

$$\phi_2(\xi) = \frac{1-\xi^2}{1-\alpha^2}$$

$$\alpha = -1 + \frac{2\delta x}{\Delta x} = -1 + 2 \frac{(x_2 - x_1)}{(x_3 - x_1)}$$

$$\phi_3(\xi) = \frac{(\xi+1)(\xi-\alpha)}{2(1-\alpha)}$$

(b) Interpolation functions

$$f(\xi) = \sum_{i=1}^N \phi_i f_i$$

(N=number of nodes)

(c) Interpolation formula

Table 4.8: Improved interpolation functions and isoparametric mappings for 1-D elements

[adapted from CELIA and GRAY 1984]



S	$\sigma_0$	$\phi \cdot m$	$\mu_0$	e	$\mu_x$	$\mu_{xx}$
10.00	264	17.44	1.0112	.25	-.0314	8.2737
	400	14.87	1.0023	.54	-.0065	1.6733
5.00	264	16.69	.9975	.32	.0073	-.7441
	400	13.07	.9994	.63	.0017	.8311
2.50	264	10.35	1.0001	.38	-.0002	.9986
	400	6.72	1.0000	.70	.0000	1.0000
2.25	264	9.16	1.0000	.38	-.0001	.9994
	400	5.67	1.0000	.70	.0000	1.0000
2.00	264	8.04	1.0000	.38	.0000	1.0000
	400	4.70	1.0000	.69	.0000	1.0000
1.75	264	7.28	1.0000	.36	.0000	1.0008
	400	4.06	1.0000	.67	.0000	1.0000
1.50	264	7.23	.9999	.34	.0001	1.0017
	400	4.13	1.0000	.64	.0000	1.0000
1.00	264	9.37	.9997	.28	.0004	1.0042
	400	6.49	1.0000	.56	.0000	1.0000

(a) Grid: 1 Interpolation scheme: 3P-LI3

S	$\sigma_0$	$\phi \cdot m$	$\mu_0$	e	$\mu_x$	$\mu_{xx}$
10.00	264	2063.32	20.6851	373.12	-53.4234	*****
	400	411.70	1.4133	48617.53	-1.0532	158.6701
5.00	264	1033.20	3.9576	*****	-8.3482	70151.5469
	400	127.09	1.2091	254.50	-.5891	70.5619
2.50	264	21.27	.9992	1.68	.0022	.5074
	400	6.62	.9999	1.34	.0003	.9740
2.25	264	15.67	1.0000	1.45	.0000	.9752
	400	5.19	1.0000	1.29	.0001	.9951
2.00	264	11.39	1.0000	1.31	-.0001	1.0068
	400	3.96	1.0000	1.23	.0000	.9988
1.75	264	8.02	.9999	1.18	.0000	1.0023
	400	2.87	1.0000	1.17	.0000	.9993
1.50	264	5.30	.9999	1.05	.0001	1.0016
	400	1.91	1.0000	1.11	.0000	.9992
1.00	264	2.55	.9997	.81	.0004	1.0032
	400	.55	.9999	1.00	.0001	.9987

(b) Grid: 1 Interpolation scheme: 5P-HL3

Table 4.9. - Accuracy measures for the BMC solution of the uniform advection of a Gauss-hill in irregular grids ( $u=0.5$  ;  $t=T=9600$ ;  $N=100$ )

S	$\sigma_0$	$\phi \cdot m$	$\mu_0$	e	$\mu_x$	$\mu_{xx}$
10.00	264	13.94	1.0983	.12	-.1109	9.3232
	400	11.99	1.0390	.27	-.0423	2.0206
5.00	264	12.27	.9920	.10	.0110	2.3045
	400	10.43	.9728	.25	.0413	1.6832
2.50	264	9.92	1.0000	.19	.0000	1.7844
	400	7.28	1.0000	.42	.0000	1.3417
2.25	264	9.50	1.0000	.21	.0000	1.7064
	400	6.78	1.0000	.46	.0000	1.3073
2.00	264	9.04	.9999	.24	.0001	1.6068
	400	6.26	1.0000	.50	.0000	1.2699
1.75	264	8.65	1.0005	.27	-.0005	1.5432
	400	5.81	1.0004	.54	-.0004	1.2357
1.50	264	8.45	.9998	.30	.0003	1.3997
	400	5.57	.9984	.58	.0017	1.1377
1.00	264	9.37	.9997	.28	.0004	1.0042
	400	6.49	1.0000	.56	.0000	1.0000

(c) Grid: 2 Interpolation scheme: 3P-LI3

S	$\sigma_0$	$\phi \cdot m$	$\mu_0$	e	$\mu_x$	$\mu_{xx}$
10.00	264	7.95	1.0252	.40	-.0272	1.3759
	400	4.40	.0000	.71	.0000	.0000
5.00	264	7.27	1.0167	.46	-.0249	1.1682
	400	3.53	.9976	.78	.0038	.9875
2.50	264	4.79	1.0000	.62	.0000	1.0016
	400	1.75	1.0000	.91	.0000	.9999
2.25	264	4.37	1.0000	.67	.0000	.9997
	400	1.48	1.0000	.93	.0000	.9999
2.00	264	3.86	1.0000	.71	.0000	.9980
	400	1.17	1.0000	.95	.0000	1.0006
1.75	264	3.19	1.0001	.77	-.0001	1.0070
	400	.85	1.0000	.98	.0000	1.0008
1.50	264	2.37	.9998	.84	.0002	.9940
	400	.56	1.0000	1.00	.0000	1.0011
1.00	264	2.55	.9997	.81	.0004	1.0032
	400	.55	.9999	1.00	.0001	.9987

(d) Grid: 2 Interpolation scheme: 5P-HL3

Table 4.9. - Cont.

S	$\sigma_0$	$\phi \cdot m$	$\mu_0$	e	$\mu_x$	$\mu_{xx}$
1.03	264	8.97	1.0000	.26	-.0007	1.5017
	400	6.09	1.0000	.53	-.0007	1.2185
1.02	264	8.49	1.0000	.30	-.0003	1.3371
	400	5.58	1.0000	.58	-.0003	1.1468
1.01	264	11.46	.9996	.22	.0006	1.0063
	400	5.68	1.0000	.59	-.0001	1.0802
1.00	264	9.37	.9997	.28	.0004	1.0042
	400	6.49	1.0000	.56	.0000	1.0000

(e) Grid: 3 Interpolation scheme: 3P-LI3

S	$\sigma_0$	$\phi \cdot m$	$\mu_0$	e	$\mu_x$	$\mu_{xx}$
1.03	264	3.15	1.0000	.79	.0000	1.0098
	400	.83	1.0000	.98	.0000	1.0036
1.02	264	2.32	1.0000	.86	.0000	1.0035
	400	.49	1.0000	1.00	.0000	1.0014
1.01	264	1.94	1.0000	.88	.0000	1.0008
	400	.40	1.0000	1.01	.0000	1.0001
1.00	264	2.55	.9997	.81	.0004	1.0032
	400	.55	.9999	1.00	.0001	.9987

(f) Grid: 3 Interpolation scheme: 5P-HL3



S	$\sigma_0$	$\phi \cdot m$	$\mu_0$	e	$\mu_x$	$\mu_{xx}$
10.00	264	13.23	1.1577	.18	-.2160	20.1242
	400	11.37	1.0097	.28	-.0137	.9561
5.00	264	12.30	1.1138	.19	-.1587	10.5447
	400	10.18	1.0070	.33	-.0104	.9556
2.50	264	10.77	1.0513	.23	-.0743	2.7430
	400	8.26	1.0032	.43	-.0052	.9687
2.25	264	10.88	1.0418	.21	-.0513	2.4784
	400	8.20	1.0026	.43	-.0026	1.0059
2.00	264	10.56	1.0317	.22	-.0383	1.9215
	400	7.83	1.0020	.46	-.0019	1.0065
1.75	264	10.20	1.0214	.23	-.0251	1.4967
	400	7.43	1.0013	.48	-.0011	1.0067
1.50	264	9.62	1.0115	.26	-.0182	1.0115
	400	6.85	1.0007	.53	-.0015	.9872
1.00	264	9.37	.9997	.28	.0004	1.0042
	400	6.49	1.0000	.56	.0000	1.0000

(g) Grid: 4

Interpolation scheme: 3P-LI3

S	$\sigma_0$	$\phi \cdot m$	$\mu_0$	e	$\mu_x$	$\mu_{xx}$
10.00	264	14.32	1.0617	.76	-.0834	2.2643
	400	7.64	1.0031	.98	-.0034	.7870
5.00	264	10.84	1.0472	.78	-.0650	1.3268
	400	5.12	1.0029	1.00	-.0042	.9505
2.50	264	5.98	1.0254	.83	-.0365	1.3571
	400	2.18	1.0016	1.01	-.0024	.9866
2.25	264	4.89	1.0109	.82	-.0128	1.0552
	400	1.73	1.0005	1.01	-.0004	.9940
2.00	264	4.15	1.0078	.82	-.0090	1.0197
	400	1.38	1.0003	1.01	-.0002	.9950
1.75	264	3.47	1.0046	.82 <sup>2</sup>	-.0050	1.0019
	400	1.04	1.0002	1.00	.0000	.9965
1.50	264	3.03	1.0070	.83	-.0106	1.0646
	400	.80	1.0004	1.00	-.0008	.9971
1.00	264	2.55	.9997	.81	.0004	1.0032
	400	.55	.9999	1.00	.0001	.9987

(h) Grid: 4

Interpolation scheme: 5P-HL3

Table 4.9. - Cont.

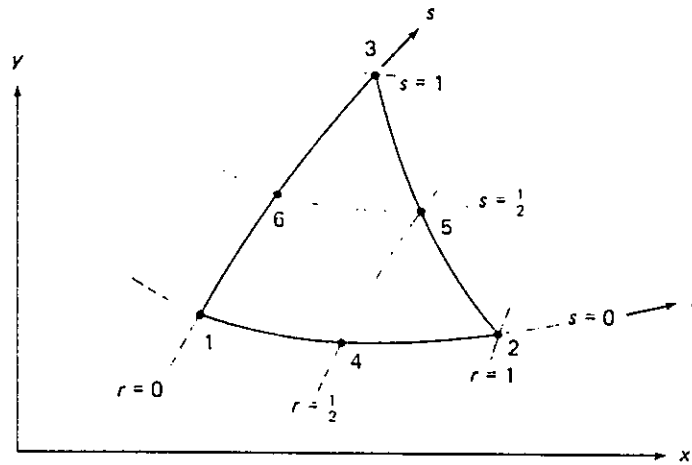
S	$\sigma_0$	$\phi \cdot m$	$\mu_0$	e	$\mu_x$	$\mu_{xx}$
10.00	264	8.45	.9998	.30	.0003	1.3997
	400	12.73	.0000	.33	.0000	.0000
5.00	264	14.09	.9999	.15	.0003	1.0080
	400	12.33	1.0000	.37	.0000	1.0000
2.50	264	13.03	.9997	.18	.0006	1.0077
	400	10.84	1.0000	.42	.0000	1.0000
2.25	264	12.78	.9996	.19	.0006	1.0075
	400	10.51	1.0000	.43	.0000	1.0000
2.00	264	12.46	.9996	.20	.0006	1.0073
	400	10.09	1.0000	.44	.0000	1.0000
1.75	264	12.04	.9996	.21	.0006	1.0068
	400	9.56	1.0000	.46	.0000	1.0000
1.50	264	11.46	.9996	.22	.0006	1.0063
	400	8.85	1.0000	.48	.0000	1.0000
1.00	264	9.37	.9997	.28	.0004	1.0042
	400	6.49	1.0000	.56	.0000	1.0000

(i) Grid: 5 Interpolation scheme: 3P-LI3

S	$\sigma_0$	$\phi \cdot m$	$\mu_0$	e	$\mu_x$	$\mu_{xx}$
10.00	264	.00	.0000	.00	.0000	.0000
	400	.00	.0000	.00	.0000	.0000
5.00	264	5.77	.9999	.57	.0002	1.0015
	400	2.54	.9998	.87	.0002	.9948
2.50	264	4.83	.9997	.61	.0005	1.0038
	400	1.92	.9999	.89	.0001	.9965
2.25	264	4.62	.9997	.62	.0005	1.0040
	400	1.78	.9999	.89	.0001	.9968
2.00	264	4.35	.9997	.63	.0005	1.0042
	400	1.62	.9999	.90	.0001	.9971
1.75	264	4.02	.9996	.65	.0005	1.0043
	400	1.41	.9999	.91	.0001	.9974
1.50	264	3.58	.9996	.68	.0005	1.0042
	400	1.14	.9999	.93	.0001	.9978
1.00	264	2.55	.9997	.81	.0004	1.0032
	400	.55	.9999	1.00	.0001	.9987

(j) Grid: 5 Interpolation scheme: 5P-HL3





(a) Reference sketch

Include only if node  $i$  is defined

		$i = 4$	$i = 5$	$i = 6$
$h_1 =$	$1-r-s$	$-\frac{1}{2}h_4$	.....	$-\frac{1}{2}h_6$
$h_2 =$	$r$	$-\frac{1}{2}h_4$	$-\frac{1}{2}h_5$	
$h_3 =$	$s$	.....	$-\frac{1}{2}h_5$	$-\frac{1}{2}h_6$
$h_4 =$	$4r(1-r-s)$			
$h_5 =$	$4rs$			
$h_6 =$	$4s(1-r-s)$			

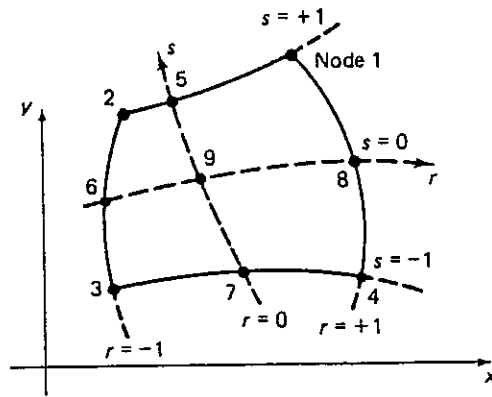
(b) Interpolation functions

$$f(r,s) = \sum_{i=1}^N h_i f_i \quad (N = \text{number of nodes})$$

(c) Interpolation formula

Table 4.10. Standard interpolation functions and isoparametric mappings for triangular elements

[adapted from BATHE 1982]



(a) Reference sketch

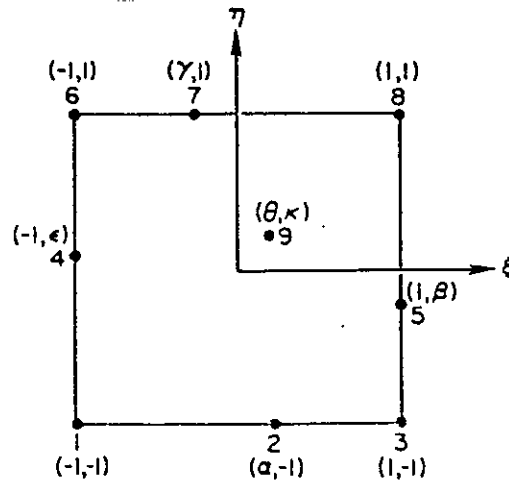
	Include only if node <i>i</i> is defined				
	<i>i</i> = 5	<i>i</i> = 6	<i>i</i> = 7	<i>i</i> = 8	<i>i</i> = 9
$h_1 = \frac{1}{4}(1+r)(1+s)$	$-\frac{1}{2}h_5$	.....	.....	$-\frac{1}{2}h_8$	$-\frac{1}{4}h_9$
$h_2 = \frac{1}{4}(1-r)(1+s)$	$-\frac{1}{2}h_5$	$-\frac{1}{2}h_6$	.....	.....	$-\frac{1}{4}h_9$
$h_3 = \frac{1}{4}(1-r)(1-s)$	.....	$-\frac{1}{2}h_6$	$-\frac{1}{2}h_7$	.....	$-\frac{1}{4}h_9$
$h_4 = \frac{1}{4}(1+r)(1-s)$	.....	.....	$-\frac{1}{2}h_7$	$-\frac{1}{2}h_8$	$-\frac{1}{4}h_9$
$h_5 = \frac{1}{2}(1-r^2)(1+s)$	.....	.....	.....	.....	$-\frac{1}{2}h_9$
$h_6 = \frac{1}{2}(1-s^2)(1-r)$	.....	.....	.....	.....	$-\frac{1}{2}h_9$
$h_7 = \frac{1}{2}(1-r^2)(1-s)$	.....	.....	.....	.....	$-\frac{1}{2}h_9$
$h_8 = \frac{1}{2}(1-s^2)(1+r)$	.....	.....	.....	.....	$-\frac{1}{2}h_9$
$h_9 = (1-r^2)(1-s^2)$	.....	.....	.....	.....	.....

(b) Interpolation functions

$$f(r,s) = \sum_{i=1}^N h_i f_i \quad (N = \text{number of nodes})$$

(c) Interpolation formula

Table 4.11. Standard interpolation functions and isoparametric mappings for quadrangular elements



(a) Reference sketch

Node co-ordinates ( $\xi_i, \eta_i$ )	$\phi_i$	Basis function
$(-1, -1)$	$\phi_1$	$\frac{1}{4}(1-\xi)(1-\eta) \left[ \frac{(1+\alpha)(1+\epsilon) - (1+\alpha)(1+\eta) - (1+\epsilon)(1+\xi)}{(1+\alpha)(1+\epsilon)} \right]$
$(\alpha, -1)$	$\phi_2$	$\frac{1}{2}(1-\eta) \left[ \frac{1-\xi^2}{1-\alpha^2} \right]$
$(1, -1)$	$\phi_3$	$\frac{1}{4}(1+\xi)(1-\eta) \left[ \frac{(1-\alpha)(1+\beta) - (1-\alpha)(1+\eta) - (1+\beta)(1-\xi)}{(1-\alpha)(1+\beta)} \right]$
$(1, \beta)$	$\phi_5$	$\frac{1}{2}(1+\xi) \left[ \frac{1-\eta^2}{1-\beta^2} \right]$
$(1, 1)$	$\phi_8$	$\frac{1}{4}(1+\xi)(1+\eta) \left[ \frac{(1-\gamma)(1-\beta) - (1-\gamma)(1-\eta) - (1-\beta)(1-\xi)}{(1-\gamma)(1-\beta)} \right]$
$(\gamma, 1)$	$\phi_7$	$\frac{1}{2}(1+\eta) \left[ \frac{1-\xi^2}{1-\gamma^2} \right]$
$(-1, 1)$	$\phi_6$	$\frac{1}{4}(1-\xi)(1+\eta) \left[ \frac{(1+\gamma)(1-\epsilon) - (1+\gamma)(1-\eta) - (1-\epsilon)(1+\xi)}{(1+\gamma)(1-\epsilon)} \right]$
$(-1, \epsilon)$	$\phi_4$	$\frac{1}{2}(1-\xi) \left[ \frac{1-\eta^2}{1-\epsilon^2} \right]$
$(\theta, \kappa)$	$\phi_9$	$\frac{(1-\xi^2)(1-\eta^2)}{(1-\theta^2)(1-\kappa^2)}$

(b) Interpolation functions

$$f(\xi, \eta) = \sum_{i=1}^N \phi_i f_i \quad (N = \text{number of nodes})$$

(c) Interpolation formula

Table 4.12. Improved interpolation functions and isoparametric mappings for 9-nodes quadrangular elements

Scheme	1-D		2-D	
	Nodes	Operations	Nodes	Operations
2P-LI2	2	4	4	12
3P-LI3	3	12	9	48
4P-LI4	4	24	16	120
4P-LR2	4	24	16	120
5P-LR3	5	40	25	240
6P-LR2	6	60	36	420
8P-LR2	8	112	64	1008
4P-HL2	4	24	16	120
5P-HL3	5	30	25	180
6P-PL2	6	36	36	252
7P-HL2	7	42	49	336
8P-PL2	8	48	64	432

Table 4.13 - Number of nodes and operations associated to alternative interpolation schemes (uniform grids)

Scheme	$\phi$	$\phi_0$	$\mu_0$	$\mu_x$	$\mu_{xx}$
3P-LI3	0.1415E-01	0.1068E-01	0.9997	0.0004	1.0040
5P-LR3	0.5656E-02	0.1700E-02	0.9998	0.0003	1.0030
5P-HL3	0.3857E-02	0.7841E-03	0.9997	0.0004	1.0040
8P-PL2	0.1857E-02	0.1835E-03	1.0000	0.0000	1.0000

(a) Pe= Di=0.0

Scheme	$\phi$	$\phi_0$	$\mu_0$	$\mu_x$	$\mu_{xx}$
3P-LI3	0.1272E-01	0.8344E-02	0.9997	0.0004	1.0040
5P-LR3	0.4673E-02	0.1123E-02	0.9998	0.0003	1.0030
5P-HL3	0.3040E-02	0.4728E-03	0.9997	0.0004	1.0030
8P-PL2	0.1435E-02	0.1060E-03	1.0000	0.0000	1.0000

(b) Pe=200 Di=0.0012

Scheme	$\phi$	$\phi_0$	$\mu_0$	$\mu_x$	$\mu_{xx}$
3P-LI3	0.5912E-02	0.1493E-02	0.9997	0.0004	1.0020
5P-LR3	0.1207E-02	0.6220E-04	0.9998	0.0003	1.0010
5P-HL3	0.5345E-03	0.1230E-04	0.9997	0.0004	1.0010
8P-PL2	0.4726E-03	0.9608E-05	1.0000	0.0000	1.0000

(c) Pe=20 Di=0.012

Scheme	$\phi$	$\phi_0$	$\mu_0$	$\mu_x$	$\mu_{xx}$
3P-LI3	0.2062E-03	0.1148E-05	0.9998	0.0003	1.0000
5P-LR3	0.3561E-04	0.3493E-07	0.9998	0.0003	1.0000
5P-HL3	0.6245E-04	0.1062E-06	0.9998	0.0003	1.0000
8P-PL2	0.2411E-04	0.1585E-07	1.0000	0.0000	1.0000

(d) Pe=2 Di=0.12

Table 5.1. Accuracy measures for the transport of a Gauss-hill in an uniform flow. An illustration of the dependence on Pe ( $Cu=0.24$ ;  $N=100$ ;  $\sigma_0/\Delta x=1.32$ ;  $t=T=9600$ )



N	$\phi$	$\phi_D$	$\mu_0$		$\mu_{xx}$
10	0.21112E-03	0.8844E-06	0.9999	*	1.0010
50	0.22979E-03	0.4768E-06	0.9999	**	1.0010
100	0.22539E-03	0.7114E-06	0.9999	**	1.0010
500	0.22603E-03	0.9474E-06	0.9999	**	1.0010
1000	0.22699E-03	0.9801E-06	0.9999	**	1.0010
10000	0.2715E-03	0.1010E-05	0.9999	*	1.0010

(a) Pe=0 Di=1.2/N Cu=0

N	$\phi$	$\phi_D$	$\mu_0$	$\mu_x$	$\mu_{xx}$
10	0.1014E-02	0.3889E-04	0.9998	0.0003	1.0010
50	0.4471E-02	0.0506E-03	0.9998	0.0003	1.0010
100	0.5912E-02	0.1493E-02	0.9997	0.0004	1.0020
500	0.6922E-02	0.2051E-02	0.9997	0.0004	1.0020
1000	0.7042E-02	0.2123E-02	0.9997	0.0004	1.0020
10000	0.7149E-02	0.2188E-02	0.9997	0.0004	1.0020

(b) Pe=20 Di=1.2/N Cu=24/N

N	$\phi$	$\phi_D$	$\mu_0$	$\mu_x$	$\mu_{xx}$
10	0.4736E-02	0.1047E-02	0.9998	0.0003	1.0030
50	0.1167E-01	0.7225E-02	0.9998	0.0003	1.0030
100	0.1415E-01	0.1068E-01	0.9997	0.0004	1.0040
500	0.1577E-01	0.1327E-01	0.9996	0.0005	1.0050
1000	0.1595E-01	0.1359E-01	0.9996	0.0005	1.0050
10000	0.1611E-01	0.1387E-01	0.9996	0.0005	1.0050

(c) Pe=∞ Di=0 Cu=24/N

N	$\phi$	$\phi_D$	$\mu_0$	$\mu_x$	$\mu_{xx}$
10	0.4361E-00	0.5247E-05	0.9998	0.0003	0.9996
50	0.1844E-03	0.9227E-06	0.9998	0.0003	1.0000
100	0.2062E-03	0.1148E-05	0.9998	0.0003	1.0000
500	0.2037E-03	0.1117E-05	0.9998	0.0003	1.0000
1000	0.2024E-03	0.1103E-05	0.9998	0.0003	1.0000
10000	0.2012E-03	0.1089E-05	0.9998	0.0002	1.0000

(d) Pe=2 Di=12/N Cu=24/N

Table 5.2. Accuracy measures for the transport of a Gauss-hill in a uniform flow, using the 3P-PLI3. An illustration of the dependence on N, for different Pe, Cu, Di ( $\sigma_0/\Delta x=1.32$ ;  $t=T=9600$ )

N	$\phi$	$\phi_0$	$\mu_0$		$\mu_{xx}$
10	0.44800E-03	0.65976E-05	0.99999	*	1.00000
50	0.79511E-04	0.20751E-06	0.99999	*	1.00000
100	0.37222E-04	0.35677E-07	0.99999	*	1.00000
500	0.25228E-04	0.13508E-08	0.99999	*	1.00000
1000	0.27041E-04	0.35099E-08	0.99999	*	1.00000
10000	0.29711E-04	0.67651E-08	0.99999	*	1.00000

(e) Pe=0 Di=6/N Cu=0

N	$\phi$	$\phi_0$	$\mu_0$		$\mu_{xx}$
10	0.45451E-03	0.56988E-05	0.99999	*	1.00000
50	0.87277E-04	0.21266E-06	0.99999	*	1.00000
100	0.41477E-04	0.47988E-07	0.99999	*	1.00000
500	0.09322E-05	0.74888E-09	0.99999	*	1.00000
1000	0.82188E-05	0.12766E-09	0.99999	*	1.00000
10000	0.96553E-05	0.50366E-09	0.99999	*	1.00000

(f) Pe=0 Di=12/N Cu=0

N	$\phi$	$\phi_0$	$\mu_0$	$\mu_x$	$\mu_{xx}$
10	0.39488E-02	0.71077E-03	0.99998	0.00003	1.00030
50	0.10344E-01	0.54977E-02	0.99998	0.00003	1.00030
100	0.12722E-01	0.83444E-02	0.99997	0.00004	1.00040
500	0.14228E-01	0.10544E-01	0.99997	0.00005	1.00040
1000	0.14466E-01	0.10888E-01	0.99996	0.00005	1.00040
10000	0.14622E-01	0.11044E-01	0.99996	0.00005	1.00050

(g) Pe=200 Di=0.12/N Cu=24/N

Table 5.2. Cont.

N	$\phi$	$\phi_0$	$\mu_0$		$\mu_{xx}$
10	0.1402E-03	0.8844E-06	0.9999	*	1.0010
50	0.1209E-03	0.4768E-06	0.9999	*	1.0010
100	0.1432E-03	0.7114E-06	0.9999	*	1.0010
500	0.1622E-03	0.9474E-06	0.9999	*	1.0010
1000	0.1646E-03	0.9801E-06	0.9999	*	1.0010
10000	0.1668E-03	0.1010E-05	0.9999	*	1.0010

(a) Pe=0 Di=1.2/N Cu=0

N	$\phi$	$\phi_0$	$\mu_0$	$\mu_x$	$\mu_{xx}$
10	0.1193E-03	0.5031E-06	0.9998	0.0002	1.0010
50	0.8758E-03	0.3257E-04	0.9999	0.0002	1.0010
100	0.1207E-02	0.6220E-04	0.9998	0.0003	1.0010
500	0.1424E-02	0.8683E-04	0.9997	0.0004	1.0020
1000	0.1448E-02	0.8974E-04	0.9997	0.0004	1.0020
10000	0.1468E-02	0.9232E-04	0.9997	0.0004	1.0020

(b) Pe=20 Di=1.2/N Cu=24/N

N	$\phi$	$\phi_0$	$\mu_0$	$\mu_x$	$\mu_{xx}$
10	0.1785E-02	0.1393E-03	0.9998	0.0002	1.0020
50	0.4642E-02	0.1136E-02	0.9999	0.0002	1.0020
100	0.5656E-02	0.1700E-02	0.9998	0.0003	1.0030
500	0.6252E-02	0.2083E-02	0.9997	0.0005	1.0030
1000	0.6314E-02	0.2125E-02	0.9996	0.0005	1.0030
10000	0.6367E-02	0.2161E-02	0.9996	0.0005	1.0030

(c) Pe= $\infty$  Di=0 Cu=24/N

Table 5.3. Accuracy measures for the transport of a Gauss-hill in a uniform flow, using the 5P-LR3. An illustration of the dependence on N, for different Pe, Cu, Di ( $\sigma_0/\Delta x=1.32$ ;  $t=T=9600$ )

N	$\phi$	$\phi_D$	$\mu_0$	$\mu_x$	$\mu_{xx}$
10	0.4543E-03	0.5663E-05	0.9998	0.0003	0.9996
50	0.8432E-04	0.1953E-06	0.9999	0.0002	1.0000
100	0.3561E-04	0.3493E-07	0.9998	0.0003	1.0000
500	0.6804E-05	0.1253E-08	0.9998	0.0002	1.0000
1000	0.9881E-05	0.2638E-08	0.9998	0.0002	1.0000
10000	0.1347E-04	0.4922E-08	0.9998	0.0002	1.0000

(d)  $Pe=2$        $Di=12/N$        $Cu=24/N$

N	$\phi$	$\phi_D$	$\mu_0$	$\mu_x$	$\mu_{xx}$
10	0.1399E-02	0.8401E-04	0.9998	0.0002	1.0020
50	0.3778E-02	0.7287E-03	0.9999	0.0002	1.0020
100	0.4673E-02	0.1123E-02	0.9998	0.0003	1.0030
500	0.5206E-02	0.1398E-02	0.9997	0.0004	1.0030
1000	0.5261E-02	0.1428E-02	0.9997	0.0005	1.0030
10000	0.5309E-02	0.1454E-02	0.9996	0.0005	1.0030

(e)  $Pe=200$        $Di=0.12/N$        $Cu=24/N$

Table 5.3. Cont.

N	$\phi$	$\phi_D$	$\mu_0$		$\mu_{xx}$
10	0.1567E-03	0.8844E-06	0.9999	*	1.0010
50	0.1158E-03	0.4768E-06	0.9999	*	1.0010
100	0.1361E-03	0.7114E-06	0.9999	*	1.0010
500	0.1541E-03	0.9474E-06	0.9999	*	1.0010
1000	0.1564E-03	0.9801E-06	0.9999	*	1.0010
10000	0.1585E-03	0.1010E-05	0.9999	*	1.0010

(a) Pe=0      Di=1.2/N      Cu=0

N	$\phi$	$\phi_D$	$\mu_0$	$\mu_x$	$\mu_{xx}$
10	0.2037E-03	0.1653E-05	0.9998	0.0003	1.0010
50	0.5439E-03	0.1246E-04	0.9998	0.0003	1.0010
100	0.5345E-03	0.1230E-04	0.9997	0.0004	1.0010
500	0.1053E-02	0.4812E-04	0.9997	0.0004	1.0020
1000	0.1140E-02	0.5632E-04	0.9997	0.0004	1.0020
10000	0.1220E-02	0.6451E-04	0.9997	0.0004	1.0020

(b) Pe=20      Di=1.2/N      Cu=24/N

N	$\phi$	$\phi_D$	$\mu_0$	$\mu_x$	$\mu_{xx}$
10	0.1233E-02	0.5564E-04	0.9998	0.0003	1.0030
50	0.3049E-02	0.4748E-03	0.9998	0.0003	1.0030
100	0.3857E-02	0.7841E-03	0.9997	0.0004	1.0040
500	0.5598E-02	0.1677E-02	0.9996	0.0005	1.0050
1000	0.5848E-02	0.1831E-02	0.9996	0.0005	1.0050
10000	0.6075E-02	0.1977E-02	0.9996	0.0005	1.0050

(c) Pe=∞      Di=0      Cu=24/N

Table 5.4. Accuracy measures for the transport of a Gauss-hill in a uniform flow, using the 5P-HL3. An illustration of the dependence on N, for different Pe, Cu, Di ( $\sigma_0/\Delta x=1.32$ ;  $t=T=9600$ )

N	$\phi$	$\phi_0$	$\mu_0$	$\mu_x$	$\mu_{xx}$
10	0.4594E-03	0.5778E-05	0.9997	0.0003	0.9996
50	0.1077E-03	0.3165E-06	0.9998	0.0003	1.0000
100	0.6245E-04	0.1062E-06	0.9998	0.0003	1.0000
500	0.2719E-04	0.2004E-07	0.9998	0.0003	1.0000
1000	0.2324E-04	0.1464E-07	0.9998	0.0003	1.0000
10000	0.1994E-04	0.1077E-07	0.9998	0.0002	1.0000

(d) Pe=2 Di=12/N Cu=24/N

N	$\phi$	$\phi_0$	$\mu_0$	$\mu_x$	$\mu_{xx}$
10	0.9360E-03	0.3156E-04	0.9998	0.0003	1.0030
50	0.2393E-02	0.2843E-03	0.9998	0.0003	1.0020
100	0.3040E-02	0.4728E-03	0.9997	0.0004	1.0030
500	0.4584E-02	0.1090E-02	0.9997	0.0005	1.0040
1000	0.4809E-02	0.1200E-02	0.9996	0.0005	1.0040
10000	0.5014E-02	0.1305E-02	0.9996	0.0005	1.0040

(e) Pe=200 Di=0.12/N Cu=24/N

Table 5.4. Cont.

N	$\phi$	$\phi_D$	$\mu_0$		$\mu_{xx}$
10	0.9648E-04	0.3883E-06	1.0000	*	1.0000
50	0.3210E-03	0.4417E-05	1.0000	**	1.0000
100	0.3499E-03	0.5254E-05	1.0000	*	1.0000
500	0.3733E-03	0.5984E-05	1.0000	**	1.0000
1000	0.3764E-03	0.6083E-05	1.0000	*	1.0000
10000	0.3822E-03	0.6272E-05	0.9998	*	1.0000

(a) Pe=0 Di=1.2/N Cu=0

N	$\phi$	$\phi_D$	$\mu_0$	$\mu_x$	$\mu_{xx}$
10	0.1357E-03	0.7769E-06	1.0000	0.0000	1.0000
50	0.5172E-03	0.1151E-04	1.0000	0.0000	1.0000
100	0.4726E-03	0.9608E-05	1.0000	0.0000	1.0000
500	0.2473E-03	0.2638E-05	1.0000	0.0000	1.0000
1000	0.2680E-03	0.3182E-05	1.0000	0.0000	1.0000
10000	0.3138E-03	0.4266E-05	1.0000	0.0000	1.0000

(b) Pe=20 Di=1.2/N Cu=24/N

N	$\phi$	$\phi_D$	$\mu_0$	$\mu_x$	$\mu_{xx}$
10	0.6522E-03	0.2104E-04	1.0000	0.0000	1.0000
50	0.1900E-02	0.1920E-03	1.0000	0.0000	1.0000
100	0.1857E-02	0.1835E-03	1.0000	0.0000	1.0000
500	0.2113E-02	0.2400E-03	1.0000	0.0000	1.0000
1000	0.2443E-02	0.3212E-03	1.0000	0.0000	1.0000
10000	0.2820E-02	0.4311E-03	1.0000	0.0000	1.0000

(c) Pe=∞ Di=0 Cu=24/N

N	$\phi$	$\phi_D$	$\mu_0$	$\mu_x$	$\mu_{xx}$
10	0.3923E-03	0.4222E-05	1.0000	0.0000	0.9997
50	0.2152E-04	0.1277E-07	1.0000	0.0000	1.0000
100	0.2411E-04	0.1585E-07	1.0000	0.0000	1.0000
500	0.5427E-04	0.8057E-07	1.0000	0.0000	1.0000
1000	0.5753E-04	0.9856E-07	1.0000	0.0000	1.0000
10000	0.6836E-04	0.9969E-07	1.0000	0.0000	1.0000

(d) Pe=2 Di=12/N Cu=24/N

Table 5.5. Accuracy measures for the transport of a Gauss-hill in a uniform flow, using the 8P-PL2. An illustration of the dependence on N, for different Pe, Cu, Di ( $\phi_0/_x=1.32$ ;  $t=T=9600$ )

N	$\phi$	$\phi_0$	$\mu_0$		$\mu_{xx}$
10	0.33353E-03	0.3611E-05	1.00000	*	1.00000
50	0.3566E-04	0.4001E-07	1.00000	*	1.00000
100	0.3261E-04	0.2170E-06	1.00000	*	1.00000
500	0.1283E-03	0.4620E-06	1.00000	*	1.00000
1000	0.1251E-03	0.5005E-06	1.00000	*	1.00000
10000	0.1310E-03	0.5407E-06	0.99990	*	0.99990

(e) Pe=0 Di=6/N Cu=0

N	$\phi$	$\phi_0$	$\mu_0$		$\mu_{xx}$
10	0.3937E-03	0.4253E-05	1.00000	*	1.00000
50	0.2826E-04	0.2201E-07	1.00000	*	1.00000
100	0.1770E-04	0.8531E-08	1.00000	*	1.00000
500	0.5456E-04	0.8143E-07	1.00000	*	1.00000
1000	0.5923E-04	0.9593E-07	1.00000	*	1.00000
10000	0.6467E-04	0.1144E-06	0.99990	*	0.99990

(f) Pe=0 Di=12/N Cu=0

N	$\phi$	$\phi_0$	$\mu_0$	$\mu_x$	$\mu_{xx}$
10	0.5747E-03	0.1616E-04	1.00000	0.00000	1.00000
50	0.1517E-02	0.1186E-03	1.00000	0.00000	1.00000
100	0.1435E-02	0.1060E-03	1.00000	0.00000	1.00000
500	0.1593E-02	0.1320E-03	1.00000	0.00000	1.00000
1000	0.1869E-02	0.1821E-03	1.00000	0.00000	1.00000
10000	0.2190E-02	0.2503E-03	1.00000	0.00000	1.00000

(g) Pe=200 Di=0.12/N Cu=24/N

Table 5.5. Cont.



Scheme	Number of time steps, N						Linear regression		
	10	50	100	500	1000	10000	a	b	p
3P-LI3	3.39	3.72	4.22	7.25	10.79	77.45	3.42	.0074	1.0000
5P-LR3	3.90	4.41	5.21	11.38	19.53	158.95	3.73	.0155	1.0000
5P-HL3	3.67	4.45	5.25	11.77	20.33	165.16	3.72	.0161	1.0000
8P-PL2	4.09	5.24	6.55	17.37	30.65	262.98	4.17	.0259	1.0000

(a) Pure advection

Scheme	Number of time steps, N						Linear regression		
	10	50	100	500	1000	10000	a	b	p
3P-LI3	3.75	4.34	5.58	13.77	24.18	198.51	3.84	.0195	1.0000
5P-LR3	3.86	5.23	5.75	14.03	24.05	204.25	3.93	.0200	1.0000
5P-HL3	3.89	4.72	5.75	14.28	24.39	202.93	3.99	.0199	1.0000
8P-PL2	3.98	4.83	5.41	10.91	16.46	126.23	4.26	.0122	1.0000

(b) Pure diffusion

Scheme	Number of time steps, N						Linear regression		
	10	50	100	500	1000	10000	a	b	p
3P-LI3	3.87	4.80	6.21	17.31	30.63	273.13	3.61	.0270	1.0000
5P-LR3	4.00	5.58	7.18	21.77	40.20	357.15	4.00	.0353	1.0000
5P-HL3	3.98	5.54	7.37	22.32	41.79	366.93	4.12	.0363	1.0000
8P-PL2	4.33	5.83	8.30	24.29	43.36	384.54	4.58	.0380	1.0000

(c) Advection-diffusion

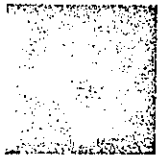
Note: Observed CPU times were adjusted through linear regression to the straight line  $cost = a + b * N$ , with correlation coefficient  $p$ . Program MINQUA by E. Oliveira, from LNEC/DH/NET, was used.

Table 5.6. CPU times (seconds) for the solution of the advection-diffusion reference problem

## APPENDIX A

REFERENCE TEST PROBLEMS AND ACCURACY MEASURES FOR  
THE CONVECTION-DIFFUSION FORUM, HELD DURING THE VI  
INTERNATIONAL CONFERENCE ON FINITE ELEMENTS IN  
WATER RESOURCES





VI International Conference on  
**Finite Elements in  
WATER RESOURCES**

**REFERENCE PROBLEMS FOR THE CONVECTION-DIFFUSION FORUM**

Document prepared by

António Melo Baptista,

Laboratório Nacional de Engenharia Civil, Portugal

October 1985

Proc. 64/13/7398

A-3



## REFERENCE PROBLEMS FOR THE CONVECTION-DIFFUSION FORUM

### 1 - INTRODUCTION

Several numerical methods have been proposed for the solution of the convection-diffusion equation. None has proved fully satisfactory, and many exhibit quite poor performances for convection-dominated problems.

A systematic comparison of available methods is felt to be a very important step to enhance further improvements. Such comparison, which constitutes a gigantic task for any individual, could be made much easier and efficient if a common reference framework was widely adopted by the technical community to demonstrate the performance of alternative methods.

The Convection-Diffusion Forum is intended to contribute to the setting-up of such a reference framework, and, in parallel, to assess the state-of-the-art in numerical modeling of the convection-dominated convection-diffusion equation.

The problems stated in the next sections are proposed as to be a starting point for a reference framework. The response of participants and the debate at the Forum will determine any further steps towards such framework.

Modellers are encouraged to use any general numerical technique to solve the proposed reference problems. To help the working group in analysing the different solutions, and preparing a comparative general report, modellers are, however, requested to closely follow the specifications for both inputs and outputs.

In addition (but not instead) modellers may present alternative outputs, or, if necessary to illustrate some important feature of their methods, even perform calculations with alternative parameters.

Modellers may elect to solve only a part of the proposed problems. The final document to be presented by each modeller should

include:

- (a) A short (about 1 page/method) but effective description of the adopted method(s), and reference to where detailed information is reported.
- (b) Fourier series analysis of the adopted method(s) -optional.
- (c) The solutions to the reference problems, as specified.
- (d) Eventual comments (e.g., on the general performance of the methods).

## 2 - PROBLEM SET #1 : TRANSPORT OF CONCENTRATION-HILLS IN UNIFORM FLOWS (1-D)

### 2.1 - General Aspects

This set of problems concerns the transport (convection-diffusion and pure-convection) of concentration-hills (a gauss and a triangle) by uniform (steady and unsteady, sinusoidal) flows.

The mathematical problem is governed by the equation

$$\frac{\partial c}{\partial t} + u \frac{\partial c}{\partial x} = D \frac{\partial^2 c}{\partial x^2} \quad \text{in } ]-\infty, +\infty[$$

with initial and boundary conditions

$$c(x,0) = c_0(x)$$

$$c(x,t) \rightarrow 0 \quad , \text{ as } |x| \rightarrow \infty$$

where

$c(x,t)$  - is the concentration field

$u$  - is the velocity field

$D$  - is a diffusion coefficient

$x, t$  - are space and time coordinates

$c_0(x)$  - is the initial concentration field, defined as:

. for the gauss-hill

$$c_0(x) = \exp\left(-\frac{(x-x_0)^2}{2\sigma_0^2}\right)$$

. for the triangle-hill

$$c_0(x) = \begin{cases} 1 - \frac{|x-x_0|}{l_0} & |x-x_0| < l_0 \\ 0 & \text{otherwise} \end{cases}$$

- $x_0$  - center of mass of the initial concentration field
- $l_0$  - half-length of the base of the triangle
- $\sigma_0$  - standard deviation of the initial concentration field

Relevant exact solutions are of the form:

. for the gauss-hill

$$c(x,t) = \frac{\sigma_0}{\sigma} \exp\left(-\frac{(x-\bar{x})^2}{2\sigma^2}\right)$$

with  $\sigma^2 = \sigma_0^2 + 2Dt$

$$\bar{x} = x_0 + \int_0^t u(\tau) d\tau$$

. for the triangle-hill, under pure convection ( $D = 0$ )

$$c(x,t) = c_0\left(x - \int_0^t u(\tau) d\tau\right)$$

Modellers should present their results, at the time indicated in section 2.2, in the form of:

- (a) A plot of the concentration profile (numerical results), covering a region of at least  $x - 6\sigma < x < x + 6\sigma^{(1)}$  and  $x - 2l_0 < x < x + 2l_0$  (for the gauss and the triangle, respectively). If any significant feature of the numerical solution (e.g., wiggles) extends outside these bounds, a larger region should be plotted as to display such feature. Concentrations at each node should be denoted by a mark (e.g., a "+"); additionally, a consistent interpolation may be used to display the (numerical) profile in a continuous form.  
Scales of the plot (units of problem/cm) should be: 200/1 horizontal<sup>(2)</sup> and 1/10 vertical
- (b) A table of  $x$  versus  $c(x)$ ; space coordinates should be written in format F6.0, and concentrations in format E10.4
- (c) The values of the accuracy measures of table 1, in format E10.4

(1) Except in problem 1C, where  $x-4\sigma < x < x+4\sigma$

(2) Except in problem 1C, where horizontal scale should be 400/1



Numerical solutions should be performed in 1-D grids<sup>(1)</sup>, referred to in each problem, and defined as follows:

. GRID 1 ( $x \in [0, 12800]$ )

$$x(i) = 200(i-1) \quad i = 1, 65$$

. GRID 2 ( $x \in [0, 12800]$ )

$$x(i) - x(i-1) = 200 - 75 \cos \frac{\pi(i-1)}{65} \quad i = 2, 65$$

where  $x(i)$  are the nodal coordinates.

The total length of the computational domain may be reduced (by changing the number of nodes, but not the nodal spacing), whenever appropriate.

## 2.2 - Specification of parameters

Units are omitted bellow, as any set of consistent units can be used

Problem 1 A:       $u = 0.5$   
                     $D = 0$   
                    grid: GRID 1  
                     $c_0(x)$ : gauss-hill, with  $x_0 = 2000$  and  $\sigma_0 = 264$   
                    boundary conditions: zero-concentration imposed in the upstream boundary; modelers are free to impose the downstream boundary condition in any consistent way

$$\Delta t = 96$$

results are requested at time 9600

Problem 1 B:      As in problem 1A, except that       $D = 2$   
Problem 1 C:      As in problem 1A, except that       $D = 50$   
Problem 1 D:      As in problem 1A, except that       $\sigma_0 = 320$   
Problem 1 E:      As in problem 1A. except that       $\sigma_0 = 400$

---

(1) If, because of code availability or otherwise, it becomes more convenient for the modeller to use a 2-D grid, he may do so, as long as he respects the specified nodal spacing in the x-direction. In this case, he should state the selected grid characteristics and transverse diffusion coefficient, and present table (b) in an extending version, covering all or a significant number of rows (to assess eventual transverse oscillations).

- Problem 1 F: As in problem 1A, except that  $u(t) = -1.50 \sin\left(\frac{2\pi t}{9600}\right)$ ; zero concentrations are imposed at the boundaries when the flow enters the domain; modellers are free to impose boundary conditions in any consistent way when the flow leaves the domain
- Problem 1 G: As in problem 1A, except that  $c_0(x)$  is a triangle-hill, with  $l_0 = 800$
- Problem 1 H: As in problem 1A, except that  $c_0(x)$  is a triangle-hill, with  $l_0 = 1000$
- Problem 1 I: As in problem 1A, except that GRID 2 should be used, and  $x_0$  should coincide with node 16
- Problem 1 J:  $u = 0.5$   
 $D = 0$   
 grid: GRID 1  
 $c_0(x)$ : gauss-hill, with  $x_0 = 600$  and  $\sigma_0 = 264$   
 boundary conditions: a concentration law
- $$c_u(t) = \exp\left(-\frac{(x_0 + ut)^2}{2\sigma_0^2}\right)$$
- is imposed at the upstream boundary; modellers are free to impose the downstream boundary condition in any consistent way
- $\Delta t = 96$   
 results are requested at time 9600
- Problem 1 K: As in problem A, except that  $\Delta t = 192$
- Problem 1 L: As in problem A, except that  $\Delta t = 960$

### 3 - PROBLEM SET #2: PURE CONVECTION OF A ROTATING CONCENTRATION-HILL (2-D)

#### 3.1 - Introduction

This set of problems concerns the transport by convection of concentration-hills (a gauss and a cone) in a flow in counterclockwise rigid body rotation.

The mathematical problem is governed by the equation

$$\frac{\partial c}{\partial t} + u \frac{\partial c}{\partial x} + v \frac{\partial c}{\partial y} = 0$$

with initial and boundary conditions

$$c(x, y, 0) = c_0(x, y)$$

$$c(x, y, t) \rightarrow 0 \quad \text{as } x^2 + y^2 \rightarrow \infty$$

where

$c(x, y, t)$  - is the concentration field

$u(y) = -\omega y$ , is the x- velocity

$v(x) = \omega x$ , is the y- velocity

$\omega$  - is the angular frequency of rotation

$c_0(x, y)$  - is the initial concentration field, defined as

. for the gauss-hill

$$c_0(x, y) = \exp \left( - \frac{(x-x_0)^2}{2\sigma_0^2} - \frac{(y-y_0)^2}{2\sigma_0^2} \right)$$

. for the cone-hill

$$c_0(x, y) = \begin{cases} 1 - \sqrt{\frac{(x-x_0)^2}{\bar{r}_0^2} + \frac{(y-y_0)^2}{\bar{r}_0^2}} & \text{if } (x-x_0)^2 + (y-y_0)^2 < \bar{r}_0^2 \\ 0 & \text{otherwise} \end{cases}$$

$x_0$  - center of mass of the initial concentration field

$\sigma_0$  - standard deviation of the initial concentration field (gauss)

$\bar{r}_0$  - radius of the initial concentration distribution (cone)

The exact solution is of the form

$$c(x, y, t) = c_0(x-ut, y-vt)$$

Modellers should present their results, at the time indicated in section 3.2, in the form of:

- (a) Plots of four concentration profiles (numerical results), passing by the instantaneous center of mass of the exact solution, and at least  $6\sigma_0$  or  $2\bar{r}_0$  long for each side of such center. One profile should be normal to the flow direction (relative to the instantaneous center of mass), the other parallel, and the remaining two at  $45^\circ$  angles. Scales (units of prob/cm): 200/1 hor.; 1/10 vert.

(b) A table of  $r$  versus  $c(r)$  for each of the above profiles ( $r$  in F7.1, and  $c(r)$  in E10.4).

(c) The values of the accuracy measures of table 2, in format E10.4.

Numerical solutions should be performed in 2-D grids, referred to in each problem, and defined as follows:

. GRID 3 ( $x, y \in [-3400, 3400]$ )

$$\begin{cases} x(i,j) = 200(i-1)-3400 & i = 1,35 \\ y(i,j) = 200(j-1)-3400 & j = 1,35 \end{cases}$$

. GRID 4 (with  $x(21,j) = y(i,21) = 0$ )

$$\begin{cases} x(i+1,j)-x(i,j) = 200-50 \cos \frac{\pi(i-1)}{35} & i = 1,35 \\ y(i,j+1)-y(i,j) = 200-50 \cos \frac{\pi(j-1)}{35} & j = 1,35 \end{cases}$$

where  $x(i,j)$ ,  $y(i,j)$  are the nodal coordinates (indices  $i$  and  $j$  refer to the  $x$ - and the  $y$ - directions, respectively). Any elements that fit these nodal coordinates may be used.

### 3.2 - Parameter specification

Problem 2 A:  $\omega = \frac{2\pi}{3000}$

grid: GRID 3

$c_0(x,y)$ : gauss-hill, with  $x_0=0$ ,  $y_0=-18000$ ,  $\sigma_0=264$

boundary conditions: zero concentration imposed

where flow enters the domain; modellers are free to specify any consistent boundary condition where flow leaves the domain

$\Delta t = 100$

results are requested after 1 revolution

Problem 2 B: As in problem 2A, except that a cone-hill, with  $r_0=800$ , should be used

Problem 2 C: As in problem 2A, except that GRID 4 should be used;  $(x_0, y_0)$  should coincide with node (21,11)

#### 4 - PROBLEM SET #3: ADVANCING FRONT (1-D)

##### 4.1 - General Aspects

In this set of problems the concentration field is imposed by a constant mass flux, specified through constant velocity and upstream concentration.

The mathematical problem is governed by the equation

$$\frac{\partial c}{\partial t} + u \frac{\partial c}{\partial x} = D \frac{\partial^2 c}{\partial x^2} \quad 0 \leq x < \infty$$

with initial and boundary conditions

$$\begin{aligned} c(x, 0) &= 0 & 0 \leq x < \infty \\ c(x, t) &= 1 & t > 0, x = 0 \\ c(x, t) & \rightarrow 0 & t > 0, x \rightarrow \infty \end{aligned}$$

where

$c(x, t)$  - is the concentration field  
 $u$  - is the velocity field  
 $D$  - is a diffusion coefficient  
 $x, t$  - are space and time coordinates

The exact solution is given by

$$c(x, t) = \frac{1}{2} \left( \operatorname{erfc} \left( \frac{x-ut}{2\sqrt{Dt}} \right) + \exp \left( \frac{ux}{D} \right) \operatorname{erfc} \left( \frac{x+ut}{2\sqrt{Dt}} \right) \right)$$

or, for  $D=0$ ,

$$c(x, t) = \begin{cases} 1 & x < ut \\ 0 & \text{otherwise} \end{cases}$$

Modellers should present their results, for time 9600, in the form of:

- (a) A plot of the concentration profile (numerical results), covering the relevant computational domain (scales: 200/1 horizontal and 1/10 vertical)<sup>(1)</sup>. Nodal concentrations should be denoted by a mark (e.g., a "+"); additionally, a consistent interpolation may be used to display the (numerical) profile in a continuous form.
- (b) A table of  $x$  versus  $c(x)$ ; space coordinates should be written in format F6.0, and concentration in format E10.4
- (c) The values of the accuracy measures of table 3, in format E10.4.

---

(1) Except in problem 3C, where the horizontal scale should be 400/1.  
Note: scales are defined as (units of problem/cm)

Numerical solutions should be performed in 1-D grids<sup>(1)</sup>, referred to in each problem, and defined as follows:

. GRID 5 ( $x \in [0, 12800]$ )

$$x(i) = 200(i-1) \quad i = 1, 65$$

. GRID 6 ( $x \in [0, 12800]$ )

$$x(i) - x(i-1) = 200 - 75 \cos \frac{\pi(i-1)}{65} \quad i = 2, 65$$

where  $x(i)$  are the nodal coordinates. The number of nodes may be reduced when appropriate

#### 4.2 - Specification of parameters

Problem 3 A:  $u = 0.5$

$$D = 0$$

grid: GRID 5

boundary conditions:  $c=1$  imposed in the upstream boundary; modellers are free to impose the downstream boundary condition in any consistent way

$$\Delta t = 96$$

Results requested at time 9600

Problem 3 B: As in probl. 3A, except that  $D = 2$

Problem 3 C: As in probl. 3A, except that  $D = 50$

Problem 3 D: As in probl. 3A, except that GRID 6 should be used.

Problem 3 E: As in probl. 3A, except that  $\Delta t = 960$

#### 5 - FINAL REMARKS

Many modellers (e.g., S.Newman, F.Holly Jr., P.Gresho, E. Varoglu, J.Benque, A. Baptista, etc.) have used the proposed or similar problems, in one form or another. The present document attempts to motivate a wide concensus on standard reference problems, with standard forms and standard accuracy measures.

The particular choices of problems and problem dimensionality, the range of controlling parameters (Peclet number, Courant number, dimensionless source size, etc.), the grid characteristics,

---

(1) Remarks made in Prob. Set #1 on 2-D grids apply

the selection of accuracy measures, etc, are by no means free of criticisms, and discussion and comments previous to and during the Forum are strongly encouraged.

It is hoped that the relatively large number of proposed parameter sets does not discourage modellers to present solutions. Modellers may decide to solve only a part of the proposed problems; in such cases, it is suggested that, within each problem, priority be given to the parameter sets with lower letters (a, b, etc).

Modellers are asked to specify the type of computer used, and the memory and CPU time requirements (optional).

**TABLES**





Table 1 - Definition of error measures for Problem 1

Symbol	Description	Definition	Comments	Value for Exact Solution
$\phi$	L-2 error norm, normalized by the total mass	$\phi(t) = \frac{1}{m(t)} \left( \int_{\Omega} [c^{nu}(x,t) - c^{ex}(x,t)]^2 dx \right)^{1/2}$	Integral measure of the overall error of the numerical solution	0
$\phi_D$	Discrete L-2 error norm, normalized by the total mass	$\phi_D(t) = \frac{1}{m(t)} \left\{ \sum_i [c_i^{nu}(t) - c_i^{ex}(x_i, t)]^2 \right\}^{1/2}$	Discrete integral measure of the overall error of the numerical solution	0
$\epsilon$	Error in the peak concentration, normalized by the exact peak concentration	$\epsilon(t) = \frac{c_{max}^{ex}(t) - c_{max}^{nu}(t)}{c_{max}^{ex}(t)}$	Point measure of the artificial damping of the numerical solution (numerical damping)	0
$\psi$	Absolute value of the maximum negative concentration, normalized by the exact peak concentration	$\psi(t) = \left  \frac{c_{max, neg}^{nu}(t)}{c_{max}^{ex}(t)} \right $	Point measure of the spurious oscillations in the numerical solution (wiggles)	0
$\xi$	Error in the position of the peak concentration, normalized by the exact travel distance	$\xi(t) = \frac{x_{max}^{ex}(t) - x_{max}^{nu}(t)}{ut}$	Point measure of the phase shift introduced in the numerical solution	0
$\mu_0$	0th moment of the concentration profile, normalized by the exact value	$\mu_0(t) = \frac{1}{m(t)} \int_{\Omega} c^{nu}(x,t) dx$	Integral measure of mass preservation	1

Table 1 - cont.

Symbol	Description	Definition	Comments	Value for Exact Solution
$\mu_x$	Error in the 1st moment of the concentration profile, normalized by the exact travel distance	$\mu_x(t) = \frac{E^{ex}(c,t) - E^{nu}(c,t)}{ut}$ <p>with</p> $E(c,t) = \frac{1}{m(t)} \int_{\Omega} xc(x,t)dx$	Integral measure of the phase shift introduced in the numerical solution	0
$\mu_{xx}$	Centered 2nd moment of the concentration profile, normalized by the exact value	$\mu_{xx}(c,t) = \frac{\int_{\Omega} [x - E^{nu}(c,t)]^2 c^{nu}(x,t) dx}{\int_{\Omega} [x - E^{ex}(c,t)]^2 c^{ex}(x,t) dx}$	Integral measure of the artificial spreading of the numerical solution (numerical spreading)	1

Table 2 - Definition of error measures for Problem 2

Symbol	Description	Definition	Comments	Value for Exact Solution
$\phi$	L-2 error norm, normalized by the total mass	$\phi(t) = \frac{1}{m(t)} \left\{ \int_{\Omega} [c^{nu}(r, \theta, t) - c^{ex}(r, \theta, t)]^2 r dr d\theta \right\}^{1/2}$	Integral measure of the overall error of the numerical solution	0
$\epsilon$	Error in the peak concentration normalized by the exact peak concentration	$\epsilon(t) = \frac{c_{max}^{ex}(t) - c_{max}^{nu}(t)}{c_{max}^{ex}(t)}$	Point measure of the artificial damping of the numerical solution (numerical damping)	0
$\psi$	Absolute value of the maximum negative concentration, normalized by the exact peak concentration	$\psi(t) = \left  \frac{c_{max, neg}^{nu}(t)}{c_{max}^{ex}(t)} \right $	Point measure of the spurious oscillations in the numerical solution (wiggles)	0
$\xi_r$	Normalized errors in the position of the peak concentration	$\xi_r(t) = \frac{r_0 - r_{max}^{nu}(t)}{r_0}$	Point measure of the phase shift introduced in the numerical solution	0
$\xi_\theta$		$\xi_\theta(t) = \frac{\theta_{max}^{ex}(t) - \theta_{max}^{nu}(t)}{2\pi(t/T)}$		
$\mu_0$	0th moment of the concentration profile, normalized by the exact value	$\mu_0(t) = \frac{1}{m(t)} \int_{\Omega} c^{nu}(r, \theta, t) r dr d\theta$	Integral measure of mass preservation	1
$\phi_D$	Discrete L-2 error norm, normalized by the total mass	$\phi_D(t) = \frac{1}{m(t)} \left\{ \sum_i c_i^{nu}(t) - c^{ex}(r_i, \theta_i, t) \right\}^2 \right\}^{1/2}$	Discrete integral measure of the overall error of the numerical solution	0

Symbol	Description	Definition	Comments	Value for Exact Solution
$\mu_r$	Normalized errors in the 1st moments of the concentration profile	$\mu_r(t) = \frac{E_r^{ex}(c,t) - E_r^{nu}(c,t)}{r_0}$ $\mu_\theta(t) = \frac{E_\theta^{ex}(c,t) - E_\theta^{nu}(c,t)}{2\pi(t/T)}$	Integral measure of the phase shift introduced in the numerical solution	0
$\mu_\theta$		with $E_r(c,t) = \frac{1}{m(t)} \int r c(r,\theta,t) r dr d\theta$ $E_\theta(c,t) = \frac{1}{m(t)} \int \theta c(r,\theta,t) r dr d\theta$		
$\mu_{rr}$	Centered 2nd moments of the concentration profile, normalized by the exact value	$\mu_{rr} = \frac{\Omega \int [r - E_r^{nu}(c,t)]^2 c^{nu}(r,\theta,t) r dr d\theta}{\Omega \int [r - E_r^{ex}(c,t)]^2 c^{ex}(r,\theta,t) r dr d\theta}$ $\mu_{\theta\theta} = \frac{\Omega \int [\theta - E_\theta^{nu}(c,t)]^2 c^{nu}(r,\theta,t) r dr d\theta}{\Omega \int [\theta - E_\theta^{ex}(c,t)]^2 c^{ex}(r,\theta,t) r dr d\theta}$	Integral measure of the artificial spreading of the numerical solution (numerical spreading)	1
$\mu_{\theta\theta}$				

Note:  $r, \theta$  are polar coordinates, with origin at the center of rotation of the flow

Table 3 - Definition of error measures for Problem 3

Symbol	Description	Definition	Comments	Value for Exact Solution
$\phi$	L-2 error norm, normalized by the total mass	$\phi(t) = \frac{1}{m(t)} \left( \int_{\Omega} [c^{nu}(x,y,t) - c^{ex}(x,y,t)]^2 dx dy \right)^{1/2}$	Integral measure of the overall error of the numerical solution	0
$\phi_D$	Discrete L-2 error norm, normalized by the total mass	$\phi_D(t) = \frac{1}{m(t)} \left( \sum_i [c_i^{nu}(t) - c^{ex}(x_i,t)]^2 \right)^{1/2}$	Discrete integral measure of the overall error of the numerical solution	0

1/1





# VI International Conference on Finite Elements in WATER RESOURCES

**Organizing Committee:**

**TECHNICAL**

A Sá da Costa  
IST - UTL, Portugal  
A. M. Baptista  
LNEC, Portugal  
C. A. Brebbia  
U. Southampton, UK  
W. G. Gray  
U. Notre Dame, USA  
G. F. Pinder  
Princeton U., USA

**EXECUTIVE:**

M. A. Falcão  
LNEC, Portugal  
A. Sá da Costa  
IST - UTL, Portugal  
A. M. Baptista  
LNEC, Portugal

73/71/77

Ref: CONVECTION-DIFFUSION FORUM

Dear Colleague :

A few misprints were brought to my attention, concerning the statement of the reference problems for the C-D Forum. They are listed below:

Page 1, line 6: "may when" should be "way when"

Page 3, line 15: " $x-6\sigma < x < x+6\sigma$ " should be " $\bar{x} - 6\sigma < x < \bar{x}+6\sigma$ "

Page 3, line 16: " $x-2l_0 < x < x+2l_0$ " should be " $\bar{x} - 2l_0 < x < \bar{x}+2l_0$ "

Page 7, line 19: " $y_0 = - 18000$ " should be " $y_0 = - 1800$ "

Table 2 : " $\phi_D(t) = \frac{1}{m(t)} \{ (\sum_i c_i^{nu}(t) - c^{ex}(x_i, \theta_i, t))^2 \}^{1/2}$ " should be

$$\phi_D(t) = \frac{1}{m(t)} \{ (\sum_i [c_i^{nu}(t) - c^{ex}(x_i, \theta_i, t)]^2 \}^{1/2}$$

I apologize for these misprints, and hope that they were not a cause of trouble.

Also, I was suggested that in Problem set #2, a smaller  $\Delta t$  should be considered, in order to allow methods that have Courant-criteria restrictions to be used. In order to accommodate this, I propose the following three additional problems:

Probl. 2D : Equal to problem 2A, except that  $\Delta t = 10$

Probl. 2E : Equal to problem 2B, except that  $\Delta t = 10$

Probl. 2F : Equal to problem 2C, except that  $\Delta t = 10$



Finally, please note that:

- $c_i^{\text{nu}}(t)$  is equivalent to  $c^{\text{nu}}(x_i, t)$  in Tables 1,3 and to  $c^{\text{nu}}(r_i, \theta_i, t)$  in Table 2.
- $m(t)$  denotes exact total mass, i.e.,

$$m(t) = \int_{\Omega} c^{\text{ex}}(x, t) dx \quad (\text{Tables 1,3})$$

$$m(t) = \int_{\Omega} c^{\text{ex}}(r, \theta, t) r dr d\theta \quad (\text{Table 2})$$

I look forward to your participation in the Forum.

Yours sincerely

Antônio Melo Baptista

Antônio Melo Baptista

APPENDIX B

A NOTE ON THE CIRCULATION MODELS TEA AND TEANL



## B.1 - Introduction

This Appendix describes fundamental concepts behind two 2-D (depth-averaged) tidal circulation models, TEA (WESTERINK et al. 1984) and TEANL (WESTERINK et al. 1985), that have been used as companions for the transport model ELA. No attempt is made to enter in the mathematical details, the reader interested in such details being referred to the original sources; emphasis is rather placed on a qualitative discussion of the frequency-domain approach adopted in these models.

## B.2 - Motivation and Concept

The well-known shallow-water equations, which often appropriately describe tidal circulation in coastal regions, involve both space and time derivatives.

Most available circulation models handle space-derivatives by a discrete technique, which is most often finite differences (FD) or finite elements (FE). Although both are suitable, FE seem more well-fitted to estuaries and coastal seas, by their superior versatility in grid discretization (which becomes extremely useful in representing irregularly shaped boundaries and in allowing local refinements in critical areas).

To handle time derivatives, most models adopt again the idea of discretization, solving the derivatives either by using some type of numerical integration scheme or by applying a combined space-time finite element scheme.

These "time-domain" models have been plagued with requirements for small time steps, necessary to insure numerical stability and/or appropriate accuracy. The maximum allowable time step decreases along with the scale of the space-discretization, making applications that require very small scales (e.g., small bays, detailed analysis of local pollutant transport) infeasible or undesirable because of the high costs involved. To keep the time step feasibly large, and still get solutions reasonably smooth, many users have adopted artificially high eddy viscosity coefficients, which has not been free of convincing criticism (e.g., see GRAY 1980).

To overcome these shortcomings of conventional "time-domain" models, investigators have lately attempted two alternative approaches:

- keep the time-domain approach, but based on the so-called wave formulation (e.g. GRAY and KINMARK 1986, LYNCH and WERNER 1986);
- adopt a frequency-domain approach, by applying harmonic method (a traditional technique before the advent of numerical modeling) in conjunction with FEM.

Models TEA and TEANL resort to this latter frequency-domain approach, which takes advantage of the periodic nature of the tidal phenomena, and of the fact that the primary frequencies of interest are known (and relatively few), to generate a set of quasi-steady (time-independent) governing equations for each

relevant frequency. Appropriate solution of these equations in space, by conventional FE (combined when necessary in an iterative procedure that accounts for non-linear interdependence of the different frequencies, and, hence, sets of governing equations), followed by a Fourier synthesis of the results, provides the desired information on tidal levels and velocities.

### B.3 - General Performance

TEA and TEANL are very attractive for the simulation of strongly tidal-dominated circulation in estuaries and coastal seas. Some of their potential merits include:

- (a) no time stepping constraints due to small element sizes are required;
- (b) eliminating the time dependence from the governing equations reduces them from the difficult and time-consuming hyperbolic type to the much more convenient elliptic type;
- (c) the results may be stored in a much more economical and convenient form for later use in a transport model;
- (d) long term residual currents are computed in a natural way;
- (e) cold-start problems, a traditional plague of "time-domain" models, are eliminated.

These models, are, however, potentially less attractive for non-tidal flows, both because a very large number of relevant frequencies may have to be handled, and because these frequencies may be randomly scattered.

Model TEA handles only the linearized forms of the governing equations and cannot account for interactions between different frequencies. Although first developed just as a core component for a fully non-linear model, TEA may be quite sufficient and very useful in relatively large and not excessively shallow water bodies, where non-linear effects do not dominate; even when a fully non-linear model will be required, using TEA first may constitute an extremely cheap and efficient way of selecting appropriate boundary conditions, detecting insufficiencies in grid discretization or bathymetry representation, helping on the set-up of field measurements, etc.

The procedure for using TEA consists in identifying dominant tidal frequencies, finding the appropriate forcing functions (tidal elevations and/or tidal flows in the model boundaries), running TEA for each frequency, and superposing results by synthesis of individual frequencies (we note that the zero-frequency can be handled, providing a useful way of simulating river or other quasi-steady flow inputs). The most delicate step (which is shared with most other models) is to define the boundary forcings, which should result from field data analysis, but often requires in complement a trial-and-error adjustment procedure.

Results from each run of TEA are in the form of space-variable amplitudes and phase shifts (relative to some pre-selected basic

phase) for flows and tidal elevations. Final results are in the form of flows (unambiguously related with depth-averaged velocities) and tidal elevations, which may vary in space and time, and may be generated for any desired tide or sequence of tides compatible with the input data.

TEANL is the fully non-linear version of TEA, and allows the handling of non-linear interactions between different frequencies (through the iterative procedure schematized in Fig. 1). This is extremely important in water bodies such as estuaries and small bays, where the astronomical tide is strongly distorted during propagation; the mechanism can be represented as the non-linear growth of harmonics of the principal astronomical constituents (e.g, DRONKERS 1964, PINGREE and GRIFFITHS 1979), resulting from finite amplitude effects entering through friction, non-linear advection and interactions with the geometry of the water body.

The inputs and outputs of TEANL are as in TEA, except by the fact that all frequencies of interest must be handled simultaneously, and therefore outputs constitute unbreakable sets. Superposition of all these frequencies to obtain final information on flow and tidal elevation is handled by harmonic synthesis, just as for TEA.



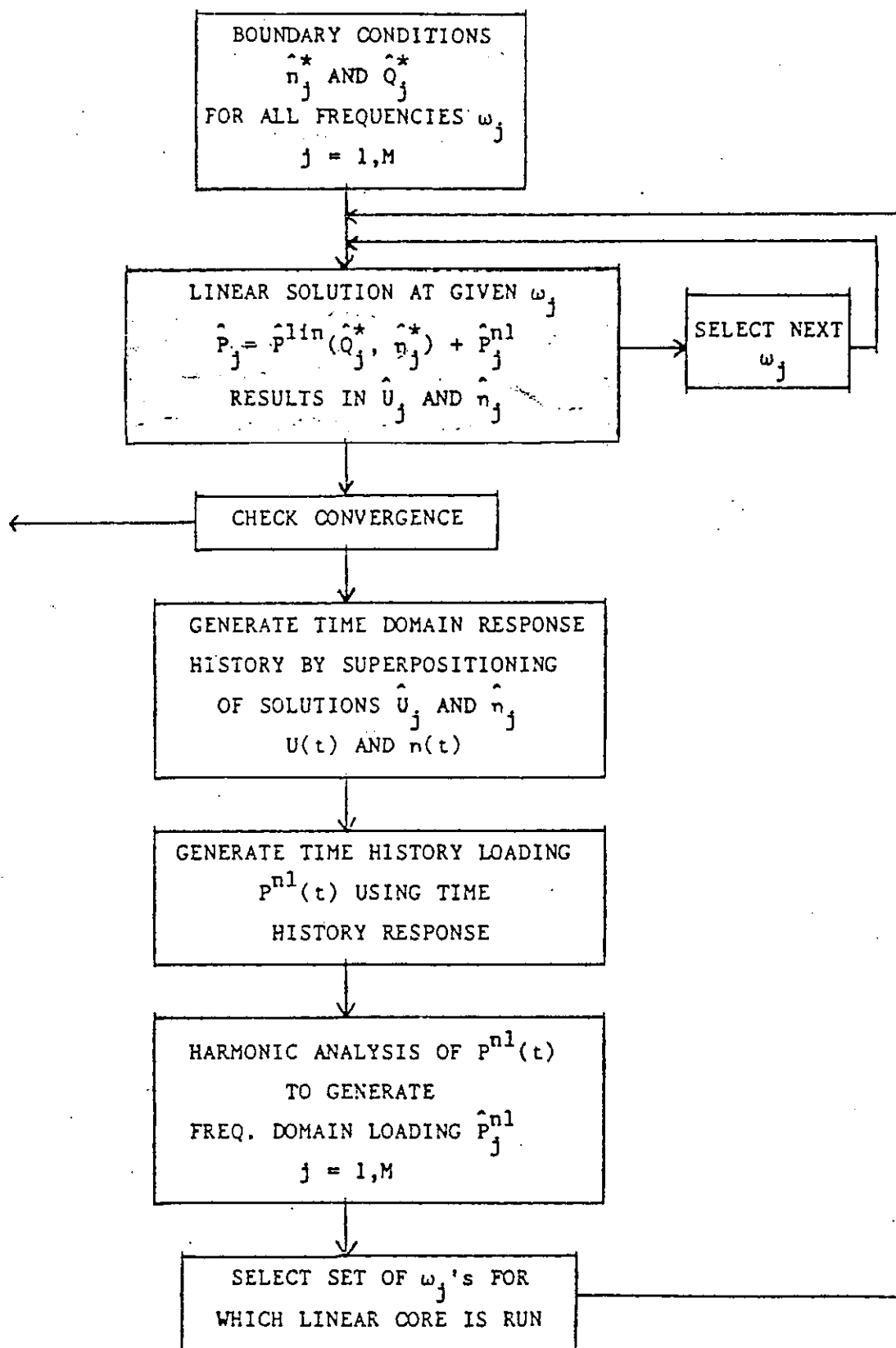


Fig. B.1. Iterative procedure for TEANL





APPENDIX C

SOURCE REPRESENTATION IN A NUMERICAL TRANSPORT  
MODEL



## SOURCE REPRESENTATION IN A NUMERICAL TRANSPORT MODEL

E. Eric Adams, Richard Kossik

Dept. of Civil Engineering, Massachusetts Institute of  
Technology, Cambridge, Massachusetts, USA

and A. Melo Baptista

Laboratório Nacional de Engenharia Civil, Lisboa, Portugal

### INTRODUCTION

Numerical models are routinely used to solve the advection diffusion equation for purposes of simulating pollutant transport in surface waters. A common difficulty in most such applications is to adequately represent concentrations in regions of high concentration gradient. For surface water calculations, strong gradients are found primarily near sources (e.g., pollutant outfalls).

One procedure for handling such problems is to represent the continuous plume near the source as the superposition of discrete puffs that are advected forward in time until they are of sufficient size to be adequately resolved with the numerical grid. Such a procedure is well suited to Lagrangian Transport Models or Eulerian-Lagrangian models in which the advection part of the advection-diffusion equation is simulated by a (Lagrangian) tracking technique.

This approach has been incorporated into the 2-D (depth-averaged) transport model ELA (Baptista et al., 1984a, b). ELA uses a split operator approach solving advection with a backwards method of characteristics using quadratic Lagrange polynomials for interpolation and using an implicit Galerkin Finite Element method for diffusion. Transformation processes such as volatilization are treated separately in a third operation. The technique is illustrated in a simulation of halocarbon concentration distributions resulting from sewage discharges into Boston Harbor.

### PROBLEM DESCRIPTION

Figure 1 illustrates a typical problem involving an outfall pipe discharging into a coastal environment discretized with a relatively uniform grid. For purposes of discussion, the near field

is defined as that region over which discharge momentum and buoyancy significantly influence local flow patterns. For a typical sewage outfall this dimension may be of order 10-100 m and no attempt is made to resolve concentrations within this region. However, it is desired to simulate realistic distributions as close to the near field as possible.

Theoretical analyses (e.g., Fourier analysis) and numerical experiments by a number of researchers have shown that the ability to successfully advect a pollutant source improves as the dimensionless source size (i.e., characteristic source size divided by characteristic grid dimension) increases. The minimum acceptable source size will depend on the numerical procedure and such parameters as Peclet and Courant number and total simulation time, but will fall in the general range of 3 to 10 (Gray and Pinder, 1976; Baptista et al., 1985). This criterion is not met, in general, for typical grid sizes of order 100-1000 m. As a result, artificial diffusion is introduced, either by the scheme itself, or by the model user who artificially introduces the mass over a larger-than-realistic region. In effect, the concentration distribution becomes artificially and instantaneously spread until it is wide enough to be advected satisfactorily. The result is erroneous prediction over an intermediate region at least as large as that required for physical processes to provide similar mixing. For tidal applications, this intermediate region can easily extend for a distance of one tidal excursion or more. For regions of strong tidal currents such as Boston Harbor, this can represent several kilometers or a significant fraction of the computational domain.

Figure 1 suggests three possible procedures for improving resolution up to the point at which physical processes have spread the pollutant enough to be resolved (i.e., the intermediate field): a) local grid refinement, b) stochastic particle tracking, and c) use of puffs.

With finite element models, grid refinement is conceptually straightforward. However, when the affected area is substantial, and multiple sources are involved, matrix size and bandwidth may increase substantially resulting in a significant increase in computational cost.

Particle tracking has been proposed as a way to resolve strong concentration gradients in Eulerian-Lagrangian models of ground-water transport (Newman, 1984). Using this approach, particles would be released at a rate corresponding to their effluent concentrations and advected by the known flow field. Diffusion can be handled by assigning a random or pseudo velocity component to the advected flow. The process is continued until the particles have diffused over sufficient elements that a smooth concentration field can be computed for subsequent discretized calculation. A major drawback with this approach is that, in order to accurately convert particle density to concentration, a large

number of particles must be tracked in relation to the number of grid points.

A third option involves the use of puffs as suggested by Adams et al. (1975) and used by Holly and Usseglio-Polatera (1984). In such an approach, the intermediate field plume is represented by a number of discrete puffs, released one at a time, with a size proportional to the near field mixing zone. As with particles, each puff is tracked forward in time. However, dispersion is handled by dispersing the puffs in accordance with a prescribed dispersion law, e.g., as determined by a tracer study or as estimated from the literature (Okubo, 1971). In contrast with particles, this may involve as little as one tracking per unit of time thus reducing costs. As illustrated below, the present approach is really a hybrid, using up to five trackings per puff in order to better define puff spreading. Nonetheless, the savings should still be substantial.

#### DETAILS

Figure 2 illustrates, schematically, puff placement for the simple case of a constant current. The elapsed time depicted is  $T = N\Delta t$  where  $\Delta t$  is the basic computational time step between alternate advection and diffusion calculations with ELA. ( $\Delta t = 3.1h$  is used in the following calculations.)

Assume  $M\Delta t$  is the minimum duration required for the puffs to mature to full size. ( $M = 1$  has been used in our calculations.) As indicated by the overlapping circular distributions, puffs are placed around the source corresponding to mass which is physically discharged during the period  $(N-M-1)\Delta t < \tau < N\Delta t$ . The most recently discharged mass is positioned first (adjacent to the source) and subsequent puffs are created to allow sufficient overlap.

Puffs created during the period of duration  $\Delta t$  from  $(N-M-1)\Delta t < \tau < (N-M)\Delta t$  are mapped onto the finite element grid at the beginning of the advection step. Younger puffs, created between  $(N-M)\Delta t < \tau < N\Delta t$ , are discarded unless a concentration printout is desired, in which case they are mapped onto a highly resolved local grid created only for contouring.

For the illustrative calculations below, symmetrical Gaussian puffs have been used implying isotropic dispersion. (However, different distributions could readily be used.) For each puff, the concentration distribution is thus

$$C = \frac{\dot{m}(t)\Delta\tau}{2\pi h \sigma^2} \exp\{-[(x-x_1)^2 + (y-y_1)^2]/2\sigma^2\} \quad (1)$$

where  $h$  is the local depth,  $\dot{m}$  is the mass loading rate,  $\Delta\tau$  is the time interval associated with the puff (see Figure 2),  $(x_1,$

$y_1$ ) is the center of mass, and  $\sigma$  is the standard deviation. Puff centers are tracked forward in time by reversing the fourth-order Runge-Kutta integration scheme used by ELA in the backward tracking of characteristics, along with the known space and time dependent variation in current speed. Thus

$$x_1(T) = x_0 + \int_{\tau}^T u \, dt \quad (2)$$

$$y_1(T) = y_0 + \int_{\tau}^T v \, dt$$

In principle, puff spreading can be computed from a relationship such as

$$\sigma^2(T) = \sigma_0^2(\tau) + 2 \int_{\tau}^T D \, dt \quad (3)$$

where  $D$  is an empirical (dispersion) coefficient and  $\sigma_0$  is the initial standard deviation at the edge of the near field.  $\sigma_0$  is determined from the near field mixing as

$$\sigma_0 = \frac{SQ_0}{\sqrt{12} |u| h} \quad (4)$$

where  $Q_0$  = effluent flow rate,  $|u|$  = instantaneous current speed, and  $S$  = near field volumetric dilution (determined from measurements or a model as a function of  $|u|$  and  $h$ ).

In a depth-integrated model,  $D$  represents physical mixing (dispersion associated with horizontal and vertical current shear as well as turbulent diffusion) plus fluid convergence/divergence effects associated with changing bottom and free surface elevation. Hence  $D$  would be expected to change with spatial position and time.

To help separate these effects, and render the intermediate field spreading of puffs similar to the far field mixing handled by finite element, an equivalent "diffusionless" puff distribution at time  $T$  can be computed by tracking  $n - 1$  additional particles. These particles are distributed initially at a distance of  $\sigma_0$  from the source center ( $x_0, y_0$ ) and are tracked along with the puff center. The equivalent  $\sigma$  is then approximated as the geometric mean of the distances between particles  $i$  and the center of mass:

$$\sigma^2 = \prod_{i=2}^n [(x_i - x_1)^2 + (y_i - y_1)^2]^{1/(n-1)} \quad (5)$$

If puffs are to be tracked over a long period of time, Equations (5) and (3) can be used sequentially over a number of time steps, with the first term on the right-hand side of Equation (3) taken to be the last value of  $\sigma^2$  from Equation (5). It is apparent that the major difference between this hybrid method and one using exclusively particles (i.e., Figure 2b) is the way in which diffusion is calculated.

#### APPLICATION

The above technique has been used to simulate the fate of treated sewage effluent discharged into Boston Harbor on the western shore of Massachusetts Bay. Boston Harbor has approximate mean width and depth of 10 km and 10 m, and is characterized by numerous islands and complicated bottom topography. Flow is primarily tidally driven with mean amplitude of about 1.4 m.

Figure 3 sketches the finite element grids that are used. The largest grid (Figure 3a) includes 888 triangular elements with linear basis functions used to compute circulation with the harmonic circulation model TEA (Westerink et al., 1985). Transport calculations are made with the inner grid (Figure 3b) comprised of triangles with quadratic interpolation functions used for the finite element (diffusion) calculations and for the interpolation component of the advection calculations. The two major effluent sources are indicated (as black dots) on Figure 3b: the Deer Island Treatment Plant (to the north) and the Nut Island Treatment plant (to the south) discharging respectively 18.4 m<sup>3</sup>/s and 5.9 m<sup>3</sup>/s.

Field measurements indicate that near field dilution is a strong function of tidal phase obeying the following approximate relations:

$$\begin{aligned} S &= 50.5|u| + 6.5 && \text{(Deer Is.)} \\ S &= 31.7|u| + 5.5 && \text{(Nut Is.)} \end{aligned} \quad (6)$$

where  $|u|$  is in m/s. For the Deer Is. outfall,  $|u|$  varies from about 0.07 to 0.61 m/s between slack tide and maximum flood resulting in almost a factor of four variation in dilution ( $10 < S < 37$ ). For Nut Is.,  $0.04 < |u| < 0.25$  m/s resulting in a factor of two variation in dilution ( $7 < S < 13$ ).

Figure 4 illustrates computed concentration contours for the compound 1,1,1-trichloroethane, an industrial solvent discharged through both outfalls at a concentration of approximately 6.7 ppb. Simulations are shown at high tide under conditions of periodic steady-state due to  $M_2$  tidal forcing (period = 12.4 hours), no wind stress (resulting in minimal residual circula-



tion), an ambient diffusion coefficient of  $10\text{m}^2/\text{s}$ , and a piston velocity of  $10\text{ cm/hr}$  describing volatilization. Measurements of halocarbon concentrations have also been taken in the harbor and substantiate the 2-D assumption. Parallel efforts are now under way aimed at a) model validation, b) establishing the viability of halocarbons as sewage tracers, and c) exploring the process of volatilization by comparing the geochemical fractionation of several related compounds both discharged and measured simultaneously. However, for present purposes, Figure 4 is presented to illustrate the sensitivity of predicted concentrations to the source representation. In particular, note the area of high concentrations west of the discharge from Deer Island and southwest of the discharge from Nut Island. These high concentrations represent effluent that was discharged during low tide when near field dilution is low and that has been advected toward shore during flood tide. Preliminary field measurements have confirmed this phenomenon. Figure 5a depicts corresponding high tide concentrations resulting from only the puffs released near the Deer Island outfall during the most recent 6.2 hours ( $M = 1$ ,  $\Delta t = 3.1$  hours) and Figure 5b shows the local grid. The factor of approximately 2.5 between concentrations at the western and eastern edges of the plume (representing discharge at low and high tide respectively) and those in the center (representing discharge during flood tide) is apparent.

The above calculations were made with a time step of 3.1 hours or one-fourth of a tidal period. As such, substantial computational savings were possible by saving, for each of the four tidal phases, both 1) the feet of the characteristic lines emanating backwards from each grid point necessary for computing far field concentration and 2) the intermediate field puff statistics ( $\Delta r$ ,  $x_1$ ,  $y_1$ ,  $\sigma$ ). Using this procedure it is estimated that the CPU time required for a two-week simulation (27 tidal cycles and the approximate time required to reach periodic steady state) is about two times that required for a single tidal cycle. While more accurate calculations would use additional tidal components, with longer repeating intervals, it is likely in many instances that transport calculations would still be required for multiple cycles, hence justifying the storage.

## CONCLUSIONS

The above description and application illustrate how puffs can be used efficiently to provide increased resolution near effluent sources in pollutant transport models. Outfall configurations, models parameters (e.g., diffusion coefficients) and puff representation have been kept simple for illustration, but more sophistication can be employed if desired and warranted by available data.

## REFERENCES

- Adams, E. E.; Stolzenbach, K. D.; and Harleman, D. R. F. (1975) Near and Far Field Analysis of Buoyant Surface Discharges into Large Bodies of Water. Report No. 205, R. M. Parsons Laboratory for Water Resources and Hydrodynamics, M.I.T., Cambridge, Mass.
- Baptista, A.; Adams, E. E.; and Stolzenbach, K. D. (1984a) Eulerian-Lagrangian Analysis of Pollutant Transport in Shallow Water. Report No. 296, R. M. Parsons Laboratory for Water Resources and Hydrodynamics, M.I.T., Cambridge, Mass.
- Baptista, A. M.; Adams, E. E., and Stolzenbach, K. D. (1984b) The 2-D Unsteady Transport Equation Solved by the Combined Use of the Finite Element Method and the Method of Characteristics. Proc. 5th Int'l Conf. on Finite Elements in Water Resources, U. of Vermont, Burlington, Vt.
- Baptista, A. M.; Adams, E. E.; and Stolzenbach, K. D. (1985) Comparison of Several Eulerian-Lagrangian Models to Solve the Advection-Diffusion Equation. Proc. 2nd Int'l Symp. on Refined Flow Modeling and Turbulence Measurements, U. of Iowa, Iowa City, Iowa.
- Gray, W. G.; and Pinder, G. F. (1976) An Analysis of the Numerical Solution of the Transport Equation. Water Resources Research, 12:547-555.
- Holly, F. M., Jr.; and Usseglio-Polatera, J.-M. (1984) Dispersion Simulation in Two-Dimensional Tidal Flow. Journal of Hydraulic Engineering, 110:905-926.
- Neuman, S. P. (1984) Adaptive Eulerian-Lagrangian Finite Element Method for Advection-Dispersion. Int'l Journal for Numerical Methods in Engineering, 20:321-337.
- Okubo, A. (1971) Oceanic Diffusion Diagrams. Deep Sea Research, 18:789-802.
- Westerink, J. J.; Stolzenbach, K. D.; and Connor, J. J. (1985) A Frequency Domain Finite Element Model for Tidal Circulation. Report No. MIT-EL 85-006, M.I.T. Energy Laboratory, Cambridge, Mass.

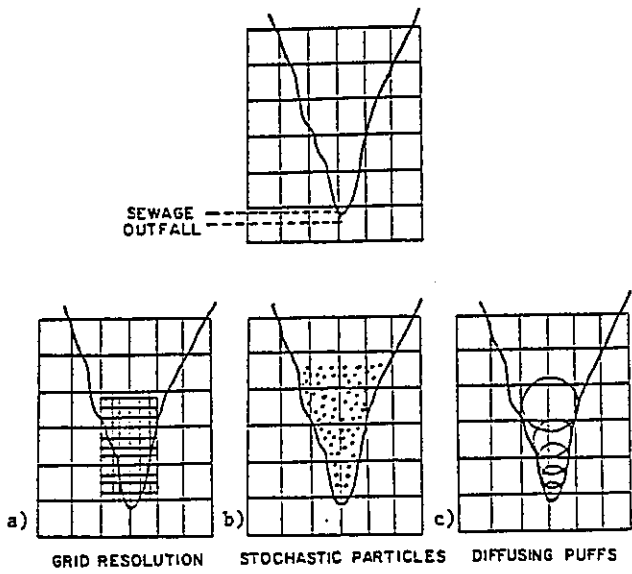


Figure 1. Techniques to Improve Near Source Resolution

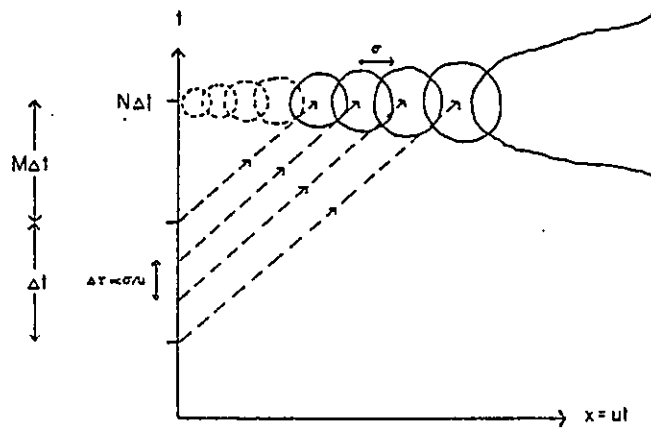


Figure 2. Schematic of Puff Placement

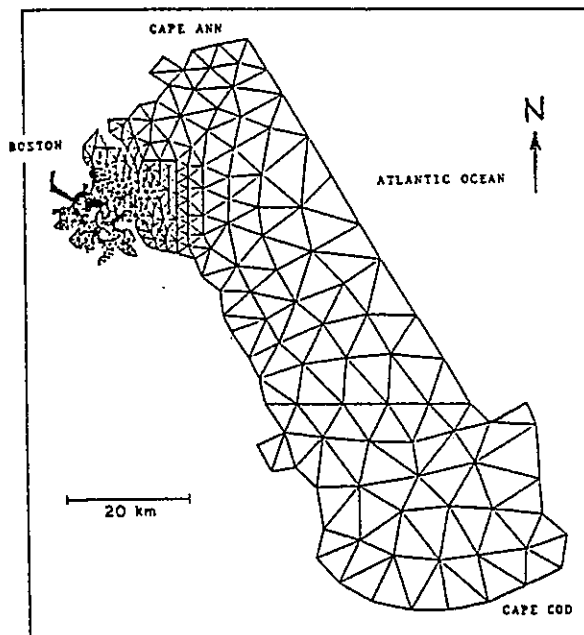


Figure 3a. Finite Element Grid of Massachusetts Bay

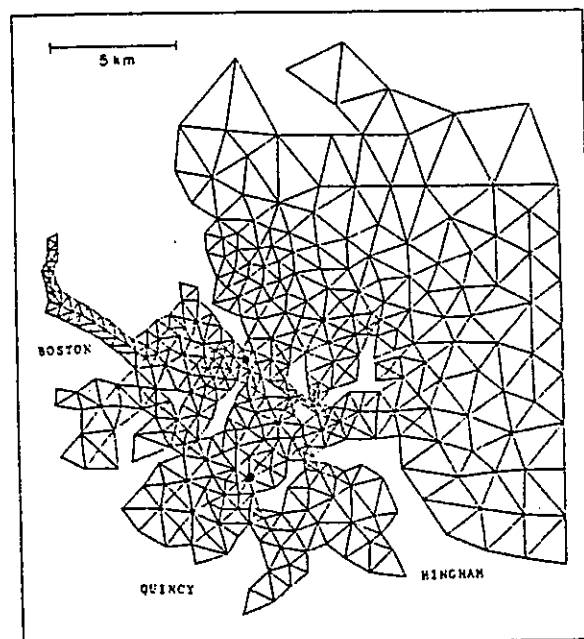


Figure 3b. Finite Element Grid—Detail of Boston Harbor

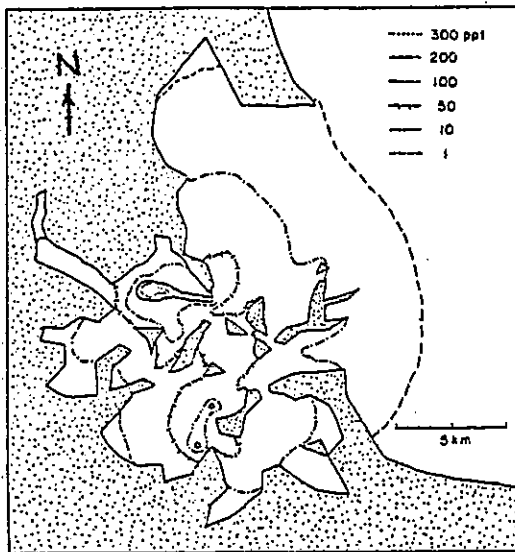


Figure 4. Simulated Intermediate and Far Field Concentration Distribution at High Tide for  $Q_0 = 24.3 \text{ m}^3/\text{s}$ ,  $C_0 = 6.7 \text{ ppb}$ ,  $K = 10 \text{ cm/hr}$ , and  $D = 10 \text{ m}^2/\text{s}$

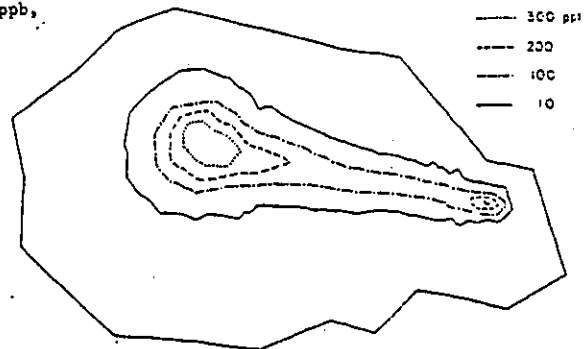


Figure 5a. Simulated Intermediate Field Concentration Distribution at High Tide (Elapsed Time = 6 hrs) Corresponding to Conditions of Figure 4

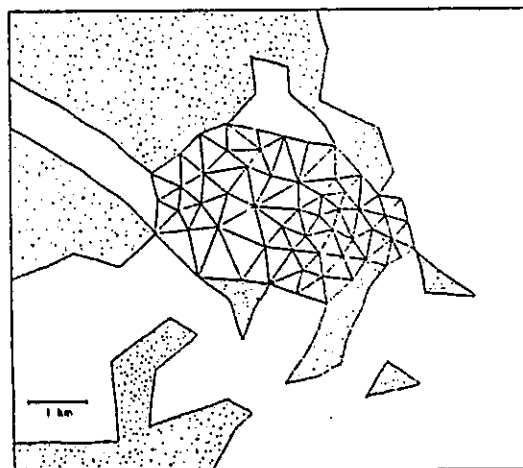


Figure 5b. Detail of Grid Within Border Shown on Figure 5a